Quaternary evolutionary persistence of Southern Ocean benthic taxa

Thesis submitted by:

Sally Cheuk Ying Lau

For the degree of Doctor of Philosophy

College of Science and Engineering
James Cook University
Townsville, Queensland
Australia

January 2022

Statement on the Contributions of Others

Intellectual Support

Thesis committee:

Professor Jan M. Strugnell	James Cook University (Australia)
Dr Nerida G. Wilson	Western Australian Museum (Australia)
Dr Catarina N.S. Silva	James Cook University (Australia)

Additional collaborators:

Chapter 2, 4:

Dr Chester J. Sands	British Antarctic Survey (United Kingdom)

Chapter 3, 5:

Professor Phillip C. Watts	University of Jyväskylä (Finland)
Dr Toni Jernfors	University of Jyväskylä (Finland)
Dr Ira R. Cooke	James Cook University (Australia)
Professor Louise Allcock	National University of Ireland, Galway (Ireland)

Chapter 6:

Professor Nick R. Golledge	Victoria University of Wellington (New Zealand)
Professor Tim R. Naish	Victoria University of Wellington (New Zealand)

Intellectual support contribution:

The core ideas of the thesis were developed from an Australian Research Council (ARC) Discovery grant received by Prof. Jan Strugnell, Dr. Nerida Wilson, Prof. Nick Golledge and Prof. Tim Naish, which *Chapter 6* particularly addressed the questions raised in the ARC grant proposal. I was responsible for formulating the other chapters of the thesis (*Chapter 1 - 5*) in order to provide research evidence to refine the research questions and methods of *Chapter 6*, with the intellectual guidance, analysis support and editorial assistance of my thesis committee and additional collaborators.

Financial support

Funding obtained by candidate:

Stipend:

James Cook University Postgraduate Research Scholarship	AUD $94,787
Antarctic Science Foundation PhD student support grant	AUD $5,000

Research support:

David Pearse Bequest – Promoting Environmental Research	AUD $12,500
Antarctic Science International Bursary	GBP £5,996
Australasian eResearch Organisations (AeRO) Cloud Grants Program	USD $1,000

James Cook University College of Science and Engineering Competitive Research Training Grant (2020)	AUD $2,700
James Cook University College of Science and Engineering Competitive Research Training Grant (2019)	AUD $3,000

Funding obtained by thesis committee:

Australian Research Council Discovery grant by Prof. Jan Strugnell, Dr. Nerida Wilson, Prof. Nick Golledge and Prof. Tim Naish	AUD $285,000
Thomas Davies Research Grant for marine, soil and plant biology awarded to Prof. Jan Strugnell	AUD $24,432

Funding obtained by additional collaborators:

Academy of Finland (award number 305532) by Prof. Phillip Watts with Prof. Jan Strugnell and Prof. Louise Allcock

James Cook University:

James Cook University provided laboratory space and infrastructures for High Performance Computing

Data collection

Biological sample loans:

Western Australian Museum (WAM)	*Chapter 2,4,6*
Museum Victoria (MV)	*Chapter 2,4,6*
Australian Antarctic Division (AAD)	*Chapter 2 - 6*
National Institute of Water and Atmospheric Research (NIWA)	*Chapter 2,4,6*
Muséum National d'Histoire Naturelle (MNHN)	*Chapter 2,4,6*
British Antarctic Survey (BAS)	*Chapter 2,4,6*
Scripps Institution of Oceanography (SIO)	*Chapter 2,4,6*
Smithsonian National Museum of Natural History (NMNH)	*Chapter 2,4,6*

Research assistance:

Jose Carvajal, Mia Hillyer and Alex Hickling (all WAM) for sequencing assistance	*Chapter 2*
Greg Rouse (SIO) for making sequences available	*Chapter 2*
Toni Jernfors (University of Jyväskylä) for sequencing assistance	*Chapter 3, 5*

Field support:

Crew, technicians and scientists on RV Investigator during IN2020_V01

Research output related to PhD thesis

Peer-reviewed publications:

Lau, S. C. Y., Wilson, N. G., Silva, C. N. S., & Strugnell, J. M. (2020). Detecting glacial refugia in the Southern Ocean. *Ecography*, **43**(11), 1639–1656. **Invited under the Ecography E4 award*

Lau, S. C. Y., Strugnell, J. M., Sands, C. J., Silva, C. N. S., & Wilson, N. G. (2021). Evolutionary innovations in Antarctic brittle stars linked to glacial refugia. *Ecology and Evolution*, **11**(23), 17428–17446.

Workshop / conference presentations:

Batch effects in the same positions, but two sequencing methods. Lightening talk at the 2021 Centre for Tropical Bioinformatics and Molecular Biology retreat. James Cook University, Australia. 29 – 31 October 2021.

Morphological innovations in brittle stars driven by sub-Antarctic glacial refugia. Online presentation at the Scientific Committee on Antarctic Research (SCAR) 2020. 3 – 7 August 2020.

Brooder and broadcast spawner in the Southern Ocean: hybridisation and spatial genetic patterns in brittle stars. Oral presentation at the 2019 Centre for Tropical Bioinformatics and Molecular Biology retreat. James Cook University, Australia. 30 September – 1 October 2019.

Brooder and broadcast spawner in the Southern Ocean: hybridisation and spatial genetic patterns in brittle stars. Oral presentation at the Society of Australian Systematic Biologists: 5th National Postgraduate Training Working in Systematics, University of Adelaide, Australia. July 2018. **Awarded the best student presentation*

Other research output during candidature

Peer-reviewed publications:

Woodings, L. N., Murphy, N. P., Liggins, G. W., Miller, M. E., Ballinger, G. M., Lau, S. C. Y., & Strugnell, J. M. (2021) Population genomics of the Eastern Rock Lobster, *Sagmariasus verreauxi*, during spawning stock recovery from over-exploitation. ICES Journal of Marine Science, **78**(7), 2448–2459.

Lau, S. C. Y., Thomas, M., Hancock, B., & Russell, B. D. (2020). Restoration potential of Asian oysters on heavily developed coastlines. *Restoration Ecology*, **28**(6), 1643–1653.

Caswell, B., Klei, E. S., Alleway, H. K., Ball, J., Botero, J., Cardinale, M., Eero, M., Engelhard, G. H., Fortibuoni, T., Giraldo, A.-J., Hentati-Sundberg, J., Jones, P., Kittinger, J. N., Frause, G., Lajus, D. L., Lau, S. C. Y., Lescrauwaet, A.-K., MacKenzie, B., McKenzie, M., ... & Thurstan, R.H. (2020) Something old, something new: historical perspectives provide lessons for blue growth agendas. *Fish and Fisheries*, **21**(4), 774–796.

Acknowledgements

I would like to firstly thank my advisory panel, Prof Jan Strugnell, Dr Nerida Wilson and Dr Catarina Silva. It was a privilege to be supervised by an all-female advisory team. Thank you for believing in my passion despite my limited background in genetics. Without your combined leadership, intellectual guidance, wisdom, compassion and patience, this PhD would not have been a success, particularly during a global pandemic. I am very grateful for the mentorship that I received, and intellectual freedoms you allowed during my candidature. Looking back the journey was hard at times but it had always been an extremely rewarding, fun and exciting ride all because of your support. I hope one day I can pass on these wonderful skills and lessons to future generations.

I would like to thank to the Marine Omics lab group and Dr Ira Cooke at James Cook University for their encouragement and guidance throughout my PhD. Every time I hit a wall, you always offered generous support and insights to help me get back on track, again and again. I would also like to thank our collaborators; Dr Ira Cooke, Dr Chester Sands, Prof Phillip Watts, Prof Louise Allcock, Prof Nick Golledge and Prof Tim Naish, for their support and feedback along the way.

This thesis would not be possible without the funders who supported my PhD, including the Australian Academy of Science, Australasian eResearch Organisations, Academy of Finland, Australian Research Council, Antarctic Science Foundation, Antarctic Science Ltd, David Pearse Bequest and James Cook University. The institutes around the world who loaned us the many biological samples used in my thesis, including those from the Western Australian Museum (AUS), Museum Victoria (AUS), Australian Antarctic Division (AUS), National Institute of Water and Atmospheric Research (NZ), Muséum National d'Histoire Naturelle (FR), British Antarctic Survey (UK), Scripps Institution of Oceanography (US) and Smithsonian National Museum of Natural History (US). I am grateful for sequencing assistance by Dr Jose Carvajal, Mia Hillyer and Alex Hickling at Western Australian Museum and Dr Toni Jernfors at the University of Jyväskylä, and Prof Greg Rouse at Scripps Institution of Oceanography for making sequences available. I would also like to thank the crew, technicians and scientists on RV Investigator during IN2020_V01 for making my first Southern Ocean expedition an incredible experience. In particular, I would like to thank Prof Mike Coffin for their support and wisdom on board, and Paige Maroni for being the best teammate/cabin buddy/friend one could ever ask for!

Thank you to my friends, both in Australia and afar, who have supported me along the way. Sara and Laura, I am thankful that I met you both at my first week at JCU. Maisy, Jes and Jo, I am very grateful that I met you all in my first year at Southampton. Thank you to my mentors whom I am fortunate enough to have met before, Dr Adam Reed and Dr Laura Grange from the UK who first introduced me to the world of Antarctica. Thank you to Dr Juan Carlos Astudillo and Dr Bayden Russell from Hong Kong, who paved the way for my early academic journey after two wonderful years of looking at bivalves, uncovering lost ecosystems, and guiding me to navigate life up until today!

Finally, thank you to my family who has always let me follow my heart and advocated for me through thick and thin over all the years. Thank you to my partner, Jonathan, for your love and patience even though I am so stubborn and no fun at times. It has been an incredible journey and I wouldn't have it any other way.

General Abstract

In this thesis I explored the complex evolutionary histories of Southern Ocean benthic taxa using molecular genetics. I investigated how the demographic history of these benthic species has been influenced by their ecology, life history, and also the physical environmental processes that occurred throughout the Quaternary. As a result, I demonstrated that by understanding the evolutionary histories of Southern Ocean benthic species, historical Antarctic Ice Sheet configurations can be reconstructed, which is crucial for accurate global sea level rise projections.

Using partial cytochrome c oxidase subunit 1 (COI) mitochondrial gene sequences and restriction-site associated DNA (RAD) loci data, I investigated the population genetic patterns of the brittle stars *Ophionotus victoriae*, *O. hexactis* and the octopus *Pareledone turqueti*, with different reproductive strategies. I explored the drivers of diversification and evolutionary innovations between *O. victoriae* (five arms, broadcaster) and *O. hexactis* (six arms, brooder). I studied whether the levels of population structure between species with different dispersal strategies might be different, including *O. victoriae, O. hexactis* and *P. turqueti* (benthic juveniles). Finally, I examined the whether the past configuration of the West Antarctic Ice Sheet (WAIS) can be deduced in two independent species, *O. victoriae* and *P. turqueti*, with contrasting reproductive strategies.

In *Chapter 2*, using COI data, I first explored species boundaries within *O. victoriae* (five arms, broadcaster), the genealogical relationship between *O. victoriae* and *O. hexactis* (six arms, brooder), and the species history for *O. victoriae* and *O. hexactis*. I found that *O. victoriae* is a single species (rather than a species complex) and is closely related to *O. hexactis* (a separate species). During periods of glacial maxima throughout the Quaternary, *O. victoriae* and *O. hexactis* likely persisted in deep-sea and Antarctic island refugia, respectively. Within *O. victoriae*, I detected clear circumpolar genetic connectivity, within and between the Antarctic continental shelf and islands, which were linked to the contemporary Antarctic Circumpolar Current and local oceanographic regimes. Finally, I suggested that survival within Antarctic island refugia was associated with an increase in arm number and a switch from broadcast spawning to brooding in *O. hexactis*. I proposed that the evolutionary innovations within *O. hexactis* could be linked to environmental changes (such as salinity) associated with intensified interglacial-glacial cycles.

Only sequence data collected at a genome-wide scale can offer high enough resolution information to resolve past changes in species demographic history. However, the widely

used reduced representation genome-wide sequencing approaches, such as RAD sequencing (RADseq), are ineffective for many Southern Ocean biological samples as they are frequently subject to DNA degradation. As a case study (*Chapter 3*), I found a target capture sequencing approach was highly effective in retrieving reads in the corresponding, previously identified double-digest RAD (ddRAD) loci in degraded samples of *P. turqueti*. When comparing reads sequenced at the exact same genomic positions obtained from ddRADseq and target capture sequencing, I found a clear batch effect between the two methods. Such a batch effect was driven by an apparent bias towards homozygous genotypes linked to allele dropout and low coverage reads in ddRADseq data. It is becoming clear that some of the detected sequencing errors within ddRADseq are not unique to this case study, and they have been reported in other published datasets sequenced from non-Southern Ocean taxa leading to biased data analyses. I demonstrated that target capture sequencing is a robust approach for generating high quality genome-wide data in degraded Southern Ocean samples, and it is associated with fewer genotyping errors compared to traditional RAD techniques.

In *Chapter 4*, I investigated the genomic signatures of past changes in demographic history in *O. victoriae* and *O. hexactis*, based on hypotheses proposed in *Chapter 2*, using RAD loci information sequenced with a target capture sequencing approach. I found that *O. victoriae* and *O. hexactis* diverged ~0.43 million years ago with interspecific gene flow in areas where their distributions overlap. This divergence time coincides with the timing of significant Antarctic Ice Sheet retreat and reduced surface salinity (Marine Isotope Stage (MIS) 11). Since then, *O. victoriae* likely persisted in deep-sea refugia, as well as within *in situ* refugia on the Antarctic continental shelf and around Antarctic islands, while *O. hexactis* likely persisted exclusively within *in situ* island refugia. In *O. victoriae*, I found contemporary gene flow can be linked to linking to the Antarctic Circumpolar Current, regional gyres and other local oceanographic regimes. In *O. hexactis*, I also found strong gene flow connecting West and East Antarctic islands near the Polar Front. The evolutionary innovations in *O. hexactis* (increase in the number of arms and switch to brooding from broadcasting) can be linked to selection under intense deglacial meltwater during MIS 11 around Antarctic islands, with strong association detected between outlier loci and salinity. This chapter provides genomic evidence indicating that intense interglacial-glacial cycles in the recent past can lead to innovative evolutionary changes and species divergence.

In *Chapter 5*, I investigated how seascape dynamics at circumpolar and regional scales can drive genomic variations in *P. turqueti*, using RAD loci information sequenced with a target capture sequencing approach. I found *P. turqueti* is biogeographically structured with clear

signatures of isolation-by-geographical distance, but long-distance genetic connectivity was also detected between East and West Antarctica. At a circumpolar scale, genomic variation of *P. turqueti* was most significantly linked to bottom water temperature. However, within the Scotia Arc (regional scale), geographical distance and isolation-by-water depth were the only significant drivers of genomic variation. I found a genotype-environmental association between warmer temperatures and samples from sub-Antarctic localities (South Georgia/Shag Rocks). I also detected a putative positive selection of hemocyanin (oxygen transport protein) around the Scotia Arc. The findings suggested a possible physiological adaptation to warmer temperatures around the sub-Antarctic in *P. turqueti*. Critically, I identified the seascape drivers of genomic variation in the Southern Ocean across circumpolar and regional scales.

Under current climate change predictions, it is unclear whether the marine-based West Antarctic Ice Sheet (WAIS) will collapse based on current trajectories in temperature rise. A complete WAIS collapse could raise global sea level by ~3.3 - 5 m. Only knowledge of what occurred during similar past climates can inform and thus constrain this uncertainty in current predictions. It is well understood that the warm interval of the Last Interglacial Period (LIG; 120,000 years ago) experienced global sea level 6 - 11 m higher than today, but the average air temperature was only 0.5 - 2°C warmer than the pre-industrial period. Whether WAIS experienced any, partial or complete collapse during LIG is still under debate due to lack of empirical data. Based on the species concepts, and evolutionary and bioinformatic context developed in *Chapters 2-5*, in *Chapter 6*, I demonstrated an innovative approach that indicated the WAIS collapsed during the LIG. Using RAD loci data of *O. victoriae* and *P. turqueti*, I found the genomic patterns of *P. turqueti* and *O. victoriae* are characterised by contemporary circumpolar gene flow and distinct signatures of historical trans-west Antarctic seaways linking the present-day Weddell Sea, Amundsen Sea and Ross Sea. Using demographic models, I inferred the historical trans-west Antarctic seaways can be dated back to LIG. Such historical connectivity was not linked to circumpolar currents; rather, it was statistically explained by the scenario of a complete WAIS collapse. My data pinpointed the thresholds of WAIS instability, which had been a significant deep uncertainty, yet a tipping point event, in future global sea level rise projections.

This thesis demonstrated the global significance of ecological and evolutionary studies of Southern Ocean taxa. I tested species concepts (*Chapter 2*) and established the robustness of sequencing technologies (*Chapter 3*). I also investigated the overall evolutionary histories of *O. victoriae* and *P. turqueti* (*Chapter 4-5*). Overall, I demonstrated that by synthesising knowledge derived from systematic, ecological and evolutionary research of Southern Ocean

taxa, applied questions of global significance can be answered, including whether the WAIS collapsed during LIG (*Chapter 6*). The findings of this thesis begin to elucidate how climatic warming experienced in Antarctica today will lead to strong increase in WAIS mass loss for centuries to come.

Table of Contents

List of Tables

List of Figures

CHAPTER 1

General Introduction

Part of this chapter is formatted for, and published in:

Lau, S. C. Y., Wilson, N. G., Silva, C. N. S. & Strugnell, J. M. (2020). Detecting glacial refugia in the Southern Ocean. *Ecography*, **43**(11), 1639–1656.

1.1 Evolutionary persistence in the Southern Ocean

Throughout the Quaternary (2.6 million years ago - now), extensive climatic oscillations caused shifts in global species distributions in a cyclical rhythm (Hewitt, 2004; Maggs et al., 2008; Provan & Bennett, 2008). During periods of glaciation, ice sheets expanded over high and mid latitude regions globally. During interglacial periods, global ice sheets contracted and were restricted to higher latitudes. In the Northern Hemisphere, biogeographic evidence suggests many Arctic and temperate taxa, from both the terrestrial and marine environments, migrated to warmer and lower latitude areas during glacial cycles. These newly colonised habitats at lower latitude would exhibit climatic conditions similar to that in their previous distributional range (Maggs et al., 2008; Provan & Bennett, 2008). In the Southern Hemisphere, the East Antarctic Ice Sheet, West Antarctic Ice Sheet and the Antarctic Peninsula Ice Sheet (collectively forming the Antarctic Ice Sheet (AIS)) also expanded and contracted throughout the Quaternary (Ingólfsson, 2004). The seafloor of the Antarctic continental shelf was repeatedly eroded by the advance and retreat of grounded ice sheets (i.e. ice sheets resting on the seabed) (Pollard & DeConto, 2009). Across the Antarctic continental shelf, these grounded ice advances are hypothesised to have catastrophically eliminated most seafloor habitat and communities, over and over again across glacial cycles (Clarke, 2008; Thatje et al., 2005).

For most benthic fauna that lived on the Southern Ocean continental shelf, migration to lower latitudes during the Quaternary glacial periods seems improbable (Thatje et al., 2005). The Southern Ocean contains the Antarctic Circumpolar Current (ACC) system with associated fronts and meridional overturning circulations that penetrate into the deep sea (Rintoul et al., 2001). These are hypothesised to have isolated most Southern Ocean fauna from other oceans since the onset of the ACC around ~34 million years ago (Clarke et al., 2004).

However, faunal migration to lower latitudes is not impossible (Clarke et al., 2004), and molecular evidence has shown an evolutionary radiation of Southern Ocean octopods into adjacent deep-sea basins (Strugnell et al., 2008). Fundamentally, the majority of palaeontological and molecular evidence suggests that many extant Southern Ocean benthic taxa appeared to have evolved, diversified and persisted *in situ* since the early to middle Eocene (Crame, 2018).

It has been argued that Southern Ocean benthic fauna likely survived glacial periods on the Antarctic continental shelf (Convey et al., 2009, 2018). However, the exact locations of glacial refugia for these fauna remain mostly unknown. The benthic fauna makes up ~88% of extant Southern Ocean marine species, and are well-represented by phyla such as Arthropoda, Bryozoa, Cnidaria, Echinodermata, Mollusca, Nematoda and Porifera (De Broyer et al., 2011). These species would have to be able to settle, mature and reproduce in a stable environment in order to persist throughout these periods. Similarly, evidence from the Antarctic terrestrial realm also suggests terrestrial biota persisted *in situ* over a multimillion year timescale (Convey et al., 2008). Ice free areas sustained by high geothermal activities are suggested to have served as local glacial refugia for some Antarctic terrestrial taxa (Fraser et al., 2014). However, these geothermal refugia appear restricted to the terrestrial realm, as marine geothermal vents tend to exclusively support small-scale endemic communities (Rogers et al., 2012; Roterman et al., 2016). If glacial advances were extensive and severe during past glacial maxima, where and how did the Southern Ocean benthic fauna survive?

Understanding how benthic fauna persisted within the Southern Ocean throughout the Quaternary, despite repeatedly challenged by environmental extremes, could provide insights into their resilience and vulnerabilities over time. Importantly, understanding how signatures of glacial survival are intertwined with signatures of species ecology, how ocean currents continuously influence dispersal, and how other historical AIS processes also determined their survival, can provide a clear picture of their evolutionary histories over a multimillion year timescale. These topics have been challenging to examine, as biological samples from this remote ecosystem are scarce, and for many years they were rarely preserved in a way that could be used for molecular sequencing. However, ‘DNA-friendly’ samples have become increasingly available following voyages to the Southern Ocean, such as those supporting the Census of Antarctic Marine Life (CAML; 2000-2010) and the International Polar Year (IPY; 2008-2009). Sequencing the ‘barcoding gene’ (partial mitochondrial cytochrome c oxidase subunit I; COI) from Southern Ocean biota was championed by the Marine Barcode of Life (BOLD) project and CAML (Grant & Linse, 2009).

These, and similar, co-ordinated sampling and sequencing initiatives have facilitated the description of emerging genetic patterns and evolutionary histories in Southern Ocean species.

This chapter first examines the current literature surrounding how Southern Ocean benthic taxa persisted through the Quaternary, particularly how they survived extreme glacial cycles in the past when most of the habitats were inhabitable. Through synthesising existing conceptual and molecular evidence, I identify and discuss current research gaps on how the genomic signatures of glacial cycles survival are intertwined with the signatures of species ecology, dispersal and other physical processes of the Southern Ocean. I highlight that there are limited data on each of these topics. I also introduce the current state of molecular analytical methods, as well as the research methods that I will use in my thesis, in order to address these research gaps.

1.2 Potential glacial refugia inferred from past Antarctic Ice Sheet reconstructions

Of all past glacial maxima, the configuration and behaviour of the AIS during the most recent Last Glacial Maximum (LGM; ~20 ka BP) is the most well-understood (Bentley et al., 2014). Since the AIS expanded across almost the entire Antarctic continental shelf during the LGM, glacial refugia for marine benthic fauna on the shelf are often suggested to be highly limited across many glacial cycles (Thatje et al., 2005). Nonetheless, various locations of glacial refugia for Southern Ocean benthic fauna have been proposed within and around the Antarctic continental shelf and adjacent regions. These hypothesised glacial refugia include unglaciated areas on the Antarctic continental shelf and deeper areas near the shelf margin, as well as the continental slope, deep sea and adjacent islands (Kott, 1969; Brey et al., 1996; Crame, 1997; Thatje et al., 2005; Convey et al., 2009). The overall locations of glacial refugia were largely proposed based on the understanding of possible ice-free areas on the shelf during the LGM. However, over repeated glacial-interglacial cycles, refugia on the Antarctic continental shelf would establish in ice-free areas during AIS expansions and subsequently dissolve during AIS retreats, when previously glaciated areas become available for colonisation. Throughout the Quaternary, the formation of ice-free refugia with the same size, at the same locations, on the shelf at each glacial maximum would require glacial periods to exhibit constant, repeated fluctuations. It is known that the total ice volume of the AIS and the magnitude of glacial extent across the continental shelf varied between glacial maximum throughout different phases of the Quaternary (Pollard & DeConto, 2009). Therefore, at each

glacial maximum, while the size of glacial refugia free from grounded ice was unlikely to be constant, whether glacial refugia located in the same areas on the shelf requires further examination of past AIS morphology in higher resolution.

Based on current ice sheet models, the amplitude of Antarctic ice volume changes over glacial-interglacial periods only became highly profound in the past one million years (Pollard & DeConto, 2009; De Boer et al., 2014; McKay et al., 2016). Similar fluctuation patterns in Antarctic atmospheric conditions between glacial-interglacial periods were also detected in the last one million years (Jouzel et al., 2007; Elderfield et al. 2012). Therefore, the AIS configuration at glacial maxima throughout the past one million years may have been similar to the LGM configuration. While it is also generally regarded that the LGM grounded ice was extensive and eroded most of the Southern Ocean continental shelf, reconstruction of the LGM AIS configuration indicates that the grounded ice did not always extend to some parts of the continental shelf break. Areas free from grounded ice present on the outer shelf during the LGM have been detected in the Eastern Weddell Sea, Bellingshausen Sea along Western Antarctic Peninsula, Eastern Ross Sea, between Adélie Land and Bruce Rise and East Antarctica, and Astrid Ridge and Gunnerus Ridge near Dronning Maud Land (Golledge et al., 2013; Bentley et al., 2014) (Fig 1.1). Even though the ice-free seabed was likely covered by floating ice shelves on the surface (Denton & Hughes, 2002), modern observations of Southern Ocean benthic communities surviving beneath the present-day ice shelves suggest faunal survival in these areas during glacial period was also possible (Dayton & Oliver, 1977; Bruchhausen et al., 1979; Riddle et al., 2007; Gutt et al., 2011).

Past AIS dynamics also offer valuable insights into whether these suggested ice-free areas were habitable. For example, modelled sediment fluxes during the LGM suggest ice free areas in the Eastern Ross Sea, Eastern Weddell Sea and Bellingshausen Sea received high cumulative sediment fluxes (> 1000 m^3 yr^{-1} per metre width) through ice streams (Golledge et al., 2013). If glacial refugia did exist in these regions, benthic fauna would likely to have only been able to survive near the shelf break away from the direct sediment flow and/or retreated into deeper areas following seafloor bathymetry. Ephemeral ice-free areas that provided additional refugia on the shelf are also known to have existed during the LGM, including polynyas, which are open marine habitats within grounded ice driven by katabatic winds (Smith et al., 2010). In addition, the timing and extent of ice sheet advance and retreat were likely to be asynchronous between different regions (Anderson et al., 2002; Hillenbrand et al., 2014; Mackintosh et al., 2014). These variable and dynamic ice-free areas on the continental shelf may have provided refugia for populations of benthic species enabling their continuous survival throughout glacial cycles (Thatje et al., 2005; Allcock & Strugnell, 2012).

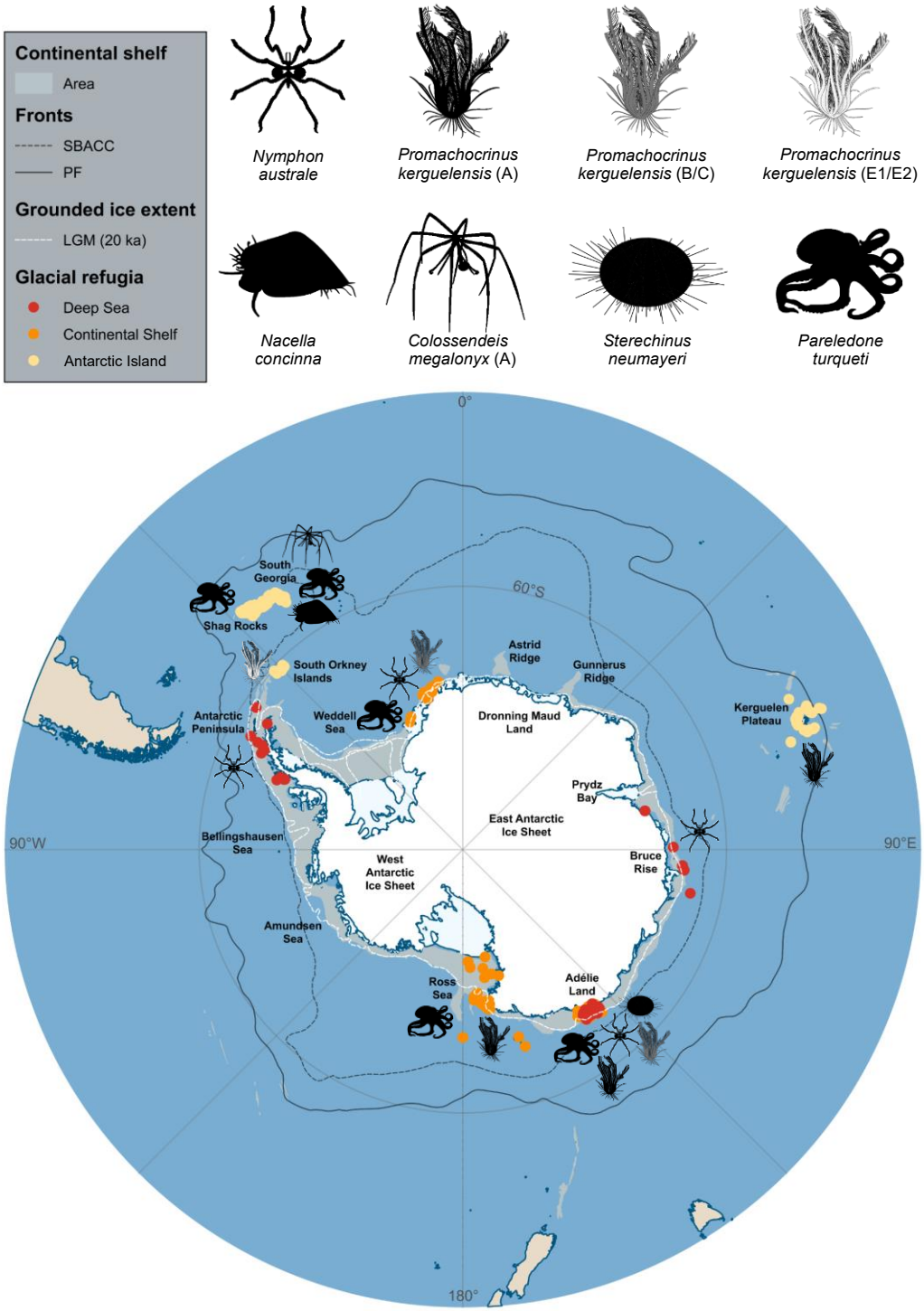

Fig 1.1 Map of Antarctica and proposed areas of Southern Ocean glacial refugia. Areas of glacial refugia were inferred from the sample locations that were associated with molecular signatures of glacial refugia, with each dot representing a sample location. Each organism on the map reflects the number of times an area was proposed as a refugium for that taxon. Data of grounded ice extent during Last Glacial Maximum (LGM) at 20 ka was extracted from model reconstruction in Bentley et al. (2014). Ice-free areas present on the outer continental shelf during the LGM are observed in the Eastern Weddell Sea, Bellingshausen Sea along Western Antarctic Peninsula, Eastern Ross Sea, between Adélie Land and Bruce Rise in East Antarctica, and Astrid Ridge and Gunnerus Ridge near Dronning Maud Land. SBACC, southern boundary of Antarctic Circumpolar Current; PF, Polar Front**.**

From the current geological evidence, it is becoming clear that ice-free areas did exist on the Antarctic continental shelf even during extreme glacial period in the Pleistocene (e.g. the LGM). Nonetheless, the spatial coverage of research effort varies across the continent, and estimates of the past AIS extent over time, remain limited and at coarse resolution (Brook & Buizert, 2018). While the potential glacial refugia inferred from past AIS reconstructions identified here provide hypotheses of refugial locations and scenarios, the knowledge identified from biological data can also be transferred vice versa.

1.3 Pathways to glacial refugia through larval dispersal

For benthic fauna to effectively retreat into glacial refugia, life history characteristics such as larval dispersal likely played an important role (Poulin et al., 2002; Thatje et al., 2005; Allcock & Strugnell, 2012). Feeding (planktotrophic) swimming larvae are normally associated with dispersal capacity over a relatively wide geographical range (Paulay & Meyer, 2006). Conversely, non-feeding (lecithotrophic) swimming larvae and non-pelagic development (i.e. benthic, direct developing juveniles) are generally believed to be associated with reduced and limited dispersal ability, respectively (Paulay & Meyer, 2006). In the Southern Ocean, since it is believed that glacial refugia on the continental shelf were small, ephemeral in nature with limited primary productivity received (Poulin et al., 2002; Thatje et al., 2005; Convey et al., 2009; Pearse et al., 2009), it has been hypothesised that direct development experienced strong positive selection (Poulin et al., 2002; Pearse et al., 2009). It has also been argued that this was likely a beneficial strategy for reproducing in low food conditions and may have been driven by allopatric speciation in isolated refugia (Poulin et al., 2002; Pearse et al., 2009).

However, genetic evidence to date indicates survival in Southern Ocean glacial refugia does not seem to be specific to a single mode of dispersal. Instead, it can be associated with both pelagic and non-pelagic development (discussed within Allcock & Strugnell (2012)). Molecular signatures of deep-sea and continental shelf refugia have been suggested for species with pelagic development including the shrimp *Nematocarcinus lanceopes* (Raupach et al., 2010), the sea urchin *Sterechinus neumayeri* (Díaz et al., 2018) and two cryptic species within the crinoid *Promachocrinus kerguelensis* (Hemery et al., 2012), as well as those with direct development including the sea spider *Nymphon australe* (Soler-Membrives et al., 2017), and the octopus *Pareledone turqueti* (Strugnell et al., 2012). Despite the apparent evolutionary success of a direct development strategy to survive glacial cycles, pelagic larvae are found in Antarctic waters from a wide range of phyla, including Arthropoda,

Bryozoa, Cnidaria, Echinodermata, Mollusca, Nematoda and Porifera (Shreeve & Peck, 1995; Stanwell-Smith et al., 1999; Sewell, 2005; Freire et al., 2006; Bowden et al., 2009; Sewell & Jury, 2011; Ameneiro et al., 2012; Gallego et al., 2015). The molecular evidence of glacial survival and modern observations of pelagic and non-pelagic development in extant benthic fauna reflect that both strategies clearly contributed unique ways of assisting fauna to persist through glacial periods.

1.4 Pelagic larval survival throughout glacial cycles

Of the pelagic larval development strategies in the Southern Ocean, lecithotrophy is hypothesised to be favoured during the food impoverished glacial maxima and therefore a trait that could be more prevalent than planktotrophy (Pearse et al., 2009). However, in recent surveys, planktotrophy and lecithotrophy were detected simultaneously all year around along the Western Antarctic Peninsula (Shreeve & Peck, 1995; Freire et al., 2006; Bowden et al., 2009). In an effort to examine whether Thorson's rule (i.e. high latitudes do not favour planktotrophy in marine invertebrates (Mileikovsky, 1971)) applies to the Western Ross Sea, Gallego et al. (2015) performed plankton surveys to measure the larval diversity characterised by planktotrophy and lecithotrophy over multiple summer seasons. This study revealed that at least 70% of the larval diversity sampled (Molecular Operational Taxonomical Units; mOTUs) during summer seasons were comprised of planktotrophic mOTUs (Gallego et al., 2015). Similarly, planktotrophic larvae were also observed in high abundance along the Western Antarctic Peninsula during austral summer, coinciding with the timing of the annual phytoplankton bloom (Bowden et al., 2009). Given the strong modern presence of planktotrophic and lecithotrophic larvae across phyla in the Southern Ocean, with planktotrophic larvae particularly dominates the larval assemblages during summer season, the current evidence indicates both planktotrophy and lecithotrophy very likely persisted throughout, and survived, glacial periods alongside non-pelagic development.

In the Southern Ocean, links between pelagic larval development and evolutionary selection have been studied in sea snails. While most non-Antarctic Capulidae snails are planktotrophic, Antarctic lineages are mostly lecithotrophic (Fassio et al., 2015), thus hints towards the links between selection and developmental strategy in the Southern Ocean. However, based on current evidence, selection for lecithotrophy does not seem to be a general trend as Antarctic Velutinidae snails appear to exhibit planktotrophy similar to other non-Antarctic lineages, although with a reduced pelagic larval duration (PLD) (Fassio et al., 2019). The persistence of planktotrophy through time could be explained by species

selection, although it is understood that over the macro-evolutionary scale, invertebrate lineages generally experience frequent evolutionary transitions to lecithotrophy (Krug et al., 2015). Therefore, the current evidence indicating of year-round presence of planktotrophic and lecithotrophic larvae, as well as a reduction in PLD in some groups, highlights that species with pelagic larvae likely possess a range of strategies that have enabled persistence throughout glacial cycles in the Southern Ocean remain to be discovered.

Instead of only favouring direct developers over species with pelagic larvae throughout glacial cycles, selection likely acted differently on pelagic and non-pelagic larval development in the Southern Ocean. The survival of direct developers could have been facilitated by isolated refugia and low primary production in the water column (Poulin et al., 2002; Pearse et al., 2009). The year round presence of lecithotrophic larvae along the Western Antarctic Peninsula (Shreeve & Peck, 1995; Freire et al., 2006; Bowden et al., 2009), and up to 30% of larval diversity (mOTUs) were found to be lecithotrophic during summer seasons in the Ross Sea (Gallego et al., 2015) when the annual summer primary production exclusively promotes planktotrophy, also highlight lecithotrophy can be a successful strategy in the Southern Ocean. More importantly, in the context of glacial period persistence, lecithotrophy and reduced PLD in planktotrophy could have also aided pelagic larvae to survive by reducing the reliance on long periods of feeding in the water column. Faunal recolonisation from the shelf break or non-shelf refugia to the inner continental shelf may seem impossible if direct development with limited dispersal ability was exclusively favoured during glacial cycles. In addition, modern observations on benthic fauna assemblages in the Weddell Sea also indicate that after local iceberg disturbance destroyed the previous benthic community, four out of the first five recolonising species were associated with pelagic larval development (Teixidó et al., 2004). After local volcanic eruptions at Deception Island, South Shetland Islands, species with planktotrophic larvae also recolonised and dominated the newly established benthic community in the caldera (Barnes et al., 2008). However, in another case study, a decade after volcanic eruptions at Southern Thule, South Sandwich Islands, species with apparent limited dispersal ability (brooding and lecithotrophy) were found to dominate the local benthic community (Kaiser et al., 2008).

Notably, although highly relevant to signatures of glacial survival, limited studies have discussed post glacial recolonisation pathways and ecological succession in relation to larval dispersal strategies throughout glacial periods. In addition, how ocean currents influence dispersal, including the ACC and regional currents, have only been examined in a handful of taxa (e.g. Thornhill et al., 2008; Wilson et al., 2009; Dambach et al., 2016; Galaska et al., 2017a, 2017b; Strugnell et al., 2017; Moore et al., 2018; Leiva et al., 2019; Muñoz-Ramírez

et al., 2020). The role of dispersal, ocean currents and seascape dynamics are also often discussed in the context of modern genetic patterns, even though these factors likely played important roles in facilitating post glacial cycles recolonisation. Nonetheless, understanding where exactly Southern Ocean benthic fauna persisted throughout glacial cycles, and by also the other drivers of genetic patterns, we can begin to understand and reconstruct the past species demographic history over time.

1.5 Locating Southern Ocean glacial refugia through demographic history

Investigating past changes in the demographic history of extant species can shed light onto how species survived repeated glacial-interglacial cycles (Clarke et al., 2004), how glacial periods selected for both pelagic and non-pelagic development (Thatje, 2012), as well as how oceanic currents and seascape dynamics have influenced population connectivity over time. Additionally, with all the above knowledge combined and synthesised, we can also use past changes in species demographic history as a proxy to investigate historical physical processes in the Southern Ocean, including ancient Antarctic Ice Sheet collapses (Strugnell et al. 2018). Fundamentally, locating Southern Ocean glacial refugia would give an important conceptual foundation for reconstructing the other elements involved in the past changes in species demographic history.

Ice sheet expansions occurring during severe glaciations in the last one million years would have been catastrophic to the Southern Ocean seafloor communities. As a result, significant changes in demography would occur according to species responses to environmental changes (Thatje et al., 2008). Individualistic species response to climate change may also lead to different strategies of survival in glacial refugia, which in turn can reflect different patterns of past species demography (Hofreiter & Stewart, 2009; Stewart et al., 2010). Such past demographic history would be encoded in the genomes of those extant species that have persisted through glacial cycles (Hewitt, 2000). Therefore, understanding the key historical processes related to persistence, migration and extinction during glacial cycles can offer testable frameworks to deduce the locations of glacial refugia in the Southern Ocean (Avise, 1989; Davis et al., 2005). For studies that detect signatures of glacial refugia in Northern Hemisphere terrestrial and marine taxa, signals of past changes in population size can indicate population persistence, and signals of shifts in species distribution can reflect migration to southernly warmer areas during glacial cycles. However, these patterns cannot be directly applied to Southern Ocean benthic fauna because of the isolated nature of the

Southern Ocean. For example, glacial cycles have been proposed as drivers of allopatric speciation in the Southern Ocean because of repeated glacial advances, retreats and refugium isolation (the Antarctic diversity pump hypothesis) (Clarke & Crame, 1989, 1992; Crame, 1997). In contrast to the Northern Hemisphere where glacial cycles were suggested to have reduced genetic diversity in terrestrial and marine taxa, repeated AIS expansions and retreats have been proposed to increase genetic diversity in the Southern Ocean (Wilson et al., 2009). Nonetheless, concepts developed from Northern Hemisphere glacial refugia research could be adapted as frameworks within the Southern Ocean context. As extant benthic fauna in the Southern Ocean could have persisted on the continental shelf or migrated to deep-sea and/or Antarctic island refugia during glacial cycles, if true, these hypothesised survival scenarios would also be reflected by different patterns in changes in population size, and population connectivity and isolation.

1.5.1 Population size

As ice-free areas on the continental shelf (such as areas along the shelf break and open marine habitats within grounded ice) could have enabled the *in situ* survival of benthic fauna, populations may have experienced demographic bottlenecks within these glacial refugia instead of complete eradication (Allcock & Strugnell, 2012). Evidence of founder effects may also be observed in individuals reaching new refugia in deeper waters and Antarctic islands for refugia, where an establishing population is based on a subset of newly colonising individuals from a source population. Given that ice sheet reconstructions suggest glacial advances did not extend beyond the continental shelf break throughout glacial cycles (Bentley et al., 2014), a supposed stable continental slope and the deep sea would have provided ice-free habitat (but see Thatje et al. (2005)). During glacial cycles, subsets of benthic shelf populations could have migrated to deeper waters for refuge following seafloor bathymetry and subsequently expanded in population size.

Individuals of species that found refuge around Antarctic islands could have dispersed via the ACC from the Antarctic continental shelf (Matschiner et al. 2009). Although larval state is typically thought of as the key dispersive stage, adults may disperse as well. Adult dispersal could be achieved via rafting and attachment to other organisms (Helmuth et al., 1994; Leese et al., 2010; Nikula et al., 2010) or to drift pieces of anchor ice (Dayton et al., 1969; Teixidó et al., 2004; Thatje, 2012). Because many of the Antarctic islands were also heavily glaciated with limited ice free areas at the LGM (Hodgson et al., 2014), newly colonising individuals were likely to experience limited expansion in population size in comparison to populations that found refuge in deep-sea areas.

1.5.2 Connectivity and isolation

If deep-sea and Antarctic island refugia were used by species, then we would expect to see some residual signals of connectivity between the shelf and these places (Clarke, 2008). However, given the Antarctic continental shelf is geographically isolated from other Antarctic islands via deep water channels, but is relatively connected to the deep sea along the seafloor bathymetry, different patterns of connectivity may be expected to be derived from surviving in deep-sea versus Antarctic island refugia. For example, repeated glacial cycles would encourage populations that were able to seek deep-sea refugia to persist and diversify on the continental slope and in the deep sea throughout glacial periods (Kaiser et al., 2011; Allcock & Strugnell, 2012). Recolonisation of the continental shelf from deep-sea refugia would also be reflected by stepwise connectivity between the deep sea and continental shelf along seafloor bathymetry. Thus, an isolation-by-distance and -depth pattern may be expected between deep-sea and continental shelf populations in extant taxa.

It could be challenging for populations that persisted in Antarctic refugia to recolonise the continental shelf as individuals would need to penetrate across different frontal boundaries within the ACC in order to reach the continent. Nonetheless, recolonisation from Antarctic island refugia is possible and has been suggested for the benthic shrimp *Chorismus antarcticus* (Raupach et al., 2010) and limpet *Nacella concinna* (González-Wevar et al., 2013). In both species, a founder effect on the continental shelf was observed, indicating connectivity between continental shelf and Antarctic islands can be achieved via a few colonist individuals.

For populations that had survived in glacial refugia on the continental shelf, those with non-pelagic development and lecithotrophic larvae would slowly expand to nearby glacial refugia or even remain isolated among refugia owing to a lower dispersal rate (Pearse et al., 1991). Pelagic development with planktotrophic larvae might enable populations to be distributed broadly and swiftly over habitable areas across long geographic distances (Pearse et al., 1991), leading to connectivity between refugia (Allcock & Strugnell, 2012). Additionally, high levels of admixture may also be seen in populations with pelagic development, as populations that were previously separated between different refugia could face secondary contact during deglaciations. Admixture (such as in the form of high genetic diversity) driven by secondary contact during post-glacial recolonisation has notably been observed in European trees and shrubs with high seed dispersal abilities (Petit et al., 2003) and in the Antarctic springtail *Desoria klovstadi* in Victoria Land, Antarctica (Stevens et al., 2007).

The degree to which dispersal strategy structures connectivity patterns appears to vary between Southern Ocean taxa, and connectivity between populations can also be influenced by seascape dynamics and ecological responses. Genetic evidence has demonstrated refugial populations of species with pelagic planktotrophic larvae (Hemery et al., 2012) and also direct development (Dietz et al., 2015) have encountered secondary contact along recolonisation routes in the Southern Ocean, despite the supposed contrasting difference in dispersal abilities. Other factors, including heterogeneous seascapes and oceanic currents, are also known to be dispersal barriers and influence population connectivity in the Southern Ocean (Thornhill et al., 2008; Wilson et al., 2009; Dambach et al., 2016; Galaska et al., 2017a, 2017b; Strugnell et al., 2017; Moore et al., 2018; Leiva et al., 2019; Muñoz-Ramírez et al., 2020). Ecological responses to glaciations may also be significant in structuring population connectivity and isolation during glacial cycles. Molecular evidence has also highlighted contrasting genetic structures between cryptic species of the Antarctic benthic amphipod genus *Eusirus*; and was proposed as a result of different species-specific survival strategies during glacial cycles (Baird et al. 2011). Similarly contrasting patterns of connectivity were detected in closely related species of Southern Ocean crinoid with pelagic development (Hemery et al., 2012) and in octopus with direct developing juveniles (Strugnell et al., 2017). Disparate patterns of population connectivity and isolation between closely related species have also been detected in other non-Antarctic marine species, and these contrasting patterns have been attributed to differences in dispersal barriers, larval duration and ecological responses (e.g. Marko, 2004; Hickerson & Cunningham, 2005; Crandall et al. 2008).

1.6 What is the current molecular evidence of glacial refugia in the Southern Ocean?

Genetic data from present-day taxa can reveal past species demography and evidence of glacial refugia (Box 1.1). Therefore, we systematically reviewed published genetic studies of Southern Ocean species to evaluate the current molecular signatures of glacial survival. A keyword search of ‘Antarctic’ AND ‘genetic’ was conducted on Web of Science on 26 September 2019. Out of the 893 journal articles that were gathered through the Web of Science search, 73 analysed the genetic patterns of Southern Ocean continental shelf benthic fauna. These articles were published between 1991 and September 2019. Of these 73 articles, only six studies used molecular data to propose locations of where Southern Ocean benthic fauna had survived glacial cycles using molecular data (Box 1.1) (Table 1.1). Other studies that did not explicitly point to locations were also discussed in the context of

how preliminary evidence can be better incorporated into investigations of the locations of glacial refugia.

Box 1.1 How to identify demographic history associated with glacial refugia?

Phylogeography (the analysis of spatially distributed genetic data, Avise et al. (1987)) has rapidly expanded since its inception, and has become one of the key disciplines in understanding the demographic and evolutionary history of species (Avise, 2009). In turn, a phylogeographic approach has been a popular tool in investigating refugia and ecological processes during glacial–interglacial cycles globally (Provan & Bennett, 2008; Gavin et al., 2014). Phylogeography connects the field of population genetics and systematics and is built upon coalescent theory (Avise et al., 1987; Avise, 2009). Coalescent theory is tightly coupled with the theories of population genetics, which assumes 1) neutral evolution, 2) that all lineages can be traced back to a single common ancestor and 3) that an idealised population should persist with random mating and neutral mutations in DNA (Rosenberg & Nordborg, 2002). Any deviations from these assumptions may signify that population structure was influenced by variations in population size and unequal gene flow between populations in the past (Hey & Machado, 2003; Grant, 2015). Several recent reviews have examined the theoretical complexities in investigating phylogeography and highlighted different methods that can offer independent lines of evidence to infer how past climate changes influenced demographic histories (Crisci et al., 2012; Cutter, 2013; Bank et al., 2014; Lowe et al., 2017). Although haplotype networks linking to alternative survival scenarios during glacial cycles and population connectivity have been widely discussed for marine taxa (Avise et al., 1987; Maggs et al., 2008; Allcock & Strugnell, 2012), other commonly reported population genetic metrics might also be useful in pinpointing possible refugial locations and scenarios.

In global animal phylogeographic studies, COI is traditionally the most commonly used genetic marker due to its low intraspecific variability but relatively high interspecifically variability (Avise et al., 1987). In the Southern Ocean phylogeographic studies, COI has frequently been sequenced due to the discounted sequencing campaigns through CAML and BOLD, as well as its widespread utility in delineating species. However, COI does not represent the multiloci genealogical evolution of the studied species. Instead, mitochondrial DNA (mtDNA) analyses only investigate the evolution of a mostly non-recombining, maternally inherited mitochondrial genome. Factors such as introgression (Ballard, 2000), hybridisation (Dowling et al., 2008), selection against assumed neutrality (Ballard & Rand, 2005) and mutation rate variations within mtDNA (Galtier et al., 2009) can violate the assumptions of coalescent theory in population genetics. Nonetheless, it is important to note that single locus studies can still offer highly transferable knowledge to establish hypotheses for future research, therefore data derived from COI data is still highly relevant in the genomic era (see Bowen et al. (2014) for detailed discussion).

Genetic variation

Genetic variation between populations (both nucleotide and haplotypic diversity) is widely used to distinguish between refugial and recolonised populations. Individuals isolated within glacial refugia are likely to experience long-term isolation and harbour more endemic diversity (private alleles). Recolonising individuals are assumed to diverge from a subset of individuals dispersed from glacial refugia, leading to lower levels of genetic diversity compared to those that persisted in refugia over multiple glacial cycles (Petit et al., 2003; Maggs et al., 2008; Provan & Bennett, 2008). Areas where colonisers from previously isolated refugia come into secondary contacts are suggested to exhibit the highest genetic diversity (Petit et al., 2003).

Neutrality tests

Population genetic data can be analysed using neutrality tests such as Tajima's D (Tajima, 1989) and Fu's Fs (Fu & Li, 1993) to test for significant deviations from neutral evolution, which can reflect past changes in population size and therefore demographic histories of refugial and recolonised populations. For example, positive and negative values derived from neutrality tests can represent historical population size reduction (loss of rare alleles) and population expansion (excess of rare alleles) respectively (Fay & Wu, 1999). However, if a bottleneck was extremely severe then neutrality tests may produce negative values; an outcome expected for population expansion because most alleles were lost to a strong bottleneck effect (Fay & Wu, 1999). Therefore, a range of methods and measurements need to be incorporated in the analyses to counteract potential method-specific errors.

Past changes in population size

Population size changes can also be investigated using the nucleotide differences between paired individuals visualised in the form of frequency distribution (pairwise/mismatch distribution) (Slatkin & Hudson, 1991; Rogers & Harpending, 1992). This pairwise difference is theorised to exhibit a unimodal distribution under the model of recent population expansion, with indication of equilibrium (i.e. constant population size) is expected to exhibit bimodal or multimodal distributions (Rogers & Harpending, 1992). In addition, a ‘ragged’ bimodal or multimodal distribution may represent deep divergences between populations (Grant, 2015). Skyline-plots are another popular demographic tool for reconstructing past population sizes through time based on estimated patterns of coalescence (Ho & Shapiro, 2011). They can reconstruct magnitude and timing of population bottleneck and subsequent expansion simultaneously.

Hypothesised refugia scenarios testing

Recent theoretical advances have also made it possible to combine genomic data derived from neutral loci with range dynamics models to reconstruct past demographic scenarios. By visualising genomic data in the form of allele frequency distribution across polymorphic sites (i.e. size frequency spectrum, SFS), the observed shape of the SFS can be used to test for deviations from neutral evolution (Rosen et al., 2018). The SFS can be computed and species demographic history can be inferred through SFS-based interface models, which can investigate complex scenarios involving divergence and historical migrations, as well as being able to distinguish which scenario scores the highest likelihood between contrasting hypothesised scenarios (Gutenkunst et al., 2009; Excoffier et al., 2013).

Table 1.1 Summary of molecular signatures of cytochrome c oxidase subunit I (COI) linked to glacial refugia in the Southern Ocean. *=significantly different from zero.

Species	Larval dispersal mode	Marker used	Area sampled	Sample depth range (m)	Proposed area of glacial refugia		Nucleotide diversity	Haplotype diversity	Fu's Fs	Pairwise difference distribution	Proportion of private haplotype	Reference
Nymphon australe	Non-pelagic	COI	South Sandwich Islands, West Antarctic Peninsula, East Weddell Sea, West Ross Sea, Davis Station, Bruce Rise, Adélie Land	25 - 1261	Deep sea	West Antarctic Peninsula	0.00538	0.7940	-17.764*	unimodal	89.7	Soler-Membrives et al., (2017)
					Deep sea	East Antarctica (Davis Station, Bruce Rise and Adélie Land)	0.00496	0.8570	-49.372*	unimodal	78.0	
					Continental shelf	East Weddell Sea	0.00133	0.4290	-3.961*	unimodal	71.4	
Colossendeis megalonyx (A)	Non-pelagic	COI	South Georgia, South Sandwich Islands, South Orkney Island, Elephant Island, South Shetland Islands	81 - 2285	Antarctic island	South Georgia	\	High	\	\	\	Dietz et al., (2015)
Promachocrinus kerguelensis (A)	Pelagic	COI, Cytb, 16S, 28S, ITS	South Georgia, South Shetland Islands, South Sandwich Islands, Bouvet Island, East Weddell Sea, West Ross Sea, Davis Station, Adélie Land, Kerguelen Plateau	106 - 541	Continental shelf	Adélie Land	0.00430	0.6855	-1.397	Unimodal	66.7	Hemery et al., (2012)
					Continental shelf	West Ross Sea	0.00480	0.6621	-3.256	Bimodal	60.0	
					Antarctic island	Kerguelen Plateau	0.00120	0.4300	-4.900*	Unimodal	85.7	
Promachocrinus kerguelensis (B/C)	Pelagic		South Orkney Island, South Shetland Island, South Sandwich Islands, West Antarctic Peninsula, East Weddell Sea, West Ross Sea, Davis Station, Adélie Land	65 - 1157	Continental shelf	Adélie Land	0.00400	0.7423	-2.056	Bimodal	64.3	
					Continental shelf	East Weddell Sea	0.00590	0.8072	-3.258	Bimodal	68.8	
Promachocrinus kerguelensis (E1/E2)	Pelagic		South Georgia, South Orkney Island, South Shetland Islands, West Ross Sea, Adélie Land	147 - 525	Antarctic island	South Orkney Islands	0.00490	0.7423	-2.056	Bimodal	64.3	
Sterechinus neumayeri	Pelagic	COI, Microsatellite	West Antarctic Peninsula, East Antarctic Peninsula, East Weddell Sea, Adélie Land	Shallow water	Continental shelf	Adélie Land	0.00115	0.4760	-2.679*	Unimodal	80.0	Díaz et al., (2018)

Nacella concinna	Pelagic	COI	South Georgia, South Orkney Island, South Shetland Islands, West Antarctic Peninsula, East Antarctic Peninsula	Intertidal	Antarctic island	South Georgia	0.00353	0.8800	-3.440*	Unimodal	72.7	González-Wevar et al., (2013)
Pareledone turqueti	Non-pelagic	COI, Microsatellite	Shag Rocks, South Georgia, South Orkney Island, South Sandwich Islands, Elephant Island, King George Island, Livingstone Island, West Antarctic Peninsula, East Antarctic Peninsula, East Weddell Sea, Prydz Bay, West Ross Sea, Adélie Land	95 - 1044	Continental shelf	Adélie Land	0.00530	0.7420	1.060	Bimodal	50.0	Strugnell et al., (2012)
					Continental shelf	West Ross Sea	0.00340	0.6270	-2.220	Multimodal	58.3	
					Continental shelf	East Weddell Sea	0.00360	0.6670	0.590	Multimodal	80.0	
					Antarctic island	Shag Rocks	0.00120	0.6130	-4.060*	Unimodal	50.0	
					Antarctic island	South Georgia	0.00050 (NW) / 0.00120 (SE)	0.3070 (NW) / 0.5830 (SE)	-3.810*	Unimodal		

Although there are only six molecular studies unequivocally proposing locations of glacial refugia in Southern Ocean benthic fauna, together they suggested multiple refugial locations on the continental shelf around Antarctica, in the deep sea, and also around Antarctic islands (Fig 1.1). Signatures of putative Southern Ocean glacial refugia have so far been inferred from the pycnogonids *Nymphon australe* (Soler-Membrives et al., 2017) and *Colossendeis megalonyx* (clade A) (Dietz et al., 2015), crinoids *Promachocrinus kerguelensis* (clade A, B/C and E1/E2) (Hemery et al., 2012), the echinoid *Sterechinus neumayeri* (Díaz et al., 2018), the gastropod *Nacella concinna* (González-Wevar et al., 2013) and the octopus *Pareledone turqueti* (Strugnell et al., 2012). These studies mainly utilised COI data to infer past species demography in species with either pelagic or non-pelagic development. The sampling distribution of these studies was either restricted to the Scotia Arc and Antarctic Peninsula or broadly-distributed taxa. The locations of glacial refugia were primarily inferred from where animals with a high number of private alleles were collected, in the form of a high proportion of private haplotypes or via high haplotypic diversity (Table 1.1). Past population size changes and population connectivity and isolation were also commonly discussed in the context of how populations were affected by glacial cycles. Even though different dispersal strategies can structure different patterns of species demography, these patterns are challenging to detect from current molecular evidence due to the limited number of studies outlined here (n = 6).

1.6.1 Evidence of shelf refugia

Although the proposed locations of refugia included the continental shelf around Antarctica (Fig 1.1), the data suggest that some Antarctic continental shelf species with island populations also persisted on the shelf areas surrounding Antarctic islands, presumably throughout glacial cycles (Table 1.1). The proposed locations of shelf refugia (Antarctic continental shelf + shelf areas surrounding islands) include Shag Rocks, South Georgia and South Orkney Islands in the Scotia Arc, and Eastern Weddell Sea, Western Ross Sea, Adélie Land, as well as the Kerguelen Plateau off East Antarctica. Some locations have been suggested as glacial refugia for multiple species, and these locations include South Georgia, Eastern Weddell Sea, Eastern Ross Sea and Adélie Land in East Antarctica. With the exception of outer shelf in the Eastern Ross Sea, these proposed glacial refugia do not correspond with the LGM ice-free areas inferred from past AIS reconstructions. This may reflect sampling effort to some extent, as these studies lacked samples collected from most of the proposed ice-free areas from past AIS reconstructions (i.e. outer shelf of Bellingshausen Sea, between Adélie Land and Bruce Rise in East Antarctica, and Astrid Ridge and Gunnerus Ridge near Dronning Maud Land). Future studies should target the

same studied species at these locations to be able to test this hypothesis directly.

Inferred changes in demographic history in relation to survival in glacial refugia have often been linked to the LGM via molecular dating (González-Wevar et al., 2013; Soler-Membrives et al., 2017), or simply hypothesised (Hemery et al., 2012; Díaz et al., 2018). Population bottlenecks during the LGM, followed by expansions during subsequent deglaciation, were suggested in species with either pelagic or non-pelagic development, and were supported by significantly negative neutrality tests and unimodal pairwise mismatch distributions (Table 1.1). These populations include *P. kerguelensis* (A) from the Kerguelen Plateau (Hemery et al., 2012), *S. neumayeri* from off Adélie Land (Díaz et al., 2018) and *N. australe* in the Weddell Sea (Soler-Membrives et al., 2017). However, other populations of *P. kerguelensis* (A) in the Western Ross Sea, as well as populations in the two other cryptic species of *P. kerguelensis* (B/C; E1/E2), also appeared to have experienced relatively stable population size in some areas on the continental shelf, most probably throughout the LGM, as indicated by non-significant negative neutrality tests and bimodal mismatch distributions (Table 1.1). In the cryptic species B/C, stable populations persisted in Adélie Land and East Weddell Sea; and in E1/E2, a stable population was detected off the South Orkney Islands.

More interestingly, past changes in the demographic history of the direct developing *P. turqueti* were dated back to the mid-Pleistocene preceding the LGM, with various populations also experiencing contrasting demographic histories (Strugnell et al., 2012). One *P. turqueti* population in the Weddell Sea had a relatively stable population size throughout glacial maxima on the continental shelf (Table 1.1). Bayesian Skyline Plot analysis of *P. turqueti* populations from off the Adélie Land and in the Ross Sea indicated *in situ* survival on the continental shelf was possibly not associated with a population bottleneck, but instead, an overall population expansion was detected in these two locations (Strugnell et al., 2012).

1.6.2 Evidence of recolonisation of the Antarctic continental shelf

Molecular evidence of recolonisation of the Southern Ocean continental shelf is limited, with only two studies so far proposing faunal recolonisation of the shelf from Antarctic island and deep-sea refugia (González-Wevar et al., 2013; Soler-Membrives et al., 2017). Recolonisation of the continental shelf from Antarctic island refugia was detected in the population history of the limpet *Nacella concinna* after the LGM (González-Wevar et al., 2013). This was demonstrated through significant genetic differentiation between Antarctic continental shelf and Antarctic island South Georgia populations, combined with an older

demographic history and a high proportion of private haplotypes in the South Georgia population (González-Wevar et al., 2013). Demographic model analysis (approximate Bayesian computation) was also employed to confirm the shelf recolonisation from Antarctic island population as a highly likely scenario (González-Wevar et al., 2013).

Signatures of shelf recolonisation from putative deep-sea refugia were suggested from the populations of *Nymphon australe* sampled mostly from the continental shelf adjacent to the Antarctic Peninsula and areas near Davis Station, Bruce Rise and Adélie Land in East Antarctica (Soler-Membrives et al., 2017). These areas were proposed as deep-sea refugia, and the sampled populations exhibited a high proportion of private haplotypes, high genetic diversity and signature of past population expansion without signs of a bottleneck (Soler-Membrives et al., 2017). The evidence of deep-sea refugia was mainly supported by signatures of population expansion, as well as high genetic variation hypothesised as a result of repeated colonisations from shelf to the deep sea (and vice versa). Although AIS reconstructions indicate the LGM grounded ice extended near the continental shelf break, limited ice-free areas were also observed on the continental shelf edge near Bruce Rise and Adélie Land (Fig 1.1). In addition, minimal samples were available (n = 8) of *N. australe* from the deeper waters (> 1000 m) to be included in the dataset. Since relatively high genetic variation and population expansion without prior bottlenecks have also been found to be associated with continental shelf refugia in other Southern Ocean benthic species (Table 1.1), the molecular signatures differentiating deep-sea and continental shelf refugia remain largely unexplored.

1.6.3 Timing of glacial refugia in the Southern Ocean

Genetic signals of glacial survival derived from syntheses on Northern Hemisphere taxa often suggest the locations of refugia were unchanged throughout glacial cycles, leading to refugial populations to exhibit long-term isolation, strong genetic differentiation and older genealogical splits from other lineages (Provan & Bennett, 2008; Bálint et al., 2011). However, given the locations and size of Southern Ocean glacial refugia were likely to be variable throughout different phases of the Quaternary, Southern Ocean taxa may not have experienced long-term isolation in a single area. From the reported genetic signatures characterising Southern Ocean glacial refugia, divergence between individuals that were sampled in putative refugia and recolonised areas can sometimes be apparent, but not definitive. For example, microsatellite data highlighted very low or no population structure between putatively refugial (Adélie Land) and non-refugial (Antarctic Peninsula and Weddell Sea) populations in *S. neumayeri* (Díaz et al., 2018). In contrast, approximate Bayesian

computation analysis based on COI data supported the scenario of continental shelf populations diverging from Antarctic island refugial population in *N. concinna* after the LGM (González-Wevar et al., 2013). The divergence of refugial and non-refugial populations in *P. turqueti* was dated back to 1.25 million years ago at the start of the Mid-Pleistocene Transition, based on COI data (Strugnell et al., 2012). Although not dated, various levels of divergence were also found between cryptic species of *P. kerguelensis* (Hemery et al., 2012). In contrast to Northern Hemisphere taxa, the current genetic evidence suggests that refugial populations in the Southern Ocean do not necessarily exhibit long-term isolation, highlighting possible evidence of glacial refugia locations being different throughout glacial cycles.

Nonetheless, current molecular data does show different divergence times between refugial and non-refugial populations in different Southern Ocean species. Different population divergence times between species could be due to taxon-specific mutation rates, but it is also likely to be the product of population-level survival and extinction events being different between species over many glacial maxima in the Quaternary (Avise, 2009; Hemery et al., 2012). Avise (2009) speculated that even though some species might have persisted in an area acting as glacial refugium, populations of a particular species (or more) could undergo extinction in the same area. During the following interglacial period, this area could be recolonised again by the species that had previously been wiped out but persisted in other refugia (Avise, 2009). Therefore, the temporal depth of lineage split could represent the last time a population faced extinction and recolonised in an area, with a shallow split representing a more recent extinction (Avise, 2009).

From the reported demographic histories in the Southern Ocean, it is clear that the effects of recent glacial cycles, particularly population bottlenecks and expansions during and post LGM, as well as connectivity driven by modern oceanic currents, have been superimposed on existing genetic patterns, thus masking the molecular signatures of older glacial events (as discussed in Maggs et al. (2008) and Grant (2015)). Phylogenetic reconstruction can also be influenced by the loci of choice, number of individuals sequenced, and population substructure (Kim et al., 2015). However, if estimated correctly, the chronology of lineage splitting appears to be able to give clues as to how multiple glacial cycles may have influenced diversification processes differently between species, and more importantly the periodicity of glacial refugia. For example, the divergence of continental shelf populations from Antarctic island populations in *N. concinna* after the LGM suggests South Georgia served as an LGM glacial refugia. The mid-Pleistocene divergence and subsequent long-term persistence of *P. turqueti* populations suggests glacial refugia for this species occurred

at Shag Rocks, South Georgia, East Weddell Sea, West Ross Sea and Adélie Land since the mid-Pleistocene.

1.6.4 The complexity of population genetic metrics

The demographic histories of extant Southern Ocean benthic fauna appear to be characterised by different combinations of population bottlenecks, expansions and stable population sizes throughout different phases of the Quaternary. These are highlighted by some species reported in Table 1.1, which do not show significantly negative neutrality tests and/or non-unimodal mismatch distributions. Although this could reflect different survival strategies of pelagic and non-pelagic development, the reported population genetic metrics may be confounded by complex evolutionary histories and sequencing biases.

While it is hypothesised that population persistence in a glacial refugium results in endemic diversity (Schmitt, 2007; Provan & Bennett, 2008), the highest genetic diversity is thought to be found in areas where colonisers from previously isolated refugia come into secondary contact along recolonisation routes (Petit et al., 2003). When comparing reported molecular population genetic metrics, proposed Southern Ocean refugial locations are not solely characterised by a similar threshold of genetic diversity. Instead, a range of intraspecific genetic diversity from low to high were found in suspected refugial populations irrespective of pelagic or non-pelagic development (Table 1.1). The wide range of genetic diversity associated with glacial refugia could be due to limited representative samples within species' distributional ranges, small sample size, and/or over pooling of samples, thus resulting incorrect estimations of genetic metrics (Goodall-Copestake et al., 2012; Bertl et al., 2018). The known widespread occurrence of grounded ice during the LGM may have induced severe population bottlenecks and therefore could even result in low genetic diversity in areas of glacial refugia (Amos & Harwood, 1998). An alternative and more persuasive explanation is that the genetic patterns of Southern Ocean benthic fauna observed today are built upon eroded signals gathered over many glacial maxima, and superimposed by the LGM and modern genetic patterns, as highlighted above. Past population and demographic histories are encoded in the genomes of extant taxa (Hewitt, 2000). However, studies employing single locus and microsatellite loci (all studies in Table 1.1) may lack power to investigate Southern Ocean benthic species with complex evolutionary histories.

The haplotype networks associated with the proposed locations of glacial refugia (Table 1.1) generally correspond to the patterns expected for species' dispersal strategy and the kind of glacial refugium as outlined in Allcock and Strugnell (2012). Additional factors likely also play

a role in shaping patterns of haplotype networks. For example, shared haplotypes between multiple regions were often detected and suggested as a result of present-day connectivity via long-distance dispersal and oceanic currents (Strugnell et al., 2012; Hemery et al., 2012; Soler-Membrives et al., 2017; Díaz et al., 2018), as well as ancient seaways from past West Antarctic Ice Sheet collapses (Strugnell et al., 2012). While signatures of glacial survival are encoded in the genome of Southern Ocean benthic taxa, other evolutionary forces are also embedded within it. These evolutionary signals range from high diversification rates as a result of rebound from extinctions associated with the formation of the Antarctic environment during the mid-Cenozoic (Dietz et al., 2015; O'Hara et al., 2019), to the evolutionary drivers associated with the local environments (e.g. water depths) (Linse et al., 2007; Strugnell et al., 2017). A better understanding of where and how the Antarctic continental shelf benthic fauna survived glacial cycles can be achieved by resolving current sampling and sequencing biases, exploiting genomic data using appropriate hypothesis driven methods.

1.6.5 The complexity of population genetic metrics

Although the studies examined here have suggested locations of glacial refugia across the continental shelf, deep sea and Antarctic islands for benthic fauna, the emerging patterns of glacial refugia may be partially a result of sampling bias. Benthic sampling in the Southern Ocean is often conducted in areas where access is relatively easy and close to supply routes to national research stations (Griffiths et al., 2014). Almost all locations suggested as glacial refugia (with the exception of Adélie Land) have been identified as benthic sampling hotspots in the Southern Ocean (Griffiths et al., 2014). Areas on the inner and outer continental shelf along the Bellingshausen Sea, Amundsen Sea, West Weddell Sea and East Antarctica are rarely sampled and therefore often excluded in the analysis of glacial refugia. Specimens from the continental slope and deep sea are also scarce, and balanced sampling designs are rarely applied. Given that molecular evidence of glacial refugium has only been suggested from eight species with inherent sampling bias, the emerging patterns of glacial refugia reported here invites continued data syntheses, sample collection from poorly sampled locations, and with respect to glacial refugia predicted from past AIS reconstructions.

The studies identified here that explicitly propose where Antarctic benthic fauna survived glacial cycles do not represent the majority of Southern Ocean molecular studies. In fact, more than 500 Southern Ocean species have been sequenced for molecular analyses (Riesgo et al., 2015) and many genetic studies have discussed some preliminary evidence of glacial refugia for benthic taxa. However, the data analysis and/or interpretation of

preliminary evidence were constrained by various factors, leaving the refugia hypotheses unanswered. Some studies suggested that evidence of glacial survival is reflected by overall genetic patterns but did not propose explicit locations of glacial refugia (Raupach et al., 2010; Dömel et al., 2015; Sromek et al., 2015; Miller et al., 2018; Leiva et al., 2019), while others had limited sample coverage (Janko et al., 2007; Baird et al., 2012; Díaz et al., 2012; Wiernes et al., 2013), and were confounded by discoveries of multiple cryptic species in datasets (Wilson et al., 2009; Allcock et al., 2011; Baird et al., 2011; Wiernes et al., 2013; Harder et al., 2016; González-Wevar et al., 2019).

1.6.6 Inferring locations of glacial refugia through speciation patterns and processes

Information related to species glacial survival can be interpreted from genetic data through different population genetic analytical methods. Interestingly, glacial cycles have been proposed as drivers of allopatric speciation in the Southern Ocean because of repeated glacial advances, retreats and refugia isolations (the Antarctic diversity pump hypothesis) (Clarke & Crame, 1989, 1992; Crame, 1997), which are relevant to the discoveries of multiple cryptic species in genetic datasets. As popular molecular methods that test for evidence of glacial refugia are based on population level processes, the discovery and inclusion of separate cryptic species could appear as an analytical dead end. Whether glacial cycles can drive allopatric speciation on the Antarctic continental shelf depends on the opportunities for refugia isolation and time since isolation within a grounded ice sheet. However, whether populations undergo speciation within isolated refugia is dependent upon reproductive isolation and genetic drift; both factors can be linked to dispersal strategies and small population size (e.g. a population bottleneck) (Palumbi, 1994; April et al., 2013). The rate of speciation is also not necessarily determined by the duration of each glacial maximum per se, as speciation could occur during a short timeframe as a result of adaptation under local selective environmental pressure (Hendry et al., 2000). Therefore, understanding whether glacial survival could drive cryptic speciation processes could lead to the discovery of glacial refugia locations, and more importantly how Southern Ocean glacial cycles influenced speciation processes.

In the Southern Ocean, it has been proposed that allopatric glacial refugia could have driven the cryptic speciation within the direct developing pycnogonid *Pallenopsis patagonica* species complex (Dömel et al., 2019). Isolation-by-glacial refugia coupled with adaptation to local predation has also been suggested to drive cryptic speciation in the direct developing sea slug *Doris kerguelenensis* in the Scotia Arc and Antarctic Peninsula regions (Wilson et al., 2009, 2013). However, it is also clear there are Southern Ocean benthic

species with populations distributed in allopatric refugia around the Southern Ocean, and across the Scotia Sea and Antarctic Peninsula, that did not speciate over glacial cycles, regardless of whether their larval type is benthic or pelagic (Table 1.1). This highlights the fact that glacial cycle survival can drive different levels of population divergence across taxa, and therefore a range of molecular signals and demographic scenarios should be expected in the analyses seeking to identify Southern Ocean glacial refugia. Increased efforts in systematic analyses, further population genetic data of Southern Ocean benthic taxa and investigations of the genetic processes driving cryptic speciation will undoubtedly unravel more mechanisms of glacial survival in the Southern Ocean.

1.7 Future directions of Southern Ocean molecular ecology

As discussed above, previous studies seeking to highlight possible signatures of glacial refugia have been restricted by sample availability, analyses using single locus, and limited examinations of potential refugium locations. Incorporation of benthic samples from rarely sampled regions in the Southern Ocean can be improved through international initiatives and cross-disciplinary collaborations. Investigating and comparing the signatures of glacial refugia in species with different dispersal strategies (direct developers, planktotrophic or lecithotrophic pelagic larvae) can offer insights into the evolutionary selection and survival of pelagic and non-pelagic development throughout glacial periods. The current collection of benthic samples and extracted genomic DNA can be re-sequenced and leveraged for more data through genomic analyses. Advances in genomic sequencing are now enabling the analysis of any regions of interest in the genome, ranging from whole genomes to the sequencing of particular regions such as the mitochondrial genome and/or exonic regions for understanding mutation rate variations and selection (Davey et al., 2011; Schraiber & Akey, 2015).

One popular method in population genetics is to use neutral and unlinked loci with single nucleotide polymorphisms (SNPs), which are sequenced across the genome to investigate past demographic processes based on neutral evolution (Schraiber & Akey, 2015). The use of SNPs can untangle past complex demographic processes at population- and species-level compared to single locus and microsatellite analyses (Morin et al., 2004; Reitzel et al., 2013; Jeffries et al., 2016). SNP data can also be used to reconstruct past changes in population size and population connectivity and isolation over time based on hypothesis testing of simulated scenarios through demographic models, and can be executed based on different mathematical assumptions (e.g. *fastsimcoal2* and *dadi*) (Gutenkunst et al., 2009;

Excoffier et al., 2013).

In Southern Ocean population genetic studies, SNPs have been employed to investigate the population divergence in the bivalve *Aequiyoldia eightsii* (Muñoz-Ramírez et al., 2020), sponge *Dendrilla antarctica* (Leiva et al., 2019), the brittle stars *Astrotoma agassizii* (Galaska et al., 2017a) and *Ophionotus victoriae* (Galaska et al., 2017b), *N. australe* (Collins et al., 2018), and the speciation processes within the *P. patagonica* species complex (Dömel et al., 2019). The use of SNPs could also be useful for investigating past AIS configurations with respect to changes in past patterns of population connectivity and demography (Strugnell et al., 2018). More importantly, genomic data can also highlight other evolutionary drivers that may be associated with survival through glacial cycles in the Southern Ocean, including physical oceanographic forces and biological adaption to environments (Halanych & Mahon, 2018). Future investigations employing SNPs will deepen our understanding of how different factors influence genetic variation and population structure, elucidate how different glacial refugial scenarios may apply across taxa, and will likely indicate pathways of recolonisation from refugia leading to present-day distributions.

Aside from selectively analysing neutral and unlinked loci, model advances have also demonstrated that detailed past evolutionary histories can be inferred through whole genome-based approaches. Whole genome approaches that are built based on sequentially Markovian coalescent (SMC), e.g. pairwise SMC (PSMC) (Li & Durbin, 2011), multiple SMC (MSMC) (Schiffels & Durbin, 2014), SMC++ (Terhorst et al., 2017), minimal-assumption genomic inference of coalescence (MAGIC) (Weissman & Hallatschek, 2017), can effectively estimate past population size and divergence from a single or multiple individuals due to the high data resolution offered by hundreds of thousands of independent loci. These SMC based approaches can investigate past population genetics and demographic processes at a much finer scale than SNPs methods, and can be effective in investigating complex evolutionary processes based on limited samples.

Detailed evolutionary histories can also be understood using approaches that dissect the genealogies of all loci within the genomes from a thousand or more samples, e.g. *Relate* (Speidel et al., 2019) and *tsinfer* (Kelleher et al., 2019). These approaches can be highly powerful in identifying mutation, natural selection and genetic drift down to a single gene and/or trait, and are more accurate in understanding modern and recent processes compared to SMC based methods (Harris, 2019). Although the investigations of Southern Ocean evolutionary histories are likely to be restricted by sample constraints, advance in genome-based approaches highlights existing methods that can detect where and how

benthic taxa persisted in the Southern Ocean over multimillion year timescales with high analytical power.

1.8 Concluding remarks

The questions of where and how Southern Ocean benthic fauna survived the Quaternary ice ages have intrigued Antarctic scientists for decades. It is important to recognise the size, and perhaps locations, of Southern Ocean glacial refugia were likely to be variable over time, and that contrasting dispersal mechanisms into and out of refugia could lead to different demographic signatures, even though these may challenge the reliability of accessing how species survived glacial periods using molecular data. The ice-free areas identified from past AIS reconstructions and the key process of how species survived through glacial periods outlined in this chapter (dispersal and patterns of past species demography) can offer testable frameworks to deduce where and how Southern Ocean benthic fauna persisted the Quaternary. Consequently, how glacial periods influenced evolutionary processes, alongside signatures of other ecological and physical processes, including ecology, dispersal influenced by oceanic currents and seascape dynamics, and other historical AIS processes, can be accurately synthesised.

These frameworks can be effectively exploited by genomic methods, which can untangle complex evolutionary histories with high analytical power. Even though only a handful of studies have proposed locations where Southern Ocean benthic fauna survived glacial cycles with potential sampling and molecular marker biases, together with other genetic studies in the Southern Ocean, they have provided essential knowledge that have progressed the critical understanding of where and how species survived glacial periods. Continued data syntheses and explorations using genomic methods (e.g. *Chapter 2-6*) will undoubtedly reveal a greater understanding of where and how Southern Ocean benthic fauna persisted over multimillion year timescales, providing insights into their resilience against climate changes in the future.

1.9 Thesis overview

1.9.1 Aims

As identified earlier in *Chapter 1*, the evolutionary histories of Southern Ocean benthic taxa can be influenced by glacial-interglacial cycles, persistence, species ecology, and species interactions with oceanic currents and seascape dynamics. Broadly, my thesis aims 1) to elucidate the unique signatures of different evolutionary processes in order to reconstruct the past changes in demographic histories in Southern Ocean benthic taxa, and 2) apply evolutionary knowledge gained to interpret historical AIS configurations.

1.9.2 Study species, their background information and biological research gaps

Only species with a wide geographical, and preferably circum-Antarctic distribution, can offer comprehensive phylogeographic patterns to answer broad evolutionary questions specific to the Southern Ocean. Additionally, a complete understanding of how historical AIS configurations influenced species distribution can only be achieved by investigating phylogeographic and demographic patterns of species with contrasting reproductive and life history strategies. Therefore, the ophiuroids *Ophionotus victoriae* (Bell, 1902), *O. hexactis* (E.A. Smith, 1876), and the octopod *Pareledone turqueti* (Joubin, 1905) were chosen as my study species.

Ophionotus victoriae is characterised by possessing five arms and a broadcast spawning strategy with pelagic larvae. It is known to be exclusively distributed south of the Antarctic Polar Front (APF) with a circumpolar distribution, and it can be found between shallow waters (scuba diving range) and depths of ~1500 m (Sands et al., 2013). *Ophionotus hexactis* is characterised by possessing six arms and brooding larvae. It is mainly distributed around Antarctic islands near the APF at depths ranging from shallow water (scuba diving range) to 459 m (Turner & Dearborn, 1979; McClintock, 1994; GBIF.org, 2019). Interestingly, a very close phylogenetic relationship between *O. victoriae* and *O. hexactis* has also been proposed by multiple genetic studies (COI and exon genomic data) (Hugall et al., 2016; Galaska et al., 2017b). Furthermore, previous studies have also suggested *O. victoriae* could be comprised of multiple cryptic species (Hunter & Halanych, 2010; Galaska et al., 2017b). Therefore, the species status of *O. victoriae*, and the relationship between *O. victoriae* and *O. hexactis*, warrant verification before analyses of population genomic patterns *(biological research gap 1)*.

Additionally, despite the close relatedness of *O. victoriae* and *O. hexactis*, they possess contrasting morphology (5 arms versus 6 arms) and reproductive strategies (broadcasting versus brooding), respectively. It is unclear how the evolutionary history of *O. victoriae* and *O. hexactis* are constructed in the context of glacial cycles survival, species' ecology and signatures of selection, the role of oceanic currents, as well as the evolutionary drivers of changes in arm numbers and reproductive strategy *(biological research gap 2)*.

Pareledone turqueti is characterised as a direct developer with benthic hatchlings (Barratt et al., 2008). It is known to be exclusively distributed south of the Antarctic Polar Front (APF) with circumpolar distribution and is known to occur at depths between shallow waters and ~1000m (Strugnell et al., 2012). Its species status has been critically evaluated by previous studies using different genetic markers, including COI and microsatellite data (Allcock et al., 2011; Strugnell et al., 2012). The genetic signatures of how *P. turqueti* persisted throughout glacial maxima have also been investigated by Strugnell et al. (2012) using COI and microsatellite data (reviewed in *Chapter 1*). Interestingly, previous work based on microsatellite data focusing on samples collected from the Scotia Arc also suggested the genetic variation of *P. turqueti* could reflect the seascape dynamics in the region, including possible signatures of isolation-by-water depth (Strugnell et al., 2017). However, it remains unclear how ocean currents and seascape dynamics contribute to the population genetic patterns of Southern Ocean benthic fauna across different spatial scales (e.g. regional and circumpolar scale), including *P. turqueti (biological research gap 3)*.

1.9.3 Bioinformatic research gaps

Biological samples collected from the Southern Ocean are often stored at room temperature in long-term museum collections (De Broyer et al., 2011), and these are frequently subject to DNA degradation; this is true for many *O. victoriae*, *O. hexactis* and *P. turqueti* samples. Typically, for non-model species, in order to sequence loci across the genome, reduced representation genomic methods (e.g. restriction-site associated DNA sequencing (RADseq), genotyping-by-sequencing (GBS)) are often employed since they do not require *a priori* information such as reference genomes. However, these methods require high quality samples with high molecular weight DNA (Puritz et al., 2014), which are not applicable for most existing samples collected from the Southern Ocean due to DNA degradation. Fortunately, it is now more feasible to obtain genomic sequence data from degraded and/or historical samples after advancement in sequencing technologies, for example using target capture sequencing approaches. The target capture approach is based on using single-stranded oligonucleotides (i.e. baits or probes) to enrich for targeted

loci in fragmented DNA and thereby sequencing genomic regions of interest across samples (Grover, Salmon, & Wendel, 2012). Bait sequences can be designed to target specific genomic positions including ultraconserved elements (UCE), exonic regions, and RAD loci based on prior knowledge (Jones & Good, 2016).

To date, studies that have incorporated target capture sequencing of RAD loci have found this technique effective in recovering loci of interest, resulting in data that is equivalent to traditional RAD-seq based methods for the purpose of downstream population genomic analyses (e.g. Boucher et al., 2016; Linck et al., 2017; Schmid et al., 2018; Dorant et al., 2019). Nonetheless, target capture sequencing of RAD loci has never been used in questions relating to Southern Ocean taxa to date (*bioinformatic research gap 1*).

More importantly, preliminary studies have also reported reads sequenced at the exact same genomic positions, generated from traditional RAD-seq methods and target capture methods, might not be directly comparable at a nucleotide bases level due to sequencing errors (Lang et al., 2020; O'Connell et al., 2021). The exact reasons driving this effect are unclear, and this could impact future studies seeking to compare and evaluate samples sequenced with either method, within and beyond Southern Ocean genomic studies (*bioinformatic research gap 2*).

1.9.4 Geophysical research gaps

A major uncertainty in future global mean sea level (GMSL) rise projections lies within the stability, or instability, of the West Antarctic ice sheet (WAIS). Under current climate change conditions, the marine-based WAIS has lost 159 ± 9 gigatons of ice mass per year between 1979 - 2017 (Rignot et al., 2019) and continues to be a major contributor to GMSL rise under all CO_2 emission scenarios (Fox-Kemper et al., 2021). It is unclear whether the WAIS is vulnerable to future collapse due to a poor understanding of the mechanisms linked to its instability. However, taking potential WAIS instability into account, modelling has suggested that GMSL could rise between 0.4 and 2.4 m under Representative Concentration Pathway (RCP) 8.5 scenario by 2100 (Fox-Kemper et al., 2021). The estimated range between 0.4 and 2.4 m reflects the wide uncertainty in WAIS instability. A constraint of this parameter is urgently needed in order to improve models of future GMSL, and their subsequent projections.

It is well understood from geological reconstructions that there were warm interglacial periods in the Pleistocene. For example, during the Last Interglacial Period (LIG; ~120,000

years ago), the average air temperature was 0.5 - 2.0 ºC warmer than today with global mean sea level (GMSL) ~6 - 11 m above present (Turney et al., 2020). During the Marine Isotope Stage (MIS) 11 (~420,000 years ago), the GMSL was ~6 - 13 m above present (Raymo & Mitrovica, 2012). Knowledge of how the WAIS was configured, during warmer periods in the recent geological past, has been identified as the most urgent data gap needed in order constrain future sea level rise projections (Gilford et al., 2020). To date, there is no direct evidence (geological or biological) indicating the stability of WAIS in the last 3 million years (*Geophysical research gap 1*).

From a biological perspective, if the WAIS did experience a partial or complete collapse at any time in the past, including the LIG, seaways that connect the present-day Weddell Sea, Amundsen Sea and Ross Sea (trans-west Antarctic seaway) would have been opened and subsequently enabled marine fauna to migrate through (Strugnell et al., 2018). So far there is some limited existing assemblage or genetic evidence indicating the presence of trans-Antarctic seaways between the Weddell Sea, Ross Sea and/or Amundsen Sea, including in studies of extant asteroids (Moreau et al., 2019), extant bryozoan (Barnes & Hillenbrand, 2010; Vaughan et al., 2011), the bivalve *Lissarca* (Linse et al., 2006), the microarthropod *Collembola* (Collins et al., 2020), as well as the species investigated within this thesis; *P. turqueti* (Strugnell et al., 2012) and *O. victoriae* (Galaska et al., 2017b). However, these studies all lacked either the sampling context necessary or the data resolution required to accurately infer demographic inferences related to past trans-west Antarctic connectivity. The sampling design needs to include spatial coverage that can distinguish the signatures of trans-west Antarctic seaways from contemporary circumpolar ocean currents. The genomic signatures of demographic histories of *P. turqueti* and *O. victoriae* including samples from East Antarctica, would need to be resolved first (*Geophysical research gap 1*).

1.9.5 Thesis outline

My thesis addresses the overall aims and the six research gaps highlighted above in five data-based chapters prepared for peer-reviewed publication (Fig 1.2).

In *Chapter 2*, I use COI data to examine i) whether *O. victoriae* contains cryptic species, ii) how genetic structure is characterised in *O. victoriae* and *O. hexactis*, iii) if there is genetic evidence indicating how *O. victoriae* and *O. hexactis* have survived glacial cycles, and finally, iv) whether the divergence between *O. victoriae* and *O. hexactis* can be linked to isolation-by-environment and present-day conditions. The results from this chapter shed light on the ecological and evolutionary context that could explain the life history and

morphological differences between *O. victoriae* and *O. hexactis*. The results from this chapter also offer hypotheses which can be tested using genomic data in *Chapter 4*.

In *Chapter 3*, I use a target capture method to sequence double-digest RAD (ddRAD) loci in *P. turqueti*. I bioinformatically integrate and compare reads from target capture sequencing and ddRAD sequencing (ddRADseq) of *P. turqueti* in two bioinformatic pipelines with contrasting genotype estimation methods. I evaluate whether biases could be found between reads derived from target capture sequencing and ddRADseq, as well as if the drivers of these biases could be identified. This chapter critically establishes the reliability of the target capture approach in retrieving ddRAD loci information utilised in *Chapter 4, 5, and 6*.

In *Chapter 4*, I use a target capture method to sequence ddRAD loci in *O. victoriae* and *O. hexactis*. I further examine the genomic signatures of i) the genealogical relationship between *O. victoriae* and *O. hexactis*, ii) whether signatures of positive selection linked to *O. hexactis* can be detected, iii) where and how *O. victoriae* and *O. hexactis* survived glacial cycles and iv) the ecological and physical drivers behind the present-day genomic structure in both species. This chapter critically identifies the various drivers behind the genomic variation of *O. victoriae*, which would offer hypotheses to test for historical WAIS collapses in *Chapter 6*.

In *Chapter 5*, I analyse the ddRAD loci sequenced with a target capture approach in *P. turqueti*. I examine i) how is the genomic variation of *P. turqueti* structured at a circumpolar scale and whether the patterns reflect those found in previous COI and microsatellite studies, ii) whether the genomic variation of *P. turqueti* can be explained by modern environmental variables and oceanic currents at both regional (e.g. Scotia Arc) and circumpolar scales, iii) whether there is signature of positive environmental association and outlier loci linked to Southern Ocean seascape dynamics in *P. turqueti*. This chapter critically examines the lesser known drivers behind the genomic variation of *P. turqueti*, and by extension, Southern Ocean benthic fauna. The knowledge from this chapter offers preliminary hypotheses to test for historical WAIS collapse in *Chapter 6*.

Lastly, in *Chapter 6*, I investigate historical admixture patterns and construct demographic models specifically designed to test for whether the WAIS collapsed during recent interglacial cycles, by analysing the ddRAD data of *P. turqueti* and *O. victoriae*. Importantly, I specifically design the methods and interpret the data around the context of the unique past changes in the demographic history of both species, building on the findings of *Chapter 2-5*.

In *Chapter 7*, I conclude that the knowledge of systematics, ecology and evolution of Southern Ocean species synthesised from *Chapter 1-5* are essential in forming testable hypotheses to pinpoint historical WAIS collapses in *Chapter 6*. I discuss the implications of how my research findings will constrain future sea level rise projections, and more importantly how the livelihoods of 10% of the global population would be affected by 2100 under current climate change. Finally, I also recommend future directions in the field of Southern Ocean genomics and interdisciplinary research.

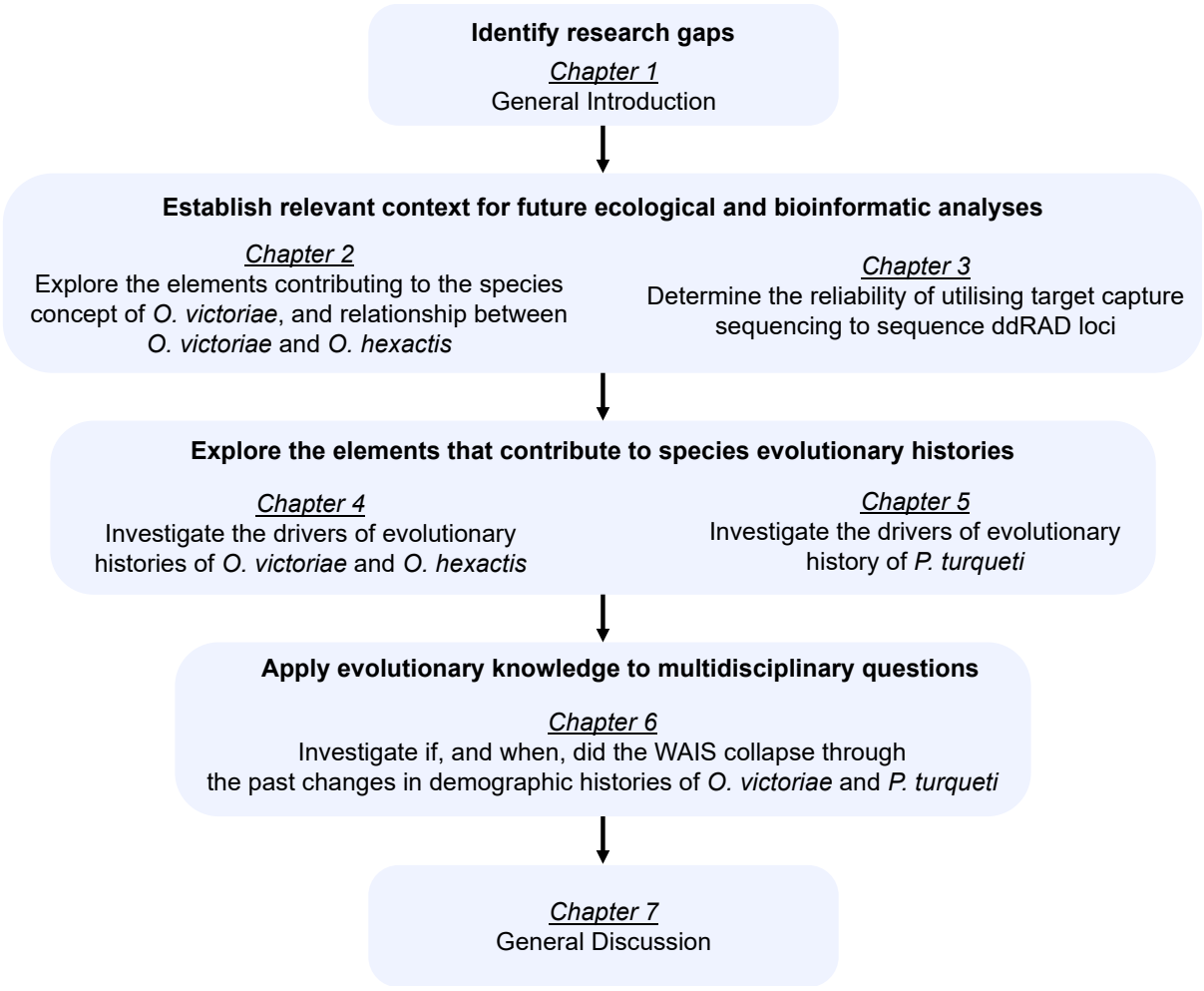

Fig 1.2 A schematic of the thesis structure. This diagram will be repeatedly used to introduce each chapter to indicate the chapter's relevance in relation to the overall thesis context.

CHAPTER 2

Evolutionary innovations in Antarctic brittle stars linked to glacial refugia

This chapter is formatted for, and is published in:

Lau, S. C. Y., Strugnell, J. M., Sands, C. J., Silva, C. N. S., & Wilson, N. G. (2021). Evolutionary innovations in Antarctic brittle stars linked to glacial refugia. *Ecology and Evolution*, **11**(23), 17428–17446.

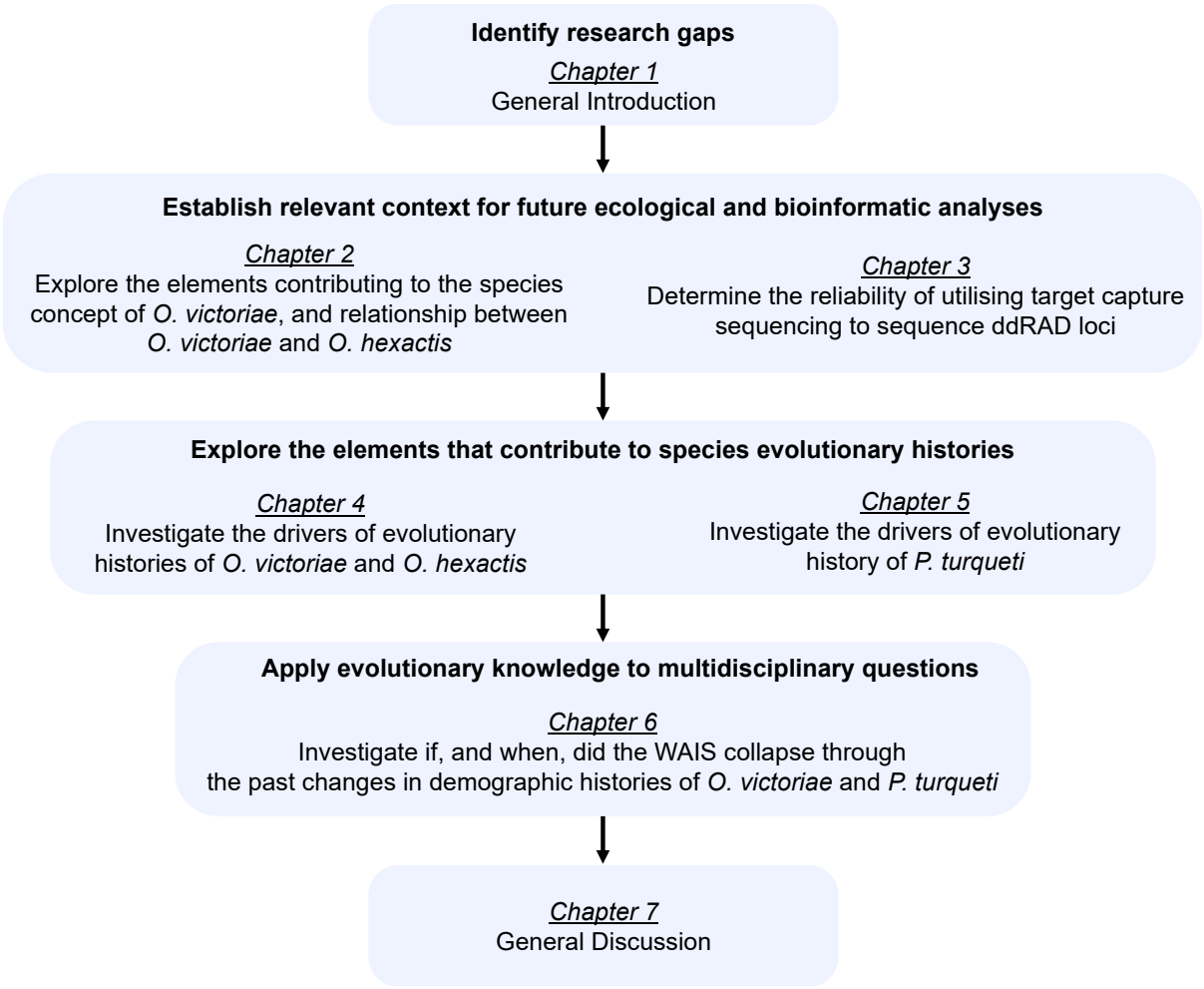

2.1 Abstract

The drivers behind evolutionary innovations such as contrasting life histories and morphological change are central questions of evolutionary biology. However, the environmental and ecological contexts linked to evolutionary innovations are generally unclear. During the Pleistocene glacial cycles, grounded ice sheets expanded across the Southern Ocean continental shelf. Limited ice-free areas remained, and fauna were isolated from other refugial populations. Survival in Southern Ocean refugia could present opportunities for ecological adaptation and evolutionary innovation. Here, we reconstructed the phylogeographic patterns of circum-Antarctic brittle stars *Ophionotus victoriae* and *O. hexactis* with contrasting life histories (broadcasting versus brooding) and morphology (five versus six arms). We examined the evolutionary relationship between the two species using cytochrome c oxidase subunit I (COI) data. COI data suggested that *O. victoriae* is a single species (rather than a species complex) and is closely related to *O. hexactis* (a separate species). Since their recent divergence in the mid-Pleistocene, *O. victoriae* and *O. hexactis* likely persisted differently throughout glacial maxima, in deep-sea and Antarctic island refugia, respectively. Genetic connectivity, within and between the Antarctic continental shelf and islands, was also observed and could be linked to the Antarctic Circumpolar Current and local oceanographic regimes. Signatures of a probable seascape corridor linking connectivity between the Scotia Arc and Prydz Bay are also highlighted. We suggest that survival in Antarctic island refugia was associated with increase in arm number and a switch from broadcast spawning to brooding in *O. hexactis*, and propose that it could be linked to environmental changes (such as salinity) associated with intensified interglacial-glacial cycles.

Keywords: contrasting life histories, evolutionary innovations, glacial refugia, morphological innovation, population genetics

2.2 Introduction

In marine invertebrates, early life-history strategy influences species dispersal potential, and this, in turn, can shape population-level gene flow and long-term evolutionary histories (Hart & Marko, 2010). Although pelagic development with planktotrophic (feeding) larvae has been suggested as the ancestral mode in most marine taxa (Strathmann, 1985), non-pelagic direct development (brooding) has been linked to evolution under increased offspring provisioning (Wray & Raff, 1991). Brooding is commonly observed as an evolutionary transition from broadcast spawning across broad lineages (Strathmann, 1985), but contrasting life histories (brooding and broadcast spawning) are also often reported between congeneric species in speciose clades, including echinoderms (Collin & Moran, 2018). The main drivers behind contrasting life histories are often unknown. However, in some reported cases, transitions from pelagic to direct development can be linked to ecological and/or environmental changes (Boissin et al., 2011). Contrasting life histories have also been observed in congeneric species in the Antarctic and Southern Ocean (e.g., Jossart et al. (2019)). If investigated, they could offer insights into variation in evolutionary processes, constrained within similar environments.

Throughout the Quaternary (2.6 million years ago - now), glacial cycles driven by climatic oscillations were significant in structuring past evolutionary histories in the terrestrial and marine realm (Hewitt, 2004; Maggs et al., 2008; Provan & Bennett, 2008). In the Northern Hemisphere, in response to ice sheet expansion and subsequent erosion of habitats, some Arctic and temperate taxa migrated to warmer, lower latitude ice-free areas for refuge, with some persisting in small-scale ice-free *in situ* refugia (Maggs et al., 2008; Provan & Bennett, 2008). In the Southern Hemisphere, the continental-based Antarctic ice sheet also expanded and eroded most of the continental shelf seafloor habitats in the Southern Ocean (Clarke & Crame, 1992; Thatje et al., 2005). However, migration to lower latitudes appears improbable for Southern Ocean fauna because of the strong Antarctic Circumpolar Current (ACC) with various frontal boundaries surrounding the Antarctic continent (Rintoul et al., 2001; Thatje et al., 2005). These ocean barriers have been suggested to play an important role in isolating Southern Ocean taxa from other ocean basins since the mid-Miocene (~14 million years ago) (Crame, 2018). Throughout the Pleistocene glacial cycles, the Southern Ocean benthic fauna are hypothesised to have either persisted in limited, isolated ice-free areas on the Antarctic continental shelf, or migrated to, and survived in, the surrounding deep sea or around Antarctic islands off the shelf (Thatje et al., 2005; Convey et al., 2009; Allcock & Strugnell, 2012).

Persistence in isolated Southern Ocean refugia has been suggested to favour non-pelagic development due to higher chances of surviving glacial periods, when the Southern Ocean experienced limited habitat availability and low primary productivity linked to permanent ice cover (Poulin et al., 2002; Thatje et al., 2005; Convey et al., 2009; Pearse et al., 2009). However, it has been suggested that pelagic development was also a successful strategy in persisting throughout glacial cycles in the Southern Ocean, and selection likely acted differently on different developmental modes throughout glacial periods (Lau et al., 2020; *Chapter 1*). Survival in allopatric refugia would present unique challenges for fauna to persist within each isolated environment, as well as providing opportunities to drive evolutionary innovations and phenotypic changes (e.g. morphological variation and reproductive specialisation) between isolated populations. Furthermore, the Quaternary glacial period was also characterised by several, but rare, "warm" climate periods (between 1 and 4°C warmer than the Holocene) (Noble et al., 2020). The environmental fluctuation between extreme conditions (glacial maxima and warm interglacial) could also promote niche diversity and ecological diversification (Clarke & Crame, 1992).

Evolutionary innovations can be represented by new traits, which often opens new ecological niches where further evolutionary changes can unfold (Wagner, 2011). New traits can include trait expression and/or novel function, and these can be a broad range of behavioural, physiological, and morphological characteristics (Love, 2003; Moczek et al., 2011), whereas key innovations are a small subset of these that are invoked as underpinning evolutionary radiations. Events such as increased diversification rate and utilisation of new and/or altered habitats have been suggested to be associated with evolutionary innovations (Dumont et al., 2012; Wilson et al., 2013). There is evidence indicating Southern Ocean glacial refugia could have provided opportunities for evolutionary innovations. First, persistence in Southern Ocean refugia has been suggested to have promoted allopatric diversification and subsequent speciation (i.e., the "species pumps" and the "Antarctic biodiversity pump" hypotheses) (Clarke & Crame, 1989; Crame, 1997; Willis & Whittaker, 2000). Cryptic speciation and/or lineage diversification linked to glacial cycles and/or glacial refugia survival has been suggested for many benthic taxa (e.g. Wilson et al., 2009; Allcock et al., 2011; Baird et al., 2011; Strugnell et al., 2012; González-Wevar et al., 2013). Second, Southern Ocean benthic taxa experienced repeated migrations to new and/or altered habitats as ice sheets expanded and contracted throughout glacial-interglacial cycles (see Lau et al. (2020); *Chapter 1* for a review). Lastly, evolutionary innovations with novel biological changes linked to survival in Southern Ocean glacial refugia have also been observed. Cryptic species within the sea slug *Doris kerguelenensis* species complex survived in allopatric refugia on the Antarctic continental shelf (Wilson et al., 2009). Over

glacial cycles, *D. kerguelenensis* underwent lineage diversification across allopatric refugia, as well as developing distinct metabolites as an adaptation to unique predation pressure within local refugial environments (Wilson et al., 2013). Nonetheless, limited examples have reported the association between evolutionary innovation and survival within glacial refugia, or past interglacial periods, to date in the global marine realm.

The brittle star genus *Ophionotus* Bell, 1902 is distributed widely throughout the Southern Ocean including the Antarctic continental shelf, deep sea, and islands within the Antarctic Polar Front (APF). *Ophionotus* is comprised of three species, including *O. victoriae* Bell, 1902, *O. hexactis* E. A. Smith, 1876, and *O. taylori* McKnight, 1967. *Ophionotus victoriae* is characterised by five arms, pelagic planktotrophic larvae (Grange et al. 2004), and a widespread distribution across the Southern Ocean at depths ranging from shallow water to 1750 m (this study; specimen IDs: WAMZ88591 - WAMZ88594). *Ophionotus hexactis* is characterised by six arms, brooding larvae, and is mainly distributed around Antarctic islands near the APF at depths ranging from shallow water to 459 m (Turner & Dearborn, 1979; McClintock, 1994; GBIF.org, 2019). However, *O. hexactis* has also been collected from the Antarctic Peninsula on the Antarctic continental shelf (Hugall et al., 2016). *Ophionotus taylori* is characterised by five arms, and its occurrence has never been reported since the type specimen was collected from Cape Hallett, Ross Sea. Compared to *O. victoriae*, *O. taylori* possesses notably coarser and thicker scales, with other taxonomic features (including arm shape, arm spines, arm plates, oral shields) different in size and shape relative to *O. victoriae* (McKnight, 1967).

Previous studies employing genetic (mitochondrial markers 16S rRNA and COI) and genomic (2b-restriction site-associated DNA (2b-RAD) sequencing) methods have suggested high genetic differentiation between distant sampling locations within *O. victoriae*, and it has been suggested to be comprised of multiple cryptic species (Hunter & Halanych, 2010; Galaska et al., 2017b). However, prior sampling efforts have been focused in some locations in West Antarctica. Samples from East Antarctica and some Antarctic islands (Shag Rocks, South Georgia, Heard Island, Scott Island, Balleny Islands) are not yet represented in genetic studies for this taxon. Therefore, the previous interpretation of cryptic species within *O. victoriae* may have been influenced by the limited and disjunct sampling of a widely distributed species, reflecting artefacts caused by isolation-by-distance. Lack of comprehensive sampling is common in Southern Ocean ecological studies. Biological samples from East Antarctica and Antarctic islands are incredibly rare, since these areas are difficult to access and are distant from most national research stations (Griffiths et al., 2014).

Given that *O. victoriae* and *O. hexactis* are characterised by overlapping distribution and wide-ranging depths in the Southern Ocean, increased sampling effort may provide a more thorough understanding of their past demographic histories. The morphology and early life history of *O. hexactis* is striking within echinoderms, as this phylum is evolutionarily primed to pentameral symmetry (i.e., five arms in brittle stars) (Rozhnov, 2012) and pelagic development with planktotrophic larvae (Gillespie & McClintock, 2007). *Ophionotus victoriae* and *O. hexactis* are currently recognised as separate species (WoRMS Editorial Board, 2021), distinguished by the number of arms (five versus six) and reproductive features (oviparous versus viviparous) (Smith, 1876; Bell, 1902). However, a single five-armed *O. hexactis* specimen from South Georgia has also been reported to exhibit brooding behaviour with six-arm juveniles (Mortensen, 1936), indicating there could be rare biological exceptions. Recent COI and exon capture data also suggest a close genetic distance between *O. victoriae* and *O. hexactis* (Hugall et al., 2016; Galaska et al., 2017b), despite their obvious morphological differences. Given the apparent close phylogenetic relationship and highly differentiated morphological variation between *O. victoriae* and *O. hexactis*, comparing their past demographic histories could provide insight into species history.

In this study, we have incorporated new *O. victoriae* samples from rarely sampled regions including East Antarctica (Prydz Bay, Davis Sea, Adélie Land) and Antarctic islands (South Georgia, Shag Rocks, Discovery Bank, Herdman Bank, Balleny Islands, Scott Islands, Heard Island) in order to holistically examine evolutionary processes across the Southern Ocean, along a geographical and circumpolar cline, in a species with a circum-Antarctic distribution. We also incorporated new *O. victoriae* samples from previously surveyed areas (Bouvet Island, Bransfield Strait, Discovery Bank, Elephant Island, Shetland Islands, South Sandwich Islands, Larsen Ice Shelf, Ross Sea, and Weddell Sea) to increase sample robustness. We used COI sequence data from samples collected from an expanded distribution to determine (a) whether *O. victoriae* contains cryptic species, (b) how genetic structure is characterised in *O. victoriae* and *O. hexactis*, (c) if there is genetic evidence indicating how *O. victoriae* and *O. hexactis* have survived glacial cycles, and finally, (d) whether the divergence between *O. victoriae* and *O. hexactis* can be linked to isolation-by-environment and present-day conditions. We used these analyses to investigate the ecological and evolutionary context that could explain the life-history and morphological differences between *O. victoriae* and *O. hexactis*.

2.3 Methods

2.3.1 Sample collection

This newly generated dataset was sequenced from individuals of *Ophionotus victoriae* (n = 443) and *O. hexactis* (n = 72) deposited at Western Australian Museum (WAM), Muséum National d'Histoire Naturelle (MNHN-IE), Museum Victoria (MV), Scripps Institution of Oceanography (SIO-BIC), and the National Institute of Water and Atmospheric Research (NIWA). Tissue samples from MNHN-IE and SIO-BIC were first sent to MV and WAM, respectively. Then, tissue sampling was performed at WAM, MV and NIWA via research visits by Sally Lau, Jan Strugnell and Nerida Wilson. All newly sequenced *O. victoriae* and *O. hexactis* samples were preserved in 50 - 100% ethanol and were identified through their readily distinguishable (and diagnostic) pentamerous and hexamerous arm symmetry, respectively. We note that it is plausible that *O. hexactis* with 5 arms exist in the dataset. Partial COI sequences of *O. victoriae* (n = 419) and *O. hexactis* (n = 1) from previous studies were also included in the data analysis (Hunter & Halanych, 2010; Galaska et al., 2017b) (see Supplementary Table 2.1 for GenBank Accession numbers). All brittle star samples (n = 935) investigated in this study were collected between the years 2004 - 2019, from depths of 34 - 1750 m during expeditions in the Southern Ocean (Fig 2.1; GenBank Accession numbers: FJ917309-FJ917354, GU227093, KU895454, KY048218- KY048268, MZ543435-MZ543949). Details of sampling information are presented in Supplementary Table 2.1).

2.3.2 Molecular sequencing

Genomic DNA of the collected samples was extracted using DNeasy Blood and Tissue Kit (Qiagen), following the manufacturer's protocol. Partial COI sequences were then amplified using genus-specific primers Op4f (5′-TAGTGACTGCCCATGCCTTC-3′) and COI_op3r (5′-TTTTTCGATCAGTGAGGAGC-3′) developed by Jose Carvajal (SIO/WAM). Each 25 µl PCR contains 5.0 µl of 5× MyTaq PCR buffer (Bioline), 0.2 µl of 5 U/µl MyTaq DNA polymerase (Bioline), 0.8 µl of each 10 µM primer (forward and reverse), 1.5 µl of template genomic DNA (5 - 20 ng/µl), and 16.8 µl of water. PCR cycling profile conditions were as follows: initial denaturation at 95°C for 3 min, 8 cycles of 95°C for 30 s, 52°C for 30 s with a touchdown which the annealing temperature was reduced by 1°C at every cycle, and 72°C for 45 s, followed by 38 cycles of 95°C for 30 s, 48°C for 30 s, and 72°C for 45 s, and a final extension step at 72°C for 5 min. PCR products were then sent to Australian Genome

Research Facility (AGRF) (Perth and Brisbane, Australia) for purification and sequencing in both directions.

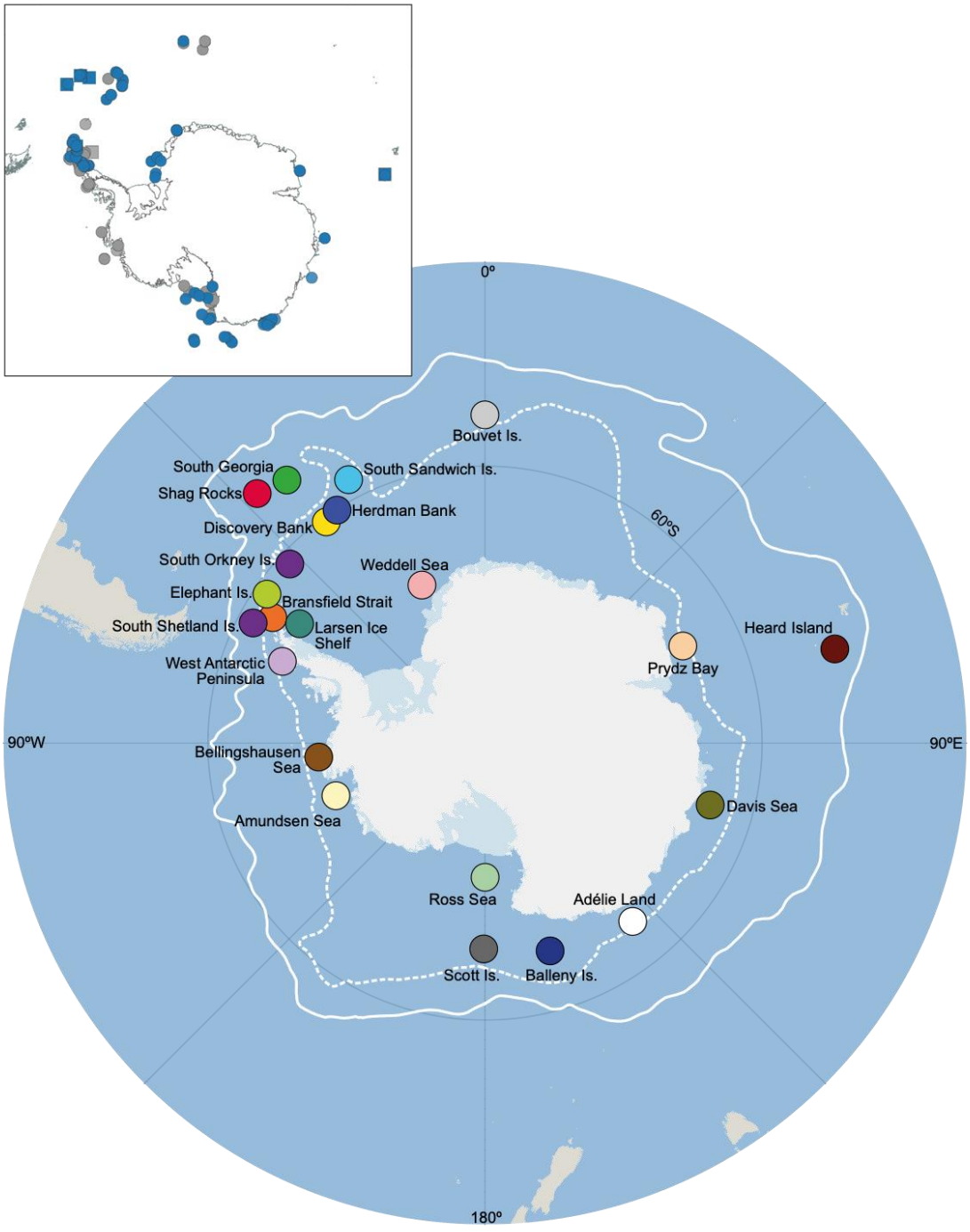

Fig 2.1 Map of Southern Ocean with sampling locations of *Ophionotus victoriae* and *O. hexactis* defined for population genetic analyses. White lines = Antarctic Polar Front (APF) (solid) and southern boundary of the Antarctic Circumpolar Current (dashed). Top left map indicates the distribution of individual samples, blue = sequences generated in this study, grey = GenBank accessions, circles = *O. victoriae*, square = *O. hexactis*.

While PCR amplification with Op4f and COI_op3r was successful in most specimens, two *O. victoriae* individuals collected from South Georgia yielded poorly amplified but detectable PCR products (ID: SIO-BIC E6408 and SIO-BIC E6420). Therefore, based on the assembled COI alignments of *O. victoriae* and *O. hexactis* collected from their overlapped distributional regions (South Georgia, Bransfield Strait and Heard Island) (see Supplementary Fig 2.1 for photos of specimens), two sets of internal primers were designed for nested PCR to target the same positions as those Op4f and COI_op3r would target in *Ophionotus* spp. The two internal primer pairs designed by this study include the following: oph_head-F (5′-TTGGGGGATTTGGAAACTGG-3′)/-R (5′-AGACCAAACAAATAAAGGAGTTCGG-3′) and oph_tail-F (5′-CCCCGGATATGGCATTTCCT-3′)/-R (5′-TTGCCCCTGCTAATACTGGT-3′). All assembled COI sequences were aligned using the Multiple Alignment using Fast Fourier Transform (MAFFT) (Katoh & Standley, 2013) plug-in *Geneious* v10.2.4 (https://www.geneious.com), using default values and trimmed to 434 base pairs (bp).

2.3.3 Network reconstruction and population genetics

A median joining (MJ) haplotype network (Bandelt et al., 1999) with epsilon = 0 was constructed using *PopART* (Leigh & Bryant, 2015) to visualise the relationships between individual samples within *O. victoriae* and *O. hexactis*, as well as relationships between species. We have also explored a MJ network with epsilon = 10 to widen the search for unobserved sequences (i.e., hypothesised haplotypes). However, the algorithm produced too many unnecessary hypothesised haplotypes and eventually broke down. Therefore, the MJ network with epsilon = 0 has achieved a sufficient level of exploration in reconstructing all possible shortest and least complex phylogenetic trees for discussion. A TCS haplotype network with a default connection limit of 95% was also constructed using *PopART* to evaluate consistency of results across different network assumptions. For population genetic analyses, COI sequences were first grouped by species and then further divided into sample localities defined in Table 2.1 (Fig 2.1). All the sampled locations are within the APF. Sample locations on the Antarctic continental shelf were considered “continental shelf,” and islands located off the Antarctic continental shelf were considered as “Antarctic islands.” Population genetic statistics including genetic diversity (nucleotide and haplotype), number of polymorphic sites, and average number of nucleotide difference were calculated for each sampling locality using *Arlequin* v3.5 (Excoffier & Lischer, 2010). Pairwise F_{ST} and subsequent analysis of molecular variance (AMOVA) based on 1,000 permutations was also calculated in *Arlequin* to examine genetic differentiation between *O. victoriae* and *O. hexactis*, as well as between sampling localities within *O. victoriae* and *O. hexactis*. The

number of private haplotypes at each locality was calculated using *Fabox* v1.5 (Villesen, 2007).

We have also examined the species boundaries and relationships between *O. victoriae* and *O. hexactis* using phylogenetic tree reconstructions (Maximum likelihood (ML) and Bayesian inference (BI)) and species delimitation methods. Our study only contains one genetic marker (mitochondrial COI gene), which may not contain sufficient information to diagnose species status (DeSalle et al., 2005). However, as species delimitation using COI may still be of interest to the wider research community (DeSalle & Goldstein, 2019) and is also useful for providing hypotheses for future studies employing nuclear data, we have presented the methods and results of species delimitation in Supplementary Note 2.1. Throughout this study, we view *O. victoriae* and *O. hexactis* as two taxonomically recognised separate species.

2.3.4 Demographic histories

The past demographic histories of *O. victoriae* and *O. hexactis* (analysed separately) were investigated via neutrality tests (Tajima's *D* and Fu's F_S), mismatch distributions (pairwise differences distributions), and past population size changes (Bayesian Skyline Plots; BSP). Tajima's *D* and Fu's F_S were calculated in *Arlequin* to examine whether data deviated from a neutral evolution model, with significance tested by 1,000 permutations. Distributions of pairwise differences to estimate parameters of demographic expansion (mismatch distribution) were calculated using the R package *adegenet* (Jombart & Ahmed, 2011) and *pegas* (Paradis, 2010) in *R* v3.3.3. Past changes in effective population size over time in *O. victoriae* and *O. hexactis* were also estimated using BSP in *BEAST* v2.5.0 (Bouckaert et al., 2019). *BEAST* was performed under the substitution model of TN+F+I+G4 (identified via Bayesian information criterion (BIC) using *ModelFinder* on the *IQ-TREE* web server (Kalyaanamoorthy et al., 2017)), uncorrelated lognormal relaxed clock and using a constant coalescent constant population tree prior (Michonneau, 2016). A Markov Chain Monte Carlo (MCMC) analysis was run for 500 million (*O. victoriae*) and 200 million (*O. hexactis*) generations sampled at every 5,000 generations. A longer MCMC was required for *O. victoriae* as the length of chain is correlated to the number of individual sequences included (n = 826 in *O. victoriae*) (Drummond et al., 2007). *Tracer* v1.7.1 (Rambaut et al., 2018) was used to inspect convergence based on trace plots and effective sample size (ESS; > 200). A substitution rate of 2.48% per million years was employed following other analyses of COI data for ophiuroids (Naughton et al., 2014; Sands et al., 2015).

2.3.5 Spatial genetic variation within *O. victoriae*

To explore how genetic variation is spatially structured in the Southern Ocean, spatial pattern detection analysis was performed within *O*. *victoriae*. Spatial pattern detection analysis was not performed for *O*. *hexactis* as the variation in sample coordinates was limited, leading to a singular matrix not suitable for a multivariate correlation analysis. For *O*. *victoriae*, a matrix of genetic *p*-distance between individual COI sequences was first calculated based on the substitution model of TN+F+I+G4 using the *APE* package in *R* (Paradis et al., 2004). The *mgQuick* function of the R package *MEMGENE* (Galpern et al., 2014) was used to extract the spatial components of genetic variation attributed to isolation-by-distance (i.e., Euclidean distances; straight linear geographical distance) between samples. *mgQuick* uses Moran's eigenvector maps (MEM) to create orthogonal eigenvectors from Euclidean distances and then uses redundancy analysis (RDA) to quantify the proportion of genetic variation explained by each eigenvector (i.e. MEMGENE variables). *MEMGENE* variables are ranked by the amount of genetic variation explained by Euclidean distances from the most to least, and the first two MEMGENE variables typically outline most of the detected spatial genetic patterns (Galpern et al., 2014). To visualise each *MEMGENE* variable, samples are first mapped based on their geographical locations. Each sample's predicted eigenvector score is then overlaid on the map to visualize the spatial component of genetic similarity or dissimilarity among individuals, thus highlighting genetic clusters linked to isolation-by-distance.

2.3.6 Isolation-by-environment between species

Isolation-by-environment was also investigated in *MEMGENE* to detect whether environmental heterogeneity (in the form of resistance surfaces) may also explain the genetic variation between *O*. *victoriae* and *O*. *hexactis*. Any significant association to environmental variables detected by isolation-by-environment may reflect non-random mating linked to environmental differences and/or local adaptation linked to selection (Sexton et al., 2013). Although including samples from both species in an IBE analysis assumes the intrinsic reproductive isolation between *O. victoriae* and *O. hexactis* is incomplete, exploring how the genetic variation between closely related species is associated with an heterogeneous environment could offer insights into how the environment could influence species differentiation (e.g., Saenz-Agudelo et al. (2015)). The environmental parameters considered in this analysis included sea surface temperature, seafloor temperature, sea surface salinity, seafloor salinity, surface current velocity (as a variable of physical transport patterns), and geological bathymetry. The resistance surfaces

representing each environmental parameter were produced from the temperature and salinity point datasets from World Ocean Atlas 2018 (Locarnini et al., 2018; Zweng et al., 2018), as well as extracted from the raster layers of Southern Ocean State Estimate (SOSE) mean surface current speed (cell resolution = 16 km) (Mazloff et al., 2010) and ETOPO1/IBCSO/RAMP2 hillshades and elevation (surface and seafloor) model (cell resolution = 1 km) (Amante & Eakins, 2009) from *Quantarctica* (Matsuoka et al., 2021) using *QGIS* (QGIS Development Team, 2019). Southern Ocean temperature and salinity data were reproduced from global point datasets (climatological means) at 1°C spatial resolution of annual average per decade between 1955 and 2010, with temperature and salinity data available at 102 depth levels ranging from 0 to 5,500 m for each point. Surface temperature and salinity data were estimated from a value at 0 m water depth for each point, whereas seafloor temperature and salinity data were estimated based on the data value at the depth interval closest to the maximum depth available for each point. All extracted temperature and salinity data were transformed to single raster layers via triangular interpolation method in *QGIS* (Interpolation plug-in).

As the raster layer of surface current speed was pre-defined with a cell resolution of 16 km in Mazloff et al. (2010), the resistance surfaces analysed in this study were interpolated (temperature and salinity) or resampled to reduce resolution (surface and seafloor elevation) to match the extent of the surface current speed layer for subsequent *mgLandscape* (*MEMGENE*) analysis (Supplementary Fig 2.2). While the interpolation of oceanic conditions may include prediction errors and deviation from true environmental conditions (especially in a heterogeneous environment) (Rellstab et al., 2015), the raster layers capture the overall dynamics of the Southern Ocean and serve as reasonable estimates for analysing genetic-environmental association at a circumpolar scale. Collinearity between selected environmental variables was checked using a pairwise Pearson correlation analysis using the R package Raster (Hijmans, 2016). The resulting correlation coefficients (r between -0.51 and 0.69) were below the threshold of collinearity ($r < 0.7$) in ecological datasets (Dormann et al., 2013) and were therefore appropriate for subsequent environmental association analysis.

The *mgLandscape* function of *MEMGENE* was used to characterise the MEM eigenvectors from the six resistance surfaces and Euclidean distances, and to relate the MEM eigenvectors to genetic distance matrix using RDA. A matrix of genetic distance between individual COI sequences (i.e., sequences of both species were pooled together) was calculated based on the substitution model of TN+F+I+G4.

For *mgQuick* (within *O. victoriae*) and *mgLandscape* (between *O. victoriae* and *O. hexactis*) analyses, forward permutations of 500 were used to test for forward selection of MEM eigenvectors and final permutations of 1,000 were used to test for significance levels at 0.05. Both *mgQuick* and *mgLandscape* produce values of adjusted R^2 (adjR^2) that estimate the overall proportion of the genetic variation that can and cannot be understood by each spatial predictor (*mgQuick*: Euclidean distances; *mgLandscape*: Euclidean distances, sea surface temperature, seafloor temperature, sea surface salinity, seafloor salinity, seafloor bathymetry, and surface current velocity).

2.4 Results

2.4.1 Haplotype networks

A total of 935 COI sequences of *O. victoriae* (n = 862) and *O. hexactis* (n = 73), comprised of 165 unique haplotypes, were included in data analysis. Median joining (MJ) network analysis of COI alignments revealed both species are highly separated but not perfectly reciprocally monophyletic groups, and that *O. victoriae* is frequently connected forming a single haplotype network (Fig 2.2). TCS network also produced an identical conclusion to the MJ network (Supplementary Fig 2.3). Here, we discuss our network results based on the MJ network. Sample distribution revealed that both species were found on the Antarctic continental shelf and around Antarctic islands, with *O. hexactis* samples much more commonly collected around Antarctic islands than on the Antarctic shelf (Fig 2.2a, b).

On the *O. victoriae* side of the haplotype network, haplotypes from different sampled locations were dispersed throughout, thus forming a diffused network (Fig 2.2c). The network also shows some, but not complete, separation of continental shelf and Antarctic island haplotypes (Fig 2.2b). However, in many cases haplotypes were shared among *O. victoriae* sampled on the continental shelf and Antarctic islands (Fig 2.2b, c). Structured populations of *O. victoriae* were also observed around Bouvet Island, Amundsen Sea, and within the Scotia Arc.

For *O. hexactis*, the differentiation between sampled locations reflected structured populations within species. Close affinities were observed between Heard Island and South Georgia haplotypes via one or few mutational steps, with South Georgia haplotypes also linked to haplotypes in Shag Rocks, Bransfield Strait, and Antarctic Peninsula via a one or few mutational steps on the haplotype network (Fig 2.2c). Importantly, one *O. victoriae*

individual from Heard Island off East Antarctica possessed the same haplotype as nine *O. hexactis* individuals collected within the same area (Fig 2.2c). The haplotypes of three *O. victoriae* individuals sampled from the Scotia Arc (two from South Georgia and one from Bransfield Strait) were also found to be nested within the *O. hexactis* haplotype network (Fig 2.2c).

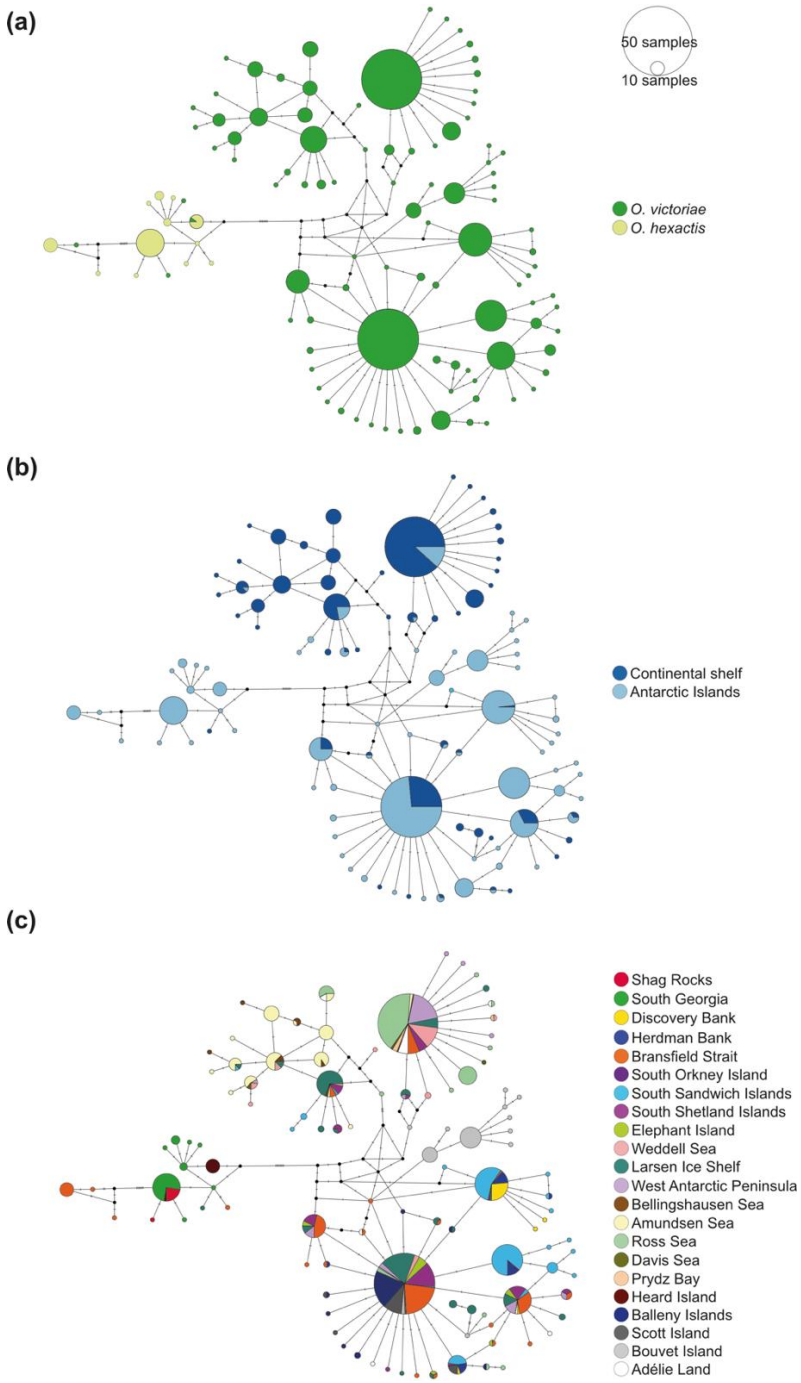

Fig 2.2 Median joining haplotype network of *Ophionotus victoriae* and *O. hexactis* COI sequences (434 bp, n = 935), separated by (a) species, (b) Antarctic continental shelf and Antarctic islands within the Antarctic Polar Front, and (c) location. Size and colour of circle represent the number of samples and sample locations associated with each haplotype. Black circle = inferred haplotype missing in the dataset. Hatch line = inferred mutation step between haplotype.

2.4.2 Population genetic metrics

Genetic diversity differed between species and sampling locations. Overall, the nucleotide diversity was similarly high in *O. victoriae* and *O. hexactis* (π = 0.01801 and 0.01276, respectively), but higher haplotype diversity was detected in *O. victoriae* compared to *O. hexactis* (Hd = 0.887 and 0.715, respectively) (Table 2.1). A higher proportion of private haplotypes was also detected within *O. victoriae* (62%) compared to *O. hexactis* (54%). For *O. victoriae*, similar levels of nucleotide and haplotype diversity were found between samples on the continental shelf and Antarctic islands. However, the proportion of private haplotypes was generally higher around Antarctic islands (72% of all haplotypes found in waters around Antarctic islands) compared to continental shelf (51% of all haplotypes found on the shelf) (Table 2.1).

Within *O. victoriae*, the lowest genetic variation was detected around Scott Island and Balleny Islands ($\pi < 0.00229$ and Hd < 0.44) (Table 2.1). Conversely, high genetic variation in *O. victoriae* was found in most areas on the continental shelf including Bellingshausen Sea, West Antarctic Peninsula, Larsen Ice Shelf, Weddell Sea, Davis Sea, and Adélie Land ($\pi > 0.01$ and Hd > 0.7) (see Goodall-Copestake et al. (2012) for global average of COI genetic diversity). However, *O. victoriae* in Prydz Bay, Ross Sea, and Amundsen Sea exhibited a relatively low level of nucleotide diversity (π between 0.00154 and 0.0069). Interestingly, while Prydz Bay and Ross Sea samples were characterised with medium level of haplotype diversity (Hd = 0.6 and 0.478, respectively), Amundsen Sea samples had a high haplotype diversity of 0.903. This low nucleotide diversity coupled with high haplotype diversity detected in Amundsen Sea samples may result from limited spatial sampling effort within the region, as all samples were collected within and around Pine Island Bay. For *O. victoriae* collected on the Antarctic continental shelf, a high proportion of private haplotypes (> 50%) was found in the Bellingshausen Sea, Ross Sea, Adélie Land, Davis Sea, and Prydz Bay (53.3%) (Table 2.1). Among the Antarctic islands, a high proportion of private haplotypes was detected from multiple island localities, including Heard Island, the Balleny Islands, Scott Island, Discovery Bank, Herdman Bank, Elephant Island, the South Sandwich Islands, Bransfield Strait, and Bouvet Island.

Table 2.1 Population statistics of *Ophionotus victoriae* and *O. hexactis* based on COI data. Antarctic islands are referred to the islands south of the Antarctic Polar Front. Hd = Haplotype diversity, Hp = Number of private haplotypes, h = Number of haplotypes, p(Hp) = Proportion of private haplotypes, S = Number of polymorphic sites, π = nucleotide diversity, Π = Average number of nucleotide difference. *statistical significance at p < 0.05.

Species	Locality	n	Hd	Hp	h	p(Hp)	S	ππ	Π	Tajima's *D*	Fu's F_S	Mismatch distribution
O. victoriae	all	862	0.887	102	165	0.62	60	0.01801	5.44006	-0.64100	-23.83934*	unimodal
	Antarctic islands	445	0.857	74	103	0.72	50	0.00994	3.01191	-1.44457*	-22.42260*	unimodal
	South Georgia	2										
	Discovery Bank	20	0.589	7	8	0.88	10	0.00308	1.33684	-1.41266	-1.083	multimodal
	Herdman Bank	20	0.811	5	8	0.63	8	0.00589	2.26842	-0.02138	11.20541	unimodal
	Bransfield Strait	97	0.835	18	28	0.64	37	0.01106	4.31508	-1.06489	-1.07556	multimodal
	South Orkney Island	1										
	South Sandwich Islands	104	0.768	25	30	0.83	29	0.00780	3.01680	-1.23021	-4.71546	unimodal
	Shetland Islands	63	0.919	10	24	0.42	30	0.01577	6.29237	0.12392	-0.07908	unimodal
	Elephant Island	17	0.890	5	10	0.50	8	0.00552	2.39706	0.04589	-3.16436	unimodal
	Heard Island	1										
	Balleny Islands	48	0.441	9	11	0.82	19	0.00229	0.99366	-2.55063	-4.10089*	multimodal
	Scott Island	25	0.410	7	9	0.78	3	0.00144	0.44000	-0.86557	-0.5395	unimodal
	Bouvet Island	47	0.732	9	13	0.69	18	0.00559	2.42738	-1.28531	-3.75045	multimodal
	Antarctic continental shelf	417	0.838	36	71	0.51	54	0.01832	6.57682	-0.09963	-11.08477	multimodal
	Weddell Sea	38	0.853	5	13	0.38	25	0.01696	7.34424	0.7998	3.40484	multimodal
	Larsen Ice Shelf	106	0.915	9	27	0.33	33	0.02003	8.67260	1.14744	-0.72463	multimodal
	West Antarctic Peninsula	56	0.716	6	13	0.46	21	0.01314	5.70455	0.78143	0.83817	multimodal
	Bellingshausen Sea	9	0.944	5	7	0.71	17	0.01140	4.83333	-1.10641	-1.31053	multimodal
	Amundsen Sea	67	0.903	9	18	0.50	24	0.00690	2.99367	-1.26273	-5.7985	multimodal
	Ross Sea	114	0.478	11	15	0.73	30	0.00638	2.30255	-1.01988	0.96876	multimodal
	Adélie Land	17	0.787	7	9	0.78	27	0.01792	7.77941	-0.1049	0.73887	multimodal
	Davis Sea	4	0.833	2	3	0.67	15	0.01728	7.50000	-0.84729	2.14949	multimodal
	Prydz Bay	6	0.600	2	3	0.67	2	0.00154	0.66667	-1.13197	-0.85842	multimodal
O. hexactis	all	73	0.715	7	13	0.54	27	0.01276	5.49500	-0.0248	1.41432	multimodal
	Antarctic islands	72	0.707	6	12	0.50	26	0.01271	5.51598	0.09727	2.02924	multimodal
	South Georgia	40	0.535	3	7	0.43	6	0.00269	1.16923	-0.45659	-1.74652	multimodal
	Shag Rocks	10	0.200	1	2	0.50	1	0.00046	0.20000	-1.11173	-0.33931	multimodal
	Bransfield Strait	12	0.295	2	3	0.67	20	0.00798	3.46154	-1.98015*	4.30689	multimodal
	Heard Island	10	0.200	1	2	0.50	3	0.00138	0.60000	-1.56222	1.22453	multimodal
	Antarctic continental shelf											
	Larsen Ice Shelf	1										

Within *O. hexactis*, the nucleotide diversity per locality was lowest around Shag Rocks (π = 0.00046) and highest on Heard Island (π = 0.00138) (Table 2.1). However, *O. hexactis* samples from Shag Rocks and Heard Island exhibited the same level of haplotypic diversity (Hd = 0.2). Although no private haplotypes were detected around Heard Island in *O. hexactis*, areas within the Scotia Arc (South Georgia, Shag Rocks, and Bransfield Strait) showed a relatively high proportion of private haplotypes (> 50%) (Table 2.1).

2.4.3 Past species demography

Overall, evidence for a past population bottleneck and subsequent expansion was inferred in *O. victoriae* from all sample locations, as seen from a significantly negative Fu's F_S value (-23.84, $p = 0.007$) and a unimodal mismatch distribution (Table 2.1). A BSP suggested a past population expansion was detected in *O. victoriae* on the shelf at around 20,000 years ago (Fig 2.3), coinciding with the timing of LGM. However, within each sample locality, signatures of past population bottlenecks and expansions appeared to be ambiguous as non-significant negative neutrality values and/or multimodal mismatch distribution were detected (Table 2.1).

In *O. hexactis*, the hypothesis of past population bottleneck and expansion was rejected due to non-significant negative neutrality tests and multimodal mismatch distribution (Table 2.1). A BSP also indicated an overall stable population size over time in *O. hexactis* (Fig 2.3).

2.4.4 Genetic differentiation within and between species

When analysing genetic structure through molecular variance, AMOVA via pairwise F_{ST} revealed a significant differentiation between species (p = .003) (Supplementary Table 2.2). However, differentiation among sample locations (within species) represented only 22.64% of the overall genetic variation (AMOVA, df = 23, sum^2 = 108.136, variance components = 0.121), and differentiation within sample locations for each species amounted to 61.48% of the overall variation (AMOVA, df = 910, sum^2 = 297.784, variance components = 0.327) (Supplementary Table 2.2). Pairwise F_{ST} showed a high and significant level of genetic differentiation between *O. victoriae* and *O. hexactis* (F_{ST} = 0.203, p < .0001) (Supplementary Table 2.3). Within *O. victoriae*, pairwise F_{ST} showed low levels of differentiation between locations that are geographically proximal, including Elephant Island, Bransfield Strait, Shetland Islands of the Scotia Arc, and Balleny Islands and Scott Island

(Supplementary Fig 2.4). Affinities between distant locations were also observed in *O. victoriae*, including West Antarctic Peninsula, Weddell Sea, Ross Sea, Adélie Land, and Prydz Bay, and also between Elephant Island, Shetland Islands, Balleny Islands, and Scott Island (Supplementary Fig 2.4). Within *O. hexactis*, pairwise F_{ST} indicated no significant differentiation between Shag Rocks and South Georgia, and Shag Rocks and Heard Island (Supplementary Fig 2.4).

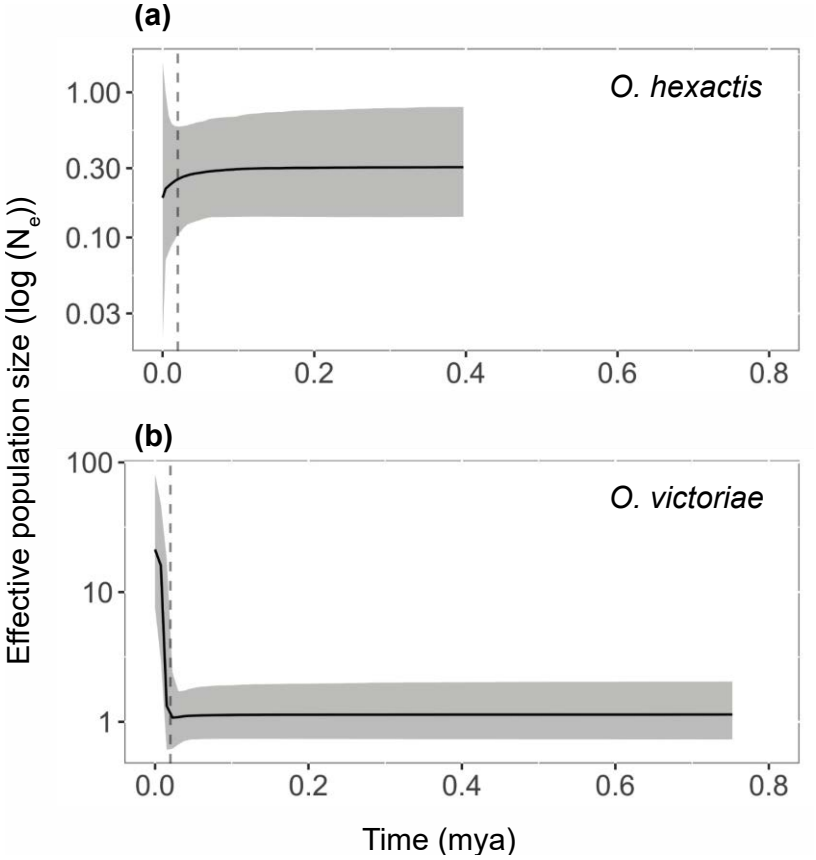

Fig 2.3 Bayesian skyline plots (BSP; $\log_{10}$ scale) of past effective population size of *Ophionotus victoriae* (a) and *O. hexactis* (b) based on COI sequences. Dashed line represents the time of the Last Glacial Maximum (~20,000 years ago).

2.4.5 Spatial pattern detection within *O.* victoriae

Spatial pattern detection analysis (*MEMGENE*) revealed that variation within *O. victoriae* was discernible when comparing genetic distance between individual COI sequences. *MEMGENE* analysis suggested 46.0% of overall genetic variation can be explained by spatial scale (adjR^2 = 0.460). *MEMGENE1*, the variable that represented the strongest spatial pattern detected by *MEMGENE* (57.2% of the adjR^2), showed clear genetic divergence between continental shelf and most island localities (Scotia Arc + Bouvet Island + Balleny Islands + Scott Island) (Fig 2.4a). However, the genetic structure of the

continental shelf and Antarctic islands does not appear to be independent of each other as *MEMGENE1* also detected genetic similarity among island localities and Prydz Bay (Fig 2.4a). Samples from Heard Island also showed genetic similarity with continental shelf samples (Fig 2.4a). *MEMGENE2*, the variable that explained the second strongest spatial pattern (31.8% of the adjR^2), further indicated relatedness between the continental shelf and Antarctic islands (Fig 2.4b). In particular, a strong regional structure was observed between Amundsen Sea, West Antarctic Peninsula, Scotia Arc, and Bouvet Island (Fig 2.4b). MEMGENE3, the variable that explained most of the remaining spatial structure in the dataset (4.78% of the adjR^2), demonstrated clear spatial structure connecting Scotia Arc, Heard Island, and Prydz Bay (Fig 2.4c).

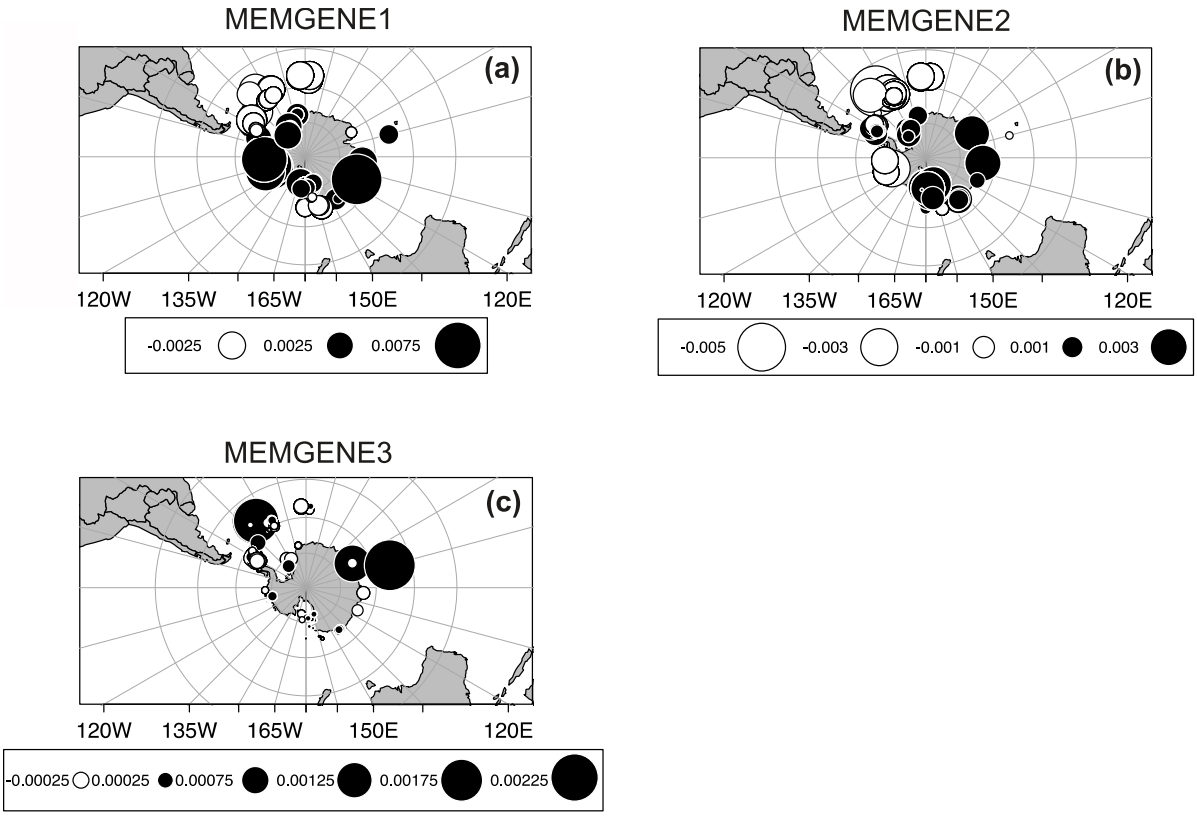

Fig 2.4 Visualisation of spatial genetic patterns among *Ophionotus victoriae* samples based on the first three *MEMGENE* variables (*mgQuick*). Values alongside circles in the legend indicates *MEMGENE* score values. Circles of similar size and the same colour represent individual sequence with similar scores on the *MEMGENE* axis (i.e. genetic similarities attributed to isolation-by-distance between samples). Overall, 46.0% of genetic variation can be explained by spatial scale (adjR^2 = 0.460). (a) *MEMGENE1* shows a strong spatial pattern of two genetic clusters distinct to the continental shelf and Antarctic islands near the Antarctic Polar Front which contributes 57.2% of the adjR^2. (b) *MEMGEN2* shows the second strongest spatial pattern of connectivity between Amundsen Sea, West Antarctic Peninsula, Scotia Arc and Bouvet Island which contributes 31.8% of the adjR^2. (c) *MEMGENE3* shows the third strongest spatial pattern demonstrating structure connecting Scotia Arc, Heard Island and Prydz Bay, which contributes 4.78% of the adjR^2.

2.4.6 Isolation-by-environment between species

Isolation-by-environment analysis (via analysing resistance surfaces) indicated that isolation-by-geographical distance (Euclidean distances), ocean surface and seafloor temperature, surface and seafloor salinity, surface current velocity, and bathymetry were all significant in explaining spatial genetic variation between *O. victoriae* and *O. hexactis* ($p < 0.001$; Table 2.2). Euclidean distances appeared to be the best spatial predictor in explaining the observed genetic variations ([a] adjR^2 = 0.426), followed by bathymetry ([a] adjR^2 = 0.390), surface temperature ([a] adjR^2 = 0.373), surface salinity ([a] adjR^2 = 0.271), surface current speed ([a] adjR^2 = 0.265), seafloor salinity ([a] adjR^2 = 0.264), and seafloor temperature ([a] adjR^2 = 0.237) (Table 2.2).

Table 2.2 Results of isolation-by-environment (*mgLandscape*) analysis comparing the proportion of spatial genetic variation between *Ophionotus victoriae* and *O. hexactis* (adjR^2) explained and not explained by environmental parameters of present-day conditions. Environmental parameters considered including isolation-by-distance (IBD), surface and seafloor temperature, surface and seafloor salinity, surface current speed and water depth. Numbers in table represent the adjR^2 explained by [abc] spatial predictors (MEM eigenvectors), [a] spatial patterns in given model, [c] coordinates, [b] confounded pattern between given model and coordinates. [d] residuals not explained by spatial predictors. P[abc], P[a], P[c] represent the significance value calculated for each proportion with significance level at p = 0.05.

Model	[abc]	P[abc]	[a]	P[a]	[c]	P[c]	[b]	[d]
IBD	0.518	0.001	0.426	0.001	0.520	0.001	0.403	0.482
Water depth (m)	0.483	0.001	0.390	0.001	0.512	0.001	0.411	0.517
Surface temperature (°C)	0.465	0.001	0.373	0.001	0.510	0.001	0.414	0.535
Surface salinity	0.364	0.001	0.271	0.001	0.198	0.001	0.725	0.636
Seafloor salinity	0.357	0.001	0.264	0.001	0.227	0.001	0.696	0.643
Surface current speed (m s^{-1})	0.357	0.001	0.265	0.001	0.211	0.001	0.712	0.643
Seafloor temperature (°C)	0.329	0.001	0.237	0.001	0.179	0.001	0.744	0.671

2.5 Discussion

2.5.1 *Ophionotus victoriae* as a single entity based on COI data

Rather than comprising multiple cryptic species as proposed by previous studies (Hunter & Halanych, 2010; Galaska et al., 2017b), the haplotype network of *O. victoriae* is frequently connected, suggesting this species is one entity with a circumpolar distribution in the Southern Ocean. In the previously published studies utilising Southern Ocean COI

datasets, *O. victoriae* had been collected from relatively few locations in West Antarctica (Hunter & Halanych, 2010; Galaska et al., 2017b). Additionally, the existing genomic dataset (2b-RAD) of *O. victoriae* is comprised of samples from an even more restricted distribution, with individuals collected from more disjunct locations (Galaska et al., 2017b). In this study, we have utilised an expanded analysis with an updated sampling coverage representing individuals collected along a geographical, circumpolar cline rather than from disjunct locations. After incorporating the additional *O. victoriae* samples (*n* = 443) to the published COI sequences in the haplotype network, *O. victoriae* is characterised by a single connected network rather than multiple clusters (as found in Galaska et al. (2017b)). Therefore, the new samples included in this study represent the missing links that connect divergent lineages described in previous studies. The previous interpretation of multiple cryptic species was likely caused by the limited spatial sampling of a genetically diverse and widely distributed species, where "individual clusters" likely represented artefacts driven by isolation-by-distance.

2.5.2 Genetic relationship between *O. victoriae* and *O. hexactis*

Although current taxonomy and previous studies (Hugall et al., 2016; Galaska et al., 2017b) recognise *O. victoriae* and *O. hexactis* are separate species, our analyses, including the haplotype network and phylogenetic trees (ML and BI), show the two taxa to be highly separated, but not perfectly reciprocally monophyletic groups. In the current dataset, the distributions of *O. victoriae* and *O. hexactis* overlap around Heard Island, as well as around Bransfield Strait and South Georgia in the Scotia Arc. We observed *O. victoriae* samples from these three areas within the *O. hexactis* clade (including all *O. victoriae* samples from Heard Island and South Georgia). Coincidentally, this dataset contains a very low sample size of *O. victoriae* from Heard Island (n = 1) and South Georgia (n = 2). However, a relatively higher sample size of *O. victoriae* from Bransfield Strait was included in this study (n = 97, including n = 67 from newly sequenced samples). Out of the 97 samples, only one sample fell within the *O. hexactis* clade (ID: SIO-BIC E5524E). Furthermore, eight other *O. victoriae* samples collected from the same trawl containing as SIO-BIC E5524E did not fall within the *O. hexactis* clade. *Ophionotus victoriae* seems to share an unusually close genetic relationship (in terms of COI data) with *O. hexactis* in locations where they overlap. However, from the sampled diversity of *O. victoriae* in Bransfield Strait, it appears that not all *O. victoriae* exhibit the similarly close genetic distance with *O. hexactis* under the same environmental opportunity.

Species-level paraphyly and haplotype affinities between *O. victoriae* and *O. hexactis* could

represent either incomplete lineage sorting or hybridisation following secondary contact (McKay & Zink, 2010). There are parallel explanations on this. First, only one haplotype shared between *O. victoriae and O*. *hexactis* was detected in this study, collected from around Heard Island. Heard Island is a remote island on the Kerguelen Plateau and is separated from the main Antarctic continental shelf and other Antarctic islands outside of the Plateau via the deep sea and a long geographical distance (Griffiths et al., 2008). It is possible that the unique environmental setting of Heard Island allowed the two species to hybridise, which enabled mitochondrial introgression to occur between species in that location, while geographical isolation prevented the shared haplotypes from spreading to other localities. Secondly, there are *O*. *victoriae* individuals possessing haplotypes within the *O*. *hexactis* clade that are not shared by the two species. This could reflect either incomplete lineage sorting, or signatures of hybridisation and introgression in the past followed by mutation.

While *O*. *victoriae* and *O*. *hexactis* exhibit contrasting reproductive strategies (broadcast spawning and brooding, respectively), previous studies have suggested sperm chemotaxis (sperm recognition of eggs) appears to be species-specific in most, but not all, brittle stars (Miller, 1998; Weber et al., 2017). Therefore, as well as the overlapping distribution of *O*. *victoriae* and *O*. *hexactis*, physiological opportunities enabling intraspecific hybridisation may also exist. Strong incomplete lineage sorting and past hybridisation have also been detected among six cryptic brittle star species *Ophioderma* spp. with brooding or broadcast spawning strategies (Weber et al., 2017). As we only utilised a single mitochondrial marker (COI) which is maternally inherited, our data could be influenced by selection, as well as bias toward the history of mitochondrial lineages that may be incongruent with species history, and the history of maternal lineages in the event of sex-biased dispersal (Sloan et al., 2017). Overall, we highlight an interesting additional case of possible incomplete lineage sorting or hybridisation between two sister taxa with contrasting morphology and life history for future multi-locus studies.

2.5.3 Contrasting signals of Southern Ocean refugia between species

Evidence of deep-sea refugia in *O*. *victoriae* is demonstrated through the overall absence of population bottleneck signatures (summary statistics), combined with signs of population expansion at the LGM (based on BSP). Results of BSP can be confounded by the effect of population structure (Heller et al., 2013); therefore, results should be interpreted with caution. However, the overall high haplotypic diversity and the “diffused” pattern in the haplotype network also suggest *O*. *victoriae* continued to diversify during glacial periods (Allcock &

Strugnell, 2012). These patterns of past population size change and population connectivity point toward the key characteristics associated with deep-sea refugia survival (Lau et al. 2020; *Chapter 1*). The deep sea was hypothesised as the only large scale, ice-free habitable area that could support a large population size and continued diversification during glacial periods; in comparison, the Antarctic continental shelf was largely covered in grounded ice (Thatje et al., 2005). While evidence of LGM grounded ice was observed around some Antarctic islands (Elephant Island, Bouvet Island, Heard Island), areas free of grounded ice were also observed around South Georgia and South Sandwich Islands during the LGM (Graham et al., 2008; Hodgson et al., 2014; Barnes et al., 2016). However, the habitable areas around Antarctic Islands are small and restricted relative to the deep sea, especially for steep, volcanic islands. Therefore, islands are unlikely to have supported the continued diversification throughout glacial periods. The eurybathic distribution of *O. victoriae* (34 – 1,750 m; the sampled depth range of this study) further supports its capability to migrate to deep-sea refugia and then subsequently recolonise the shelf after the LGM. Association between eurybathic distributions and deep-sea refugia was also suggested in the Southern Ocean shrimp *Nematocarcinus lanceopes* (Raupach et al., 2010) and the sea spider *Nymphon australe* (Soler-Membrives et al., 2017).

Evidence of Antarctic island refugia for *O. hexactis* is demonstrated through a stable population structure throughout glacial maxima, as seen from the lack of strong population bottlenecks and the absence of population expansion (summary statistics and BSP). The structured populations between distant locations (e.g., Heard Island and the Scotia Arc) reflected in the haplotype network are also suggestive of *in situ* survival within these locations. The known depth and range distribution of *O. hexactis*, which is restricted to the shallow Southern Ocean mainly around Antarctic islands (0–459 m (GBIF.org, 2019)), also support the case of *in situ* survival within island refugia. Given that connectivity between the Scotia Arc and Heard Island are detected on the haplotype network (i.e., haplotypes from both locations separated by one mutation step), this long-distance connectivity is probably facilitated by rafting, as suggested in other Southern Ocean benthic fauna also with brooding characteristic (Helmuth et al., 1994; Leese et al., 2010; Nikula et al., 2010) and the Antarctic terrestrial springtail (Hawes et al., 2008).

Isolation-by-environment analysis also indicated the spatial genetic patterns between *O. victoriae* and *O. hexactis* were most associated with geographic distance and water depth, suggesting isolation-by-geographical distance and -depth. Isolation-by-distance and -depth are expected when populations have been stable over time, with gene flow occurring more often between spatially neighbouring populations, as well as selective

ecological forces and reproductive barrier between diverging populations (Wright, 1943). Since the depth range of *O. victoriae* extends into the deep sea while *O. hexactis* is only known from relatively shallow waters, the isolation-by-depth pattern might reflect a stepwise recolonisation pattern in *O. victoriae* from deep-sea refugia to the continental shelf along the seafloor bathymetry after the LGM. Given that there is also a distributional difference between *O. victoriae* and *O. hexactis*, whereby *O. victoriae* inhabits the deep sea, Antarctic continental shelf and Antarctic islands, and *O. hexactis* is mainly observed around Antarctic islands, the strong isolation-by-distance pattern detected likely reflects genetic differentiation between the two species.

2.5.4 Evolutionary implications of different refugial use in the Southern Ocean

In the Southern Ocean, glacial cycles have been hypothesised to drive allopatric speciation due to populations being contained within isolated refugia on the continental shelf (i.e., the Antarctic biodiversity pump hypothesis) (Clarke & Crame, 1989, 1992; Crame, 1997). In the case of *Ophionotus* spp., the evidence suggests that *O. victoriae* and *O. hexactis* have taken refuge within independent, largely non-overlapping environments (the deep sea and islands, respectively). Interestingly, a recent study also presented a seemingly similar case to *Ophionotus*, in which a brooding clade (clade V) was reported in the Antarctic brittle star *Astrotoma agassizii* species complex around South Georgia, with a broadcast spawning sister clade (clade I) distributed on both the Antarctic continental shelf and around South Georgia (Jossart et al., 2019). Both sympatric cryptic species are also characterised by a clear size dimorphism (larger and smaller body size in clade I and V, respectively) (Jossart et al., 2019). These clades with contrasting life-history strategies were also previously reported in Galaska et al. (2017a) but were not known then to be sympatric. Although the evolutionary history of the Southern Ocean *A. agassizii* complex was not examined by Jossart et al. (2019), the reported significantly negative values obtained from neutrality tests (Tajima's *D* and Fu's F_S) indicate both clades exhibited signatures of strong population bottlenecks, suggesting *in situ* persistence throughout glacial cycles. The star-like haplotype networks of clade I and V of *A. agassizii* also support a likely scenario of *in situ* refugia in these areas (discussed within Allcock and Strugnell (2012)). The current data suggest South Georgia served as a sub-Antarctic glacial refugia for both *A. agassizii* (clade I and V) and *O. hexactis*. For the Southern Ocean ophiuroids that are currently living on the continental shelf, *O. victoriae* historically found refuge in the deep sea while *A. agassizii* (clade I) likely persisted on the shelf over glacial periods, highlighting that refugium survival can be different between brittle stars with the same reproductive strategy (broadcast spawning).

Both the cases of the Southern Ocean *Ophionotus* spp. and *A. agassizii* (Clades I and V) show different morphologic traits are observed between closely related species, including size dimorphism between the two clades in *A. agassizii*, and different arm numbers in *O. victoriae* and *O. hexactis*. For the case of *A. agassizii*, the two closely related species cannot coexist in sympatry without evolving character displacement (competitive exclusion principle) (Hardin, 1960). However, survival in independent glacial refugia (deep-sea and Antarctic islands) is also associated with character changes between *O. victoriae* and *O. hexactis*. Our data highlight that species histories can vary among Southern Ocean taxa, even within the same class (i.e., the case of ophiuroids presented here). Another interesting aspect common in both cases is that brooding as a reproductive trait is mostly exclusive to Antarctic islands, indicating brooding could be positively selected around the islands.

2.5.5 Connectivity and isolation between the continental shelf and Antarctic islands

Spatial pattern detection analysis (*mgQuick*) and the haplotype network within *O. victoriae* support signatures of both isolation and connectivity, within and between, the Antarctic continental shelf and Antarctic islands that could also be linked to physical transports in the Southern Ocean. First, the strong spatial genetic structures detected by *MEMGENE1* that separate the continental shelf and some Antarctic islands (Scotia Arc, Bouvet Island, Balleny Islands, Scott Islands) coincide with the southern frontal structure of the ACC (southern boundary ACC and southern ACC) in the Southern Ocean (Sokolov & Rintoul, 2009). However, as detected by *MEMGENE1*, *2*, and *3* within *O. victoriae*, patterns connecting continental shelf localities (Prydz Bay and Amundsen Sea) and Antarctic islands were also observed, indicating a permeable barrier between the two environments.

Within *O. victoriae*, similarity was detected between the Scotia Arc, Bouvet Island, and Prydz Bay in *MEMGENE1*, and between the Scotia Arc, Heard Island, and Prydz Bay in *MEMGENE3*. Connectivity between the Scotia Arc and Bouvet Island has been observed in the notothenioid *Lepidonotothen larseni* (Damerau et al., 2014). Also, a Scotia Arc - Prydz Bay connection pathway has also been previously described in other Southern Ocean taxa including the asteroid *Glabraster antarctica* (Moore et al., 2018), the octopod *Pareledone turqueti* (Strugnell et al., 2012), the amphipod *Eusirus giganteus* (Baird et al., 2011), and the crinoid *Promachocrinus* phylogroup C and F (Hemery et al., 2012), highlighting a probable seascape corridor that enables gene flow between Antarctic islands and continental shelf in some Southern Ocean benthic taxa. Given that the Scotia Arc, Bouvet Island, Prydz Bay, and Heard Island are separated by a long geographical distance, there are likely unsampled

regions between these areas that contribute to this proposed long-distance connectivity. The regional spatial genetic structure detected by *MEMGENE2*, found between the Amundsen Sea, Antarctic Peninsula, Scotia Arc, and Bouvet Island, also likely reflects the influence of local oceanographic dynamics into and beyond the Scotia Arc including the eastward flowing ACC (Maldonado et al., 2003).

2.5.6 Life history and morphological innovation in *O. hexactis* during glacial periods

In echinoderms, brooding has often emerged under environmental stressful conditions during species selection over macroevolutionary timeframes (Lawrence & Herrera, 2000), even though this strategy requires higher maternal investment compared with pelagic larval development (Fernández et al., 2000). Previous studies have also suggested that, after a shift to hyper-oligotrophy in the Eastern Mediterranean region, the brittle star *Ophioderma zibrowii* with a brooding characteristic emerged from a broadcast spawning lineage (Boissin et al., 2011; Weber et al., 2019; Stöhr et al., 2020), suggesting brooding character can emerge due to historical environmental changes. Furthermore, in the Southern Ocean, brooding as a characteristic has also been hypothesised as a result of selection from non-present-day environmental conditions, rather than an adaptation to generic polar conditions (Pearse et al., 2009). However, an increase in arm number in echinoderms has yet to be linked to changes in past environmental conditions. Nonetheless, laboratories experiments have reported exposure to high salinity and low pH can result in arm number changes in the asteroid *Echinaster* sp. and in the ophiuroid *Ophiothrix fragilis*, respectively, under experimental conditions (Watts et al., 1983; Dupont et al., 2008). Furthermore, an increase in arm number (more than 5 arms) in ophiuroids is positively correlated to coordinated locomotion (Clark et al., 2019) and can be linked to increasingly random escape patterns (thus non-predictable escape strategies) (Wakita et al., 2020). Therefore, the six-arm innovation in *O. hexactis* could be related to selective forces linked to changes in environmental conditions (such as salinity or pH) or ecological settings that would require increased coordination. We suggest that the morphological and life-history differences observed between *O. victoriae* and *O. hexactis* could be linked to strong environmental stressors in the past.

While the modern Southern Ocean seafloor is characterised by marked gradients of low temperature (-2.1 to 2.8°C) and salinity (34.2 - 34.7 practical salinity unit (psu)), the surface of the Southern Ocean is comprised of a series of sharp temperature (< 1.5 - 4°C) and salinity (33.6 - 34.4) fronts that divide the subtropical (warmer water, saline in the North) and polar fronts (colder, fresher water in the South) (Locarnini et al., 2018; Zweng et al., 2018).

Isolation-by-environment analysis indicated the spatial genetic pattern between *O. victoriae* and *O. hexactis* showed stronger associations with sea surface temperature + salinity gradients, compared to associations with seafloor temperature + salinity gradients, despite the two species being benthic species. *Ophionotus victoriae* and *O. hexactis* have been suggested to have diverged at 1.64 million years ago (mya; 0.53 - 5.79 mya) during the Pleistocene, based on exon phylogenetic data (O'Hara et al., 2019). Therefore, it is unlikely that the morphological innovation in *O. hexactis* was influenced by modern temperature and salinity patterns. Instead, the results likely reflect the divergence between *O. victoriae* and *O. hexactis* is linked to strong environmental gradients separating the two species in the past. For example, the prolonged glacial-interglacial cycles, or fluctuation in salinity and overall lower salinity throughout the late Pleistocene, or other environmental changes linked to intensified glacial-interglacial cycles, were likely the key environmental drivers linked to evolutionary innovations in *O. hexactis*. Notably, in the past 1.5 million years, the glacial-interglacial cycles transitioned from 41 kyr cycles with low amplitude to 100 kyr cycles with intensification in climatic cycles after the mid-Pleistocene transition (Clark et al., 2006). Since *O. hexactis* persisted in Antarctic island refugia in the shallow Southern Ocean, which would have been directly exposed to the prolonged, as well as intensified elements of glaciations and interglacial periods. Additionally, the rapid deglaciation at the beginning of each interglacial cycle should lead to a rapid and steep decline in salinity in the surface Southern Ocean. *Ophionotus hexactis* around Antarctic islands would have been directly and repeatedly exposed to deglacial meltwater after each glacial maximum. It has also been recently suggested that the surface Southern Ocean consisted of a lower level of salinity during glacial maxima (~33.4 psu relative to ~34.56 psu in the deep sea) (Hasenfratz et al., 2019). Therefore, it is also plausible that the rapid and steep decline in salinity during intensified interglacial cycles could have driven the character changes in *O. hexactis*, and the overall lower salinity during glacial cycles also maintained such innovations.

Alternatively, an increase in arm number and brooding strategy may not be directly linked to the proposed selective forces during the Pleistocene. The increase in arm number could be linked to ecosystem dynamics around Antarctic islands leading to enhanced coordination or could have simply arisen as a by-product of vicariance. The advantageous nature of brooding during glacial periods, when the Southern Ocean experienced limited habitat availability and low primary productivity, is more widely accepted (Poulin et al., 2002; Thatje et al., 2005; Convey et al., 2009; Pearse et al., 2009). Nonetheless, the establishment of the morphological difference between *O. victoriae* and *O. hexactis* could have occurred prior, during, or after lineage splitting. The two characteristic morphological changes

in *O*. *hexactis* might also not have happened simultaneously, as arm number and reproductive mode are functionally different. Each innovation leading to ecological success would have been driven by different ecological opportunities, and possibly occurred on independent occasions.

2.6 Conclusion

This study suggests that *O*. *victoriae* is a single species and is closely related to *O. hexactis* based on COI data. Although there could be incomplete lineage sorting, or hybridisation between *O. victoriae* and *O*. *hexactis*, the contrasting morphology and life-history traits support the current taxonomic recognition of two species. The broader implications of this study demonstrate how glacial cycles and oceanic currents have structured genetic patterns in Southern Ocean benthic taxa. While *O. victoriae* and *O. hexactis* appear to have found refuge in different environments during glacial periods (the deep sea and Antarctic islands, respectively), we highlight that Southern Ocean species with similar life histories can survive in different types of glacial refugia (e.g., the parallel case of *A*. *agassizii* (clade I) and *O. victoriae*).

Our data also demonstrate distinct genetic clusters between the Antarctic continental shelf and Antarctic islands near the Antarctic Polar Front, coinciding with the frontal boundary of the ACC in the Southern Ocean. However, genetic connectivity between the Scotia Arc and Prydz Bay was also detected, suggesting connectivity between the Antarctic islands and the Antarctic continental shelf is ongoing. Genetic structure observed between the Scotia Arc and neighbouring regions (Bellingshausen Sea, Antarctic Peninsula, Weddell Sea, and Bouvet Island) also highlights the role of the ACC and Weddell gyre in structuring regional genetic patterns.

Finally, our work also discussed that the morphological and life-history innovation in *O. hexactis* (an increase in arm number and brooding as reproductive strategy) can be linked to selection from environmental conditions in the past, which was first proposed by Pearse et al. (2009). Further work examining genetic structure in *O. victoriae* and *O. hexactis* using nuclear data should provide a thorough understanding of the genetic relationship between the two species, and signatures of past environmental selection.

CHAPTER 3

Target capture sequencing is better than ddRADseq for population studies

Lau, S.C.Y., Watts, P.C., Cooke, I.R., Wilson, N.G., Allcock, A.L., Silva, C.N.S., Jernfors, T., Strugnell, J.M.

This chapter is formatted for *Molecular Ecology Resources*.

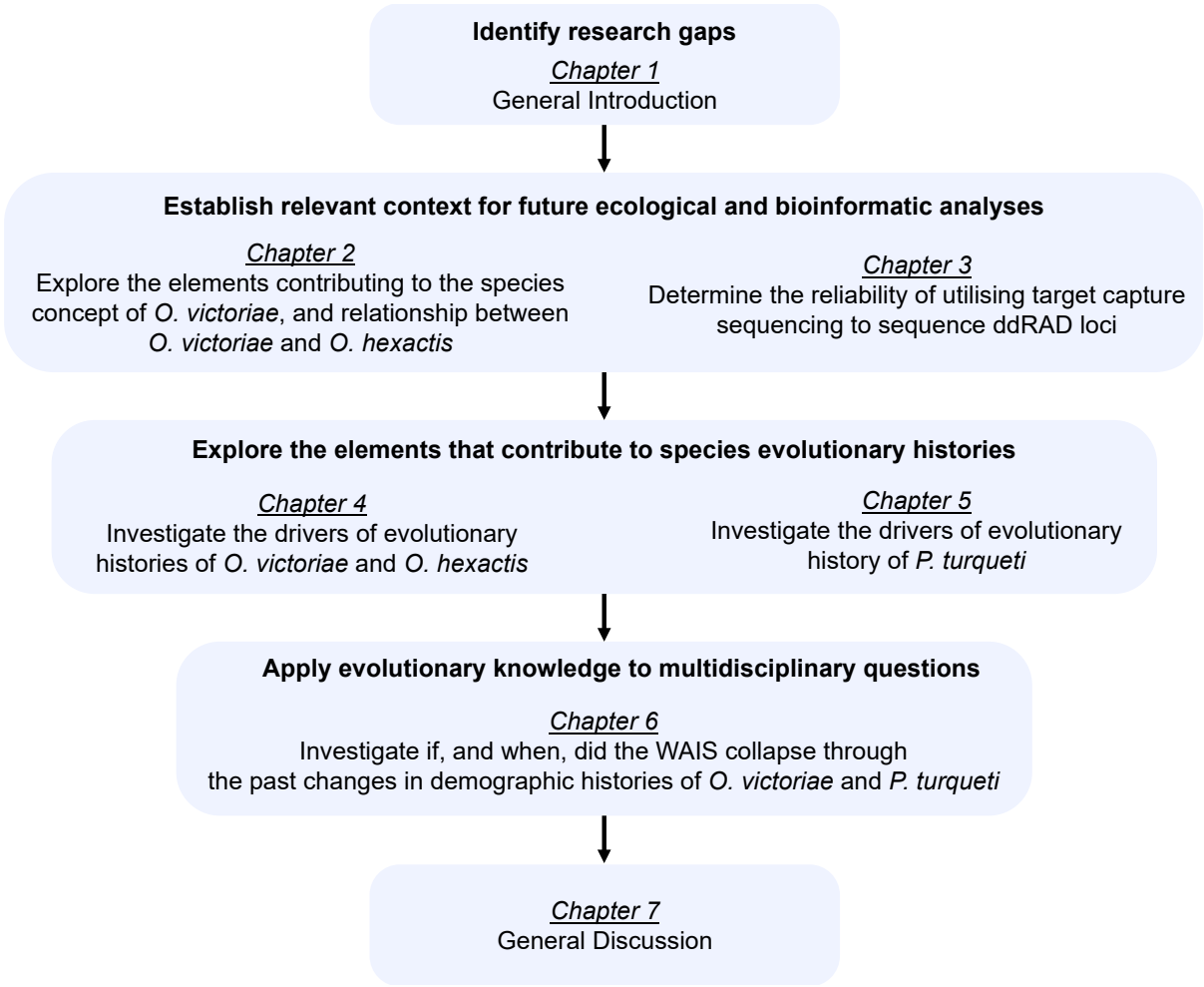

3.1 Abstract

Many non-model species have been sequenced at genome-wide scales via reduced-representation approaches such as restriction site-association sequencing (RADseq). However, existing datasets are limited to modern samples as RADseq requires high quality DNA. Target capture sequencing is known to be effective in retrieving RAD loci in degraded samples such as historical or rare specimens. By combining new target capture datasets into existing RADseq datasets, broad questions related to temporal and spatial genetic variations can be better explored. Here, we sequenced the circum-Antarctic Southern Ocean octopus *Pareledone turqueti* via double-digest RADseq (ddRADseq) and then carried out subsequent target capture sequencing of corresponding ddRAD loci. We found a clear batch effect between ddRADseq and target capture data even when analyses were restricted to genomic positions sequenced by both methods. We used bioinformatic pipelines encompassing both hard genotype calling (*mpileup*) and genotype likelihood estimation (*ANGSD*) approaches to address and rule out reasons that could explain the differences between sequencing methods. We showed that the observed differences were not related to DNA degradation, geographical or temporal genetic structure, variations in missing data, filtering thresholds or presence of paralogous sequences. However, we detected an apparent bias towards homozygous genotypes in ddRADseq data linked to allele dropout that could not be resolved through the use of genotype likelihood-based analyses. Additionally, ddRADseq data were characterised by low read depth, which could have reduced the ability in detecting heterozygotes. Finally, we do not recommend studies to directly combine reads derived from ddRADseq and target capture sequencing at this stage. It is becoming clear that different genotyping errors (e.g. allele drop out, low coverage) uniquely affect different proportions of loci, which may be detected and filtered by *ANGSD*. Future pipelines should focus on identifying loci affected by different types of genotyping errors, as well as establishing frameworks for filtering erroneous loci while maintaining data integrity.

Keywords: allele dropout, batch effect, ddRADseq, genotyping error, hybridisation capture, museum genomics, target enrichment

3.2 Introduction

Population genomic information can now be readily harnessed to answer questions of interest to ecology, evolution, conservation and fisheries and aquaculture, with many traditional “non-model” species having now been sequenced at a genomic scale (Feder & Mitchell-Olds, 2003; Ellegren, 2014; Bernatchez et al., 2017; Hohenlohe et al., 2021). While previous genomic data have been limited to high quality, fresh tissue samples, it is becoming increasingly feasible to obtain genomic sequence data from degraded and/or historical samples such as museum samples thanks to the advancement in sequencing technologies. By synthesising both historical and modern data, as well as including samples collected from rarely collected/remote regions, a wealth of information on ecological and evolutionary processes over temporal and/or spatial scales can be interrogated. Much existing genomic data have been publicly archived to maintain reproducibility (De-Kayne et al., 2021), thus offering opportunities for studies focusing on historical samples and/or degraded samples to sequence regions that have been captured before, in order to integrate new information with existing datasets. Consequently, questions that rely on low quality samples, such as those pertaining to temporal genetic variation, response to anthropogenic changes in the past century, local extinction, and genetic patterns in remote ecosystems (e.g. Antarctica, deep sea) (Bi et al., 2013; Taylor & Roterman, 2017; Lau et al., 2020; Layton et al., 2020) are beginning to be addressed in population genomic studies.

Among the existing population genomics studies, restriction site-association sequencing (RADseq) has been one of the most popular next generation sequencing methods in detecting genome-wide single-nucleotide polymorphisms (SNPs) in non-model species (Andrews et al., 2016). RADseq is a reduced representation sequencing technique that relies on restriction enzymes to target a fraction of the genome across many individuals or populations (Davey et al., 2011; Wang et al., 2012). This enables thousands, to hundreds of thousands, of SNP genotypes across samples to be compared on a genome-wide scale. The analyses of RAD loci do not require a reference genome, and assembly can be performed *de novo* (Catchen et al., 2011; Eaton, 2014; Sovic et al., 2015), which makes the method highly applicable to species without high quality reference genomes. RADseq typically relies on restriction enzymes but specific protocols can differ in enzyme digestion, adaptor ligation, barcoding or size selection steps (Puritz et al., 2014). The high versatility and resolution of the genotypic information derived from a RADseq-based approach can be applied to address a diversity of topics ranging from phylogenetics, population structure, pedigree reconstruction, association analyses, to genomic scans (Peterson et al., 2012).

Samples from historical collections or remote regions are typically un- or underrepresented in genomic analyses as they are characterised by short DNA fragments due to degradation in long-term storage and/or non-optimal DNA preservation media (Holmes et al., 2016). RAD-seq based approaches are practically ineffective for these samples as this approach relies on relatively long DNA fragments for adaptor ligations and/or are limited by fragment size selection (Puritz et al., 2014). As a result, RAD-seq based approaches are constrained to samples with high molecular weight DNA (i.e. fresh or well-preserved samples). However, recent advancement of target capture (or 'sequence capture', 'targeted enrichment', 'hybridisation capture', 'hybrid enrichment') sequencing approaches has been emphasised as an alternative approach to retrieve genomic loci in degraded samples. These methods are based on using single-stranded oligonucleotides (i.e. baits or probes) to enrich for targeted loci and thereby sequence genomic regions of interest across samples (see Grover et al. (2012) for a technical review). Bait sequences can be designed to target specific genomic positions including ultraconserved elements (UCE), exonic regions, and RAD loci based on prior knowledge (Jones & Good, 2016). More importantly, one set of bait sequences can be applicable to species across a taxonomic range (e.g. within genera or class) (Hugall et al., 2016; Souza et al., 2017; Bossert & Danforth, 2018), with high target success (between 55 and 77% of target regions) having been achieved between species with ~< 5% sequence divergence (Souza et al., 2017). Recent proof-of-concept studies have demonstrated the efficiency and reliability of target capture techniques in retrieving RAD loci from samples with degraded DNA (e.g. RADcap (Hoffberg et al., 2016), hyRAD (Suchan et al., 2016), RAPTURE (Ali et al., 2016), ddRAD target enriched sequencing (Souza et al., 2017)). Importantly, target capture sequencing of RAD loci circumvents errors that are associated with traditional RAD-seq based methods, including restriction fragment length bias and allele dropout at heterozygous restriction sites (discussed within Davey et al. (2013)). Target capture sequencing has proven to be successful in obtaining useful sequences in degraded samples for population genomic inferences that would otherwise be excluded in traditional RAD-seq based methods.

To date, studies that have incorporated target capture sequencing of RAD loci have found this technique effective in recovering the target loci, resulting in data that are equivalent to traditional RAD-seq based methods for the purpose of downstream population genomic analyses (e.g. Boucher et al. 2016; Linck et al. 2017; Schmid et al. 2018; Dorant et al. 2019). Combining and integrating reads containing the same genomic positions derived from target capture sequencing (e.g. degraded samples) and RADseq approaches (e.g. high quality/fresh samples, from existing sequence databases) within a single bioinformatic pipeline for expanded analyses have also been explored (Lang et al., 2020; O'Connell et al.,

2021). However, batch effects have been observed between RADseq and target capture sequencing data when analysed together (Lang et al., 2020; O'Connell et al., 2021), although the exact reasons driving this effect are unclear. The challenges of incorporating degraded samples relative to fresh samples have also been highlighted in the literature, including exogenous DNA contamination (Burrell et al., 2015), post-mortem DNA degradation (Linck et al., 2017) and/or missing data (Boucher et al., 2016). Biases linked to genetic variation between historical and modern samples could also exist, as the collection year difference could represent temporal genetic variation. This is especially likely in cases of rapid environmental change where historical samples could represent populations that have declined, become extinct or hybridised so that they would not be represented in a modern dataset (Boucher et al., 2016). These technical (e.g. contamination, DNA misincorporation from damage) and ecological factors (e.g. geographical bias, temporal genetic patterns) often intertwine and can be difficult to distinguish (Linck et al., 2017; Schmid et al., 2018), and could explain the batch effect observed between sequencing methods in Lang et al. (2020) and O'Connell et al. (2021). An alternative possibility, that is yet to be thoroughly examined, is that variability in sequencing technology and protocol bias, such as allele dropout specific to RAD-seq based approaches could be responsible for such batch effects.

Here, we developed a bait set that captures thousands of double-digest RAD (ddRAD) loci in the Southern Ocean octopus *Pareledone turqueti* based on information obtained from prior ddRAD sequencing (ddRADseq). We then performed target capture sequencing of ddRAD loci in degraded samples of Southern Ocean octopus *P. turqueti*, and integrated reads from target capture sequencing and previous ddRAD sequencing in two bioinformatic pipelines, involving genotype calling (*bcftools mpileup*) (Li, 2011) and genotype likelihood estimation methods (*ANGSD*) (Korneliussen et al., 2014). As a case study, our aim was to evaluate whether biases could be found between reads derived from target capture sequencing and ddRADseq. Upon discovery of these biases, a secondary aim was to determine whether the drivers of these biases could be identified.

3.3 Methods

3.3.1 Reference genome sequencing and assembly

A reference genome of *P. turqueti* was sequenced from two individuals collected from Elephant Island (ID: PT186) and the South Orkney Islands (ID: PT244) (Supplementary Table 3.1). Total genomic DNA of both of these samples (gDNA) was extracted using a

DNeasy Blood and Tissue Kit (Qiagen), following the manufacturer's protocol. Sample PT186 was sequenced on PacBio SequeI system (20 K insert library) with three cells which generated a total read volume of 28 Gigabase pair (Gbp). Both 200 base pair (bp) and 500 bp insert libraries were sequenced on an Illumina HiSeq X ten in 150 bp paired-end mode across one flow cell for the 200 bp library and two flow cells for the 500 bp. Genome size was estimated at between 3.7 Gb and 8.1 Gb based on the Illumina reads using Genomescope 2.0 (Ranallo-Benavidez et al., 2020). Genome assembly was performed with *Flye* v2.4.2 (Kolmogorov et al., 2019) using the long-reads from PT186 and then error corrected using reads from PT244 with *Pilon* (Walker et al., 2014). The final assembly had a total length of 5.1 Gb from 38,290 contigs with the largest contig of 146 Kb and N50 of 16.9 Kb.

3.3.2 ddRAD library preparation, sequencing and SNP calling

As part of a wider effort to perform ddRAD sequencing across different Southern Ocean octopus species, 418 Southern Ocean octopus specimens (*Adelieledone polymorpha*, *A. adelieana*, *Adelieledone* sp., *Pareledone turqueti*, *P. aequipapillae*, *P. prydzensis*, *P. cornuta*, *P. subtilis*, *Pareledone* sp., *Megaleledone setebos* and *Graneledone* sp.) (Supplementary Table 3.2) were selected for ddRADseq library preparation and sequencing. ddRADseq libraries were prepared at the Beijing Genomics Institute (BGI) Tech Solutions Co. Limited (Hong Kong) following Peterson et al. (2012). Briefly, genomic DNA of each sample was digested with MseI and EcoRI restriction enzymes, ligated with barcoded adapters, pooled digested ligated fragments were size selected using Blue Pippin and divided into libraries. Twenty-two technical replicates were also included across libraries, resulting in a total of 440 samples sequenced for ddRADseq (see Supplementary Table 3.2). All libraries were amplified via PCR using indexed primers and sequenced on a HiSeq X ten (at BGI).

Raw ddRAD reads were demultiplexed with barcodes and adapters removed by BGI using their in-house pipeline. Reads with phred quality less than 20 ($Q < 20$) were also discarded using *fastp* v0.20 (Chen et al., 2018). Potential contaminants (human and microorganisms) were identified using *Kraken* v1.0 (Wood & Salzberg, 2014), and reads that matched those of the contaminant database were removed. Cleaned and trimmed reads were checked for quality using *fastQC* v0.11.7 (Andrews, 2019), and mapped to the reference genome of *Pareledone turqueti* using *bowtie2* v2.3.4.1 (--very-sensitive-local) (Langmead & Salzberg, 2012). Local alignment (--very-sensitive-local) was used, following Souza et al. (2017), since the ddRADseq dataset contains a wide variety of Southern Ocean octopod taxa that may contain structural rearrangements or variants at either ends of reads that are different from

the reference genome (*P. turqueti*). *Samtools* v1.7 (Li et al., 2009) was used to sort the alignments (BAM files) by coordinates. ddRAD loci were built from aligned and sorted reads, and SNPs were called, using the *Stacks* v2.3d *gstacks* module with default settings (Catchen et al., 2013).

3.3.3 ddRAD loci discovery for target capture sequencing of *Pareledone turqueti*

Initial assessment of raw genotype calls from *Stacks* indicated 155 out of 440 Southern Ocean octopus samples suffered from a high amount of missing data (> 80%), with 92 out of these 155 samples identified as *P. turqueti*. Samples with high levels of missing data were likely degraded due to long term storage. Then, a target capture bait set was designed with the intention of capturing a high proportion of the same loci in the degraded samples that were included in the ddRADseq (non-degraded) dataset. Loci discovery for this purpose was performed using a total of 285 samples (with 17 technical replicates across libraries included) comprising those with missing data less than 80% and included samples from the following species: *A. adelieana*, *A. polymorpha*, *Adelieledone* sp., *P. turqueti*, *P. aequipapillae*, *Pareledone* sp., *M. setebos*, *Graneledone* sp. (Supplementary Table 3.2). The *Stacks population* module was then performed to retain sites that were present in 50% of the remaining samples (-R 0.5) with at least a minor allele frequency of 0.01 (*--min-maf* 0.01), which resulted in 31,142 loci retained. Discriminant analysis of principal components (DAPC) was performed via the R package *adegenet* v2.1.3 (Jombart & Ahmed, 2011) to visualise potential batch effects between libraries (no batch effect was found). When the technical replicates were paired together, the replicate with the highest amount of missing data was removed.

The consensus fasta sequences of the 31,142 loci were then aligned back to the reference *P. turqueti* genome using *bowtie2* with end-to-end alignment (--sensitive). Of the 31,142 loci, 8,942 loci were aligned back to the genome exactly once were retained for target capture bait design, to avoid paralogous genes which can compromise phylogenetic inference (Andermann et al., 2020). Lost loci may also represent reads in repetitive areas as they would be expected to be missing from the genome assembly.

3.3.4 Target capture sequencing of ddRAD loci in degraded *P. turqueti* samples

3.3.4.1 Bait design

The consensus sequences of the filtered ddRAD loci (n = 8,942) were used for custom biotinylated RNA bait manufacturing at Arbor Bioscience (Ann Arbor, MI, USA). Input

sequences were soft-masked (0.5%) for simple repeats and low-complexity regions using Repeat Masker (Smit et al., 2015), and candidate bait sequences were designed based on bait length (70 nucleotides per bait) and 3 X tiling per locus. Candidate baits were removed if, 1) they were greater than 25% soft-masked for simple repeats, 2) had hits to regions of the *P. turqueti* genome (this study) and the common octopus *Octopus vulgaris* genome (GenBank assembly accession: GCA_003957725.1) (Zarrella et al., 2019) that were greater than 25% soft-masked, or 3) failed Arbor Bioscience in-house moderate Basic Local Alignment Search Tool (BLAST) parameters, which take into account the BLAST hit for a bait and predicted melting temperatures. The final myBaits® (Arbor Bioscience) panel contained 86,422 baits that targeted 8,877 ddRAD loci with at least one bait.

3.3.4.2 Library preparation and target capture sequencing

Genomic DNA of 87 *P. turqueti* samples were sent to Arbor Biosciences for library preparation and target capture sequencing (Supplementary Table 3.3). None of the *P. turqueti* individuals sequenced with target capture sequencing were used for the discovery of ddRAD loci, because they were excluded prior to SNP calling while processing ddRADseq data. We did not include the standard DNA shearing step as these samples had already been identified as having degraded DNA. Libraries with unique index adapters were built and pooled into single capture reactions (six libraries per capture). All libraries were enriched in capture reactions using myBaits® following the manufacturer's protocol and the resulting capture reactions were sequenced on a single Illumina NovaSeq S4 flow cell with 150 bp paired end reads.

3.3.4.3 Target capture reads cleaning

Raw target capture reads were demultiplexed with barcodes removed using *process_shortreads* in *Stacks*. Reads with phred quality less than 20 (Q < 20) were also discarded, and polyG in read tails (a problem with NovaSeq output) were trimmed, using *fastp*. Potential contaminants (human and microorganisms) were screened for and removed using *Kraken*. Reads were then truncated to a final read length of 140 bp. Cleaned and trimmed reads were checked for quality using *fastQC*.

3.3.5 Variant calling

3.3.5.1 Read mapping and variant calling for ddRAD and target-capture data

Variants were called across ddRAD (*P. turqueti* samples only sequenced with ddRAD sequencing; n = 219) and target capture samples (n = 87) (see Fig 3.1 for sample locations). All cleaned, raw ddRAD and target capture reads were mapped to the consensus sequences of ddRAD loci used for bait design using *bwa mem* with default parameters (Li & Durbin, 2009). *Samtools* was used to sort alignments (BAM files) by coordinates. For both ddRAD and target capture reads, PCR duplicates were marked and removed using *picard* v2.18.1 (Broad Institute, 2019). Variants and short indels were called across all samples using *bcftools* v1.7 *mpileup* (Li et al., 2009).

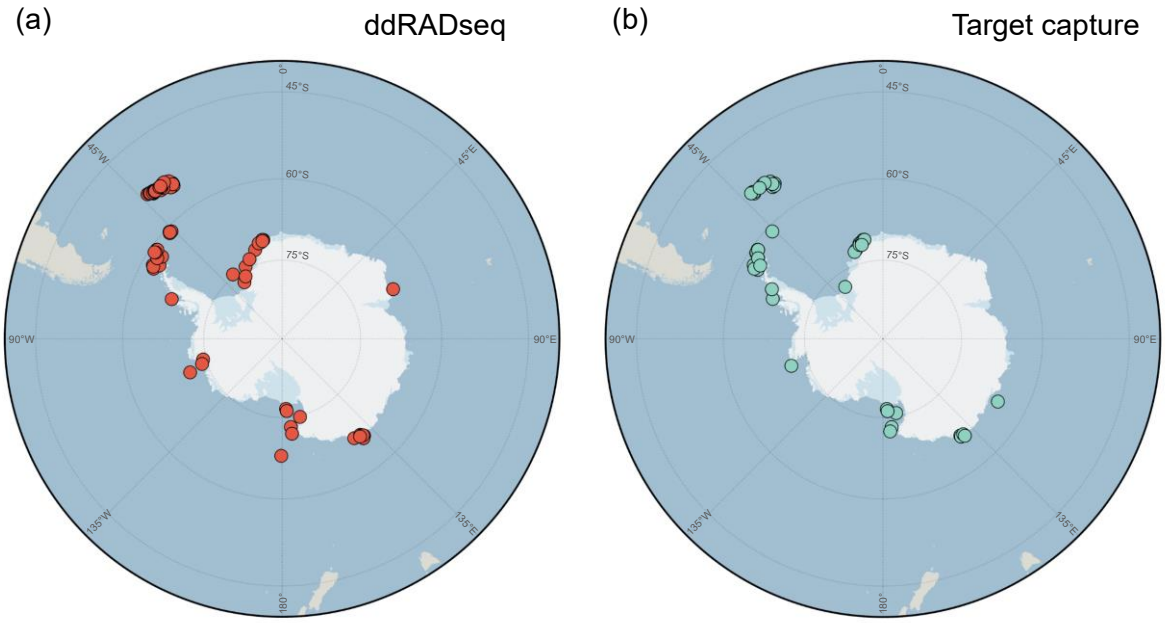

Fig 3.1 Sample locations of *Pareledone turqueti* sequenced via (a) ddRADseq (n = 219) and (b) target capture sequencing (n = 87) compared in this study.

3.3.5.2 Variant filtering

VCFtools v0.1.16 (Danecek et al., 2011) was used to perform variant filtering on the raw variants called across ddRAD and target capture samples via *mpileup*. Variant filtering was performed based on different thresholds of missing genotypes across all samples (10 - 50%) to evaluate their respective effects on downstream genetic structure analyses. Indels and samples with > 80% sites without a genotype call (n = 14) were first removed, and high quality SNPs were retained based on the following steps. Sites with Phred scaled site quality score more than 30 were kept (--minQ 30). Sites with mean read depth of less than 10x and

greater than 50x (=2*average depth (24.9)) were removed (--min-meanDP 10, --max-meanDP 50). Only biallelic sites were kept (--min-alleles 2, --max-alleles 2). Sites were kept if present in 90, 80, 70, 60 and 50% of all samples (--max-missing 0.9, 0.8, 0.7, 0.6, 0.5), based on presence/absence of a genotype call. Sites with a minor allele frequency of at least 5% were kept (--maf 0.05). To remove sites that could belong to paralogous sequences, only sites with a maximum observed heterozygosity of 0.5 were kept (identified via the R package *adegenet*) (Hohenlohe et al., 2011). Finally, only one site per locus was kept (--thin 1000; an arbitrary length larger than the longest contig in the ddRAD reference of the bait set).

We also explored the effects of different minor allele frequency thresholds on downstream analyses; SNP filtering criteria was kept as above. The threshold of missing data was fixed at --max-missing 0.8 (SNPs were kept if present in 80% of all samples). SNPs were filtered with a minor allele frequency of at least 2, 5% or 10% (--maf 0.02, 0.05, 0.1).

3.3.6 Genotype likelihood estimation

Even though the variant calling method (*mpileup*, *VCFtools*) enabled us to keep a minimum depth of coverage for ddRAD and target capture data (10x; see above), the genotype likelihood estimation method was used as an alternative strategy to variant calling, which would enable us to retain reads with low depth while accounting for genotype uncertainty and error rates (Korneliussen et al., 2014). Genotype likelihood estimation has been found to be successful in handling low coverage data. In addition, among the raw variant calls directly derived from *mpileup*, ddRAD samples were associated with lower read depths (median = 2.3x, average = 8.5x) than target capture (median = 30.2x, average = 66.2x). Given that genotypes called from low coverage data are associated with high uncertainty, *ANGSD* v0.931 (Korneliussen et al., 2014) was also used to estimate genotype likelihoods across ddRAD and target capture *P. turqueti* samples so that genotype uncertainty could be accounted for in downstream analyses.

Sorted BAM files of ddRAD and target capture samples from *Samtools* (prior to variant calling using *mplieup*) were processed in *ANGSD* for genotype likelihood estimation under different filtering thresholds (varying across the percentage of missing data and minor allele frequency). The *samtools* genotype likelihood model (GL 1) was used to estimate genotype likelihoods from the mapped reads. Reads were removed when they mapped to multiple loci (-uniqueOnly), were considered non-primary, failed or duplicated (-remove_bads 1; remove reads with SAM flag > 255), had a mapping score of less than 10 (-minMapQ 10) or a minimum base quality score of less than 20 (-minQ 20). Genotype posterior probabilities

were estimated using a uniform prior (-doPost 2). Major and minor alleles, and minor allele frequencies were estimated from genotype likelihoods (-doMajorMinor 1, -doMaf 1). Sites were required to be present in at least 90, 80, 70, 60 or 50% of all samples (-minInd) and with a minor allele frequency of at least 5% (-minMaf 0.05). Polymorphic sites were called if the SNP p-value was $\leq 1x10^{-6}$ (-SNP_pval 1e-6). Similar to *mpileup* SNP filtering, we also explored the effects of different minor allele frequency thresholds on downstream population genetic analyses, with SNPs filtered with a minor allele frequency of at least 2, 5 or 10%, as well as if present in 80% of all samples.

3.3.7 Data evaluation with genotype calling and genotype likelihood approaches

3.3.7.1 Genetic structure between sequencing methods

Genetic structure of both datasets generated from genotype calling (*mpileup*) and genotype likelihood (*ANGSD*) approaches were examined using Principal Component Analysis (PCA). For both *mpileup* and *ANGSD* datasets, PCA was also visualised with different missing data and maf thresholds. For SNPs derived from *mpileup*, PCA was performed using the R package *adegenet* (Jombart & Ahmed, 2011). For genotype likelihoods at variant sites identified via ANGSD, *PCAngsd* v1.0 (Meisner & Albrechtsen, 2018) was used to infer covariance matrix between individuals while taking into the account for uncertainty in low depth data. Individual level PCA was then visualised by computing eigenvectors from the covariance matrix using the R package *RcppCNPy* v0.2.10 (Eddelbuettel & Wu, 2016). All analyses on R were performed in *RStudio* v1.1.456 (Rstudio, 2020).

3.3.7.2 Quantification of DNA damage from degradation

mapDamage v2.0 (Jónsson et al., 2013) was used to evaluate whether samples used in ddRADseq and target capture sequencing suffered from nucleotide misincorporation patterns due to DNA damage, such as fragmentation and degradation. A typical post-modern damage would indicate an excess of C to T substitutions at the 5' end terminal and G to A substitutions at the 3' end terminal, with the level of substitution declining exponentially inwards along the first five positions (Jónsson et al., 2013). Cleaned, raw, paired-end ddRAD and target capture reads were merged into single-end reads using *PEAR* v0.9.11 (Zhang et al., 2014). Merged reads were then mapped against the bait reference using *bwa mem* with default parameters, and BAM files were sorted using *Samtools*. Sorted BAM files were processed using *mapDamage* to compute and compare damage pattern between ddRADseq and target capture sequencing.

3.3.7.3 Genotyping error estimation

Allele dropout and genotyping errors can cause departures from Hardy-Weinberg Equilibrium (HWE) (Chen et al., 2017). To detect and remove these errors, we filtered for departure from HWE in the datasets derived from *mpileup* and *ANGSD* (maf 0.05, 20% missing data allowed). HWE-departure was considered significant with $p \leq 0.05$.

We further explored genotyping errors between ddRADseq and target capture sequencing, and estimated the % per-allele genotype errors in homozygote and heterozygote calls between the two sequencing methods. We used *Tiger* (Bresadola, 2020) to evaluate the % genotyping errors in the filtered called SNPs generated from *mpileup*. We estimated the % genotyping errors the datasets filtered with maf of 0.05, missing data of 20%, with and without filter applied for HWE-departure with $p \leq 0.05$. *Tiger* was performed based on the assumption that the populations of *P. turqueti* are in HWE, with sample locations defined as 'populations'.

3.3.7.4 Heterozygosity estimation

Genome wide heterozygosity was calculated using *mpileup* dataset and compared between sequencing methods. For the *mpileup* dataset, heterozygosity per locus was estimated using the data filtered with maf of 0.05, missing data of 20%, with and without filter applied for HWE-departure with $p \leq 0.05$. For the *mpileup* dataset, observed and expected heterozygosity (i.e. proportion of observed and expected heterozygous sites in biallelic SNP data) were calculated for each sample using *VCFtools* after SNP filtering. Observed and expected heterozygosity per locus was also calculated per sequencing method using the R package *adegenet* after SNP filtering.

3.4 Results

3.4.1 Variant filtering and genotype likelihood estimation

In the datasets where *P. turqueti* samples (ddRADseq and target capture sequencing) were processed via *mpileup* (reference calling), 745,569 raw SNPs were detected. After SNP filtering with various missing data (10 - 50% missingness allowed) and maf thresholds (maf 0.02 - 0.1), the final filtered datasets included 292 *P. turqueti* individuals with 3585 - 4807 SNPs retained; Supplementary Table 3.4). In the datasets where samples were processed

via *ANGSD* (genotype likelihood estimations), the filtered datasets included 306 *P. turqueti* individuals with 100,258 - 243,619 sites retained (10 - 50% missing data, maf 0.02 - 0.1; Supplementary Table 3.4). Further filtering based on HWE-departure ($p \leq 0.05$) with 20% missing data and maf of 0.05 resulted 292 *P. turqueti* individuals with 2,293 SNPs detected in *mpileup*, and 306 *P. turqueti* individuals with 36,960 sites (*ANGSD*) retained.

3.4.2 Genetic structure between sequencing and read processing methods

Both PCA plots from *PCAngsd* (Fig 3.2a) and *mpileup* (Fig 3.2b) recovered a similar pattern where a clear separation was found between samples derived from ddRADseq and target capture on the PC1 axis. Samples separating based on sequencing method was also observed when sites were additionally filtered for HWE-departure on the PC1 axis, via *PCAngsd* (Fig 3.2c) and *mpileup* (Fig 3.2d). However, samples were not separated on the PC2 axis of the PCA plots from *mpileup* and *PCAngsd* (Fig 3.2a, b, c, d). On the PC2 axis, *PCAngsd* suggested limited variation can be observed between target capture samples compared to ddRADseq samples (Fig 3.2a, c). Based on *mpileup* and *ANGSD*, on the PC2 axis, ddRADseq samples appeared to be more variable relative to target capture samples (Fig 3.2) Between bioinformatic pipelines, on the PC2 axis, target capture samples were associated with higher level of variation in *mpileup* relative to *ANGSD* (Fig 3.2b, d).

Regardless of whether reads were processed via *ANGSD* or *mpileup*, as well as the difference in filtering thresholds applied for missing data and maf, similar population structure was observed across sequencing methods (Supplementary Fig 3.1-3.4). Overall, on the PC2 axis, a gradient of variation can be observed along sample locations. The greatest difference was observed between samples from Shag Rocks + South Georgia versus the continental shelf. Samples from the Scotia Arc (South Orkney Island, Elephant Island, Livingston Island, Deception Island, King George Island, Robert Island) appear to connect the samples from Shag Rocks + South Georgia and the continental shelf along the PC axis.

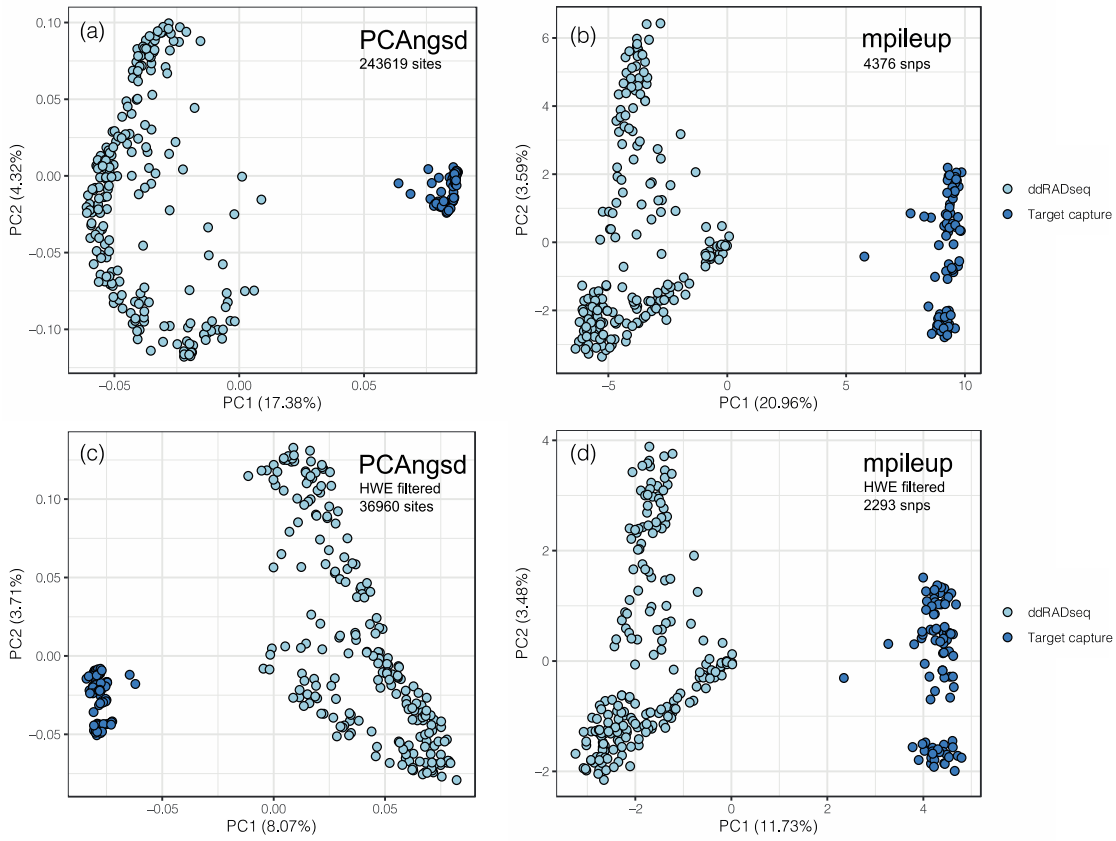

Fig 3.2 Principal Component Analysis of ddRADseq and target capture sequencing of ddRAD loci in *Pareledone turqueti*. Reads derived from both methods were processed together in a single bioinformatic pipeline via genotype likelihood estimation with *PCAngsd* (a, c) and reference calling with *mpileup* (b, d). Both pipelines were filtered with a minor allele frequency of at least 0.05 and 20% missing data allowed, as well as filtering for Hardy-Weinberg departure (HWE) with $p \leq 0.05$ in (c, d).

3.4.3 Post-mortem damage and genotyping error estimation

Analysis of nucleotide misincorporation pattern (*mapDamage*) showed no signatures of post-modern damage in *P. turqueti* samples sequenced by ddRADseq or target capture sequencing (Fig 3.3). However, a slight increase in G to A substitutions (average = 0.052 $\pm$ SD 0.023 SD and 0.048 $\pm$ SD 0.022 for ddRADseq and target capture sequencing, respectively) at the first base pair (bp) from the at 3' end (Fig 3.3). Since 2nd to 5th bp from the 3' end are characterised by limited frequency of G to A substitutions in both methods, which do not follow the typical nucleotide misincorporation pattern, the G to A substitution at the 1st bp was likely not an indication of post-modern damage but true nucleotide difference in some samples (consistent across both sequencing methods) (van der Valk et al., 2019). Overall, neither ddRADseq nor target capture samples are characterised by the distinct nucleotide misincorporation pattern that can be related the obvious batch effect.

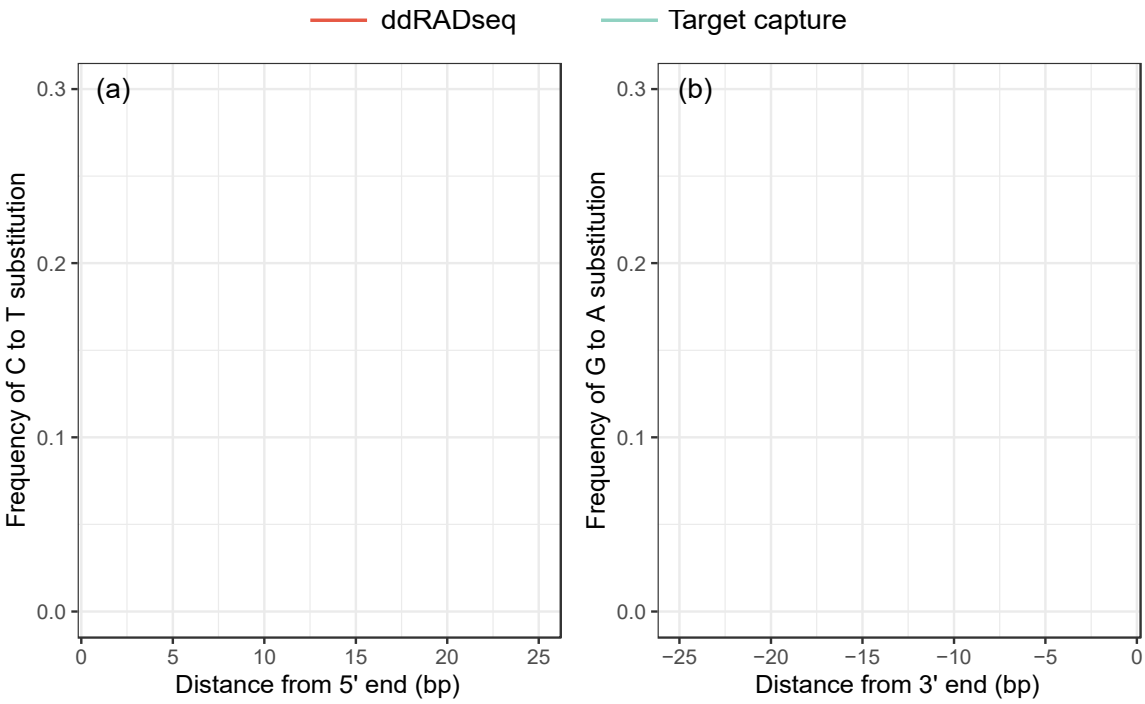

Fig 3.3 *mapDamage* analysis of reads derived from ddRADseq and target capture sequencing of ddRAD loci in *Pareledone turqueti*. A typical base substitution pattern due to post-mortem damage would reflect an increase of C -> T substitution at the terminal region from 5' end and G -> A substitution at the terminal region from 3' end. No evidence of post-mortem damage is observed in samples used in ddRADseq and target capture sequencing. Each lines represent a sample.

Table 3.1 Allele error rates estimated for *Pareledone turqueti* samples sequenced via ddRADseq and target capture sequencing. Reads derived from both methods were processed via reference calling with *mpileup*. Error rates were calculated in sites that were present after filtering for 20% missing data and a minor allele frequency of 0.05, with or without filtering for Hardy-Weinberg equilibrium (HWE) departure with $p \leq 0.05$.

		Allele error rate	
		Homozygous calls	Heterozygous calls
No HWE filter	ddRADseq	0.051	0.081
	Target capture	0.042	0.057
HWE filter	ddRADseq	0.046	0.098
	Target capture	0.039	0.071

In the reference calling dataset derived from *mpileup*, when SNPs were not filtered for HWE-departure, % allele error rates were estimated to be at 5.1% for homozygous genotypes and 8.1% for heterozygous genotypes in ddRADseq samples, and 4.2% for homozygous genotypes and 5.7% for heterozygous genotypes in target capture samples (Table 3.1). When SNPs were filtered for HWE-departure, % allele error rates were estimated to be at 4.6% for homozygous genotypes and 9.8% for heterozygous genotypes in ddRADseq

samples, and 3.9% for homozygous genotypes and 7.1% for heterozygous genotypes in target capture samples (Table 3.1). Regardless of whether SNPs were filtered for HWE-departure, the highest % error rate was observed for heterozygous genotypes in ddRADseq samples, indicating a general bias towards homozygous genotype calls in ddRADseq.

3.4.4 Heterozygosity estimation

Estimations of observed heterozygosity per locus via *mpileup* and *VCFtools* indicated there was no significant difference between ddRADseq and target capture, regardless of whether the data was filtered with or without HWE-departure (Fig 3.4). However, from visualising the values of observed heterozygosity per locus between ddRADseq and target capture, there is a noticeable difference between observed and expected heterozygosity values between methods (Fig 3.5). An overall higher level of observed and expected heterozygosity was observed in target capture relative to ddRADseq, regardless of whether data were filtered with or without HWE-departure.

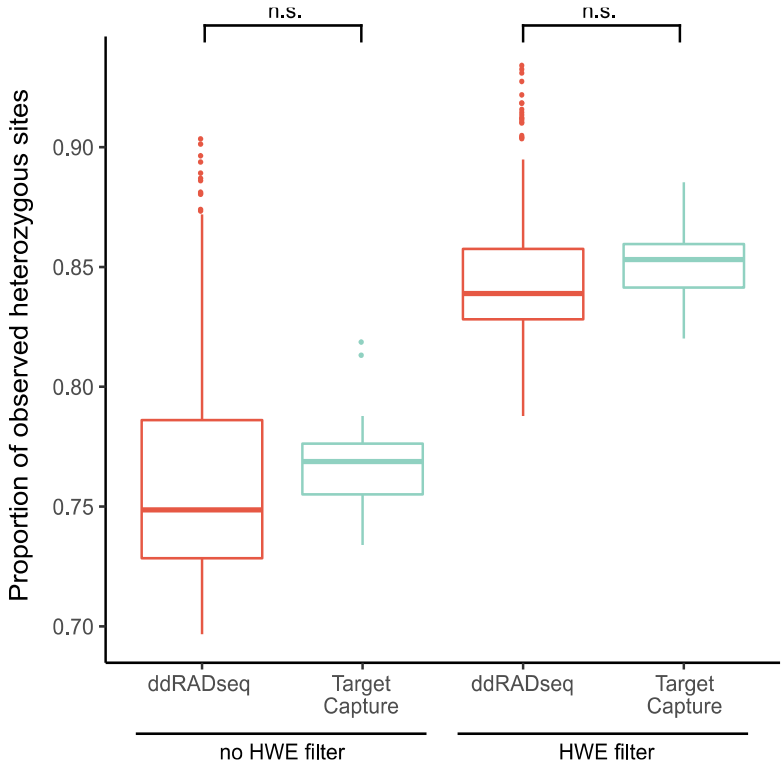

Fig 3.4 Proportion of observed heterozygous sites in the biallelic SNP data of *Pareledone turqueti* sequenced via ddRADseq and target capture sequencing. Reads derived from both methods were processed via reference calling with *mpileup*. Estimates were calculated per sample, and only considered sites that were present after filtering for 20% missing data and a minor allele frequency of 0.05, with or without filtering for Hardy-Weinberg equilibrium (HWE) departure with $p \leq 0.05$. n.s. = not significant at $p = 0.025$. Box = first and third quantiles, line within the box = median, upper and lower whisker = maximum and minimum values within the 1.5x interquartile range, respectively, dots = outlier values outside of the 1.5x interquartile range.

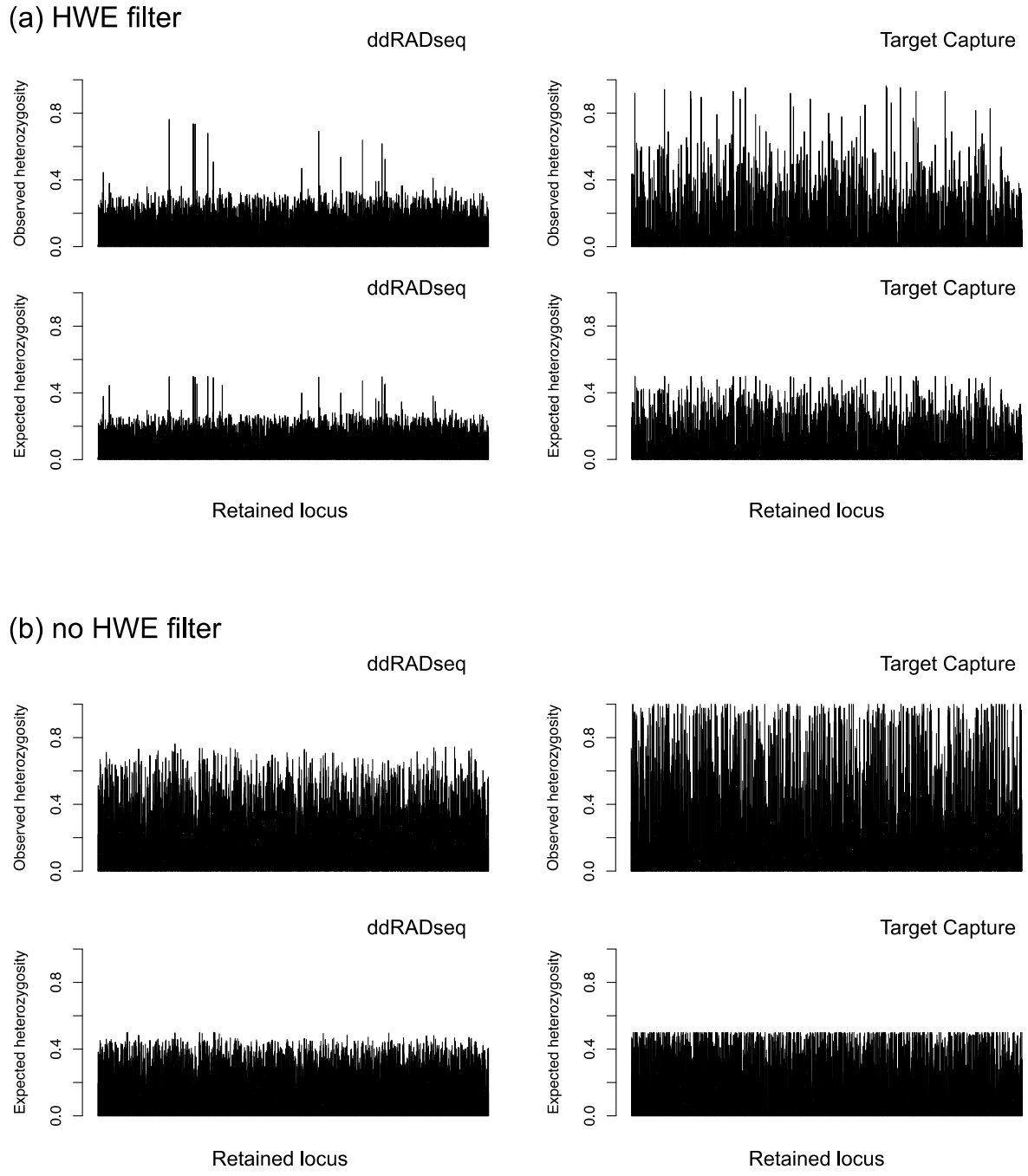

Fig 3.5 Observed and expected heterozygosity per locus in the biallelic SNP data of *Pareledone turqueti* sequenced via ddRADseq and target capture sequencing. Reads derived from both methods were processed via reference calling with *mpileup*. Estimates were per locus, with each bar represents a locus. Only sites that were present after filtering for 20% missing data and a minor allele frequency of 0.05, with (a) or without (b) filtering for Hardy-Weinberg equilibrium (HWE) departure with $p \leq 0.05$ were analysed.

3.5 Discussion

Here, a clear signal of read incompatibility between ddRADseq and target capture sequencing is reported, despite both methods being used to sequence the same genomic positions (ddRAD loci). This study accounted for previously proposed challenges associated with biases that could explain such a batch effect and found that none of them were responsible for the observed difference. The overall results indicated a bias towards homozygous genotypes in ddRADseq (i.e. excess homozygous calls) could be distinguished, and suggest there are technical issues, such as low read coverage and allele dropout, leading to genotypes derived from ddRADseq, which cannot be directly compared to other sequencing methods (e.g. target capture sequencing).

The differences between ddRADseq and target capture data are typically discussed alongside geographical and temporal sampling bias (Linck et al., 2017; Schmid et al., 2018; Lang et al., 2020), as well as the sample quality associated with each method (fresh samples for ddRADseq versus degraded samples for target capture sequencing). Additionally, degraded samples could also be associated with read quality bias linked to DNA degradation (Linck et al., 2017), missing data (Boucher et al., 2016), read depth (Fountain et al., 2016; Ewart et al., 2019) or reduced alignment efficiency (Rowe et al., 2011). In this study, we recognise that no technical replicates across sequencing methods were included. However, both ddRADseq and target capture datasets included samples collected from the same expedition cruises, locations from around the Southern Ocean, as well as fresh and degraded samples collected between year 2003 and 2016. Therefore, any systematic biases in genetic structure due to geographical or temporal sampling can be ruled out. Post-mortem DNA damage analysis also indicated samples employed in ddRADseq and target capture sequencing did not suffer from typical nucleotide misincorporation patterns caused by DNA degradation. While a clear difference in read depth was observed between ddRADseq (low depth) and target capture sequencing (high depth), genotype likelihood estimations (*ANGSD*/*PCAngsd*) that accounted for biases in low and variable sequencing depth also reflected a clear batch effect between both methods. Finally, the stringency in missing data and minor allele frequency thresholds, as well as filtering for Hardy-Weinberg departure, did not overcome the observed batch effect. Overall, our bioinformatic pipelines ruled out most of the possibilities proposed in literature that could lead to differences between ddRADseq and target capture sequencing of the same genomic positions.

Similar batch effects to those observed in the present study have been reported in recent studies which have attempted to merge reads of the same genomic positions derived from

ddRADseq and target capture sequencing (Lang et al., 2020; O'Connell et al., 2021). A recent study has also discussed differences between SNPs derived from ddRADseq and target capture sequencing that were linked to variation in heterozygous and homozygous calls (O'Connell et al., 2021). Although the authors did not conclude on the source of errors, they discussed that the errors could be linked to either 1) the presence of paralogous sequences in target capture data that was causing false heterozygous calls at homozygous sites, or 2) allele dropout in ddRADseq data leading to false homozygous calls at heterozygous restriction sites. In this study, we particularly selected ddRAD loci that aligned back to the *P. turqueti* genome only once when designing target capture bait set, as well as applied a strict SNP filtering threshold to further remove putative paralogous sequences (in *mpileup* datasets). Nonetheless, despite accounting for presence of paralogous sequences via a two-step approach, the batch effect still persisted, as evidenced on the PCA plots (Fig 3.2). Therefore, the observed differences between the two methods are likely linked to biases within ddRADseq, with issues specific to this study and issues typically found across studies. Technical issues in RADseq (including ddRADseq) have been extensively discussed and reviewed in the literature (e.g. Davey et al., 2013; Puritz et al., 2014; Andrews et al., 2016), these errors include false homozygote calls due to allele dropout at heterozygous restriction sites (Gautier et al., 2013), amplification bias towards reads with high GC content (PCR duplicates) (DaCosta & Sorenson, 2014), and variation in read depth (Fountain et al., 2016). Since PCR duplicates were also mitigated and removed bioinformatically (*Picard MarkDuplicates*), and variation in read depth was accounted for via genotype likelihood estimation, the genotyping error observed within ddRADseq in this study is likely driven by allele dropout at restriction sites and overall low read coverage.

Based on genotyping error rate estimations, the highest error rate was detected in heterozygous calls within ddRADseq of *P. turqueti*, suggesting an apparent bias towards homozygous calls within ddRADseq. It should be noted that in this study, genotyping error rate estimation was performed based on the assumption that populations are under Hardy-Weinberg equilibrium. Previous studies based on microsatellite data have suggested *P. turqueti* could be under selection and/or exhibit population substructure linked to seascape dynamics in the Southern Ocean (Strugnell et al., 2017), which would violate HWE assumptions (Chen et al., 2017). Indeed, genotyping error estimation also detected errors within target capture sequencing under the assumption of HWE. Therefore, error rates estimated in this study could be an overestimation, and might not reflect an accurate quantification of true genotyping error rates, or that reads derived from target capture sequencing also suffer from a level of genotyping error such as errors from sequencing platforms (Wall et al., 2014). Furthermore, while *mapDamage* indicated target capture and

ddRADseq samples do not follow typical misincorporation patterns linked to DNA degradation, noticeable frequencies in nucleotide misincorporation are observed within the reads. This pattern could reflect either true mutations or read inaccuracy (Eisenhofer et al., 2017; van der Valk et al., 2019), and the latter could also support the cause of genotyping error in both methods. Nonetheless, since the highest percentage error rate was observed for heterozygous calls within ddRADseq, it appears the data contains a level of genotyping error specific to ddRADseq, supporting the case of allele dropout as a driver of the batch effect in this study. Additionally, the overall low coverage reads in ddRADseq, a problem specific to this study, could also be associated with the possibility of not sampling the alternate allele, thus leading to bias towards homozygous genotypes (Barbanti et al., 2020).

In the dataset where reference calling (*mpileup*) followed by variant filtering was performed by *VCFtools*, no significant difference was found in observed heterozygosity (defined as "the proportion of observed heterozygous sites in biallelic SNP calls after filtering") between samples derived from ddRADseq and target capture sequencing. When observed and expected heterozygosity were visualised per locus between methods, there was a noticeable difference between methods, with an overall higher level of heterozygosity observed across loci. This means the batch effect could be driven by specific loci within each method. It is assumed that allele dropout would generally lead to a reduction in heterozygosity estimates in RAD data (Gautier et al., 2013; Flanagan & Jones, 2018). The same principle would also be applicable to the problem of low coverage reads that would result in bias towards homozygous genotypes. Even though no statistical differences between heterozygosity in ddRADseq and target capture data were detected in this study, there is, however, a noticeable reduction in heterozygosity in ddRADseq data. It is clear from the further downstream analyses in this study, biases between ddRADseq and target capture sequencing are present in this study. Genotype error estimation also indicated an ~10% error rate in heterozygous calls in ddRADseq of *P. turqueti*. In comparison to other ddRAD studies, where a 4 - 11% error rate in heterozygous calls was suggested (Luca et al., 2011; Mastretta-Yanes et al., 2015; Miklós et al., 2021; Woodings et al., 2021), or up to an extreme level where a 50% error rate was estimated (Bresadola et al., 2020). Therefore, the level of genotyping error detected in this study appears to be in agreement with other ddRAD data in the literature. Although we recognised that the ddRAD data in this study suffer from low read coverage, which can contribute towards genotyping errors, it is plausible that issues commonly found across ddRADseq studies, such as allele dropout, could already affect downstream analyses. In this sense, genotypes derived from ddRADseq cannot be directly compared to other sequencing methods less prone to genotyping errors such as target capture, even when errors are not reflected via heterozygosity estimates. Since it is likely

that other ddRADseq studies could also suffer from similar percentage error rate in heterozygous calls, this study highlights the (un)reliability of ddRADseq in achieving accurate genotype calls.

Our study does not undermine the power of ddRADseq in population genomics inference, which is a widely-used, popular method among non-model species investigations (Andrews et al., 2016). *Pareledone turqueti* is characterised by large effective population size (N_e up to $1e^8$; based on cytochrome c oxidase subunit I (COI) data) (Strugnell et al., 2012). Based on simulated data, it has been suggested that allele dropout likely only becomes problematic in species with $N_e > 1e^5$ (Gautier et al., 2013). Our ddRADseq data also suffered from generally low coverage reads, which could have been avoided by increasing sequencing depth per sample. For *P. turqueti*, both ddRADseq and target capture sequencing also recovered consistent patterns in population structure across different filtering thresholds and genotyping calling methods, which were also supported by previous microsatellite and COI data of *P. turqueti* (Strugnell et al., 2012). Therefore, compared to results derived from target capture sequencing, allele dropout in ddRADseq does not appear to affect its power of general genetic structure inference. However, given the inherent bias in ddRADseq, data might not be reliable for downstream analyses that rely on accurate genotype calls (e.g. outlier loci detection, environmental association analyses, site frequency spectrum based inferences).

The variety of filtering strategies and genotype calling methods applied in this study suggest it is unlikely that the bias towards homozygous calls in ddRADseq can be mitigated using existing bioinformatic pipelines. Therefore, we do not recommend studies directly combine reads derived from ddRADseq and target capture sequencing at present. However, it is becoming clear that different technical causes of batch effects, such as allele dropout and low read coverage, only affect certain sites and thus these can be excluded during filtering process (Lou & Therkildsen, 2021). These sites can be detected and reviewed via specially designed and carefully considered approaches (Lou & Therkildsen, 2021). Additionally, methods based on carefully designed outlier loci detection analyses could be applied to remove putative SNPs that drive the batch effects. However, so far, there is no standard bioinformatic pipeline or practice that mitigate batch effects resulting from technical issues. It is also unclear to what extent the removal of these sites would affect downstream population genetic and biological inference. In the future, to integrate reads generated from different sequencing methods, a reproducible approach would require bioinformatic pipelines specifically designed to mitigate the batch effect linked to genotyping errors (e.g. low read coverage, allele drop out in ddRADseq) with clear justifications and reasonings.

Alternatively, since target capture methods do not incorporate restriction enzymes and can avoid issues linked to allele dropout, target capture sequencing could be extended to recovering ddRAD loci in both non-degraded and degraded samples, as also suggested within O'Connell et al. (2021). However, RADseq has been one of the most popular next generation sequencing methods performed in non-model species across the world, and much of these genomic data in existing repositories cannot be ignored. Target capture methods are also more costly to perform compared to RADseq. It is also inevitable that RADseq methods are ineffective for degraded samples, and that target capture sequencing offers an alternative approach for sequencing the same genomic positions as RADseq methods would in degraded samples. Overall, with the rapid advancement of molecular techniques and genomic analyses, emphasis should be focused on achieving genotyping calls with high accuracy to ensure the longevity of datasets, as well as reproducibility across sequencing methods.

3.6 Conclusion

This study highlights target capture sequencing is the preferable approach with relatively limited sequencing errors, compared to ddRADseq, for sequencing genomic loci in samples (degraded or non-degraded). As a case study using *P. turqueti* samples, we outline a clear batch effect between ddRADseq and target capture data even when analysis was restricted to genomic positions sequenced by both methods. By employing both hard genotype calling (*mpileup*) and genotype likelihood estimation (*ANGSD*) approaches to deduce the drivers of the observed batch effect, we showed that observed differences were not related to DNA degradation, geographical or temporal genetic structure, variations in missing data, filtering thresholds or presence of paralogous sequences. However, an apparent bias towards homozygous genotypes in ddRADseq data was found, linked to allele dropout, and this could not be resolved using existing bioinformatic tools. Additionally, ddRADseq data obtained from *P. turqueti* were characterised by low read depth, which could have reduced the ability in detecting heterozygotes. Future pipelines should be designed to specifically combine reads derived from ddRADseq and target capture sequencing. Different genotyping errors (e.g. allele drop out, low coverage) likely uniquely affect different proportions of loci, and future pipelines should focus on identifying and removing loci affected by different types of genotyping errors, as well as establishing frameworks for filtering erroneous loci while maintaining data integrity.

CHAPTER 4

Evolutionary divergence and innovations driven by a historical warm interglacial: genomic insights from Antarctic brittle stars

Lau, S.C.Y., Strugnell, J.M., Sands, C.J., Silva, C.N.S. Wilson, N.G.

This chapter is formatted for *Molecular Ecology*.

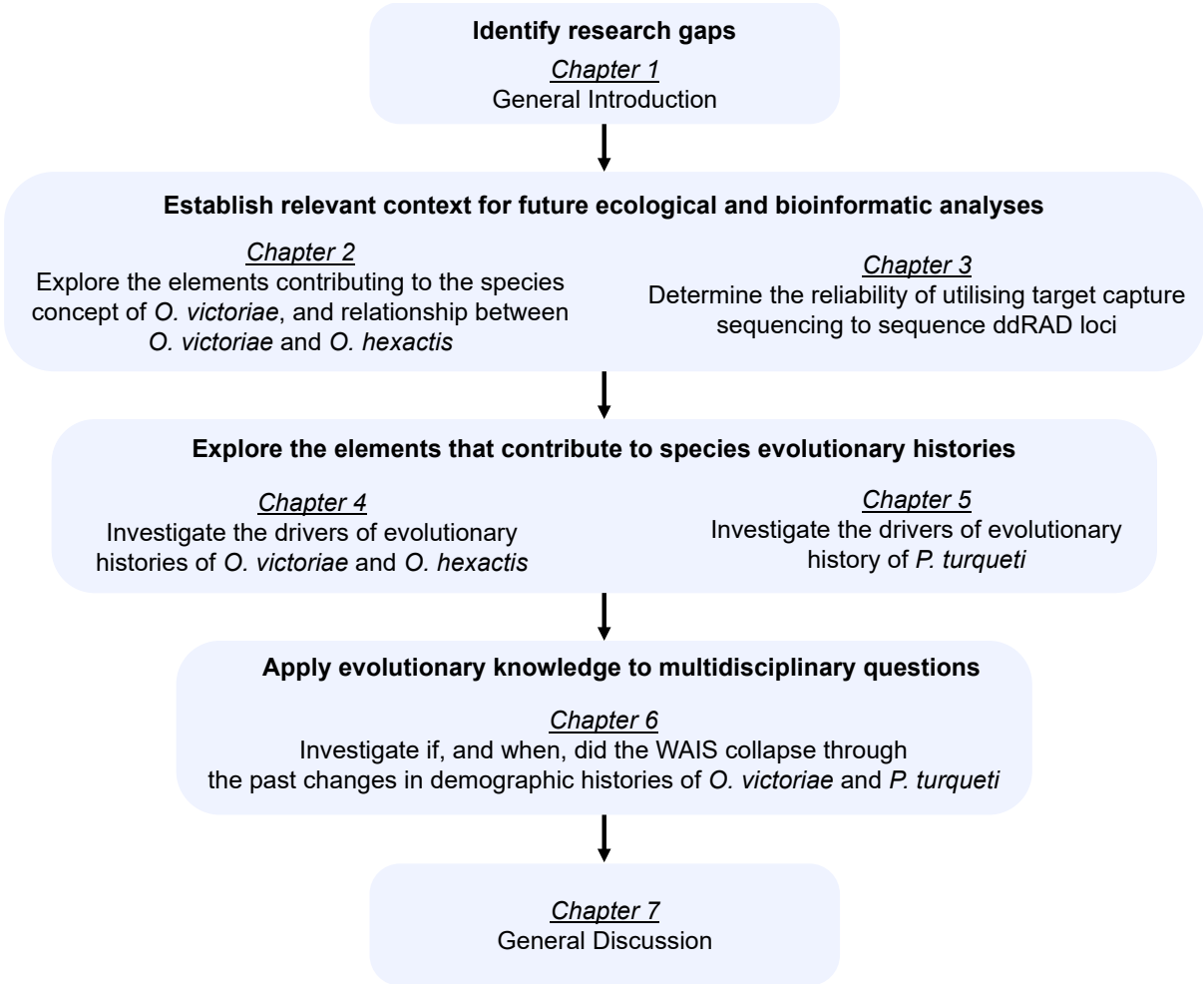

4.1 Abstract

Understanding the drivers of evolutionary innovations provide a crucial perspective of how evolutionary processes unfold across taxa and ecological systems. It has been hypothesised that the Southern Ocean provided ecological opportunities for innovations the past. However, the drivers of innovations are challenging to pinpoint as the evolutionary genetics of Southern Ocean fauna are influenced by signatures of Quaternary glacial-interglacial cycles, oceanic currents and species ecology. Here we examined the genome-wide single nucleotide polymorphisms of the Southern Ocean brittle stars *Ophionotus victoriae* (five arms, broadcaster) and *O. hexactis* (six arms, brooder). We found that *O. victoriae* and *O. hexactis* diverged at ~0.43 million years ago with interspecific gene flow. The species divergence time also coincides with the timing of significant Antarctic Ice Sheet retreat and reduced surface salinity (Marine Isotope Stage [MIS] 11). Since then, *O. victoriae* persisted in deep-sea refugia and *in situ* refugia on the Antarctic continental shelf and around Antarctic islands; *O. hexactis* persisted exclusively within *in situ* island refugia. Within *O. victoriae*, contemporary gene flow linking to the Antarctic Circumpolar Current, regional gyres and other local oceanographic regimes was observed. Gene flow connecting West and East Antarctic islands near the Polar Front was also detected in *O. hexactis*. The evolutionary innovations in *O. hexactis* (increase in arm number and switch to brooding from broadcasting) were linked to selection under intense deglacial meltwater during MIS 11 within Antarctic island refugia, with strong association detected between outlier loci and salinity. Our study highlights that intense interglacial-glacial cycles in the recent past can lead to innovative evolutionary changes and species divergence.

Keywords: evolutionary innovations, glacial refugia, interglacial period, Marine Isotope Stage 11, museum genomics, RAD loci, target capture sequencing

4.2 Introduction

Evolutionary innovation fuels the complexity among species differences and the overall diversity in the global ecosystem, and is one of the fundamental concepts in evolutionary biology. Innovations influence the speciation and radiation of global taxa (marine and terrestrial) (McGee et al., 2015; Arnold & Kunte, 2017) and its definition can be broad; it is commonly defined as trait expression or novel function across a broad range of behavioural, physiological and morphological characteristics (Love, 2003; Moczek et al., 2011). Although innovations can be found everywhere in the natural world, ranging from plants to species with complex nervous systems, the drivers of innovations are often unclear as processes are different across taxa and ecological systems (Wagner, 2011). Understanding evolutionary innovation between closely-related species offers valuable opportunities to pinpoint past demographic events and genotypic signatures of innovations, which in turn can reveal the unique environmental and biological 'building blocks' of evolutionary processes. Evolutionary innovation among closely related species has been discussed within specific environmental and/or ecological contexts, and very often, are presented as case studies within a particular system (e.g. Boissin et al., 2011; Foster et al. 2020). There is evidence that the Southern Ocean could have provided ecological opportunities for evolutionary innovation the past, with cases linked to the Pleistocene glacial cycles (e.g. Wilson et al., 2013; Lau et al., 2021), however, this idea has rarely been explored using genomic techniques.

Understanding the drivers of evolutionary innovation requires knowledge of past and ongoing drivers of genetic patterns, in order to reconstruct demographic events that can explain innovations. The Southern Ocean contains a high diversity of marine benthic fauna (~88% of total Antarctic marine species) (De Broyer et al., 2011), and the majority of modern taxa has diversified and persisted *in situ* since the Mid-Miocene (c. 14 Mya) (Crame, 2018). However, the apparent ecological success of the Southern Ocean benthic fauna has been structured by various environmental changes over time. In the past, their persistence was challenged by the Quaternary glacial-interglacial period, when the Antarctic ice sheet (AIS) repeatedly expanded and contracted over glacial-interglacial cycles. At extreme glacial cycles (e.g. Last Glacial Maximum (LGM, ~20,000 years ago)), the AIS expanded with grounded ice (i.e. ice resting on the seafloor) reaching the edge of the Antarctic continental shelf (Anderson et al., 2002), which in turn completely eroded most of the continental shelf seafloor. Throughout glacial maxima, Southern Ocean benthic fauna could have remained within *in situ* small-scale ice-free areas on the shelf, migrated to the deep sea or to Antarctic islands off the shelf for refuge (Kott, 1969; Brey et al., 1996; Crame, 1997; Thatje et al., 2005; Convey et al., 2009). At extreme interglacial cycles (e.g. Marine Isotope Stage (MIS) 5e, 11), parts of the

AIS likely experienced significant retreats (Dutton et al., 2015). Throughout extreme interglacial cycles, Southern Ocean benthic fauna would have experienced climate change associated with significant ice loss, including temporary habitat expansion for migrations (Strugnell et al., 2018). Evidence regarding where and how benthic taxa survived the Pleistocene glacial-interglacial period remains limited (see review by Lau et al. (2020); *Chapter 1*). Over time, species diversification and gene flow have also been influenced by regional oceanography (e.g. Antarctic Slope Current around the Antarctic Peninsula) (Muñoz-Ramírez et al., 2020) and the Antarctic Circumpolar Current (ACC) (González-Wevar et al., 2017; Moore et al., 2018). More importantly, how different events and processes (e.g. glacial-interglacial survival + oceanic currents + species dispersal and adaptation) structured genetic patterns simultaneously over time and across spatial scales are unclear.

Only species with a wide geographical, circum-Antarctic distribution can offer comprehensive phylogeographic patterns to answer broad evolutionary questions specific to the Southern Ocean. However, these have rarely been investigated thoroughly due to limited sample availability from the region, and a lack of prior knowledge of species ecology and evolutionary history. Many key Southern Ocean regions, particularly East Antarctica (two-thirds of the Antarctic continent), Antarctic islands and the deep sea, are scarcely sampled as they are located away from often-visited national research stations (Griffiths et al., 2014). Biological samples are often stored at room temperature in long-term museum collections (De Broyer et al., 2011), which is generally associated with DNA degradation. Investigation of questions around innovation also requires further effort in order to comprehensively collect and sample closely-related species with known innovations. This presents additional challenges as it would require prior knowledge of both species life histories and evolutionary distance between multiple species, which has only been examined for a handful of Southern Ocean benthic taxa (discussed within Riesgo et al., 2015 and Xavier et al., 2016).

The Southern Ocean brittle stars *Ophionotus victoriae* and *O. hexactis* are closely-related species with known morphological (five arms versus six arms) and reproductive differences (broadcaster vs brooder). They are excellent candidates to test for multiple evolutionary forces across the Southern Ocean. The brittle star *Ophionotus victoriae* Bell, 1902 is commonly found on the Antarctic continental shelf and around Antarctic islands south of the Polar Front (PF) (Sands et al., 2013). It has a circumpolar distribution and has been collected from shallow depths to the deep sea (Lau et al. 2021; *Chapter 2*). *Ophionotus hexactis* is commonly found around Antarctic islands near the PF and is mainly distributed at shallow depths between 0 - 302 m (McClintock 1994; this study). Furthermore, a close phylogenetic relationship between *O. victoriae* and *O. hexactis* E. A. Smith, 1876, has also been proposed

by multiple genetic studies (cytochrome c oxidase subunit I [COI] and exon genomic data) (Hugall et al., 2016; Galaska et al., 2017b), with incomplete lineage sorting between them based on COI data (Lau et al. 2021; *Chapter 2*). The genetic closeness between *O. victoriae* and *O. hexactis* is striking, as the two species have different morphological and functional traits; *O. victoriae* is characterised by five arms and pelagic planktotrophic larvae (Grange et al., 2004), and *O. hexactis* by six arms and brooding larvae (Turner & Dearborn, 1979). Given that echinoderms (including brittle stars) are evolutionarily primed to pentameral symmetry (five arms in brittle stars) (Rozhnov, 2012) and pelagic planktotrophic larvae (Gillespie & McClintock, 2007), it has been hypothesised that the divergent characteristics of *O. hexactis* could be evolutionary innovations linked to survival within glacial refugia around Antarctic islands throughout the Pleistocene (Lau et al. 2021; *Chapter 2*).

Here, we investigate the genetic structure of *O. victoriae* and *O. hexactis* with double-digest restriction-associated DNA (ddRAD) loci, using samples collected throughout most of their distributional range at depths between shallow water and 1,750 m. We utilised a target capture approach to sequence ddRAD-identified loci in degraded samples, which enabled comprehensive sampling of *O. victoriae* and *O. hexactis* collected from around the Southern Ocean, even if samples had been stored in collections over decades. Specifically, we examined i) the genealogical relationship between *O. victoriae* and *O. hexactis*, ii) whether signatures of positive selection linked to *O. hexactis* can be detected, iii) where and how *O. victoriae* and *O. hexactis* survived glacial-interglacial cycles and iv) the drivers behind the present-day genetic structure.

4.3 Methods

4.3.1 ddRAD library preparation and loci discovery for target capture sequencing

Eight mitochondrially divergent *Ophionotus* individuals with high quality gDNA (*Ophionotus victoriae*, n = 6, accession numbers SIOBICE4802C, SIOBICE4777D, WAMZ43231, WAMZ44940, WAMZ44947, WAMZ88551, WAMZ88565; and *O. hexactis*, n = 2, accession numbers SIOBICE4798A, WAMZ43231) were selected for ddRADseq library preparation and sequencing. ddRADseq libraries were prepared at the Australian Genomic Research Facility (AGRF), Brisbane, Australia, following Peterson et al. (2012). Briefly, 250 ng genomic DNA of each sample was digested with restriction enzymes ecoR1 and hpych4IV, ligated with barcoded adapters, pooled digested ligated fragments were size selected using Blue Pippin and the library was amplified via PCR using indexed primers. The library of eight samples

was sequenced on a single lane of the Illumina NextSeq 500 with 150 cycles in MID-output (single end) at AGRF.

Raw ddRAD reads were processed and single nucleotide polymorphisms (SNPs) were called by AGRF using their genotyping-by-sequencing (GBS) in house Perl script based on *Stacks* v1.47 (Catchen et al., 2011). Raw reads were first trimmed and demultiplexed using *process_radtags*. ddRAD loci were assembled *de novo* with each module (*ustacks*, *cstacks*, *sstacks*, *genotypes*, *population*) executed individually. Reads were aligned and sorted with a maximum distance of two nucleotides between stacks (-M 2), minimum stack depth of two (-m 2), maximum distance of four nucleotides allowed to align secondary reads to primary stacks (-N 4) (values recommended by Catchen et al. (2011)), as well as disabling haplotype calls from secondary reads in *ustacks*. A loci catalog was built with one mismatch allowed between sample tags (-n 1) in *cstacks*, and samples were verified against the catalog in *sstacks*. Sample genotypes from common variants were then identified in *genotypes* with automated corrections (-c), a minimum of one progeny required per marker (-r 1), a minimum of five reads to call homozygous genotype (--*min_hom_seqs* 5). The options --min_het_seqs (0.05) and --max_het_seqs (0.1) were used to check that the genotype was correctly called based on ratio of the depth of the smaller allele to the bigger allele. The *population* module was performed to retain genotype calls with at least 10x coverage. Reads were then further filtered using *VCFtools* v0.1.16 (Danecek et al., 2011), with sites only retained if present across all samples (--max-missing 1) and with at least a minor allele frequency of 0.01 (--*maf* 0.01). A total of 8,113 ddRAD loci shared across all eight *Ophionotus* individuals were identified and selected for target capture bait design.

4.3.2 Bait design for target capture sequencing

The consensus sequence (140 base pair [bp]) of the filtered ddRAD loci were used for custom biotinylated RNA bait manufacturing at Arbor Bioscience (Ann Arbor, MI, USA). Input sequences were soft-masked (0.5%) for simple repeats using *RepeatMasker* v4.0 (Smit et al., 2015), and candidate bait sequences were designed based on bait length (90 nucleotides per bait) and 2 X tiling per locus. Candidate baits were BLAST filtered against the provided sequences based on hybridisation temperatures and were retained if they have most ten hits between 62.5 - 65ºC and two hits above 65ºC, and fewer than two passing baits on each flank. The final myBaits® (Arbor Bioscience) panel contained 16,061 baits and targeted 8,075 loci with at least one bait.

4.3.3 Sample collection and DNA extraction for target capture sequencing

Tissue samples of *Ophionotus victoriae* (n = 218) and *O. hexactis* (n = 40) deposited at Western Australian Museum (WAM), Museum Victoria (MV), Scripps Institution of Oceanography (SIO-BIC) and the National Institute of Water and Atmospheric Research (NIWA) were sequenced in this study (Fig 4.1). All *Ophionotus* samples were a subset of a previous study which analysed their COI data (Lau et al. 2021; *Chapter 2*).

4.4.4 Library preparation and target capture sequencing

Genomic DNA of all *Ophionotus* samples (n = 258) were sent to Arbor Biosciences for library preparation and target enriched sequencing. The DNA shearing step was avoided as most samples experienced DNA degradation. Samples were converted into libraries with unique index adapters and libraries were pooled into capture reactions (six libraries per capture). Twelve *O. victoriae* samples with extremely degraded DNA were identified during DNA quantification after extraction (< 0.04 ng/µL). Their libraries were not multiplexed with other samples (Supplementary Table 4.1); their libraries were processed in individual capture reactions to avoid capture bias that can occur against extremely degraded samples. All libraries were enriched in capture reactions using myBaits® following the manufacturer's protocol and resulting capture reactions were sequenced on Illumina NovaSeq S4 with 150 bp paired end reads.

4.4.5 Target capture reads processing, mapping and variant calling

Raw data were demultiplexed with barcodes removed using *process_shortreads* in *Stacks* v2.3d (Catchen et al., 2013). Reads with phred quality less than 20 (Q < 20) were discarded, and polyG in read tails (a problem with NovaSeq due to 2-colour chemistry) were trimmed, using *fastp* v0.20 (Chen et al., 2018). Potential contaminants (human and microorganisms) were identified using *Kraken* v1.0 (Wood & Salzberg, 2014), and reads that matched those of the contaminant database were removed. Reads were then truncated to a final read length of 140 bp. Cleaned and trimmed reads were checked for quality using *fastQC* v0.11.7 (Andrews, 2019), and mapped to the consensus sequences of ddRAD loci used for bait design using *bwa* v0.7.17 *mem* with default parameters (Li & Durbin, 2009). *Samtools* v1.7 (Li et al., 2009) was used to sort alignments by coordinates, and PCR duplicates were marked and removed using *picard* v2.18.1 (Broad Institute, 2019). Variants and short indels were called across all samples using *bcftools* v1.7 *mpileup* (Li et al., 2009).

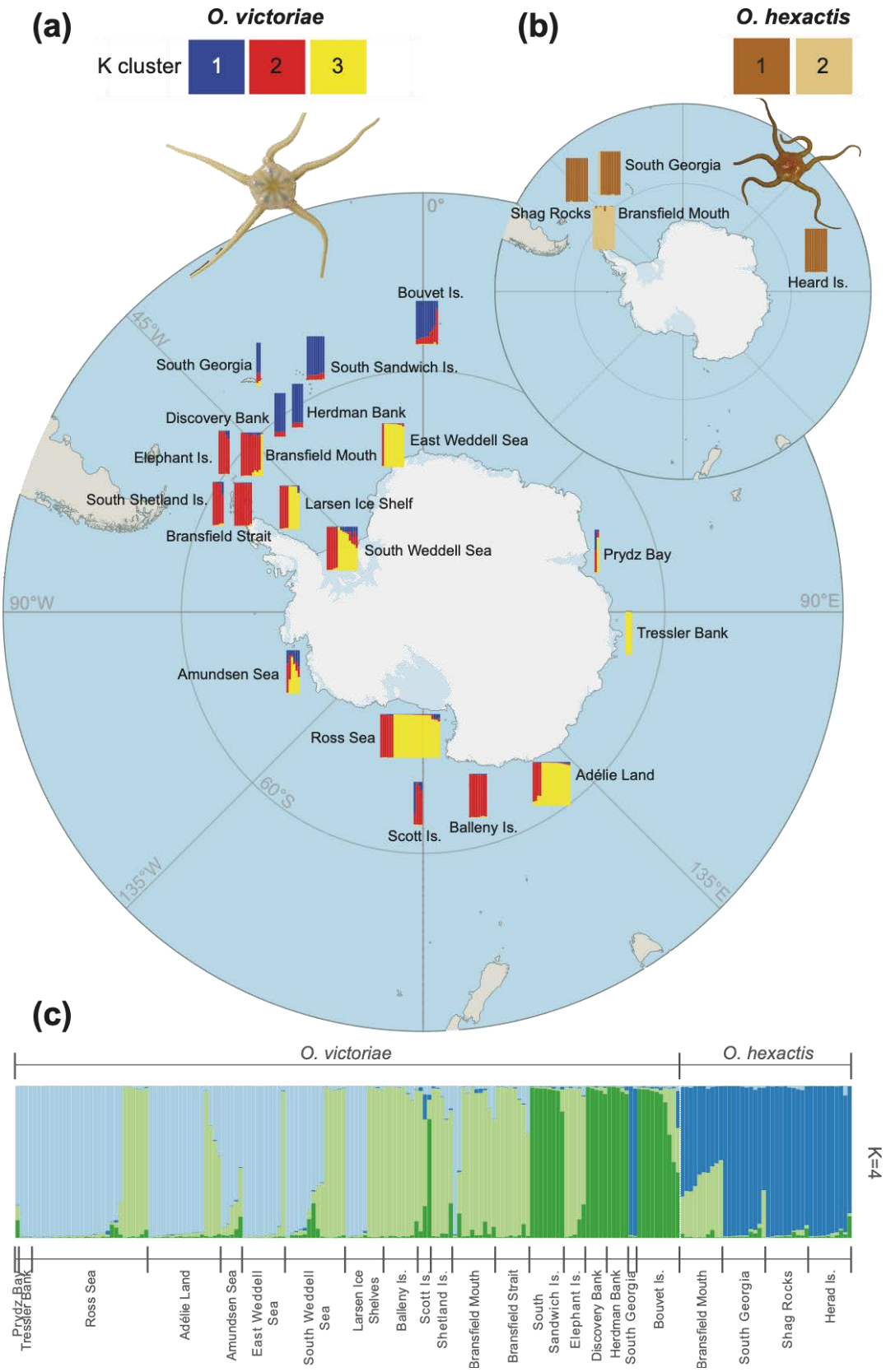

Fig 4.1 Map of Southern Ocean with sampling locations and admixture proportions, based on ddRAD loci data, within (a) *Ophionotus victoriae* (n = 158) and (b) *O. hexactis* (n = 40). (c) Admixture proportions between *O. victoriae* and *O. hexactis* (n = 195). Each vertical bar represents one individual sample, colours correspond to admixture proportion estimations derived from *Structure* analyses (only optimal values of *K* are presented in the main figure).

Three SNPs datasets were created for subsequent analyses, and *VCFtools* was used to perform variant filtering on the raw variant calls. Prior to SNP filtering, the first dataset included all samples from both *O. victoriae* and *O. hexactis* (n = 258), the second dataset included only samples from *O. victoriae* (n = 218), and the third dataset included only samples from *O. hexactis* (n = 40). Within all three datasets, indels and samples with high missing data on an individual basis (> 80%) were first removed, and high quality SNPs were retained based on the following steps. First, sites with Phred quality score more than 30 were kept (--minQ 30). Then, sites with mean read depth of less than 10x and greater than 32x (=2*average depth (15.8x)) were removed (--min-meanDP 10, --max-meanDP 32). Sites were kept if they were biallelic (--min-alleles 2, --max-alleles 2), and if present in 70% of all samples (--max-missing 0.7), and with a minor allele frequency of at least 2% were kept (--maf 0.02). To remove sites that likely belonged to paralogous loci and therefore artificial SNPs, only sites with a maximum observed heterozygosity of 0.5 were kept, following Hohenlohe et al. (2011) and Gargiulo et al. (2020), identified via the R package *adegenet* v2.1.3 (Jombart & Ahmed, 2011). Lastly, only one site per locus was kept (--thin 140). The final datasets included *O. victoriae* (n = 155) and *O. hexactis* (n = 40) with 1,781 SNPs in dataset 1, *O. victoriae* (n = 158) with 1,653 SNPs in dataset 2, and *O. hexactis* (n = 40) with 2,209 SNPs in dataset 3.

4.4.6 Data analyses

4.4.6.1 Genetic structure between and within species

The overall levels of genetic differentiation between species, and among sample locations within species, were assessed via population statistics. Observed (H_o) and expected (H_e) heterozygosities, and the fixation index, were calculated using *GenoDive* v3.0 (Meirmans, 2020). Neutrality test, Tajima's D, was calculated using the R package *PopGenome* v2.7.5 (Pfeifer et al., 2014). Values of H_o, H_e and Tajima's D between species were also calculated excluding samples that exhibited strong signatures of intraspecific admixture, i.e. *O. victoriae* from South Georgia (n = 2) and *O. hexactis* from Bransfield Mouth (n = 10).

Principal Component Analysis (PCA) was performed using *adegenet* to examine the species boundaries between *O. victoriae* and *O. hexactis* (dataset 1), and whether genetically distinct clusters were present within species (dataset 2 and 3). The alleles contributing the most to the discriminant functions (at 0.999 quantile) between *O. victoriae* and *O. hexactis* (dataset 1) were examined using Discriminant Analysis of Principal Components (DAPC; *loadingplot*) via *adegenet*. Genetic structure between species (using dataset 1), and among sample

locations within species (using dataset 2 and 3) were also examined via *Structure* v2.3.4 (Pritchard et al., 2000). *Structure* was performed to assign individuals to genetic clusters (*K*). *Structure* was run for *K* = 1 - 10 with ten replicates per *K* via *Structure_threader* (Pina-Martins et al., 2017). Each run was performed with 500,000 iterations and burn-in of 100,000. As preliminary runs without prior information found weak genetic structure in all datasets, prior information of species information (dataset 1) or sample locations (dataset 2 and 3) was used to assist clustering in all *Structure* runs (LOCPRIOR 1). LOCPRIOR models are useful as they do not artificially inflate genetic structure. They assume prior information may be informative regarding ancestries and are able to ignore prior information when they are not correlated with individual samples' ancestries (Pritchard et al., 2000). The meaningful *K* per dataset was evaluated based on the highest mean log likelihood [mean LnP(*K*)] and delta*K* statistics using *Structure Harvester* v0.6.94 (Earl & VonHoldt, 2012).

4.4.6.2 Population tree with admixture

TreeMix v1.13 (Pickrell & Pritchard, 2012) was performed to infer a maximum likelihood (ML) tree topology within each species, as well as to calculate a covariance matrix to infer historical splits and mixture between populations, using dataset 1 (1,781 SNPs). *TreeMix* is a complimentary method to *Structure*, while *Structure* assigns individuals into discrete genetic clusters, *TreeMix* models how the populations may have arisen and outlines the genealogical relationship between populations (Pickrell & Pritchard, 2012). For *TreeMix* analysis within *O. victoriae*, all individuals *of O. hexactis* were assigned as outgroup for tree rooting. Populations within *O. victoriae* were classified by clustering individuals from neighbouring sample locations with similar admixture proportions based on the *Structure* analysis (optimal *K* = 4 in dataset 1). This approach was also utilised in other studies where populations were not clearly defined by discrete geographical locations (e.g. Thom et al., 2020). For *TreeMix* analysis within *O. hexactis*, all individuals *of O. victoriae* were assigned as outgroup. Populations within *O. hexactis* were classified by sample sites, as the genetic structure of *O. hexactis* can be defined by geographical locations (based on *Structure* analysis of dataset 1).

Migration edges (m) were modelled between 0 and 10 in *O. victoriae*, and between 0 and 5 in *O. hexactis*. Ten replicates per each migrant edge were generated using the bootstrap option with a block size of 1. The best *TreeMix* model with the optimal number of migration edges for each species was evaluated based on residuals of the covariance matrix, as well as the simple exponential and non-linear least square model (threshold = 0.05) using the R package *OptM* v0.1.3 (Fitak, 2019). Confidence of migration events was also evaluated using

jackknife p values, f_3 and f_4 statistics implemented within *TreeMix*. For detailed description of *TreeMix*, see the "Population tree with admixture" section in Supplementary Note 4.1.

4.4.6.3 Gene flow between and within species

Genetic differentiation between species (dataset 1) and among locations within species (dataset 2 and 3) was examined with pairwise F_{ST} values, calculated using *GenoDive* with 10,000 permutations to test for significance. Post hoc Bonferroni correction was applied to account for multiple pairwise comparisons. When calculating pairwise F_{ST} between locations within O*. victoriae*, samples from South Georgia were excluded due to low sample size (n = 2). Samples of O*. victoriae* from Tressler Bank (n = 3) and Prydz Bay (n = 2) were also pooled together and defined as 'East Antarctica' in order to increase overall sample size, and to evaluate the genetic differentiation between East Antarctica versus West Antarctic and Antarctic island localities.

Directional relative migration and among locations within species (dataset 2 and 3), was also examined using *divMigrate* (Sundqvist et al., 2016) via the R package *DiveRsity* v1.9.89 (Keenan et al., 2013). *divMigrate* evaluates the directional migration rates by comparing the geometric means of allele frequencies between user defined populations (Sundqvist et al., 2016). For *O. victoriae* and *O. hexactis divMigrate* analyses, genetic differentiation, between and within species, were calculated using *Nm* (i.e. effective number of migrants) (Alcala et al., 2014), which incorporates information from both G_{ST} (i.e. genetic differentiation based on allele fixation) and *D* (i.e. genetic differentiation based on genetic composition). Ten thousand bootstrap iterations were used to assess whether gene flow between populations was significantly asymmetric. However, it should be noted that *divMigrate* might not be able to accurately estimate the directionality of gene flow when migration rates are high (Melosik et al., 2019). When comparing gene flow between locations within *O. victoriae*, locations with n > 5 were randomly subsampled to n = 5, samples from Tressler Bank (n = 3) and Prydz Bay (n = 2) were also pooled together and defined as 'East Antarctica' (i.e. n = 5), and samples from Scott Island (n = 4) and South Georgia (n = 2) were excluded from analysis.

4.4.6.4 Genotype environmental association analysis

Redundancy analysis (RDA) was performed to detect genome-wide adaptations to environmental variables in the Southern Ocean, specifically the proportion of genetic variation explained by each identified environmental predictor within a multivariate environment, as well as the putative outlier SNPs with significant statistical association with

environmental predictors. Environmental data (sea surface temperature and salinity, bottom water temperature and salinity, water depths, latitudes and longitudes) were extracted from existing datasets or sample information.

RDA was performed using the R package *vegan* v2.5-6 (Oksanen et al., 2013), and separate RDA was performed a) between samples of *O. victoriae* and *O. hexactis* (dataset 1), b) among samples, within *O. victoriae*, with samples separated by deep continental shelf (> 1000 m), shallow continental shelf (< 1000 m) and Antarctic islands (dataset 2), and c) among sample locations within *O. hexactis* (dataset 3). Within each RDA, multicollinearity between environmental predictors was assessed using the R package *psych* v1.9.12 (Revelle, 2020) (cut-off threshold at r = 0.7). All environmental variables were retained in the analyses between *O. victoriae* and *O. hexactis*, and within *O. victoriae*. However, for the analysis of *O. hexactis*, strong correlations were observed so only the variables of bottom salinity, bottom sea water temperature and water depths were retained in the final RDA.

Environmental data from each sample location (sea surface temperature and salinity, water bottom temperature and salinity) were extracted from World Ocean Atlas 2018 (Locarnini et al., 2018; Zweng et al., 2018), using *QGIS* (QGIS Development Team, 2019), following Lau et al. (2021; *Chapter 2*). Information of water depths, latitudes and longitudes were provided based on sampling information. One sample collected from Amundsen Sea (JR179 cruise; sample ID: SL-5) was omitted from genotype environmental association analysis as the precise sampling location was lost.

The significance (at $\alpha = 0.05$) of each full RDA model was assessed via ANOVA with 999 permutations, and Variance Inflation Factors were assessed for further evidence of multicollinearity between environmental predictors within each RDA model. RDA was also used to identify the SNP loadings in the ordination space to assess whether SNPs are associated with environmental predictors (i.e. SNPs under selection as a function of environmental predictors). Outlier SNPs were identified through the distribution of SNP loadings on each significant RDA axis. SNPs that exhibit more than ± 3 standard deviations from the mean loading were identified as outliers, a threshold that minimises type I and II error as suggested in Forester et al. (2018). Associations between putative outlier SNPs and environmental variables were evaluated using Pearson correlation coefficient.

4.4.6.5 Outlier loci detection and gene ontology

Loci under putative selection between species and within species were identified using

genetic differentiation outlier analyses; *OutFLANK* v.02 (Whitlock & Lotterhos, 2015), *BayeScan* v2.1 (Foll & Gaggiotti, 2008), *PCAdapt* v4.3.2 (Privé et al., 2020) and RDA. For *OutFLANK* and *BayeScan*, individuals can be pre-defined as different populations and thus samples were grouped between species (dataset 1) and within species (dataset 2 and 3). Between species (dataset 1), samples for *O. victoriae* from South Georgia were categorised as *O. hexactis* due their limited genetic differentiation from *O. hexactis*. Within *O. victoriae* (dataset 2), samples were separated among those collected from the deep continental shelf (> 1000 m), shallow continental shelf (< 1000 m) and around Antarctic islands. Within the *O. hexactis* (dataset 3), samples were separated among sample locations.

For *BayeScan* analyses, prior odds were set to 100, followed by 20 pilot runs and 100,000 iterations with 5,000 samples, burn-in length of 50,000 and thinning interval of 10. *OutFLANK* analyses were performed default parameters and a *q*-value threshold of 0.01. *PCAdapt* analyses were performed with scree plots used to select the optimal principal component (*K*), and outlier SNPs were determined via the Benjamini-Hochberg Procedure with a p-value threshold (alpha) of 0.01.

Loci that were identified as outliers by two or more tests (*OutFLANK*, *BayeScan*, *PCAdapt*, RDA) were considered to be putatively under selection. The consensus sequences (140 bp) of all putative outlier loci were compared within the National Center for Biotechnology Information (NCBI) database (Agarwala et al., 2018) using the BLASTx (Altschul et al., 1990) search tool to determine their identities. Hits returned with a maximum E value of 1×10^{-3} and a percent identity of at least 80% were considered as significant matches. The consensus sequences of outlier loci were also translated to protein sequences in all six reading frames (standard code), and were searched against the *InterPro* (Blum et al., 2020) protein database using *InterProScan* (Jones et al., 2014) in *Geneious* (https://www.geneious.com). *InterProScan* results were also used to infer gene ontology IDs.

4.4.6.7 Variant filtering - additional filtering for SFS-based inferences

For past demographic inference (*dadi* v2.1.1) (Gutenkunst et al., 2009) using dataset 1, and *StairwayPlot* v2.1.1 (Liu & Fu, 2015, 2020) analyses using dataset 2 and 3, SNPs were converted into folded site frequency spectrums (SFS) (i.e. no outgroup information was used). Filtering thresholds were relaxed in order to retain the maximum number of informative loci for demographic events, as the signals of true demographic events would be much stronger than a few erroneous loci (Gargiulo et al., 2020). Instead of filtering for minor allele frequency of at least 2%, sites with a minor allele count of one (--mac 1) were kept in

order to only exclude singletons. A heterozygosity cut-off of 0.7 was applied following Gargiulo et al. (2020). All SNPs per locus were retained in order to maximise the number of sites in the observed SFSs. For SFS-based inferences, a generation time of ten years was assumed based on information about minimum disc size at sexual maturity (based on females) (Grange et al., 2004) and average disc size across age of *O. victoriae* (Dahm & Brey, 1998). A mutation rate of 1.43×10^{-8} per site per generation was used based on the tip substitution rate of the *O. victoriae* and *O. hexactis* branch among global ophiuroid species (0.0015924; substitution/site/myr) (O'Hara et al., 2019)

4.4.6.8 Past population size changes within species

Past effective population size (N_e) changes within *O. victoriae* (using dataset 2; n = 158 with 10,572 SNPS) and *O. hexactis* (using dataset 3; n = 40 with 11,416 SNPs) were reconstructed using *StairwayPlot*. *StairwayPlot* is a model flexible method that infers past population size changes over specific points in a genealogy through 1-dimensional site frequency spectrum (1d-SFS). *Stairway plot* was chosen to further explore past population size changes within species instead of demographic models (e.g. *dadi*) as it is not constrained by a-priori information, which can in turn explore a larger model space than parameterised demographic models (Liu & Fu, 2015). For *StairwayPlot* input, folded 1d-SFSs were generated using easySFS.py (https://github.com/isaacovercast/easySFS) with down projection to 222 and 56 haploid samples, respectively, in order to maximise the number of segregating sites. For model input, the total sequence length of 277,760 and 345,660 was applied for *O. victoriae* and *O. hexactis* respectively. The total sequence length was defined as the number of loci retained after SNP filtering (=1,984 in O*. victoriae* and 2,469 in *O. hexactis*) x length of locus (140 bp). Each run was performed with a random starting seed. The percentage of sites used for training was 67%, and the number of random break points for each run were (nseq-2)/4, (nseq-2)/2, (nseq-2)*3/4, nseq-2, based on default values.

4.4.6.9 Demographic modelling between *O. victoriae* and *O. hexactis*

The divergence and connectivity between *O. victoriae* and *O. hexactis* were investigated via the diffusion approximation framework within *dadi*. We explored the relationship between *O. victoriae* and *O. hexactis* using all samples of dataset 1 (n = 195), but excluded samples with signals of strong interspecific admixture, i.e. *O. victoriae* from South Georgia (n = 2) and *O. hexactis* from Bransfield Mouth (n = 10). Thus, the total sample size was n = 183 with 24,649 SNPs. A total of nine demographic models were fitted against the folded 2-dimensional joint site frequency spectrum (2d-SFS) between *O. victoriae* and *O. hexactis*. The examined

demographic models ranged from simple (three parameters) to complex (ten parameters) biologically relevant scenarios, including divergence followed by strict isolation, continuous migration, ancient migration, secondary contact and past population size changes (Supplementary Fig 4.1).

For *dadi* input, folded 2d-SFS was generated using easySFS.py. The haploid sample size of [*O. victoriae*, *O. hexactis*] in the input dataset was down projected [144, 32] in order to maximise the number of segregating sites for *dadi*, as recommended by Gutenkunst et al. (2009). Each *dadi* model was run with four consecutive rounds of optimisation using the *dadi_pipeline* v3.1.6 with default features (Portik et al., 2017). Parameters of the best fit models were converted into biologically meaningful units. For detailed description of *dadi* inference and model evaluations, see the "*dadi* inference between *O. victoriae* and *O. hexactis*" section in Supplementary Note 4.2.

4.4 Results

4.4.1 Read quality

A total of 83,789,628 raw reads were obtained from the eight *Ophionotus* samples during ddRAD loci discovery, with an average of 10,473,704 reads ± 2,042,156 SD per sample. After SNP filtering with no missing data allowed and maf of at least 1%, the loci discovery dataset included 8,113 ddRAD loci for target capture bait design. After target capture sequencing of all *Ophionotus* samples (n = 258), a total of 847,967,674 raw reads were obtained, with an average of 4,583,609 reads ± 2,543,496 SD per sample, as well as an average depth of 15.8x (across sites per sample).

4.4.2 Genetic diversity and population structure

Both *O. victoriae* and *O. hexactis* exhibited higher observed than expected heterozygosity, as well as negative inbreeding coefficients (Table 4.1). Within each species, samples at each locality also demonstrated higher observed than expected heterozygosity and negative inbreeding coefficients (Table 4.1). Removal of samples exhibiting strong intraspecific admixture led to lower levels of observed and expected heterozygosity and inbreeding coefficients. Both species and all their respective samples localities were associated with negative Tajima's D values.

Table 4.1 Genetic diversity and neutrality tests of *Ophionotus victoriae* and *O. hexactis* across geographical locations based on target capture sequencing of ddRAD loci.

		Sampled depth range (m)	Number of samples	Observed heterozygosity (H_o)	Expected heterozygosity (H_e)	Inbreeding coefficient (F_{IS})	Tajima's D
O. victoriae	all samples	0-1750	158	0.157	0.136	-0.157	-1.272
	all but excluding South Georgia	0-1750	156	0.148	0.131	-0.127	-0.607
Continental shelf	Prydz Bay	213-270	2	0.160	0.144	-0.109	NA
	Tressler Bank	758-779	3	0.154	0.135	-0.14	-1.106
	Ross Sea	0-1376	27	0.155	0.136	-0.141	-1.169
	Adélie Land	22-1204	17	0.151	0.133	-0.138	-1.284
	Amundsen Sea	998-1208	6	0.180	0.151	-0.196	-0.150
	East Weddell Sea	250-615	10	0.167	0.145	-0.152	-1.077
	South Weddell Sea	282-1750	14	0.148	0.131	-0.133	-1.272
	Larsen Ice Shelves	320-682	9	0.155	0.136	-0.133	-1.276
Antarctic islands	Balleny Islands	85-350	8	0.159	0.138	-0.146	-1.113
	Scott Island	144-403	4	0.188	0.157	-0.194	NA
	South Shetland Islands	183	5	0.153	0.133	-0.148	-0.940
	Bransfield Mouth	302-349	10	0.162	0.141	-0.15	-0.893
	Bransfield Strait	213-292	8	0.153	0.134	-0.142	-1.162
	South Sandwich Islands	116-230	8	0.152	0.130	-0.164	-1.047
	Elephant Island	143-202	5	0.149	0.131	-0.134	-1.183
	Discovery Bank	439	5	0.154	0.13	-0.185	-0.876
	Herdman Bank	600	5	0.156	0.132	-0.182	-0.512
	South Georgia	167-190	2	0.164	0.137	-0.195	NA
	Bouvet Island	300	10	0.146	0.126	-0.164	-0.872
O. hexactis	all	131-302	40	0.170	0.148	-0.144	-1.188
	all but excluding Bransfield Mouth	131-203	30	0.152	0.130	-0.172	-0.984
Antarctic islands	Bransfield Mouth	302	10	0.170	0.145	-0.168	-0.969
	South Georgia	119	10	0.169	0.149	-0.132	-1.244
	Shag Rocks	131-180	10	0.174	0.152	-0.138	-1.169
	Heard Island	203	10	0.166	0.146	-0.137	-1.188

PCA indicated an overall separation between *O. victoriae* and *O. hexactis*, with 4.35% of the total genetic variance explained by the first two PCs (Fig 4.2a). Two *O. victoriae* samples (ID: SIOBICE6508 and SIOBICE6420) from South Georgia were observed within the *O. hexactis* cluster (Fig 4.2a). On PC1 and PC2 axes, individuals of *O. victoriae* from Scott Island, Bouvet Island and Bransfield Mouth showed close proximity to *O. hexactis* from Bransfield Mouth (Supplementary Fig 4.2a).

Genotypic clustering using *Structure* suggested that *K* = 2 and *K* = 4 are useful indications of admixture proportions across *O. victoriae* and *O. hexactis* samples (Fig 4.1c, Supplementary Fig 4.3). The *K* = 4 model was favoured as the preferred *K* value as the levels of admixture observed between species and within species were also observed within the PCA (Fig 4.2). At *K* = 4, *O. hexactis* was represented overall by a distinct genetic cluster, but *O. victoriae* from South Georgia cannot be differentiated from *O. hexactis* (Fig 4.1c). Individuals of *O. hexactis* from Bransfield Mouth were distinct from *O. hexactis* from other locations by displaying genetic admixture with *O. victoriae* (most notably from Bransfield Mouth, Bransfield Strait, Elephant Island, South Shetland Islands and Balleny Islands). Three loci (CLocus-61907, CLocus-137845 and CLocus-172167) were identified as the most contributing variables to the discriminant functions at 0.999 quantile (Supplementary Fig 4.4). Major and minor allele frequency at these three loci were also examined between species, with *O. victoriae* from South Georgia and *O. hexactis* from Bransfield Mouth also visualised as separate clusters. At CLocus-61907, *O. victoriae* from South Georgia share similar allele frequencies with *O. hexactis* samples (overall and from Bransfield Mouth). At CLocus-137845 and CLocus-172167, similar major and minor allele frequencies were observed between *O. victoriae* (overall) and *O. hexactis* from Bransfield Mouth. Similar allele frequencies were also shared between *O. hexactis* (overall) and *O. victoriae* from South Georgia (Supplementary Fig 4.4).

Within *O. victoriae*, PCA indicated samples from South Sandwich Islands, Discovery Bank and Herdman Bank are slightly separated from the rest of sampled localities (Supplementary Fig 4.2b). *Structure* suggested *K* = 2 and *K* = 3 admixture models within *O. victoriae* (Fig 4.1a, Supplementary Fig 4.5). The *K* = 3 model was favoured as the preferred K as the admixture patterns captured are also supported by the PCA (Fig 4.2). When samples were grouped by depth-related habitats (i.e. those collected from the deep continental shelf [> 1000 m], shallow continental shelf [< 1000 m] and around Antarctic islands), samples from all three habitats showed close proximity to each other on PC1 and PC2 axes, with divergence observed within shallow continental shelf and Antarctic islands. *Structure* suggested that at *K* = 3, *O. victoriae* individuals from the continental shelf and Antarctic islands were generally separated by distinct genetic clusters, with connectivity between the

two regions (Fig 4.1a). *Ophionotus victoriae* samples from deep continental shelf (> 1000 m) also exhibited unique admixture with samples from Antarctic islands, as observed on the PCA (Supplementary Fig 4.2b).

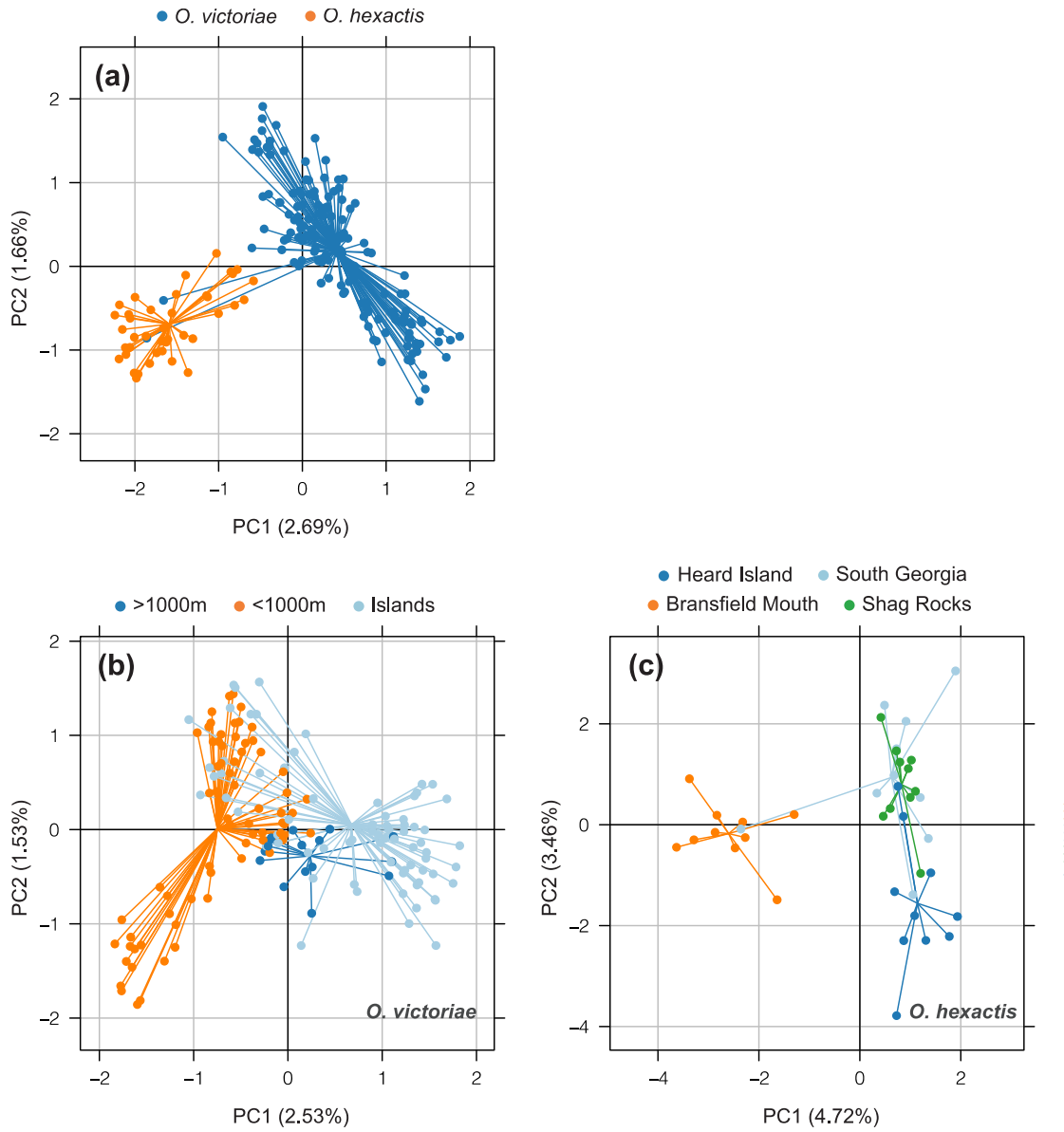

Fig 4.2 Principal component analysis (PCA) results on the first two axes including (a) samples of *Ophionotus victoriae* and *O. hexactis* (n = 195); (b) within *O. victoriae* with samples grouped by those collected on the deep Antarctic continental shelf (> 1000 m), shallow Antarctic continental shelf (<1000 m) and around Antarctic islands (off the shelf, south of Polar Front) (islands) (n = 158); (c) within *O. hexactis* with samples grouped by geographical locations (n = 40).

Within *O. hexactis*, PCA indicated an overall difference between samples from Bransfield Mouth and other locations (South Georgia, Shag Rocks and Heard Island) (Fig 4.2c). One sample from South Georgia was found within the Bransfield Mouth cluster. A lack of genetic differentiation was observed between samples from South Georgia and Shag Rocks.

Samples from South Georgia and Shag Rocks also showed limited differentiation to those from Heard Island. *Structure* suggested *K* = 1 and *K* = 2 admixture models within *O. hexactis* samples (Fig 4.1b, Supplementary Fig 4.6). The *K* = 2 model was preferred as the PCA also indicated samples from Bransfield Mouth can be distinguished as an isolated genetic cluster (Fig 4.2c). *Structure* suggested that at *K* = 2, samples from Bransfield Mouth (+ one sample from South Georgia) were characterised by a distinct genetic cluster, with no differentiation observed between samples from South Georgia, Shag Rocks and Heard Island (Fig 4.1b).

4.4.3 Population tree with admixture within species

TreeMix revealed samples of *O. victoriae* from South Georgia were closely related to *O. hexactis* (Fig 4.3a). Post hoc evaluation (non-linear least squares and simple exponential models) supported m = 1 as the optimal number of migration edges within *TreeMix* threshold modelling. A jackknife significance test also indicated m = 1 significantly improved the model fit to the observed allele frequency data. The final *TreeMix* model with m = 1 explained 90.2% of the total variance. On the ML population tree of *O. victoriae*, short internal branches with limited genetic drift were observed at each locality (Fig 4.3a). Stepwise population splits were observed between Scott Island, Discovery Bank + Herdman Bank + South Sandwich Islands (grouped together), and Bouvet Island. Samples from the Ross Sea, East Weddell Sea and Amundsen Sea form a distinct cluster, with migration detected from the Amundsen Sea to the South Weddell Sea. Gene flow between the Amundsen Sea and the South Weddell Sea was further supported by f_3- and f_4 statistics (Z-score < -3) (Supplementary Table 4.2-4.3). The range of the *TreeMix* residuals was small (up to ± 4.4 SE) and most were close to zero between paired localities within species (Supplementary Fig 4.7a, b), suggesting the final *TreeMix* models were a good fit to the observed data.

TreeMix also revealed *O. hexactis* formed two separate clades, with individuals from Bransfield Mouth grouped in a single clade, and individuals from Shag Rocks, South Georgia and Heard Island grouped in a separate clade. Overall, *O. hexactis* from Bransfield Mouth were most closely related to *O. victoriae* on the ML tree (Fig 4.3b). Post hoc evaluation (non-linear least squares and simple exponential models) supported m = 2 and m = 1 as the optimal number of migration edges within *TreeMix* threshold modelling, respectively. However, a jackknife significance test showed migration edges did not significantly improve the model fit to the observed allele frequency data. No admixture between populations was detected in f_3-statistics (Supplementary Table 4.4). f_4-statistics indicated gene flow either between *O. victoriae* and *O. hexactis* from Bransfield Mouth, or between Shag Rocks, South Georgia and Heard Island within *O. hexactis*. (Supplementary

Table 4.5). The final *TreeMix* model of *O. hexactis* included no migration edge and explained 96.7% of the total variance.

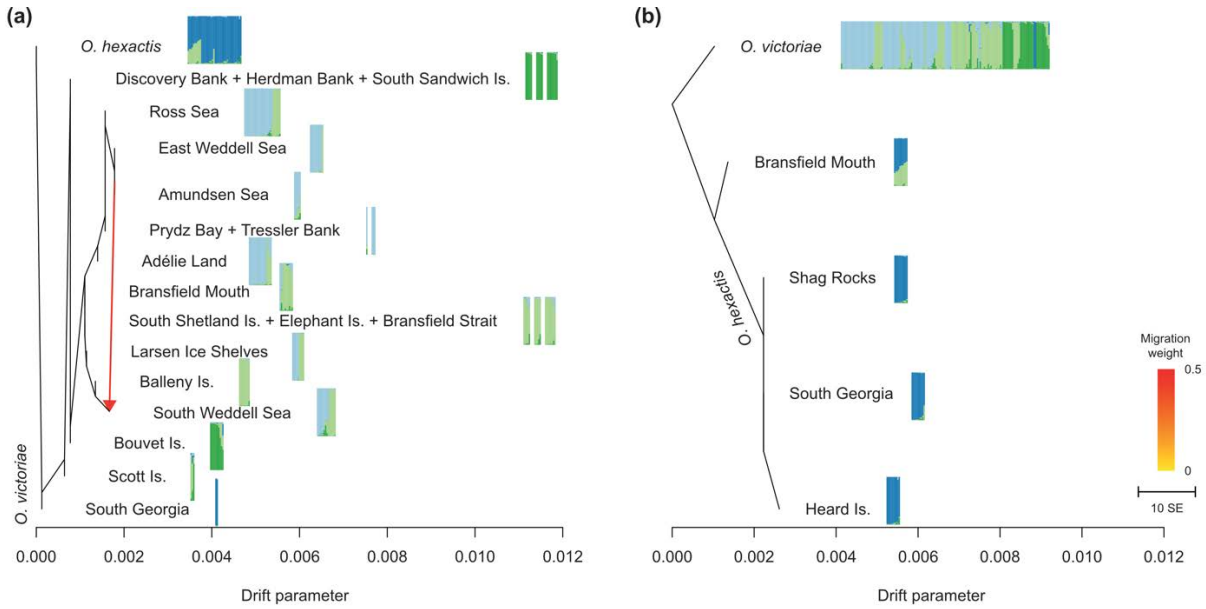

Fig 4.3 *TreeMix* maximum likelihood (ML) tree of (a) *Ophionotus victoriae* (n = 165) rooted with *O. hexactis* (n = 40), and (b) *O. hexactis* (n = 40) rooted with *O. victoriae* (n = 165). Terminal nodes are subdivided based on neighbouring geographical locations with similar admixture proportions estimated by *Structure* (preferred *K* = 4). Horizontal branch lengths are proportional to the amount of genetic drift occurred on each branch. In the bar plots, each vertical bar represents one individual sample from the corresponding geographic location/s, with colours corresponding to admixture proportion estimations. (a) Optimal migration edge of 1 (Amundsen Sea -> South Weddell Sea) was inferred by simple exponential and non-linear least square model, and was also supported by f_4-statistic and jackknife significance test (p = 0.0005). (b) Optimal migration edge of 0 was inferred by simple exponential and non-linear least square model and was also supported by f_4-statistic and jackknife significance test. Migration edge was coloured based on migration weight, which corresponds to the % ancestry in the sink population originated from the source population.

4.4.4 Environmental association analyses

When comparing *O. victoriae* and *O. hexactis* (with two *O. victoriae* samples from South Georgia included as *O. hexactis*) in the RDA, constrained ordination significantly explained 2.17% (adjusted R^2, $p < 0.001$) of the overall genetic variation with all six environmental variables. The first three constrained PC axes significantly explained 39.0, 16.3 and 13.3% of the total adjusted R^2 ($p < 0.001$). On PC1 and 2, between species, *O. hexactis* showed a general positive association with water temperature (Fig 4.5a). Within *O. victoriae*, constrained ordination significantly explained 0.88% (adjusted R^2, $p < 0.001$) of the overall genetic variation with five environmental variables. The first two constrained PC axes

significantly explained 27.3 and 19.7% of the total adjusted R^2 ($p < 0.001$). On PC1 and 2, within *O. victoriae*, samples from the deep continental shelf (> 1000 m) exhibited a positive association with water depth, and those collected around Antarctic islands exhibited a positive association with sea surface temperature (Fig 4.5b). Within *O. hexactis*, constrained ordination significantly explained 2.26% (adjusted R^2, $p < 0.001$) of the overall genetic variation with three environmental variables. The first three constrained PC significantly explained 40.9%, 31.1% and 28.0% of the total adjusted R^2 ($p < 0.05$). On PC1 and 2, samples of *O. hexactis* from the Bransfield Mouth showed a positive association with water depth, but negative associations with bottom water salinity were observed in samples from Heard Island (Fig 4.5c).

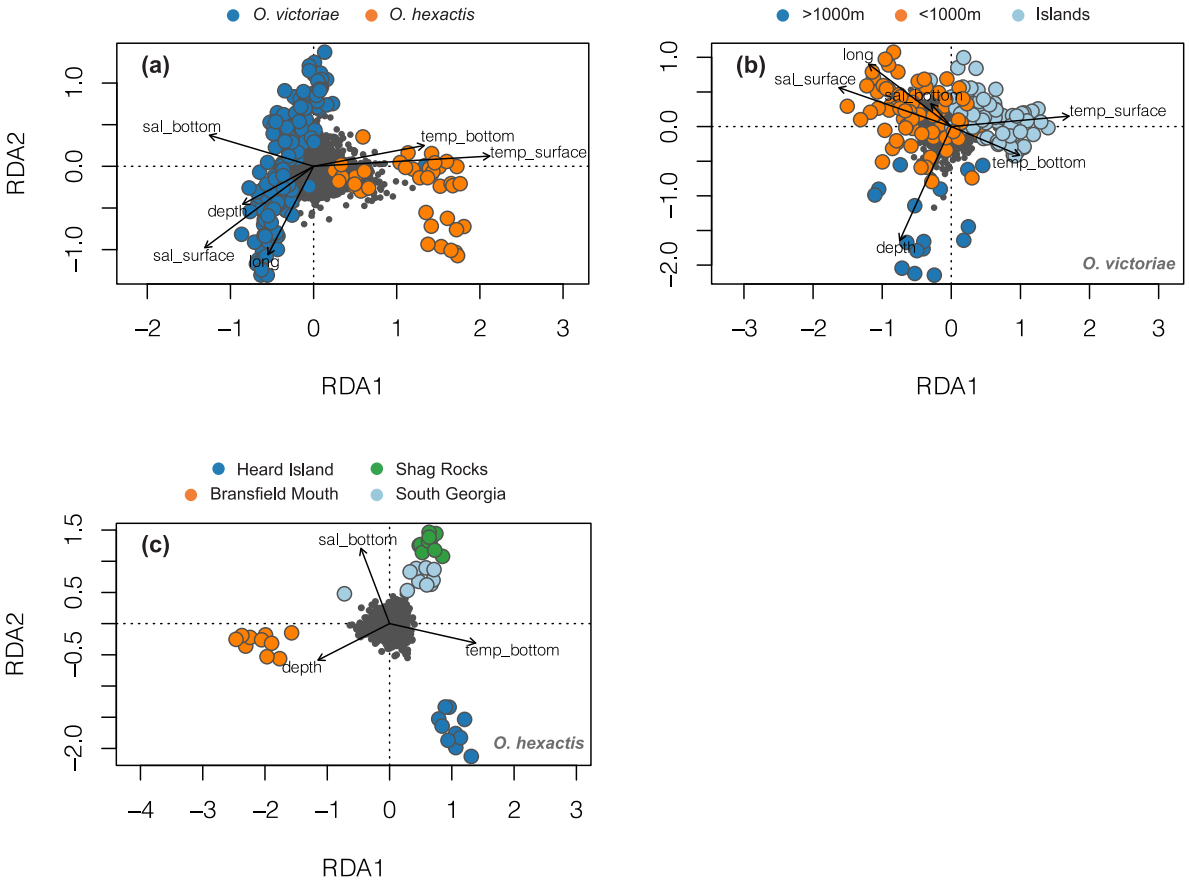

Fig 4.4 Redundancy analysis (RDA) showing genotype-environment association in *Ophionotus victoriae* and *O. hexactis* on the first two constrained axes. Grey dots represent SNPs, and coloured circles represent individual sample defined by assigned labels. Vectors represent environmental predictors, including surface water salinity (sal_surface), bottom water salinity (sal_bottom), surface water temperature (temp_surface), bottom water temperature (temp_bottom), water depth (depth). (a) Samples of *O. victoriae* and *O. hexactis* defined by species (n = 195). (b) Samples of *O. victoriae* defined by deep continental shelf (>1000 m), shallow continental shelf (<1000 m) and Antarctic islands (n = 158). (c) Samples of *O. hexactis* defined by geographical locations (n = 40).

4.4.5 Outlier loci

Based on the outlier loci detected by at least two methods (*PCAdapt*, *OutFLANK*, *RDA* and *BayeScan*), a total of 30, 25 and 11 loci were identified as putative outliers between species, within *O. victoriae* and within *O. hexactis*, respectively (Supplementary Fig 4.8, Supplementary Table 4.6). No outlier loci were matched with the BLASTx database under the search criteria. One outlier locus (Clocus-186281) detected between species had a positive match to the InterPro database with GO annotations (Ionotropic glutamate receptor, InterPro ID: IPR001320) (Supplementary Table 4.7). RDA also predicted outlier loci correlated with selected environment variables on the significant constrained axes. When comparing *O. victoriae* and *O. hexactis* samples, outlier loci were correlated with bottom water salinity (n = 22), surface water salinity (n = 16), water depth (n = 14), sea bottom temperature (n = 7) and longitude (n = 3) (Supplementary Table 4.6). Within *O. victoriae*, outlier loci were correlated with water depth (n = 14), sea surface temperature (n = 8) and sea surface salinity (n = 5) (Supplementary Table 4.6). Within *O. hexactis*, outlier loci were correlated with bottom water temperature (n = 9), bottom water salinity (n = 7) and water depth (n = 4) (Supplementary Table 4.6).

4.4.6 Gene flow within species

Within *O. victoriae*, various levels of gene flow (*Nm* between 0.21 and 1) were observed between all locations (Fig 4.5a, Supplementary Table 4.8), and no significant asymmetric gene flow was detected by *divMigrate*. Relatively high gene flow (*Nm* > 0.8) was inferred within and between the Antarctic continental shelf and Antarctic island localities. Pairwise F_{ST} values also supported the overall gene flow estimation by *divMigrate*, where no significant differentiation was observed in most areas detected with high gene flow (Supplementary Table 4.9).

Within *O. hexactis*, an overall high level of gene flow was observed between locations (*Nm* between 0.54 and 1), with no significant asymmetric gene flow detected by *divMigrate* (Fig 4.5b, Supplementary Table 4.10). Relatively high gene flow (*Nm* > 0.8) was inferred between South Georgia, Shag Rocks and Heard Island (Fig 4.5b). However, pairwise F_{ST} values suggested significant differentiation between individual sample localities ($p < 0.001$; Supplementary Table 4.11).

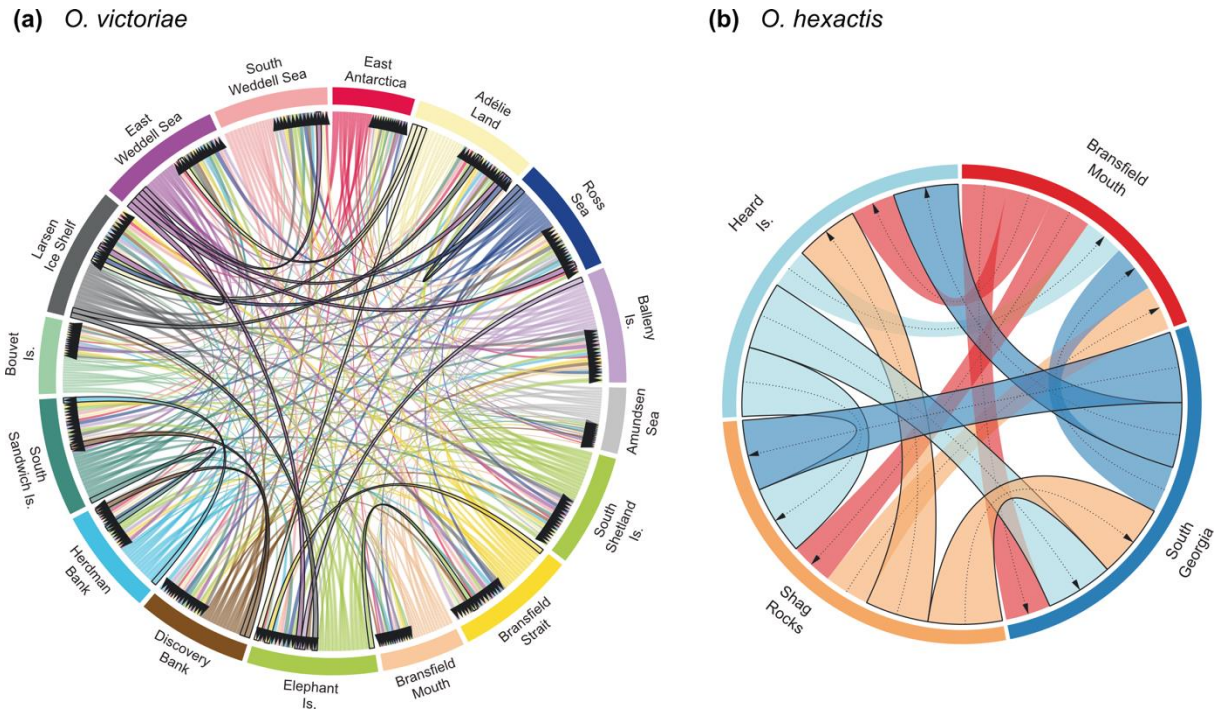

Fig 4.5 Relative migration (*Nm*) estimated by *divMigrate* within (a) *Ophionotus victoriae* and (b) *O. hexactis*. East Antarctica included samples from Prydz Bay and Tressler Bank. Sample sizes were balanced between locations within species after random sub-sampling (a) n = 5, (b) n = 10. Arrows indicate the direction of gene flow. Black borders highlight migration values above 0.8 for better visualisation of source-sink populations with high gene flow. No significant asymmetric migration was observed between locations within species (10,000 bootstrap iterations).

4.4.7 Demographic modelling between species

Out of the nine models that examined the divergence and gene flow between *O. victoriae* and *O. hexactis*, isolation with migration (IM) returned as the best model based on AIC values (5604.34), model score (1.00) and residual plots compared to observed data (Supp Fig 4.6, supplementary Table 4.12). With this model, *O. victoriae and O. hexactis* diverged at 434,307 years ago (95% confidence interval between 433,399 and 435,212), with continuous asymmetric gene flow between species (Table 4.2).

Upon inspecting the 1d-SFS of the observed *O. victoriae* and *O. hexactis* data (excluding samples with strong interspecific admixture), both species are characterised by a W-shaped SFS with internal peak at intermediate frequencies; a stronger peak was observed within *O. victoriae* (Fig 4.6a). The observed 2d-SFS between *O. victoriae* and *O. hexactis* also indicated a lack of intermediate frequencies SNPs shared between *O. victoriae and O. hexactis* (Fig 4.6a, b). However, *dadi* attempted to model these missing SNPs, leading to high residual values at sites with intermediate frequencies (Fig 4.6b).

Table 4.2 Parameter estimates of the best demographic model explaining the divergence and gene flow between *Ophionotus victoriae* and *O. hexactis* (with 95% confidence intervals presented). 95% confidence intervals were generated from 100 block-bootstrapped datasets. Analysed dataset excluded samples with strong intraspecific admixture, including *O. victoriae* samples from South Georgia and *O. hexactis* samples from Bransfield Mouth. Values are scaled to biological meaningful units.

Model	Nref	nu1	nu2	m12	m21	T
IM	1658.05 (1596.05 - 1722.47)	49356.79 (49347.91 - 49365.68)	3885.15 (3840.55 - 3930.27)	4.764×10^{-6} (4.748×10^{-6} - 4.781×10^{-6})	1.523×10^{-3} (1.403×10^{-3} - 1.5654×10^{-3})	434307.40 (433399.15 - 435217.55)

Abbreviations:
Nref: The effective size of the ancestral population before split
nu1: The effective size of *O. victoriae*
nu2: The effective size of *O. hexactis*
T: The time of divergence between split and present in years
m12: The neutral movement of genes from *O. hexactis* to *O. victoriae* in units of 2Nref generations
m21: The neutral movement of genes from *O. victoriae* to *O. hexactis* in units of 2Nref generations

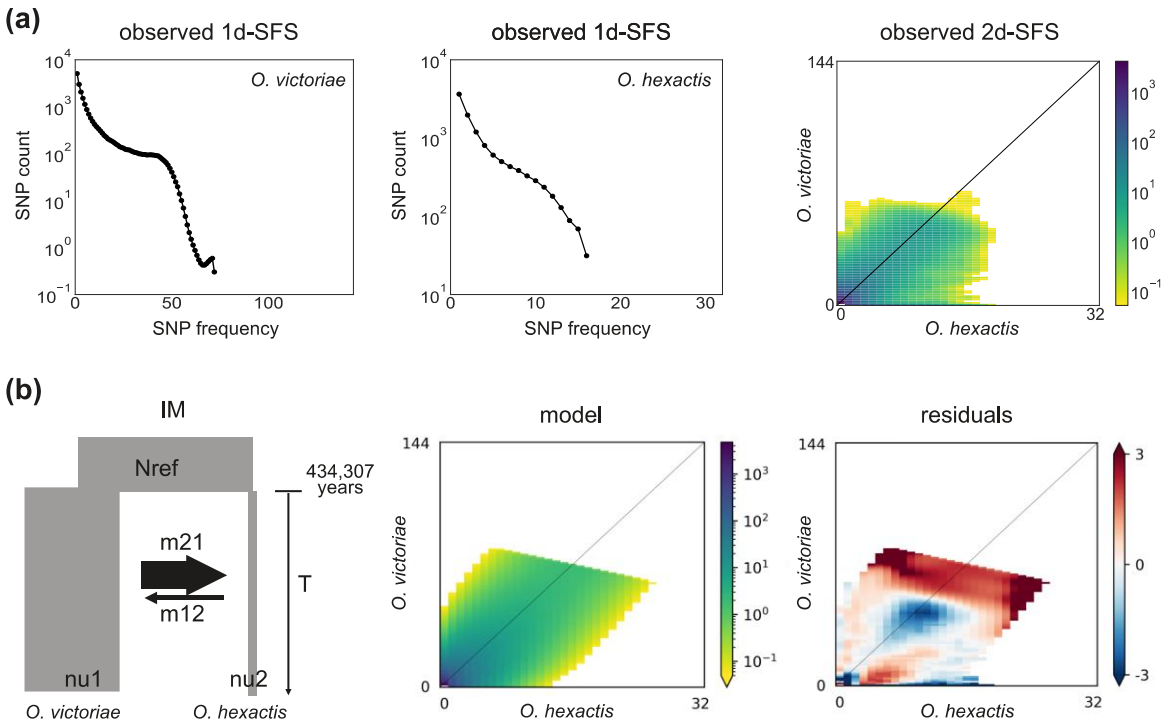

Fig 4.6 Summary of the site frequency spectrums (SFS) of the best supported demographic model (IM) and observed data sampled from *Ophionotus victoriae* and *O. hexactis*, excluding samples of *O. victoriae* from South Georgia and *O. hexactis* from Bransfield Mouth with strong interspecific admixture. (a) One-dimensional (1d-) and two-dimensional (2d-) SFS of the observed data. (b) 2d-SFS of the schematic presentation of the best fit model, 2d-SFS predicted from model and the model residuals compared to the observed data. IM: isolation with continuous migration. Arrows represent migration rates, with thicker line represented by higher migration rates. Width of boxes represents the effective population size of ancestral population (Nref), and of *O. victoriae* (nu1) and *O. hexactis* (nu2). T = time of divergence with continuous migration until present time.

4.4.8 Past changes in effective population size within species

Within *O. victoriae*, when samples were grouped by deep continental shelf (> 1000m), shallow continental shelf (< 1000 m) or Antarctic islands, a recent population bottleneck was inferred in shallow continental shelf (< 1000 m) and Antarctic islands (Fig 4.7a). Samples of *O. victoriae* from the deep continental shelf were associated with a population size decline since ~350,000 years ago, with gradual increase in population size since ~100,000 years ago (Fig 4.7a). Within *O. hexactis*, for samples from the Bransfield Mouth, a gradual population decline was inferred at ~150,000 years ago, followed by a stable population size since ~70,000 years ago (Fig 4.7b). A recent and sharp population bottleneck was observed in samples from South Georgia + Shag Rocks + Heard Island (grouped together) (Fig 4.7b).

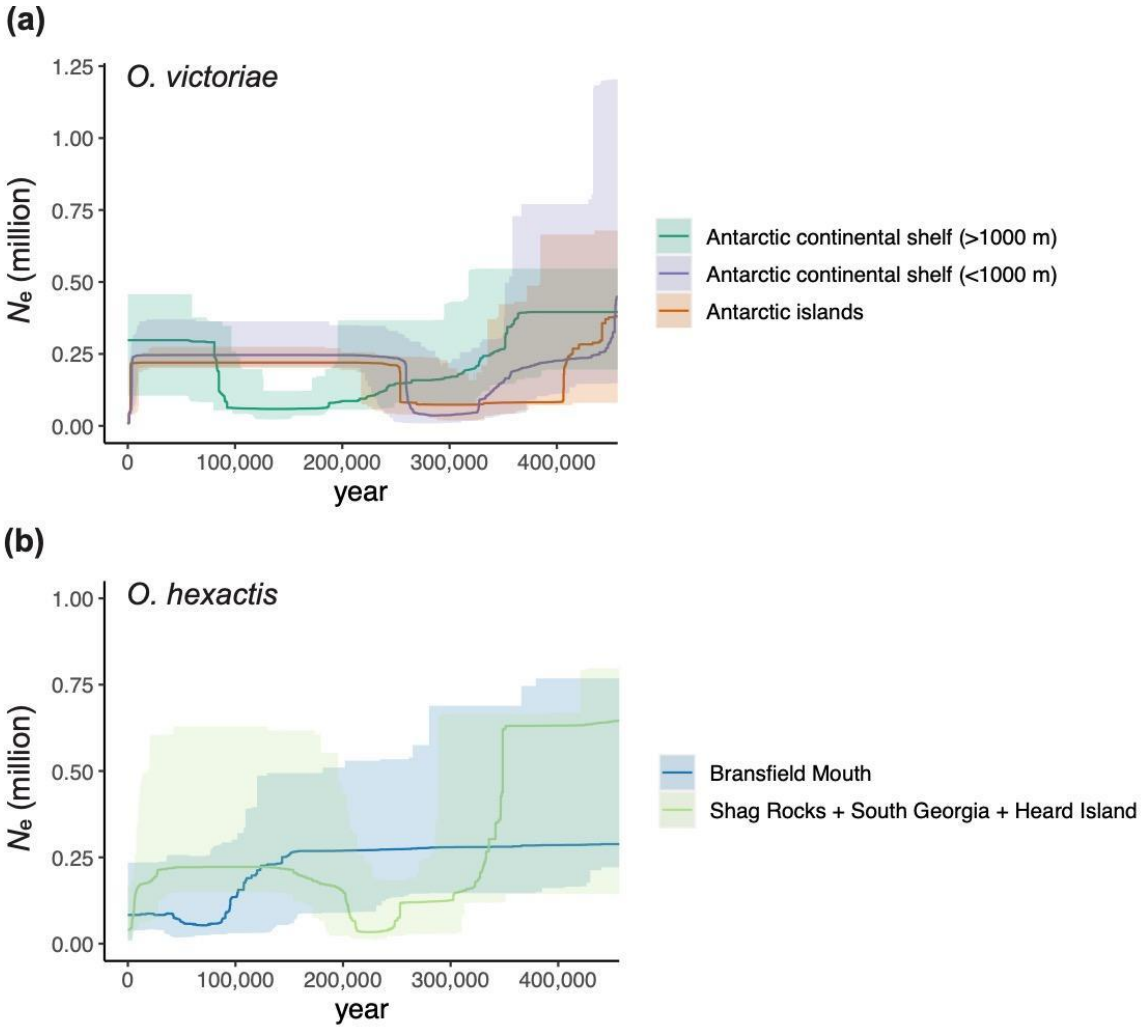

Fig 4.7 *StairwayPlot* estimates of past effective population size (N_e) changes over multiple epochs (a) within *Ophionotus victoriae* with samples defined by deep continental shelf (> 1000 m), shallow continental shelf (< 1000 m) and Antarctic islands, and (b) within *O. hexactis* with samples defined by geographical locations. Shaded areas represent 95% confidence intervals. Lines represent median values.

4.5 Discussion

4.5.1 Gene flow between *Ophionotus victoriae* and *O. hexactis*

The target capture of ddRAD loci data presented here suggest *Ophionotus victoriae* and *O. hexactis* are closely related species with evidence of ongoing gene flow. A previous study based on mitochondrial (COI) and 2b-RAD data focusing on samples from West Antarctica suggested *O. victoriae* contains up to four distinct lineages, possibly representing multiple cryptic species (Galaska et al., 2017b). A later study based on COI data focusing on samples from both West and East Antarctica suggested *O. victoriae* constitutes a single species with a circumpolar distribution (Lau et al. 2021; *Chapter 2*). The genomic data here also supports *O. victoriae* as a single species with a circumpolar distribution containing multiple (three) intraspecific admixed lineages. Based on PCA, these lineages do not represent cryptic species as there is no disjunct structure within *O. victoriae*, thus indicating *O. victoriae* is a genetically diverse and widely distributed species across the Southern Ocean.

The genomic data also suggest some *O. victoriae* individuals from Bransfield Mouth, and all individuals from South Georgia, show evidence of admixture with *O. hexactis* where they overlap. Distinctly different admixture signals were observed at the Bransfield Mouth and South Georgia, possibly indicating independent occasions (over time and/or across spatial scale) of gene flow between species. Additionally, at the three most differentiated loci contributing to the discriminant functions, *O. victoriae* from South Georgia share similar major and minor allele frequencies with *O. hexactis*, with *O. hexactis* from Bransfield Mouth also share similar major and minor allele frequencies with *O. victoriae*. Excluding samples with interspecific admixture, demographic modelling further suggested stronger migration rate from *O. victoriae* to *O. hexactis* since species divergence, suggesting opportunities for admixture could be greater in one direction than the other.

Interestingly, the observed 1d-SFS of both species are associated with a peak at intermediate frequencies across genome wide data (W-shaped SFS), which can be linked to a high admixture rate with more than one ancestral allele being introduced at previously fixed sites (Marchi & Excoffier, 2020), balancing selection (Cheng & Degiorgio, 2020), associative overdominance (heterozygous advantage at neutral loci) (Gilbert et al., 2020) or a recent bottleneck (Charlesworth & Jain, 2014). The alleles associated with this peak appear to be species specific, as a lack of alleles at intermediate frequencies was shared between *O. victoriae* and *O. hexactis*. We could not distinguish the drivers behind such peak, as *O. victoriae* and *O. hexactis* have experienced dramatic changes in demographic

history linked to the Pleistocene glacial-interglacial cycles that could lead to any of the above scenarios (see below). In this case, we highlight that SFS-based inference could be limited by historical demographic processes involving allele frequency changes beyond model assumptions.

4.5.2 Genetic connectivity within *O. victoriae* with pelagic larvae

Individual admixture proportions showed strong admixture across geographical locations in *O. victoriae,* highlighting the species' potential for dispersal, possibly driven by current dynamics. Overall, *Structure* suggests *O. victoriae* can be characterised by three distinct genetic groups, with two separate genetic groups (genetic cluster 1 and 2 of $K = 3$; blue and red on Fig 4.1a) linked to the Scotia Arc and Antarctic islands, and one genetic cluster (cluster 3) mainly found on the Antarctic continental shelf. Genetic cluster 1 was distinct to the islands away from the Antarctic continental shelf, possibly highlighting uncharacterised or stochastic local oceanographic regimes linking these areas near the Polar Front.

The genetic structure of *O. victoriae* in genetic cluster 2 as most frequently represented genetic cluster, also reflects circumpolar connectivity between the Antarctic continental shelf and Antarctic islands. Many of the island locations of genetic cluster 2 coincide with the southern boundary of the ACC (sbACC) (Sokolov & Rintoul, 2009), suggesting the distribution of cluster 2 could be driven by the eastward flowing ACC. In addition, the biogeography of cluster 2 in the central Scotia Arc, Larsen Ice shelf and South Weddell Sea coincides with the circulation pattern of Antarctic Slope Current that travels from the Larsen Ice Shelves to the West Antarctic Peninsula (WAP) (Collares et al., 2018). Gene flow related to the Antarctic Slope Current along the WAP has been reported in the Antarctic bivalve *Aequiyoldia eightsii* (Muñoz-Ramírez et al., 2020). The presence of genetic cluster 2 in the Ross Sea also suggests a relationship between sbACC and the Ross Gyre in larval dispersal. Although the sbACC does not penetrate through the Ross Sea, it connects to the contours of the Ross Gyre (Dotto et al., 2018). The Ross Gyre is a cyclonic regional gyre in the Southern Ocean which connects the ACC to the Ross Sea continental shelf, which would explain the presence of cluster 2 connecting Adélie Land, the Balleny Islands, Scott Island and the Ross Sea. Strong gene flow was also detected from the Ross Sea to Adélie Land by *divMigrate*, further suggesting the directionality of the Ross Gyre (from West to East against the ACC), and its role structuring gene flow in the region.

Further evidence of circularity could also be observed in *O. victoriae* on the Antarctic continental shelf. Samples collected from the shelf are characterised by a single genetic cluster (genetic cluster 3 of $K = 3$; yellow on Fig 4.1a), suggesting genetic homogeneity

around the shelf. Connectivity around the Antarctic continental shelf has also been observed in other Southern Ocean benthic species with pelagic larvae linking to the ACC (Matschiner et al., 2009; Raupach et al., 2010; Hemery et al., 2012; Sands et al., 2015). Alternatively, circulatory genetic pattern could also be explained by the Antarctic Slope Current (counter clockwise circumpolar current), which has recently been found to drive circumpolar connectivity in Southern Ocean benthic species (*Chapter 6*).

4.5.3 Genetic connectivity within *O. hexactis* with benthic larvae

As for *O. hexactis*, both strong population structure and admixture were observed among locations across the Southern Ocean. In particular, distinct population structure was observed within Bransfield Mouth, which separates this location from other localities (South Georgia, Shag Rocks and Heard Island). Strong admixture was also observed among South Georgia, Shag Rocks and Heard Island (additionally supported by high gene flow detected between these areas), even though some of these locations are separated by long geographical distance across the Southern Ocean. Together, the evidence suggests both long-distance dispersal and genetic isolation are possible for Southern Ocean benthic species with non-pelagic dispersal.

Previous studies have highlighted that Southern Ocean benthic brooders can be characterised by geographical structure due to their limited dispersal ability across the vast Southern Ocean (Moreau et al., 2017, 2019). However, most of the current genetic evidence outlining distinct segregated population structure in Southern Ocean brooding species or species with benthic juveniles are linked to the islands within the Scotia Arc (Linse et al., 2007; Hoffman et al., 2011a; Strugnell et al., 2017). Additionally, it has been argued that some brooding species exhibit genetic connectivity across the Southern Ocean (reviewed within Halanych & Mahon (2018)). For *O. hexactis*, around West Antarctica, it appears that locations within (Shag Rocks and South Georgia) and outside (Bransfield Mouth) of the Scotia Arc are highly separated, indicating the physical seascape dynamics within the Scotia Arc system could promote genetic isolation and diversification, as suggested for other Southern Ocean species (Demarchi et al., 2010; Hoffman et al., 2011b; Verheye et al., 2016). However, the barriers linked to isolation within Bransfield Mouth are permeable, as one *O. hexactis* sample from South Georgia also falls within the genetic cluster distinct to Bransfield Mouth.

Beyond the Bransfield Strait, individuals sampled around South Georgia, Shag Rocks and Heard Island were associated with long-distance connectivity. This likely reflects the abilities of *O. hexactis* to travel long-distances as adults, for example via rafting along the ACC,

which has also been observed in other Southern Ocean brooding species (Nikula et al., 2010). It must be said that *O. hexactis* are mostly found on flat muddy substrates and do not typically wrap their arms around other organisms or substrates, yet the dispersal signals are nonetheless apparent.

4.5.4 Genomic signatures of Southern Ocean glacial cycle survival

4.5.4.1 Deep-sea refugia in *O. victoriae*

During glacial maxima, the deep seafloor of the Southern Ocean was not impacted by the continentally-grounded ice sheets. The large deep-sea habitable area was hypothesised to enable refugial populations to persist, maintain and/or expand in size and diversify (Allcock & Strugnell, 2012). In *O. victoriae*, a strong genotype-environmental association with depth was observed in deep-water samples (> 1000 m), suggesting isolation-by-water depth. Isolation-by-depth is expected when populations have been stable over time, spatially neighbouring populations are more genetically similar to each other, and diverging populations are isolated by selective forces on ecology and reproductive barriers (Wright, 1943). Therefore, the strong genotype association with depth is likely linked to long-term diversification within deep-sea refugia. Population expansion was also detected in samples collected from > 1000 m after ~100,000 years ago, corroborating the hypothesis that populations in deep water could maintain population size throughout glacial cycles, including during the LGM.

It is likely that signatures of deep-water refugia represent a single connected refugium. Samples of *O. victoriae* from the deep continental shelf (> 1000 m) are observed in sites that are separated by long-distances across the Southern Ocean (Ross Sea, Adélie Land, Amundsen Sea and South Weddell Sea). If deep-water refugia were geographically structured within *O. victoriae*, isolation-by-distance and subsequent genetic drift would be expected to create distinct structure associated with each refugium. When samples of *O. victoriae* from > 1000 m were analysed together, these samples are highly connected while strong signals of deep-water refugia were highlighted by separate analyses (RDA, *StairwayPlot*).

4.5.4.2 *in situ* shelf and island refugia

Even during the most extreme glacial maxima (such as the LGM), where the grounded ice from the AIS eroded most of the Antarctic continental shelf habitat, pockets of ice-free areas have been proposed to exist along the continental shelf edge around the Southern Ocean,

as well as around some Antarctic islands (Thatje et al., 2005). *In situ* refugia in the Southern Ocean were hypothesised to enable small populations to persist throughout glacial cycles and would be characterised by signatures of bottlenecks followed by population expansion (Allcock & Strugnell, 2012). For *O. victoriae*, the overall negative neutrality tests (all sequences pooled) suggest this species experienced population bottleneck followed by expansion. *StairwayPlot* further indicated a recent strong bottleneck in *O. victoriae* from shallow continental shelf sites (< 1000 m) and around Antarctic islands, suggesting *O. victoriae* also persisted *in situ* on the Antarctic continental shelf and around the Antarctic islands. Although genetic structure distinct to either the continental shelf or Antarctic islands was observed within *O. victoriae*, location-specific structure was not detected, likely due to the low and uneven sample size between locations. Therefore, the exact locations of *in situ* glacial refugia cannot yet be pinpointed. Moreover, observed heterozygosity is higher than expected heterozygosity at all locations in *O. victoriae*, which could be possible indications of admixture between previously isolated populations (the isolate-breaking effect; Karamanlidis et al., 2018). After the LGM, benthic fauna that persisted in Southern Ocean glacial refugia are hypothesised to have recolonised ice-free areas during deglaciation (Thatje et al., 2005). However, the extent and pathways of recolonisation from Southern Ocean refugia are unclear. At least in *O. victoriae*, the higher-than-expected heterozygosity observed at all locations, and high gene flow between locations, suggest recolonisation could have been widespread across the continental shelf and Antarctic islands following gene flow driven by oceanic currents (see above), and that each location could have received migrants from differing refugial populations.

As for *O. hexactis*, signatures of *in situ* refugia were detected around Antarctic Islands. Negative neutrality tests and *StairwayPlot* showed *O. hexactis* appeared to have experienced population bottlenecks at all sampled locations, suggesting signatures of *in situ* refugial survival. Interestingly, *O. hexactis* from Bransfield Strait is characterised by stable population structure since ~70,000 years ago, as well as with an association with water depth. The current evidence possibly highlights that the LGM grounded ice sheets did not completely erode the deeper habitable areas in Bransfield Strait where *O. hexactis* could have persisted. Ice sheet reconstructions also indicate areas where *O. hexactis* could have found refuge (Bransfield Mouth, Shag Rocks and Heard Island) that were not (or only partially) impacted by grounded ice (Hodgson et al., 2014; Simms et al., 2011), further supporting the case of *in situ* refugia in these areas.

Inference of population size changes via *StairwayPlot* appears to have limited power in detecting repeated bottlenecks, and that very often, only the most recent bottleneck would be inferred by the model (Liu & Fu, 2015). Therefore, the signatures of population

bottlenecks detected in *O. victoriae* and *O. hexactis* are possibly linked to the LGM, the last time when most of the shelf and some island habitats were destroyed by grounded ice. However, *dadi* suggested both species diverged at approximately at ~434,307 years ago, spanning multiple interglacial-glacial cycles. It is likely then that *O. victoriae* and *O. hexactis* did persist in their respective refugia throughout the late Pleistocene. While the population size inference of *O. victoriae* and *O. hexactis* could be related to LGM refugia, the current evidence does not preclude the possibilities of prior population bottlenecks and *in situ* refugia reflecting older glacial cycles. Additionally, since *StairwayPlot* detected population bottlenecks continuing to the present, it could be that *O. victoriae* and *O. hexactis* have adapted to the colder waters of glacial conditions, with a few short warm interglacial periods, including the Holocene, throughout their species history. A previous study has also demonstrated *O. victoriae* is incapable of acclimating to +2 °C (Peck et al., 2009). In this sense, the decline in population size could be linked to the current Holocene condition, which might not be ideal for their survival.

4.5.5 Evolutionary innovations in *O. hexactis* linked to a historical warm interglacial

The divergence time between *O. victoriae* and *O. hexactis* estimated by *dadi* was approximately at ~434,307 years ago. Interestingly, based on exon data, the node that joins *O. hexactis* to *O. victoriae* was dated to 1.64 (0.53 – 5.79) mya (O'Hara et al., 2017), where our divergence estimation concurs with the lower range of this uncertainty. This is likely due to exonic regions being highly conserved relative to the highly variable RAD loci, thus exonic data are suitable in detecting deep time phylogenetic signals whilst RAD loci are more suitable for detecting population and species level divergence (Carter et al., 2021). Nonetheless, both exon and RAD data converge upon a recent species divergence time. Around 428,000 - 397,000 years ago (Marine Isotope Stage [MIS] 11), the global climate was experiencing an unusually long interglacial period, when the air temperature was 2 °C warmer than the preindustrial period with sea level 6 to 13 m higher than today (Dutton et al., 2015). The divergence of *O. victoriae* and *O. hexactis* likely coincided with an extremely warm interglacial period in the past.

It has been hypothesised that the Antarctic Ice sheet could have experienced significant melting during MIS 11 (Raymo & Mitrovica, 2012), which would result in lower-salinity outflow towards the upper Southern Ocean (Jacobs et al., 1996). *Ophionotus hexactis* persisted *in situ* around Antarctic islands at relatively shallow depths (0 - 302 m) throughout the late Pleistocene. Therefore, the innovations of six arms and brooding of *O. hexactis* were likely influenced by the low salinity meltwater given that this species would have been directly exposed to the deglacial meltwater, with environmental association analysis (RDA)

also detected 61% of the outlier loci were linked to salinity. The evolutionary innovations of six arms and brooding in *O. hexactis* could reflect its ecological success within the Pleistocene Southern Ocean under low salinity regime and island refugia. In brittle stars, increased in arm numbers are related to water pumping motions of solid matter transport, escape strategies and coordination (Clark et al., 2019; Wakita et al., 2019, 2020). The decentralised nervous system in brittle stars also mean that any arm can act as the responsive leading arm upon stimulus sensing, thus individuals with higher number of arms (six or seven) can lead to a more random escape pattern compared to those with 5 arms (Wakita et al., 2020). Arm numbers are also positively related to coordinated locomotion in brittle stars (Clark et al., 2019). Finally, one of the outlier loci identified between *O. hexactis* and *O. victoriae* matched with the protein-coding gene of ionotropic glutamate receptor. This receptor has been found to be a chemoreceptor gene within the olfactory organs of a crown-of-thorns starfish (Roberts et al., 2018), as well as arm autotomy in crinoid *Antedon mediterranea* (Wilkie et al., 2010), suggesting possible selection for enhanced prey sensing and/or escape responses. Interestingly, it has been reported that, when under captivity, *O. victoriae* exhibits a stress response with a lack of feeding behaviour and a high degree of arm autotomy (Fratt & Dearborn, 1984). The increase in arm number within *O. hexactis*, based on all of the benefits discussed above, could reflect improved response and movement coordination, within its presumably stressful environment.

It is recognised that there is an unusually high proportion of echinoderms with brooding relative to broadcast spawning strategies in the Southern Ocean (Poulin & Féral, 1996). The prevalence of brooding in Southern Ocean echinoderms is likely not an adaptation to current polar conditions, but rather linked to environmental conditions in the past (Pearse et al., 2009). In particular, it was hypothesised that brooding species could be carried to new habitats by the ACC across the Drake Passage and the Scotia Arc, where, over time, isolation-by-distance and limited dispersal ability would have led to diversification and speciation among brooding echinoderms (Pearse et al., 2009). Brooding could also reflect a general adaptation to lack of primary productivity and limited habitat availability for successful pelagic larval development during glacial cycles (Poulin et al., 2002). However, emerging studies have also highlighted that contrasting life histories can be found between closely-related ophiuroid species in the Southern Ocean, with brooding strategies mainly found around Antarctic islands and broadcasting strategies mainly observed on the Antarctic continental shelf (Jossart et al., 2019; Sands et al., 2015; this study). It is likely that some of the proposed environmental drivers of innovations within island environments, such as low salinity in the past driven by extreme interglacial periods, could explain the brooding mechanism in *O. hexactis*, and could be extended to other ophiuroid species with similar evolutionary histories as *Ophionotus*.

4.6 Conclusion

We found that *O. victoriae* and *O. hexactis* are closely-related species that diverged at ~434,000 years ago coinciding the onset of MIS 11, with interspecific admixture observed in locations where they overlap. The genome-wide data also revealed multiple evolutionary forces influencing population genetic patterns in the Southern Ocean. The genetic structure of *O. victoriae* indicate the effect of glacial cycles, such as survival in *in situ* shelf refugia and deep-water refugia, appeared to have played a major role in shaping the present-day distribution and genetic structure of *O. victoriae*. In addition, while the ACC is discussed as the main driver of circumpolar genetic connectivity in *O. victoriae*, local current dynamics also appear to distinctively structure the species' connectivity patterns.

Similar to *O. victoriae*, the genetic pattern of *O. hexactis* is likely driven by the combination of glacial refugia survival and oceanic currents. Significant genetic differentiation was detected between all locations in *O. hexactis*, suggesting a level of genetic structure specific to each location, despite apparent high gene flow. As *O. hexactis* likely persisted in *in situ* refugia at sampled locations, significant genetic differentiation could reflect genetic drift within each glacial refugium throughout glacial cycles. Overall, the genetic patterns of *O. victoriae* and *O. hexactis* are likely driven by the combination of survival in glacial refugia in the past with modern oceanic currents. The evolutionary innovations in *O. hexactis* (increase in arm number and a switch to brooding from broadcasting) were likely an evolutionary response to unique environmental changes within Antarctic islands, resulting from hypothesised intense deglacial meltwater during MIS 11. Antarctic islands also subsequently, and exclusively, served as glacial refugia for *O. hexactis* leading to its present-day distribution. Our results highlight that evolutionary divergence and innovative changes can be driven by a relatively recent intense interglacial cycle when the air temperature was 2 ^{o}C warmer than the preindustrial period.

CHAPTER 5

Circumpolar and regional seascape drivers of genomic variation in a Southern Ocean octopus

Lau, S.C.Y., Watts, P.C., Cooke, I.R., Wilson, N.G., Allcock, A.L., Silva, C.N.S., Jernfors, T., Strugnell, J.M.

This chapter is formatted for *Molecular Ecology*.

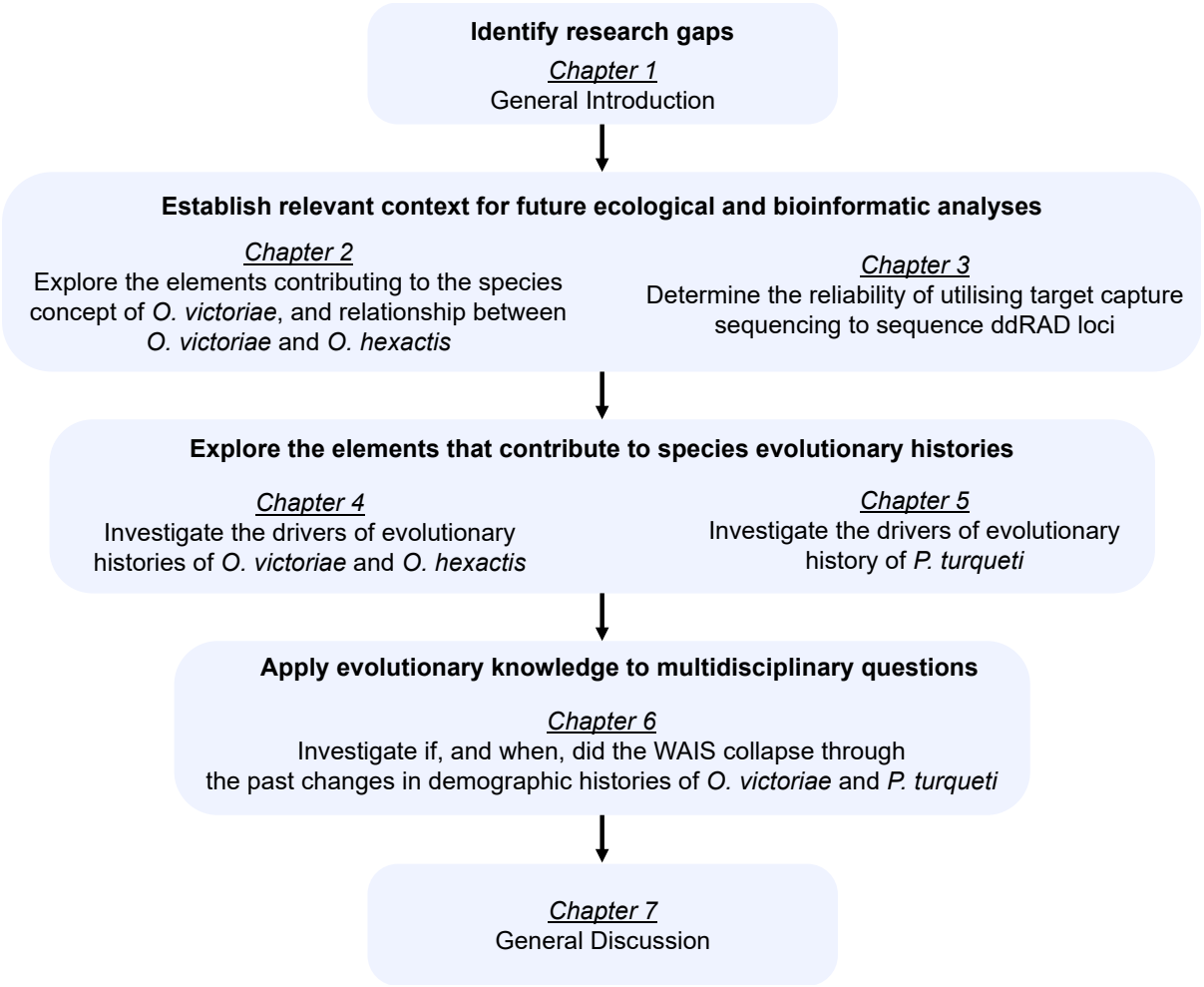

5.1 Abstract

Understanding how ecological, environmental, and geographic features structure population genetic patterns provides crucial insights into a species' evolutionary history, as well as their vulnerability or resilience under climate change. The circumpolar and regional seascape dynamics in the Southern Ocean influence population genetic variation differently across spatial scales. However, comprehensive analyses testing the relative importance of different environmental and geographic variables on genomic variation, across these scales, are generally lacking in the Southern Ocean. Here, we examined genome-wide single nucleotide polymorphisms of the Southern Ocean octopus *Pareledone turqueti* collected from across the Scotia Arc and the Antarctic continental shelf, at depths between 102 - 1,342 m, throughout most of the species distribution. We found that the circumpolar distribution of *P. turqueti* is biogeographically structured with a clear signature of isolation-by-geographical distance. However, long-distance genetic connectivity was also detected between locations in East and West Antarctica. The genomic variation of *P. turqueti* was primarily linked to bottom water temperature at a circumpolar scale. However, within the Scotia Arc, geographical distance and isolation-by-water depth were the only significant drivers of genomic variation at a regional scale. A genotype-environmental association was also detected between warmer temperatures and South Georgia/Shag Rocks, with putative positive selection of hemocyanin (oxygen transport protein) indicated, suggesting possible physiological adaptation to warmer temperatures around sub-Antarctic localities. We identified seascape drivers of genomic variation in the Southern Ocean at circumpolar and regional scales in *P. turqueti* and contextualised the roles of environmental adaptations in the species' evolutionary history.

Keywords: adaptation, biogeography, isolation-by-geographical distance, isolation-by-water depth, seascape dynamics, temperature

5.2 Introduction

Understanding spatial genetic structure provides information about key evolutionary processes that occurred during a species' history, and is particularly important for building roadmaps for species' conservation and management (Selkoe et al., 2016). In the marine environment, seascape genomics provides a conceptual framework for understanding how environmental and geographic features influence contemporary patterns of neutral and adaptive variation, which in turn, can highlight how the seascape has influenced a species' evolutionary history and reveal the potential for a species to adapt to future environmental changes (Liggins et al., 2019). A putative consequence of current global climate change is that genetic diversity will be reduced or restructured (Pauls et al., 2013; Provan, 2013; Hoffmann et al., 2021). It is also forecast that future climate change could outpace the ability of some species to adapt (Visser, 2008; Diniz-Filho et al., 2019). However, it is uncertain how marine ecosystems as a whole will respond due to the variability of individual species responses, as well as the synergistic effects between different climate drivers (Henson et al., 2017). Therefore, understanding the seascape drivers of population genomic variation is urgently needed in order to accurately characterise species and ecosystem responses, including vulnerability or adaptive potential, to any future changes.

The Southern Ocean is beginning to experience rapid environmental changes with about 86% of its ecosystem projected to experience adverse climate change stressors by 2100, including significant warming (Gutt et al., 2015). The Southern Ocean covers ~10% of the world's oceans, and encompasses diverse habitats (e.g. islands, the Antarctic continental shelf, pelagic and deep-sea habitats) and complex variation in environmental, oceanographic and geographic conditions (Post et al., 2014; Xavier et al., 2016). However, the underlying combined physical and ecological dynamics of these ecoregions are vulnerable to climate change (Fabri-Ruiz et al., 2020), and this impacts current conservation efforts that are directed towards protecting distinct ecoregions. For example, at the present day, the Southern Ocean is characterised as being thermally stable with limited seasonal variation, albeit with thermal gradients associated with latitude and between shelf and deep-sea habitats (Clarke et al., 2009; Post et al., 2014). Future changes, such as warming, will impact benthic habitats and their associated biota (Constable et al., 2014; Chapman et al., 2020). It is generally unclear how Southern Ocean benthic fauna will respond to temperature or other future environmental changes resulting from climate change, at a functional or molecular level (Ingels et al., 2012; Gutt et al., 2018; Brasier et al., 2021). Since many Southern Ocean benthic species are distributed across diverse habitats, including some species with a circumpolar distribution, understanding the relationship between seascape dynamics and ecology, within and across ecoregions at different spatial scales, could help

explain and forecast biological responses to this rapidly changing environment in support of comprehensive conservation efforts.

Species with a non-pelagic larval or juvenile phase are typically characterised as having less dispersal capacity than those with a pelagic larval phase. As a result, they tend to show more spatially-structured populations (Moreau et al., 2019). The relationship between seascape dynamics and population genetic variation is often discussed in the context of oceanic currents and dispersal strategies, including the circumpolar current (ACC) (Raupach et al., 2010; Hemery et al., 2012; Moore et al., 2018) and regional currents (Galaska et al., 2017b; Muñoz-Ramírez et al., 2020; Levicoy et al., 2021). However, genetic variation in the Southern Ocean has also been linked to other seascape variables. For example, the Scotia Sea contains an island arc system separated by deep-water channels (> 1000 m), crossed by the ACC and is also influenced by local current regimes with various circulatory patterns (Thompson et al., 2009). Previous studies have highlighted oceanographic current dynamics driving regional gene flow patterns (Hoffman et al., 2012; Muñoz-Ramírez et al., 2020; Levicoy et al., 2021) or genetic discontinuities (Linse et al., 2007; Hoffman et al., 2011b; Moore et al., 2018) in some species within the Scotia Arc. Other studies have also highlighted that isolation-by-bathymetry could also be the driver of genetic variation in the Scotia Arc (Linse et al., 2007; Strugnell et al., 2017). However, it has been reported that closely-related species with similar life histories can exhibit contrasting patterns of genetic differentiation across the Scotia Arc (Strugnell et al., 2017). Beyond the Scotia Arc, fine-scale population structure in benthic taxa has also been observed in other parts of the Southern Ocean such as East Antarctica, possibly linked to regional seascape patterns (Baird et al., 2011, 2012; Soler-Membrives et al., 2017; Collins et al., 2018). Contemporary evidence suggests population genetic variation can be structured differently across spatial scales in the Southern Ocean, with dispersal strategies and species specific and/or evolutionary responses playing an important role. How Southern Ocean population genetic variation might have been structured by historical connectivity and demographic history have been discussed and/or examined in a number of studies across different taxa (e.g. Allcock & Strugnell, 2012; Díaz et al., 2018; Dietz et al., 2015; González-Wevar et al., 2013; Hemery et al., 2012; Lau et al., 2020, 2021; Soler-Membrives et al., 2017; Strugnell et al., 2012, 2018; Wilson et al., 2009). Nonetheless, comprehensive analyses testing for the relative importance of different modern seascape variables on genomic variation, across regional and circumpolar scales, are scarce in the Southern Ocean benthic realm (Brasier et al., 2021).

The Southern Ocean octopus *Pareledone turqueti* is an excellent model to examine the influence of circumpolar and regional seascape dynamics on genomic variation. *Pareledone*

turqueti has a circumpolar distribution and occurs around Antarctic islands south of the Polar Front and on the Antarctic continental shelf between shallow waters and ~1,000 m (Strugnell et al., 2012). This species is a direct developer with benthic hatchlings (Barratt et al., 2008), and is therefore associated with limited dispersal capability. A previous study based on ten microsatellite markers focusing on samples collected from the Scotia Arc suggested the genetic variation of *P. turqueti* reflected the seascape dynamics in the region, including possible signatures of isolation-by-water depth (Strugnell et al., 2017). However, the way in which the Southern Ocean seascape structures the genetic variation of benthic species, at both a regional (e.g. Scotia Arc) and a circumpolar scale, remains to be investigated at a genomic level.

Here, we investigate the population genomic variation of *P. turqueti* with double-digest restriction-associated DNA (ddRAD) loci, using samples collected throughout most of their distributional range at depths between 102 and 1,342 m. We used a target capture sequencing approach to sequence ddRAD loci, as this method is efficient in recovering genomic loci in degraded samples. Specifically, we examined i) how the genomic variation of *P. turqueti* is structured at a circumpolar scale and whether the patterns reflect those found in previous studies focusing on mitochondrial gene cytochrome c oxidase subunit I (COI) and microsatellite data, ii) whether the genomic variation of *P. turqueti* can be explained by modern environmental variables and oceanic currents at both regional (e.g. Scotia Arc) and circumpolar scales, iii) whether there is signature of genotype-environmental association linked to Southern Ocean seascape dynamics in *P. turqueti*.

5.3 Methods

5.3.1 Sample collection and target capture sequencing of ddRAD loci

The genomic data of this chapter was generated in *Chapter 3*. In brief, tissue samples of *Pareledone turqueti* (n = 87) collected around the Antarctic continental shelf and Antarctic islands, between the depths of 102 - 1342 m (Fig 5.1; Supplementary Table 5.1), were sequenced with target capture sequencing with probes designed from previously identified ddRADseq loci (n = 8,942). Two outgroup species (*P. aequipapillae*; ID: 44064_1 *and P. cornuta*; ID: CT931) collected from the Ross Sea and Adélie Land, respectively, were also included in the target capture dataset (Supplementary Table 5.1). Fifty-six out of the 87 *P. turqueti* samples and the two outgroup samples, were also included in previous studies which analysed their COI and microsatellite data (Strugnell et al., 2012, 2017) (Supplementary Table 5.1).

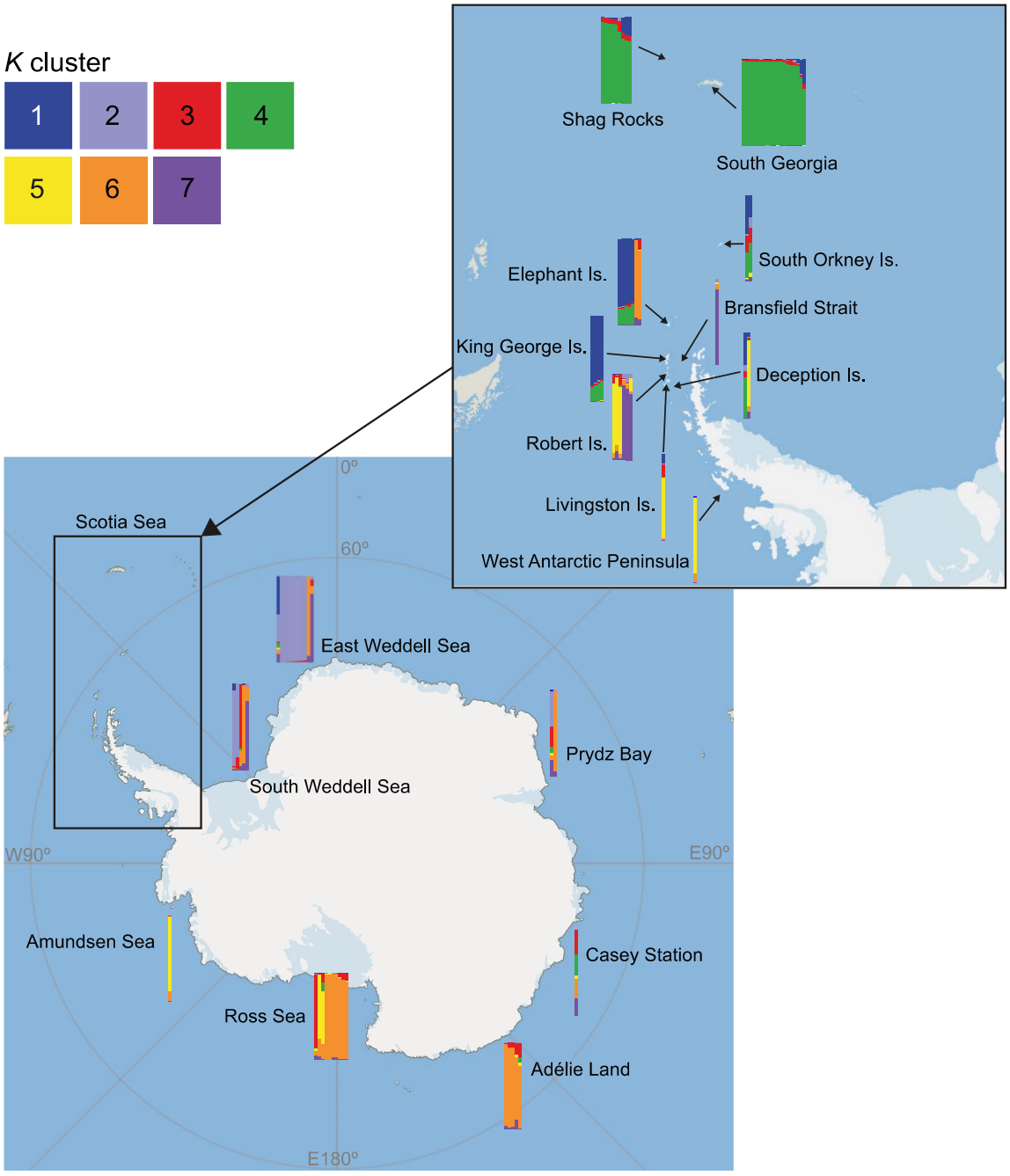

Fig 5.1 Map of Southern Ocean with sampling locations and admixture proportions within *Pareledone turqueti* (n = 87) based on ddRAD loci data. Each vertical bar represents one individual sample, colours correspond to admixture proportion estimations derived from *Structure* analyses (only the optimal value of *K* = 7 is presented in the main figure).

Raw target capture reads were demultiplexed with adapters and barcodes removed using *process_shortreads* in *Stacks* v2.3d (Catchen et al., 2013). Reads with phred quality less than 20 (Q < 20) were also discarded, and polyG in read tails (a problem with NovaSeq due to 2-colour chemistry) were trimmed, using *fastp* v0.20 (Chen et al., 2018). Potential contaminants (human and microorganisms) were identified using *Kraken* v1.0 (Wood & Salzberg, 2014) and reads that matched those of the contaminant database were removed. Cleaned and trimmed reads were checked for quality using *fastQC* v0.11.7 (Andrews, 2019)

5.3.2 Read mapping and variant calling

Cleaned target capture reads were mapped to the consensus sequences of the ddRAD loci used for bait design using *bwa* v0.7.17 *mem* with default parameters (Li & Durbin, 2009). *Samtools* v1.7 (Li et al., 2009) was used to sort alignments by coordinates, and PCR duplicates were marked and removed using *picard* v2.18.1 (Broad Institute, 2019). Variants and short indels were called across all samples using *bcftools* v1.7 *mpileup* (Li, 2011).

Variant filtering was performed in *VCFtools* v0.1.13 (Danecek et al., 2011) for downstream analyses. First, indels and samples with high missing data on an individual basis (> 80%) were first removed, and high quality SNPs were retained based on the following steps. Sites with Phred scaled site quality score more than 30 were kept (--minQ 30). Then, sites with a mean read depth of less than 14x (=average depth (43.7x)/3) and greater than 87x (=2*average depth (43.7x)) were removed (--min-meanDP 14, --max-meanDP 87). Only biallelic sites were kept (--min-alleles 2, --max-alleles 2). Sites were kept if present in 50% of all samples (--max-missing 0.5). Sites with a minor allele frequency of at least 5% were kept (--maf 0.05). To remove sites that were likely belonged to paralogous loci, and therefore artificial SNPs, those with excess observed heterozygosity were filtered. Only sites with a maximum observed heterozygosity of 0.5 were kept (Hohenlohe et al., 2011; Gargiulo et al., 2020), identified via the R package *adegenet* v2.1.3 (Jombart & Ahmed, 2011). Lastly, only one site per locus was kept (--thin 1000; an arbitrary number larger than the longest contig (in bp) used in the bait set). Subsets of this dataset were also generated by removing individuals, based on including 1) all *P. turqueti* samples (n = 87) without outgroups, and 2) *P. turqueti* samples from the Scotia Arc (n = 52). Unless otherwise stated, the analyses of target capture data were performed with the dataset comprising of one SNP per locus.

5.3.3 Genetic structure

Principal Component Analyses (PCA) analysis was performed using *adegenet* to explore the population structure of *P. turqueti*. Genetic differentiation between sample locations was examined with pairwise F_{ST} values, calculated using *GenoDive* v3.0 (Meirmans, 2020) with 10,000 permutations to test for significance. Locations with low sample size ($\leq$ two samples) were omitted from F_{ST} analysis. Post hoc Bonferroni correction was applied to account for multiple pairwise comparisons. Individual admixture proportions were also estimated via *Structure* v2.3.4 (Pritchard et al., 2000). *Structure* was run between *K* = 1 and 10, with ten replicates per *K* via *Structure_threader* (Pina-Martins et al., 2017). Each run was performed with 500,000 iterations and burn-in of 100,000. The meaningful K was evaluated based on

the highest mean log likelihood [mean LnP(*K*)] and delta*K* statistics using *Structure Harvester* (Earl & VonHoldt, 2012).

As a complimentary method to *Structure*, *TreeMix* v1.13 (Pickrell & Pritchard, 2012) was performed to generate a maximum likelihood (ML) tree topology of *P. turqueti*, as well as to model the historical splits and mixtures between locations and the amount genetic drift experienced at each location. While *Structure* assigns individuals into discrete genetic clusters, *TreeMix* models how the populations may have arisen and outlines the genealogical relationship between populations (Pickrell & Pritchard, 2012). For *TreeMix* analysis of *P. turqueti*, outgroup species (*P. aequipapillae* and *P. cornuta*) were included for tree rooting. *TreeMix* input was generated using the R package *dartR* v1.1.11 (Gruber et al., 2018). Within *TreeMix*, migration edges (m) were modelled between 0 and 10, with 10 replicates per m using the bootstrap option with a block size of 1 (assuming loci are unlinked as the input dataset contained a one SNP per locus). The optimal number of m was evaluated using the simple exponential and non-linear least square model (threshold = 0.05) via the R package *OptM* v0.1.3 (Fitak, 2019). The final best m (after *OptM* evaluation) was chosen based on the highest amount of variance explained. Among the 10 replicate runs of the best m, the replicate with the least residuals was presented. In addition, only significant migration edges, evaluated using jackknife p values (significance level at 0.05), were presented. Each migration edge was weighted based on the ancestry fraction in the sink population originated from each source population (Pickrell & Pritchard, 2012).

5.3.4 Isolation-by-environment

To evaluate whether the genetic variation of *P. turqueti* can be explained by isolation-by-distance (IBD) and -environment (IBE), generalised dissimilarity modelling (GDM) was performed. GDM is a multivariate statistical method that uses a nonlinear matrix regression to model the dissimilarity between genetic differentiation versus geographic distances and environmental variables (Ferrier et al., 2007) (hereafter predictors). GDM models 1) the variation in the rate of non-stationary compositional turnover (i.e. genetic distance in this study) at different positions along a given predictor gradient, and 2) the curvilinear relationship between genetic dissimilarity and increasing environmental or geographical distance between sample locations.

In the GDM analysis, each predictor variable is first transformed using the default three I-spline basis functions, and models are fitted using maximum-likelihood estimation. Variables are also standardised so their resulting coefficients can be compared. The overall model significance and the significance of each predictor was quantified using matrix permutation

via the function *gdm.varImp* within the R package *gdm* v1.4.2.2 (Fitzpatrick et al., 2021). During permutation testing (n = 999), a full model containing all predictors was first considered, followed by iteratively removing the predictor with the lowest coefficient and recalculating the model fit and significance values. Permutation testing is repeated until all non-significant predictors are removed. In the final GDM plot, only the relationships between genetic distance and significant predictors are visualised. The maximum height of each I-spline represents the total amount of genetic variation turnover associated with each significant predictor (while holding other significant predictors constant) (Fitzpatrick & Keller, 2015). The slope of each I-spline represents the rate of genetic turnover, as well as how the rate varies along the associated environmental gradient. The characteristics of each I-spline explore the amount of genetic variation linked to environmental change and possible ecological adaptation (Fitzpatrick & Keller, 2015).

Separate GDM analyses were performed for 1) all *P. turqueti* samples and 2) *P. turqueti* samples from the Scotia Arc. For both datasets, pairwise genetic distance between samples were estimated via *ngsDist* (Vieira et al., 2016) using all SNPs across retained ddRAD loci. For predictor inputs, geographical distances between samples (Euclidean distance; straight direct distance between sample locations) were calculated directly from geographical coordinates within GDM. The environmental variables considered for all GDM analyses included water depth, seafloor water temperature, seafloor water salinity, as well as silicate, phosphate, nitrate and dissolved oxygen (winter and summer values, at the surface and 500 m). Information on water depth, latitude and longitude were obtained from the sampling information. Values of seafloor water temperature and salinity were calculated from the decadal means of annual average seafloor temperature and salinity at 1°C spatial resolution between 1955 and 2010 from World Ocean Atlas 2018 (Locarnini et al., 2018; Zweng et al., 2018). Seafloor temperature and salinity data were estimated based on the information at the depth interval closest to the maximum depth available for each point using QGIS. Values of silicate, phosphate, nitrate and dissolved oxygen (summer and winter values, at the surface and 500 m) were extracted from existing interpolated GIS layers from *Quantarctica* (Matsuoka et al., 2021), generated based on World Ocean Atlas 2013 datasets (Garcia et al., 2013, 2018), gridded at 25 km spatial resolution. These values were extracted from existing GIS layers from *Quantarctica* rather than directly from World Ocean Atlas as they required additional care on achieving the statistically best interpolations, which was performed within *Quantarctica*. Since Southern Ocean seafloor temperature and salinity exhibit limited seasonal variation, decadal means of annual averages were used in this study. However, Southern Ocean biological production varies seasonally following summer sea ice melt (which influences nutrient parameters) (Post et al., 2014), therefore, both summer and winter values of nutrient profiles at different depths were utilised in this study.

Multicollinearity between environmental predictors was assessed using the R package *psych* v1.9.12 (Revelle, 2020), and predictors with low collinearity ($r < 0.7$) were kept for GDM. For both datasets, after checking for collinearity, only water depth, seafloor temperature, seafloor salinity and summer nitrate level at 0 m were kept as GDM environmental predictor inputs.

5.3.5 Genotype environmental association analysis

Redundancy analyses (RDAs) were performed to detect genome-wide adaptations to environmental variables in the Southern Ocean (Forester et al., 2018). RDA is a constrained ordination approach that uses multiple linear regression to summarise the linear relationships between genotypes by a set of explanatory environmental predictors. RDAs were performed using the R package *vegan* v2.5-6 (Oksanen et al., 2013), and separate RDAs were performed for 1) all *P. turqueti* samples, 2) *P. turqueti* samples from the Scotia Arc. Within each RDA, after checking for collinearity ($r < 0.7$), the environmental variables considered included longitude, water depth, seafloor temperature, seafloor salinity and summer nitrate level at 0 m.

For each RDA model, significance (at $\alpha = 0.05$) was assessed with ANOVA (999 permutations), and Variance Inflation Factors were examined for possible further indication of multicollinearity between environmental predictors. SNP loadings in the ordination space were also identified to assess whether certain SNPs might be associated with environmental predictors (i.e. SNPs under selection as a function of environmental predictors). Outlier SNPs were identified via the distribution of SNP loadings on each significant RDA axis, with SNPs that exhibited more than ± 3 standard deviations from the mean loading identified as putative outliers, a threshold suggested within Forester et al. (2018). Pearson's correlation coefficient was used to evaluate associations between putative outlier SNPs and environmental predictors.

5.3.6 Outlier SNP detection and gene ontology

SNPs under putative selection were identified using outlier detection analyses including *OutFLANK* v.02 (Whitlock & Lotterhos, 2015), *BayeScan* v2.1 (Foll & Gaggiotti, 2008), *PCAdapt* v4.3.2 (Privé et al., 2020), *FastPCA* (Meisner et al., 2021) and RDA. Outlier detection analyses were performed separately across 1) all *P. turqueti* samples and 2) *P. turqueti* samples from the Scotia Arc.

For *OutFLANK* and *BayeScan*, individuals can be pre-defined as different populations. For

outlier detection analyses across all *P. turqueti* samples, samples were grouped between the Scotia Arc or Antarctic continental shelf. For outlier detection analyses across *P. turqueti* from the Scotia Arc, samples were grouped among sample locations.

OutFLANK analyses were performed using default parameters and a *q*-value threshold of 0.05. *BayeScan* analyses were performed with prior odds set to 100, followed by 20 pilot runs and 100,000 iterations with 5,000 samples, burn-in length of 50,000 and thinning interval of 10. *PCAdapt* analyses were performed with scree plots used to select the optimal principal component (*K*), and outlier SNPs were determined via the Benjamini-Hochberg Procedure with a p-value threshold (alpha) of 0.05. *FastPCA* (Galinsky et al., 2016) analyses were performed via *PCAngsd* v1.03 (-selection) (Meisner & Albrechtsen, 2018), with the resulting statistic being chi-square distributed with one degree of freedom and a *p* value calculated for each variant. The final *FastPCA* results were corrected for inflation factor (λ), and the significance level was adjusted with Bonferroni correction (i.e. 0.05 / number of sites tested for each dataset), in order to minimise false discoveries in the data following François et al. (2015). SNPs that were identified as outliers by two or more tests (*OutFLANK*, *BayeScan*, *PCAdapt*, *FastPCA*, RDA) were considered to be putatively under selection in order to minimise false positives (Ahrens et al., 2021).

All contigs containing putative outlier SNPs were queried against the National Center for Biotechnology Information (NCBI) database (Agarwala et al., 2018) using the BLASTx (Altschul et al., 1990) search tool to determine whether homologous sequences were present with a known function. Hits that were returned with a maximum E value of 1×10^{-5} were considered as significant matches. Gene ontology (GO) functional annotations of the significant matches were assigned using the *QuickGO* webserver (GO version 2021-07-22) (Binns et al., 2009). To visualise GO terms, redundant GO terms were filtered and clustered based on semantic similarity, using *REViGO* (Supek et al., 2011).

Contigs containing outlier SNPs, identified across 1) all *P. turqueti* samples (n = 125) and 2) *P. turqueti* from the Scotia Arc (n = 65), were also annotated using *RepeatModeler* (Smit & Hubley, 2015) (*RMBlast*) and masked with *RepeatMasker* (Smit et al., 2015) to identify whether they may contain transposable elements. In addition, 125 and 65 neutral contigs retained after SNP filtering, containing no outlier SNPs, were randomly selected for each dataset. The selected neutral contigs were also annotated using *RepeatModeler* and masked with *RepeatMasker*. A Fisher's exact test (one-sided) was applied to each dataset to evaluate whether the outlier contigs may contain a significant higher proportion of TE compared to neutral contigs. For 1) all *P. turqueti* samples and 2) *P. turqueti* samples from the Scotia Arc, for each dataset, neutral contigs were randomly selected five times, and

compared to outlier contigs via Fisher's exact test five times to ensure consistency. For the evaluation of each dataset, the p-value was adjusted with Bonferroni correction, and a one-sided p-value threshold of 0.01 (= 0.05/5) was used to determine significance.

5.4 Results

5.4.1 Read quality

A total of 1,300,258,985 raw reads were obtained from 87 *P. turqueti* samples and two outgroup samples (*P. aequipapillae* and *P. cornuta*) during target capture sequencing of ddRAD loci, with an average of 14,609,652 reads (± 5,612,687 SD) per sample. After SNP filtering, the final dataset included *P. turqueti* (n = 87) and outgroups (n = 2) with 37,698 SNPs (all SNPs per locus included) and 5,437 SNPs (single SNP per locus only).

5.4.2 Population structure

Genotypic clustering using *Structure* suggested all *P. turqueti* samples can be represented by *K* = 2 or 7, based on delta*K* and log-likelihood values, respectively (Fig 5.1, Supplementary Fig 5.1). At *K* = 2, samples from Shag Rocks and South Georgia were distinct from the rest of the locations, with some locations within the Scotia Arc (Deception Island, Elephant Island and King George Island) exhibiting a high level of admixture with Shag Rocks and South Georgia (Supplementary Fig 5.1). At *K* = 7, samples from Shag Rocks and South Georgia were also distinct from other sampled locations, with a low level of admixture detected with Deception Island, Elephant Island, King George Island, South Orkney Islands (Fig 5.1). The model of *K* = 7 was chosen as the preferred model as it corroborates the genetic structure detected within *TreeMix* and PCA. Furthermore, within *K* = 7, two distinct admixture signals between Bransfield Strait, Livingston Island, Robert Island, Deception Island, Amundsen Sea and West Antarctic Peninsula were also observed (Fig 5.1). When grouped by water depths, these two distinct admixture signals can be differentiated by depths across these locations (Supplementary Fig 5.2). On the Antarctic continental shelf, strong admixture is observed between Ross Sea and Adélie Land, as well as some South Weddell Sea individuals (Fig 5.1). Admixture was also detected between East and South Weddell Sea, with one individual from either location exhibiting admixture with Scotia Arc localities (Fig 5.1). The interpretation of the individual admixture proportions at Prydz Bay and Casey Station should be treated with caution as both locations were characterised by one or two samples. However, one sample from Prydz Bay cannot be differentiated from Ross Sea and Adélie Land individuals, while other samples from Casey

Station and Prydz Bay appeared to be associated with multiple genetic clusters.

PCA detected structured populations within *P. turqueti*, with the first PC axis (PC1) explaining 10.59% of the overall genetic variance. Samples collected from Shag Rocks and South Georgia clustered together and were distinct from other locations (Fig 5.2). The second PC axis (PC2), explaining 5.08% of the overall genetic variance, indicated a clear differentiation between most samples from East Weddell Sea and Ross Sea / Adélie Land. Some samples from East Weddell Sea, South Weddell Sea, Prydz Bay and Elephant Island exhibited limited differentiation from Ross Sea / Adélie Land samples on the PC2 (Fig 5.2). Pairwise F_{ST} indicated samples from South Georgia and Shag Rocks exhibited significant differentiation between all sample locations (F_{ST} between 0.036 and 0.152) (except between Shag Rocks and King George Island) (Supplementary Table 5.2). Within and around the Scotia Arc, a lack of significant differentiation was detected between Elephant Island, King George Island, Robert Island and South Weddell Sea (F_{ST} between 0.006 and 0.092). Connectivity between the Antarctic continental shelf and the Scotia Arc can be observed via a lack of significant differentiation detected between Adélie Land and Elephant Island / King George Island / Robert Island (F_{ST} between 0.018 and 0.095). On the Antarctic continental shelf, a lack of significant differentiation was detected between East and South Weddell Sea localities (F_{ST} = 0.001), as well as between the Ross Sea and South Weddell Sea (F_{ST} = 0.039) and between the Ross Sea and Adélie Land (F_{ST} = 0.018).

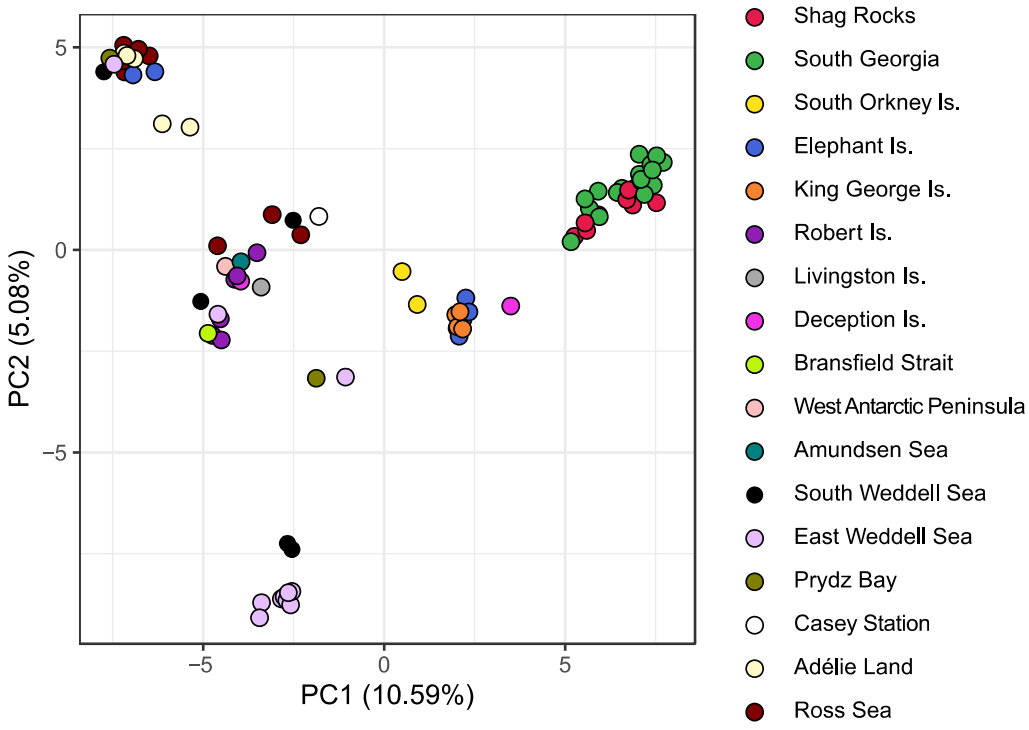

Fig 5.2 Principal Component (PC) Analysis results on the first two axes of *Pareledone turqueti* (n = 87) based on ddRAD loci data.

5.4.3 Population tree with admixture

TreeMix analysis, and subsequent post hoc evaluation, supported m = 5 and 6 as the optimal number of migration edges within *TreeMix* threshold modelling. Upon evaluating the model with the highest proportion of genetic variance explained and lowest residual values, the *TreeMix* with m = 6 model, explaining 96.1% of the total variance and up to ± 5.3 SE in residuals, was selected (Supplementary Fig 5.3). At m = 6, a further jackknife significance test indicated only four out of six migration edges significantly improved the model fit to the observed allele frequency data ($p < 0.004$, Fig 5.3).

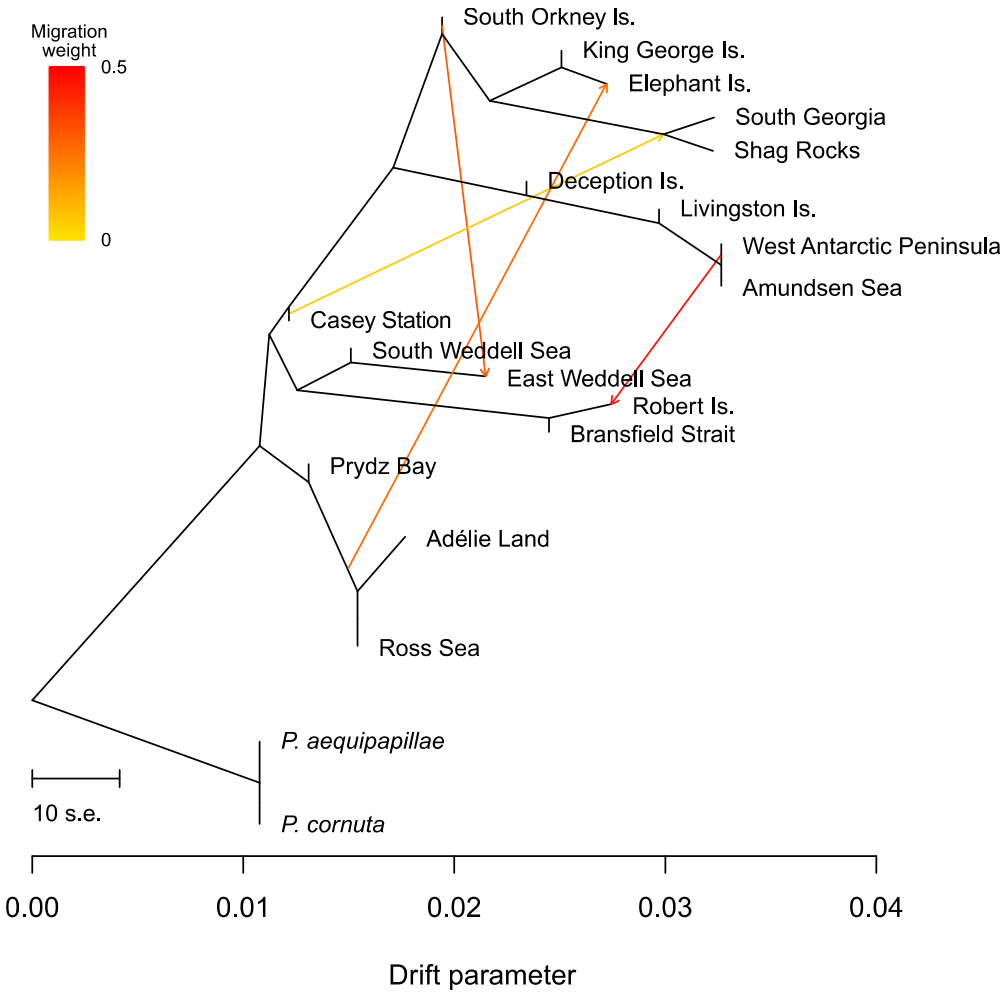

Fig 5.3 *TreeMix* maximum likelihood (ML) tree of *Pareledone turqueti* (n = 87) rooted with *P. cornuta and P. aequipapillae*, based on ddRAD loci data. Terminal nodes are subdivided based on sampled geographical locations. Horizontal branch lengths are proportional to the amount of genetic drift occurred on each branch. Only significant migration edges are shown (coloured arrows, n = 4) after evaluation via simple exponential and non-linear least square models and jackknife significance test. Migration edge was coloured based on migration weight, which corresponds to the % ancestry in the sink population originated from the source population.

The final *TreeMix* model suggested that *P. turqueti* can be separated into four clades (Fig 5.3), largely corresponding to the individual admixture similarities suggested by *Structure* (at *K* = 7). In *TreeMix*, locations within and around the Scotia Arc were separated into three clades, corresponding to their geographical range (Fig 5.3). One clade mostly contains locations along the Scotia Arc system including Shag Rocks, South Georgia, South Orkney Island, Elephant Island as well as King George Island. The second clade mostly contains locations adjacent to the Antarctic Peninsula including Deception Island, Livingston Island, West Antarctic Peninsula and Amundsen Sea. The third clade contains locations around the Weddell Sea including Robert Island, Bransfield Strait, South and East Weddell Sea, with Casey Station showing affinity with this clade. Finally, Ross Sea, Adélie Land and Prydz Bay were grouped as a separate clade. Based on *TreeMix*, strong historical gene flow was detected from the West Antarctic Peninsula to Robert Island; relatively less historical gene flow was detected from South Orkney Island to East Weddell Sea, and from Adélie Land + Ross Sea to Elephant Island; and the relatively least historical gene flow was detected from Casey Station to South Georgia + Shag Rocks.

5.4.4 Isolation-by-environment

GDM found evidence of significant isolation-by-geographical distance (IBD) and isolation-by-environment (IBE) based on pairwise genetic distance between *P. turqueti* individuals, for both datasets including 1) all *P. turqueti* samples and also 2) *P. turqueti* samples collected from the Scotia Arc (Table 5.1, Fig 5.4a, b). For the dataset including all samples, significant environmental predictors (n = 4) explained 32.4% of total genetic variance ($p < 0.0001$), with bottom water temperature as the most important predictor, followed by water depth, geographical distance and bottom water salinity (Table 5.1). Based on the I-splines of each significant predictor, while holding other predictors constant, the rate of genetic turnover increased exponentially with increasing temperature (Fig 5.4a). For other predictors (water depth, geographical distance and bottom water salinity), the rate of genetic turnover appeared to increase rapidly near the low ends of these gradients but plateaued as the values increased (Fig 5.4a).

For the dataset which only included samples from the Scotia Arc, significant environmental predictors (n = 2) explained 41.2% of total genetic variance ($p < 0.0001$), with geographical distance found to be the most important predictor, followed by water depth (Table 5.1). For this dataset, the rate of genetic turnover exhibited an almost proportional increase with farther geographical distance (Fig 5.4b). In comparison, the rate of genetic turnover increased slightly with increasing water depth (Fig 5.4b).

Table 5.1 Model fit and relative importance of isolation-by-environment variables in generalised dissimilarity modelling (GDM) for target capture of ddRAD loci data of *Pareledone turqueti* (37,698 linked SNPs). Importance was defined by the % in deviance explained by the full model after permutation. Variable significance was determined with 999 permutations with significance level at 0.05. Non-significant variables are represented by —.

Overall model	All circumpolar samples (n = 83)	Only samples from Scotia Arc (n = 52)
Model deviance	8.78	2.45
Percentage explained	32.39	41.16
p-value	<0.0001	<0.0001
Relative parameter importance (bootstrapped p-value)		
Geographic distance	12.43 (<0.001)	35.07 (<0.001)
Water depth	13.03 (0.013)	3.81 (0.042)
Bottom water temperature	27.38 (0.001)	—
Bottom water salinity	10.72 (0.044)	—
Surface nitrate (summer)	—	—

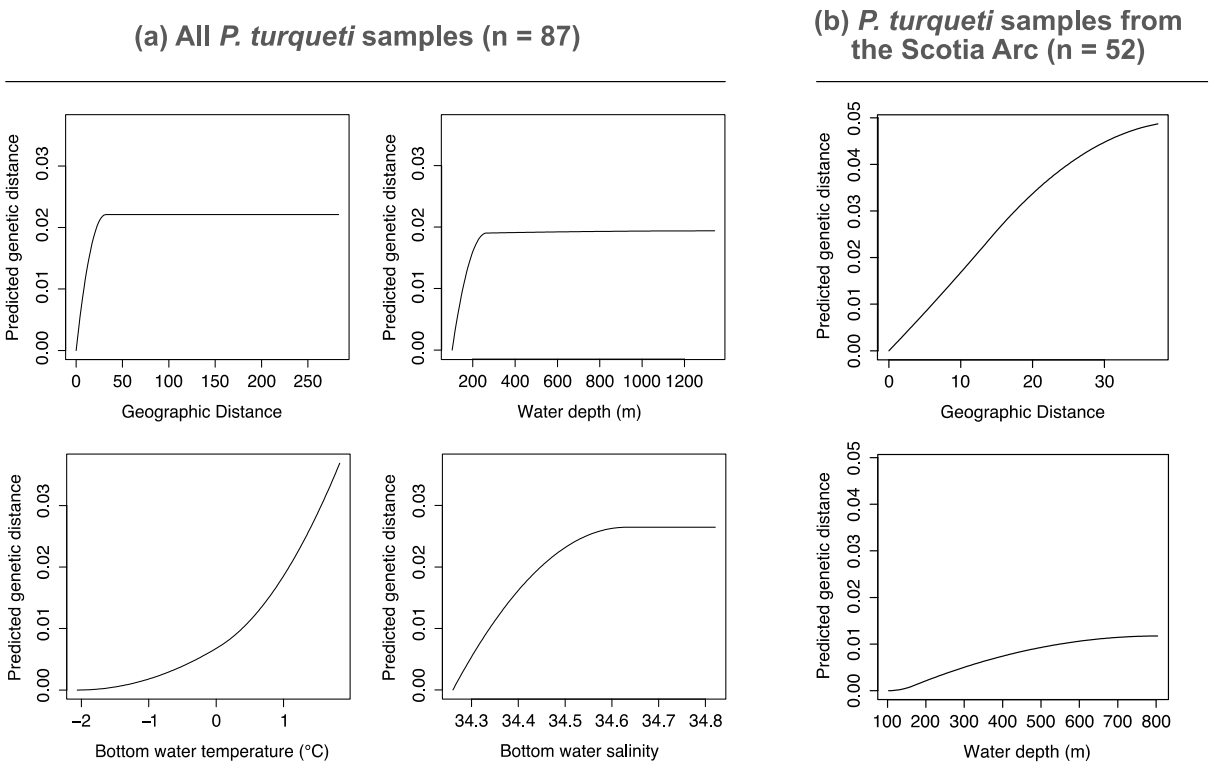

Fig 5.4 I-Spline plots for generalised dissimilarity models (GDM) analysing all *Pareledone turqueti* samples across the Southern Ocean (a) and only *P. turqueti* samples from the Scotia Arc (b), based on ddRAD loci data (37,698 linked SNPs). Each predicted spline illustrates the estimated relationship between genetic distance and the environmental variable that was significantly associated with genetic variation, while holding other variables constant. The maximum height of each I-spline shows the amount of genetic turnover associated with each environmental variable. The shape of each I-spline curve shows the rate of genetic turnover across the sampled environmental gradient.

5.4.5 Genotype-environmental association analyses

When comparing individuals collected along the circumpolar scale in the RDA, constrained ordination explained 7.87% (adjusted R^2, $p < 0.001$) of the overall genetic variation with all five environmental predictors (longitude, water depth, bottom water salinity, bottom water temperature, surface nitrate values). The first four constrained PCs significantly explained 48.1% ($p < 0.001$), 19.9% ($p < 0.001$), 12.3% ($p = 0.002$) and 11.4% ($p < 0.001$) of the total adjusted R^2. On PC1 and 2, individual genotypes of Shag Rocks and South Georgia exhibited a strong association with temperature, and genotypes of Ross Sea and Adélie Land were strongly associated with longitude (Fig 5.5a, b). Two individuals from Elephant Island, and one individual from East Weddell Sea, Ross Sea and Prydz Bay, also showed association with salinity (Fig 5.5a, b).

When comparing individuals collected within the Scotia Arc in the RDA, constrained ordination significantly explained 8.80% (adjusted R^2, $p < 0.001$) of the overall genetic variation with all five environmental predictors. The first three constrained PCs explained 44.4%, 19.5% and 15.6% of the total adjusted R^2 ($p < 0.001$). On RDA1 and 2, genotypes of Shag Rocks and South Georgia showed association with longitude and temperature, but stronger association was detected between Shag Rocks and longitude, and between South Georgia and temperature (Fig 5.5c). Individuals of Robert Island exhibited a strong association with water depth, and two individuals from Elephant Island showed association with salinity and nitrate (Fig 5.5c)

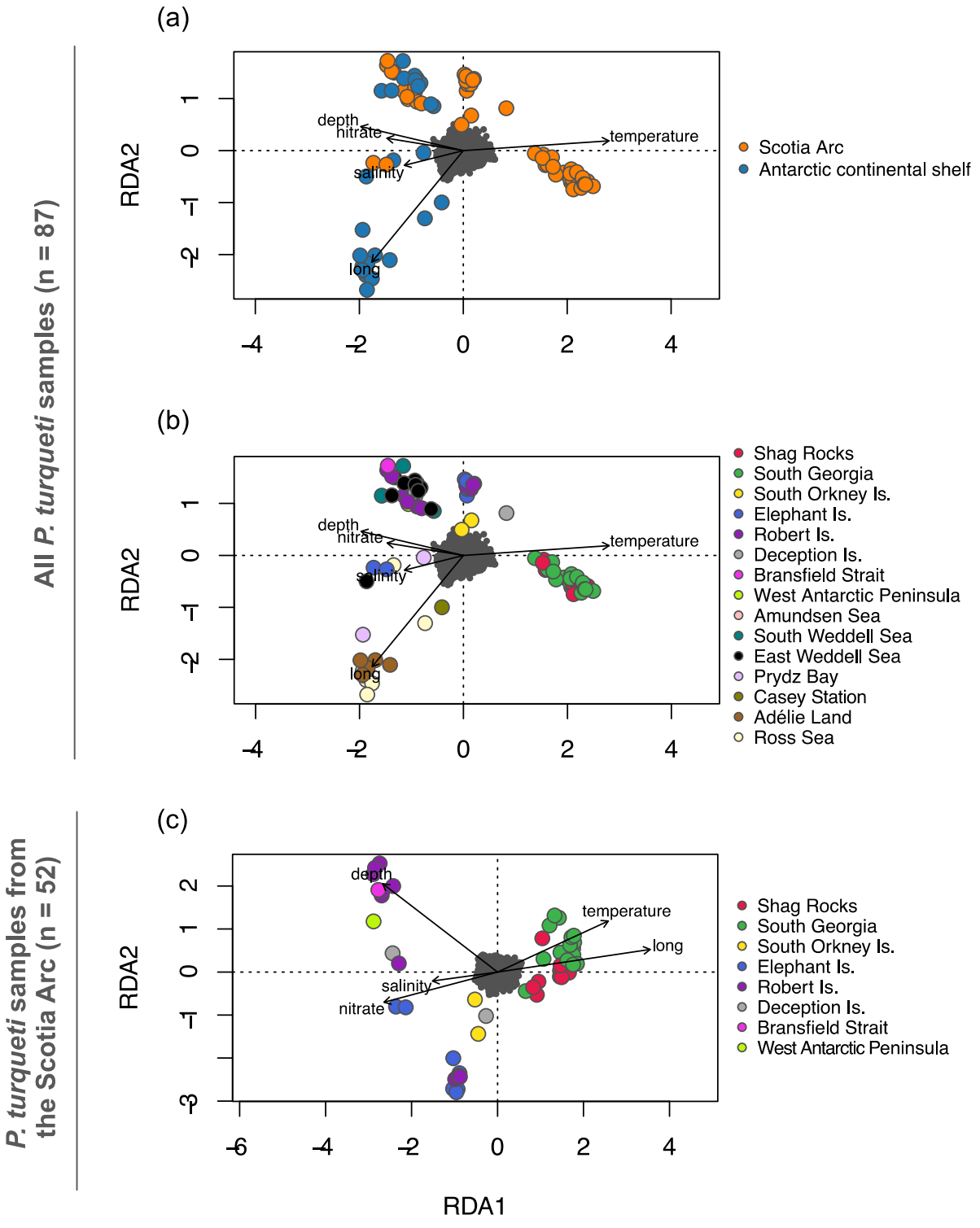

Fig 5.5 Redundancy analysis (RDA) showing genotype-environment association in *Pareledone turqueti* on the first two constrained axes based on ddRAD loci data. (a, b) RDA of *P. turqueti* samples collected across the Southern Ocean (n = 87), (c) RDA of *P. turqueti* samples from the Scotia Arc only (n = 52). Grey dots represent SNPs, and coloured circles represent individual sample defined by assigned labels. Vectors represent environmental predictors, including bottom water temperature (temperature), bottom water salinity (salinity), nitrate (summer nitrate values at 0m), water depth (depth) and longitudes (long).

5.4.6 Outlier SNP detection and gene ontology

Based on the outlier SNPs detected by at least two methods (*FastPCA*, *OutFLANK*, *BayeScan*, *PCAdapt* and RDA), a total of 125 contigs containing putative outlier SNPs were identified when samples were separated between Scotia Arc and Antarctic continental shelf (dataset of 1) all *P. turqueti* samples) (Supplementary Fig 5.4a). In the full dataset, 31 contigs were annotated with support of the BLASTx database under the search criteria (Supplementary Table 5.3). Among the annotated 31 contigs, 17 were proteins related to transposable elements (TE), including retrotransposons (long interspersed nuclear elements (LINE), long terminal repeat (LTR); n = 7), DNA transposons (terminal inverted repeat (TIR), n = 2), domesticated TE (n = 4), proteins known to interact with TE (n = 2) and proteins known to repress TE (n = 2) (Supplementary Fig 5.5). Of the identified outlier contigs associated with environmental variables, identified via RDA, a retrotransposon (LINE; n = 1) was associated with water depth, and retrotransposons (LINE; n = 2) and domesticated TE (n = 1) were associated with temperature (Supplementary Fig 5.6a). In the remaining annotated contigs (n = 13) that were not related to TE, GO annotations identified multiple levels of biological processes, including cellular component organisation, response to stimulus, biological regulation, developmental processes and metabolic processes (Supplementary Fig 5.7).

In the dataset containing only *P. turqueti* samples from the Scotia Arc, a total of 65 contigs containing putative outlier SNPs were identified when individuals were separated between sample locations (Supplementary Fig 5.4b). Of the 65 contigs, 19 were annotated with support of the BLASTx database under the search criteria, and seven were related to TE, including TE repressor (n = 1) was associated with temperature, retrotransposons (LINE; n = 1) was associated with salinity, and retrotransposons (LINE, LTR; n = 4), DNA transposon (TIR; n = 1), domesticated TE (n = 3), TE interactor (n = 1) and TE repressor (n = 1) were associated with longitude (Supplementary Fig 5.6b). In the remaining annotated contigs (n = 6) that were not related to TE, GO annotations identified multiple levels of biological processes, including organelle organisation, response to stimulus, establishment of localisation, regulation of biological processes, RNA processing, metabolic processes, reproductive processes and developmental processes (Supplementary Fig 5.7).

Finally, there was no significant difference in the proportion of TEs between outlier and neutral contigs, in the datasets containing all *P. turqueti* individuals (Fisher's exact tests, $p > 0.01$) and only *P. turqueti* individuals from the Scotia Arc (Fisher's exact tests, $p > 0.01$).

5.5 Discussion

The Southern Ocean is a vast and complex ecosystem containing Antarctic islands, the Antarctic continental shelf and the deep sea, which tends to partition benthic fauna between taxon-specific biogeographical regions (Griffiths et al., 2008; Moreau et al., 2017). However, there is limited understanding of how benthic fauna associate with the underlying biogeographic dynamics across the circumpolar scale at a genomic level. Here, we used a target capture sequencing approach to sequence ddRAD-identified loci in a circumpolar Southern Ocean octopus, *Pareledone turqueti*, with samples collected across the Scotia Arc and the Antarctic continental shelf throughout most of the species' distribution. The genetic structure of *P. turqueti* coincides with general biogeographic patterns across the Southern Ocean. Different selective pressures linked to isolation-by-environment (IBE) were also found to be significant in driving genetic variation across spatial scales, most notably temperature, at a circumpolar scale but geographical distance and water depth were the only significant drivers within the Scotia Arc. Signatures of putative adaptive loci also revealed possible environmental adaptations to warmer temperatures around Shag Rocks and South Georgia in the Scotia Arc.

5.5.1 Biogeographic structure with long-distance connectivity in *P. turqueti*

The benthic habitats of the Southern Ocean can be separated into distinct bioregions based on geomorphic features, temperature, sea ice extent and productivity, which can act as barriers to biological dispersal (Douglass et al., 2014). Additionally, isolation-by-geographical distance (IBD) leading to genetic differentiation between geographically distant locations is expected for direct developing species in the Southern Ocean (Poulin & Féral, 1996). The geographical barriers between ecoregions, combined with IBD, likely simultaneously limit the dispersal range of Southern Ocean direct developing species, including *P. turqueti*. Genetic dissimilarity between distant locations has also previously been reported across different Southern Ocean benthic taxa with a non-pelagic dispersal strategy (Baird et al., 2011; Hoffman et al., 2011a; Collins et al., 2018; Moreau et al., 2019), including species of *Pareledone* (Allcock et al., 2011), and was also supported here. The distinct genomic structure observed within *P. turqueti* also correspond to known ecoregions (e.g. Antarctic Peninsula, South Georgia, South Orkney Islands), or connectivity between neighbouring ecoregions (e.g. Ross Sea - Adélie Land [Oates]), consistent with the view that Southern Ocean direct developers generally do not disperse far.

However, connectivity over long-distances was also detected in the present study and has been reported in other Southern Ocean benthic taxa that have direct development or benthic

larvae (Leese et al., 2010; González-Wevar et al. 2018; Lau et al. 2021; *Chapter 2, 4*). These observed patterns often involve connectivity between locations separated by the deep sea that are outside of the depth range of the focal species, as well as over long geographical distances. For *P. turqueti*, the detected long-distance connectivity is superimposed on an overall genetic structure that reflects biogeographical patterns. A previous study focusing on COI and microsatellite data of *P. turqueti* similarly reported that the overall genetic variation of *P. turqueti* is highly structured, with long-distance admixture also detected between South Georgia and Prydz Bay (Strugnell et al., 2012). It was hypothesised that the long-distance dispersal in *P. turqueti* could have been facilitated via adults or egg masses rafting on floating substrates, or that their benthic egg masses could become dislodged and disperse through the currents (Strugnell et al., 2012). Connectivity between the Ross Sea and the Antarctic Peninsula, excluding the Amundsen Sea or Bellingshausen Sea, has also been reported in other Southern Ocean species with both pelagic and benthic larvae, hypothesised to be linked to the role of the ACC in gene flow (Galaska et al., 2017b; Collins et al., 2018). In this study, from the directionality of gene flow and the geographical locations of the receiving population observed (i.e. Elephant Island and South Georgia), it also appears that the long-distance connectivity could have been facilitated by oceanic currents. For example, Elephant Island has been described as a "choke point" for ocean current drifters entering the Scotia Arc, suggesting this area has the potential to receive biological migrants coming from outside the Scotia Arc via current advections (Thompson et al., 2009; Renner et al., 2012). Genetic connectivity between South Georgia and East Antarctic locations (including Heard Island and Prydz Bay) has also been reported in a variety of Southern Ocean benthic taxa (Baird et al., 2011; Hemery et al., 2012; Strugnell et al., 2012; Moore et al., 2018; Lau et al., 2021; *Chapter 2*), with a probable current-driven seascape corridor linking the two regions (Lau et al., 2021; *Chapter 2*). Oceanographic modelling has also suggested that long-distance dispersal is possible for marine invertebrates rafting on kelp to drift from South Georgia to locations around the Antarctic continental shelf, including East Antarctica (Fraser et al., 2018). Direct observations of biological migration and estimations of gene flow directionality between these source-sink locations would be necessary to finally verify the role of oceanic currents in facilitating long-distance connectivity in Southern Ocean benthic taxa.

5.5.2 Seascape drivers of *P. turqueti* divergence at circumpolar scale

From the empirical data in this study, the overall genetic structure of *P. turqueti* can also be explained by variation in seafloor temperature, with Generalised Dissimilarity Modelling (GDM) identifying an exponential increase in genetic distance between samples following increasing seafloor temperature. Given that seafloor temperature is associated with latitudes

in the Southern Ocean (Clarke et al., 2009), the observed association between temperature and genetic variation in *P. turqueti* could reflect neutral processes (Wang & Bradburd, 2014), such as the influence of circumpolar-scale biogeographic patterns on genetic differentiation, as observed in the overall genetic patterns of this species. However, the current evidence suggests that *P. turqueti* likely exhibits local adaptation to temperature. Evidence of temperature adaptation include the locus containing the coding sequence of Hemocyanin G-type (units Oda to Odg), which was found to be under selection between samples collected from the Scotia Arc and Antarctic continental shelf. RDA also detected correlation between the same locus linked to Hemocyanin G-type (units Oda to Odg) and seafloor temperature, and that samples from South Georgia and Shag Rocks (the northernmost range of *P. turqueti*'s distribution, thus warmer water habitat) were positively associated with seafloor temperature. Together, the evidence suggests possible selection for Hemocyanin G-type (units Oda to Odg) at warmer seafloor temperatures in the Scotia Arc.

Hemocyanins are copper-binding oxygen transport proteins that are found in arthropods and molluscs (Kato et al., 2018), notably responsible for the blue blood pigment upon oxygen binding. A previous study examining the blood oxygen binding capacity in the Antarctic octopus *P. charcoti*, a closely-related species to *P. turqueti*, suggested hemocyanin in *P. charcoti* is thermally sensitive, and can release most of the bound oxygen and maintain oxygen supply at warmer water temperatures up to 10°C (Oellermann et al., 2015a). Consequently, at warmer temperatures, hemocyanin in *P. charcoti* can buffer oxygen demands and reduces the workload for other circulatory organs that can be affected by temperature increase, thus supporting the eurythermal ability of this species to survive in warmer temperatures (Oellermann et al., 2015a). A further study also indicated that even though the phylogenetic distance of haemocyanin G type are diverse across global octopods, limited differentiation was found between *P. charcoti* and *P. turqueti* (Oellermann et al., 2015b), suggesting the physiological functions of hemocyanins observed in *P. charcoti* could be applicable to *P. turqueti*.

In *P. turqueti*, the putative positive selection of hemocyanin around the warmer Scotia Arc localities (e.g. South Georgia and Shag Rocks), could represent the species potential physiological adaptation to the current, and possibly future, warmer temperatures at lower latitudes. It has been suggested that some Southern Ocean species and regions might respond significantly negatively or positively to predicted warming seafloor temperatures (Griffiths et al., 2017). For the case of *P. turqueti*, it appears that some populations in the Scotia Arc might have the abilities to potentially tolerate warming seafloor temperatures. Conversely, given the apparent genetic differentiation between the Scotia Arc and some continental shelf samples (e.g. East Weddell Sea, Ross Sea, Casey Station, Prydz Bay), as

well as the apparent lack of selection for hemocyanin on the Antarctic continental shelf, *P. turqueti* from these areas may be more vulnerable to warming temperatures in the future.

In addition to *P. turqueti*'s association with temperature, the genetic variation of this species was also found to be associated with lower seafloor salinity and longitude. GDM indicated the genetic differentiation between samples increased rapidly along the lower range of the salinity sampled in this study (up to ~34.5‰), suggesting lower salinity might drive genetic variation. In particular, when comparing samples collected between Scotia Arc locations, the coding sequence of one of the outlier loci was identified as the Baculoviral IAP repeat-containing protein 2 (BIRC2), while RDA also identified the locus linked to BIRC2 was significantly associated with salinity. In the clam *Cyclina sinensis*, BIRC2 is an immune response gene that is down regulated upon low salinity stress from 25‰ to 8‰ (Ni et al., 2021). Finally, longitude was also found to be positively correlated with samples from the Ross Sea and Adélie Land. Association with longitude likely represents genetic isolation from other localities, supporting IBD as a significant driver of genetic variation at a circumpolar scale.

5.5.3 Seascape drivers of *P. turqueti* divergence within the Scotia Arc

Five out of seven genetic clusters (of $K = 7$ in Fig 5.1) observed across all sampled *P. turqueti* had a major presence within the Scotia Arc, supporting high genetic diversity can be found in this area (Strugnell et al., 2017). The distinct distributions of genetic clusters within the region also appear to be linked to different oceanographic regimes known from the Scotia Arc and surrounding areas. For example, the connectivity observed between Amundsen Sea, West Antarctic Peninsula, Livingston Island, Deception Island and Robert Island coincides with the pathway of Circumpolar Deep Water intrusion onto the continental shelf of the Amundsen and Bellingshausen Seas, over West Antarctic Peninsula and along South Shetland islands (Nakayama et al., 2018; Dotto et al., 2021). The close affinities observed between East and South Weddell Sea, Bransfield Strait and Robert Island also coincide with the direction of the Antarctic Slope Current (Collares et al., 2018; Moffat & Meredith, 2018). Finally, a strong connectivity between King George Island and Elephant Island was detected, which could be attributed to the fast moving near-surface circulation between the two areas (Bartlett et al., 2021).

The observed genetic structure in *P. turqueti* within the Scotia Arc, is striking, and is hypothesised to be linked to ocean currents in this study. The influence of regional currents, such as those associated with the Scotia Arc, on gene flow is often discussed in the context of pelagic dispersal (Galaska et al., 2017a; Muñoz-Ramírez et al., 2020; Lau et al., 2021;

Chapter 2, 4). However, the ddRAD loci data of this study also suggest a level of genetic structure linked to genetic isolation across the Scotia Arc. Genetic isolation between Scotia Arc islands has been reported in direct developing species (Linse et al., 2007; Wilson et al., 2009; Lörz et al., 2012), and sometimes in species with pelagic larval dispersal (Demarchi et al., 2010; Young et al., 2015). A recent study examining the genetic divergence of Southern Ocean octopus *Pareledone* spp. (including *P. turqueti*) across the Scotia Arc using microsatellite data, found the genetic differentiation among island groups differed between closely related species (Strugnell et al., 2017), indicating the levels of genetic differentiation in the Scotia Arc might not necessary be strictly related to dispersal strategies. In addition, based on microsatellite data, the genetic differentiation among samples of *P. turqueti* from Antarctic Peninsula, Elephant Island and Signy Island was reported to be associated with sampling collection depth (Strugnell et al., 2017). Interestingly, in this present study, GDM also suggested genetic variation in the Scotia Arc was significantly associated with water depths, but only limited to a small proportion of the total genetic variation (3.81%). *Structure* analysis further indicated genetic clusters 5 and 7 of $K = 7$ (yellow and purple on Fig 5.1) were only found at depths > 350 m around Bransfield Strait, Robert Island, Deception Island, Livingston Island and West Antarctic Peninsula. RDA also highlighted samples from Robert Island and Bransfield Strait were positively associated with water depth. The sampling distribution of *P. turqueti* in the Scotia Arc in the present study was more comprehensive than previous analyses of *P. turqueti* (Strugnell et al., 2012, 2017). The present study suggests that water depth may only be a driver of genetic variation of *P. turqueti* in parts of the Scotia Arc region (e.g. West Antarctic Peninsula, South Shetland islands and Bransfield Strait). Alternatively, water depths could be a proxy for other unaccounted factors that drive the genetic variation of *P. turqueti* around the Scotia Arc. For example, factors such as the stochastic and/or ephemeral historical connectivity and isolation driven by the Quaternary glacial-interglacial periods could influence genetic structure but were not accounted for in this study.

Within the sampled South Shetland island group (King George Island, Robert Island, Livingston Island and Deception Island), a sharp genetic discontinuity was observed between King George Island and other sampled localities. A genetic break between King George Island and other islands within the South Shetland Islands group has also recently been reported in the sponge *Dendrilla antarctica* using neutral ddRAD loci (Leiva et al., 2019). Given the genetic differentiation of *D. antarctica* did not appear to be driven by IBD, Leiva et al (2019) hypothesised that the observed genetic break could be explained by other unknown factors. For the case of *P. turqueti*, the genetic discontinuity between King George Island and Robert Island (and other South Shetland localities) does not seem to be explained by oceanic barriers, as previous drifter data indicated that water can travel from

the north of King George Island to Robert Island within 10 days (Bartlett et al., 2021). Within the South Shetland Islands group, King George Island and Robert Island are separated by Nelson Strait (Capella et al., 1992). However, the waters of Nelson Strait do not exceed ~500 m and its seafloor habitat are characterised by bedrocks and thin sediments (Simms et al., 2011), which are within the distributional and habitat range of *P. turqueti*. Given that the *P. turqueti* samples from King George Island were collected at shallow depths of 111 m, and samples from Robert Island, Livingston Island and Deception Island were collected at depths between 352 - 804 m, a plausible explanation of this genetic break could be genetic isolation-by-water depth within the South Shetland island group.

5.5.4 Seascape dynamics and genomic diversification in *P. turqueti*

Although no significant difference in the proportion of transposable elements (TEs) was detected between outlier and neutral loci, eight out of 42 unique outlier loci detected in *P. turqueti* were related to proteins that are known to interact or repress TEs, or are a form of domesticated TEs (i.e. non-mobile TE). Overall, outlier loci analyses suggest a level of potential selective signals related to genome interactions with transposition in *P. turqueti*. Transposable elements are mobile genetic sequences that have the ability to change positions within a genome and are major components across eukaryotic genomes (Etchegaray et al., 2021), including cephalopods (Whitelaw et al., 2020). TE activity can lead to potential deleterious insertions and genomic instability (Bourque et al., 2018). Within an ecological context, TEs are also hypothesised to promote genotypic variations leading to diversification within and between species (Serrato-Capuchina & Matute, 2018; Niu et al., 2019). The propagation of TEs has been hypothesised to be favoured during local adaptation (Serrato-Capuchina & Matute, 2018), genetic isolation and drift (Jurka et al., 2011), small population size (Belyayev, 2014), and/or response to environmental stress (Pimpinelli & Piacentini, 2020). The identified outlier loci with potential homologous functions in interacting with TEs in this study include DNA repair and recombination protein RAD54-like (Romeijn et al., 2005), and those with potential functions in repressing TEs include Structure-specific endonuclease subunit SLX4 (Lagisquet et al., 2021) and Zinc finger protein 726 (a Kruppel-associated box zinc-finger protein; KRAB-ZFP) (Huntley et al., 2006). In particular, KRAB-ZFPs are thought to have emerged in the last common ancestor of coelacanths and tetrapods, and are believed to be locked in a co-evolutionary ‘arms race’ in response to increasingly diverse TEs across mammalian genomes (Huntley et al., 2006). The selection for TEs and related genes in *P. turqueti* potentially unlocks a new genomic perspective on understanding the long-standing questions regarding the mechanisms of diversification and evolution in the Southern Ocean. Although seascape dynamics may structure the genetic variation of *P. turqueti* across different spatial scales, the detection of

TE-related outlier loci could hint towards the underlying genomic mechanisms leading to diversification across Southern Ocean seascape. Future whole genome sequencing would be required to investigate how TE and TE-interacting genes contribute to genome evolution across evolutionary timeframe and the physical seascape dynamics within the Southern Ocean.

5.6 Conclusion

We found that the genomic variation of *P. turqueti* coincides with the general biogeographic patterns across the Southern Ocean. However, long-distance genetic connectivity was also observed between West and East Antarctica. At the circumpolar scale, bottom water temperature was the most important factor in driving the genomic variation of *P. turqueti*. However, within the Scotia Arc, geographical distance and isolation-by-water depth were the only significant drivers of genomic variation at regional scale. Furthermore, signature of isolation-by-water depth was likely only associated with genetic structure within parts of the Scotia Arc.

Genotype-environmental association was also detected between warmer temperatures and South Georgia/Shag Rocks, with putative positive selection of hemocyanin (oxygen transport protein) indicated, suggesting possible physiological adaptation to warmer temperatures around sub-Antarctic localities. Finally, our work also proposed a link between possible selection for genes that interact or repress transposable elements and the drivers of genomic variations in the Southern Ocean, including seascape dynamics. Future work examining the genome architecture of Southern Ocean taxa, including *P. turqueti*, using whole genome sequencing should provide a thorough understanding of the genomic mechanisms leading to diversification across the Southern Ocean.

CHAPTER 6

Genomic evidence of West Antarctic Ice Sheet collapse during the Last Interglacial Period

Lau, S.C.Y., Wilson, N.G., Golledge, N.R., Naish, T.R., Silva, C.N.S., Strugnell, J.M.

This chapter is formatted for *Nature*.

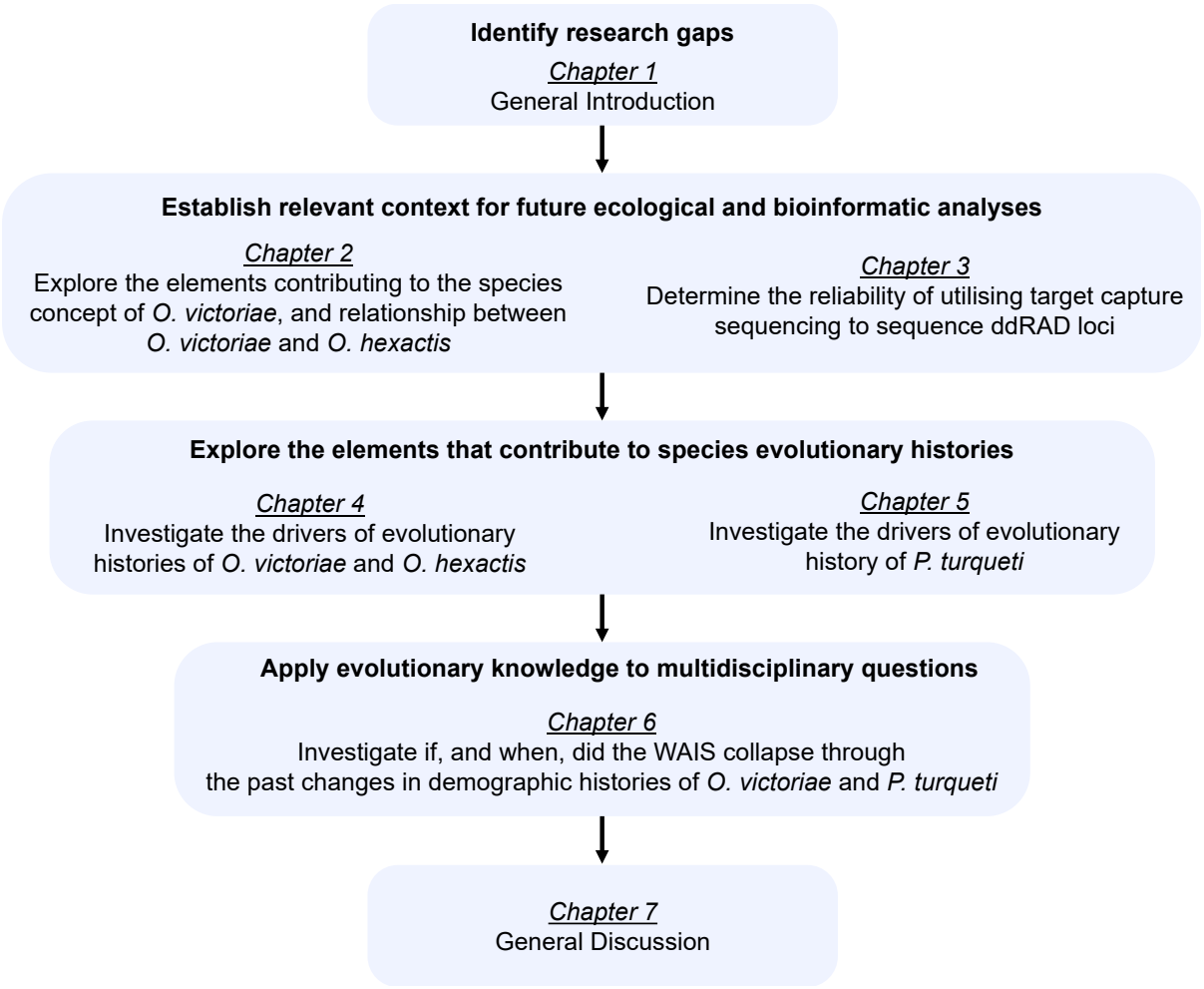

6.1 Abstract

The marine-based West Antarctic Ice Sheet (WAIS) is vulnerable to collapse based on current trajectories in temperature rise. However, the tipping point of WAIS collapse is unclear, and knowledge of the degree of ice loss during similar past climates can inform, and thus constrain this uncertainty. It is well understood that the warm interval of the Last Interglacial Period (LIG; ~120,000 years ago) experienced global sea level 6 -11 m higher than today, but the average temperature was only 0.5 - 2.0°C warmer than the pre-industrial period. Using genome-wide single-nucleotide-polymorphisms of species with circum-Antarctic distributions, the octopus *Pareledone turqueti* and the brittle star *Ophionotus victoriae*, we present direct empirical evidence indicating the WAIS collapsed during the LIG. The genomic patterns of *P. turqueti* and *O. victoriae* support both contemporary circumpolar gene flow and also distinct signatures of historical trans-west Antarctic seaways linking the present-day Weddell Sea, Amundsen Sea and Ross Sea. We infer the historical trans-west Antarctic seaways can be dated back to LIG, and such historical connectivity was facilitated by a complete WAIS collapse. Our results outline that the tipping point of WAIS instability could potentially be reached under current climate change trajectories. Models that are used to project global sea level rise should incorporate the probable collapse of the WAIS in order to accurately inform the future changes of the world's coastlines.

Keywords: admixture, demographic modelling, population genomics, Last Interglacial Period, MIS 5e, West Antarctic Ice Sheet collapse

6.2 Introduction

A major uncertainty in global mean sea level (GMSL) rise projections lies within the stability of the West Antarctic ice sheet (WAIS) (Golledge et al., 2015; DeConto & Pollard, 2016; Fox-Femper et al., 2021). The marine-based WAIS has lost 159 ± gigatons of ice mass per year between 1979 - 2017 (Rignot et al., 2019), and continues to be a major contributor to GMSL rise under all CO_2 emission scenarios (Fox-Femper et al., 2021). It is unclear whether the WAIS is vulnerable to future collapse due to poor understanding of the mechanisms linked to marine ice-sheet instability (MISI) (Steig & Neff, 2018; Robel et al., 2019; Garbe et al., 2020). A complete WAIS collapse could raise global sea level by ~3.3 - 5 m (Vaughan, 2008; Bamber et al., 2009). Knowledge of how the WAIS was configured during warmer periods in the recent geological past is urgently needed to constraint MISI and future sea level rise projections (Harrison et al., 2015; Kemp et al., 2015; Gilford et al., 2020).

Geological reconstructions indicate that during the Last Interglacial Period (LIG) in the Pleistocene (Marine Isotope Stage [MIS] 5e, ~129 - 116 thousand years ago [ka]), the average air temperature was 0.5 - 2.0°C warmer than the pre-industrial period with GSML 6.6 - 11.4 m higher than the present day (Turney et al., 2020). So far, marine drill core records of WAIS configuration remain inconclusive (Scherer et al., 2008; Naish et al., 2009). Existing ice sheet models have yielded conflicting WAIS reconstructions during the LIG, ranging from no collapse (Holloway et al., 2016), to partial (Golledge et al., 2021) or full collapse (Steig et al., 2015; DeConto & Pollard, 2016). To date, there is no empirical evidence indicating the stability of the WAIS in last three million years since the MIS 31 (Grant et al., 2019).

A complete historical collapse of the WAIS would lead to the opening of trans-west Antarctic seaways linking the present-day Weddell Sea (WS), Amundsen Sea (AS) and Ross Sea (RS) (Strugnell et al., 2018). Such historic seaways would have allowed marine animals to migrate and/or inhabit across the opened straits, thus leaving genetic signatures of past connectivity in the genomes of their descendent, extant populations (hereafter seaway populations) (Strugnell et al., 2018). Previous biological studies have supported the existence of trans-west Antarctic seaways; these studies were based on species assemblage data at macro-evolutionary scales (Linse et al., 2006; Barnes & Hillenbrand, 2010; Vaughan et al., 2011; Moreau et al., 2019) or low resolution genetic data that are based on single locus or microsatellite data (Held & Wägele, 2005; Linse et al., 2007; Strugnell et al., 2012; Collins et al., 2020) that cannot support accurate demographic analysis. Importantly, all of these studies lacked sample sizes or spatial coverage that could distinguish the signatures of trans-west Antarctic seaways from contemporary circumpolar

ocean currents. Here we used a comprehensive sampling strategy to robustly test for the presence of trans-west Antarctic seaways using genome-wide single-nucleotide-polymorphisms (SNPs) data in two marine benthic animals with circum-Antarctic distributions, the octopus *Pareledone turqueti* and the brittle star *Ophionotus victoriae*.

6.3 Evidence of circumpolar gene flow and historical seaway connectivity

We sequenced genome-wide SNPs derived from double-digest restriction site-associated DNA (ddRAD) loci from 89 *P. turqueti* and 158 *O. victoriae* indiviudals collected from around the Southern Ocean. The datasets represent both species' circumpolar genomic variation, which underlies their contemporary connectivity driven by oceanic currents, mainly the Antarctic circumpolar current (ACC; clockwise) and the Antarctic Slope Current (ASC; counter-clockwise) (Fig 6.1), as well as historical connectivity linked to past trans-west Antarctic seaways. We used reduced SNP datasets (one SNP per locus) to analyse population structure, which included 1,653 and 5,437 unlinked SNPs for *O. victoriae* and *P. turqueti*, respectively. Using *Structure* (Fig 6.1) and PCA (Supplementary Fig 6.1), we confirm both species exhibit contrasting levels of genetic structure. *Pareledone turqueti* is characterised by benthic crawling juveniles, and its population genomic variation is characterised by biogeographically structured populations across the Southern Ocean (Fig 6.1b, Supplementary Fig 6.1a). In *P. turqueti*, long-distance connectivity linking East and West Antarctica, across the Antarctic continental shelf and Antarctic islands, is also observed (e.g. admixture between Prydz Bay, Adélie Land, RS, Elephant Is. and South WS). *Ophionotus victoriae* is characterised by broadcasting free-swimming larvae, and we found that its population genomic variation is highly dispersed and is explained by three components (Fig 6.1c, Supplementary Fig 6.1b): (1) distinct circumpolar connectivity linking all Antarctic continental shelf localities, (2) distinct circumpolar connectivity between Antarctic islands off the Antarctic continental shelf, and (3) admixture within Antarctic continental shelf and Antarctic islands. In both species, admixture is observed between WS, AS and RS. However, admixture at circumpolar scale is also detected (more pronounced in *O. victoriae*), likely reflecting the well-established role of circumpolar currents in driving gene flow in Southern Ocean benthic species.

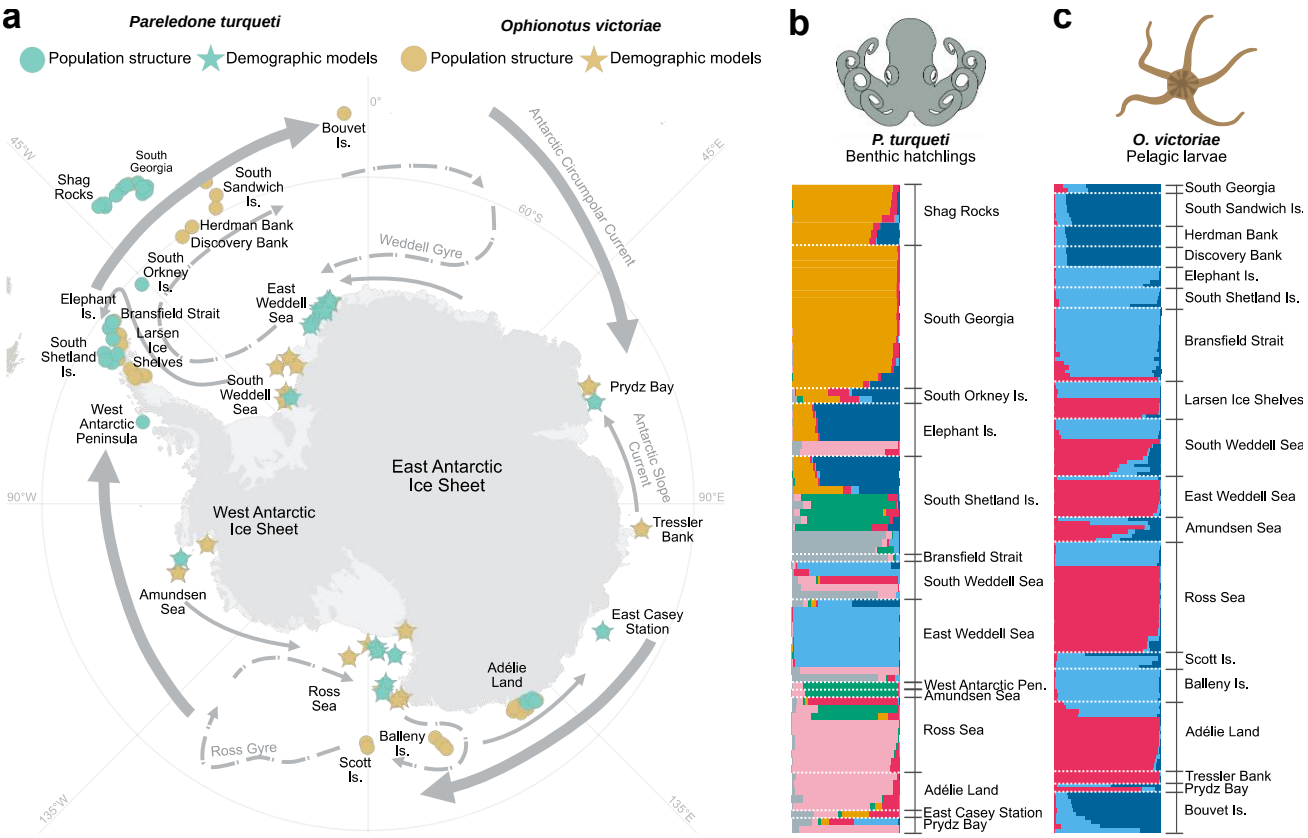

Fig 6.1 Sampled locations of *Pareledone turqueti* and *Ophionotus victoriae* with *Structure* analyses. (a) Map of sample locations including the directionalities of the major circumpolar currents (Antarctic Circumpolar Current, Antarctic Slope Current) and regional currents (Weddell Gyre, Ross Gyre) in the Southern Ocean. Colours = species. Circles = samples used for analyses of population structure. Stars = samples used for demographic modelling to test for the existence of historical trans-west Antarctic seaways. (b, c) Clustering analysis using *Structure* method inferred $K = 7$ for *P. turqueti* and $K = 4$ for *O. victoriae*. Each horizontal bar represents an individual sample, bars are grouped by geographical locations within species, colours correspond to the proportion of each genetic cluster in the individual within species.

To ascertain whether there is a distinct historical relationship between WS-AS-RS in relation to other Southern Ocean localities, we generated admixture graphs using *TreeMix* using reduced SNP datasets (Supplementary Fig 6.2). In *P. turqueti*, *TreeMix* did not suggest a clear affinity between WS-AS-RS (Supplementary Fig 6.2a). Instead, four clusters were inferred, largely corresponding to the levels of admixture proportions suggested by *Structure* (Fig 6.1b), indicating a strong signal of isolation-by-geographical distance as expected in species with structured populations. In *O. victoriae*, short internal branch lengths were observed, likely linked to the species' high dispersal ability with persistent gene flow driven by oceanic currents (Supplementary Fig 6.2b). In *O. victoriae*, *TreeMix* also shows that RS, East WS and AS form a distinct clade, with gene flow inferred from AS to South WS, supporting a unique connectivity signal between WS-AS-RS.

We further examined distinct admixture signals between WS-AS-RS with respect to South Shetland Islands (SHE) and East Antarctica (EA) samples using 26,769 and 101,346 linked SNPs (all SNPs kept across loci), in *O. victoriae* and *P. turqueti*, respectively. SHE and EA are known to be influenced by both the ACC and ASC, but are irrelevant to the historical trans-west Antarctic connectivity; thus these are ideal locations that can separate present-day connectivity along WAIS and East Antarctic Ice Sheet (EAIS) from historical signals.

We used the *D*-statistic to characterise excess derived allele sharing between populations, as well as the outgroup-f_3-statistic to measure shared genetic drift between pairs of populations since they diverged from a common outgroup. In *P. turqueti*, we find that when SHE is the sister lineage to AS/RS and WS (*D*(AS/RA, SHE, WS, outgroup)), we find excess allele sharing between SHE and WS (Fig 6.2a). When EA is treated as sister lineage to AS/RS and WS (*D*(AS/RA, EA, WS, outgroup)), excess allele sharing between EA-WS is observed (Fig 6.2a). However, the least amount of drift is detected between RS and WS, and the highest level of drift between SHE and WS/AS (Fig 6.2b). In *O. victoriae*, we detected excess allele sharing between RS and WS, and between AS and WS, when SHE is the sister lineage (Fig 6.2a). However, the least amount of genetic drift is detected between SHE to other tested populations (Fig 6.2b). When EA is treated as sister lineage, we find no significant allele sharing between *O. victoriae* populations (Fig 6.2a), but the highest amount of drift was detected between EA and seaway populations (Fig 6.2b). These results confirm that in *P. turqueti*, the unusually short shared evolutionary time between RS-WS suggests signal of historical seaway connectivity in a species that is characterised by biogeographically structured populations. In *O. victoriae*, there is also distinct admixture between seaway populations around the WAIS, but signals are insignificant around EAIS. In both species, given the close affinities between seaway locations and SHE/EA, signals of seaway admixture are likely also masked by circumpolar gene flow.

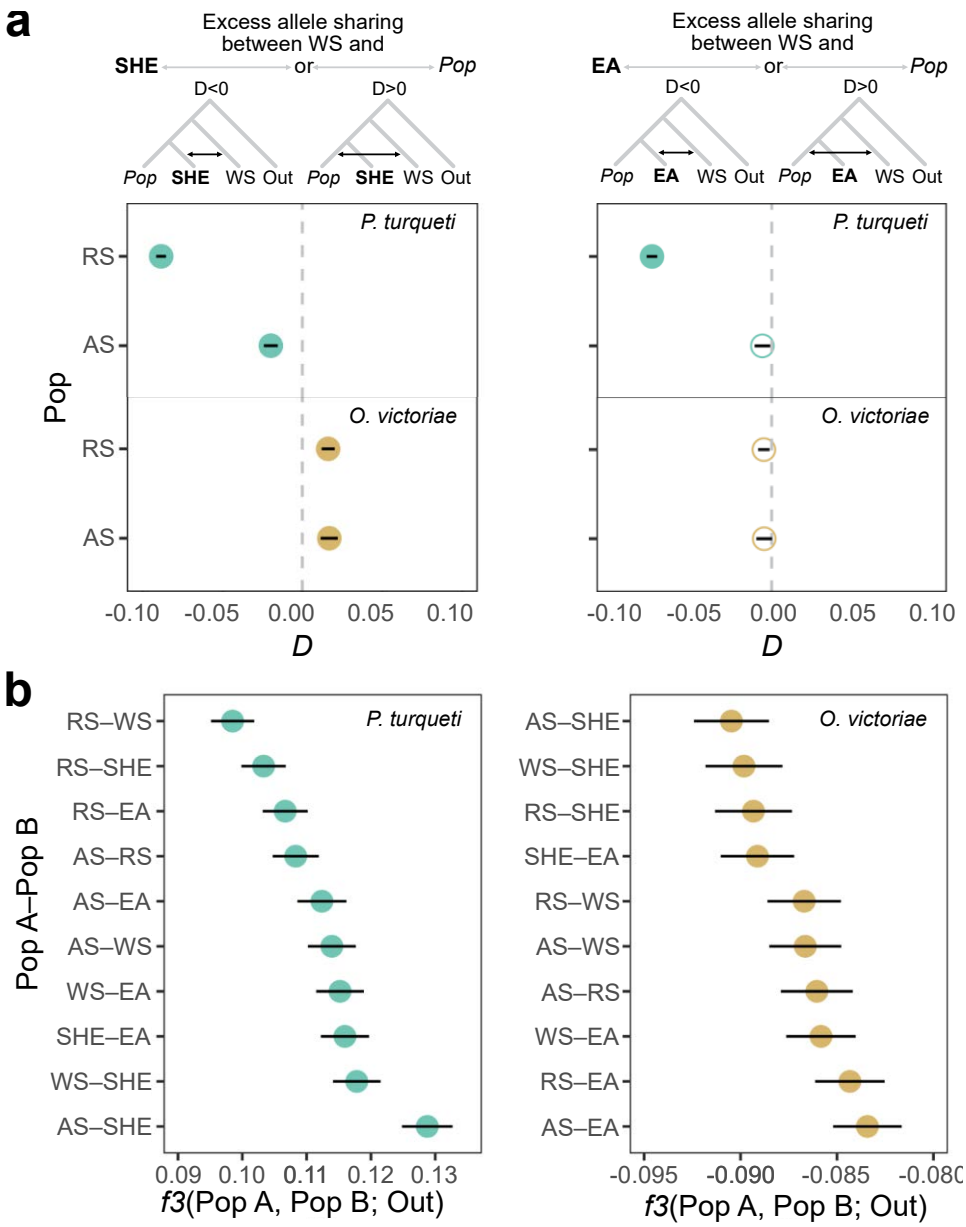

Fig 6.2 Evidence of distinct admixture between Weddell Sea (WS), Amundsen Sea (AS) and Ross Sea (RS), as well as contemporary gene flow, in *Pareledone turqueti* and *Ophionotus victoriae*. Error bars = standard errors, filled circles = significant (Z-score values > 3 or < -3), empty circles = not significant (Z-score values between -3 and 3). (a) In *P. turqueti*, D-statistic shows significant excess of allele sharing between WS and South Shetland Islands (SHE) (left panel), and between WS and East Antarctica (EA) (right panel). In *O. victoriae*, D-statistic also shows significant excess of allele sharing between WS-RS, WS-AS relative to SHE (left panel). However, signature of allele sharing between WS-RS became insignificant in *O. victoriae* relative to EA (right panel). (b) Outgroup-f_3-statistics between pairs of populations with less shared drift between pairs of population following decreasing f_3 values. In *P. turqueti* (right panel), RS and WS shared the least amount of genetic drift, indicative of distinct admixture unexplained by contemporary genetic patterns. In *O. victoriae* (left panel), SHE showed limited drift with AS, WS, RS, indicating strong circumpolar gene flow.

6.4 Dating West Antarctic Ice Sheet collapse during the Last Interglacial Period

We used a site-frequency-spectrum (SFS)-based, coalescent demographic modelling framework to test for the hypothesis of whether historical trans-west Antarctic seaways existed followed by contemporary circumpolar gene flow. For demographic modelling, we included samples from WS, AS, RS and EA, with 30,182 and 115,022 linkage disequilibrium (LD)-pruned SNPs across loci in *O. victoriae* and *P. turqueti*, respectively. We employed a hierarchical approach to test for WAIS collapse scenarios while incorporating modern circumpolar gene flow in the models (Supplementary Fig 6.3-6.4). We first determined the phylogenetic relationship between WS, AS, RS and EA (Supplementary Fig 6.3a). Then, based on the best topology, we compared contrasting scenarios of past WAIS configurations. For the models, we hypothesised that since population divergence, WS, AS, RS experienced no, partial, or complete connectivity, followed by modern circumpolar gene flow linking between WS, EA, RS and AS (Supplementary Fig 6.3b, c, Supplementary Fig 6.4a, b). For circumpolar gene flow, we considered both directionalities of the ACC and ASC (clockwise and counter-clockwise) (Supplementary Fig 6.3c, Supplementary Fig 6.4b). For *O. victoriae*, the dataset did not have enough power (i.e. low number of SNPs) to model all aspects of ecologically realistic scenarios, therefore we could only consider simpler models that included the directionality of ACC (clockwise) (Supplementary Fig 6.3b, Supplementary Fig 6.4a).

For *P. turqueti* and *O. victoriae*, the observed SFSs were best explained by the scenario of a complete historical WAIS collapse, followed by modern circumpolar gene flow (Supplementary Notes 6.1). For *P. turqueti*, the ancestral population of *P. turqueti*'s seaway and EA populations experienced a population expansion at 2.76 (95% confidence interval [CI] between 1.47 and 5.65) million years ago (Fig 6.3a, Supplementary Table 6.1), corresponding to the previous estimated timing of the species' continental shelf clade emergence based on mitochondrial data (Strugnell et al., 2012). Then, AS was split from the ancestral population of WS, RS and EA at 373,945 (95% CI between 158,500 and 1,071,228) years ago, and direct gene flow between WS-AS, AS-RS and WS-RS was detected at 107,237 years ago (95% CI between 57,855 and 162,553). Finally, contemporary gene flow following to the directionality of the ACC and ASC began at modern times (95% CI between 0 and 0 years ago).

For *O. victoriae* (Fig 6.3b, Supplementary Table 6.2), the ancestral population of *O. victoriae* experienced a population expansion at 3.82 million years ago (95% CI between 3.14 and 9.05). Then, AS was split from the ancestral population of WS, RS and EA at 3,770 years

ago (95% CI between 2.74 and 7.28 million years ago). The discordance between the maximised AS divergence time from ancestral population and 95% CI ranges is likely caused by the impacts of severe recent bottleneck on parameter scaling. Direct gene flow between WS-AS, AS-RS and WS-RS was dated back to 1,250 years ago (95% CI between 286 and 13,943). Finally, contemporary gene flow following to the directionality of the ACC began at modern times (95% CI between 0 and 0 years ago).

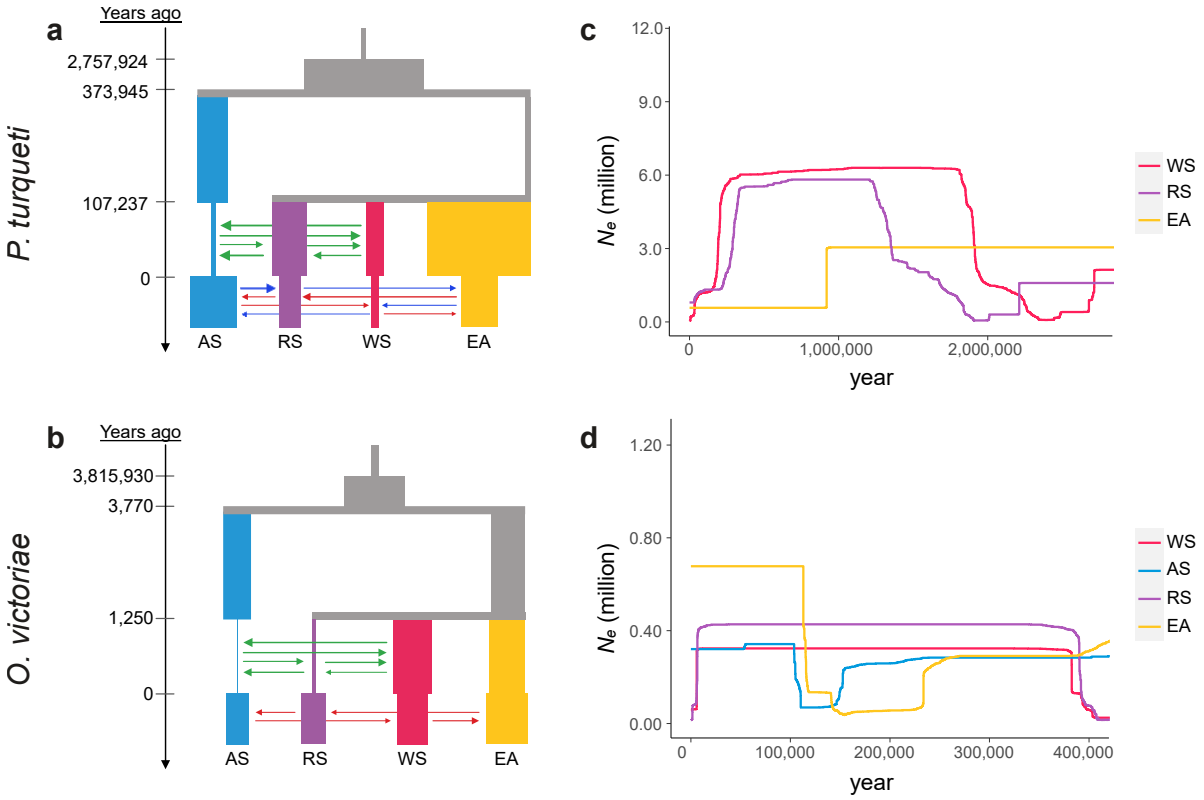

Fig 6.3 Demographic models of *Pareledone turqueti* and *Ophionotus victoriae* indicating a complete historical West Antarctic Ice Sheet collapse scenario, supplemented by *StairwayPlot* indicating past changes in population size throughout species history. (a, b) Maximum likelihood model for *P. turqueti* (a) and *O. victoriae* (b) including Amundsen Sea (AS), Ross Sea (RS), Weddell Sea (WS) and East Antarctica (EA) populations. Parameter estimates and 95% confidence intervals (CI) are reported in Supplementary Table 6.1- 6.2. Time of the events modelled are shown on the left and values represent those maximised the likelihoods. The width of the bars is proportional to the effective population size of the population. Arrows indicate asymmetric migration between populations (forward in time), with the width of the arrows proportional to the strength of migration. (c, d) *StairwayPlot* reconstruction of past changes in effective population size over time in *P. turqueti* (c) and *O. victoriae* (d) since species divergence. Solid vertical line represents timing of the Last Interglacial Period (125,000 years ago). Dashed line represents timing of the Last Glacial Maximum (12,000 years ago).

Our demographic modelling approach was specifically designed to test whether historical trans-west Antarctic seaways existed in the past that could be detected with simple contrasting models. The evolutionary histories of *P. turqueti* and *O. victoriae* are highly complex with unique demographic changes associated with each glacial-interglacial cycle

throughout the Quaternary. Our models did not sequentially reconstruct their past changes in population size and connectivity patterns to avoid over-parameterisation in limited SNP datasets (i.e. RAD loci). We applied our method to define a broad model of demographic changes in Southern Ocean benthic fauna that refine our knowledge of Antarctic history and raise interesting questions. A similar approach has been performed in interpreting human migration history; a broad, simplified "out-of-Africa" model was first verified by Gutenkunst et al. (2009) and Excoffier et al. (2013), and subsequently acted as a foundational basis for more complex demographic models involving additional human populations and refined sampling approaches (e.g. Rasmussen et al., 2011; Choin et al., 2021).

Importantly, during the LIG, large areas of newly ice-free habitats would have become available for benthic fauna to colonise and permit population size expansion. During the subsequent Last Glacial Maximum (LGM, ~20,000 years ago) following the LIG, the AIS expanded across the Antarctic continental shelf, and the marine shelf habitats would likely be reduced to small, isolated pockets of *in situ* ice-free refugia (Thatje et al., 2005; Convey et al., 2009) leading to severe population bottleneck events (Allcock & Strugnell, 2012). Such dramatic bottlenecks during the LGM were most apparent for RS and WS populations of *O. victoriae* (Fig 6.3c), indicating both lineages likely persisted in *in situ* ice free refugia in the areas. Therefore, the young event ages detected in the demographic models of *O. victoriae* likely do not reflect the accurate timing of modelled events (e.g. historical WAIS connectivity); rather, the shallow tree length was expected to be caused by recent severe bottlenecks in some populations. A severe recent bottleneck would produce many coalescence events at the same time point, leading to a reduction in the overall tree length (Excoffier et al., 2013; Terhorst & Song, 2015), thus confounding the parameter scaling of time, population size and migration rates (Excoffier et al., 2013). Nonetheless, variation in tree length does not preclude the conclusion of genealogy (i.e. model choice) (Excoffier et al., 2013; Gattepaille et al., 2013), thus ensuring our connectivity conclusions were still robust. Finally, *O. victoriae* and its sister species *O. hexactis* diverged around the onset of MIS 11 (434,307 years ago ± 433,399 and 435,212 (95% CI)) (*Chapter 4*). In *O. victoriae*, the only subsequent ecological and geological opportunity that would most likely enable gene flow linking to a full WAIS collapse scenario would be during the LIG.

Another observation that reflects the complex evolutionary histories of Southern Ocean fauna is that signatures of deep-sea refugia (in the form of population expansion) were also observed in *O. victoriae* in AS and EA (Fig 6.3c). Gradual population decline was observed across all modelled populations in *P. turqueti* (Fig 6.3d), despite this species having likely exclusively persisted within *in situ* shelf refugia during the LGM (Strugnell et al., 2012). These species-specific characteristics of glacial refugial survival mechanisms have also

been previously reported (Strugnell et al., 2012; Lau et al., 2021). These signatures were not accurately detected by *Fastsimcoal*, as *StairwayPlot* is a model flexible method that can explore a wider, continuous model space than model-constrained methods (e.g. *fastsimcoal*), which pre-specify the breakpoints in demographic changes (Liu & Fu, 2015). We particularly utilised a target capture approach to sequence reduced representation genomic data in samples with DNA degradation, and inferred signatures of historical WAIS collapse alongside gene flow driven by contemporary circumpolar currents. We also identified that signatures of historical LIG WAIS connectivity were likely masked by the signatures of LGM glacial cycle survival. Importantly, different species (*P. turqueti* versus *O. victoriae*), and different populations within a species (*O. victoriae*), can experience contrasting changes in coalescence rates over time due to various survival strategies during the LGM. Future whole genome sequencing can offer even higher resolution data to resolve contrasting population and species histories under a coalescence framework, and to sequentially reconstruct past changes in demographic histories throughout modern times, through the LGM, LIG and beyond. Regardless of the overall challenge of demographic modelling for Southern Ocean species, signatures of a complete WAIS collapse, likely during the LIG, were clear enough to be inferred in two independent Southern Ocean species with contrasting reproductive strategies. Such conclusions would not be possible without prior understanding of the overall species evolutionary context, and how LGM survival can significantly impact simple demographic inference.

6.5 Implications for future sea level rise projection

Here we provide empirical evidence indicating the WAIS collapsed during the LIG. The statistically significant observed likelihood of direct LIG seaway connectivity between WS-AS-RS cannot be explained by circumpolar currents (ACC and ASC) in either *P. turqueti* or *O. victoriae*. For *P. turqueti*, a higher level of biological migrations was detected among Weddell Sea, Amundsen Sea and Ross Sea during the LIG relative to present day. This indicates that suitable habitat for marine benthic taxa was available across the area that today is covered by the WAIS, thus providing support for a complete WAIS collapse. The current uncertainty of near-future sea level rise largely lies within the undetermined tipping point of MISI (Golledge et al., 2015; DeConto & Pollard, 2016; Robel et al., 2019). By demonstrating that the WAIS collapsed in the last interglacial when the air temperature was 0.5 - 2.0°C warmer than the pre-industrial period, we have identified a tipping point of WAIS stability, and by extension MISI, as a palaeo-constraint. Currently, MISI is only considered under high CO_2 emissions scenarios, e.g. Representative Concentration Pathway (RCP) 8.5 scenario (air temperature increase between 3.3 - 5.7 ºC by 2100), in which sea level is projected to rise to ~1 m by 2100 and ~3.5 m by 2150 (Fox-Femper et al., 2021). Under the

current likely RCP 4.5 scenario, the air temperature projection is also projected to reach 2.1-3.5 ºC by 2100 (Fox - Femper et al., 2021), which could also potentially be within the tipping point of future WAIS collapse. Importantly, MISI is regulated by a self-reinforcing mechanism (Garbe et al., 2020), meaning that the collapse of WAIS is irreversible for centuries once underway (Weber et al., 2021). Future global sea level rise projections should incorporate the potential collapse of the WAIS as a crucial parameter under relevant RCP scenarios in order to accurately project future sea level rise, as well informing decisions regarding socioeconomic, demographic, institutional, and political policies of the future of global coastal communities.

6.6 Methods

6.6.1 Target capture sequencing of ddRAD loci in *P. turqueti*

The genomic data of this chapter was generated in *Chapter 3*. In brief, tissue samples of *Pareledone turqueti* (n = 87) collected around the Antarctic continental shelf and Antarctic islands, between the depths of 102 - 1342 m, were sequenced with target capture sequencing with probes designed from previously identified ddRADseq loci (Fig 6.1a; Supplementary Table 6.3). Two outgroup species (*P. aequipapillae*; ID: 44064_1 *and P. cornuta*; ID: CT931) collected from the Ross Sea was also included in the target capture dataset. Target capture sequencing of 8,942 ddRAD loci of all *P. turqueti* and outgroup samples were detailed in *Chapter 3*. In addition, 56 out of the 87 *P. turqueti* samples, as well as the two outgroup samples, were also included in previous studies which analysed their COI and microsatellite data (Strugnell et al., 2012, 2017).

6.6.2 Target capture data processing, reads mapping and variant calling (*P. turqueti*)

Raw target capture reads were demultiplexed with adapters and barcodes removed using *process_shortreads* in *Stacks* v2.3d (Catchen et al., 2013). Reads with phred quality less than 20 (Q < 20) were also discarded, and polyG in read tails were trimmed, using *fastp* v0.20 (Chen et al., 2018). Potential contaminants (human and microorganisms) were identified using *Kraken* v1.0 (Wood & Salzberg, 2014), and reads that matched those of the contaminant database were removed. Cleaned and trimmed reads were then checked for quality using *fastQC* v0.11.7 (Andrews, 2019).

Cleaned target capture reads were mapped to the consensus sequences of ddRAD loci that were used for bait design using *bwa* v0.7.17 *mem* with default parameters (Li & Durbin, 2009). *Samtools* v1.7 (Li et al., 2009) was used to sort alignments by coordinates, and PCR

duplicates were marked and removed using *picard* v2.18.1 (Broad Institute, 2019). Sites were called across all samples using *bcftools* v1.7 *mpileup* (Li, 2011). Then, indels and samples with high missing data on an individual basis (> 80%) were first removed, and only sites with Phred scaled site quality score more than 30 were kept (--minQ 30). Further SNP filtering were performed based on the conditions of data analyses using *VCFtools* v0.1.16 (Danecek et al., 2011).

For the inference of population structure and relationship at a circumpolar scale (Principal Component Analysis (PCA)), *Structure* v.2.3.4 (Pritchard et al., 2000), *TreeMix* v.1.13 (Pickrell & Pritchard, 2012), we included all *P.* samples (n = 87), as well as outgroup species (n = 2). We reduced the dataset to unlinked 5,437 biallelic SNPs, filtered based on the following steps: Sites with mean read depth of less than 14x and greater than 87x (=2*average depth (43.7x)) were removed (--min-meanDP 14, --max-meanDP 87). Only biallelic sites were kept (--min-alleles 2, --max-alleles 2). Sites were kept if present in 50% of all samples (--max-missing 0.5). Sites with a minor allele frequency of at least 5% were kept (--maf 0.05). To remove sites that were likely belong to paralogous loci and therefore artificial SNPs, only sites with a maximum observed heterozygosity of 0.5 were kept (Hohenlohe et al., 2011; Gargiulo et al., 2020), identified via the R package *adegenet* v2.1.3 (Jombart & Ahmed, 2011). Lastly, only one site per locus were kept (--thin 1000; an arbitrary number larger than the longest contig (in basepair (bp)) in the bait set).

For the inference of admixture and past population demography (*AdmixTools* v7.0.1 (Patterson et al., 2012), *StairwayPlot* v2 (Liu & Fu, 2015, 2020)), we included *P.* samples (in diploids) from Weddell Sea (WS) (n = 16), Amundsen Sea (AS) (n = 1), Ross Sea (RS) (n = 10), South Shetland Islands (SHE) (n = 11) and East Antarctica (EA) (n = 3), as well as outgroup species (n = 2). East Antarctic localities included Prydz Bay and East Casey Station in *P. turqueti*. We excluded Adélie Land from EA samples as *Structure*, PCA, and *TreeMix* indicated uniquely strong admixture between Adélie Land and RS in *P. turqueti*. The observed Adélie Land - RS connectivity could be linked to regional currents, thus confounding the interpretation of historical trans-west Antarctic connectivity while considering for the effects of circumpolar gene flow using EA samples. Filtering thresholds were relaxed in order to retain maximum number of informative SNPs about demographic events, as the signals of true demographic events would be much stronger than a few erroneous loci (Gargiulo et al., 2020). We reduced the dataset to linked 101,346 biallelic SNPs, filtered based on the following steps: Sites with mean read depth of less than 16x and greater than 96x (=2*average depth (48.0x)) were removed (--min-meanDP 16, --max-meanDP 96). Only biallelic sites were kept (--min-alleles 2, --max-alleles 2). Sites were kept if present in 50% of all samples (--max-missing 0.5). Sites with a minor allele count of at

least 1 were kept (--mac 1) in order to exclude singletons. Only sites with a maximum observed heterozygosity of 0.7 were kept (Hohenlohe et al., 2011; Gargiulo et al., 2020), identified via the R package *adegenet*. For *StairwayPlot*, we did not project the spectra downward as the number of segregating sites are already maximised at existing sample size per population.

For demographic modelling using *fastsimcoal* v2.6 (Excoffier et al., 2013), we included *P. turqueti* samples (in diploids) from WS (n = 16), AS (n = 1), RS (n = 10) and EA (n = 3; excluding Adélie Land). We reduced the dataset to unlinked 115,022 biallelic SNPs with 195,120 monomorphic sites, filtered based on the following steps: Sites with mean read depth of less than 16x and greater than 96x (=2*average depth (48.0x)) were removed (--min-meanDP 16, --max-meanDP 96). Only sites with a maximum of two alleles were (--min-alleles 1, --max-alleles 2). Sites were kept if present in 50% of all samples (--max-missing 0.5). Only sites with a maximum observed heterozygosity of 0.7 were kept (Hohenlohe et al., 2011; Gargiulo et al., 2020), identified via the R package *adegenet*. Next, we randomly resampled a fixed number of diploid genotypes from each locality (WS: 13, AS: 1, RS: 8, EA: 3) to a dataset without missing data while maximising the number of SNPs and genotypes across localities, using a python script fastsimcoal/sampleKgenotypesPerPop.py. Then, within each RAD locus, SNPs with linkage were removed based on $r^2 > 0.95$, identified via --geno-r2 (--min-r2 0.95), following Marques et al. (2019). We also randomly removed a number of monomorphic sites proportional to the retained number of SNPs after linkage pruning.

6.6.3 Target capture sequencing of ddRAD loci in *O. victoriae*

Target capture sequencing of ddRAD loci in *O. victoriae* was detailed in *Chapter 4*. In brief, tissue samples of the brittle star *Ophionotus victoriae* (n = 169) deposited at Western Australian Museum (WAM), Museum Victoria (MV), and Scripps Institution of Oceanography (SIO-BIC) and the National Institute of Water and Atmospheric Research (NIWA) were sequenced via target capture approach and analysed in this study (Fig 6.1a; Supplementary Table 6.4). One outgroup species (*O. hexactis*; ID: SIO-BICE5246) collected from Shag Rocks was also included in the target capture dataset. All *Ophionotus* samples were a subset of a previous study which analysed their partial mitochondrial cytochrome oxidase I (COI) data (Lau et al. 2021; *Chapter 2*).

6.6.4 Target capture data processing, reads mapping and variant calling (*O. victoriae*)

Raw data were demultiplexed with barcodes removed using *process_shortreads* in *Stacks*. Reads with phred quality less than 20 (Q < 20) were discarded, and polyG in read tails were trimmed, using *fastp*. Potential contaminants (human and microorganisms) were identified using *Kraken*, and reads that matched those of the contaminant database were removed. Reads were then truncated to a final read length of 140 bp. Cleaned and trimmed reads were checked for quality using *fastQC*, and mapped to the consensus sequences of ddRAD loci used for bait design using *bwa mem* with default parameters. *Samtools* was used to sort alignments by coordinates, and PCR duplicates were marked and removed using *picard*. Sites were called across all samples using *bcftools mpileup*. Then, indels and samples with high missing data on an individual basis (> 80%) were first removed, and only sites with Phred scaled site quality score more than 30 were kept (--minQ 30). Further SNP filtering were performed based on the conditions of data analyses using *VCFtools*.

For the inference of population structure and relationship at a circumpolar scale (PCA, *Structure*, *TreeMix*), we included *O. victoriae* samples (n = 166), as well as outgroup species (n = 1). We reduced the dataset to unlinked 1,653 biallelic SNPs, filtered based on the following steps: Sites with mean read depth of less than 10x and greater than 32x (=2*average depth (15.8x)) were removed (--min-meanDP 10, --max-meanDP 32). Only biallelic sites were kept (--min-alleles 2, --max-alleles 2). Sites were kept if present in 70% of all samples (--max-missing 0.7). Sites with a minor allele frequency of at least 2% were kept (--maf 0.02). To remove sites that were likely belong to paralogous loci and therefore artificial SNPs, only sites with a maximum observed heterozygosity of 0.5 were kept (Hohenlohe et al., 2011; Gargiulo et al., 2020), identified via the R package *adegenet*. Lastly, only one site per locus were kept (--thin 140).

For the inference of admixture and past population demography (*AdmixTools*, *StairwayPlot*), we included *O. victoriae* samples (in diploids) from WS (n = 24), AS (n = 11), RS (n = 30), SHE (n = 5) and EA (n = 8), as well as outgroup species (n = 1). East Antarctic localities included Prydz Bay and Tressler Bank in *O. victoriae*. We excluded Adélie Land from EA samples as *Structure*, *PCA*, and *TreeMix* indicated uniquely strong admixture between Adélie Land and RS in *O. victoriae*. The observed Adélie Land - RS connectivity could be linked to regional currents, thus confounding the interpretation of historical trans-west Antarctic connectivity while considering for the effects of circumpolar gene flow using EA samples. Filtering thresholds were relaxed in order to retain maximum number of informative SNPs about demographic events, as the signals of true demographic events would be much stronger than a few erroneous loci (Gargiulo et al., 2020). We reduced the dataset to linked 26,769 biallelic SNPs, filtered based on the following steps: Sites with mean read depth of less than 10x and greater than 39x (=2*average depth (19.2x)) were removed (--min-

meanDP 10, --max-meanDP 39). Only biallelic sites were kept (--min-alleles 2, --max-alleles 2). Sites were kept if present in 50% of all samples (--max-missing 0.5). Sites with a minor allele count of at least 1 were kept (--mac 1) in order to only exclude singletons. Only sites with a maximum observed heterozygosity of 0.7 were kept (Hohenlohe et al., 2011; Gargiulo et al., 2020), identified via the R package *adegenet*. For *StairwayPlot*, we projected the spectra downward in AS (to haploid n = 16), RS (to haploid n = 56) and EA (to haploid n = 12), in order to maximise the number of segregating sites for population size change inferences.

For demographic modelling using *fastsimcoal*, we included *O. victoriae* samples (in diploids) from WS (n = 24), AS (n = 11), RS (n = 30) and EA (n = 8; excluding Adélie Land). We reduced the dataset to unlinked 30,182 biallelic SNPs with 39,205 monomorphic sites, filtered based on the following steps: Sites with mean read depth of less than 10x and greater than 39 x (=2*average depth (19.2 x)) were removed (--min-meanDP 10, --max-meanDP 39). Only sites with a maximum of two alleles were (--min-alleles 1, --max-alleles 2). Sites were kept if present in 50% of all samples (--max-missing 0.5). Only sites with a maximum observed heterozygosity of 0.7 were kept (Gargiulo et al., 2020; Hohenlohe et al., 2011b), identified via the R package *adegenet*. Next, we randomly resampled a fixed number of diploid genotypes from each locality (WS: 20, AS: 7, RS: 25, EA: 6) to a dataset without missing data while maximising the number of SNPs and genotypes across localities, using a python script fastsimcoal/sampleKgenotypesPerPop.py (https://github.com/marqueda/SFS-scripts/blob/master/sampleKgenotypesPerPop.py). Then, within each RAD locus, SNPs with linkage were removed based on r^2 >0.95, identified via --geno-r2 (--min-r2 0.95), following Marques et al. (2019). We also randomly removed a number of monomorphic sites proportional to the retained number of SNPs after linkage pruning.

6.6.5 Genetic structure of *P. turqueti* and *O. victoriae*

To visualise the overall genetic structure of *P. turqueti* and *O. victoriae* at a circumpolar scale, PCA was performed using *adegenet* across all samples per species. Individual admixture proportions were also estimated via *Structure*. *Structure* was run between *K* = 1 and 10, with ten replicates per *K* via *Structure_threader* (Pina-Martins et al., 2017). Each run was performed with 500,000 iterations and burn-in of 100,000. The meaningful *K* was evaluated based on the highest mean log likelihood [mean LnP(*K*)] and delta*K* statistics using *Structure Harvester* (Earl & VonHoldt, 2012).

6.6.6 Patterns of population splits and mixtures using *TreeMix*

We used the heuristic approach in *TreeMix* to explore the phylogenetic history of WS, AS and RS in the broader context of historical splits and mixture between locations across the Southern Ocean. *TreeMix* was also designed as a complimentary method to *Structure*; while *Structure* assigns individuals into discrete genetic clusters, *TreeMix* models how the populations may have arisen and outlines the genealogical relationship between populations (Pickrell & Pritchard, 2012). Given the high similarity in shared admixture proportions between neighbouring locations in *O. victoriae* (a highly admixed species), in order to improve the accuracy of population genetic interpretation, some neighbouring locations with similar admixture proportions (estimated with *Structure*) were clustered together, following Thom et al. (2020). This is particularly important as *TreeMix* assumes the input population labels largely represent a tree-like population structure; when the number of admixed "populations" is high relative to the number of unadmixed "populations", the assumption of tree-ness breaks down (Pickrell & Pritchard, 2012). Conversely, given biogeographical substructure was observed in *P. turqueti* (a highly structured species), some locations were further divided into smaller scale local geographical populations in *TreeMix*.

For *TreeMix* analysis of *P. turqueti* and *O. victoriae*, outgroup species were included for tree rooting. *TreeMix* input was generated using the R package *dartR* v1.1.11 (Gruber et al., 2018). Within *TreeMix*, migration edges (m) were modelled between 0 and 10, with 10 replicates per m using the bootstrap option with a block size of 1 (assuming loci are unlinked as the input dataset contained a one SNP per locus). The optimal number of m was evaluated using the simple exponential and non-linear least square model (threshold = 0.05) via the R package *OptM* v0.1.3 (Fitak, 2019). The final best m (after *OptM* evaluation) was chosen based on the highest amount of variance explained. Among the 10 replicate runs of the best m, the replicate with the least amount of residuals was presented. In addition, only the significant migration edges, evaluated using jackknife p values (significance level at 0.05), were presented. Each migration edge was weighted based on the ancestry fraction in the sink population originated from each source population (Pickrell & Pritchard, 2012).

6.6.7 Allele frequency correlations between seaway populations

To further explore whether there is direct admixture between seaway populations despite circumpolar gene flow driven by the Antarctic Circumpolar Current (ACC) and Antarctic Slope Current (ASC), *D*-statistic (i.e. ABBA-BABA) (Durand et al., 2011) and outgroup-f_3-statistic (Raghavan et al., 2014) were performed using *AdmixTools*. Both tests were performed for *P. turqueti* and *O. victoriae*, and between WS-AS-RS populations, with respect to locations (SHE and EA) situated in between WS-AS-RS as well as are known to receive migrants travelled through either current. For both tests, common outgroup was also

incorporated to discriminate ancestral and derived alleles. Z-score values > 3 or < 3 were considered significantly different from 0 for both tests.

D-statistic examines whether there are excess allele sharing between two of the three ingroup populations, with respect to a common outgroup. We considered the hypotheses of whether there was a partial collapse across WAIS which would result connectivity between WS and AS, and whether there was a full collapse across WAIS which would result connectivity between WS and RS. When testing for excess allele sharing between WS and AS or RS, considering SHE or EA, we computed the *D*-statistic of the following form: *D*(seaway population, circumpolar current population, WS, outgroup), where seaway population represents AS or RS, and circumpolar current population represents SHE or EA.

Outgroup-f_3-statistic examines the branch length (shared genetic drift) between pairs of population with respect to a common outgroup. We computed the outgroup-f_3-statistic of the following form: f_3(Outgroup; A, B), where A and B represent pairs of population between WS, AS, RS, SHE and EA. For *D*-statistic and outgroup f_3 statistic, standard errors were computed with block-jackknife procedures, with blocks representing the length of RAD loci.

6.6.8 SFS based inferences – mutation rate and generation time

For site frequency spectrum (SFS) based inferences (*StairwayPlot*, *fastsimcoal*), for *P. turqueti*, a generation time of 12 years was assumed based on the species' approximated life span (Schwarz et al., 2018; Schwarz et al., 2019), as female octopods (including cold water deep-sea octopus) are known to exhibit a single reproductive period followed by death in their lifetime (Robison et al., 2014; Schwarz et al., 2018). A mutation rate of 2.4×10^{-9} per site per generation was used based the genome-wide mutation rate estimated for the Southern blue-ringed octopus (*Hapalochlaena maculosa*) (Whitelaw et al., 2020), as it is the only mutation rate estimated for any cephalopod genome to date. For *O. victoriae*, a generation time of ten years was assumed based on information about minimum disc size at sexual maturity (based on females) (Grange et al., 2004) and average disc size across age of *O. victoriae* (Dahm & Brey, 1998). A mutation rate of 1.43×10^{-8} per site per generation was used based on the tip substitution rate of the *O. victoriae* and *O. hexactis* branch among global ophiuroid species (0.0015924; substitution/site/myr) (O'Hara et al., 2019).

6.6.9 Past population size changes

Past effective population size (N_e) changes within WS, AS, RS and EA populations, of *P. turqueti* and *O. victoriae*, were reconstructed using *StairwayPlot*. *StairwayPlot* is a model flexible method that infers past population size changes over specific points in a genealogy through 1-dimensional SFS (1d-SFS). *StairwayPlot* was chosen to further explore past population size changes within species instead of demographic models (e.g. *fastsimcoal*) as it is not constrained by a-priori information, which can in turn explore a larger model space than parametrised demographic models (Liu & Fu, 2015). *StairwayPlot* is also known to reconstruct recent population size changes with high accuracy compared to Sequentially Markovian Coalescent (SMC)-based methods (Patton et al., 2019). For *StairwayPlot*, we first polarised SNPs using outgroup information. Then, unfolded 1d-SFS per locality was generated via easySFS.py (https://github.com/isaacovercast/easySFS#easysfs). Total sequence length was defined as the length of genome explored after SNP filtering (= number of loci x length of locus). The percentage of sites used for training was 67% and the number of random break points for each run were (nseq-2)/4, (nseq-2)/2, (nseq-2)*3/4, nseq-2 based on default values. Each run was performed with a random starting seed.

6.6.10 Demographic modelling

We used demographic modelling to explicitly evaluate whether they were ancient migrations linking to no, partial or complete collapse of the WAIS preceding modern-day gene flow in *P. turqueti* and *O. victoriae*. Demographic modelling was performed using the coalescent simulations based framework in *fastsimcoal*. For demographic modelling, we only considered WS, AS, RS and EA in our models (4 population model), as the model evaluation is based on composite likelihoods which requires a single multidimensional SFS (i.e. four dimensional (4d)-SFS in this study). In a multidimensional SFS with > 4 populations, the number of zero entries will increase which makes it challenging for *fastsimcoal* to fit the observed data (Bagley et al., 2017). EA samples are chosen to be included in the models instead of SHE as samples from across EA are considered of particular importance in representing clear signatures of circumpolar gene flow (Strugnell et al., 2018), because they are geographically separated from the WAIS but are also directly influenced by both ACC and ASC.

Because there are an unlimited number of demographic models to be explored, especially when a high number of populations is incorporated (i.e. four in this study), we used a hypothesis driven, hierarchical approach to reconstruct simple, contrasting demographic models involving no, partial or complete historical collapse of WAIS using *fastsimcoal*

(Supplementary Fig 6.3). We explored simpler models and subsequently added more complex parameters to improve the fit to the observed data, as recommended by Marchi et al. (2021), with a hierarchical framework constructed following Marques et al. (2019). First, we established the phylogenetic relationship among WS, AS, RS and EA. Then, building on top of the best model evaluated in the first step, we compared six different models comprising of different no, partial or complete WAIS collapse scenarios, while modelling for contemporary gene flow driven by the circumpolar currents. These included six main conditions: 1) continuous circumpolar gene flow since population divergence (no collapse scenario), 2) strict isolation followed by circumpolar gene flow (no collapse scenario), 3) gene flow between WS-AS followed by circumpolar gene flow (partial collapse scenario), 4) gene flow between AS-RS followed by circumpolar gene flow (partial collapse scenario), 5) gene flow between WS-RS followed by circumpolar gene flow (full collapse scenario), and 6) gene flow between WS-AS-RS followed by circumpolar gene flow (full collapse scenario). For dataset that does not have enough information to model all aspects of ecologically realistic scenarios (i.e. low number of SNPs in *O. victoriae*), we considered simpler models (level 2) that only included the directionality of ACC (clockwise). For dataset that has higher number of SNPs and thus more ecologically realistic scenarios can be inferred (*P. turqueti*), we considered complex models (level 3) that included the directionality of ACC (clockwise) and ASC (counter-clockwise). (Supplementary Fig 6.3-6.4).

6.6.11 Model selection

For *fastsimcoal* analyses, we first polarised SNPs using outgroup information. Then, we converted the datasets into unfolded multidimensional SFS for model evaluation using a python script fastsimcoal/vcf2sfs.py (https://github.com/marqueda/SFS-scripts/blob/master/vcf2sfs.py). For each model, we performed 100 independent runs of random starting parameter combinations, with each run pooling SFS entries with less than 10 SNPs in order to avoid overfitting (-C 10), consisting of 40 ECM optimisation cycles and using 200,000 coalescent simulations. We then re-estimated the likelihoods of each model, based on the maximum-likelihood estimates obtained from the best run (*_maxL.par), again with 100 independent runs and 200,000 coalescent simulations. The re-calculated likelihoods should closely approximate the true likelihoods as they are maximised under each model scenario, and the distribution of the re-calculated likelihoods should reflect the inherent stochasticity of coalescent simulations (Excoffier et al., 2013).

For each step, model fit was evaluated based on the lowest deltaLikelihood, Akaike's information criterion (AIC) and AIC weights. We also visualised the distributions of re-estimated AIC values in order to assess the variance of approximation, and a clear overlap

among models would indicate no significant differences. For the final best model, we visually inspected the fit of the observed versus expected SFS, as well as the residuals in model fitting, to evaluate whether the final selected model for each species could reproduce the observed data.

6.6.12 Parameter estimation of the final best model

Parameters of the best final model for each species were estimated using joint pairwise two dimensional (2d)-SFS. Instead of a single multidimensional SFS (which fits under the assumption of composite likelihoods for AIC comparisons), multiple joint pairwise 2d-SFSs were used as they reduce the overall SFS size, as well as the number of zero entries, which is more appropriate for estimating parameters for complex models with high number of populations (e.g. this study) (Excoffier et al., 2013; Bagley et al., 2017). The parameter estimates of the best final model for each species were calculated with 100 independent runs of random starting parameter combinations, with each run pooling SFS entries with less than 10 SNPs in order to avoid overfitting (-C 10), consisting of 40 ECM optimisation cycles and using 200,000 coalescent simulations. We introduced parameter upper bound for the parameter T1 (divergence time estimate) for both species as the model runs were detecting ancestral signals beyond species history, thus likely to confound with estimation of recent parameter estimates (Momigliano et al., 2021). Introducing an upper bound of divergence estimates would also reduce the parameter space within the time period of interest (i.e. history since speciation) in complex models (Marques et al., 2019; Choin et al., 2021). The upper bound of T1 was constrained by known conservative (median) estimate of species divergence time, which were 4 and 1.64 million years ago for *P. turqueti* (Strugnell et al., 2012) and *O. victoriae* (Hugall et al., 2016; O'Hara et al., 2017), respectively. These divergence estimates were chosen as they were calculated using different markers than RAD loci; these divergence times were estimated using mitochondrial and exon phylogenetic data in *P. turqueti* (Strugnell et al., 2012) and *O. victoriae* (Hugall et al., 2016; O'Hara et al., 2017), respectively. The final parameter estimates were obtained from the best run with the highest likelihoods.

The 95% confidence intervals (CI) of parameters of the best model were calculating using 53 and 16 replicates (*P. turqueti* and *O. victoriae*, respectively) of non-parametric block-bootstrapped joint pairwise 2d-SFSs. Bootstrapped replicates were generated via vcf2sfs.py. The length of each block was defined as the length of RAD locus. Within each replicate, the parameters under the best model scenario were estimated with 100 independent runs of block-bootstrapped SFSs. The parameter estimates of the best run from each bootstrapped

replicate were used to compute the confidence interval. For the final manuscript publication, we will estimate 95% CI using 100 block-bootstrapped replicates in each species.

CHAPTER 7

General Discussion

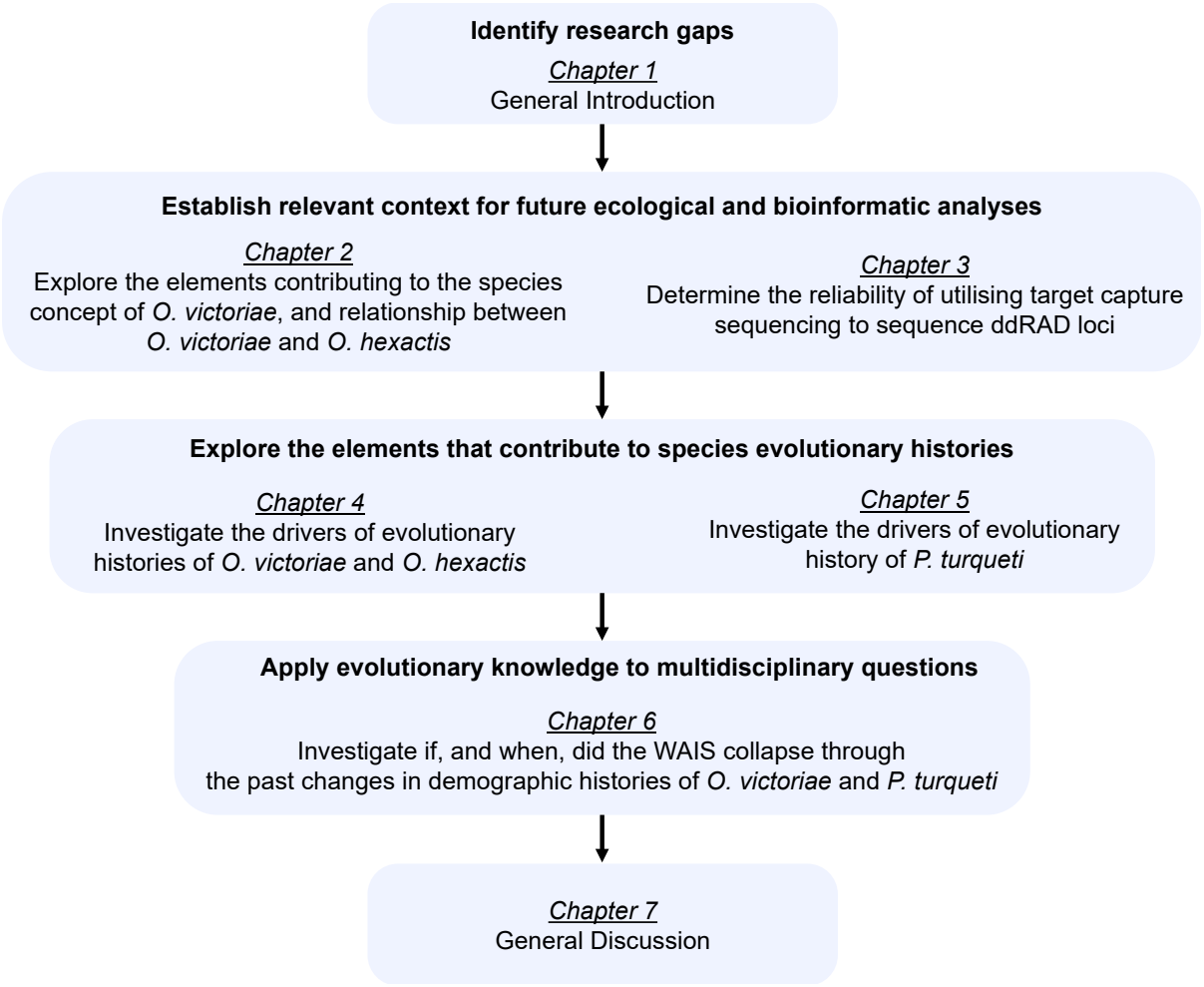

7.1 Thesis overview

The biological and physical processes of Antarctica have had profound influences on the global biodiversity and climate throughout the Quaternary until the present day (Clarke & Crame, 1992; Pollard & DeConto, 2009). However, knowledge of how Southern Ocean benthic fauna have persisted through time is limited, and empirical evidence indicating past Antarctic Ice Sheet behaviour over the Quaternary is also scarce. My thesis demonstrates that by testing species concepts and investigating evolutionary histories of Southern Ocean benthic fauna, we can shed light on both the biological and physical past of the Southern Ocean. In turn, by examining the past, we can better understand the present and future biological and physical changes that are being, and will be, experienced in Antarctica.

My thesis chapters collectively show that species history throughout the Quaternary, as well as the genomic patterns that underpin these signatures, are highly complex in the Southern Ocean. More importantly, species history contrasts between taxa (e.g. ophiuroid and cephalopod; *Chapter 2, 4, 5, 6*) and closely-related species (e.g. *Ophionotus* spp. (*Chapter 2, 4*). Thus, the outlined framework in *Chapter 1* on detecting how benthic fauna would have survived glacial cycles, based on generalised changes in population connectivity, isolation and population size, may seem oversimplified. However, as proposed in *Chapter 1*, each species' population genomic signatures are comprised of past demographic changes, linked to different phases of the Quaternary, which are superimposed on top of each other. *Chapter 1* offered valuable testable frameworks for my subsequent data chapters to evaluate these intertwined signals of Quaternary persistence.

Throughout my thesis, I have deconstructed the evolutionary histories of the brittle stars *O. victoriae* and *O. hexactis,* and the octopus *P. turqueti*. I also showed that target capture is efficient in retrieving genomic data from degraded Southern Ocean samples (*Chapter 3*). Importantly, the literature suggests that the past distribution and connectivity of Southern Ocean benthic fauna could be proxies for reconstructing past AIS configurations, such as verifying whether the WAIS collapsed during the Quaternary (Barnes & Hillenbrand, 2010; Linse et al., 2006; Vaughan et al., 2011; Strugnell et al., 2018; Moreau et al., 2019; Collins et al., 2020). My thesis demonstrated that this idea is executable with a robust sampling and sequencing approach, and offered genomic evidence indicating that the WAIS collapsed during the Last Interglacial Period (LIG). However, echoing the overarching aims of this thesis, the application of genomic data on applied questions of global significance would not be possible without first 1) elucidating the unique signatures of different evolutionary processes in order to reconstruct the past changes in demographic histories, and 2) applying evolutionary knowledge gained to interpret historical AIS configurations.

7.2 Revisiting the drivers of circumpolar connectivity

Here I demonstrate clear, long-distance circumpolar connectivity can be observed in three different species with contrasting reproductive strategies using high resolution genomic data, including *O. victoriae*, which possesses pelagic larvae, *O. hexactis* with brooding larvae and *P. turqueti* with direct developing juveniles (*Chapter 2, 4, 5, 6*). In the Southern Ocean, long-distance biological connectivity is expected to be feasible primarily in species with pelagic larval dispersal; conversely, for species without a pelagic dispersal phase, connectivity is assumed to be relatively limited (Thatje, 2012; Moon et al., 2017, but see Leese et al. (2010)). Emerging genetic studies have shown that some brooding species exhibit genetic connectivity throughout the Southern Ocean (reviewed within Halanych & Mahon (2018)). Together, the genomic evidence presented within this thesis suggests that long-distance connectivity is occurring in species that exhibit both pelagic and non-pelagic dispersal strategies.

My thesis demonstrates general dispersal routes with long-distance connectivity throughout the Southern Ocean. Most notably, a direct genetic connection was detected between the Scotia Arc and Prydz Bay/Heard Island for *O. victoriae*, *O. hexactis* and *P. turqueti*. This potential connectivity pathway has also been previously observed in other Southern Ocean taxa based on low resolution single locus data, including in the asteroid *Glabraster antarctica* (Moore et al., 2018), the amphipod *Eusirus giganteus* (Baird et al., 2011) and the crinoid *Promachocrinus* phylogroups C and F (Hemery et al., 2012). The detection of this Scotia Arc and Prydz Bay/Heard Island connectivity route using high resolution genomic data across taxa in this thesis verifies the existence of this generic connectivity route, which is supported by a Southern Ocean circulation model incorporating the Antarctic Circumpolar Current (ACC), mesoscale eddies and surface waves (Fraser et al., 2018). Based on the surface ocean current model presented in Fraser et al. (2018), particles released from South Georgia could reach the Antarctic continental shelf, including East Antarctica, within two years. Although it is plausible for species with pelagic larvae to disperse along with the current, for species without a pelagic dispersal phase, it was suggested that this surface circulatory pattern could facilitate circumpolar dispersal of Antarctic benthic fauna via rafting on detached kelp, pumice and icebergs (Fraser et al., 2018). The Scotia Arc - Prydz Bay/Heard Island genetic connectivity, explained by the hypothesis of rafting and surface ocean currents, seems plausible for species that are generally associated with kelp habitats and can survive in the kelp holdfasts for an extended time period (i.e. years).

However, whether non-kelp associating benthic species with a non-pelagic dispersal strategy, such as *O. hexactis* and *P. turqueti* could disperse across wide geographical distances via kelp rafting remains highly uncertain. Both *O. hexactis* and *P. turqueti* are mostly found in habitats that are far away from the coastal, shallow kelp forests. For the case of *O. hexactis*, this species is known to be generally associated with flat muddy substrates (Chester Sands, pers. comm.) and has also been observed to actively move away from, or seek shelter in, areas with strong currents (Fratt & Dearborn, 1983). Therefore, any dispersal of *O. hexactis* via kelp rafting along the ACC would be highly stochastic and likely very rare occurrences, which should lead to some, but limited, admixture between long-distance locations. Nonetheless, empirical genomic evidence presented within this thesis suggests strong homogeneity was observed across Heard Island, Shag Rocks and South Georgia in *O. hexactis*, which cannot seem to be explained by the restricted ecological opportunities of rafting experienced by this species. Furthermore, for the case of *P. turqueti*, gene flow was detected between Casey Station and Shag Rocks / South Georgia. However, this connectivity is also unlikely to be explained by kelp rafting via surface currents, as samples from these locations were collected at depths at which kelp forests do not exist (113 - 903 m). In the literature, it has been suggested that long-distance dispersal in *P. turqueti* could have been facilitated via adults or egg masses rafting on floating substrates, or that their benthic egg masses could become dislodged and disperse through the currents (Strugnell et al., 2012). Dispersal via floating egg masses also seem ecologically improbable, as this scenario implies that the egg masses would be separated from the mother, yet the necessary survival of unhatched eggs depends on constant maternal care to prevent fouling and suffocation (Boletzky, 1994). Additionally, only small-sized octopus (e.g. juvenile *Octopus bimaculatus* and adult *O. micropyrsus* with a mantle length between 20 - 25 mm) have so far been reported to live in kelp holdfast globally (Ambrose, 1982; Boyle & Rodhouse, 2008); such sizes are equivalent to the early juvenile stage of *P. turqueti*. Therefore, opportunities for *P. turqueti* to dispersal via kelp rafting would likely only be limited to a brief period of this species development. Although not impossible, the ecological opportunities of *P. turqueti* being dispersed via rafting also seem to be quite limited. Overall, it is becoming clear that rafting, or the ACC itself, cannot easily explain the molecular signatures of long-distance connectivity in the Southern Ocean.

Much of the existing work focusing on establishing the drivers of long-distance connectivity (e.g. Fraser et al., 2018; Moore et al., 2018), including this thesis, have mostly regarded the ACC as the general driver of circumpolar connectivity. However, existing molecular evidence has also hinted that long-distance connectivity in the Southern Ocean can also be linked to factors other than the ACC, such as historical events that occurred over evolutionary timeframes. Based on COI data, the Antarctic brittle star *Ophiuroglypha lymani* was

suggested to have migrated from South America to Antarctica (South Georgia) multiple times against the directionality of the ACC in the Quaternary (Sands et al., 2015). The case of *O. lymani* highlights that long-distance connectivity could be linked to unique evolutionary events that are not part of the ACC regime. However, Sands et al. (2015) was based on low resolution single locus data (COI), which might be subjected to biases that do not reflect true connectivity (see *Chapter 2* for more details). In this thesis, I also detected long-distance connectivity between the Ross Sea and the Weddell Sea that could be linked to historical WAIS collapse using genomic data (*Chapter 6*). Together the evidence suggests long-distance connectivity between extant populations could have been driven by events in the past.

Results from this study also detected another general route of long-distance connectivity that cannot be explained by the ACC. Instead, this connectivity could be linked to historical biological connectivity during the Last Glacial Maximum (LGM). A strong, genetic connection between the Ross Sea and South Shetland Islands/Elephant Island, while mostly bypassing locations between these two areas (e.g. Amundsen Sea, Bellingshausen Sea), was detected in both *Ophionotus victoriae* (*Chapter 3*) and *P. turqueti* (*Chapter 5*). Interestingly, this direct connectivity pathway between the Ross Sea and South Shetland Islands/Elephant Island was also observed in previous studies analysing the 2b-RAD data of *O. victoriae* and *Astrotoma agassizii* (Galaska et al. 2017a, 2017b). This dispersal pathway does not seem to reflect the surface current patterns modelled in Fraser et al. (2018). In addition, this dispersal pathway cannot be explained by the ACC as the ACC crosses over the Ross Sea, Amundsen Sea and Bellingshausen Sea into the Scotia Sea (Sokolov & Rintoul, 2009). Therefore, any ACC-driven circumpolar connectivity should lead to admixture between the Ross Sea, Amundsen Sea, Bellingshausen Sea and South Shetland Islands/Elephant Island. For *O. victoriae*, *P. turqueti* and *A. agassizii*, although connectivity along West Antarctica linked to the ACC was detected in some species (*O. victoriae* and *P. turqueti*), a distinct admixture signal was also detected between the Ross Sea and South Shetland Islands/Elephant Island within all three species, which cannot be explained by the boundary of the ACC (Sokolov & Rintoul, 2009). One hypothesis is that the distinct admixture between the Ross Sea and South Shetland Islands/Elephant Island can be linked to connectivity between *in situ* refugia during the LGM. The shelf areas along both the Amundsen Sea and Bellingshausen Sea have been highlighted as mostly inhabitable during the LGM due to heavy sedimentation inputs (Golledge et al., 2013), while the Ross Sea and islands within the Scotia Sea likely contained open habitats and served as *in situ* glacial refugia for Southern Ocean benthic species during that same LGM time period. Therefore, the distinct admixture signal between the Ross Sea and South Shetland Islands/Elephant Island likely represents migration between *in situ* refugia during the LGM, which was an ecological

process hypothesised for benthic taxa seeking *in situ* refugia on the Antarctic continental shelf (Thatje et al., 2005). Alternatively, such signals could represent subsequent and immediate post-LGM colonisation from *in situ* refugia to new shelf habitats. For example, the shelf refugia areas in Ross Sea and South Shetland Islands/Elephant Island were already open throughout the LGM and presumably were immediately ready to receive newly colonising migrants after deglaciation. Similar long-distance admixture signals between LGM refugia have also been recently observed in Central African tree species with a high dispersal potential (Piñeiro et al., 2021). In this example, a clear distinct admixture was detected between Northern and Southern LGM refugial lineages, with the authors hypothesising that the long-distance connectivity between the two refugia could be due to the habitats presumably were immediately ready to receive newly colonising migrants following deglaciation (Piñeiro et al., 2021).

Finally, my thesis also demonstrates long-distance circumpolar connectivity can be driven by oceanic forces other than the ACC. *Chapter 6* of my thesis is one of the few studies that has established the role of Antarctic Slope Current (ASC) in driving circumpolar gene flow. Previously, many studies have erroneously assumed that the ACC was the only driver at work (e.g. Griffiths et al., 2008; Raupach et al., 2010; Hemery et al., 2012; Moore et al., 2018; Lau et al., 2021). Therefore, long-distance connectivity in the Southern Ocean can be driven by the ASC as well as other uncharacterised large-scale currents. Future studies would also need to consider the role of 1) evolutionary events and 2) both the ACC and ASC in driving circumpolar gene flow. Direct observations of biological migration, and/or estimations of how gene flow changes temporally between each location, would be necessary to finally verify the physical and temporal facilitators of long-distance connectivity in Southern Ocean benthic taxa.

7.3 Drivers of genetic structure in the Scotia Arc

By employing comprehensive sampling, this thesis shows that *O. victoriae* and *P. turqueti* exhibit contrasting genomic patterns within the Scotia Arc (*Chapter 2, 4, 5*). Although contrasting genetic patterns could reflect different modes of reproductive strategy, the genetic patterns detected across many islands in the region also hint towards the idea that different factors could be acting on each dispersal strategy in the region. Firstly, in *O. victoriae*, a sharp genetic break was observed along the Scotia Arc, separating the locations north of Discovery Bank and south of Elephant Island into two distinct clusters (Fig 4.1). However, in *P. turqueti*, a gradual isolation-by-geographical distance pattern was observed along the Scotia Arc (Fig 5.1). Although the sharp genetic break observed in *O. victoriae* is not expected given that it possesses a pelagic dispersal phase, this signature is also not

observed in *P. turqueti* with non-pelagic dispersal, suggesting an unknown factor that is acting on the pelagic dispersal of *O. victoriae*. Secondly, within the South Shetland islands group, while genetic homogeneity was observed between the islands within this group in *O. victoriae*, a sharp genetic discontinuity was observed between King George Island and other islands in *P. turqueti*. While a sharp genetic break is consistent with a lack of pelagic dispersal phase, further evaluation indicated the observed genetic discontinuity in *P. turqueti* could be linked to isolation-by-water depth, which was not detected in *O. victoriae* within this region (nor in some octopus species such as *Pareledone charcoti* and *Adelieledone polymorpha* in this area as reported in Strugnell et al., 2017).

Previous genetic studies have highlighted that the seascape dynamics within the Scotia Arc might promote genetic differentiation across different taxa, including amphipods (Verheye et al., 2016), ascidians (Demarchi et al., 2016), bivalves (Linse et al., 2007), limpets (Hoffman et al., 2011b) and octopus (Strugnell et al., 2017). However, Strugnell et al. (2017) also reported that contrasting genetic structure can be observed in closely related species in the Scotia Arc. Therefore, it is likely that physical seascape dynamics are not the sole generic drivers of genetic differentiation across taxa in the Scotia Arc. The genomic patterns observed in *O. victoriae* and *P. turqueti* also reflect that their dispersal might be constrained by different seascape factors in the region. For example, the connectivity between South Georgia, Discovery Bank, Herdman Bank and Bouvet Island in *O. victoriae* likely reflect uncharacterised or stochastic local oceanographic regimes linking these areas near the Polar Front, which was not detected in *P. turqueti* or other Southern Ocean species. In addition, *P. turqueti* exhibits putative genetic signals of adaptation to warmer temperatures around Shag Rocks and South Georgia that could also contribute to the genetic structure detected in this region. Furthermore, these similar signatures were not detected in *O. victoriae*. Further sampling, discoveries and investigations into the genetic structure of different benthic taxa within the Scotia Sea will help reveal why physical seascape dynamics might not act as generic drivers of genetic differentiation in the region.

7.4 Robust Southern Ocean species delimitation in the genomics era

The results of my thesis demonstrate that the previous interpretation of cryptic species in *O. victoriae* was incorrect. The conclusion of multiple species was driven by a pattern of isolation-by-geographical distance and patchy sampling of a genetically diverse and widely distributed species. Therefore, care must be taken when discussing species status if comprehensive sampling is not yet available.

Lack of comprehensive sampling is a particularly significant challenge in studies that seek to

interpret species status of Southern Ocean benthic taxa. Importantly, one of the longstanding hypotheses of Southern Ocean evolutionary processes is that survival in allopatric glacial refugia could serve as a "biodiversity pump" for cryptic speciation in the Southern Ocean (Clarke & Crame, 1989, 1992; Crame 1997, Wilson et al., 2009). Over the last decade, since the Marine Barcode of Life and Census of Antarctic Marine Life (2000-2010), and International Polar Year projects (2008-2009), were launched, many Southern Ocean molecular studies have also reported evidence of cryptic species across a variety of benthic taxa, including amphipods (Lörz et al., 2009; Baird et al., 2011; Havermans et al., 2011), asteroids (Janosik et al., 2011), bivalves (González-Wevar et al., 2019), crinoids (Wilson et al., 2007; Hemery et al., 2012), isopods (Held & Wägele, 2005; Raupach & Wägele, 2006; Leese & Held, 2008), nematodes (Lee et al., 2017), octopus (Allcock et al., 2011), ophiuroids (Hunter & Halanych, 2008, 2010; Heimeier et al., 2010; Galaska et al., 2017a, 2017b; Jossart et al., 2019), ostracods (Brandão et al., 2010), polychaetes (Brasier et al., 2016), sea cucumbers (O'Loughlin et al., 2011), sea slugs (Wilson et al., 2009, 2013) and sea spiders (Arango et al., 2011; Dietz et al., 2015; Collins et al., 2018). Although Antarctica does not appear to have a higher than usual level of cryptic species (Pfenniger & Schwenk, 2007), there is an increasing weight of studies reporting cryptic species in many Southern Ocean taxa (De Broyer et al., 2011). However, the majority of these studies reporting cryptic species are characterised by patchy sampling between disjunct locations separated by long geographical distances (e.g. Held & Wägele, 2005; Leese & Held, 2008; Lörz et al., 2009; Brandão et al., 2010; Hunter & Halanych, 2010; Arango et al., 2011; Baird et al., 2011; Havermans et al., 2011; Brasier et al., 2016; Collins et al., 2018; González-Wevar et al., 2019). Although cryptic speciation is likely a true phenomenon for some Southern Ocean taxa, it is unclear whether the interpretation of cryptic species in some studies has been biased by sampling artefacts.

Regardless of the variations in species concept definition, the large discussion of cryptic speciation in the literature points toward a gradual continuum of genetic isolation across geographical distance in many Southern Ocean taxa. Such a description also seems fitting for the genomic patterns detected in this thesis, including the lineages within *O. victoriae*, lineages within *P. turqueti*, and the relationship between *O. victoriae* and *O. hexactis*. Although both *O. victoriae* and *P. turqueti* appear to be single species based on samples taken from individuals collected across their circumpolar distributions, both exhibit gradual signatures of isolation-by-geographical distance. In turn, based on *Structure* analyses, the relatively high genetic differentiation between distant locations within each species has also led to geographically-separated populations likely to exhibit no gene flow between each other (e.g. between Bouvet Island and Ross Sea in *O. victoriae*, and between Shag Rocks and Amundsen Sea in *P. turqueti*). Nonetheless, these signals do not represent

reproductively-isolated lineages, as these areas also exhibit gene flow with nearby geographical locations. Thus, the genetic patterns of *O. victoriae* and *P. turqueti* are characterised by a gradual continuum of genetic isolation, which is expected in widely distributed species (Helbig 2005).

Furthermore, for *O. victoriae* and *O. hexactis*, although both species can be genetically and morphologically distinguished as two separate species, there is strong intraspecific gene flow observed in areas where their distributions are overlapping (e.g. Bransfield Mouth). Therefore, the gradual genetic differentiation observed between *O. victoriae* and *O. hexactis* likely represents a transitional stage along a speciation continuum. This is potentially problematic for existing species concepts in the Southern Ocean realm, as speciation in this region is often viewed as a single, already completed event (e.g. De Broyer et al., 2011; Brasier et al., 2016, but see Sands et al. 2021 for a call for integrated species delimitation in the Southern Ocean). Nonetheless, the cases of *O. victoriae* and *P. turqueti* illustrate that isolation-by-geographical distance likely plays an important role in driving genetic structure in the Southern Ocean. Importantly, when discussing species concepts, geographical isolation only represents reduction in migration rate; it does not represent reproductive isolation leading to speciation (Helbig 2005; Stankowski & Ravinet, 2021). The relationship between *O. victoriae* and *O. hexactis* further illustrates speciation in the Southern Ocean can also be a gradual process. Therefore, future studies seeking to explore species concepts in the Southern Ocean should acknowledge that 1) geographical isolation is likely a key characteristic of population genetic patterns in the Southern Ocean, and that 2) speciation can be an ongoing, continuous process. To thoroughly understand species boundaries across continuums in the Southern Ocean, future studies should further characterise how population divergence and speciation processes unfold in a range of taxa (Stankowski & Ravinet, 2021).

7.5 Interglacial cycles influence Southern Ocean evolutionary history

Throughout this thesis, I demonstrate that persistence through recent extreme interglacial cycles strongly influenced species history in the Southern Ocean, including past population connectivity (*Chapter 6*), ecological divergence and evolutionary innovations (*Chapter 2, 4*). Furthermore, the divergence of *O. victoriae* and *O. hexactis* can be dated back to a historically warm interglacial period at ~0.43 million years ago, when the West Antarctic Ice Sheet (WAIS) has been proposed to experience complete collapse leading to intense influx of deglacial meltwater to the surrounding Antarctic island environments. Outlier loci detection analyses of sequences of *P. turqueti* also revealed that lineages that persisted around Antarctic islands can be associated with low salinity stress (*Chapter 5*). Since the WAIS also

likely experienced a more recent complete collapse in the last interglacial period (LIG) at ~125,000 years ago (*Chapter 6*), it is possible that species that persisted around Antarctic islands were repeatedly exposed to low salinity stress driven by extreme interglacial cycles throughout the Quaternary. However, in the literature, most studies focusing on how Southern Ocean benthic species survived through the Quaternary often only discuss where and how benthic fauna could have survived recent extreme glacial cycles in the past (Allcock & Strugnell, 2012; Clarke & Crame, 1989, 1992; Crame, 1997, 2018; Lau et al., 2018, 2021; Thatje et al., 2005, 2008; *Chapter 1, 2*). Overall, I argue that recent interglacial cycles also strongly influenced Southern Ocean species history, particularly species that are distributed around Antarctic islands.

Particularly, I also suggest that species persistence through strong interglacial periods in the recent past could be linked to the emergence of a brooding strategy in the Southern Ocean. Studies investigating the life history of Antarctic benthic invertebrates mostly focus on echinoderm species (Pearse et al., 1991), with a widely-discussed consensus suggesting an unusually high number of brooding species in this region (Pearse et al., 1991, 2009; Poulin & Féral, 1996; Poulin et al., 2002). The prevalence of a brooding strategy in echinoderms within the Southern Ocean has long been discussed, and widely accepted, as a general adaptation to a lack of primary productivity and limited habitat availability for successful pelagic larval development during glacial cycles (Poulin et al., 2002). However, it has been reported that a higher proportion of echinoderm species with a brooding strategy can be found around islands within the Scotia Arc (65%) relative to the Antarctic continent and sub-Antarctic islands (42% each) (Pearse & Bosch, 1994; reported within Pearse et al. (1991)). Nonetheless, the species concepts behind these numbers should be re-examined using molecular data for better accuracy, and that not all echinoderm species have been examined for their reproductive strategies in the Southern Ocean. Emerging studies have also highlighted that between closely related Southern Ocean ophiuroid species with contrasting life histories (brooding versus broadcasting), a brooding strategy is mostly exclusive to the Antarctic islands including the Scotia Sea (Sands et al., 2015; Jossart et al., 2019; Lau et al., 2021; *Chapter 4*). Antarctic islands, especially the islands within the Scotia Sea, would be more likely to be the habitats that were directly exposed to the low salinity meltwater from putative WAIS collapse in the past extreme interglacial cycles compared to the continent. In addition, in echinoderms, brooding has often emerged under stressful environmental conditions during lineage transition over macroevolutionary timeframes (Lawrence & Herrera, 2000), even though this strategy requires higher maternal investment compared with pelagic larval development (Fernández et al., 2000). Therefore, it can be argued that the prevalence of brooding in the Southern Ocean could also be explained by low salinity selection driven by intense interglacial periods in the past.

Finally, from the case study of *O. victoriae* and *O. hexactis*, the divergence of both species can be dated back to a historically extreme interglacial period (*Chapter 4)*. However, the subsequent persistence within mostly non-overlapping glacial refugia, including Antarctic island refugia for *O. hexactis* and deep-sea and Antarctic continental shelf refugia for *O. victoriae*, likely created opportunities for reproductive isolation thus reinforcing the divergence between *O. victoriae* and *O. hexactis*. In this sense, repeated survival through glacial-interglacial cycles likely has synergistic effects on species evolutionary histories in the Southern Ocean.

7.6 Reconstructing past West and East Antarctic Ice Sheet collapses throughout the Quaternary

The final chapter of my thesis demonstrates that the WAIS likely experienced a complete collapse in the last interglacial period (LIG) when the average air temperature was only 0.5 - 2^{o}C warmer than the pre-industrial period (Dutton et al., 2015). This finding produces empirical evidence confirming the longstanding hypothesis of Marine Ice Sheet Instability (MISI), where marine ice sheets may become unstable due to global warming (Robel et al., 2019). So far, only the collapse of the WAIS has been considered under very high, but increasingly realistic, CO_2 emissions scenarios (Representative Concentration Pathway (RCP) 8.5; the 'business as usual scenario' that is widely reported by the popular media. According to the Intergovernmental Panel on Climate Change (IPCC) Sixth Assessment Report (Fox-Kemper et al., 2021), under the RCP 8.5 scenario without incorporating MISI, global sea level is predicted to reach ~0.77 m by 2100, and ~1.32 m by 2150. However, when including MISI driven by potential WAIS collapse, the global sea level is expected to reach ~0.99 m by 2100, and ~3.48 m by 2150. My thesis indicates the WAIS was sensitive enough to collapse under a 0.5 - 2^{o}C increase in air temperature during the LIG relative to the pre-industrial period, which is a level of temperature increase included in all RCP scenarios (RCP 2.6 - 8.5; low to high emission). Therefore, future global sea level rise projections should incorporate the likely collapse of the WAIS as a crucial parameter under all RCP scenarios in order to offer realistic projections of future events.

However, there are also other marine-based ice sheets in Antarctica that are vulnerable to collapse based on current trajectories in temperature rise, such as the Wilkes Land sector of the East Antarctic Ice Sheet (EAIS) (Joughin & Alley, 2011; Weber et al., 2021). The global consequences of marine-based ice sheet collapse are often discussed around the future of WAIS (Dutton et al., 2015), including the most recent IPCC Sixth Assessment Report (Fox-Kemper et al., 2021). Although a complete WAIS collapse could raise global sea level by

~3.3 - 5 m (Vaughan, 2008; Bamber et al., 2009), a collapse of the EAIS within the Wilkes Land sector could additionally raise global sea level by ~3 - 4 m (Mengel & Levermann, 2014). Together, the potential future collapse of both the WAIS and EAIS could raise global sea level up to ~9 m.

Accurate projections of future sea level rise require the knowledge of past and future EAIS stability, which is a parameter that is yet to be considered in any current RCP scenarios. This is due to the fact that the subglacial geology and past geological history of the Wilkes Land sector around the EAIS are unclear (Cook et al., 2013; Aitken et al., 2014; Noble et al., 2020). Nonetheless, it has been suggested that the Wilkes Land sector of the EAIS could have experienced partial collapse in mid-Pliocene at ~3 million years ago (Hill et al., 2007), indicating this sector was vulnerable to collapse in the past. Before presenting the molecular evidence of WAIS collapse in the LIG in *Chapter 6*, the last confirmed collapse of the WAIS was at ~3 million years ago in mid-Pliocene (Grant et al., 2019). Therefore, investigations of the past EAIS collapse should be urgent and are executable using molecular methods, and the implications of those findings would have critical global significance.

Since I have demonstrated that investigations of population demographic histories are effective in determining signatures of past WAIS collapse, these methods can also be extended and designed to answer additional questions related to the tempo and extent of past WAIS and EAIS collapses throughout the Quaternary. For example, accurate inferences of past population size changes in some locations can reveal past changes in habitat availability over time. By characterising the habitat availability (e.g. in the form of historical population expansion or stable population size proxies) around Wilkes Land during LIG, this could reveal whether parts of the EAIS also collapsed in the recent past and whether they will also be susceptible to future collapse under current climate change projections. Only a thorough understanding of WAIS configurations throughout the many different interglacial periods in the Quaternary can supplement and constrain the mathematical models behind WAIS collapse for future comprehensive projections. By further understanding the sequential changes in population demographic histories across the WAIS, the number of times the WAIS collapsed in the Quaternary can also be reconstructed.

Finally, Marine Ice Sheet Instability (MISI) is suggested to be regulated by a self-reinforcing mechanism (Garbe et al., 2020), meaning that future sea level rise is irreversible and will continue to increase following projections once the WAIS and EAIS begin to collapse. It has been estimated that in the event of a 2 m increase in global sea level by 2100, 630 million people, i.e. 10% of the world's population, whose livelihoods are dependent on the world's coastlines would be at risk for displacement (Kulp & Strauss, 2019). This outcome is likely

by 2150 if CO_2 emissions continue to be “business as usual”. Importantly, this statistic within the proposed timeframe (by 2100) is likely attainable if the EAIS is also vulnerable to collapse in the near future. By employing interdisciplinary research, my thesis demonstrates it is now feasible to understand the sensitivity of WAIS and EAIS to future warming. Understanding future WAIS and EAIS changes are not only important to the numerical projections of future sea level rise, their implications are also crucial to studies that seek to predict future human migrations, as well as informing future decisions regarding socioeconomic, demographic, institutional, and political policies linked to future sea level rise (McMichael et al. 2020).

7.7 Future directions of Southern Ocean molecular research

Based on my thesis, as well as the current literature of population genomics, in this section I have outlined the future directions of Southern Ocean genomic research from data collection to sequencing and analyses. I also emphasised the data gaps in biological data, as well as a lack of synthesis of Southern Ocean evolutionary histories in theoretical population genetics. Overall, they should be addressed in order to achieve a holistic understanding of Southern Ocean genomics.

7.7.1 Data sampling and museum curation

Increased effort in data sampling, curation and interpretation are needed in order to accurately understand the past persistence, current challenges and future vulnerability of Southern Ocean benthic fauna. Firstly, *Chapter 2* outlined a critical problem of patchy sampling of a genetically diverse species which could lead to biased data interpretation, such as incorrectly concluding the presence of cryptic species. Since sampling locations of Southern Ocean benthic fauna are concentrated near national research stations, as well as the routes taken by supply vessels (Griffiths et al., 2014), the problem of patchy sampling confounding the interpretation of species status is likely applicable to many Southern Ocean benthic fauna, particularly those with a circumpolar distribution. Careful interpretation of data is required when sampling distributions do not represent the species’ full distributional range.

However, sampling challenges can be resolved by improved and continued coordination of international collaborations to facilitate effective loaning of existing samples (Xavier et al., 2016). Ensuring samples are accessioned into museum collections (and are not retained in individual laboratories) is the best way to ensure the correct sample information (e.g. field IDs, water depth, latitude, longitude, habitat type etc) are easily accessible for future data analyses. When sampling gaps are clearly identified, dedicated expeditions could also be

undertaken to perform biological sampling in poorly surveyed regions, including the Amundsen Sea and East Antarctica.

Future investment in museums is also needed in order to ensure samples are easily retrievable and continuously stored in appropriate, stable conditions in order to ensure the longevity and effective analysis of these samples. For example, care needs to be taken to ensure frozen samples and extracted DNA do not suffer from freezer failures, and preserved (e.g. ethanol) samples need to be regularly inspected to ensure the preservative is at optimal quantity and concentration. Efforts to establish museum vouchering of DNA samples can also ensure genetic studies are reproducible in the future (Buckner et al., 2021). Finally, museums are also crucial stakeholders in ensuring samples are correctly catalogued and accessible for valuable global biodiversity analyses.

7.7.2 Quality control of genomic data

To date, the cleaning and filtering of existing genomic data of Southern Ocean benthic invertebrates has been poorly executed. The steps taken in data cleaning and filtering rarely follow community-defined standards (e.g. O'Leary et al., 2018). For example, many studies rarely report and filter for sample and read depth, as well as minor allele frequency filtering thresholds (e.g. Galaska et al., 2017a, 2017b; Collins et al., 2018; Leiva et al., 2019; Muñoz-Ramírez et al., 2020). It should be noted that these steps are essential in removing putative genotyping errors, and are standard requirements for common downstream analyses (e.g. *Structure*, Prichard et al., 2000; outlier loci detection analysis, Whitlock & Lotterhos, 2015). This incomplete SNP filtering is likely influenced by the high-level of DNA degradation in Southern Ocean samples, as existing (but inadequately filtered) datasets often only contain a few hundreds to a few thousand SNPs to begin with (e.g. Galaska et al., 2017a, 2017b; Collins et al., 2018; Leiva et al., 2019; Muñoz-Ramírez et al., 2020). Thus, filtering for these thresholds would likely further reduce the number of SNPs retained for downstream analyses. However, most poorly-filtered Southern Ocean SNP datasets (or studies that did not accurately report their filtering steps) were bioinformatically processed using a hard genotype calling approach, which might not be optimal for the degraded nature of Southern Ocean benthic fauna. These datasets could have been analysed differently, for example, by using genotype likelihood methods that can account for read uncertainty driven by DNA degradation (Korneliussen et al., 2014), in order to maximise the number of sites, and thus the amount of information sequenced. Overall, the consequence of inadequate genomic data processing is that the resulting data will be "of little value in a comparative sense", as outlined in a recent progress report on the Southern Ocean omics research by the National Academies of Sciences, Engineering, and Medicine (2021). As the community strives to take

advantage of genomic advancement, opportunities for additional training can be achieved via community building, regular workshops and open access of bioinformatic resources.

7.7.3 Technical strategies for whole genome sequencing in Southern Ocean benthic taxa

My thesis highlights that target capture sequencing is highly effective in retrieving reduced representation genomic data (e.g. RAD loci) in degraded samples. However, reduced representation genomic methods only explore a small fraction (~1 - 5%) of the genome that can answer broad evolutionary questions (Fuentes-Pardo & Ruzzante, 2017). In order to thoroughly understand Southern Ocean evolutionary history, as well as underlying genomic mechanisms, whole genome sequencing is the obvious next step in advancing Southern Ocean genomic research.

First, for species of interest, a high quality reference genome would need to be sequenced via *de novo* assembly, annotated for gene functions, as well as detected for SNPs, indels and copy number variation (CNVs) for future whole genome sequence alignment (Ekblom & Wolf, 2014; Montero-Mendieta et al., 2017; Jung et al., 2020). A high quality and well-annotated reference genome can allow accurate inference of population genomic patterns, structural variations and post-translational modifications including DNA methylation or histone modification (Jung et al., 2020). To ensure the success of a high quality reference genome construction, ideally, tissues from populations that experienced a strong bottleneck in the LGM should be used in order to limit the amount of heterozygous positions in the genome. Library preparations should also be performed using high quality DNA extraction input (Ekblom & Wolf, 2014). A high-quality reference genome should be constructed from a large set of minimally overlapping large inserts with limited gaps and artificial errors (Stemple, 2013). Therefore, the reference genome should be sequenced via long reads platforms (e.g. Pacific Biosciences, IonTorrent, Illumina sequencing or Oxford Nanopore, between 5 to 30 kb) (Jung et al., 2020). A reference genome can also be constructed via the combinations of long read and short read sequencing (e.g. Sanger sequencing, < 500 bp) to ensure the resulting assembly is not fragmented (Jung et al., 2020).

Once a high quality reference genome is assembled and annotated, samples from different populations can be sequenced using whole genome sequencing for population genomic analyses. In order to achieve high sample sizes within and across populations, which is particularly important yet costly for species with circumpolar distributions, large-scale shallow whole genome sequencing (< 10x) can be used as an effective approach as it is cost-effective for comparative analyses of hundreds of samples (Lou et al., 2021). As

analyses of shallow whole genome sequencing expect low sequencing depth data, the degraded nature of existing samples deposited at museum collections around the world can be utilised with this method (van der Valk et al., 2019). However, the overall DNA degradation of many museum samples can still present limitations for downstream analyses including nucleotide misincorporation (Jónsson et al., 2013) and reads with extremely low sequencing depth (van der Valk et al., 2019; *Chapter 3*). An alternative approach is to perform whole genome sequencing in the field after collecting fresh samples, which can be easily achieved on cruises or research stations with a dry lab fitted for DNA extraction and a mobile MinION sequencer (Oxford Nanopore) (Jain et al., 2016). However, this approach is likely impractical for population genomic analyses across a large spatial scale, as a single expedition often only visit a small regional part of the Southern Ocean per research season. Overcoming technical challenges associated with sequencing is crucial to the success of Southern Ocean molecular research as samples from this region are incredibly rare and expensive to collect.

7.7.4 Analytical strategies for whole genome sequencing in Southern Ocean population genomics

Once whole genome sequencing and appropriate dataset preparation are successfully executed for population genomic inferences, a wealth of information can be leveraged with different types of analyses optimised to answer unresolved questions of evolutionary histories of Southern Ocean benthic taxa.

7.7.4.1 Haplotype phasing and linkage disequilibrium

Firstly, haplotype estimations (i.e. haplotype phasing) can be achieved with high accuracy using long read whole genome sequencing data. Compared to SNPs, haplotype phasing offers even higher resolution of data as it identifies the specific alleles on each copy of homologous chromosomes within a sample (Al Bkhetan et al., 2019). Importantly, haplotype similarities between samples can be inferred (e.g. Identity-by-Descent [IBD] and Identity-by-State [IBS]), and the relationships across and between different IBD and IBS blocks across samples reflect different levels of coalescence events across recent and ancient timescales (Zheng et al., 2014; Al Bkhetan et al., 2019). The application of haplotype phased data should resolve severe bottlenecks events, as well as events prior to the bottleneck, that reduced representation genomic data have limited power to reconstruct (identified as an issue within *Chapter 6*). In turn, demographic inferences (e.g. *dadi,* Gutenkunst et al., 2009; *fastsimcoal*, Excoffier et al., 2013) could accurately infer past changes in populations size within populations, as well as migration between populations, over multiple epochs.

Additionally, programs based on sequentially Markovian coalescent methods, including pairwise sequentially Markovian coalescent (PSMC) (Li & Durbin, 2011) and multiple sequentially Markovian coalescent (MSMC) (Schiffels & Durbin, 2014), can leverage haplotype-resolved coalescent events to reconstruct population splits and continuous population size change over time. For the analyses of Southern Ocean benthic taxa, this could reflect changes in past demography linked to different glacial-interglacial cycles throughout the Pleistocene. Accurate inferences of past population size changes in some locations could reveal past changes in habitat availability over time, including around the Wilkes Land margin of the EAIS. This could be pivotal in revealing whether parts of the EAIS also collapsed in the recent past and whether they will be susceptible to future collapse under current climate change projections.

Further, because allelic information is understood from haplotype phasing, information regarding linkage disequilibrium (LD) can also be detected. Information on LD reveals the correlations between neighbouring linked loci across the genome (Slatkin, 2008). When examining LD across samples and populations, LD can reveal temporal and spatial variations of gene flow between populations (Pfaff et al., 2001). Analyses such as admixture tracts can calculate dispersal distance between samples (Leitwein et al., 2020), which is useful for detecting connectivity distance and pathways, as well as establishing the role of the ASC and ACC in driving population connectivity, in Southern Ocean benthic taxa. This would also be useful in characterising designated bioregions and Marine Protected Areas (MPA) in the Southern Ocean based on genetic data (Leitwein et al., 2020).

Additionally, interpretations of LD patterns are highly effective in revealing admixture histories (Loh et al., 2013). Examples range from detecting archaic admixture between human, Neanderthal and Denisovan genomes (Schaefer et al., 2021), to reconstructing and dating recent admixture pulses between populations within *Drosophila melanogaster* (Medina et al., 2018) and modern human populations (Zhou et al., 2017). By interrogating LD information in admixture studies of Southern Ocean benthic fauna, signatures of gene flow or isolation linked to contemporary ocean currents, recolonisation from LGM glacial refugia leading to present-day distribution, survival in different types and locations of glacial refugia during LGM, ancient AIS collapses and archaic admixture between sister species can be sequentially reconstructed.

7.7.4.2 Genome-wide association studies

The high resolution of whole genome sequencing data can allow genomic scans such as genome-wide association studies (GWAS) to be performed. Firstly, GWAS can be used to answer questions behind the framework of genomic islands of differentiation. Secondly, GWAS can tease out genomic regions that could be under selection linked to phenotypic variations (Santure & Garant, 2018). For example, there are emerging common observations of contrasting characteristics (five arms versus six arms, broadcasting versus brooding) between Antarctic island and continental shelf localities in closely related species within Ophiuroidea (Sands et al., 2015; Jossart et al., 2019; Lau et al., 2021). By understanding the genomic regions under selection linked to the different phenotypic variations and environments, across different pairs of ophiuroid species, long standing questions such as the drivers of brooding in the Southern Ocean (Poulin & Féral, 1996; Poulin et al., 2002; Pearse et al., 2009), and whether this is related to selection in the past (Pearse et al., 2009; Lau et al. 2021; *Chapter 2, 4*), can be answered. These genomic regions under selection can also be isolated and the timing of differentiation linked to putative selective pressure can be dated using carefully designed demographic modelling approaches (e.g. Tine et al., 2014). In turn, understanding the genomic histories of regions under selection can reveal whether they could be linked to events in the past.

7.7.4.3 Genomic islands of differentiation

From a population genetic perspective, understanding the underlying genomic mechanisms behind the continuum of genetic isolation and/or speciation in the Southern Ocean could offer key insights into the fundamental theory of genomic islands of differentiation. This is a framework illustrating that the genomic landscape that underpins differentiation between lineages should be heterogeneous, with pockets of genomic regions (i.e. islands) experiencing elevated differentiation leading to genetic isolation while other regions may still experience low differentiation and continuous gene flow (Wolf & Ellegren, 2017; Duranton et al., 2018). So far, in global ecology and evolution studies, the data linked to genomic islands of differentiation suffer from various limitations, leading to very few case studies that have successfully demonstrated (uncontested) signatures of genomic islands of differentiation in the terrestrial or marine realm (Wolf & Ellegren, 2017). These limitations include a lack of spatial scale and/or sample collection across the continuum, lack of robust whole genome sequencing data, lack of thorough understanding of past changes in population and species histories, as well as confounding factors due to unaccounted signatures of selection (i.e. non-neutral processes) (Wolf & Ellegren, 2017).

The Southern Ocean serves as an ideal natural laboratory to critically explore the processes that underpin genomic islands of differentiation. It is clear that the continuum of reproductive isolation and/or speciation exists for many Southern Ocean taxa (i.e. studies that have reported signatures of cryptic speciation), including the species examined in this thesis. These observed continuums are likely characterised by gradual steps leading to isolation facilitated by a level of isolation-by-geographical distance in the vast Southern Ocean. For some benthic lineages and species, the drivers of diversification and speciation have already been understood, including adaption to seascape dynamics in *P. turqueti* (Strugnell et al., 2017; *Chapter 5*) and survival strategies of glacial-interglacial cycles in *Ophionotus* (*Chapter 2, 4*). Future studies could employ a clear, comprehensive regime across the genetic isolation/speciation continuum in order to accurately detect signatures of genomic islands of differentiation at a whole genome scale.

Importantly, my thesis has highlighted additional insights behind diversification in the Southern Ocean that could further characterise mechanisms linked to genomic islands of differentiation at a nucleotide base level. For example, the selection for genes linked to suppression or interaction of transposable elements (TE) across seascape dynamics in *P. turqueti* could indicate TE could be linked to diversification across the Southern Ocean. Alternatively, TE could be merely a by-produce of genomic variance across the Southern Ocean in *P. turqueti*. Transposable elements are mobile genetic sequences that have the ability to change positions within a genome (Etchegaray et al., 2021). The role of TE in diversification has also long been hypothesised to promote genotypic variations leading to diversification within and between species, but has rarely been demonstrated in empirical studies, as discussed within Jurka et al., 2011 and Serrato-Capuchina & Matute, 2018 (but see Niu et al., 2019 as an empirical case study). Additionally, in *Chapter 5*, the number of TE was not significantly different between outlier loci and neutral loci in *P. turqueti*, indicating any possible genomic differentiations driven by TE would be linked to neutral processes. So far, the hypothesis of TE in driving differentiation in *P. turqueti* fits most of the assumptions of finding genomic islands of differentiations. Nonetheless, to my knowledge, the connection between TE and genomic islands of differentiation is rarely discussed in the literature. Analyses of future whole genome sequencing could also aim to understand structural variations in genomes linked to TE, in *P. turqueti* or other Southern Ocean species, when searching for genomic islands of differentiation.

7.7.4.4 Interpretation of whole genome sequencing data is not possible without understanding the fundamentals

Whole genome sequencing is a powerful and effective approach in understanding evolutionary histories of Southern Ocean benthic taxa, and the implications can be of global significance. For example, past demographic changes in Southern Ocean benthic taxa can inform past and future Antarctic Ice Sheet collapses. The underlying genomic mechanisms of diversification remains an unresolved puzzle of global evolutionary studies and Southern Ocean benthic taxa are ideal for testing these theories. However, analyses of whole genome sequencing data are not possible without first understanding fundamental biological data. For example, inferences using a molecular clock heavily rely on accurate information of mutation rate, generation time and life span. Furthermore, analyses and interpretation of genetic connectivity can only be robust if the species reproductive strategies and pelagic larval duration (when applicable) are known. So far, only a handful of Southern Ocean benthic taxa species have been studied for their life histories including reproduction (e.g. Pearse et al., 1991; Brey & Hain, 1992; Chiantore et al., 2002; Tyler et al., 2003; Grange et al., 2004, 2007, 2011; Higgs et al., 2009; Reed et al., 2013; Lau et al., 2018). Knowledge of general species ecology, such as feeding habits and habitat preference, would also be needed in order to search for, and interpret, signatures of evolutionary histories at an ecosystem scale.

Finally, most genomic inferences are built based on diffusion processes (Wright–Fisher diffusion for genetic drift looking forward in time; Fisher, 1930, Wright, 1931) or coalescent theory (based on the Kingman Coalescent for coalescence events looking backward in time; Kingman, 2000). However, it is becoming clear the evolutionary histories of Southern Ocean benthic taxa have been influenced by many events following the cyclicity of glacial-interglacial cycles, leading to many unique demographic changes associated with each event in the past. Existing diffusion and coalescent analytical frameworks are often constructed based on the condensed evolutionary histories in model species (e.g. ‘out-of-Africa’ event in human populations). Therefore, the genomic signatures of different past events in the Southern Ocean are often difficult to tease out using existing frameworks. Therefore, the theoretical interpretations of diffusion processes and coalescent theory may need to be expanded and considered for the unique evolutionary context of the Southern Ocean benthic fauna. Future research on statistical genomics with a Southern Ocean focus could offer valuable frameworks for accurately understanding species evolutionary histories in the Southern Ocean.

7.8 Closing remarks

This thesis provides novel insights into the evolutionary persistence of Sothern Ocean benthic taxa throughout the Quaternary period. By testing species concepts, establishing the

robustness of the sequencing approach, and investigating the overall evolutionary histories of *O. victoriae*, *O. hexactis* and *P. turqueti*, knowledge derived from Southern Ocean systematics, ecology and evolution research can be used to answer applied questions of global significance. Using genomic data, my thesis offers direct empirical evidence indicating the WAIS collapsed during the last interglacial period, and thus pinpoints the thresholds of WAIS instability. This has been a significant deep uncertainty, and a tipping point event, in future global sea level rise projections. By understanding the genomic signatures that underpin the evolutionary histories of Southern Ocean benthic fauna, we can begin to elucidate the global consequences of future changes in Antarctica.

References

Agarwala, R., Barrett, T., Beck, J., Benson, D. A., Bollin, C., Bolton, E., Bourexis, D., Brister, J. R., Bryant, S. H., Canese, K., Cavanaugh, M., Charowhas, C., Clark, K., Dondoshansky, I., Feolo, M., Fitzpatrick, L., Funk, K., Geer, L. Y., … Zbicz, K. (2018). Database resources of the National Center for Biotechnology Information. *Nucleic Acids Research*, **44**(D1), D7-19.

Ahrens, C. W., Jordan, R., Bragg, J., Harrison, P. A., Hopley, T., Bothwell, H., Murray, K., Steane, D. A., Whale, J. W., Byrne, M., Andrew, R., & Rymer, P. D. (2021). Regarding the F-word: The effects of data filtering on inferred genotype-environment associations. *Molecular Ecology Resources*, **21**(5), 1460–1474.

Aitken, A. R. A., Young, D. A., Ferraccioli, F., Betts, P. G., Greenbaum, J. S., Richter, T. G., Roberts, J. L., Blankenship, D. D., & Siegert, M. J. (2014). The subglacial geology of Wilkes Land, East Antarctica. *Geophysical Research Letters*, **41**(7), 2390–2400.

Al Bkhetan, Z., Zobel, J., Kowalczyk, A., Verspoor, K., & Goudey, B. (2019). Exploring effective approaches for haplotype block phasing. *BMC Bioinformatics*, **20**, 540.

Alcala, N., Goudet, J., & Vuilleumier, S. (2014). On the transition of genetic differentiation from isolation to panmixia: What we can learn from GST and D. *Theoretical Population Biology*, **93**, 75–84.

Ali, O. A., O'Rourke, S. M., Amish, S. J., Meek, M. H., Luikart, G., Jeffres, C., & Miller, M. R. (2016). Rad capture (Rapture): Flexible and efficient sequence-based genotyping. *Genetics*, **202**(2), 389–400.

Allcock, A. L., Barratt, I., Eléaume, M., Linse, K., Norman, M. D., Smith, P. J., Steinke, D., Stevens, D. W., & Strugnell, J. M. (2011). Cryptic speciation and the circumpolarity debate: A case study on endemic Southern Ocean octopuses using the COI barcode of life. *Deep-Sea Research Part II: Topical Studies in Oceanography*, **58**(1–2), 242–249.

Allcock, A. L., & Strugnell, J. M. (2012). Southern Ocean diversity: New paradigms from molecular ecology. *Trends in Ecology and Evolution*, **27**(9), 520–528.

Altschul, S. F., Gish, W., Miller, W., Myers, E. W., & Lipman, D. J. (1990). Basic local alignment search tool. *Journal of Molecular Biology*, **215**(3), 403–410.

Amante, C., & Eakins, B. W. (2009). *ETOPO1 1 Arc-Minute Global Relief Model: Procedures, Data Sources and Analysis*. *NOAA Technical Memorandum NESDIS NGDC-24*. National Geophysical Data Center.

Ambrose, R. F. (1982). Shelter Utilization by the Molluscan Cephalopod *Octopus bimaculatus*. *Marine Ecology Progress Series*, **7**(1), 67–73.

Ameneiro, J., Mouriño-Carballido, B., Parapar, J., & Vázquez, E. (2012). Abundance and distribution of invertebrate larvae in the Bellingshausen Sea (West Antarctica). *Polar Biology*, **35**, 1359–1373.

Amos, W., & Harwood, J. (1998). Factors affecting levels of genetic diversity in natural populations. *Philosophical Transactions of the Royal Society B: Biological Sciences*, **353**(1366), 177–186.

Andermann, T., Torres Jiménez, M. F., Matos-Maraví, P., Batista, R., Blanco-Pastor, J. L., Gustafsson, A. L. S., Kistler, L., Liberal, I. M., Oxelman, B., Bacon, C. D., & Antonelli, A. (2020). A Guide to Carrying Out a Phylogenomic Target Sequence Capture Project. *Frontiers in Genetics*, **10**, 1407.

Anderson, J. B., Shipp, S. S., Lowe, A. L., Wellner, J. S., & Mosola, A. B. (2002). The Antarctic Ice Sheet during the Last Glacial Maximum and its subsequent retreat history:

a review. *Quaternary Science Reviews*, **21**(1–3), 49–70.
Andrews, K. R., Good, J. M., Miller, M. R., Luikart, G., & Hohenlohe, P. A. (2016). Harnessing the power of RADseq for ecological and evolutionary genomics. *Nature Reviews Genetics*, **17**, 81–92.
Andrews, S. (2019). FastQC: A Quality Control tool for High Throughput Sequence Data. [tool source] Retrieved from http://www.bioinformatics.babraham.ac.uk/projects/fastqc
April, J., Hanner, R. H., Dion-Côté, A.-M., & Bernatchez, L. (2013). Glacial cycles as an allopatric speciation pump in north-eastern American freshwater fishes. *Molecular Ecology*, **22**(2), 409–422.
Arango C. P., Soler-Membrives, A., & Miller, K. J. (2011). Genetic differentiation in the circum-Antarctic sea spider *Nymphon australe* (Pycnogonida; Nymphonidae). *Deep Sea Research Part II: Topical Studies in Oceanography*, **58**(1-2), 212–219.
Arnold, M. L., & Kunte, K. (2017). Adaptive Genetic Exchange: A Tangled History of Admixture and Evolutionary Innovation. *Trends in Ecology and Evolution*, **32**(8), 601–611.
Avise, J. C. (1989). Gene Trees and Organismal Histories: A Phylogenetic Approach to Population Biology. *Evolution*, **43**, 1192–1208.
Avise, J. C. (2009). Phylogeography: retrospect and prospect. *Journal of Biogeography*, **36**(1), 3–15.
Avise, J. C., Arnold, J., Ball, R. M., Bermingham, E., Lamb, T., Neigel, J. E., Reeb, C. A., Saunders, N. C. (1987). INTRASPECIFIC PHYLOGEOGRAPHY: The Mitochondrial DNA Bridge Between Population Genetics and Systematics. *Annual Review of Ecology and Systematics*, **18**, 489–522.
Bagley, R. K., Sousa, V. C., Niemiller, M. L., & Linnen, C. R. (2017). History, geography and host use shape genomewide patterns of genetic variation in the redheaded pine sawfly (*Neodiprion lecontei*). *Molecular Ecology*, **26**(4), 1022–1044.
Baird, H. P., Miller, K. J., & Stark, J. S. (2011). Evidence of hidden biodiversity, ongoing speciation and diverse patterns of genetic structure in giant Antarctic amphipods. *Molecular Ecology*, **20**(16), 3439–3454.
Baird, H. P., Miller, K. J., & Stark, J. S. (2012). Genetic Population Structure in the Antarctic Benthos: Insights from the Widespread Amphipod, *Orchomenella franklini*. *PLoS ONE*, **7**(3), e34363.
Bálint, M., Domisch, S., Engelhardt, C. H. M., Haase, P., Lehrian, S., Sauer, J., Theissinger, K., Pauls, S. U., & Nowak, C. (2011). Cryptic biodiversity loss linked to global climate change. *Nature Climate Change*, **1**, 313–318.
Ballard, J. W. O. (2000). When One Is Not Enough: Introgression of Mitochondrial DNA in *Drosophila*. *Molecular Biology and Evolution*, **17**(7), 1126–1130.
Ballard, J. W. O., & Rand, D. M. (2005). The Population Biology of Mitochondrial DNA and Its Phylogenetic Implications. *Annual Review of Ecology, Evolution, and Systematics*, **36**, 621–642.
Bamber, J. L., Riva, R. E. M., Vermeersen, B. L. A., & Lebrocq, A. M. (2009). Reassessment of the potential sea-level rise from a collapse of the west Antarctic ice sheet. *Science*, **324**(5929), 901–903.
Bandelt, H. J., Forster, P., & Röhl, A. (1999). Median-joining networks for inferring intraspecific phylogenies. *Molecular Biology and Evolution*, **16**(1), 37–48.
Bank, C., Ewing, G. B., Ferrer-Admettla, A., Foll, M., & Jensen, J. D. (2014). Thinking too positive? Revisiting current methods of population genetic selection inference. *Trends in Genetics*, **30**(12), 540–546.
Barbanti, A., Torrado, H., Macpherson, E., Bargelloni, L., Franch, R., Carreras, C., & Pascual, M. (2020). Helping decision making for reliable and cost-effective 2b-RAD

sequencing and genotyping analyses in non-model species. *Molecular Ecology Resources*, **20**(3), 795–806.
Barnes, D. K. A., & Hillenbrand, C. D. (2010). Faunal evidence for a late quaternary trans-Antarctic seaway. *Global Change Biology*, **16**(12), 3297–3303.
Barnes, D. K. A., Linse, K., Enderlein, P., Smale, D., Fraser, K. P. P., & Brown, M. (2008). Marine richness and gradients at Deception Island, Antarctica. *Antarctic Science*, **20**(3), 272–280.
Barnes, D. K. A., Sands, C. J., Hogg, O. T., Robinson, B. J. O., Downey, R. V., & Smith, J. A. (2016). Biodiversity signature of the Last Glacial Maximum at South Georgia, Southern Ocean. *Journal of Biogeography*, **43**(12), 2391–2399.
Barratt, I. M., Johnson, M. P., Collins, M. A., & Allcock, A. L. (2008). Female reproductive biology of two sympatric incirrate octopod species, *Adelieledone polymorpha* (Robson 1930) and *Pareledone turqueti* (Joubin 1905) (Cephalopoda: Octopodidae), from South Georgia. *Polar Biology*, **31**, 583–594.
Bartlett, J. C., Convey, P., Hughes, K. A., Thorpe, S. E., & Hayward, S. A. L. (2021). Ocean currents as a potential dispersal pathway for Antarctica's most persistent non-native terrestrial insect. *Polar Biology*, **44**, 209–216.
Bell, F. J. (1902). VIII. Echinoderma. In Southern Cross Exploring Vessel Voyage 1898 (Ed.), *Reports on the collections of Natural History made in the Antarctic regions during the voyage of the "Southern Cross"* (pp. 214–220). British Museum (Natural History).
Belyayev, A. (2014). Bursts of transposable elements as an evolutionary driving force. *Journal of Evolutionary Biology*, **27**(12), 2573–2584.
Bentley, M. J., Ocofaigh, C., Anderson, J. B., Conway, H., Davies, B., Graham, A. G. C., Hillenbrand, C.-D., Hodgson, D. A., Jamieson, S. S. R., Larter, R. D., Mackintosh, A., Smith, J. A., Verleyen, E., Ackert, R. P., Bart, P. J., Berg, S., Brunstein, D., Canals, M., Colhoun, E. A, … Zwartz, D. (2014). A community-based geological reconstruction of Antarctic Ice Sheet deglaciation since the Last Glacial Maximum. *Quaternary Science Reviews*, **100**, 1–9.
Bernatchez, L., Wellenreuther, M., Araneda, C., Ashton, D. T., Barth, J. M. I., Beacham, T. D., Maes, G. E., Martinsohn, J. T., Miller, K. M., Naish, K. A., Ovenden, J. R., Primmer, C. R., Suk, H. Y., Therkildsen, N. O., & Withler, R. E. (2017). Harnessing the Power of Genomics to Secure the Future of Seafood. *Trends in Ecology and Evolution*, **32**(9), 665–680.
Bertl, J., Ringbauer, H., & Blum, M. G. B. (2018). Can secondary contact following range expansion be distinguished from barriers to gene flow? *PeerJ*, **6**, e5325.
Bi, K., Linderoth, T., Vanderpool, D., Good, J. M., Nielsen, R., & Moritz, C. (2013). Unlocking the vault: Next-generation museum population genomics. *Molecular Ecology*, **22**(24), 6018–6032.
Binns, D., Dimmer, E., Huntley, R., Barrell, D., O'Donovan, C., & Apweiler, R. (2009). QuickGO: A web-based tool for Gene Ontology searching. *Bioinformatics*, **25**(22), 3045–3056.
Blum, M., Chang, H.-Y., Chuguransky, S., Grego, T., Kandasaamy, S., Mitchell, A., Nuka, G., Paysan-Lafosse, T., Qureshi, M., Raj, D., Richardson, L., Salazar, G. A., Williams, L., Bork, P., Bridge, A., Gough, J., Haft, D. H., Letunic, I., Marchler-Bauer, A., … Finn, R. D. (2020). The InterPro protein families and domains database: 20 years on. *Nucleic Acids Research*, **49**(D1), D344–D354.
Boissin, E., Stöhr, S., & Chenuil, A. (2011). Did vicariance and adaptation drive cryptic speciation and evolution of brooding in *Ophioderma longicauda* (Echinodermata: Ophiuroidea), a common Atlanto-Mediterranean ophiuroid? *Molecular Ecology*, **20**(22), 4737–4755.

Boletzky, S. V. (1994). Embryonic development of cephalopods at low temperatures. *Antarctic Science*, **6**(2), 139–142.

Bossert, S., & Danforth, B. N. (2018). On the universality of target-enrichment baits for phylogenomic research. *Methods in Ecology and Evolution*, **9**(6), 1–8.

Boucher, F. C., Casazza, G., Szövényi, P., & Conti, E. (2016). Sequence capture using RAD probes clarifies phylogenetic relationships and species boundaries in *Primula* sect. *Auricula*. *Molecular Phylogenetics and Evolution*, **104**, 60–72.

Bouckaert, R., Vaughan, T. G., Barido-Sottani, J., Duchêne, S., Fourment, M., Gavryushkina, A., Heled, J., Jones, G., Kühnert, D., De Maio, N., Matschiner, M., Mendes, F. K., Müller, N. F., Ogilvie, H. A., du Plessis, L., Popinga, A., Rambaut, A., Rasmussen, D., Siveroni, I., … Drummond, A. J. (2019). BEAST 2.5: An advanced software platform for Bayesian evolutionary analysis. *PLoS Computational Biology*, **15**(4), e1006650.

Bourque, G., Burns, K. H., Gehring, M., Gorbunova, V., Seluanov, A., Hammell, M., Imbeault, M., Izsvák, Z., Levin, H. L., Macfarlan, T. S., Mager, D. L., Feschotte, C. (2018). Ten things you should know about transposable elements. *Genome Biology*, **19**, 199.

Bowden, D. A., Clarke, A., & Peck, L. S. (2009). Seasonal variation in the diversity and abundance of pelagic larvae of Antarctic marine invertebrates. *Marine Biology*, **156**(10), 2033–2047.

Bowen, B. W., Shanker, K., Yasuda, N., Maria, M. C., Von Der Heyden, S., Paulay, G., Rocha, L. A., Selkoe, K. A., Barber, P. H., Williams, S. T., Lessios, H. A., Crandall, E. D., Bernardi, G., Meyer, C. P., Carpenter, K. E, & Toonen, R. J. (2014). Phylogeography unplugged: Comparative surveys in the genomic era. *Bulletin of Marine Science*, **90**(1), 13–46.

Boyle, P., & Rodhouse, P. (2005). *Cephalopods: Ecology and Fisheries*. Blackwell Science Ltd.

Brandão, S. N., Sauer, J., & Schön, I. (2010). Circumantarctic distribution in Southern Ocean benthos? A genetic test using the genus *Macroscapha* (Crustacea, Ostracoda) as a model. *Molecular Phylogenetics and Evolution*, **55**(3), 1055–1069.

Brasier, M. J., Wiklund, H., Neal, L., Jeffreys, R., Linse, K., Ruhl, H., & Glover, A. G. (2021). DNA barcoding uncovers cryptic diversity in 50% of deep-sea Antarctic polychaetes. *Royal Society Open Science*, **3**, 160432.

Brasier, M. J., Barnes, D., Bax, N., Brandt, A., Christianson, A. B., Constable, A. J., Downey, R., Figuerola, B., Griffiths, H., Gutt, J., Lockhart, S., Morley, S. A., Post, A. L., Van de Putte, A., Saeedi, H., Stark, J. S., Sumner, M., & Waller, C. L. (2021). Responses of Southern Ocean Seafloor Habitats and Communities to Global and Local Drivers of Change. *Frontiers in Marine Science*, **8**, 622721.

Bresadola, L., Link, V., Buerkle, C. A., Lexer, C., & Wegmann, D. (2020). Estimating and accounting for genotyping errors in RAD-seq experiments. *Molecular Ecology Resources*, **20**(4), 856–870.

Brey, T., Dahm, C., Gorny, M., Klages, M., Stiller, M., & Arntz, W. E. (1996). Do Antarctic benthic invertebrates show an extended level of eurybathy? *Antarctic Science*, **8**(1), 3–6.

Brey, Thomas, & Hain, S. (1992). Growth, reproduction and production of *Lissarca notorcadensis* (Bivalvia: Philobryidae) in the Weddell Sea, Antarctica. *Marine Ecology Progress Series*, **82**, 219–226.

Broad Institute. (2019). Picard Toolkit. [tool source] Retrieved from http://broadinstitute.github.io/picard/

Brook, E. J., & Buizert, C. (2018). Antarctic and global climate history viewed from ice cores.

Nature, **558**, 200–208.
Bruchhausen, P. M., Raymond, J. A., Jacobs, S. S., Devries, A. L., Thorndike, E. M., & DeWitt, H. H. (1979). Fish, Crustaceans, and the Sea Floor Under the Ross Ice Shelf. *Science*, **203**(4379), 449–451.
Burrell, A. S., Disotell, T. R., & Bergey, C. M. (2015). The use of museum specimens with high-throughput DNA sequencers. *Journal of Human Evolution*, **79**, 35–44.
Capella, J. E., Ross, R. M., Quetin, L. B., & Hofmann, E. E. (1992). A note on the thermal structure of the upper ocean in the Bransfield Strait-South Shetland Islands region. *Deep Sea Research Part A, Oceanographic Research Papers*, **39**(7–8), 1221–1229.
Carter, J., Spellman, G., Kimball, R., Safran, R., Funk, E., Schield, D., & Kane, N. (2021). Estimating phylogenies from genomes: A review of commonly used genomic data in phylogenomics. *Authorea*. Preprint.
Catchen, J., Hohenlohe, P. A., Bassham, S., Amores, A., & Cresko, W. A. (2013). Stacks: An analysis tool set for population genomics. *Molecular Ecology*, **22**(11), 3124–3140.
Catchen, J. M., Amores, A., Hohenlohe, P., Cresko, W., & Postlethwait, J. H. (2011). Stacks: Building and genotyping loci de novo from short-read sequences. *G3: Genes, Genomes, Genetics*, **1**(3), 171–182.
Chapman, C. C., Lea, M. A., Meyer, A., Sallée, J.-B., & Hindell, M. (2020). Defining Southern Ocean fronts and their influence on biological and physical processes in a changing climate. *Nature Climate Change*, **10**, 209–219.
Charlesworth, B., & Jain, K. (2014). Purifying selection, drift, and reversible mutation with arbitrarily high mutation rates. *Genetics*, **198**(4), 1587–1602.
Chen, B., Cole, J. W., & Grond-Ginsbach, C. (2017). Departure from Hardy Weinberg Equilibrium and Genotyping Error. *Frontiers in Genetics*, **8**, 167.
Chen, S., Zhou, Y., Chen, Y., & Gu, J. (2018). fastp: an ultra-fast all-in-one FASTQ preprocessor. *Bioinformatics*, **34**(17), i884–i890.
Cheng, X., & Degiorgio, M. (2020). Flexible Mixture Model Approaches That Accommodate Footprint Size Variability for Robust Detection of Balancing Selection. *Molecular Biology and Evolution*, **37**(11), 3267–3291.
Chiantore, M., Cattaneo-Vietti, R., Elia, L., Guidetti, M., & Antonini, M. (2002). Reproduction and condition of the scallop *Adamussium colbecki* (Smith 1902), the sea-urchin *Sterechinus neumayeri* (Meissner 1900) and the sea-star *Odontaster validus* Koehler 1911 at Terra Nova Bay (Ross Sea): different strategies relate. *Polar Biology*, **25**, 251–255.
Choin, J., Mendoza-Revilla, J., Arauna, L. R., Cuadros-Espinoza, S., Cassar, O., Larena, M., Ko, A. M. S., Harmant, C., Laurent, R., Verdu, P., Laval, G., Boland, A., Olaso, R., Deleuze, J.-F., Valentin, F., Ko, Y. C., Jakobsson, M., Gessain, A., Excoffier, L. … Quintana-Murci, L. (2021). Genomic insights into population history and biological adaptation in Oceania. *Nature*, **592**, 583–589.
Clark, E. G., Kanauchi, D., Kano, T., Aonuma, H., Briggs, D. E. G., & Ishiguro, A. (2019). The function of the ophiuroid nerve ring: How a decentralized nervous system controls coordinated locomotion. *Journal of Experimental Biology*, **222**(2), jeb192104.
Clark, P. U., Archer, D., Pollard, D., Blum, J. D., Rial, J. A., Brovkin, V., Mix, A. C., Pisias, N. G., & Roy, M. (2006). The middle Pleistocene transition: characteristics, mechanisms, and implications for long-term changes in atmospheric pCO_2. *Quaternary Science Reviews*, **25**(23–24), 3150–3184.
Clarke, A. (2008). Antarctic marine benthic diversity: patterns and processes. *Journal of Experimental Marine Biology and Ecology*, **366**(1–2), 48–55.
Clarke, A., Aronson, R. B., Crame, J. A., Gili, J.-M., & Blake, D. B. (2004). Evolution and diversity of the benthic fauna of the Southern Ocean continental shelf. *Antarctic*

Science, **16**(4), 559–568.
Clarke, A., & Crame, J. A. (1989). The origin of the Southern Ocean marine fauna. *Geological Society, London, Special Publications*, **47**, 2253–268.
Clarke, A., & Crame, J. A. (1992). The Southern Ocean benthic fauna and climate change: a historical perspective. *Philosophical Transactions of the Royal Society B: Biological Sciences*, **338**(1285), 299–309.
Clarke, A., Griffiths, H. J., Barnes, D. K. A., Meredith, M. P., & Grant, S. M. (2009). Spatial variation in seabed temperatures in the Southern Ocean: Implications for benthic ecology and biogeography. *Journal of Geophysical Research: Biogeosciences*, **114**(G3), G03003.
Collares, L. L., Mata, M. M., Kerr, R., Arigony-Neto, J., & Barbat, M. M. (2018). Iceberg drift and ocean circulation in the northwestern Weddell Sea, Antarctica. *Deep-Sea Research Part II: Topical Studies in Oceanography*, **149**, 10–24.
Collin, R., & Moran, A. (2018). Evolutionary transitions in mode of development. In T. J. Carrier, A. M. Reitzel, & A. Heyland (Eds.), *Evolutionary Ecology of Marine Invertebrate Larvae* (pp. 50–66). Oxford University Press.
Collins, E. E., Galaska, M. P., Halanych, K. M., & Mahon, A. R. (2018). Population Genomics of *Nymphon australe* Hodgson, 1902 (Pycnogonida, Nymphonidae) in the Western Antarctic. *The Biological Bulletin*, **234**(3), 180–191.
Collins, G. E., Hogg, I. D., Convey, P., Sancho, L. G., Cowan, D. A., Lyons, W. B., Adams, B. J., Wall, D. H, & Green, T. G. A. (2020). Genetic diversity of soil invertebrates corroborates timing estimates for past collapses of the West Antarctic Ice Sheet. *Proceedings of the National Academy of Sciences of the United States of America*, **117**(36), 22293–22302.
Constable, A. J., Melbourne-Thomas, J., Corney, S. P., Arrigo, K. R., Barbraud, C., Barnes, D. K. A., Bindoff, N. L., Boyd, P. W., Brandt, A., Costa, D. P., Davidson, A. T., Ducklow, H. W., Emmerson, L., Fukuchi, M., Gutt, J., Hindell, M. A., Hofmann, E. E., Hosie, G. W., Iida, T., … Ziegler, P. (2014). Climate change and Southern Ocean ecosystems I: How changes in physical habitats directly affect marine biota. *Global Change Biology*, **20**(10), 3004–3025.
Convey, P., Bowman, V. C., Chown, S. L., Francis, J. E., Fraser, C., & Smellie, J. L. (2018). Ice-Bound Antarctica: Biotic Consequences of the Shift from a Temperate to a Polar Climate. In C. Hoorn, A. Perrigo, & A. Antonelli (Eds.), *Mountains, Climate and Biodiversity* (pp. 355–373). Oxford, UK: John Wiley & Sons.
Convey, P., Gibson, J. A. E., Hillenbrand, C. D., Hodgson, D. A., Pugh, P. J. A., Smellie, J. L., & Stevens, M. I. (2008). Antarctic terrestrial life - Challenging the history of the frozen continent? *Biological Reviews*, **82**(2), 103–117.
Convey, P., Stevens, M. I., Hodgson, D. A., Smellie, J. L., Hillenbrand, C.-D., Barnes, D. K. A., Clarke, A., Pugh, P. J. A., Linse, K., & Cary, S. C. (2009). Exploring biological constraints on the glacial history of Antarctica. *Quaternary Science Reviews*, **28**(27–28), 3035–3048.
Cook, C. P., Van De Flierdt, T., Williams, T., Hemming, S. R., Iwai, M., Kobayashi, M., Jimenez-Espejo, F. J., Escutia, C., González, J. J., Khim, B. K., McKay, R. M., Passchier, S., Bohaty, S. M., Riesselman, C. R., Tauxe, L., Sugisaki, S., Galindo, A. L., Patterson, M. O., Sangiorgi, F., … Yamane, M. (2013). Dynamic behaviour of the East Antarctic ice sheet during Pliocene warmth. *Nature Geoscience*, **6**, 765–769.
Crame, J. A. (1997). An evolutionary framework for the polar regions. *Journal of Biogeography*, **24**(1), 1–9.
Crame, J. A. (2018). Key stages in the evolution of the Antarctic marine fauna. *Journal of Biogeography*, **45**(5), 986–994.

Crandall, E. D., Frey, M. A., Grosberg, R. K., & Barber, P. H. (2008). Contrasting demographic history and phylogeographical patterns in two Indo-Pacific gastropods. *Molecular Ecology*, **17**(2), 611–626.

Crisci, J. L., Poh, Y.-P., Bean, A., Simkin, A., & Jensen, J. D. (2012). Recent progress in polymorphism-based population genetic inference. *Journal of Heredity*, **103**(2), 287–296.

Cutter, A. D. (2013). Integrating phylogenetics, phylogeography and population genetics through genomes and evolutionary theory. *Molecular Phylogenetics and Evolution*, **69**(3), 1172–1185.

DaCosta, J. M., & Sorenson, M. D. (2014). Amplification Biases and Consistent Recovery of Loci in a Double-Digest RAD-seq Protocol. *PLoS ONE*, **9**(9), e106713.

Dahm, C., & Brey, T. (1998). Determination of growth and age of slow growing brittle stars (Echinodermata: Ophiuroidea) from natural growth bands. *Journal of the Marine Biological Association of the United Kingdom*, **78**(3), 941–951.

Dambach, J., Raupach, M. J., Leese, F., Schwarzer, J., & Engler, J. O. (2016). Ocean currents determine functional connectivity in an Antarctic deep-sea shrimp. *Marine Ecology*, **37**(6), 1336–1344.

Damerau, M., Salzburger, W., & Hanel, R. (2014). Population genetic structure of *Lepidonotothen larseni* revisited: *cyb* and microsatellites suggest limited connectivity in the Southern Ocean. *Marine Ecology Progress Series*, **517**, 251–263.

Danecek, P., Auton, A., Abecasis, G., Albers, C. A., Banks, E., DePristo, M. A., Handsaker, R. E., Lunter, G., Marth, G. T., Sherry, S. T., McVean, G., & Durbin, R. (2011). The variant call format and VCFtools. *Bioinformatics*, **27**(15), 2156–2158.

Davey, J. W., Cezard, T., Fuentes-Utrilla, P., Eland, C., Gharbi, K., & Blaxter, M. L. (2013). Special features of RAD Sequencing data: Implications for genotyping. *Molecular Ecology*, **22**(11), 3151–3164.

Davey, J. W., Hohenlohe, P. A., Etter, P. D., Boone, J. Q., Catchen, J. M., & Blaxter, M. L. (2011). Genome-wide genetic marker discovery and genotyping using next-generation sequencing. *Nature Reviews Genetics*, **12**, 499–510.

Davis, M. B., Shaw, R. G., & Etterson, J. R. (2005). Evolutionary responses to changing climate. *Ecology*, **86**(7), 1704–1714.

Dayton, P. K., & Oliver, J. S. (1977). Antarctic soft-bottom benthos in oligotrophic and eutrophic environments. *Science*, **197**, 55–58.

Dayton, P. K., Robilliard, G. A., & Devries, A. L. (1969). Anchor Ice Formation in McMurdo Sound, Antarctica, and Its Biological Effects. *Science*, **163**(3864), 273–274.

De-Kayne, R., Frei, D., Greenway, R., Mendes, S. L., Retel, C., & Feulner, P. G. D. (2021). Sequencing platform shifts provide opportunities but pose challenges for combining genomic data sets. *Molecular Ecology Resources*, **21**(3), 653–660.

De Boer, B., Lourens, L. J., & Van De Wal, R. S. W. (2014). Persistent 400,000-year variability of antarctic ice volume and the carbon cycle is revealed throughout the plio-pleistocene. *Nature Communications*, **5**, 2999.

De Broyer, C., Danis, B., Louise, A., Martin, A., Claudia, A., Tom, A., David, B., Marthan, B., Kasia, B. S., Magda, B., Jens, B., Nunes, B. S., Angelika, B., Bruno, D., Bruno, D., De Claude, B., de Miguel, S., Marc, E., Christian, E., & Wolfgang, Z. (2011). How many species in the Southern Ocean? Towards a dynamic inventory of the Antarctic marine species. *Deep-Sea Research Part II: Topical Studies in Oceanography*, **58**(1–2), 5–17.

DeConto, R. M., & Pollard, D. (2016). Contribution of Antarctica to past and future sea-level rise. *Nature*, **531**, 591–597.

Demarchi, M., Chiappero, M. B., Tatián, M., & Sahade, R. (2010). Population genetic structure of the Antarctic ascidian *Aplidium falklandicum* from Scotia Arc and South

Shetland Islands. *Polar Biology*, **33**(11), 1567–1576.
Denton, G. H., & Hughes, T. J. (2002). Reconstructing the Antarctic Ice Sheet at the Last Glacial Maximum. *Quaternary Science Reviews*, **21**(1–3), 193–202.
DeSalle, R., Egan, M. G., & Siddall, M. (2005). The unholy trinity: Taxonomy, species delimitation and DNA barcoding. *Philosophical Transactions of the Royal Society B: Biological Sciences*, **360**(1462), 1905–1916.
DeSalle, R., & Goldstein, P. (2019). Review and Interpretation of Trends in DNA Barcoding. *Frontiers in Ecology and Evolution*, **7**, 302.
Díaz, A., Gérard, K., Claudio, G. W., Maturana, C., Féral, J. P., David, B., Saucède, T., & Poulin, E. (2018). Genetic structure and demographic inference of the regular sea urchin *Sterechinus neumayeri* (Meissner, 1900) in the Southern Ocean: The role of the last glaciation. *PLoS ONE*, **13**(6), e0197611.
Díaz, A., González-Wevar, C. A., Maturana, C. S., Palma, Á. T., Poulin, E., & Gerard, K. (2012). Restricted geographic distribution and low genetic diversity of the brooding sea urchin *Abatus agassizii* (Spatangoidea: Schizasteridae) in the South Shetland Islands: A bridgehead population before the spread to the northern Antarctic Peninsula? *Revista Chilena de Historia Natural*, **85**(4), 457–468.
Dietz, L., Arango, C. P., Dömel, J. S., Halanych, K. M., Harder, A. M., Held, C., Mahon, A. R., Mayer, C., Melzer, R. R., Rouse, G. W., Weis, A., Wilson, N. G., & Leese, F. (2015). Regional differentiation and extensive hybridization between mitochondrial clades of the Southern Ocean giant sea spider *Colossendeis megalonyx*. *Royal Society Open Science*, **2**(7), 140424.
Diniz-Filho, J. A. F., Souza, K. S., Bini, L. M., Loyola, R., Dobrovolski, R., Rodrigues, J. F. M., Lima-Ribeiro, S., Terribile, L. C., Rangel, T. F., Bione, I., Freitas, R., Machado, I. F., Rocha, T., Lorini, M. L., Vale, M. M., Navas, C. A., Maciel, N. M., Villalobos, F., Olalla-Tarraga, M. A., & Gouveia, S. (2019). A macroecological approach to evolutionary rescue and adaptation to climate change. *Ecography*, **42**(6), 1124–1141.
Dömel, J. S., Convey, P., & Leese, F. (2015). Genetic Data Support Independent Glacial Refugia and Open Ocean Barriers to Dispersal for the Southern Ocean Sea Spider *Austropallene cornigera* (Möbius, 1902). *Journal of Crustacean Biology*, **35**(4), 480–490.
Dömel, J. S., Macher, T.-H., Dietz, L., Duncan, S., Mayer, C., Rozenberg, A., Wolcott, K., Leese, F., & Melzer, R. R. (2019). Combining morphological and genomic evidence to resolve species diversity and study speciation processes of the *Pallenopsis patagonica* (Pycnogonida) species complex. *Frontiers in Zoology*, **16**, 36.
Dorant, Y., Benestan, L., Rougemont, Q., Normandeau, E., Boyle, B., Rochette, R., & Bernatchez, L. (2019). Comparing Pool-seq, Rapture, and GBS genotyping for inferring weak population structure: The American lobster (*Homarus americanus*) as a case study. *Ecology and Evolution*, **9**(11), 6606–6623.
Dormann, C. F., Elith, J., Bacher, S., Buchmann, C., Carl, G., Carré, G., Marquéz, J. R. G., Gruber, B., Lafourcade, B., Leitão, P. J., Münkemüller, T., Mcclean, C., Osborne, P. E., Reineking, B., Schröder, B., Skidmore, A. K., Zurell, D., & Lautenbach, S. (2013). Collinearity: a review of methods to deal with it and a simulation study evaluating their performance. *Ecography*, **36**(1), 27–46.
Dotto, T. S., Mata, M. M., Kerr, R., & Garcia, C. A. E. (2021). A novel hydrographic gridded data set for the northern Antarctic Peninsula. *Earth System Science Data*, **13**(2), 671–696.
Dotto, T. S., Naveira Garabato, A., Bacon, S., Tsamados, M., Holland, P. R., Hooley, J., Frajka-Williams, E., Ridout, A., & Meredith, M. P. (2018). Variability of the Ross Gyre, Southern Ocean: Drivers and Responses Revealed by Satellite Altimetry. *Geophysical*

Research Letters, **45**(12), 6195–6204.
Douglass, L. L., Turner, J., Grantham, H. S., Kaiser, S., Constable, A., Nicoll, R., Raymond, B., Post, A., Brandt, A., & Beaver, D. (2014). A hierarchical classification of benthic biodiversity and assessment of protected areas in the Southern Ocean. *PLoS ONE*, **9**(7), e100551.
Dowling, D. K., Friberg, U., & Lindell, J. (2008). Evolutionary implications of non-neutral mitochondrial genetic variation. *Trends in Ecology and Evolution*, **23**(10), 546–554.
Drummond, A. J., Ho, S. Y. W., Rawlence, N., & Rambaut, A. (2007). *A rough guide to BEAST 1.4*. University of Auckland.
Dumont, E. R., Dávalos, L. M., Goldberg, A., Santana, S. E., Rex, K., & Voigt, C. C. (2012). Morphological innovation, diversification and invasion of a new adaptive zone. *Proceedings of the Royal Society B: Biological Sciences*, **279**, 1797–1805.
Dupont, S., Havenhand, J., Thorndyke, W., Peck, L., & Thorndyke, M. (2008). Near-future level of CO_2-driven ocean acidification radically affects larval survival and development in the brittlestar *Ophiothrix fragilis*. *Marine Ecology Progress Series*, **373**, 285–294.
Durand, E. Y., Patterson, N., Reich, D., & Slatkin, M. (2011). Testing for ancient admixture between closely related populations. *Molecular Biology and Evolution*, **28**(8), 2239–2252.
Duranton, M., Allal, F., Fraïsse, C., Bierne, N., Bonhomme, F., & Gagnaire, P. A. (2018). The origin and remolding of genomic islands of differentiation in the European sea bass. *Nature Communications*, **9**, 2518.
Dutton, A., Carlson, A. E., Long, A. J., Milne, G. A., Clark, P. U., Deconto, R., Horton, B. P., Rahmstorf, S., & Raymo, M. E. (2015). Sea-level rise due to polar ice-sheet mass loss during past warm periods. *Science*, **349**(6244), aaa4019.
Earl, D. A., & VonHoldt, B. M. (2012). STRUCTURE HARVESTER: A website and program for visualizing STRUCTURE output and implementing the Evanno method. *Conservation Genetics Resources*, **4**, 359–361.
Eaton, D. A. R. (2014). PyRAD: assembly of *de novo* RADseq loci for phylogenetic analyses. *Bioinformatics*, **30**(13), 1844–1849.
Eddelbuettel, D., & Wu, W. (2016). RcppCNPy: Read-Write Support for NumPy Files in R. *The Journal of Open Source Software*, **1**, 55.
Eisenhofer, R., Cooper, A., & Weyrich, L. S. (2017). Reply to Santiago-Rodriguez et al.: Proper authentication of ancient DNA is essential. *FEMS Microbiology Ecology*, **93**(5), fix042.
Ekblom, R., & Wolf, J. B. W. (2014). A field guide to whole-genome sequencing, assembly and annotation. *Evolutionary Applications*, **7**(9), 1026–1042.
Elderfield, H., Ferretti, P., Greaves, M., Crowhurst, S., McCave, I. N., Hodell, D., & Piotrowski, A. M. (2012). Evolution of Ocean Temperature and Ice Volume Through the Mid-Pleistocene Climate Transition. *Science*, **337**(6095), 704–709.
Ellegren, H. (2014). Genome sequencing and population genomics in non-model organisms. *Trends in Ecology and Evolution*, **29**(1), 51–63.
Etchegaray, E., Naville, M., Volff, J.-N., & Haftek-Terreau, Z. (2021). Transposable element-derived sequences in vertebrate development. *Mobile DNA*, **12**, 1.
Ewart, K. M., Johnson, R. N., Ogden, R., Joseph, L., Frankham, G. J., & Lo, N. (2019). Museum specimens provide reliable SNP data for population genomic analysis of a widely distributed but threatened cockatoo species. *Molecular Ecology Resources*, **19**(6), 1578–1592.
Excoffier, L., Dupanloup, I., Huerta-Sánchez, E., Sousa, V. C., & Foll, M. (2013). Robust Demographic Inference from Genomic and SNP Data. *PLoS Genetics*, **9**(10), e1003905.

Excoffier, L., & Lischer, H. E. L. (2010). Arlequin suite ver 3.5: a new series of programs to perform population genetics analyses under Linux and Windows. *Molecular Ecology Resources*, **10**(3), 564–567.

Fabri-Ruiz, S., Danis, B., Navarro, N., Koubbi, P., Laffont, R., & Saucède, T. (2020). Benthic ecoregionalization based on echinoid fauna of the Southern Ocean supports current proposals of Antarctic Marine Protected Areas under IPCC scenarios of climate change. *Global Change Biology*, **26**(4), 2161–2180.

Fassio, G., Modica, M. V., Alvaro, M. C., Buge, B., Salvi, D., Oliverio, M., & Schiaparelli, S. (2019). An Antarctic flock under the Thorson's rule: Diversity and larval development of Antarctic Velutinidae (Mollusca: Gastropoda). *Molecular Phylogenetics and Evolution*, **132**, 1–13.

Fassio, G., Modica, M. V., Alvaro, M. C., Schiaparelli, S., & Oliverio, M. (2015). Developmental trade-offs in Southern Ocean mollusc kleptoparasitic species. *Hydrobiologia*, **761**(1), 121–141.

Fay, J. C., & Wu, C.-I. (1999). A human population bottleneck can account for the discordance between patterns of mitochondrial versus nuclear DNA variation. *Molecular Biology and Evolution*, **16**(7), 1003–1005.

Feder, M. E., & Mitchell-Olds, T. (2003). Evolutionary and ecological functional genomics. *Nature Reviews Genetics*, **4**, 649–655.

Fernández, M., Bock, C., & Pörtner, H.-O. (2000). The cost of being a caring mother: The ignored factor in the reproduction of marine invertebrates. *Ecology Letters*, **3**(6), 487–494.

Ferrier, S., Manion, G., Elith, J., & Richardson, K. (2007). Using generalized dissimilarity modelling to analyse and predict patterns of beta diversity in regional biodiversity assessment. *Diversity and Distributions*, **13**(3), 252–264.

Fisher, R. A. (1930). *The genetical theory of natural selection*. *Oxford University Press*. Oxford: Oxford University Press.

Fitak, R. R. (2019). *OptM*: Estimating the Optimal Number of Migration Edges from *Treemix*. *Biology Methods and Protocols*, **6**(1), bpab017.

Fitzpatrick, M. C., & Keller, S. R. (2015). Ecological genomics meets community-level modelling of biodiversity: Mapping the genomic landscape of current and future environmental adaptation. *Ecology Letters*, **18**(1), 1–16.

Fitzpatrick, M. C., Mokany, K., Manion, G., Lisk, M., Ferrier, S., & Nieto-Lugilde, D. (2021). gdm: Generalized Dissimilarity Modeling. *R Package Version 1.4.2.2.* [tool source] Retreived from https://rdrr.io/cran/gdm/

Flanagan, S. P., & Jones, A. G. (2018). Substantial differences in bias between single-digest and double-digest RAD-seq libraries: A case study. *Molecular Ecology Resources*, **18**(2), 264–280.

Foll, M., & Gaggiotti, O. (2008). A Genome-Scan Method to Identify Selected Loci Appropriate for Both Dominant and Codominant Markers: A Bayesian Perspective. *Genetics*, **180**(2), 977–993.

Forester, B. R., Lasky, J. R., Wagner, H. H., & Urban, D. L. (2018). Comparing methods for detecting multilocus adaptation with multivariate genotype–environment associations. *Molecular Ecology*, **27**(9), 2215–2233.

Foster, C. S. P., Thompson, M. B., Van Dyke, J. U., Brandley, M. C., & Whittington, C. M. (2020). Emergence of an evolutionary innovation: Gene expression differences associated with the transition between oviparity and viviparity. *Molecular Ecology*, **29**(7), 1315–1327.

Fountain, E. D., Pauli, J. N., Reid, B. N., Palsbøll, P. J., & Peery, M. Z. (2016). Finding the right coverage: the impact of coverage and sequence quality on single nucleotide

polymorphism genotyping error rates. *Molecular Ecology Resources*, **16**(4), 966–978.
Fox-Kemper, B., Hewitt, H. T., Xiao, C., Aðalgeirsdóttir, G., Drijfhout, S. S., Edwards, T. L., Golledge, N. R., Hemer, M., Kopp, R. E., Krinner, G., Mix, A., Notz, D., Nowicki, S., Nurhati, I. S., Ruiz, L., Sallée, J.-B., Slangen, A. B. A., & Yu, Y. (2021). Ocean, Cryosphere and Sea Level Change. In V. MassonDelmotte, P. Zhai, A. Pirani, S. L. Connors, C. Péan, S. Berger, Caud, N., Chen, Y., Goldfarb, L., Gomis, M. I., Huang, M., Leitzell, K., Lonnoy, E., Matthews, J. B. R., Maycock, T. K., Waterfield, T., Yelekçi, O., Yu, R., & B. Zhou (Eds.), *Climate Change 2021: The Physical Science Basis. Contribution of Working Group I to the Sixth Assessment Report of the Intergovernmental Panel on Climate Change*. Cambridge University Press.
François, O., Martins, H., Caye, K., & Schoville, S. D. (2015). Controlling false discoveries in genome scans for selection. *Molecular Ecology*, **25**(2), 454–469.
Fraser, C. I., Morrison, A. K., Hogg, A. M. C., Macaya, E. C., van Sebille, E., Ryan, P. G., Padovan, A., Jack, C., Valdivia, N., & Waters, J. M. (2018). Antarctica's ecological isolation will be broken by storm-driven dispersal and warming. *Nature Climate Change*, **8**, 704–708.
Fraser, C. I., Terauds, A., Smellie, J., Convey, P., & Chown, S. L. (2014). Geothermal activity helps life survive glacial cycles. *Proceedings of the National Academy of Sciences*, **111**(15), 5634–5639.
Fratt, D. B., & Dearborn, J. H. (1984). Feeding biology of the Antarctic brittle star *Ophionotus victoriae* (Echinodermata: Ophiuroidea). *Polar Biology*, **3**, 127–139.
Freire, A. S., Absher, T. M., Cruz-Kaled, A. C., Kern, Y., & Elbers, K. L. (2006). Seasonal variation of pelagic invertebrate larvae in the shallow Antarctic waters of Admiralty Bay (King George Island). *Polar Biology*, **29**(4), 294–302.
Fu, Y. X., & Li, W. H. (1993). Statistical tests of neutrality of mutations. *Genetics*, **133**(3), 693–709.
Fuentes-Pardo, A. P., & Ruzzante, D. E. (2017). Whole-genome sequencing approaches for conservation biology: Advantages, limitations and practical recommendations. *Molecular Ecology*, **26**(20), 5369–5406.
Galaska, M. P., Sands, C. J., Santos, S. R., Mahon, A. R., & Halanych, K. M. (2017a). Crossing the Divide: Admixture Across the Antarctic Polar Front Revealed by the Brittle Star *Astrotoma agassizii*. *The Biological Bulletin*, **232**(3), 198–211.
Galaska, M. P., Sands, C. J., Santos, S. R., Mahon, A. R., & Halanych, K. M. (2017b). Geographic structure in the Southern Ocean circumpolar brittle star *Ophionotus victoriae* (Ophiuridae) revealed from mtDNA and single-nucleotide polymorphism data. *Ecology and Evolution*, **7**(2), 475–485.
Galinsky, K. J., Bhatia, G., Loh, P. R., Georgiev, S., Mukherjee, S., Patterson, N. J., & Price, A. L. (2016). Fast Principal-Component Analysis Reveals Convergent Evolution of ADH1B in Europe and East Asia. *American Journal of Human Genetics*, **98**(3), 456–472.
Gallego, R., Heimeier, D., Lavery, S., & Sewell, M. A. (2015). The meroplankton communities from the coastal Ross Sea: a latitudinal study. *Hydrobiologia*, **761**(1), 195–209.
Galpern, P., Peres-Neto, P. R., Polfus, J., & Manseau, M. (2014). MEMGENE: Spatial pattern detection in genetic distance data. *Methods in Ecology and Evolution*, **5**(10), 1116–1120.
Galtier, N., Nabholz, B., GlÉmin, S., & Hurst, G. D. D. (2009). Mitochondrial DNA as a marker of molecular diversity: a reappraisal. *Molecular Ecology*, **18**(22), 4541–4550.
Garbe, J., Albrecht, T., Levermann, A., Donges, J. F., & Winkelmann, R. (2020). The hysteresis of the Antarctic Ice Sheet. *Nature*, **585**, 538–544.

Garcia, H. E., Locarnini, R. A., Boyer, T. P., Antonov, J. I., Baranova, O. K., Zweng, M. M., Reagan, J. R., & Johnson, D. R. (2013). World Ocean Atlas 2013, Vol. 4 : Dissolved Inorganic Nutrients (phosphate, nitrate, silicate). In D. Levitus & A. Mishonov (Eds.), *NOAA Atlas NESDIS 76* (p. 25).

Garcia, H. E., Weathers, K. W., Paver, C. R., Smolyar, I., Boyer, T. P., Locarnini, R. A., Zweng, M. M., Mishonov, A. V., Baranova, O. K., Seidov, D., & Reagan, J. R. (2018). World Ocean Atlas 2018. Vol. 3: dissolved oxygen, apparent oxygen utilization, and oxygen saturation. In S. Levitus & A. Mishonov (Eds.), *NOAA Atlas NESDIS 75* (p. 27).

Gargiulo, R., Kull, T., & Fay, M. F. (2020). Effective double-digest RAD sequencing and genotyping despite large genome size. *Molecular Ecology Resources*, **21**(4), 1037–1055.

Gattepaille, L. M., Jakobsson, M., & Blum, M. G. B. (2013). Inferring population size changes with sequence and SNP data: Lessons from human bottlenecks. *Heredity*, **110**, 409–419.

Gautier, M., Gharbi, K., Cezard, T., Foucaud, J., Kerdelhué, C., Pudlo, P., Cornuet, J.-M., & Estoup, A. (2013). The effect of RAD allele dropout on the estimation of genetic variation within and between populations. *Molecular Ecology*, **22**(11), 3165–3178.

Gavin, D. G., Fitzpatrick, M. C., Gugger, P. F., Heath, K. D., Rodríguez-Sánchez, F., Dobrowski, S. Z., Hampe, A., Hu, F. S., Ashcroft, M. B., Bartlein, P. J., Blois, J. L., Carstens, B. C., Davis, E. B., de Lafontaine, G., Edwards, M. E., Fernandez, M., Henne, P. D., Herring, E. M., Holden, Z. A., … Williams, J. W. (2014). Climate refugia: joint inference from fossil records, species distribution models and phylogeography. *New Phytologist*, **204**(1), 37–54.

GBIF.org. (2019). *GBIF Occurrence Download* [Data set]. https://doi.org/10.15468/dl.fb26rb.

Gilbert, K. J., Pouyet, F., Excoffier, L., & Peischl, S. (2020). Transition from Background Selection to Associative Overdominance Promotes Diversity in Regions of Low Recombination. *Current Biology*, **30**(1), 101-107.e3.

Gilford, D. M., Ashe, E. L., DeConto, R. M., Kopp, R. E., Pollard, D., & Rovere, A. (2020). Could the Last Interglacial Constrain Projections of Future Antarctic Ice Mass Loss and Sea-Level Rise? *Journal of Geophysical Research: Earth Surface*, **125**(10), e2019JF005418.

Gillespie, J. M., & McClintock, J. B. (2007). Brooding in echinoderms: How can modern experimental techniques add to our historical perspective? *Journal of Experimental Marine Biology and Ecology*, **342**(2), 191–201.

Golledge, N. R., Clark, P. U., He, F., Dutton, A., Turney, C. S. M., Fogwill, C. J., Naish, T. R., Levy, R. H., McKay, R. M., Lowry, D. P., Bertler, N. A.N., Dunbar, G. B., & Carlson, A. E. (2021). Retreat of the Antarctic Ice Sheet During the Last Interglaciation and Implications for Future Change. *Geophysical Research Letters*, **48**(17), e2021GL094513.

Golledge, N. R., Levy, R. H., McKay, R. M., Fogwill, C. J., White, D. A., Graham, A. G. C., Smith, J. A., Hillenbrand, C.-D., Licht, K. J., Denton, G. H., Ackert, R. P., Maas, S. M., & Hall, B. L. (2013). Glaciology and geological signature of the Last Glacial Maximum Antarctic ice sheet. *Quaternary Science Reviews*, **78**, 225–247.

Golledge, N. R., Kowalewski, D. E., Naish, T. R., Levy, R. H., Fogwill, C. J., & Gasson, E. G. W. (2015). The multi-millennial Antarctic commitment to future sea-level rise. *Nature*, **526**, 421–425.

González-Wevar, C. A., Gérard, K., Rosenfeld, S., Saucède, T., Naretto, J., Díaz, A., Morley, S. A., Brickle, P., & Poulin, E. (2019). Cryptic speciation in Southern Ocean *Aequiyoldia eightsii* (Jay, 1839): Mio-Pliocene trans-Drake Passage separation and diversification. *Progress in Oceanography*, **174**, 44–54.

González-Wevar, C. A., Hüne, M., Segovia, N. I., Nakano, T., Spencer, H. G., Chown, S. L., Saucède, T., Johnstone, G., Mansilla, A., & Poulin, E. (2017). Following the Antarctic Circumpolar Current: patterns and processes in the biogeography of the limpet *Nacella* (Mollusca: Patellogastropoda) across the Southern Ocean. *Journal of Biogeography*, **44**(4), 861–874.

González-Wevar, C. A., Saucède, T., Morley, S. A., Chown, S. L., & Poulin, E. (2013). Extinction and recolonization of maritime Antarctica in the limpet *Nacella concinna* (Strebel, 1908) during the last glacial cycle: toward a model of Quaternary biogeography in shallow Antarctic invertebrates. *Molecular Ecology*, **22**, 5221–5236.

González-Wevar, C. A., Segovia, N. I., Rosenfeld, S., Ojeda, J., Hüne, M., Naretto, J., Saucède, T., Brickle, P., Morley, S., Féral, J.-P., Spencer, H. G., & Poulin, E. (2018). Unexpected absence of island endemics: Long-distance dispersal in higher latitude sub-Antarctic *Siphonaria* (Gastropoda: Euthyneura) species. *Journal of Biogeography*, **45**(4), 874–884.

Goodall-Copestake, W. P., Tarling, G. A., & Murphy, E. J. (2012). On the comparison of population-level estimates of haplotype and nucleotide diversity: a case study using the gene *cox1* in animals. *Heredity*, **109**, 50–56.

Graham, A. G. C., Fretwell, P. T., Larter, R. D., Hodgson, D. A., Wilson, C. K., Tate, A. J., & Morris, P. (2008). A new bathymetric compilation highlighting extensive paleo-ice sheet drainage on the continental shelf, South Georgia, sub-Antarctica. *Geochemistry, Geophysics, Geosystems*, **9**(7), Q07011.

Grange, L. J., Peck, L. S., & Tyler, P. A. (2011). Reproductive ecology of the circumpolar Antarctic nemertean *Parborlasia corrugatus*: No evidence for inter-annual variation. *Journal of Experimental Marine Biology and Ecology*, **404**(1–2), 98–107.

Grange, L. J., Tyler, P. A., & Peck, L. S. (2007). Multi-year observations on the gametogenic ecology of the Antarctic seastar *Odontaster validus*. *Marine Biology*, **153**, 15–23.

Grange, L. J., Tyler, P. A., Peck, L. S., & Cornelius, N. (2004). Long-term interannual cycles of the gametogenic ecology of the Antarctic brittle star *Ophionotus victoriae*. *Marine Ecology Progress Series*, **278**, 141–155.

Grant, G. R., Naish, T. R., Dunbar, G. B., Stocchi, P., Kominz, M. A., Kamp, P. J. J., Tapia, C. A., McKay, R. M., Levy, R. H., & Patterson, M. O. (2019). The amplitude and origin of sea-level variability during the Pliocene epoch. *Nature*, **574**, 237–241.

Grant, R. A., & Linse, K. (2009). Barcoding Antarctic Biodiversity: current status and the CAML initiative, a case study of marine invertebrates. *Polar Biology*, **32**, 1629–1637.

Grant, W. S. (2015). Problems and Cautions With Sequence Mismatch Analysis and Bayesian Skyline Plots to Infer Historical Demography. *Journal of Heredity*, **106**(4), 333–346.

Griffiths, H. J., Barnes, D. K. A., & Linse, K. (2008). Towards a generalized biogeography of the Southern Ocean benthos. *Journal of Biogeography*, **36**(1), 162–177.

Griffiths, H. J., Meijers, A. J. S., & Bracegirdle, T. J. (2017). More losers than winners in a century of future Southern Ocean seafloor warming. *Nature Climate Change*, **7**, 749–754.

Griffiths, H. J., Van de Putte, A. P., & Danis, B. (2014). Data distribution: Patterns and implications. In C De Broyer, P. Koubbi, H. Griffiths, B. Raymond, C. d'Udekem d'Acoz, A. Van de Putte, B. Danis, B. David, S. Grant, J. Gutt, C. Held, G. Hosie, F. Huettmann, A. Post, & Y. Ropert-Coudert (Eds.), *Biogeographic Atlas of the Southern Ocean* (pp. 16–26). Cambridge: Scientific Committee on Antarctic Research.

Grover, C. E., Salmon, A., & Wendel, J. F. (2012). Targeted sequence capture as a powerful tool for evolutionary analysis. *American Journal of Botany*, **99**(2), 312–319.

Gruber, B., Georges, A., Mijangos, J. L., Unmack, P. J., Berry, O., Clark, L. V., & Devloo-

Delva, F. (2018). dartR: Importing and analysing SNP and silicodart data generated by genome-wide restriction fragment analysis. [tool source] Retrieved from https://cran.r-project.org/package=dartR

Gutenkunst, R. N., Hernandez, R. D., Williamson, S. H., & Bustamante, C. D. (2009). Inferring the joint demographic history of multiple populations from multidimensional SNP frequency data. *PLoS Genetics*, **5**(10), e1000695.

Gutt, J., Barratt, I., Domack, E., d'Udekem d'Acoz, C., Dimmler, W., Grémare, A., Heilmayer, O., Isla, E., Janussen, D., Jorgensen, E., Kock, K. H., Lehnert, L. S., López-Gonzáles, P., Langner, S., Linse, K., Manjón-Cabeza, M. E., Meißner, M., Montiel, A., Raes, M., … Smith, C. (2011). Biodiversity change after climate-induced ice-shelf collapse in the Antarctic. *Deep-Sea Research Part II: Topical Studies in Oceanography*, **58**(1–2), 74–83.

Gutt, J., Bertler, N., Bracegirdle, T. J., Buschmann, A., Comiso, J., Hosie, G., Isla, E., Schloss, I. R., Smith, C. R., Tournadre, J., & Xavier, J. C. (2015). The Southern Ocean ecosystem under multiple climate change stresses - an integrated circumpolar assessment. *Global Change Biology*, **21**(4), 1434–1453.

Gutt, J., Isla, E., Bertler, A. N., Bodeker, G. E., Bracegirdle, T. J., Cavanagh, R. D., Comiso, J. C., Convey, P., Cummings, V., Deconto, R., De Master, D., di Prisco, G., D'Ovidio, F., Griffiths, H. J., Khan, A. L., López-Martínez, J., Murray, A. E., Nielsen, U. N., Ott, S., … Xavier, J. C. (2018). Cross-disciplinarity in the advance of Antarctic ecosystem research. *Marine Genomics*, **37**, 1–17.

Halanych, K. M., & Mahon, A. R. (2018). Challenging Dogma Concerning Biogeographic Patterns of Antarctica and the Southern Ocean. *Annual Review of Ecology, Evolution, and Systematics*, **49**, 355–378.

Havermans, C., Nagy, Z. T., Sonet, G., De Broyer, C., & Martin, P. (2011). DNA barcoding reveals new insights into the diversity of Antarctic species of *Orchomene sensu lato* (Crustacea: Amphipoda: Lysianassoidea). *Deep Sea Research Part II: Topical Studies in Oceanography*, **58**(5), 230–241.

Harder, A. M., Halanych, K. M., & Mahon, A. R. (2016). Diversity and distribution within the sea spider genus *Pallenopsis* (Chelicerata: Pycnogonida) in the Western Antarctic as revealed by mitochondrial DNA. *Polar Biology*, **39**, 677–688.

Hardin, G. (1960). The Competitive Exclusion Principle. *Science*, **131**(3409), 1292–1297.

Harris, K. (2019). From a database of genomes to a forest of evolutionary trees. *Nature Genetics*, **51**, 1306–1307.

Harrison, S. P., Bartlein, P. J., Izumi, K., Li, G., Annan, J., Hargreaves, J., Braconnot, P., & Kageyama, M. (2015). Evaluation of CMIP5 palaeo-simulations to improve climate projections. *Nature Climate Change*, **5**, 735–743.

Hart, M. W., & Marko, P. B. (2010). It's about time: Divergence, demography, and the evolution of developmental modes in marine invertebrates. *Integrative and Comparative Biology*, **50**(4), 643–661.

Hasenfratz, A. P., Jaccard, S. L., Martínez-García, A., Sigman, D. M., Hodell, D. A., Vance, D., Bernasconi, S. M., Kleiven, H. F., Haumann, F. A., & Haug, G. H. (2019). The residence time of Southern Ocean surface waters and the 100,000-year ice age cycle. *Science*, **363**(6431), 1080–1084.

Hawes, T. C., Worland, M. R., Bale, J. S., & Convey, P. (2008). Rafting in Antarctic Collembola. *Journal of Zoology*, **274**, 44–50.

Helbig, A. J. (2005). Evolutionary genetics: A ring of species. *Heredity*, **95**, 113–114.

Held, C., & Wägele, J. W. (2005). Cryptic speciation in the giant Antarctic isopod *Glyptonotus antarcticus* (Isopoda: Valvifera: Chaetiliidae). *Scientia Marina*, **69**(S2), 175–181.

Heller, R., Chikhi, L., & Siegismund, H. R. (2013). The Confounding Effect of Population Structure on Bayesian Skyline Plot Inferences of Demographic History. *PLoS ONE*, **8**(5), e62992.

Helmuth, B., Veit, R. R., & Holberton, R. (1994). Long-distance dispersal of a subantarctic brooding bivalve (*Gaimardia trapesina*) by kelp-rafting. *Marine Biology*, **120**(3), 421–426.

Hemery, L. G., Eléaume, M., Roussel, V., Améziane, N., Gallut, C., Steinke, D., Cruaud, C., Couloux, A., & Wilson, N. G. (2012). Comprehensive sampling reveals circumpolarity and sympatry in seven mitochondrial lineages of the Southern Ocean crinoid species *Promachocrinus kerguelensis* (Echinodermata). *Molecular Ecology*, **21**(10), 2502–2518.

Hendry, A. P., Wenburg, J. K., Bentzen, P., Volk, E. C., & Quinn, T. P. (2000). Rapid Evolution of Reproductive Isolation in the Wild: Evidence from Introduced Salmon. *Science*, **290**(5491), 516–518.

Henson, S. A., Beaulieu, C., Ilyina, T., John, J. G., Long, M., Séférian, R., Tjiputra, J., & Sarmiento, J. L. (2017). Rapid emergence of climate change in environmental drivers of marine ecosystems. *Nature Communications*, **8**, 14682.

Hewitt, G. (2000). The genetic legacy of the Quaternary ice ages. *Nature*, **405**, 907–913.

Hewitt, G. M. (2004). Genetic consequences of climatic oscillations in the Quaternary. *Philosophical Transactions of the Royal Society B: Biological Sciences*, **359**(1442), 183–195.

Hey, J., & Machado, C. A. (2003). The study of structured populations - New hope for a difficult and divided science. *Nature Reviews Genetics*, **4**, 535–543.

Hickerson, M. J., & Cunningham, C. W. (2005). Contrasting quaternary histories in an ecologically divergent sister pair of low-dispersing intertidal fish (*Xiphister*) revealed by multilocus DNA analysis. *Evolution*, **59**(2), 344–360.

Higgs, N. D., Reed, A. J., Hooke, R., Honey, D. J., Heilmayer, O., & Thatje, S. (2009). Growth and reproduction in the Antarctic brooding bivalve *Adacnarca nitens* (Philobryidae) from the Ross Sea. *Marine Biology*, **156**, 1073–1081.

Hijmans, R. J. (2016). Raster: Geographic Data Analysis and modeling. *R Package Version 2.5-8.* [tool source] Retreived from *https://CRAN.R-Project.Org/Package=raster*

Hill, D. J., Haywood, A. M., Hindmarsh, R. C. A., & Valdes, P. J. (2014). Characterizing ice sheets during the Pliocene: evidence from data and models. In M. Williams, A. M. Haywood, F. J. Gregory, & D. N. Schmidt (Eds.), *Deep-time perspectives on climate change: marrying the signal from computer models and biological proxies* (pp. 517–538). London, Geological Society of London (Micropalaeontological Society special publications).

Hillenbrand, C. D., Bentley, M. J., Stolldorf, T. D., Hein, A. S., Kuhn, G., Graham, A. G. C., Fogwill, C. J., Kristoffersen, Y., Smith, J. A., Anderson, J. B., Larter, R. D., Melles, M., Hodgson, D. A., Mulvaney, R., & Sugden, D. E. (2014). Reconstruction of changes in the Weddell Sea sector of the Antarctic Ice Sheet since the Last Glacial Maximum. *Quaternary Science Reviews*, **100**, 111–136.

Ho, S. Y. W., & Shapiro, B. (2011). Skyline-plot methods for estimating demographic history from nucleotide sequences. *Molecular Ecology Resources*, **11**(3), 423–434.

Hodgson, D. A., Graham, A. G. C., Roberts, S. J., Bentley, M. J., Cofaigh, C. Ó., Verleyen, E., Vyverman, W., Jomelli, V., Favier, V., Brunstein, D., Verfaillie, D., Colhoun, E. A., Saunders, K. M., Selkirk, P. M., Mackintosh, A., Hedding, D. W., Nel, W., Hall, K., McGlone, M. S., … Smith, J. A. (2014). Terrestrial and submarine evidence for the extent and timing of the Last Glacial Maximum and the onset of deglaciation on the maritime-Antarctic and sub-Antarctic islands. *Quaternary Science Reviews*, **100**, 137–158.

Hoffberg, S. L., Kieran, T. J., Catchen, J. M., Devault, A., Faircloth, B. C., Mauricio, R., & Glenn, T. C. (2016). RADcap: sequence capture of dual-digest RADseq libraries with identifiable duplicates and reduced missing data. *Molecular Ecology Resources*, **16**(5), 1264–1278.

Hoffman, J. I., Clarke, A., Clark, M. S., Fretwell, P., & Peck, L. S. (2012). Unexpected fine-scale population structure in a broadcast-spawning Antarctic marine mollusc. *PLoS ONE*, **7**(3), e32415.

Hoffman, J. I., Clarke, A., Linse, K., & Peck, L. S. (2011a). Effects of brooding and broadcasting reproductive modes on the population genetic structure of two Antarctic gastropod molluscs. *Marine Biology*, **158**, 287–296.

Hoffman, J. I., Peck, L. S., Linse, K., & Clarke, A. (2011b). Strong population genetic structure in a broadcast-spawning Antarctic marine invertebrate. *Journal of Heredity*, **102**(1), 55–66.

Hoffmann, A. A., Weeks, A. R., & Sgrò, C. M. (2021). Opportunities and challenges in assessing climate change vulnerability through genomics. *Cell*, **184**(6), 1420–1425.

Hofreiter, M., & Stewart, J. (2009). Ecological Change, Range Fluctuations and Population Dynamics during the Pleistocene. *Current Biology*, **19**(14), R584–R594.

Hohenlohe, P. A., Amish, S. J., Catchen, J. M., Allendorf, F. W., & Luikart, G. (2011). Next-generation RAD sequencing identifies thousands of SNPs for assessing hybridization between rainbow and westslope cutthroat trout. *Molecular Ecology Resources*, **11**(s1), 117–122.

Hohenlohe, P. A., Funk, W. C., & Rajora, O. P. (2021). Population genomics for wildlife conservation and management. *Molecular Ecology*, **30**(1), 62–82.

Holloway, M. D., Sime, L. C., Singarayer, J. S., Tindall, J. C., Bunch, P., & Valdes, P. J. (2016). Antarctic last interglacial isotope peak in response to sea ice retreat not ice-sheet collapse. *Nature Communications*, **7**, 12293

Holmes, M. W., Hammond, T. T., Wogan, G. O. U., Walsh, R. E., Labarbera, K., Wommack, E. A., Martins, F. M., Crawford, J. C., Mack, K. L., Bloch, L. M., & Nachman, M. W. (2016). Natural history collections as windows on evolutionary processes. *Molecular Ecology*, **25**(4), 864–881.

Hugall, A. F., O'Hara, T. D., Hunjan, S., Nilsen, R., & Moussalli, A. (2016). An Exon-Capture System for the Entire Class Ophiuroidea. *Molecular Biology and Evolution*, **33**(1), 281–294.

Hunter, R. L., & Halanych, K. M. (2008). Evaluating connectivity in the brooding brittle star *Astrotoma agassizii* across the Drake Passage in the Southern Ocean. *Journal of Heredity*, **99**(2), 137–148.

Hunter, R. L., & Halanych, K. M. (2010). Phylogeography of the Antarctic planktotrophic brittle star *Ophionotus victoriae* reveals genetic structure inconsistent with early life history. *Marine Biology*, **157**(8), 1693–1704.

Huntley, S., Baggott, D. M., Hamilton, A. T., Tran-Gyamfi, M., Yang, S., Kim, J., Gordon, L., Branscomb, E., & Stubbs, L. (2006). A comprehensive catalog of human KRAB-associated zinc finger genes: Insights into the evolutionary history of a large family of transcriptional repressors. *Genome Research*, **16**(5), 669–677.

Ingels, J., Vanreusel, A., Brandt, A., Catarino, A. I., David, B., De Ridder, C., Dubois, P., Gooday, A. J., Martin, P., Pasotti, F., & Robert, H. (2012). Possible effects of global environmental changes on Antarctic benthos: a synthesis across five major taxa. *Ecology and Evolution*, **2**(2), 453–485.

Ingólfsson, Ó. (2004). Quaternary glacial and climate history of Antarctica. *Developments in Quaternary Science*, **2**(Part C), 3–43.

Jacobs, S. S., Hellmer, H. H., & Jenkins, A. (1996). Antarctic Ice Sheet melting in the

southeast Pacific. *Geophysical Research Letters*, **23**(9), 957–960.
Jain, M., Olsen, H. E., Paten, B., & Akeson, M. (2016). The Oxford Nanopore MinION: delivery of nanopore sequencing to the genomics community. *Genome Biology*, **17**, 239.
Janko, K., Lecointre, G., DeVries, A., Couloux, A., Cruaud, C., & Marshall, C. (2007). Did glacial advances during the Pleistocene influence differently the demographic histories of benthic and pelagic Antarctic shelf fishes? – Inferences from intraspecific mitochondrial and nuclear DNA sequence diversity. *BMC Evolutionary Biology*, **7**, 220.
Janosik, A., Mahon, A., & Halanych, K. (2011). Evolutionary history of Southern Ocean *Odontaster* sea star species (Odontasteridae; Asteroidea). *Polar Biology*, **34**, 575–586.
Jeffries, D. L., Copp, G. H., Handley, L. L., Olsén, K. H. K., Sayer, C. D., & Hänfling, B. (2016). Comparing RADseq and microsatellites to infer complex phylogeographic patterns, an empirical perspective in the Crucian carp, *Carassius carassius*, L. *Molecular Ecology*, **25**(13), 2997–3018.
Jombart, T., & Ahmed, I. (2011). adegenet 1.3-1: New tools for the analysis of genome-wide SNP data. *Bioinformatics*, **27**(21), 3070–3071.
Jonas, M., Albrechtsen, A., & Hanghøj, K. (2021). Detecting selection in low-coverage high-throughput sequencing data using principal component analysis. *BMC Bioinformatics*, **22**, 270.
Jones, M. R., & Good, J. M. (2016). Targeted capture in evolutionary and ecological genomics. *Molecular Ecology*, **25**(1), 185–202.
Jones, P., Binns, D., Chang, H.-Y., Fraser, M., Li, W., McAnulla, C., McWilliam, H., Maslen, J., Mitchell, A., Nuka, G., Pesseat, S., Quinn, A. F., Sangrador-Vegas, A., Scheremetjew, M., Yong, S.-Y., Lopez, R., & Hunter, S. (2014). InterProScan 5: Genome-scale protein function classification. *Bioinformatics*, **30**(9), 1236–1240.
Jónsson, H., Ginolhac, A., Schubert, M., Johnson, P. L. F., & Orlando, L. (2013). mapDamage2.0: fast approximate Bayesian estimates of ancient DNA damage parameters. *Bioinformatics*, **29**(13), 1682–1684.
Jossart, Q., Sands, C. J., & Sewell, M. A. (2019). Dwarf brooder versus giant broadcaster: combining genetic and reproductive data to unravel cryptic diversity in an Antarctic brittle star. *Heredity*, **123**, 622–633.
Joughin, I., & Alley, R. B. (2011). Stability of the West Antarctic ice sheet in a warming world. *Nature Geoscience*, **4**, 506–513.
Jouzel, J., Masson-Delmotte, V., Cattani, O., Dreyfus, G., Falourd, S., Hoffmann, G., Minster, B., Nouet, J., Barnola, J. M., Chappellaz, J., Fischer, H., Gallet, J. C., Johnsen, S., Leuenberger, M., Loulergue, L., Luethi, D., Oerter, H., Parrenin, F., Raisbeck, G., … Wolff, E. W. (2007). Orbital and Millennial Antarctic Climate Variability over the Past 800,000 Years. *Science*, **317**(5839), 793–796.
Jung, H., Ventura, T., Chung, J. S., Kim, W.-J., Nam, B.-H., Kong, H. J., Kim, Y.-O., Jeon, M.-S., & Eyun, S. (2020). Twelve quick steps for genome assembly and annotation in the classroom. *PLOS Computational Biology*, **16**(11), e1008325.
Jurka, J., Bao, W., & Kojima, K. K. (2011). Families of transposable elements, population structure and the origin of species. *Biology Direct*, **6**, 44.
Kaiser, S., Barnes, D. K. A., Linse, K., & Brandt, A. (2008). Epibenthic macrofauna associated with the shelf and slope of a young and isolated Southern Ocean island. *Antarctic Science*, **20**(3), 281–290.
Kaiser, S., Griffiths, H. J., Barnes, D. K. A., Brandão, S. N., Brandt, A., & O'Brien, P. E. (2011). Is there a distinct continental slope fauna in the Antarctic? *Deep-Sea Research Part II: Topical Studies in Oceanography*, **58**(1–2), 91–104.
Kalyaanamoorthy, S., Minh, B. Q., Wong, T. K. F., Von Haeseler, A., & Jermiin, L. S. (2017).

ModelFinder: Fast model selection for accurate phylogenetic estimates. *Nature Methods*, **14**(6), 587–589.
Karamanlidis, A. A., Skrbinšek, T., De Gabriel Hernando, M., Krambokoukis, L., Munoz-Fuentes, V., Bailey, Z., Nowak, C., & Stronen, A. V. (2018). History-driven population structure and asymmetric gene flow in a recovering large carnivore at the rear-edge of its European range. *Heredity*, **120**, 168–182.
Kato, S., Matsui, T., Gatsogiannis, C., & Tanaka, Y. (2018). Molluscan hemocyanin: structure, evolution, and physiology. *Biophysical Reviews*, **10**(2), 191–202.
Katoh, K., & Standley, D. M. (2013). MAFFT multiple sequence alignment software version 7: Improvements in performance and usability. *Molecular Biology and Evolution*, **30**(4), 772–780.
Keenan, K., Mcginnity, P., Cross, T. F., Crozier, W. W., & Prodöhl, P. A. (2013). DiveRsity: An R package for the estimation and exploration of population genetics parameters and their associated errors. *Methods in Ecology and Evolution*, **4**(8), 782–788.
Kelleher, J., Wong, Y., Wohns, A. W., Fadil, C., Albers, P. K., & McVean, G. (2019). Inferring whole-genome histories in large population datasets. *Nature Genetics*, **51**, 1330–1338.
Kemp, A. C., Dutton, A., & Raymo, M. E. (2015). Paleo Constraints on Future Sea-Level Rise. *Current Climate Change Reports*, **1**, 205–215.
Kim, J., Mossel, E., Rácz, M. Z., & Ross, N. (2015). Can one hear the shape of a population history? *Theoretical Population Biology*, **100**, 26–38.
Kingman, J. F. C. (2000). Origins of the coalescent: 1974-1982. *Genetics*, **156**(4), 1461–1463.
Kolmogorov, M., Yuan, J., Lin, Y., & Pevzner, P. A. (2019). Assembly of long, error-prone reads using repeat graphs. *Nature Biotechnology*, **37**, 540–546.
Korneliussen, T. S., Albrechtsen, A., & Nielsen, R. (2014). ANGSD: Analysis of Next Generation Sequencing Data. *BMC Bioinformatics*, **15**, 356.
Kott, P. (1969). Zoogeographic Discussion. In *Antarctic Ascidiacea* (pp. 193–208). American Geophysical Union (AGU).
Krug, P. J., Vendetti, J. E., Ellingson, R. A., Trowbridge, C. D., Hirano, Y. M., Trathen, D. Y., Rodriguez, A. K., Swennen, C., Wilson, N. G., & Valdés, Á. A. (2015). Species Selection Favors Dispersive Life Histories in Sea Slugs, but Higher Per-Offspring Investment Drives Shifts to Short-Lived Larvae. *Systematic Biology*, **64**(6), 983–999.
Kulp, S. A., & Strauss, B. H. (2019). New elevation data triple estimates of global vulnerability to sea-level rise and coastal flooding. *Nature Communications*, **10**, 4844.
Lagisquet, J., Zuber, K., & Gramberg, T. (2021). Recognize Yourself—Innate Sensing of Non-LTR Retrotransposons. *Viruses*, **13**(1), 94.
Lang, P. L. M., Weiß, C. L., Kersten, S., Latorre, S. M., Nagel, S., Nickel, B., Meyer, M., & Burbano, H. A. (2020). Hybridization ddRAD-sequencing for population genomics of nonmodel plants using highly degraded historical specimen DNA. *Molecular Ecology Resources*, **20**, 1228–1247.
Langmead, B., & Salzberg, S. L. (2012). Fast gapped-read alignment with Bowtie 2. *Nature Methods*, **9**, 357–359.
Lau, S. C. Y., Grange, L. J., Peck, L. S., & Reed, A. J. (2018). The reproductive ecology of the Antarctic bivalve *Aequiyoldia eightsii* (Protobranchia: Sareptidae) follows neither Antarctic nor taxonomic patterns. *Polar Biology*, **41**, 1693–1706.
Lau, S. C. Y., Strugnell, J. M., Sands, C. J., Silva, C. N. S., & Wilson, N. G. (2021). Evolutionary innovations in Antarctic brittle stars linked to glacial refugia. *Ecology and Evolution*, **11**(23), 17428–17446.
Lau, S. C. Y., Wilson, N. G., Silva, C. N. S., & Strugnell, J. M. (2020). Detecting glacial refugia in the Southern Ocean. *Ecography*, **43**(11), 1639–1656.

Lawrence, J. M., & Herrera, J. (2000). Stress and Deviant Reproduction in Echinoderms. *Zoological Studies*, **39**(3), 151–171.

Layton, K. K. S., Carvajal, J. I., & Wilson, N. G. (2020). Mimicry and mitonuclear discordance in nudibranchs: New insights from exon capture phylogenomics. *Ecology and Evolution*, **10**(21), 11966–11982.

Lee, M. R., Canales-Aguirre, C. B., Nuñez, D., Pérez, K., Hernández, C. E., & Brante, A. (2017). The identification of sympatric cryptic free-living nematode species in the Antarctic intertidal. *PLoS ONE*, **12**(10), e0186140.

Leese, F., Agrawal, S., & Held, C. (2010). Long-distance island hopping without dispersal stages: Transportation across major zoogeographic barriers in a Southern Ocean isopod. *Naturwissenschaften*, **97**, 583–594.

Leese, F., & Held, C. (2008). Identification and characterization of microsatellites from the Antarctic isopod *Ceratoserolis trilobitoides*: nuclear evidence for cryptic species. *Conservation Genetics*, **9**, 1369–1372.

Leigh, J. W., & Bryant, D. (2015). POPART: full-feature software for haplotype network construction. *Methods in Ecology and Evolution*, **6**(9), 1110–1116.

Leitwein, M., Duranton, M., Rougemont, Q., Gagnaire, P. A., & Bernatchez, L. (2020). Using Haplotype Information for Conservation Genomics. *Trends in Ecology and Evolution*, **35**(3), 245–258.

Leiva, C., Taboada, S., Kenny, N. J., Combosch, D., Giribet, G., Jombart, T., & Riesgo, A. (2019). Population substructure and signals of divergent adaptive selection despite admixture in the sponge *Dendrilla antarctica* from shallow waters surrounding the Antarctic Peninsula. *Molecular Ecology*, **29**(13), 3151–3170.

Levicoy, D., Flores, K., Rosenfeld, S., & Cárdenas, L. (2021). Phylogeography and genetic diversity of the microbivalve *Kidderia subquadrata*, reveals new data from West Antarctic Peninsula. *Scientific Reports*, **11**, 5705.

Li, H. (2011). A statistical framework for SNP calling, mutation discovery, association mapping and population genetical parameter estimation from sequencing data. *Bioinformatics*, **27**(11), 2987–2993.

Li, H., & Durbin, R. (2009). Fast and accurate short read alignment with Burrows-Wheeler transform. *Bioinformatics*, **25**(14), 1754–1760.

Li, H., & Durbin, R. (2011). Inference of human population history from individual whole-genome sequences. *Nature*, **475**, 493–496.

Li, H., Handsaker, B., Wysoker, A., Fennell, T., Ruan, J., Homer, N., Marth, G., Abecasis, G., Durbin, R., & 1000 Genome Project Data Processing Subgroup. (2009). The Sequence Alignment/Map format and SAMtools. *Bioinformatics*, **25**(16), 2078–2079.

Liggins, L., Treml, E. A., & Riginos, C. (2019). Seascape Genomics: Contextualizing Adaptive and Neutral Genomic Variation in the Ocean Environment. In M. Oleksiak & O. Rajora (Eds.), *Population Genomics: Marine Organisms* (pp. 171–218). Springer, Cham.

Linck, E. B., Hanna, Z. R., Sellas, A., & Dumbacher, J. P. (2017). Evaluating hybridization capture with RAD probes as a tool for museum genomics with historical bird specimens. *Ecology and Evolution*, **7**(13), 4755–4767.

Linse, K., Cope, T., Lörz, A.-N., & Sands, C. (2007). Is the Scotia Sea a centre of Antarctic marine diversification? Some evidence of cryptic speciation in the circum-Antarctic bivalve *Lissarca notorcadensis* (Arcoidea: Philobryidae). *Polar Biology*, **30**(8), 1059–1068.

Linse, K., Griffiths, H. J., Barnes, D. K. A., & Clarke, A. (2006). Biodiversity and biogeography of Antarctic and sub-Antarctic mollusca. *Deep-Sea Research Part II: Topical Studies in Oceanography*, **53**(8–10), 985–1008.

Liu, X., & Fu, Y.-X. (2015). Exploring population size changes using SNP frequency spectra. *Nature Genetics*, **47**, 555–559.

Liu, X., & Fu, Y.-X. (2020). Stairway Plot 2: demographic history inference with folded SNP frequency spectra. *Genome Biology*, **21**, 280.

Locarnini, R. A., Mishonov, A. V., Baranova, O. K., Boyer, T. P., Zweng, M. M., Garcia, H. E., Reagan, J. R., Seidov, D., Weathers, K., Paver, C. R., & Smolyar, I. (2018). World Ocean Atlas 2018, Volume 1: Temperature. In A. Mishonov (Ed.), *NOAA Atlas NESDIS 75* (p. 52).

Loh, P.-R., Lipson, M., Patterson, N., Moorjani, P., Pickrell, J. K., Reich, D., & Berger, B. (2013). Inferring admixture histories of human populations using linkage disequilibrium. *Genetics*, **193**, 1233–1254.

Lörz, A.-N., Maas, E. W., Linse, K., & Coleman, C. O. (2009). Do circum-Antarctic species exist in peracarid Amphipoda? A case study in the genus *Epimeria* Costa, 1851 (Crustacea, Peracarida, Epimeriidae). *ZooKeys*, **18**, 91–128.

Lörz, A.-N., Smith, P., Linse, K., & Steinke, D. (2012). High genetic diversity within *Epimeria georgiana* (Amphipoda) from the southern Scotia Arc. *Marine Biodiversity*, **42**, 137–159.

Lou, R. N., Jacobs, A., Wilder, A. P., & Therkildsen, N. O. (2021). A beginner's guide to low-coverage whole genome sequencing for population genomics. *Molecular Ecology*, **30**(23), 5966–5993.

Lou, R. N., & Therkildsen, N. O. (2021). Batch effects in population genomic studies with low-coverage whole genome sequencing data: causes, detection, and mitigation. *Molecular Ecology Resources* (In Press).

Love, A. C. (2003). Evolutionary Morphology, Innovation, and the Synthesis of Evolutionary and Developmental Biology. *Biology and Philosophy*, **18**, 309–345.

Lowe, W. H., Kovach, R. P., & Allendorf, F. W. (2017). Population Genetics and Demography Unite Ecology and Evolution. *Trends in Ecology and Evolution*, **32**(2), 141–152.

Luca, F., Hudson, R. R., Witonsky, D. B., & Di Rienzo, A. (2011). A reduced representation approach to population genetic analyses and applications to human evolution. *Genome Research*, **21**(7), 1087–1098.

Mackintosh, A. N., Verleyen, E., O'Brien, P. E., White, D. A., Jones, R. S., McKay, R., Dunbar, R., Gore, D. B., Fink, D., Post, A. L., Miura, H., Leventer, A., Goodwin, I., Hodgson, D. A., Lilly, K., Crosta, X., Golledge, N. R., Wagner, B., Berg, S., … Masse, G. (2014). Retreat history of the East Antarctic Ice Sheet since the Last Glacial Maximum. *Quaternary Science Reviews*, **100**, 10–30.

Maggs, C. A., Castilho, R., Foltz, D., Henzler, C., Jolly, M. T., Kelly, J., Olsen, J., Perez, K. E., Stam, W., Väinölä, R., Viard, F., & Wares, J. (2008). Evaluating signatures of glacial refugia for north atlantic benthic marine taxa. *Ecology*, **89**(sp11), S108–S122.

Maldonado, A., Barnolas, A., Bohoyo, F., Galindo-Zaldívar, J., Hernández-Molina, J., Lobo, F., Rodríguez-Fernández, J., Somoza, L., & Vázquez, J. T. (2003). Contourite deposits in the central Scotia Sea: the importance of the Antarctic Circumpolar Current and the Weddell Gyre flows. *Palaeogeography, Palaeoclimatology, Palaeoecology*, **198**(1–2), 187–221.

Marchi, N., & Excoffier, L. (2020). Gene flow as a simple cause for an excess of high-frequency-derived alleles. *Evolutionary Applications*, **13**, 2254–2263.

Marchi, N., Schlichta, F., & Excoffier, L. (2021). Demographic inference. *Current Biology*, **31**(6), R276–R279.

Marko, P. B. (2004). 'What's larvae got to do with it?' Disparate patterns of post-glacial population structure in two benthic marine gastropods with identical dispersal potential. *Molecular Ecology*, **13**(3), 597–611.

Marques, D. A., Lucek, K., Sousa, V. C., Excoffier, L., & Seehausen, O. (2019). Admixture between old lineages facilitated contemporary ecological speciation in Lake Constance stickleback. *Nature Communications*, **10**, 4240.

Mastretta-Yanes, A., Arrigo, N., Alvarez, N., Jorgensen, T. H., Piñero, D., & Emerson, B. C. (2015). Restriction site-associated DNA sequencing, genotyping error estimation and de novo assembly optimization for population genetic inference. *Molecular Ecology Resources*, **15**(1), 28–41.

Matschiner, M., Hanel, R., & Salzburger, W. (2009). Gene flow by larval dispersal in the Antarctic notothenioid fish *Gobionotothen gibberifrons*. *Molecular Ecology*, **18**(12), 2574–2587.

Matsuoka, K., Skoglund, A., Roth, G., de Pomereu, J., Griffiths, H., Headland, R., Herried, B., Katsumata, K., Le Brocq, A., Licht, K., Morgan, F., Neff, P. D., Ritz, C., Scheinert, M., Tamura, T., Van de Putte, A., Van Den Broeke, M., von Deschwanden, A., Deschamps-Berger, C., … Melvær, Y. (2021). Quantarctica, an integrated mapping environment for Antarctica, the Southern Ocean, and sub-Antarctic islands. *Environmental Modelling and Software*, **140**, 105015.

Mazloff, M. R., Heimbach, P., & Wunsch, C. (2010). An eddy-permitting Southern Ocean state estimate. *Journal of Physical Oceanography*, **40**(5), 880–899.

McClintock, J. B. (1994). Trophic biology of Antarctic shallow-water echinoderms. *Marine Ecology Progress Series*, **111**, 191–202.

McGee, M. D., Borstein, S. R., Neches, R. Y., Buescher, H. H., Seehausen, O., & Wainwright, P. C. (2015). A pharyngeal jaw evolutionary innovation facilitated extinction in Lake Victoria cichlids. *Science*, **350**(6264), 1077–1079.

McKay, B. D., & Zink, R. M. (2010). The causes of mitochondrial DNA gene tree paraphyly in birds. *Molecular Phylogenetics and Evolution*, **54**(2), 647–650.

McKay, R. M., Barrett, P. J., Levy, R. H., Naish, T. R., Golledge, N. R., & Pyne, A. (2016). Antarctic Cenozoic climate history from sedimentary records: ANDRILL and beyond. *Philosophical Transactions of the Royal Society A: Mathematical, Physical and Engineering Sciences*, **374**(2059), 20140301.

McKnight, D. G. (1967). Echinoderms from Cape Hallett, ross sea. *New Zealand Journal of Marine and Freshwater Research*, **1**(3), 314–323.

McMichael, C., Dasgupta, S., Ayeb-Karlsson, S., & Kelman, I. (2020). A review of estimating population exposure to sea-level rise and the relevance for migration. *Environmental Research Letters*, **15**, 123005.

Medina, P., Thornlow, B., Nielsen, R., & Corbett-Detig, R. (2018). Estimating the timing of multiple admixture pulses during local ancestry inference. *Genetics*, **210**(3), 1089–1107.

Meirmans, P. G. (2020). GENODIVE version 3.0: Easy-to-use software for the analysis of genetic data of diploids and polyploids. *Molecular Ecology Resources*, **20**(4), 1126–1131.

Meisner, J., & Albrechtsen, A. (2018). Inferring population structure and admixture proportions in low-depth NGS data. *Genetics*, **210**(2), 719–731.

Melosik, I., Walczak, U., Staszak, J., Winnicka, K., & Baraniak, E. (2019). Is there a host-associated molecular and morphological differentiation between sympatrically occurring individuals of the invasive leaf miner *Cameraria ohridella*? *Arthropod-Plant Interactions*, **13**, 853–864.

Mengel, M., & Levermann, A. (2014). Ice plug prevents irreversible discharge from East Antarctica. *Nature Climate Change*, **4**, 451–455.

Michonneau, F. (2016). Using GMYC for species delination. *Zenodo*. Retrieved from http://doi.org/10.5281/zenodo.838260

Miklós, M., Laczkó, L., Sramkó, G., Sebestyén, F., Barta, Z., & Tökölyi, J. (2021). Phenotypic plasticity rather than genotype drives reproductive choices in *Hydra* populations. *Molecular Ecology*, **30**(5), 1206–1222.

Mileikovsky, S. A. (1971). Types of larval development in marine bottom invertebrates, their distribution and ecological significance: a re-evaluation. *Marine Biology: International Journal on Life in Oceans and Coastal Waters*, **10**, 193–213.

Miller, K. J., Baird, H. P., Van Oosterom, J., Mondon, J., & King, C. K. (2018). Complex genetic structure revealed in the circum-Antarctic broadcast spawning sea urchin *Sterechinus neumayeri*. *Marine Ecology Progress Series*, **601**, 153–166.

Miller, R. L. (1998). Specificity of sperm chemotaxis among Great Barrier Reef shallow-water Holothurians and Ophiuroids. *Journal of Experimental Zoology*, **279**(2), 189–200.

Moczek, A. P., Sultan, S., Foster, S., Ledón-Rettig, C., Dworkin, I., Nijhout, H. F., Abouheif, E., & Pfennig, D. W. (2011). The role of developmental plasticity in evolutionary innovation. *Proceedings of the Royal Society B: Biological Sciences*, **278**(1719), 2705–2713.

Moffat, C., & Meredith, M. (2018). Shelf-ocean exchange and hydrography west of the Antarctic Peninsula: A review. *Philosophical Transactions of the Royal Society A: Mathematical, Physical and Engineering Sciences*, **376**(2122), 20170164.

Momigliano, P., Florin, A. B., & Merilä, J. (2021). Biases in Demographic Modeling Affect Our Understanding of Recent Divergence. *Molecular Biology and Evolution*, **38**(7), 2967–2985.

Montero-Mendieta, S., Grabherr, M., Lantz, H., De la Riva, I., Leonard, J. A., Webster, M. T., & Vilà, C. (2017). A practical guide to build de-novo assemblies for single tissues of non-model organisms: The example of a Neotropical frog. *PeerJ*, **5**, e3702.

Moon, K. L., Chown, S. L., & Fraser, C. I. (2017). Reconsidering connectivity in the sub-Antarctic. *Biological Reviews*, **92**(4), 2164–2181.

Moore, J. M., Carvajal, J. I., Rouse, G. W., & Wilson, N. G. (2018). The Antarctic Circumpolar Current isolates and connects: Structured circumpolarity in the sea star *Glabraster antarctica*. *Ecology and Evolution*, **8**(21), 10621–10633.

Moreau, C., Danis, B., Jossart, Q., Eléaume, M., Sands, C., Achaz, G., Agüera, A., & Saucède, T. (2019). Is reproductive strategy a key factor in understanding the evolutionary history of Southern Ocean Asteroidea (Echinodermata)? *Ecology and Evolution*, **9**(15), 8465–8478.

Moreau, C., Saucède, T., Jossart, Q., Agüera, A., Brayard, A., & Danis, B. (2017). Reproductive strategy as a piece of the biogeographic puzzle: a case study using Antarctic sea stars (Echinodermata, Asteroidea). *Journal of Biogeography*, **44**(4), 848–860.

Morin, P. A., Luikart, G., & Wayne, R. K. (2004). SNPs in ecology, evolution and conservation. *Trends in Ecology and Evolution*, **19**(4), 208–216.

Mortensen, T. H. (1936). Echinoidea and Ophiuroidea. *Discovery Reports*, **12**, 199–348.

Muñoz-Ramírez, C. P., Barnes, D. K. A., Cárdenas, L., Meredith, M. P., Morley, S. A., Roman-Gonzalez, A., Sands, C. J., Scourse, J., & Brante, A. (2020). Gene flow in the Antarctic bivalve *Aequiyoldia eightsii* (Jay, 1839) suggests a role for the Antarctic Peninsula Coastal Current in larval dispersal. *Royal Society Open Science*, **7**(9), 200603.

Naish, T., Powell, R., Levy, R., Wilson, G., Scherer, R., Talarico, F., Pompilio, M., Wilson, T., Carter, L., DeConto, R., Huybers, P., McKay, R., Pollard, D., Ross, J., Winter, D., Barrett, P., Browne, G., … Williams, T. (2009). Obliquity-paced Pliocene West Antarctic ice sheet oscillations. *Nature*, **458**, 322–328.

Nakayama, Y., Menemenlis, D., Zhang, H., Schodlok, M., & Rignot, E. (2018). Origin of

Circumpolar Deep Water intruding onto the Amundsen and Bellingshausen Sea continental shelves. *Nature Communications*, **9**, 3403.
National Academies of Sciences, Engineering, and Medicine (2021). *Mid-Term Assessment of Progress on the 2015 Strategic Vision for Antarctic and Southern Ocean Research*. The National Academies Press. https://doi.org/10.17226/26338
Naughton, K. M., O'Hara, T. D., Appleton, B., & Cisternas, P. A. (2014). Antitropical distributions and species delimitation in a group of ophiocomid brittle stars (Echinodermata: Ophiuroidea: Ophiocomidae). *Molecular Phylogenetics and Evolution*, **78**, 232–244.
Ni, Q., Li, W., Liang, X., Liu, J., Ge, H., & Dong, Z. (2021). Gill transcriptome analysis reveals the molecular response to the acute low-salinity stress in *Cyclina sinensis*. *Aquaculture Reports*, **19**, 100564.
Nikula, R., Fraser, C. I., Spencer, H. G., & Waters, J. M. (2010). Circumpolar dispersal by rafting in two subantarctic kelp-dwelling crustaceans. *Marine Ecology Progress Series*, **405**, 221–230.
Niu, X.-M., Xu, Y.-C., Li, Z.-W., Bian, Y.-T., Hou, X.-H., Chen, J.-F., Zou, Y.-P., Jiang, J., Wu, Q., Ge, S., Balasubramanian, S., & Guo, Y.-L. (2019). Transposable elements drive rapid phenotypic variation in *Capsella rubella*. *Proceedings of the National Academy of Sciences of the United States of America*, **116**(14), 6908–6913.
Noble, T. L., Rohling, E. J., Aitken, A. R. A., Bostock, H. C., Chase, Z., Gomez, N., Jong, L. M., King, M. A., Mackintosh, A. N., McCormack, F. S., McKay, R. M., Menviel, L., Phipps, S. J., Weber, M. E., Fogwill, C. J., Gayen, B., Golledge, N. R., Gwyther, D. E., Hogg, A. McC., … Williams, T. (2020). The Sensitivity of the Antarctic Ice Sheet to a Changing Climate: Past, Present, and Future. *Reviews of Geophysics*, **58**(4), e2019RG000663.
O'Connell, K., Mulder, K., Wynn, A., de Queiroz, K., & Bell, R. (2021). Genomic library preparation and hybridization capture of formalin-fixed tissues and allozyme supernatant for population genomics and considerations for combining capture- and RADseq-based single nucleotide polymorphism data sets. *Molecular Ecology Resources*, **22**(2), 487–502.
O'Hara, T. D., Hugall, A. F., Thuy, B., Stöhr, S., & Martynov, A. V. (2017). Restructuring higher taxonomy using broad-scale phylogenomics: The living Ophiuroidea. *Molecular Phylogenetics and Evolution*, **107**, 415–430.
O'Hara, T. D., Hugall, A. F., Woolley, S. N. C., Bribiesca-Contreras, G., & Bax, N. J. (2019). Contrasting processes drive ophiuroid phylodiversity across shallow and deep seafloors. *Nature*, **565**, 636–639.
O'Leary, S. J., Puritz, J. B., Willis, S. C., Hollenbeck, C. M., & Portnoy, D. S. (2018). These aren't the loci you'e looking for: Principles of effective SNP filtering for molecular ecologists. *Molecular Ecology*, **27**(16), 3193–3206.
O'Loughlin, P. M., Paulay, G., Davey, N., & Michonneau, F. (2011). The Antarctic region as a marine biodiversity hotspot for echinoderms: Diversity and diversification of sea cucumbers. *Deep-Sea Research Part II: Topical Studies in Oceanography*, **58**(1-2), 264–275.
Oellermann, M., Lieb, B., Pörtner, H. O., Semmens, J. M., & Mark, F. C. (2015a). Blue blood on ice: Modulated blood oxygen transport facilitates cold compensation and eurythermy in an Antarctic octopod. *Frontiers in Zoology*, **12**, 6.
Oellermann, M., Strugnell, J. M., Lieb, B., & Mark, F. C. (2015b). Positive selection in octopus haemocyanin indicates functional links to temperature adaptation. *BMC Evolutionary Biology*, **15**, 133.
Oksanen, J., Blanchet, F. G., Friendly, M., Kindt, R., Legendre, P., McGlinn, D., Minchin, P.

R., O'Hara, R. B., Simpson, G. L., Solymos, P., Henry, M., Stevens, H., Szoecs, E., & Wagner, H. (2013). vegan: Community Ecology Package. *R Package Version 2.5-6*. [tool source] Retrieved from https://cran.r-project.org/package=vegan

Palumbi, S. R. (1994). Genetic Divergence, Reproductive Isolation, and Marine Speciation. *Annual Review of Ecology and Systematics*, **25**, 547–572.

Paradis, E. (2010). pegas: an R package for population genetics with an integrated–modular approach. *Bioinformatics*, **26**(3), 419–420.

Paradis, E., Claude, J., & Strimmer, K. (2004). APE: Analyses of phylogenetics and evolution in R language. *Bioinformatics*, **20**(2), 289–290.

Patterson, N., Moorjani, P., Luo, Y., Mallick, S., Rohland, N., Zhan, Y., Genschoreck, T., Webster, T., & Reich, D. (2012). Ancient admixture in human history. *Genetics*, **192**(3), 1065–1093.

Patton, A. H., Margres, M. J., Stahlke, A. R., Hendricks, S., Lewallen, K., Hamede, R. K., Ruiz-Aravena, M., Ryder, O., McCallum, H. I., Jones, M. E., Hohenlohe, P. A., & Storfer, A. (2019). Contemporary Demographic Reconstruction Methods Are Robust to Genome Assembly Quality: A Case Study in Tasmanian Devils. *Molecular Biology and Evolution*, **36**(12), 2906–2921.

Paulay, G., & Meyer, C. (2006). Dispersal and divergence across the greatest ocean region: Do larvae matter? *Integrative and Comparative Biology*, **46**(3), 269–281.

Pauls, S. U., Nowak, C., Bálint, M., & Pfenninger, M. (2013). The impact of global climate change on genetic diversity within populations and species. *Molecular Ecology*, **22**(4), 925–946.

Pearse, J. S., & Bosch, I. (1994). Brooding in the Antarctic: Östergren had it nearly right. In B. David, A. Guille, J.-P. Féral, & M. Roux (Eds.), *Echinoderms through Time* (pp. 111–120). CPC Press.

Pearse, J. S., McClintock, J. B., & Bosch, I. (1991). Reproduction of Antarctic Benthic Marine Invertebrates: Tempos, Modes, and Timing. *Integrative and Comparative Biology*, **31**(1), 65–80.

Pearse, J. S., Mooi, R., Lockhart, S. J., & Brandt, A. (2009). Brooding and Species Diversity in the Southern Ocean: Selection for Brooders or Speciation within Brooding Clades? In I. Krupnik, M. A. Lang, & S. E. Miller (Eds.), *Smithsonian at the Poles: Contributions to International Polar Year Science* (pp. 181–196). Smithsonian Institution Scholarly Press.

Peck, L. S., Massey, A., Thorne, M. A. S., & Clark, M. S. (2009). Lack of acclimation in *Ophionotus victoriae*: Brittle stars are not fish. *Polar Biology*, **32**, 399–402.

Peterson, B. K., Weber, J. N., Kay, E. H., Fisher, H. S., & Hoekstra, H. E. (2012). Double digest RADseq: An inexpensive method for de novo SNP discovery and genotyping in model and non-model species. *PLoS ONE*, **7**(5), e37135.

Petit, R. J., Aguinagalde, I., De Beaulieu, J. L., Bittkau, C., Brewer, S., Cheddadi, R., Ennos, R., Fineschi, S., Grivet, D., Lascoux, M., Mohanty, A., Müller-Starck, G., Demesure-Musch, B., Palmé, A., Martín, J. P., Rendell, S., & Vendramin, G. G. (2003). Glacial refugia: Hotspots but not melting pots of genetic diversity. *Science*, **300**(5625), 1563–1565.

Pfaff, C. L., Parra, E. J., Bonilla, C., Hiester, K., McKeigue, P. M., Kamboh, M. I., Hutchinson, R. G., Ferrell, R. E., Boerwinkle, E., & Shriver, M. D. (2001). Population structure in admixed populations: Effect of admixture dynamics on the pattern of linkage disequilibrium. *American Journal of Human Genetics*, **68**(1), 198–207.

Pfeifer, B., Wittelsbürger, U., Ramos-Onsins, S. E., & Lercher, M. J. (2014). PopGenome: An efficient swiss army knife for population genomic analyses in R. *Molecular Biology and Evolution*, **31**(7), 1929–1936.

Pfenninger, M., & Schwenk, K. (2014). Cryptic animal species are homogeneously distributed among taxa and biogeographical regions. *BMC Ecology and Evolution*, **7**, 121.

Pickrell, J. K., & Pritchard, J. K. (2012). Inference of Population Splits and Mixtures from Genome-Wide Allele Frequency Data. *PLoS Genetics*, **8**(11), e1002967.

Pimpinelli, S., & Piacentini, L. (2020). Environmental change and the evolution of genomes: Transposable elements as translators of phenotypic plasticity into genotypic variability. *Functional Ecology*, **34**(2), 428–441.

Pina-Martins, F., Silva, D. N., Fino, J., & Paulo, O. S. (2017). *Structure_threader*: An improved method for automation and parallelization of programs STRUCTURE, FASTSTRUCTURE and *MavericK* on multicore CPU systems. *Molecular Ecology Resources*, **17**(6), e268–e274.

Pina-Martins, F., Silva, D. N., Fino, J., & Paulo, O. S. (2017). *Structure_threader*: An improved method for automation and parallelization of programs STRUCTURE, FASTSTRUCTURE and *MavericK* on multicore CPU systems. *Molecular Ecology Resources*, **17**(6), e268–e274.

Piñeiro, R., Hardy, O. J., Tovar, C., Gopalakrishnan, S, Vieira, F. G., & Gilbert, M. T. P. (2021). Contrasting genetic signal of recolonization after rainforest fragmentation in African trees with different dispersal abilities. *Proceedings of the National Academy of Sciences of the United States of America*, **118**(27), e2013979118.

Pollard, D., & DeConto, R. M. (2009). Modelling West Antarctic ice sheet growth and collapse through the past five million years. *Nature*, **458**, 329–332.

Portik, D. M., Leaché, A. D., Rivera, D., Barej, M. F., Burger, M., Hirschfeld, M., Rödel, M. O., Blackburn, D. C., & Fujita, M. K. (2017). Evaluating mechanisms of diversification in a Guineo-Congolian tropical forest frog using demographic model selection. *Molecular Ecology*, **26**(19), 5245–5263.

Post, A. L., Meijers, A. J. S., Fraser, A. D., Meiners, K. M., Ayers, J., Bindoff, N. L., Griffiths, H. J., Van de Putte, A. P., O'Brien, P. E., Swadling, K. M., & Raymond, B. (2014). PART 4. ENVIRONMENTAL SETTING. In C De Broyer, P. Koubbi, H. J. Griffiths, B. Raymond, & C. Udekem d'Acoz (Eds.), *Biogeographic Atlas of the Southern Ocean* (pp. 46–64). Cambridge: Scientific Committee on Antarctic Research.

Poulin, É., & Féral, J.-P. (1996). Why are there so many species of brooding antarctic echinoids? *Evolution*, **50**(2), 820–830.

Poulin, E., Palma, A. T., & Feéral, J. P. (2002). Evolutionary versus ecological success in Antarctic benthic invertebrates. *Trends in Ecology and Evolution*, **17**(5), 218–222.

Pritchard, J. K., Stephens, M., & Donnelly, P. (2000). Inference of Population Structure Using Multilocus Genotype Data. *Genetics*, **155**(2), 945–959.

Privé, F., Luu, K., Vilhjálmsson, B. J., & Blum, M. G. B. (2020). Performing Highly Efficient Genome Scans for Local Adaptation with R Package pcadapt Version 4. *Molecular Biology and Evolution*, **37**(7), 2153–2154.

Provan, J. (2013). The effects of past, present and future climate change on range-wide genetic diversity in northern North Atlantic marine species. *Frontiers of Biogeography*, **5**(1), 60–66.

Provan, J., & Bennett, K. D. (2008). Phylogeographic insights into cryptic glacial refugia. *Trends in Ecology and Evolution*, **23**(10), 564–571.

Puritz, J. B., Matz, M. V., Toonen, R. J., Weber, J. N., Bolnick, D. I., & Bird, C. E. (2014). Demystifying the RAD fad. *Molecular Ecology*, **23**(24), 5937–5942.

QGIS Development Team. (2019). QGIS Geographic Information System. *Open Source Geospatial Foundation Project*. [tool source] Retrieved from http://qgis.osgeo.org

Raghavan, M., Skoglund, P., Graf, K. E., Metspalu, M., Albrechtsen, A., Moltke, I.,

Rasmussen, S., Stafford, T. W., Orlando, L., Metspalu, E., Karmin, M., Tambets, K., Rootsi, S., Mägi, R., Campos, P. F., Balanovska, E., Balanovsky, O., Khusnutdinova, E., Litvinov, S., … Willerslev, E. (2014). Upper Palaeolithic Siberian genome reveals dual ancestry of Native Americans. *Nature*, **505**, 87–91.

Rambaut, A., Drummond, A. J., Xie, D., Baele, G., & Suchard, M. A. (2018). Posterior Summarization in Bayesian Phylogenetics Using Tracer 1.7. *Systematic Biology*, **67**(5), 901–904.

Ranallo-Benavidez, T. R., Jaron, K. S., & Schatz, M. C. (2020). GenomeScope 2.0 and Smudgeplot for reference-free profiling of polyploid genomes. *Nature Communications*, **11**, 1432.

Rasmussen, M., Guo, X., Wang, Y., Lohmueller, K. E., Rasmussen, S., Albrechtsen, A., Skotte, L., Lindgreen, S., Metspalu, M., Jombart, T., Kivisild, T., Zhai, W., Eriksson, A., Manica, A., Orlando, L., De La Vega, F. M., Tridico, S., Metspalu, E., Nielsen, K., … Willerslev, E. (2011). An Aboriginal Australian Genome Reveals Separate Human Dispersals into Asia. *Science*, **334**(6052), 94–98.

Raupach, M. J., Thatje, S., Dambach, J., Rehm, P., Misof, B., & Leese, F. (2010). Genetic homogeneity and circum-Antarctic distribution of two benthic shrimp species of the Southern Ocean, *Chorismus antarcticus* and *Nematocarcinus lanceopes*. *Marine Biology*, **157**, 1783–1797.

Raymo, M. E., & Mitrovica, J. X. (2012). Collapse of polar ice sheets during the stage 11 interglacial. *Nature*, **483**, 453–456.

Reed, A. J., & Thatje, S. (2015). Long-term acclimation and potential scope for thermal resilience in Southern Ocean bivalves. *Marine Biology*, **162**, 2217–2224.

Reed, A. J., Thatje, S., & Linse, K. (2013). An unusual hermaphrodite reproductive trait in the Antarctic brooding bivalve *Lissarca miliaris* (Philobryidae) from the Scotia Sea, Southern Ocean. *Polar Biology*, **36**, 1–11.

Reitzel, A. M., Herrera, S., Layden, M. J., Martindale, M. Q., & Shank, T. M. (2013). Going where traditional markers have not gone before: Utility of and promise for RAD sequencing in marine invertebrate phylogeography and population genomics. *Molecular Ecology*, **21**(11), 2953–2970.

Rellstab, C., Gugerli, F., Eckert, A. J., Hancock, A. M., & Holderegger, R. (2015). A practical guide to environmental association analysis in landscape genomics. *Molecular Ecology*, **24**(17), 4348–4370.

Renner, A. H. H., Thorpe, S. E., Heywood, K. J., Murphy, E. J., Watkins, J. L., & Meredith, M. P. (2012). Advective pathways near the tip of the Antarctic Peninsula: Trends, variability and ecosystem implications. *Deep-Sea Research Part I: Oceanographic Research Papers*, **63**, 91–101.

Revelle, W. (2020). psych: Procedures for Personality and Psychological Research. [tool source] Retreived from *https://CRAN.R-Project.Org/Package=psych*

Riddle, M. J., Craven, M., Goldsworthy, P. M., & Carsey, F. (2007). A diverse benthic assemblage 100 km from open water under the Amery Ice Shelf, Antarctica. *Paleoceanography*, **22**(1), PA1204.

Riesgo, A., Taboada, S., & Avila, C. (2015). Evolutionary patterns in Antarctic marine invertebrates: An update on molecular studies. *Marine Genomics*, **23**, 1–13.

Rignot, E., Mouginot, J., Scheuchl, B., Van Den Broeke, M., Van Wessem, M. J., & Morlighem, M. (2019). Four decades of Antarctic ice sheet mass balance from 1979–2017. *Proceedings of the National Academy of Sciences of the United States of America*, **115**(4), 1095–1103.

Rintoul, S. R., Hughes, C. W., & Olbers, D. (2001). Chapter 4.6 The Antarctic circumpolar current system. *International Geophysics*, **77**, 271–302.

Robel, A. A., Seroussi, H., & Roe, G. H. (2019). Marine ice sheet instability amplifies and skews uncertainty in projections of future sea-level rise. *Proceedings of the National Academy of Sciences of the United States of America*, **116**(30), 14887–14892.

Roberts, R. E., Powell, D., Wang, T., Hall, M. H., Motti, C. A., & Cummins, S. F. (2018). Putative chemosensory receptors are differentially expressed in the sensory organs of male and female crown-of-thorns starfish, *Acanthaster planci*. *BMC Genomics*, **19**, 853.

Robison, B., Seibel, B., & Drazen, J. (2014). Deep-sea octopus (*Graneledone boreopacifica*) conducts the longest-known egg-brooding period of any animal. *PLoS ONE*, **9**(7), e103437.

Rogers, A. D., Tyler, P. A., Connelly, D. P., Copley, J. T., James, R., Larter, R. D., Linse, K., Mills, R. A., Garabato, A. N., Pancost, R. D., Pearce, D. A., Polunin, N. V. C., German, C. R., Shank, T., Boersch-Supan, P. H., Alker, B. J., Aquilina, A., Bennett, S. A., Clarke, A., … Zwirglmaier, K. (2012). The Discovery of New Deep-Sea Hydrothermal Vent Communities in the Southern Ocean and Implications for Biogeography. *PLoS Biology*, **10**(1), e1001234.

Rogers, A. R., & Harpending, H. C. (1992). Population growth makes waves in the distribution of pairwise genetic differences. *Molecular Biology and Evolution*, **9**(3), 552–559.

Romeijn, R. J., Gorski, M. M., Van Schie, M. A., Noordermeer, J. N., Mullenders, L. H., Ferro, W., & Pastink, A. (2005). Lig4 and Rad54 are required for repair of DNA double-strand breaks induced by P-element excision in *Drosophila*. *Genetics*, **169**(2), 795–806.

Rosen, Z., Bhaskar, A., Roch, S., & Song, Y. S. (2018). Geometry of the Sample Frequency Spectrum and the Perils of Demographic Inference. *Genetics*, **210**(2), 665–682.

Rosenberg, N. A., & Nordborg, M. (2002). Genealogical trees, coalescent theory and the analysis of genetic polymorphisms. *Nature Reviews Genetics*, **3**, 380–390.

Roterman, C. N., Copley, J. T., Linse, K. T., Tyler, P. A., & Rogers, A. D. (2016). Connectivity in the cold: The comparative population genetics of vent-endemic fauna in the Scotia Sea, Southern Ocean. *Molecular Ecology*, **25**(5), 1073–1088.

Rowe, K. C., Singhal, S., Macmanes, M. D., Ayroles, J. F., Morelli, T. L., Rubidge, E. M., Bi, K., & Moritz, C. C. (2011). Museum genomics: low-cost and high-accuracy genetic data from historical specimens. *Molecular Ecology Resources*, **11**(6), 1082–1092.

Rozhnov, S. V. (2012). Development of Symmetry and Asymmetry in the Early Evolution of the Echinoderms. *Paleontological Journal*, **48**(8), 780–792.

Rstudio, T. (2020). RStudio: Integrated Development for R. *Rstudio Team, PBC, Boston, MA.* [tool source] Retreived from *http://Www.Rstudio.Com/*. doi:10.1145/3132847.3132886

Saenz-Agudelo, P., DiBattista, J. D., Piatek, M. J., Gaither, M. R., Harrison, H. B., Nanninga, G. B., & Berumen, M. L. (2015). Seascape genetics along environmental gradients in the Arabian Peninsula: Insights from ddRAD sequencing of anemonefishes. *Molecular Ecology*, **24**(24), 6241–6255.

Sands, C. J., Griffiths, H. J., Downey, R. V., Barnes, D. K. A., Linse, K., & Martín-Ledo, R. (2013). Observations of the ophiuroids from the West Antarctic sector of the Southern Ocean. *Antarctic Science*, **25**(1), 3–10.

Sands, C. J., O'Hara, T. D., Barnes, D. K. A., & Martín-Ledo, R. (2015). Against the flow: Evidence of multiple recent invasions of warmer continental shelf waters by a Southern Ocean brittle star. *Frontiers in Ecology and Evolution*, **3**, 63.

Sands, C. J., O'Hara, T. D., & Martín-Ledo, R. (2021). Pragmatic Assignment of Species Groups Based on Primary Species Hypotheses: The Case of a Dominant Component of the Southern Ocean Benthic Fauna. *Frontiers in Marine Science*, **9**, 723328.

Santure, A. W., & Garant, D. (2018). Wild GWAS—association mapping in natural

populations. *Molecular Ecology Resources*, **18**(4), 729–739.
Schaefer, N. K., Shapiro, B., & Green, R. E. (2021). An ancestral recombination graph of human, Neanderthal, and Denisovan genomes. *Science Advances*, **7**(29), eabc0776.
Scherer, R. P., Bohaty, S. M., Dunbar, R. B., Esper, O., Flores, J. A., Gersonde, R., Harwood, D. M., Roberts, A. P., & Taviani, M. (2008). Antarctic records of precession-paced insolation-driven warming during early Pleistocene Marine Isotope Stage 31. *Geophysical Research Letters*, **35**(3), L03505.
Schiffels, S., & Durbin, R. (2014). Inferring human population size and separation history from multiple genome sequences. *Nature Genetics*, **46**, 919–925.
Schmid, S., Neuenschwander, S., Pitteloud, C., Heckel, G., Pajkovic, M., Arlettaz, R., & Alvarez, N. (2018). Spatial and temporal genetic dynamics of the grasshopper *Oedaleus decorus* revealed by museum genomics. *Ecology and Evolution*, **8**(3), 1480–1495.
Schmitt, T. (2007). Molecular biogeography of Europe: Pleistocene cycles and postglacial trends. *Frontiers in Zoology*, **4**, 11.
Schraiber, J. G., & Akey, J. M. (2015). Methods and models for unravelling human evolutionary history. *Nature Reviews Genetics*, **16**, 727–740.
Schwarz, R., Hoving, H.-J., Noever, C., & Piatkowski, U. (2019). Life histories of Antarctic incirrate octopods (Cephalopoda: Octopoda). *PLoS ONE*, **14**(7), e0219694.
Schwarz, R., Piatkowski, U., & Hoving, H. J. T. (2018). Impact of environmental temperature on the lifespan of octopods. *Marine Ecology Progress Series*, **605**, 151–164.
Selkoe, K. A., D'Aloia, C. C., Crandall, E. D., Iacchei, M., Liggins, L., Puritz, J. B., von der Heyden, S., & Toonen, R. J. (2016). A decade of seascape genetics: contributions to basic and applied marine connectivity. *Marine Ecology Progress Series*, **554**, 1–19.
Serrato-Capuchina, A., & Matute, D. R. (2018). The role of transposable elements in speciation. *Genes*, **15**(9), 254.
Sewell, M. A. (2005). Examination of the meroplankton community in the south-western Ross Sea, Antarctica, using a collapsible plankton net. *Polar Biology*, **28**, 119–131.
Sewell, M. A., & Jury, J. A. (2011). Seasonal patterns in diversity and abundance of the high antarctic meroplankton: Plankton sampling using a Ross Sea desalination plant. *Limnology and Oceanography*, **56**(5), 1667–1681.
Sexton, J. P., Hangartner, S. B., & Hoffmann, A. A. (2013). Genetic isolation by environment or distance: Which pattern of gene flow is most common? *Evolution*, **68**(1), 1–15.
Shreeve, R., & Peck, L. (1995). Distribution of pelagic larvae of benthic marine invertebrates in the Bellingshausen Sea. *Polar Biology*, **15**(5), 369–374.
Simms, A. R., Milliken, K. T., Anderson, J. B., & Wellner, J. S. (2011). The marine record of deglaciation of the South Shetland Islands, Antarctica since the Last Glacial Maximum. *Quaternary Science Reviews*, **30**(13–14), 1583–1601.
Slatkin, M. (2008). Linkage disequilibrium — understanding the evolutionary past and mapping the medical future. *Nature Reviews Genetics*, **9**, 477–485.
Slatkin, M., & Hudson, R. R. (1991). Pairwise comparisons of mitochondrial DNA sequences in stable and exponentially growing populations. *Genetics*, **129**(2), 555–562.
Sloan, D. B., Havird, J. C., & Sharbrough, J. (2017). The on-again, off-again relationship between mitochondrial genomes and species boundaries. *Molecular Ecology*, **26**(8), 2212–2236.
Smit, A. F. A., & Hubley, R. (2008-2015). *RepeatModeler* open-1.0. [tool source] Retrieved from http://www.repeatmasker.org
Smit, A. F. A., Hubley, R., & Green, P. (2013-2015). *RepeatMasker* Open-4.0. [tool source] Retrieved from http://www.repeatmasker.org
Smith, E. A. (1876). Descriptions of species of Asteridae and Ophiuridae from Kerguelen

Islands. *Annals and Magazine of Natural History. 4th Series*, **17**, 105–113.
Smith, J. A., Hillenbrand, C.-D., Pudsey, C. J., Allen, C. S., & Graham, A. G. C. (2010). The presence of polynyas in the Weddell Sea during the Last Glacial Period with implications for the reconstruction of sea-ice limits and ice sheet history. *Earth and Planetary Science Letters*, **296**(3–4), 287–298.
Sokolov, S., & Rintoul, S. R. (2009). Circumpolar structure and distribution of the Antarctic Circumpolar Current fronts: 1. Mean circumpolar paths. *Journal of Geophysical Research: Oceans*, **114**(C11), C11018.
Soler-Membrives, A., Linse, K., Miller, K. J., & Arango, C. P. (2017). Genetic signature of last glacial maximum regional refugia in a circum-Antarctic sea spider. *Royal Society Open Science*, **4**(10), 170615.
Souza, C. A., Murphy, N., Villacorta-Rath, C., Woodings, L. N., Ilyushkina, I., Hernandez, C. E., Green, B. S., Bell, J. J., & Strugnell, J. M. (2017). Efficiency of ddRAD target enriched sequencing across spiny rock lobster species (Palinuridae: *Jasus*). *Scientific Reports*, **7**, 6781.
Sovic, M. G., Fries, A. C., & Gibbs, H. L. (2015). AftrRAD: A pipeline for accurate and efficient de novo assembly of RADseq data. *Molecular Ecology Resources*, **15**(5), 1163–1171.
Speidel, L., Forest, M., Shi, S., & Myers, S. R. (2019). A method for genome-wide genealogy estimation for thousands of samples. *Nature Genetics*, **51**, 1321–1329.
Sromek, L., Lasota, R., & Wolowicz, M. (2015). Impact of glaciations on genetic diversity of pelagic mollusks: Antarctic *Limacina antarctica* and Arctic *Limacina helicina*. *Marine Ecology Progress Series*, **525**, 143–152.
Stankowski, S., & Ravinet, M. (2021). Defining the speciation continuum. *Evolution*, **75**(6), 1256–1273.
Stanwell-Smith, D., Peck, L. S., Clarke, A., Murray, A. W. A., & Todd, C. D. (1999). The distribution, abundance and seasonality of pelagic marine invertebrate larvae in the maritime Antarctic. *Philosophical Transactions of the Royal Society B: Biological Sciences*, **354**(1382), 471–484.
Steig, E. J., Huybers, K., Singh, H. A., Steiger, N. J., Ding, Q., Frierson, D. M. W., Popp, T., & White, J. W. C. (2015). Influence of West Antarctic Ice Sheet collapse on Antarctic surface climate. *Geophysical Research Letters*, **42**(12), 4862–4868.
Steig, E. J., & Neff, P. D. (2018). The prescience of paleoclimatology and the future of the Antarctic ice sheet. *Nature Communications*, **9**, 2730.
Stemple, D. L. (2013). So, you want to sequence a genome... *Genome Biology*, **14**(7), 128.
Stevens, M. I., Frati, F., McGaughran, A., Spinsanti, G., & Hogg, I. D. (2007). Phylogeographic structure suggests multiple glacial refugia in northern Victoria Land for the endemic Antarctic springtail *Desoria klovstadi* (Collembola, Isotomidae). *Zoologica Scripta*, **36**(2), 201–212.
Stewart, J. R., Lister, A. M., Barnes, I., & Dalén, L. (2010). Refugia revisited: Individualistic responses of species in space and time. *Proceedings of the Royal Society B: Biological Sciences*, **227**(1628), 661–671.
Stöhr, S., Weber, A. A.-T., Boissin, E., & Chenuil, A. (2020). Resolving the *Ophioderma longicauda* (Echinodermata: Ophiuroidea) cryptic species complex: Five sisters, three of them new. *European Journal of Taxonomy*, **600**, 1–37.
Strathamnn, R. R. (1985). Feeding and nonfeeding larval development and life-history evolution in marine invertebrates. *Annual Review of Ecology and Systematics*, **16**, 339–361.
Strugnell, J. M., Allcock, A. L., & Watts, P. C. (2017). Closely related octopus species show different spatial genetic structures in response to the Antarctic seascape. *Ecology and*

Evolution, **7**(19), 8087–8099.
Strugnell, J. M., Pedro, J. B., & Wilson, N. G. (2018). Dating Antarctic ice sheet collapse: Proposing a molecular genetic approach. *Quaternary Science Reviews*, **179**, 153–157.
Strugnell, J. M., Rogers, A. D., Prodöhl, P. A., Collins, M. A., & Allcock, A. L. (2008). The thermohaline expressway: the Southern Ocean as a centre of origin for deep-sea octopuses. *Cladistics*, **24**(6), 853–860.
Strugnell, J. M., Watts, P. C., Smith, P. J., & Allcock, A. L. (2012). Persistent genetic signatures of historic climatic events in an Antarctic octopus. *Molecular Ecology*, **21**(11), 2775–2787.
Suchan, T., Pitteloud, C., Gerasimova, N. S., Kostikova, A., Schmid, S., Arrigo, N., Pajkovic, M., Ronikier, M., & Alvarez, N. (2016). Hybridization Capture Using RAD Probes (hyRAD), a New Tool for Performing Genomic Analyses on Collection Specimens. *PLoS ONE*, **11**(3), e0151651.
Sundqvist, L., Keenan, K., Zackrisson, M., Prodöhl, P., & Kleinhans, D. (2016). Directional genetic differentiation and relative migration. *Ecology and Evolution*, **6**(11), 3461–3475.
Supek, F., Bošnjak, M., Škunca, N., & Šmuc, T. (2011). REVIGO Summarizes and Visualizes Long Lists of Gene Ontology Terms. *PLoS ONE*, **6**(7), e21800.
Sutter, J., Eisen, O., Werner, M., Grosfeld, K., Kleiner, T., & Fischer, H. (2020). Limited Retreat of the Wilkes Basin Ice Sheet During the Last Interglacial. *Geophysical Research Letters*, **47**(13), e2020GL088131.
Tajima, F. (1989). Statistical method for testing the neutral mutation hypothesis by DNA polymorphism. *Genetics*, **123**(3), 585–595.
Taylor, M. L., & Roterman, C. N. (2017). Invertebrate population genetics across Earth's largest habitat: The deep-sea floor. *Molecular Ecology*, **26**(19), 4872–4896.
Teixidó, N., Garrabou, J., Gutt, J., & Arntz, W. E. (2004). Recovery in Antarctic benthos after iceberg disturbance: Trends in benthic composition, abundance and growth forms. *Marine Ecology Progress Series*, **278**, 1–16.
Terhorst, J., Kamm, J. A., & Song, Y. S. (2017). Robust and scalable inference of population history from hundreds of unphased whole genomes. *Nature Genetics*, **49**, 303–309.
Terhorst, J., & Song, Y. S. (2015). Fundamental limits on the accuracy of demographic inference based on the sample frequency spectrum. *Proceedings of the National Academy of Sciences of the United States of America*, **112**(25), 7677–7682.
Thatje, S. (2012). Effects of Capability for Dispersal on the Evolution of Diversity in Antarctic Benthos. *Integrative and Comparative Biology*, **52**(4), 470–482.
Thatje, S., Hillenbrand, C.-D., Mackensen, A., & Larter, R. (2008). Life hung by a thread: Endurance of Antarctic fauna in glacial periods. *Ecology*, **89**(3), 682–692.
Thatje, S., Hillenbrand, C. D., & Larter, R. (2005). On the origin of Antarctic marine benthic community structure. *Trends in Ecology and Evolution*, **20**(10), 534–540.
Thom, G., Xue, A. T., Sawakuchi, A. O., Ribas, C. C., Hickerson, M. J., Aleixo, A., & Miyaki, C. (2020). Quaternary climate changes as speciation drivers in the Amazon floodplains. *Science Advances*, **6**(11), eaax4718.
Thompson, A. F., Heywood, K. J., Thorpe, S. E., Renner, A. H. H., & Trasviña, A. (2009). Surface circulation at the tip of the Antarctic Peninsula from drifters. *Journal of Physical Oceanography*, **39**(1), 3–26.
Thornhill, D. J., Mahon, A. R., Norenburg, J. L., & Halanych, K. M. (2008). Open-ocean barriers to dispersal: a test case with the Antarctic Polar Front and the ribbon worm *Parborlasia corrugatus* (Nemertea: Lineidae). *Molecular Ecology*, **17**(23), 5104–5117.
Tine, M., Kuhl, H., Gagnaire, P.-A., Louro, B., Desmarais, E., Martins, R. S. T., Hecht, J., Knaust, F., Belkhir, K., Klages, S., Dieterich, R., Stueber, K., Piferrer, F., Guinand, B., Bierne, N., Volckaert, F. A. M., Bargelloni, L., Power, D. M., Bonhomme, F., …

Reinhardt, R. (2014). European sea bass genome and its variation provide insights into adaptation to euryhalinity and speciation. *Nature Communications*, **5**, 5770.
Turner, R. L., & Dearborn, J. H. (1979). Organic and inorganic composition of post-metamorphic growth stages of *Ophionotus hexactis* (E.A. Smith) (Echinodermata: Ophiuroidea) during intraovarian incubation. *Journal of Experimental Marine Biology and Ecology*, **36**, 41–51.
Turney, C. S. M., Jones, R. T., McKay, N. P., Van Sebille, E., Thomas, Z. A., Hillenbrand, C.-D., & Fogwill, C. J. (2020). A global mean sea surface temperature dataset for the Last Interglacial (129–116 ka) and contribution of thermal expansion to sea level change. *Earth System Science Data*, **12**(12), 3341–3356.
Tyler, P. A., Reeves, S., Peck, L., Clarke, A., & Powell, D. (2003). Seasonal variation in the gametogenic ecology of the Antarctic scallop *Adamussium colbecki*. *Polar Biology*, **26**, 2003.
van der Valk, T., Díez-del-Molino, D., Marques-Bonet, T., Guschanski, K., & Dalén, L. (2019). Historical Genomes Reveal the Genomic Consequences of Recent Population Decline in Eastern Gorillas. *Current Biology*, **29**(1), 165-170.e6.
Vaughan, D. G. (2008). West Antarctic Ice Sheet collapse - The fall and rise of a paradigm. *Climatic Change*, **91**, 65–79.
Vaughan, D. G., Barnes, D. K. A., Fretwell, P. T., & Bingham, R. G. (2011). Potential seaways across West Antarctica. *Geochemistry, Geophysics, Geosystems*, **12**(10), Q10004.
Verheye, M. L., Backeljau, T., & D'Acoz, C. d'Udekem. (2016). Looking beneath the tip of the iceberg: diversification of the genus *Epimeria* on the Antarctic shelf (Crustacea, Amphipoda). *Polar Biology*, **39**, 925–945.
Vieira, F. G., Lassalle, F., Korneliussen, T. S., & Fumagalli, M. (2016). Improving the estimation of genetic distances from Next-Generation Sequencing data. *Biological Journal of the Linnean Society*, **117**(1), 139–149.
Villesen, P. (2007). FaBox: an online toolbox for FASTA sequences. *Molecular Ecology Notes*, **7**(6), 965–968.
Visser, M. E. (2008). Keeping up with a warming world; assessing the rate of adaptation to climate change. *Proceedings of the Royal Society B: Biological Sciences*, **275**(1635), 649–659.
Wagner, A. (2011). The molecular origins of evolutionary innovations. *Trends in Genetics*, **27**(10), 397–410.
Wakita, D., Hayase, Y., & Aonuma, H. (2019). Different Synchrony in Rhythmic Movement Caused by Morphological Difference between Five- and Six-armed Brittle Stars. *Scientific Reports*, **9**, 8298.
Wakita, D., Kagaya, K., & Aonuma, H. (2020). A general model of locomotion of brittle stars with a variable number of arms. *Journal of the Royal Society Interface*, **17**(162), 20190374.
Walker, B. J., Abeel, T., Shea, T., Priest, M., Abouelliel, A., Sakthikumar, S., Cuomo, C. A., Zeng, Q., Wortman, J., Young, S. K., & Earl, A. M. (2014). Pilon: An integrated tool for comprehensive microbial variant detection and genome assembly improvement. *PLoS ONE*, **9**(11), e112963.
Wall, J. D., Tang, L. F., Zerbe, B., Kvale, M. N., Kwok, P.-Y., Schaefer, C., & Risch, N. (2014). Estimating genotype error rates from high-coverage next-generation sequence data. *Genome Research*, **24**(11), 1734–1739.
Wang, I. J., & Bradburd, G. S. (2014). Isolation by environment. *Molecular Ecology*, **23**(23), 5649–5662.
Wang, S., Meyer, E., Mckay, J. K., & Matz, M. V. (2012). 2b-RAD: a simple and flexible

method for genome-wide genotyping. *Nature Methods*, **9**, 808–810.
Watts, S. A., Scheibling, R. E., Marsh, A. G., & McClintock, J. B. (1983). Induction of Aberrant Ray Numbers in *Echinaster* sp. (Echinodermata: Asteroidea) by High Salinity. *Florida Scientist*, **46**(2), 125–128.
Weber, A. A.-T., Abi-Rached, L., Galtier, N., Bernard, A., Montoya-Burgos, J. I., & Chenuil, A. (2017). Positive selection on sperm ion channels in a brooding brittle star: consequence of life-history traits evolution. *Molecular Ecology*, **26**(14), 3744–3759.
Weber, A. A.-T., Stöhr, S., & Chenuil, A. (2019). Species delimitation in the presence of strong incomplete lineage sorting and hybridization: Lessons from *Ophioderma* (Ophiuroidea: Echinodermata). *Molecular Phylogenetics and Evolution*, **131**, 138–148.
Weber, M. E., Golledge, N. R., Fogwill, C. J., Turney, C. S. M., & Thomas, Z. A. (2021). Decadal-scale onset and termination of Antarctic ice-mass loss during the last deglaciation. *Nature Communications*, **12**, 6683.
Weissman, D. B., & Hallatschek, O. (2017). Minimal-assumption inference from population-genomic data. *ELife*, **6**, e24836.
Whitelaw, B. L., Cooke, I. R., Finn, J., Da Fonseca, R. R., Ritschard, E. A., Gilbert, M. T. P., Simakov, O., & Strugnell, J. M. (2020). Adaptive venom evolution and toxicity in octopods is driven by extensive novel gene formation, expansion, and loss. *GigaScience*, **9**(11), giaa120.
Whitlock, M. C., & Lotterhos, K. E. (2015). Reliable Detection of Loci Responsible for Local Adaptation: Inference of a Null Model through Trimming the Distribution of F_{ST}. *American Naturalist*, **186**, S24–S36.
Wiernes, M. P., Sahade, R., Tatián, M., & Chiappero, M. B. (2013). Genetic variability and differentiation among polymorphic populations of the genus *Synoicum* (Tunicata, Ascidiacea) from the South Shetland Islands. *Polar Biology*, **36**(6), 871–883.
Wilkie, I. C., Barbaglio, A., Maclaren, W. M., & Candia Carnevali, M. D. (2010). Physiological and immunocytochemical evidence that glutamatergic neurotransmission is involved in the activation of arm autotomy in the featherstar *Antedon mediterránea* (Echinodermata: Crinoidea). *Journal of Experimental Biology*, **213**(12), 2104–2115.
Willis, K. J., & Whittaker, R. J. (2000). The Refugial Debate. *Science*, **287**(5457), 1406–1407.
Wilson, N. G., Hunter, R. L., Lockhart, S. J., & Halanych, K. M. (2007). Multiple lineages and absence of panmixia in the "circumpolar" crinoid *Promachocrinus kerguelensis* from the Atlantic sector of Antarctica. *Marine Biology*, **152**(4), 895–904.
Wilson, N. G., Maschek, J. A., & Baker, B. J. (2013). A Species Flock Driven by Predation? Secondary Metabolites Support Diversification of Slugs in Antarctica. *PLoS ONE*, **8**(11), e80277.
Wilson, N. G., Schrödl, M., & Halanych, K. M. (2009). Ocean barriers and glaciation: Evidence for explosive radiation of mitochondrial lineages in the Antarctic sea slug *Doris kerguelenensis* (Mollusca, Nudibranchia). *Molecular Ecology*, **18**(5), 965–984.
Wolf, J. B. W., & Ellegren, H. (2017). Making sense of genomic islands of differentiation in light of speciation. *Nature Reviews Genetics*, **18**(18), 87–100.
Wood, D. E., & Salzberg, S. L. (2014). Kraken: ultrafast metagenomic sequence classification using exact alignments. *Genome Biology*, **15**, R46.
Woodings, L. N., Murphy, N. P., Liggins, G. W., Miller, M. E., Ballinger, G. M., Lau, S. C. Y., & Strugnell, J. M. (2021). Population genomics of the Eastern Rock Lobster, *Sagmariasus verreauxi*, during spawning stock recovery from over-exploitation. *ICES Journal of Marine Science*, **78**(7), 2448–2459.
WoRMS Editorial Board. (2021). World Register of Marine Species. [tool source] Retreived from doi:10.14284/170

Wray, G. A., & Raff, R. A. (1991). The evolution of developmental strategy in marine invertebrates. *Trends in Ecology and Evolution*, **6**(2), 45–50.

Wright, S. (1931). Evolution in Mendelian Populations. *Genetics*, **16**(2), 97–159.

Wright, S. (1943). Isolation by Distance. *Genetics*, **28**(2), 114–138.

Xavier, J. C., Brandt, A., Ropert-Coudert, Y., Badhe, R., Gutt, J., Havermans, C., Jones, C., Costa, E. S., Lochte, K., Schloss, I. R., Kennicutt, M. C., & Sutherland, W. J. (2016). Future Challenges in Southern Ocean Ecology Research. *Frontiers in Marine Science*, **3**, 94.

Young, E. F., Belchier, M., Hauser, L., Horsburgh, G. J., Meredith, M. P., Murphy, E. J., Pascoal, S., Rock, J., Tysklind, N., & Carvalho, G. R. (2015). Oceanography and life history predict contrasting genetic population structure in two Antarctic fish species. *Evolutionary Applications*, **8**(5), 486–509.

Zarrella, I., Herten, K., Maes, G. E., Tai, S., Yang, M., Seuntjens, E., Ritschard, E A., Zach, M., Styfhals, R., Sanges, R., Simakov, O., Ponte, G., & Fiorito, G. (2019). The survey and reference assisted assembly of the *Octopus vulgaris* genome. *Scientific Data*, **6**(3), 13.

Zhang, J., Kobert, K., Flouri, T., & Stamatakis, A. (2014). PEAR: A fast and accurate Illumina Paired-End reAd mergeR. *Bioinformatics*, **30**(5), 614–620.

Zheng, C., Kuhner, M. K., & Thompson, E. A. (2014). Joint inference of identity by descent along multiple chromosomes from population samples. *Journal of Computational Biology*, **21**(3), 185–200.

Zhou, Y., Yuan, K., Yu, Y., Ni, X., Xie, P., Xing, E. P., & Xu, S. (2017). Inference of multiple-wave population admixture by modeling decay of linkage disequilibrium with polynomial functions. *Heredity*, **118**, 503–510.

Zweng, M. M., Reagan, J. R., Seidov, D., Boyer, T. P., Antonov, J. I., Locarnini, R. A., Garcia, H. E., Mishonov, A. V., Baranova, O. K., Weathers, K. W., Paver, C. R., & Smolyar, I. V. (2018). *World Ocean Atlas 2018, Volume 2: Salinity*. (A. Mishonov, Ed.), *World Ocean Atlas 2018*. NOAA Atlas NESDIS 82.

Supplementary Material

[blank page]

Supplementary Table 2.1 Sample information of all collected samples newly sequenced for this study, and GenBank accessions and associated sampling information from previous studies used in *Chapter 2*.

Genus	Species	Field ID	Registration ID	Sample locality (defined in this study)	Haplotype number in this study	GenBank accession from previous studies (if applicable)	Collection year	Expedition	Station ID	Event number	Latitude	Longitude	Collection depth (m)
Ophionotus	victoriae		IE.2009.4672	Adélie Land	1		2008	CEAMARC	70EV451		-66.409	140.508	1204
Ophionotus	victoriae		IE.2009.4676	Adélie Land	1		2008	CEAMARC	70EV451		-66.409	140.508	1204
Ophionotus	victoriae		IE.2009.4679	Adélie Land	1		2008	CEAMARC	70EV451		-66.409	140.508	1204
Ophionotus	victoriae		IE.2009.4690	Adélie Land	1		2007	CEAMARC	40EV152		-66.651	142.957	637
Ophionotus	victoriae		IE.2009.4726	Adélie Land	1		2007	CEAMARC	39EV141		-66.550	142.959	875
Ophionotus	victoriae		IE.2009.4734	Adélie Land	1		2008	CEAMARC	31EV268		-66.539	144.973	451
Ophionotus	victoriae		IE.2009.4753	Adélie Land	1		2008	CEAMARC	71EV447		-66.389	140.429	791
Ophionotus	victoriae		IE.2009.4763	Adélie Land	1		2008	CEAMARC	59EV259		-66.739	144.307	954
Ophionotus	victoriae		IE.2009.4675	Adélie Land	3		2008	CEAMARC	22EV503		-65.991	139.307	485
Ophionotus	victoriae		IE.2009.4754	Adélie Land	6		2007	CEAMARC	30EV66		-66.004	143.716	440
Ophionotus	victoriae	IE.2009.4687A	IE.2009.4687	Adélie Land	49		2008	CEAMARC	10EV420		-66.335	141.273	227
Ophionotus	victoriae		IE.2009.4702	Adélie Land	49		2007	CEAMARC	9EV117		-66.535	141.983	521
Ophionotus	victoriae		IE.2009.4703	Adélie Land	50		2008	CEAMARC	3EV411		-66.000	142.014	248
Ophionotus	victoriae		IE.2009.4707	Adélie Land	51		2008	CEAMARC	1EV405		-66.004	142.314	240
Ophionotus	victoriae		IE.2009.4713	Adélie Land	52		2007	CEAMARC	9EV117		-66.535	141.983	521
Ophionotus	victoriae		IE.2009.4731	Adélie Land	53		2007	CEAMARC	30EV66		-66.004	143.716	440
Ophionotus	victoriae		IE.2009.4767	Adélie Land	54		2007	CEAMARC	4EV112		-66.316	142.000	257
Ophionotus	victoriae	DSOPH2346		Amundsen Sea	1	FJ917337	2008	JR179	BIO6-AGT-1B		-71.152	-110.013	1491
Ophionotus	victoriae	DSOPH2571		Amundsen Sea	1	FJ917337	2008	JR179	BIO6-AGT-2A		-71.175	-109.863	1080
Ophionotus	victoriae	DSOPH2204		Amundsen Sea	14	FJ917310	2008	JR179	BIO6-AGT-2A		-71.175	-109.863	1080
Ophionotus	victoriae	DSOPH2257		Amundsen Sea	25	FJ917319	2008	JR179	BIO6-AGT-2C		-71.182	-109.926	987
Ophionotus	victoriae	DSOPH2568		Amundsen Sea	43	FJ917348	2008	JR179	BIO4-AGT-2C		-74.477	-104.257	1151
Ophionotus	victoriae	DSOPH2203		Amundsen Sea	49	KY048234	2008	JR179	BIO6-AGT-2A		-71.175	-109.863	1080
Ophionotus	victoriae	DSOPH2207		Amundsen Sea	49	KY048234	2008	JR179	BIO6-AGT-2A		-71.175	-109.863	1080
Ophionotus	victoriae	DSOPH2218		Amundsen Sea	49	KY048234	2008	JR179	BIO6-AGT-2A		-71.175	-109.863	1080
Ophionotus	victoriae	DSOPH2198		Amundsen Sea	58	KY048231	2008	JR179	BIO6-AGT-2B		-71.179	-109.894	998
Ophionotus	victoriae	DSOPH2212		Amundsen Sea	58	KY048231	2008	JR179	BIO6-AGT-2A		-71.175	-109.863	1080

Ophionotus	victoriae	DSOPH2251	Amundsen Sea	58	KY048231	2008	JR179	BIO6-AGT-2C	-71.182	-109.926	987
Ophionotus	victoriae	DSOPH2678	Amundsen Sea	58	KY048231	2008	JR179	BIO4-AGT-2C	-74.477	-104.257	1151
Ophionotus	victoriae	DSOPH2685	Amundsen Sea	58	KY048231	2008	JR179	BIO4-AGT-2C	-74.477	-104.257	1151
Ophionotus	victoriae	DSOPH2734	Amundsen Sea	58	KY048231	2008	JR179	BIO6-AGT-2B	-71.179	-109.894	998
Ophionotus	victoriae	DSOPH2186	Amundsen Sea	62	KY048226	2008	JR179	BIO6-AGT-2B	-71.179	-109.894	998
Ophionotus	victoriae	DSOPH2215	Amundsen Sea	62	KY048226	2008	JR179	BIO6-AGT-2A	-71.175	-109.863	1080
Ophionotus	victoriae	DSOPH2217	Amundsen Sea	62	KY048226	2008	JR179	BIO6-AGT-2A	-71.175	-109.863	1080
Ophionotus	victoriae	DSOPH2254	Amundsen Sea	62	KY048226	2008	JR179	BIO6-AGT-2C	-71.182	-109.926	987
Ophionotus	victoriae	DSOPH2256	Amundsen Sea	62	KY048226	2008	JR179	BIO6-AGT-2C	-71.182	-109.926	987
Ophionotus	victoriae	DSOPH2258	Amundsen Sea	62	KY048226	2008	JR179	BIO6-AGT-2C	-71.182	-109.926	987
Ophionotus	victoriae	DSOPH2684	Amundsen Sea	62	KY048226	2008	JR179	BIO4-AGT-2C	-74.477	-104.257	1151
Ophionotus	victoriae	DSOPH2699	Amundsen Sea	62	KY048226	2008	JR179	BIO6-AGT-2A	-71.175	-109.863	1080
Ophionotus	victoriae	DSOPH2743	Amundsen Sea	62	KY048226	2008	JR179	BIO6-AGT-2B	-71.179	-109.894	998
Ophionotus	victoriae	DSOPH2187	Amundsen Sea	63	KY048227	2008	JR179	BIO6-AGT-2B	-71.179	-109.894	998
Ophionotus	victoriae	DSOPH2191	Amundsen Sea	64	KY048228	2008	JR179	BIO6-AGT-2B	-71.179	-109.894	998
Ophionotus	victoriae	DSOPH2199	Amundsen Sea	64	KY048228	2008	JR179	BIO6-AGT-2A	-71.175	-109.863	1080
Ophionotus	victoriae	DSOPH2229	Amundsen Sea	64	KY048228	2008	JR179	BIO6-AGT-2A	-71.175	-109.863	1080
Ophionotus	victoriae	DSOPH2255	Amundsen Sea	64	KY048228	2008	JR179	BIO6-AGT-2C	-71.182	-109.926	987
Ophionotus	victoriae	DSOPH2273	Amundsen Sea	64	KY048228	2008	JR179	BIO6-AGT-2C	-71.182	-109.926	987
Ophionotus	victoriae	DSOPH2566	Amundsen Sea	64	KY048237	2008	JR179	BIO4-AGT-2A	-74.479	-104.237	1208
Ophionotus	victoriae	DSOPH2733	Amundsen Sea	64	KY048228	2008	JR179	BIO6-AGT-2B	-71.179	-109.894	998
Ophionotus	victoriae	DSOPH2736	Amundsen Sea	64	KY048228	2008	JR179	BIO6-AGT-2B	-71.179	-109.894	998
Ophionotus	victoriae	DSOPH2193	Amundsen Sea	65	KY048229	2008	JR179	BIO6-AGT-2B	-71.179	-109.894	998
Ophionotus	victoriae	DSOPH2206	Amundsen Sea	65	KY048229	2008	JR179	BIO6-AGT-2A	-71.175	-109.863	1080
Ophionotus	victoriae	DSOPH2208	Amundsen Sea	65	KY048229	2008	JR179	BIO6-AGT-2A	-71.175	-109.863	1080
Ophionotus	victoriae	DSOPH2211	Amundsen Sea	65	KY048229	2008	JR179	BIO6-AGT-2A	-71.175	-109.863	1080
Ophionotus	victoriae	DSOPH2216	Amundsen Sea	65	KY048229	2008	JR179	BIO6-AGT-2A	-71.175	-109.863	1080
Ophionotus	victoriae	DSOPH2230	Amundsen Sea	65	KY048229	2008	JR179	BIO6-AGT-2A	-71.175	-109.863	1080

Ophionotus	victoriae	DSOPH2252	Amundsen Sea	65	KY048229	2008	JR179	BIO6-AGT-2C	-71.182	-109.926	987
Ophionotus	victoriae	DSOPH2259	Amundsen Sea	65	KY048229	2008	JR179	BIO6-AGT-2C	-71.182	-109.926	987
Ophionotus	victoriae	DSOPH2272	Amundsen Sea	65	KY048229	2008	JR179	BIO6-AGT-2C	-71.182	-109.926	987
Ophionotus	victoriae	DSOPH2676	Amundsen Sea	65	KY048229	2008	JR179	BIO4-AGT-2B	-74.480	-104.255	1163
Ophionotus	victoriae	DSOPH2738	Amundsen Sea	65	KY048229	2008	JR179	BIO6-AGT-2B	-71.179	-109.894	998
Ophionotus	victoriae	DSOPH2195	Amundsen Sea	66	KY048230	2008	JR179	BIO6-AGT-2B	-71.179	-109.894	998
Ophionotus	victoriae	DSOPH2213	Amundsen Sea	66	KY048230	2008	JR179	BIO6-AGT-2A	-71.175	-109.863	1080
Ophionotus	victoriae	DSOPH2253	Amundsen Sea	66	KY048230	2008	JR179	BIO6-AGT-2C	-71.182	-109.926	987
Ophionotus	victoriae	DSOPH2260	Amundsen Sea	66	KY048230	2008	JR179	BIO6-AGT-2C	-71.182	-109.926	987
Ophionotus	victoriae	DSOPH2264	Amundsen Sea	66	KY048230	2008	JR179	BIO6-AGT-2C	-71.182	-109.926	987
Ophionotus	victoriae	DSOPH2359	Amundsen Sea	66	KY048230	2008	JR179	BIO6-AGT-1A	-71.146	-109.971	1531
Ophionotus	victoriae	DSOPH2680	Amundsen Sea	66	KY048230	2008	JR179	BIO4-AGT-2C	-74.477	-104.257	1151
Ophionotus	victoriae	DSOPH2730	Amundsen Sea	66	KY048230	2008	JR179	BIO6-AGT-2B	-71.179	-109.894	998
Ophionotus	victoriae	DSOPH2732	Amundsen Sea	66	KY048230	2008	JR179	BIO6-AGT-2B	-71.179	-109.894	998
Ophionotus	victoriae	DSOPH2747	Amundsen Sea	66	KY048230	2008	JR179	BIO6-AGT-2B	-71.179	-109.894	998
Ophionotus	victoriae	DSOPH2753	Amundsen Sea	66	KY048230	2008	JR179	BIO6-AGT-2B	-71.179	-109.894	998
Ophionotus	victoriae	DSOPH678	Amundsen Sea	66	KY048230	2008	JR179	BIO5-AGT-3C	-73.986	-107.390	542
Ophionotus	victoriae	DSOPH2200	Amundsen Sea	67	KY048232	2008	JR179	BIO6-AGT-2A	-71.175	-109.863	1080
Ophionotus	victoriae	DSOPH2276	Amundsen Sea	67	KY048232	2008	JR179	BIO6-AGT-2C	-71.182	-109.926	987
Ophionotus	victoriae	DSOPH2201	Amundsen Sea	68	KY048233	2008	JR179	BIO6-AGT-2A	-71.175	-109.863	1080
Ophionotus	victoriae	DSOPH2202	Amundsen Sea	68	KY048233	2008	JR179	BIO6-AGT-2A	-71.175	-109.863	1080
Ophionotus	victoriae	DSOPH2209	Amundsen Sea	68	KY048233	2008	JR179	BIO6-AGT-2A	-71.175	-109.863	1080
Ophionotus	victoriae	DSOPH2731	Amundsen Sea	68	KY048233	2008	JR179	BIO6-AGT-2B	-71.179	-109.894	998
Ophionotus	victoriae	DSOPH2752	Amundsen Sea	68	KY048233	2008	JR179	BIO6-AGT-2B	-71.179	-109.894	998
Ophionotus	victoriae	DSOPH2205	Amundsen Sea	69	KY048235	2008	JR179	BIO6-AGT-2A	-71.175	-109.863	1080
Ophionotus	victoriae	DSOPH2275	Amundsen Sea	70	KY048236	2008	JR179	BIO6-AGT-2C	-71.182	-109.926	987
Ophionotus	victoriae	DSOPH2567	Amundsen Sea	71	KY048238	2008	JR179	BIO4-AGT-2B	-74.480	-104.255	1163
Ophionotus	victoriae	DSOPH2729	Amundsen Sea	72	KY048239	2008	JR179	BIO6-AGT-2B	-71.179	-109.894	998

Ophionotus	victoriae	DSOPH2742		Amundsen Sea	73	KY048240	2008	JR179	BIO6-AGT-2B		-71.179	-109.894	998
Ophionotus	victoriae	N0098	NIWA84670	Balleny Islands	1		2006	TAN0602		448	-66.557	162.570	85
Ophionotus	victoriae	81991A	NIWA81991	Balleny Islands	24		2001	TAN0102		K0807	-67.568	164.958	148
Ophionotus	victoriae	81991B	NIWA81991	Balleny Islands	24		2001	TAN0102		K0807	-67.568	164.958	148
Ophionotus	victoriae	94857A	NIWA94857	Balleny Islands	24		2004	TAN0402		233	-67.418	163.915	227
Ophionotus	victoriae	94857B	NIWA94857	Balleny Islands	24		2004	TAN0402		233	-67.418	163.915	227
Ophionotus	victoriae	N0081	NIWA84670	Balleny Islands	24		2006	TAN0602		448	-66.557	162.570	85
Ophionotus	victoriae	N0083	NIWA84670	Balleny Islands	24		2006	TAN0602		448	-66.557	162.570	85
Ophionotus	victoriae	N0084	NIWA84670	Balleny Islands	24		2006	TAN0602		448	-66.557	162.570	85
Ophionotus	victoriae	N0085	NIWA84670	Balleny Islands	24		2006	TAN0602		448	-66.557	162.570	85
Ophionotus	victoriae	N0086	NIWA84670	Balleny Islands	24		2006	TAN0602		448	-66.557	162.570	85
Ophionotus	victoriae	N0088	NIWA84670	Balleny Islands	24		2006	TAN0602		448	-66.557	162.570	85
Ophionotus	victoriae	N0089	NIWA84670	Balleny Islands	24		2006	TAN0602		448	-66.557	162.570	85
Ophionotus	victoriae	N0090	NIWA84670	Balleny Islands	24		2006	TAN0602		448	-66.557	162.570	85
Ophionotus	victoriae	N0091	NIWA84670	Balleny Islands	24		2006	TAN0602		448	-66.557	162.570	85
Ophionotus	victoriae	N0092	NIWA84670	Balleny Islands	24		2006	TAN0602		448	-66.557	162.570	85
Ophionotus	victoriae	N0093	NIWA84670	Balleny Islands	24		2006	TAN0602		448	-66.557	162.570	85
Ophionotus	victoriae	N0095	NIWA84670	Balleny Islands	24		2006	TAN0602		448	-66.557	162.570	85
Ophionotus	victoriae	N0096	NIWA84670	Balleny Islands	24		2006	TAN0602		448	-66.557	162.570	85
Ophionotus	victoriae	N0097	NIWA84670	Balleny Islands	24		2006	TAN0602		448	-66.557	162.570	85
Ophionotus	victoriae	WAMZ44963	WAMZ44963	Balleny Islands	24		2017	ACE 2016/17	46	1209	-66.174	162.203	350
Ophionotus	victoriae	WAMZ44964	WAMZ44964	Balleny Islands	24		2017	ACE 2016/17	46	1209	-66.174	162.203	350
Ophionotus	victoriae	WAMZ44966	WAMZ44966	Balleny Islands	24		2017	ACE 2016/17	46	1209	-66.174	162.203	350
Ophionotus	victoriae	WAMZ44967	WAMZ44967	Balleny Islands	24		2017	ACE 2016/17	46	1209	-66.174	162.203	350
Ophionotus	victoriae	WAMZ44968	WAMZ44968	Balleny Islands	24		2017	ACE 2016/17	46	1209	-66.174	162.203	350
Ophionotus	victoriae	WAMZ44970	WAMZ44970	Balleny Islands	24		2017	ACE 2016/17	46	1209	-66.174	162.203	350
Ophionotus	victoriae	WAMZ44971	WAMZ44971	Balleny Islands	24		2017	ACE 2016/17	46	1209	-66.174	162.203	350
Ophionotus	victoriae	WAMZ44972	WAMZ44972	Balleny Islands	24		2017	ACE 2016/17	46	1209	-66.174	162.203	350
Ophionotus	victoriae	WAMZ44973	WAMZ44973	Balleny Islands	24		2017	ACE 2016/17	46	1209	-66.174	162.203	350
Ophionotus	victoriae	WAMZ44974	WAMZ44974	Balleny Islands	24		2017	ACE 2016/17	46	1209	-66.174	162.203	350
Ophionotus	victoriae	WAMZ44975	WAMZ44975	Balleny Islands	24		2017	ACE 2016/17	46	1209	-66.174	162.203	350
Ophionotus	victoriae	WAMZ44976	WAMZ44976	Balleny Islands	24		2017	ACE 2016/17	46	1209	-66.174	162.203	350
Ophionotus	victoriae	WAMZ44977	WAMZ44977	Balleny Islands	24		2017	ACE 2016/17	46	1209	-66.174	162.203	350
Ophionotus	victoriae	WAMZ44978	WAMZ44978	Balleny Islands	24		2017	ACE 2016/17	46	1209	-66.174	162.203	350
Ophionotus	victoriae	WAMZ44979	WAMZ44979	Balleny Islands	24		2017	ACE 2016/17	46	1209	-66.174	162.203	350
Ophionotus	victoriae	WAMZ44980	WAMZ44980	Balleny Islands	24		2017	ACE 2016/17	46	1209	-66.174	162.203	350
Ophionotus	victoriae	WAMZ44982	WAMZ44982	Balleny Islands	24		2017	ACE 2016/17	46	1209	-66.174	162.203	350
Ophionotus	victoriae	WAMZ44983	WAMZ44983	Balleny Islands	24		2017	ACE 2016/17	46	1209	-66.174	162.203	350
Ophionotus	victoriae	WAMZ44984	WAMZ44984	Balleny Islands	24		2017	ACE 2016/17	46	1209	-66.174	162.203	350
Ophionotus	victoriae	WAMZ44969	WAMZ44969	Balleny Islands	93		2017	ACE 2016/17	46	1209	-66.174	162.203	350

Ophionotus	victoriae	N0078	NIWA84670	Balleny Islands	96		2006	TAN0602		448	-66.557	162.570	85
Ophionotus	victoriae	WAMZ44965	WAMZ44965	Balleny Islands	96		2017	ACE 2016/17	46	1209	-66.174	162.203	350
Ophionotus	victoriae	N0079	NIWA84670	Balleny Islands	97		2006	TAN0602		448	-66.557	162.570	85
Ophionotus	victoriae	N0080	NIWA84670	Balleny Islands	98		2006	TAN0602		448	-66.557	162.570	85
Ophionotus	victoriae	N0082	NIWA84670	Balleny Islands	99		2006	TAN0602		448	-66.557	162.570	85
Ophionotus	victoriae	N0087	NIWA84670	Balleny Islands	100		2006	TAN0602		448	-66.557	162.570	85
Ophionotus	victoriae	N0094	NIWA84670	Balleny Islands	101		2006	TAN0602		448	-66.557	162.570	85
Ophionotus	victoriae	WAMZ44962	WAMZ44962	Balleny Islands	156		2017	ACE 2016/17	46	1209	-66.174	162.203	350
Ophionotus	victoriae	WAMZ44981	WAMZ44981	Balleny Islands	157		2017	ACE 2016/17	46	1209	-66.174	162.203	350
Ophionotus	victoriae	Op531_3E_11		Bellingshausen Sea	1	FJ917337	2013	NBP-12-10	3		-71.699	-93.694	670
Ophionotus	victoriae	Op531_3E_6		Bellingshausen Sea	62	KY048226	2013	NBP-12-10	3		-71.699	-93.694	670
Ophionotus	victoriae	Op531_3E_13		Bellingshausen Sea	64	KY048228	2013	NBP-12-10	3		-71.699	-93.694	670
Ophionotus	victoriae	Op531_3E_9		Bellingshausen Sea	64	KY048228	2013	NBP-12-10	3		-71.699	-93.694	670
Ophionotus	victoriae	Op531_3E_4		Bellingshausen Sea	72	KY048239	2013	NBP-12-10	3		-71.699	-93.694	670
Ophionotus	victoriae	Op531_3E_8		Bellingshausen Sea	72	KY048239	2013	NBP-12-10	3		-71.699	-93.694	670
Ophionotus	victoriae	Op531_3E_10		Bellingshausen Sea	88	KY048258	2013	NBP-12-10	3		-71.699	-93.694	670
Ophionotus	victoriae	OP531_3E_12		Bellingshausen Sea	89	KY048259	2013	NBP-12-10	3		-71.699	-93.694	670
Ophionotus	victoriae	Op531_3E_5		Bellingshausen Sea	90	KY048260	2013	NBP-12-10	3		-71.699	-93.694	670
Ophionotus	victoriae	196.1E.10		Bouvet Island	4	FJ917313	2006	LMG-04-14	50		-56.007	2.601	648
Ophionotus	victoriae	WAMZ44952	WAMZ44952	Bouvet Island	4		2017	ACE 2016/17	98	2765	-54.419	-3.494	300
Ophionotus	victoriae	WAMZ44954	WAMZ44954	Bouvet Island	4		2017	ACE 2016/17	98	2765	-54.419	-3.494	300
Ophionotus	victoriae	177.1E.01		Bouvet Island	28	FJ917324	2004	LMG-04-14	58		-54.817	-3.500	169
Ophionotus	victoriae	177.1E.05		Bouvet Island	28	FJ917324	2004	LMG-04-14	58		-54.817	-3.500	169
Ophionotus	victoriae	196.1E.07		Bouvet Island	28	FJ917324	2006	LMG-04-14	50		-56.007	2.601	684
Ophionotus	victoriae	DSOPH3146		Bouvet Island	28	FJ917324	2011	Polarstern ANT-XXVII/3	PS77_312-4		-54.481	3.189	300
Ophionotus	victoriae	SA6 (haplotype ID)		Bouvet Island	29	FJ917325	2004	Nathaniel B. Palmer			-54.817	-3.500	169
Ophionotus	victoriae	WAMZ44951	WAMZ44951	Bouvet Island	29		2017	ACE 2016/17	98	2765	-54.419	-3.494	300
Ophionotus	victoriae	WAMZ44953	WAMZ44953	Bouvet Island	29		2017	ACE 2016/17	98	2765	-54.419	-3.494	300
Ophionotus	victoriae	WAMZ44947	WAMZ44947	Bouvet Island	30		2017	ACE 2016/17	98	2765	-54.419	-3.494	300
Ophionotus	victoriae	WAMZ44948	WAMZ44948	Bouvet Island	30		2017	ACE 2016/17	98	2765	-54.419	-3.494	300
Ophionotus	victoriae	WAMZ44949	WAMZ44949	Bouvet Island	30		2017	ACE 2016/17	98	2765	-54.419	-3.494	300
Ophionotus	victoriae	WAMZ44950	WAMZ44950	Bouvet Island	30		2017	ACE 2016/17	98	2765	-54.419	-3.494	300
Ophionotus	victoriae	WAMZ44957	WAMZ44957	Bouvet Island	30		2017	ACE 2016/17	98	2765	-54.419	-3.494	300
Ophionotus	victoriae	WAMZ44958	WAMZ44958	Bouvet Island	30		2017	ACE 2016/17	98	2765	-54.419	-3.494	300
Ophionotus	victoriae	WAMZ44961	WAMZ44961	Bouvet Island	30		2017	ACE 2016/17	98	2765	-54.419	-3.494	300

Ophionotus	victoriae	196.1E.03		Bouvet Island	37	FJ917336	2006	LMG-04-14	50		-56.007	2.601	548
Ophionotus	victoriae	DSOPH3044		Bouvet Island	77	KY048245	2011	Polarstern ANT-XXVII/3	PS77_312-2		-54.470	3.185	296
Ophionotus	victoriae	DSOPH3158		Bouvet Island	80	KY048249	2011	Polarstern ANT-XXVII/3	PS77_312-3		-54.502	3.225	264
Ophionotus	victoriae	DSOPH3159		Bouvet Island	81	KY048250	2011	Polarstern ANT-XXVII/3	PS77_312-3		-54.502	3.225	264
Ophionotus	victoriae	DSOPH3226		Bouvet Island	82	KY048251	2011	Polarstern ANT-XXVII/3	PS77_312-2		-54.470	3.185	296
Ophionotus	victoriae	WAMZ44955	WAMZ44955	Bouvet Island	152		2017	ACE 2016/17	98	2765	-54.419	-3.494	300
Ophionotus	victoriae	WAMZ44956	WAMZ44956	Bouvet Island	153		2017	ACE 2016/17	98	2765	-54.419	-3.494	300
Ophionotus	victoriae	WAMZ44959	WAMZ44959	Bouvet Island	154		2017	ACE 2016/17	98	2765	-54.419	-3.494	300
Ophionotus	victoriae	WAMZ44960	WAMZ44960	Bouvet Island	155		2017	ACE 2016/17	98	2765	-54.419	-3.494	300
Ophionotus	victoriae	177.1E.02		Bouvet Island	29	FJ917327	2004	LMG-04-14	58		-54.817	-3.500	169
Ophionotus	victoriae	177.1E.06		Bouvet Island	29	FJ917327	2004	LMG-04-14	58		-54.817	-3.500	169
Ophionotus	victoriae	177.1E.09		Bouvet Island	29	FJ917327	2004	LMG-04-14	58		-54.817	-3.500	169
Ophionotus	victoriae	177.1E.11		Bouvet Island	29	FJ917327	2004	LMG-04-14	58		-54.817	-3.500	169
Ophionotus	victoriae	DSOPH3144		Bouvet Island	29	FJ917327	2001	Polarstern ANT-XXVII/3	PS77_312-4		-54.481	3.189	300
Ophionotus	victoriae	177.1E.04		Bouvet Island	30	FJ917326	2004	LMG-04-14	58		-54.817	-3.500	169
Ophionotus	victoriae	177.1E.07		Bouvet Island	30	FJ917326	2004	LMG-04-14	58		-54.817	-3.500	169
Ophionotus	victoriae	177.1E.10		Bouvet Island	30	FJ917326	2004	LMG-04-14	58		-54.817	-3.500	169
Ophionotus	victoriae	177.1E.12		Bouvet Island	30	FJ917326	2004	LMG-04-14	58		-54.817	-3.500	169
Ophionotus	victoriae	196.1E.01		Bouvet Island	30	FJ917326	2004	LMG-04-14	50		-56.007	2.601	648
Ophionotus	victoriae	196.1E.04		Bouvet Island	30	FJ917326	2004	LMG-04-14	50		-56.007	2.601	648
Ophionotus	victoriae	196.1E.05		Bouvet Island	30	FJ917326	2004	LMG-04-14	50		-56.007	2.601	648
Ophionotus	victoriae	196.1E.06		Bouvet Island	30	FJ917326	2004	LMG-04-14	50		-56.007	2.601	648
Ophionotus	victoriae	196.1E.08		Bouvet Island	30	FJ917326	2004	LMG-04-14	50		-56.007	2.601	648
Ophionotus	victoriae	DSOPH3043		Bouvet Island	30	FJ917326	2011	Polarstern ANT-XXVII/3	PS77_312-2		-54.470	3.185	296
Ophionotus	victoriae	DSOPH3045		Bouvet Island	30	FJ917326	2011	Polarstern ANT-XXVII/3	PS77_312-2		-54.470	3.185	296
Ophionotus	victoriae	DSOPH3046		Bouvet Island	30	FJ917326	2011	Polarstern ANT-XXVII/3	PS77_312-2		-54.470	3.185	296
Ophionotus	victoriae	DSOPH3145		Bouvet Island	30	FJ917326	2011	Polarstern ANT-XXVII/3	PS77_312-4		-54.481	3.189	300
Ophionotus	victoriae	DSOPH3147		Bouvet Island	30	FJ917326	2011	Polarstern ANT-XXVII/3	PS77_312-4		-54.481	3.189	300
Ophionotus	victoriae	DSOPH3157		Bouvet Island	30	FJ917326	2011	Polarstern ANT-XXVII/3	PS77_312-3		-54.502	3.225	264
Ophionotus	victoriae	DSOPH3160		Bouvet Island	30	FJ917326	2011	Polarstern ANT-XXVII/3	PS77_312-3		-54.502	3.225	264
Ophionotus	victoriae	SIOBICP00524B	SIOBICE5524	Bransfield Strait	1		2012	Polarstern ANT-XXVIII/4		79279	-62.278	-55.833	324
Ophionotus	victoriae	SIOBICP00524I	SIOBICE5524	Bransfield Strait	1		2012	Polarstern ANT-XXVIII/4		79279	-62.278	-55.833	324
Ophionotus	victoriae	E82.2C.01		Bransfield Strait	1	FJ917339	2004	LMG-04-14	47		-62.850	-59.460	900
Ophionotus	victoriae	E82.2C.02		Bransfield Strait	1	FJ917339	2004	LMG-04-14	47		-62.850	-59.460	900

Ophionotus	victoriae	E82.2C.04		Bransfield Strait	1	FJ917337	2006	LMG-04-14	47		-62.850	-59.460	900
Ophionotus	victoriae	E82.2C.05		Bransfield Strait	1	FJ917337	2006	LMG-04-14	47		-62.850	-59.460	900
Ophionotus	victoriae	Op877_2E_1		Bransfield Strait	1	FJ917339	2013	LMG-13-12	4		-62.996	-58.599	320
Ophionotus	victoriae	Op877_2E_3		Bransfield Strait	1	FJ917337	2013	LMG-13-12	4		-62.996	-58.599	320
Ophionotus	victoriae	Op877_2E_7		Bransfield Strait	1	FJ917337	2013	LMG-13-12	4		-62.996	-58.599	320
Ophionotus	victoriae	Op877_2E_8		Bransfield Strait	1	FJ917339	2013	LMG-13-12	4		-62.996	-58.599	320
Ophionotus	victoriae	Op877_2E_9		Bransfield Strait	1	FJ917337	2013	LMG-13-12	4		-62.996	-58.599	320
Ophionotus	victoriae	Op877_2E_5		Bransfield Strait	3	FJ917340	2013	LMG-13-12	4		-62.996	-58.599	320
Ophionotus	victoriae	92.10C		Bransfield Strait	4	FJ917313	2004	LMG-04-14	51		-63.384	-60.060	277
Ophionotus	victoriae	SIOBICP00496A	SIOBICE5492	Bransfield Strait	4		2012	Polarstern ANT-XXVIII/4		79273	-62.367	-55.961	349
Ophionotus	victoriae	SIOBICP00496R	SIOBICE5492	Bransfield Strait	4		2012	Polarstern ANT-XXVIII/4		79273	-62.367	-55.961	349
Ophionotus	victoriae	92.16C		Bransfield Strait	5	FJ917320	2004	LMG-04-14	51		-63.384	-60.060	277
Ophionotus	victoriae	SIOBICP00496B	SIOBICE5492	Bransfield Strait	5		2012	Polarstern ANT-XXVIII/4		79273	-62.367	-55.961	349
Ophionotus	victoriae	SIOBICP00496D	SIOBICE5492	Bransfield Strait	5		2012	Polarstern ANT-XXVIII/4		79273	-62.367	-55.961	349
Ophionotus	victoriae	SIOBICP00496F	SIOBICE5492	Bransfield Strait	5		2012	Polarstern ANT-XXVIII/4		79273	-62.367	-55.961	349
Ophionotus	victoriae	SIOBICP00496H	SIOBICE5492	Bransfield Strait	5		2012	Polarstern ANT-XXVIII/4		79273	-62.367	-55.961	349
Ophionotus	victoriae	SIOBICP00496K	SIOBICE5492	Bransfield Strait	5		2012	Polarstern ANT-XXVIII/4		79273	-62.367	-55.961	349
Ophionotus	victoriae	SIOBICP00496N	SIOBICE5492	Bransfield Strait	5		2012	Polarstern ANT-XXVIII/4		79273	-62.367	-55.961	349
Ophionotus	victoriae	SIOBICP00496O	SIOBICE5492	Bransfield Strait	5		2012	Polarstern ANT-XXVIII/4		79273	-62.367	-55.961	349
Ophionotus	victoriae	SIOBICP00496T	SIOBICE5492	Bransfield Strait	5		2012	Polarstern ANT-XXVIII/4		79273	-62.367	-55.961	349
Ophionotus	victoriae	Op877_2E_10		Bransfield Strait	5	FJ917320	2013	LMG-13-12	4		-62.996	-58.599	320
Ophionotus	victoriae	Op877_2E_4		Bransfield Strait	5	FJ917320	2013	LMG-13-12	4		-62.996	-58.599	320
Ophionotus	victoriae	Op877_2E_6		Bransfield Strait	5	FJ917320	2013	LMG-13-12	4		-62.996	-58.599	320
Ophionotus	victoriae	SIOBICS6316F	SIOBICE4770	Bransfield Strait	5		2011	Scotia 2011	BS2	89	-63.343	-59.910	213
Ophionotus	victoriae	SIOBICS6338B	SIOBICE4781	Bransfield Strait	5		2011	Scotia 2011	BS2	90	-63.283	-59.903	290
Ophionotus	victoriae	SIOBICS6338F	SIOBICE4781	Bransfield Strait	5		2011	Scotia 2011	BS2	90	-63.283	-59.903	290
Ophionotus	victoriae	SIOBICS6760B	SIOBICE4777	Bransfield Strait	5		2011	Scotia 2011	BS1	87	-62.753	-57.322	292
Ophionotus	victoriae	SIOBICS6760G	SIOBICE4777	Bransfield Strait	5		2011	Scotia 2011	BS1	87	-62.753	-57.322	292
Ophionotus	victoriae	92.14C		Bransfield Strait	6	FJ917309	2004	LMG-04-14	51		-63.384	-60.060	277
Ophionotus	victoriae	92.9C		Bransfield Strait	6	FJ917309	2004	LMG-04-14	51		-63.384	-60.060	277
Ophionotus	victoriae	SIOBICP00496C	SIOBICE5492	Bransfield Strait	6		2012	Polarstern ANT-XXVIII/4		79273	-62.367	-55.961	349
Ophionotus	victoriae	SIOBICP00496G	SIOBICE5492	Bransfield Strait	6		2012	Polarstern ANT-XXVIII/4		79273	-62.367	-55.961	349
Ophionotus	victoriae	SIOBICP00496I	SIOBICE5492	Bransfield Strait	6		2012	Polarstern ANT-XXVIII/4		79273	-62.367	-55.961	349
Ophionotus	victoriae	SIOBICP00524A	SIOBICE5524	Bransfield Strait	6		2012	Polarstern ANT-XXVIII/4		79279	-62.278	-55.833	324

Ophionotus	victoriae	SIOBICS6316D	SIOBICE4770	Bransfield Strait	6		2011	Scotia 2011	BS2	89	-63.343	-59.910	213
Ophionotus	victoriae	SIOBICS6316H	SIOBICE4770	Bransfield Strait	6		2011	Scotia 2011	BS2	89	-63.343	-59.910	213
Ophionotus	victoriae	SIOBICS6338D	SIOBICE4781	Bransfield Strait	6		2011	Scotia 2011	BS2	90	-63.283	-59.903	290
Ophionotus	victoriae	SIOBICS6760C	SIOBICE4777	Bransfield Strait	6		2011	Scotia 2011	BS1	87	-62.753	-57.322	292
Ophionotus	victoriae	SIOBICS6905B	SIOBICE5162	Bransfield Strait	6		2011	Scotia 2011	BS1	86	-62.870	-57.217	247
Ophionotus	victoriae	SIOBICS6905K	SIOBICE5162	Bransfield Strait	6		2011	Scotia 2011	BS1	86	-62.870	-57.217	247
Ophionotus	victoriae	SIOBICP00496E	SIOBICE5492	Bransfield Strait	7		2012	Polarstern ANT-XXVIII/4		79273	-62.367	-55.961	349
Ophionotus	victoriae	SIOBICP00496J	SIOBICE5492	Bransfield Strait	7		2012	Polarstern ANT-XXVIII/4		79273	-62.367	-55.961	349
Ophionotus	victoriae	SIOBICP00496P	SIOBICE5492	Bransfield Strait	7		2012	Polarstern ANT-XXVIII/4		79273	-62.367	-55.961	349
Ophionotus	victoriae	SIOBICS6316G	SIOBICE4770	Bransfield Strait	7		2011	Scotia 2011	BS2	89	-63.343	-59.910	213
Ophionotus	victoriae	SIOBICS6338C	SIOBICE4781	Bransfield Strait	7		2011	Scotia 2011	BS2	90	-63.283	-59.903	290
Ophionotus	victoriae	SIOBICS6338G	SIOBICE4781	Bransfield Strait	7		2011	Scotia 2011	BS2	90	-63.283	-59.903	290
Ophionotus	victoriae	SIOBICS6338J	SIOBICE4781	Bransfield Strait	7		2011	Scotia 2011	BS2	90	-63.283	-59.903	290
Ophionotus	victoriae	SIOBICS6760F	SIOBICE4777	Bransfield Strait	7		2011	Scotia 2011	BS1	87	-62.753	-57.322	292
Ophionotus	victoriae	SIOBICS6905A	SIOBICE5162	Bransfield Strait	7		2011	Scotia 2011	BS1	86	-62.870	-57.217	247
Ophionotus	victoriae	SIOBICS6905D	SIOBICE5162	Bransfield Strait	7		2011	Scotia 2011	BS1	86	-62.870	-57.217	247
Ophionotus	victoriae	SIOBICS6905E	SIOBICE5162	Bransfield Strait	7		2011	Scotia 2011	BS1	86	-62.870	-57.217	247
Ophionotus	victoriae	SIOBICS6905L	SIOBICE5162	Bransfield Strait	7		2011	Scotia 2011	BS1	86	-62.870	-57.217	247
Ophionotus	victoriae	92.11C		Bransfield Strait	8	FJ917316	2004	LMG-04-14	51		-63.384	-60.060	277
Ophionotus	victoriae	92.13C		Bransfield Strait	8	FJ917316	2004	LMG-04-14	51		-63.384	-60.060	277
Ophionotus	victoriae	92.15C		Bransfield Strait	8	FJ917316	2004	LMG-04-14	51		-63.384	-60.060	277
Ophionotus	victoriae	92.17C		Bransfield Strait	8	FJ917316	2004	LMG-04-14	51		-63.384	-60.060	277
Ophionotus	victoriae	92.5C		Bransfield Strait	8	FJ917316	2004	LMG-04-14	51		-63.384	-60.060	277
Ophionotus	victoriae	92.6C		Bransfield Strait	8	FJ917316	2004	LMG-04-14	51		-63.384	-60.060	277
Ophionotus	victoriae	SIOBICP00496L	SIOBICE5492	Bransfield Strait	8		2012	Polarstern ANT-XXVIII/4		79273	-62.367	-55.961	349
Ophionotus	victoriae	SIOBICP00496Q	SIOBICE5492	Bransfield Strait	8		2012	Polarstern ANT-XXVIII/4		79273	-62.367	-55.961	349
Ophionotus	victoriae	Op877_2E_2		Bransfield Strait	8	FJ917316	2013	LMG-13-12	4		-62.996	-58.599	320
Ophionotus	victoriae	SIOBICS6316A	SIOBICE4770	Bransfield Strait	8		2011	Scotia 2011	BS2	89	-63.343	-59.910	213
Ophionotus	victoriae	SIOBICS6316C	SIOBICE4770	Bransfield Strait	8		2011	Scotia 2011	BS2	89	-63.343	-59.910	213
Ophionotus	victoriae	SIOBICS6338I	SIOBICE4781	Bransfield Strait	8		2011	Scotia 2011	BS2	90	-63.283	-59.903	290
Ophionotus	victoriae	SIOBICS6760A	SIOBICE4777	Bransfield Strait	8		2011	Scotia 2011	BS1	87	-62.753	-57.322	292
Ophionotus	victoriae	SIOBICP00496M	SIOBICE5492	Bransfield Strait	9		2012	Polarstern ANT-XXVIII/4		79273	-62.367	-55.961	349
Ophionotus	victoriae	SIOBICP00496S	SIOBICE5492	Bransfield Strait	10		2012	Polarstern ANT-XXVIII/4		79273	-62.367	-55.961	349
Ophionotus	victoriae	SIOBICP00524C	SIOBICE5524	Bransfield Strait	14		2012	Polarstern ANT-XXVIII/4		79279	-62.278	-55.833	324
Ophionotus	victoriae	SIOBICP00524D	SIOBICE5524	Bransfield Strait	14		2012	Polarstern ANT-XXVIII/4		79279	-62.278	-55.833	324
Ophionotus	victoriae	SIOBICP00524G	SIOBICE5524	Bransfield Strait	14		2012	Polarstern ANT-XXVIII/4		79279	-62.278	-55.833	324

Ophionotus	victoriae	SIOBICP00524E	SIOBICE5524	Bransfield Strait	15		2012	Polarstern ANT-XXVIII/4		79279	-62.278	-55.833	324
Ophionotus	victoriae	SIOBICP00524F	SIOBICE5524	Bransfield Strait	16		2012	Polarstern ANT-XXVIII/4		79279	-62.278	-55.833	324
Ophionotus	victoriae	SIOBICP00524H	SIOBICE5524	Bransfield Strait	17		2012	Polarstern ANT-XXVIII/4		79279	-62.278	-55.833	324
Ophionotus	victoriae	92.3C		Bransfield Strait	21	FJ917314	2004	LMG-04-14	51		-63.384	-60.060	900
Ophionotus	victoriae	92.4C		Bransfield Strait	22	FJ917315	2004	LMG-04-14	51		-63.384	-60.060	900
Ophionotus	victoriae	92.7C		Bransfield Strait	23	FJ917317	2004	LMG-04-14	51		-63.384	-60.060	277
Ophionotus	victoriae	92.8C		Bransfield Strait	24	FJ917318	2004	LMG-04-14	51		-63.384	-60.060	277
Ophionotus	victoriae	SIOBICS6316B	SIOBICE4770	Bransfield Strait	24		2011	Scotia 2011	BS2	89	-63.343	-59.910	213
Ophionotus	victoriae	SIOBICS6760H	SIOBICE4777	Bransfield Strait	24		2011	Scotia 2011	BS1	87	-62.753	-57.322	292
Ophionotus	victoriae	92.12C		Bransfield Strait	25	FJ917319	2004	LMG-04-14	51		-63.384	-60.060	277
Ophionotus	victoriae	SIOBICS6338H	SIOBICE4781	Bransfield Strait	25		2011	Scotia 2011	BS2	90	-63.283	-59.903	290
Ophionotus	victoriae	SIOBICS6905C	SIOBICE5162	Bransfield Strait	25		2011	Scotia 2011	BS1	86	-62.870	-57.217	247
Ophionotus	victoriae	SIOBICS6905I	SIOBICE5162	Bransfield Strait	32		2011	Scotia 2011	BS1	86	-62.870	-57.217	247
Ophionotus	victoriae	SIOBICS6760D	SIOBICE4777	Bransfield Strait	39		2011	Scotia 2011	BS1	87	-62.753	-57.322	292
Ophionotus	victoriae	SIOBICS6905G	SIOBICE5162	Bransfield Strait	39		2011	Scotia 2011	BS1	86	-62.870	-57.217	247
Ophionotus	victoriae	E82.2C.03		Bransfield Strait	47	FJ917354	2006	LMG-04-14	47		-62.850	-59.460	900
Ophionotus	victoriae	SIOBICS6760E	SIOBICE4777	Bransfield Strait	84		2011	Scotia 2011	BS1	87	-62.753	-57.322	292
Ophionotus	victoriae	SIOBICS6316E	SIOBICE4770	Bransfield Strait	138		2011	Scotia 2011	BS2	89	-63.343	-59.910	213
Ophionotus	victoriae	SIOBICS6338A	SIOBICE4781	Bransfield Strait	139		2011	Scotia 2011	BS2	90	-63.283	-59.903	290
Ophionotus	victoriae	SIOBICS6338E	SIOBICE4781	Bransfield Strait	140		2011	Scotia 2011	BS2	90	-63.283	-59.903	290
Ophionotus	victoriae	SIOBICS6338K	SIOBICE4781	Bransfield Strait	141		2011	Scotia 2011	BS2	90	-63.283	-59.903	290
Ophionotus	victoriae	SIOBICS6905H	SIOBICE5162	Bransfield Strait	142		2011	Scotia 2011	BS1	86	-62.870	-57.217	247
Ophionotus	victoriae	SIOBICS6905J	SIOBICE5162	Bransfield Strait	143		2011	Scotia 2011	BS1	86	-62.870	-57.217	247
Ophionotus	victoriae	PNG708	PNG708	Davis Sea	1		2010	AAD	Tressler2	BTC15	-64.560	95.317	779
Ophionotus	victoriae	PNG710	PNG710	Davis Sea	1		2010	AAD	Tressler2	BTC15	-64.560	95.317	779
Ophionotus	victoriae	WAMZ43206	WAMZ43206	Davis Sea	68		2016	AAD		59	-65.067	113.778	1331
Ophionotus	victoriae	PNG703	PNG703	Davis Sea	112		2010	AAD	Tressler2	BTC17	-64.560	95.320	758
Ophionotus	victoriae	SIOBICS4306	SIOBICE5221	Discovery Bank	32		2011	Scotia 2011	DB1	58	-60.111	-34.827	439
Ophionotus	victoriae	SIOBICS4307	SIOBICE5169	Discovery Bank	32		2011	Scotia 2011	DB1	58	-60.111	-34.827	439
Ophionotus	victoriae	SIOBICS4309	SIOBICE5168	Discovery Bank	32		2011	Scotia 2011	DB1	58	-60.111	-34.827	439
Ophionotus	victoriae	SIOBICS4310	SIOBICE5183	Discovery Bank	32		2011	Scotia 2011	DB1	58	-60.111	-34.827	439
Ophionotus	victoriae	SIOBICS4311	SIOBICE5239	Discovery Bank	32		2011	Scotia 2011	DB1	58	-60.111	-34.827	439
Ophionotus	victoriae	SIOBICS4314	SIOBICE5179	Discovery Bank	32		2011	Scotia 2011	DB1	58	-60.111	-34.827	439
Ophionotus	victoriae	SIOBICS4315	SIOBICE5258	Discovery Bank	32		2011	Scotia 2011	DB1	58	-60.111	-34.827	439
Ophionotus	victoriae	SIOBICS4316	SIOBICE5261	Discovery Bank	32		2011	Scotia 2011	DB1	58	-60.111	-34.827	439
Ophionotus	victoriae	SIOBICS4318	SIOBICE5222	Discovery Bank	32		2011	Scotia 2011	DB1	58	-60.111	-34.827	439
Ophionotus	victoriae	SIOBICS4319	SIOBICE5259	Discovery Bank	32		2011	Scotia 2011	DB1	58	-60.111	-34.827	439
Ophionotus	victoriae	SIOBICS4320	SIOBICE5231	Discovery Bank	32		2011	Scotia 2011	DB1	58	-60.111	-34.827	439
Ophionotus	victoriae	SIOBICS4323	SIOBICE5240	Discovery Bank	32		2011	Scotia 2011	DB1	58	-60.111	-34.827	439

Ophionotus	victoriae	SIOBICS4325	SIOBICE5264	Discovery Bank	32		2011	Scotia 2011	DB1	58	-60.111	-34.827	439
Ophionotus	victoriae	SIOBICS4321	SIOBICE5260	Discovery Bank	33		2011	Scotia 2011	DB1	58	-60.111	-34.827	439
Ophionotus	victoriae	SIOBICS4324	SIOBICE5263	Discovery Bank	35		2011	Scotia 2011	DB1	58	-60.111	-34.827	439
Ophionotus	victoriae	SIOBICS4308	SIOBICE5194	Discovery Bank	130		2011	Scotia 2011	DB1	58	-60.111	-34.827	439
Ophionotus	victoriae	SIOBICS4312	SIOBICE5218	Discovery Bank	131		2011	Scotia 2011	DB1	58	-60.111	-34.827	439
Ophionotus	victoriae	SIOBICS4313	SIOBICE5224	Discovery Bank	132		2011	Scotia 2011	DB1	58	-60.111	-34.827	439
Ophionotus	victoriae	SIOBICS4317	SIOBICE5188	Discovery Bank	133		2011	Scotia 2011	DB1	58	-60.111	-34.827	439
Ophionotus	victoriae	SIOBICS4322	SIOBICE5262	Discovery Bank	134		2011	Scotia 2011	DB1	58	-60.111	-34.827	439
Ophionotus	victoriae	SIOBICS1312K	SIOBICE4771	Elephant Island	4		2011	Scotia 2011	EI1	81	-61.218	-54.255	202
Ophionotus	victoriae	SIOBICS1312A	SIOBICE4771	Elephant Island	5		2011	Scotia 2011	EI1	81	-61.218	-54.255	202
Ophionotus	victoriae	SIOBICS1312B	SIOBICE4771	Elephant Island	5		2011	Scotia 2011	EI1	81	-61.218	-54.255	202
Ophionotus	victoriae	SIOBICS1312F	SIOBICE4771	Elephant Island	5		2011	Scotia 2011	EI1	81	-61.218	-54.255	202
Ophionotus	victoriae	SIOBICS1312H	SIOBICE4771	Elephant Island	5		2011	Scotia 2011	EI1	81	-61.218	-54.255	202
Ophionotus	victoriae	SIOBICS6775A	SIOBICE4803	Elephant Island	5		2011	Scotia 2011	EI2	84	-61.304	-55.708	170
Ophionotus	victoriae	SIOBICS1312I	SIOBICE4771	Elephant Island	6		2011	Scotia 2011	EI1	81	-61.218	-54.255	202
Ophionotus	victoriae	SIOBICS6741	SIOBICE5209	Elephant Island	6		2011	Scotia 2011	EI2	83	-61.339	-55.625	143
Ophionotus	victoriae	SIOBICS6779	SIOBICE5289	Elephant Island	6		2011	Scotia 2011	EI2	83	-61.339	-55.625	143
Ophionotus	victoriae	SIOBICS1312C	SIOBICE4771	Elephant Island	7		2011	Scotia 2011	EI1	81	-61.218	-54.255	202
Ophionotus	victoriae	SIOBICS1312J	SIOBICE4771	Elephant Island	7		2011	Scotia 2011	EI1	81	-61.218	-54.255	202
Ophionotus	victoriae	SIOBICS1312D	SIOBICE4771	Elephant Island	8		2011	Scotia 2011	EI1	81	-61.218	-54.255	202
Ophionotus	victoriae	SIOBICS1312E	SIOBICE4771	Elephant Island	8		2011	Scotia 2011	EI1	81	-61.218	-54.255	202
Ophionotus	victoriae	SIOBICS6743	SIOBICE5237	Elephant Island	24		2011	Scotia 2011	EI2	83	-61.339	-55.625	143
Ophionotus	victoriae	SIOBICS1312L	SIOBICE4771	Elephant Island	25		2011	Scotia 2011	EI1	81	-61.218	-54.255	202
Ophionotus	victoriae	AP43 (haplotype ID)		Elephant Island	44	FJ917349	2008	JR179	BIO6-AGT-2A		-61.200	-54.733	239
Ophionotus	victoriae	SIOBICS1312G	SIOBICE4771	Elephant Island	84		2011	Scotia 2011	EI1	81	-61.218	-54.255	202
Ophionotus	victoriae	PNG635	PNG635	Heard Island	111			AAD	SC50	H257	-52.385	75.052	240
Ophionotus	victoriae	SIOBICS4494	SIOBICE5353	Herdman Bank	5		2011	Scotia 2011	HB1	51	-59.899	-32.451	520
Ophionotus	victoriae	SIOBICS4491	SIOBICE5210	Herdman Bank	11		2011	Scotia 2011	HB1	51	-59.899	-32.451	520
Ophionotus	victoriae	SIOBICS4472K	SIOBICE4791	Herdman Bank	31		2011	Scotia 2011	HB1	50	-59.863	-32.470	600
Ophionotus	victoriae	SIOBICS4472L	SIOBICE4791	Herdman Bank	31		2011	Scotia 2011	HB1	50	-59.863	-32.470	600
Ophionotus	victoriae	SIOBICS4472N	SIOBICE4791	Herdman Bank	31		2011	Scotia 2011	HB1	50	-59.863	-32.470	600
Ophionotus	victoriae	SIOBICS4472Q	SIOBICE4791	Herdman Bank	31		2011	Scotia 2011	HB1	50	-59.863	-32.470	600
Ophionotus	victoriae	SIOBICS4472R	SIOBICE4791	Herdman Bank	31		2011	Scotia 2011	HB1	50	-59.863	-32.470	600
Ophionotus	victoriae	SIOBICS4472T	SIOBICE4791	Herdman Bank	31		2011	Scotia 2011	HB1	50	-59.863	-32.470	600
Ophionotus	victoriae	SIOBICS4493	SIOBICE5352	Herdman Bank	32		2011	Scotia 2011	HB1	51	-59.899	-32.451	520
Ophionotus	victoriae	SIOBICS4495	SIOBICE5354	Herdman Bank	32		2011	Scotia 2011	HB1	51	-59.899	-32.451	520
Ophionotus	victoriae	SIOBICS4496	SIOBICE5355	Herdman Bank	32		2011	Scotia 2011	HB1	51	-59.899	-32.451	520
Ophionotus	victoriae	SIOBICS4497	SIOBICE5356	Herdman Bank	32		2011	Scotia 2011	HB1	51	-59.899	-32.451	520
Ophionotus	victoriae	SIOBICS4498	SIOBICE5357	Herdman Bank	32		2011	Scotia 2011	HB1	51	-59.899	-32.451	520
Ophionotus	victoriae	SIOBICS4472M	SIOBICE4791	Herdman Bank	34		2011	Scotia 2011	HB1	50	-59.863	-32.470	600

Ophionotus	victoriae	SIOBICS4472O	SIOBICE4791	Herdman Bank	35		2011	Scotia 2011	HB1	50	-59.863	-32.470	600
Ophionotus	victoriae	SIOBICS4472P	SIOBICE4791	Herdman Bank	35		2011	Scotia 2011	HB1	50	-59.863	-32.470	600
Ophionotus	victoriae	SIOBICS4472S	SIOBICE4791	Herdman Bank	35		2011	Scotia 2011	HB1	50	-59.863	-32.470	600
Ophionotus	victoriae	SIOBICS4499	SIOBICE5358	Herdman Bank	35		2011	Scotia 2011	HB1	51	-59.899	-32.451	520
Ophionotus	victoriae	SIOBICS4500	SIOBICE5360	Herdman Bank	121		2011	Scotia 2011	HB1	51	-59.899	-32.451	520
Ophionotus	victoriae	SIOBICS4492	SIOBICE5351	Herdman Bank	135		2011	Scotia 2011	HB1	51	-59.899	-32.451	520
Ophionotus	victoriae	DSOPH2904		Larsen Ice Shelf	1	FJ917337	2011	Polarstern ANT-XXVII/3	PS77_250-6		-65.384	-61.548	567
Ophionotus	victoriae	DSOPH3807		Larsen Ice Shelf	1	FJ917337	2011	Polarstern ANT-XXVII/3	PS77_239-3		-66.200	-60.171	360
Ophionotus	victoriae	DSOPH3810		Larsen Ice Shelf	1	FJ917337	2011	Polarstern ANT-XXVII/3	PS77_239-3		-66.200	-60.171	360
Ophionotus	victoriae	DSOPH3859		Larsen Ice Shelf	1	FJ917337	2011	Polarstern ANT-XXVII/3	PS77_233-3		-65.558	-61.622	324
Ophionotus	victoriae	DSOPH3871		Larsen Ice Shelf	1	FJ917337	2011	Polarstern ANT-XXVII/3	PS77_233-3		-65.558	-61.622	324
Ophionotus	victoriae	WAMZ88551	WAMZ88551	Larsen Ice Shelf	1		2011	Polarstern ANT-XXVII/3	PS77_228-3		-64.903	-60.490	570
Ophionotus	victoriae	WAMZ88553	WAMZ88553	Larsen Ice Shelf	1		2011	Polarstern ANT-XXVII/3	PS77_228-4		-64.933	-60.560	329
Ophionotus	victoriae	WAMZ88560	WAMZ88560	Larsen Ice Shelf	1		2011	Polarstern ANT-XXVII/3	PS77_233-3		-65.558	-61.623	320
Ophionotus	victoriae	WAMZ88574	WAMZ88574	Larsen Ice Shelf	1		2011	Polarstern ANT-XXVII/3	PS77_233-3		-65.558	-61.623	320
Ophionotus	victoriae	57.3C.13		Larsen Ice Shelf	4	FJ917313	2004	LMG-04-14	40		-63.667	-57.329	335
Ophionotus	victoriae	Op913_3E_7		Larsen Ice Shelf	4	FJ917313	2013	LMG-13-12	8		-64.134	-56.860	310
Ophionotus	victoriae	Op917_3E_1		Larsen Ice Shelf	4	KY048266	2013	LMG-13-12	10		-63.686	-56.859	400
Ophionotus	victoriae	Op917_3E_5		Larsen Ice Shelf	4	FJ917313	2013	LMG-13-12	10		-63.686	-56.859	400
Ophionotus	victoriae	Op917_3E_8		Larsen Ice Shelf	4	FJ917313	2013	LMG-13-12	10		-63.686	-56.859	400
Ophionotus	victoriae	Op917_3E_9		Larsen Ice Shelf	4	FJ917313	2013	LMG-13-12	10		-63.686	-56.859	400
Ophionotus	victoriae	DSOPH2924		Larsen Ice Shelf	5	FJ917320	2011	Polarstern ANT-XXVII/3	PS77_231-3		-64.914	-60.515	314
Ophionotus	victoriae	DSOPH3837		Larsen Ice Shelf	5	FJ917320	2011	Polarstern ANT-XXVII/3	PS77_226-7		-64.914	-60.621	226
Ophionotus	victoriae	DSOPH3839		Larsen Ice Shelf	5	FJ917320	2011	Polarstern ANT-XXVII/3	PS77_226-7		-64.914	-60.621	226
Ophionotus	victoriae	WAMZ88561	WAMZ88561	Larsen Ice Shelf	5		2011	Polarstern ANT-XXVII/3	PS77_226-7		-64.913	-60.624	226
Ophionotus	victoriae	WAMZ88566	WAMZ88566	Larsen Ice Shelf	5		2011	Polarstern ANT-XXVII/3	PS77_226-7		-64.913	-60.624	226
Ophionotus	victoriae	57.3C.03		Larsen Ice Shelf	6	FJ917309	2004	LMG-04-14	40		-63.667	-57.329	335
Ophionotus	victoriae	57.3C.14		Larsen Ice Shelf	6	FJ917309	2004	LMG-04-14	40		-63.667	-57.329	335
Ophionotus	victoriae	DSOPH3838		Larsen Ice Shelf	6	KY048254	2011	Polarstern ANT-XXVII/3	PS77_226-7		-64.914	-60.621	226
Ophionotus	victoriae	Op895_3E_5		Larsen Ice Shelf	6	FJ917309	2013	LMG-13-12	6		-64.302	-56.136	290
Ophionotus	victoriae	Op895_3E_7		Larsen Ice Shelf	6	FJ917309	2013	LMG-13-12	6		-64.302	-56.136	290
Ophionotus	victoriae	WAMZ88567	WAMZ88567	Larsen Ice Shelf	6		2011	Polarstern ANT-XXVII/3	PS77_226-7		-64.913	-60.624	226
Ophionotus	victoriae	DSOPH2918		Larsen Ice Shelf	7	FJ917322	2011	Polarstern ANT-XXVII/3	PS77_237-2		-66.209	-60.162	383

Ophionotus	victoriae	DSOPH3809		Larsen Ice Shelf	7	FJ917322	2011	Polarstern ANT-XXVII/3	PS77_239-3	-66.200	-60.171	360
Ophionotus	victoriae	DSOPH3876		Larsen Ice Shelf	7	FJ917322	2011	Polarstern ANT-XXVII/3	PS77_233-3	-65.558	-61.622	324
Ophionotus	victoriae	Op895_3E_10		Larsen Ice Shelf	7	KY048263	2013	LMG-13-12	6	-64.302	-56.136	290
Ophionotus	victoriae	WAMZ88556	WAMZ88556	Larsen Ice Shelf	7		2011	Polarstern ANT-XXVII/3	PS77_237-2	-66.208	-60.161	362
Ophionotus	victoriae	DSOPH3848		Larsen Ice Shelf	8	FJ917316	2011	Polarstern ANT-XXVII/3	PS77_228-3	-64.918	-60.537	280
Ophionotus	victoriae	DSOPH3892		Larsen Ice Shelf	8	FJ917316	2011	Polarstern ANT-XXVII/3	PS77_228-4	-64.929	-60.565	316
Ophionotus	victoriae	WAMZ88557	WAMZ88557	Larsen Ice Shelf	8		2011	Polarstern ANT-XXVII/3	PS77_228-4	-64.933	-60.560	329
Ophionotus	victoriae	57.3C.11		Larsen Ice Shelf	10	FJ917312	2004	LMG-04-14	40	-63.667	-57.329	335
Ophionotus	victoriae	DSOPH2923		Larsen Ice Shelf	10	KY048244	2011	Polarstern ANT-XXVII/3	PS77_231-3	-64.914	-60.515	314
Ophionotus	victoriae	Op914_3E_10		Larsen Ice Shelf	10	FJ917312	2013	LMG-13-12	9	-63.742	-57.432	692
Ophionotus	victoriae	321.2C.04		Larsen Ice Shelf	14	FJ917310	2006	LMG-06-05	21	-64.350	-57.077	146
Ophionotus	victoriae	57.3C.05		Larsen Ice Shelf	14	FJ917310	2004	LMG-04-14	40	-63.667	-57.329	335
Ophionotus	victoriae	57.3C.10		Larsen Ice Shelf	14	FJ917310	2004	LMG-04-14	40	-63.667	-57.329	335
Ophionotus	victoriae	57.3C.12		Larsen Ice Shelf	14	FJ917310	2004	LMG-04-14	40	-63.667	-57.329	335
Ophionotus	victoriae	59.2C.03		Larsen Ice Shelf	14	FJ917310	2004	LMG-04-14	40	-63.667	-57.329	335
Ophionotus	victoriae	59.2C.06		Larsen Ice Shelf	14	FJ917310	2004	LMG-04-14	40	-63.667	-57.329	335
Ophionotus	victoriae	59.2C.07		Larsen Ice Shelf	14	FJ917310	2004	LMG-04-14	40	-63.667	-57.329	335
Ophionotus	victoriae	DSOPH2888		Larsen Ice Shelf	14	FJ917310	2011	Polarstern ANT-XXVII/3	PS77_248-3	-65.924	-60.332	443
Ophionotus	victoriae	DSOPH3835		Larsen Ice Shelf	14	FJ917310	2011	Polarstern ANT-XXVII/3	PS77_226-7	-64.914	-60.621	226
Ophionotus	victoriae	Op913_3E_1		Larsen Ice Shelf	14	FJ917310	2013	LMG-13-12	8	-64.134	-56.860	310
Ophionotus	victoriae	Op913_3E_2		Larsen Ice Shelf	14	FJ917310	2013	LMG-13-12	8	-64.134	-56.860	310
Ophionotus	victoriae	Op913_3E_4		Larsen Ice Shelf	14	FJ917310	2013	LMG-13-12	8	-64.134	-56.860	310
Ophionotus	victoriae	Op913_3E_5		Larsen Ice Shelf	14	FJ917310	2013	LMG-13-12	8	-64.134	-56.860	310
Ophionotus	victoriae	Op913_3E_6		Larsen Ice Shelf	14	FJ917310	2013	LMG-13-12	8	-64.134	-56.860	310
Ophionotus	victoriae	Op913_3E_9		Larsen Ice Shelf	14	FJ917310	2013	LMG-13-12	8	-64.134	-56.860	310
Ophionotus	victoriae	Op914_3E_8		Larsen Ice Shelf	14	FJ917310	2013	LMG-13-12	9	-63.742	-57.432	692
Ophionotus	victoriae	Op914_3E_9		Larsen Ice Shelf	14	FJ917310	2013	LMG-13-12	9	-63.742	-57.432	692
Ophionotus	victoriae	Op917_3E_10		Larsen Ice Shelf	14	FJ917310	2013	LMG-13-12	10	-63.686	-56.859	400
Ophionotus	victoriae	Op917_3E_4		Larsen Ice Shelf	14	FJ917310	2013	LMG-13-12	10	-63.686	-56.859	400
Ophionotus	victoriae	Op917_3E_6		Larsen Ice Shelf	14	FJ917310	2013	LMG-13-12	10	-63.686	-56.859	400
Ophionotus	victoriae	Op917_3E_7		Larsen Ice Shelf	14	FJ917310	2013	LMG-13-12	10	-63.686	-56.859	400
Ophionotus	victoriae	WAMZ88564	WAMZ88564	Larsen Ice Shelf	14		2011	Polarstern ANT-XXVII/3	PS77_233-3	-65.558	-61.623	320
Ophionotus	victoriae	WAMZ88565	WAMZ88565	Larsen Ice Shelf	14		2011	Polarstern ANT-XXVII/3	PS77_233-3	-65.558	-61.623	320
Ophionotus	victoriae	WAMZ88572	WAMZ88572	Larsen Ice Shelf	14		2011	Polarstern ANT-XXVII/3	PS77_248-3	-65.928	-60.335	433

Ophionotus	victoriae	WAMZ88581	WAMZ88581	Larsen Ice Shelf	14		2011	Polarstern ANT-XXVII/3	PS77_226-7	-64.913	-60.624	226
Ophionotus	victoriae	57.3C.08		Larsen Ice Shelf	20	FJ917311	2004	LMG-04-14	40	-63.667	-57.329	335
Ophionotus	victoriae	Op917_3E_2		Larsen Ice Shelf	20	FJ917311	2013	LMG-13-12	10	-63.686	-56.859	400
Ophionotus	victoriae	321.2C.01		Larsen Ice Shelf	24	FJ917318	2006	LMG-06-05	21	-64.350	-57.077	146
Ophionotus	victoriae	DSOPH3808		Larsen Ice Shelf	24	FJ917318	2011	Polarstern ANT-XXVII/3	PS77_239-3	-66.200	-60.171	360
Ophionotus	victoriae	DSOPH3847		Larsen Ice Shelf	24	FJ917318	2011	Polarstern ANT-XXVII/3	PS77_228-3	-64.918	-60.537	280
Ophionotus	victoriae	DSOPH3850		Larsen Ice Shelf	24	FJ917318	2011	Polarstern ANT-XXVII/3	PS77_228-3	-64.918	-60.537	280
Ophionotus	victoriae	DSOPH3851		Larsen Ice Shelf	24	FJ917318	2011	Polarstern ANT-XXVII/3	PS77_228-3	-64.918	-60.537	280
Ophionotus	victoriae	Op914_3E_6		Larsen Ice Shelf	24	FJ917318	2013	LMG-13-12	9	-63.742	-57.432	692
Ophionotus	victoriae	Op914_3E_7		Larsen Ice Shelf	24	FJ917318	2013	LMG-13-12	9	-63.742	-57.432	692
Ophionotus	victoriae	WAMZ88568	WAMZ88568	Larsen Ice Shelf	24		2011	Polarstern ANT-XXVII/3	PS77_252-7	-64.704	-60.530	343
Ophionotus	victoriae	321.2C.03		Larsen Ice Shelf	25	FJ917319	2006	LMG-06-05	21	-64.350	-57.077	146
Ophionotus	victoriae	321.2C.06		Larsen Ice Shelf	25	FJ917319	2006	LMG-06-05	21	-64.350	-57.077	146
Ophionotus	victoriae	Op895_3E_2		Larsen Ice Shelf	25	FJ917319	2013	LMG-13-12	6	-64.302	-56.136	290
Ophionotus	victoriae	Op895_3E_4		Larsen Ice Shelf	25	FJ917319	2013	LMG-13-12	6	-64.302	-56.136	290
Ophionotus	victoriae	Op895_3E_8		Larsen Ice Shelf	25	FJ917319	2013	LMG-13-12	6	-64.302	-56.136	290
Ophionotus	victoriae	Op913_3E_8		Larsen Ice Shelf	25	FJ917319	2013	LMG-13-12	8	-64.134	-56.860	310
Ophionotus	victoriae	Op914_3E_2		Larsen Ice Shelf	25	FJ917319	2013	LMG-13-12	8	-64.134	-56.860	310
Ophionotus	victoriae	Op917_3E_3		Larsen Ice Shelf	25	KY048267	2013	LMG-13-12	10	-63.686	-56.859	400
Ophionotus	victoriae	Op895_3E_3		Larsen Ice Shelf	32	KY048264	2013	LMG-13-12	6	-64.302	-56.136	290
Ophionotus	victoriae	321.2C.02		Larsen Ice Shelf	38	FJ917341	2006	LMG-06-05	21	-64.350	-57.077	146
Ophionotus	victoriae	Op913_3E_3		Larsen Ice Shelf	55	KY048218	2013	LMG-13-12	8	-64.134	-56.860	310
Ophionotus	victoriae	Op913_3E_10		Larsen Ice Shelf	58	KY048231	2013	LMG-13-12	8	-64.134	-56.860	310
Ophionotus	victoriae	DSOPH2903		Larsen Ice Shelf	64	KY048228	2011	Polarstern ANT-XXVII/3	PS77_250-6	-65.384	-61.548	567
Ophionotus	victoriae	WAMZ88582	WAMZ88582	Larsen Ice Shelf	64		2011	Polarstern ANT-XXVII/3	PS77_250-6	-65.381	-61.557	581
Ophionotus	victoriae	DSOPH2867		Larsen Ice Shelf	74	KY048241	2011	Polarstern ANT-XXVII/3	PS77_252-3	-64.694	-60.518	316
Ophionotus	victoriae	WAMZ88555	WAMZ88555	Larsen Ice Shelf	74		2011	Polarstern ANT-XXVII/3	PS77_255-3	-64.833	-60.597	682
Ophionotus	victoriae	DSOPH2902		Larsen Ice Shelf	75	KY048242	2011	Polarstern ANT-XXVII/3	PS77_250-6	-65.384	-61.548	567
Ophionotus	victoriae	DSOPH2905		Larsen Ice Shelf	75	KY048242	2011	Polarstern ANT-XXVII/3	PS77_250-6	-65.384	-61.548	567
Ophionotus	victoriae	DSOPH2906		Larsen Ice Shelf	75	KY048242	2011	Polarstern ANT-XXVII/3	PS77_250-6	-65.384	-61.548	567
Ophionotus	victoriae	WAMZ88578	WAMZ88578	Larsen Ice Shelf	75		2011	Polarstern ANT-XXVII/3	PS77_250-6	-65.381	-61.557	581
Ophionotus	victoriae	DSOPH2914		Larsen Ice Shelf	76	KY048243	2011	Polarstern ANT-XXVII/3	PS77_235-8	-65.528	-61.552	449
Ophionotus	victoriae	DSOPH3872		Larsen Ice Shelf	76	KY048243	2011	Polarstern ANT-XXVII/3	PS77_233-3	-65.558	-61.622	324

Ophionotus	victoriae	WAMZ88569	WAMZ88569	Larsen Ice Shelf	76		2011	Polarstern ANT-XXVII/3	PS77_233-3		-65.558	-61.623	320
Ophionotus	victoriae	DSOPH3873		Larsen Ice Shelf	83	KY048252	2011	Polarstern ANT-XXVII/3	PS77_233-3		-65.558	-61.622	324
Ophionotus	victoriae	WAMZ88573	WAMZ88573	Larsen Ice Shelf	83		2011	Polarstern ANT-XXVII/3	PS77_248-3		-65.928	-60.335	433
Ophionotus	victoriae	WAMZ88575	WAMZ88575	Larsen Ice Shelf	83		2011	Polarstern ANT-XXVII/3	PS77_233-3		-65.558	-61.623	320
Ophionotus	victoriae	DSOPH3836		Larsen Ice Shelf	84	KY048253	2011	Polarstern ANT-XXVII/3	PS77_226-7		-64.914	-60.621	226
Ophionotus	victoriae	DSOPH3849		Larsen Ice Shelf	85	KY048255	2011	Polarstern ANT-XXVII/3	PS77_228-3		-64.918	-60.537	280
Ophionotus	victoriae	WAMZ88563	WAMZ88563	Larsen Ice Shelf	85		2011	Polarstern ANT-XXVII/3	PS77_228-3		-64.903	-60.490	570
Ophionotus	victoriae	Op914_3E_3		Larsen Ice Shelf	92	KY048265	2013	LMG-13-12	9		-63.742	-57.432	692
Ophionotus	victoriae	Op914_3E_5		Larsen Ice Shelf	92	KY048265	2013	LMG-13-12	9		-63.742	-57.432	692
Ophionotus	victoriae	DSOPH3811		Larsen Ice Shelf	93	KY048268	2011	Polarstern ANT-XXVII/3	PS77_239-3		-66.200	-60.171	360
Ophionotus	victoriae	WAMZ88552	WAMZ88552	Larsen Ice Shelf	158		2011	Polarstern ANT-XXVII/3	PS77_250-6		-65.381	-61.557	581
Ophionotus	victoriae	WAMZ88562	WAMZ88562	Larsen Ice Shelf	159		2011	Polarstern ANT-XXVII/3	PS77_228-4		-64.933	-60.560	329
Ophionotus	victoriae	AAD107	AAD107	Prydz Bay	1		2001	AAD	AL27-130	58.4.2	-66.791	62.442	213
Ophionotus	victoriae	AAD140	AAD140	Prydz Bay	1		2001	AAD	AL27-127	58.4.2	-66.792	62.096	270
Ophionotus	victoriae	AAD141	AAD141	Prydz Bay	1		2001	AAD	AL27-127	58.4.2	-66.792	62.096	270
Ophionotus	victoriae	AAD143	AAD143	Prydz Bay	1		2001	AAD	AL27-127	58.4.2	-66.792	62.096	270
Ophionotus	victoriae	AAD139	AAD139	Prydz Bay	2		2001	AAD	AL27-127	58.4.2	-66.792	62.096	270
Ophionotus	victoriae	AAD145	AAD145	Prydz Bay	3		2001	AAD	AL27-127	58.4.2	-66.792	62.096	270
Ophionotus	victoriae	36968A	NIWA36968	Ross Sea	1		2008	TAN0802		100	-76.202	176.248	447
Ophionotus	victoriae	36968B	NIWA36968	Ross Sea	1		2008	TAN0802		100	-76.202	176.248	447
Ophionotus	victoriae	36968C	NIWA36968	Ross Sea	1		2008	TAN0802		100	-76.202	176.248	447
Ophionotus	victoriae	36968E	NIWA36968	Ross Sea	1		2008	TAN0802		100	-76.202	176.248	447
Ophionotus	victoriae	36968F	NIWA36968	Ross Sea	1		2008	TAN0802		100	-76.202	176.248	447
Ophionotus	victoriae	37157A	NIWA37157	Ross Sea	1		2008	TAN0802		117	-72.590	175.342	175
Ophionotus	victoriae	37157B	NIWA37157	Ross Sea	1		2008	TAN0802		117	-72.590	175.342	175
Ophionotus	victoriae	94866B	NIWA94866	Ross Sea	1		2004	TAN0402		132	-71.648	170.180	172
Ophionotus	victoriae	N0065	NIWA85184	Ross Sea	1		2008	TAN0802		61	-75.622	169.805	521
Ophionotus	victoriae	N0068	NIWA85184	Ross Sea	1		2008	TAN0802		61	-75.622	169.805	521
Ophionotus	victoriae	N0069	NIWA85184	Ross Sea	1		2008	TAN0802		61	-75.622	169.805	521
Ophionotus	victoriae	N0072	NIWA85184	Ross Sea	1		2008	TAN0802		61	-75.622	169.805	521
Ophionotus	victoriae	N0073	NIWA85184	Ross Sea	1		2008	TAN0802		61	-75.622	169.805	521
Ophionotus	victoriae	N0075	NIWA85184	Ross Sea	1		2008	TAN0802		61	-75.622	169.805	521
Ophionotus	victoriae	N0099	NIWA85183	Ross Sea	1		2008	TAN0802		77	-76.833	179.950	664
Ophionotus	victoriae	N0100	NIWA85183	Ross Sea	1		2008	TAN0802		77	-76.833	179.950	664
Ophionotus	victoriae	N0101	NIWA84672	Ross Sea	1		2008	TAN0802		77	-76.833	179.950	664
Ophionotus	victoriae	N0105	NIWA84672	Ross Sea	1		2008	TAN0802		77	-76.833	179.950	664

Ophionotus	victoriae	N0106	NIWA84672	Ross Sea	1		2008	TAN0802		77	-76.833	179.950	664
Ophionotus	victoriae	N0107	NIWA84672	Ross Sea	1		2008	TAN0802		77	-76.833	179.950	664
Ophionotus	victoriae	N0108	NIWA84672	Ross Sea	1		2008	TAN0802		77	-76.833	179.950	664
Ophionotus	victoriae	Op762_2E		Ross Sea	1	FJ917337	2013	NBP-12-10	21		-78.063	-169.991	549
Ophionotus	victoriae	Op762_4C_1		Ross Sea	1	KY048262	2013	NBP-12-10	21		-78.063	-169.991	549
Ophionotus	victoriae	Op762_5C_1		Ross Sea	1	FJ917337	2013	NBP-12-10	21		-78.063	-169.991	549
Ophionotus	victoriae	Op762_6C_1		Ross Sea	1	FJ917337	2013	NBP-12-10	21		-78.063	-169.991	549
Ophionotus	victoriae	Op762_6C_2		Ross Sea	1	FJ917337	2013	NBP-12-10	21		-78.063	-169.991	549
Ophionotus	victoriae	Op787_5C_1		Ross Sea	1	FJ917337	2013	NBP-12-10	22		-76.998	-175.093	541
Ophionotus	victoriae	Op787_5C_2		Ross Sea	1	FJ917337	2013	NBP-12-10	22		-76.998	-175.093	541
Ophionotus	victoriae	Op787_5C_3		Ross Sea	1	FJ917337	2013	NBP-12-10	22		-76.998	-175.093	541
Ophionotus	victoriae	Op787_5C_4		Ross Sea	1	FJ917337	2013	NBP-12-10	22		-76.998	-175.093	541
Ophionotus	victoriae	Op787_6C_1		Ross Sea	1	FJ917337	2013	NBP-12-10	22		-76.998	-175.093	541
Ophionotus	victoriae	Op787_6C_2		Ross Sea	1	FJ917337	2013	NBP-12-10	22		-76.998	-175.093	541
Ophionotus	victoriae	Op787_6C_3		Ross Sea	1	FJ917337	2013	NBP-12-10	22		-76.998	-175.093	541
Ophionotus	victoriae	Op787_6C_5		Ross Sea	1	FJ917337	2013	NBP-12-10	22		-76.998	-175.093	541
Ophionotus	victoriae	Op803_3C_1		Ross Sea	1	FJ917337	2013	NBP-12-10	23		-76.245	174.504	604
Ophionotus	victoriae	Op803_3C_2		Ross Sea	1	FJ917337	2013	NBP-12-10	23		-76.245	174.504	604
Ophionotus	victoriae	Op803_3C_3		Ross Sea	1	FJ917337	2013	NBP-12-10	23		-76.245	174.504	604
Ophionotus	victoriae	Op803_3C_4		Ross Sea	1	FJ917337	2013	NBP-12-10	23		-76.245	174.504	604
Ophionotus	victoriae	Op803_3C_5		Ross Sea	1	FJ917337	2013	NBP-12-10	23		-76.245	174.504	604
Ophionotus	victoriae	Op803_3C_6		Ross Sea	1	FJ917337	2013	NBP-12-10	23		-76.245	174.504	604
Ophionotus	victoriae	Op803_4C_2		Ross Sea	1	FJ917337	2013	NBP-12-10	23		-76.245	174.504	604
Ophionotus	victoriae	Op803_4C_3		Ross Sea	1	FJ917337	2013	NBP-12-10	23		-76.245	174.504	604
Ophionotus	victoriae	Op806_2E		Ross Sea	1	FJ917337	2013	NBP-12-10	24		-76.904	169.965	764
Ophionotus	victoriae	Op806_3C_3		Ross Sea	1	FJ917337	2013	NBP-12-10	24		-76.904	169.965	764
Ophionotus	victoriae	Op806_3C_4		Ross Sea	1	FJ917337	2013	NBP-12-10	24		-76.904	169.965	764
Ophionotus	victoriae	Op806_8C_2		Ross Sea	1	FJ917337	2013	NBP-12-10	24		-76.904	169.965	764
Ophionotus	victoriae	Op806_8C_3		Ross Sea	1	FJ917337	2013	NBP-12-10	24		-76.904	169.965	764
Ophionotus	victoriae	Op806_8C_4		Ross Sea	1	FJ917337	2013	NBP-12-10	24		-76.904	169.965	764
Ophionotus	victoriae	Op818_3C_1		Ross Sea	1	FJ917337	2013	NBP-12-10	25		-75.833	166.505	552
Ophionotus	victoriae	Op818_3C_2		Ross Sea	1	FJ917337	2013	NBP-12-10	25		-75.833	166.505	552
Ophionotus	victoriae	Op818_3C_4		Ross Sea	1	FJ917337	2013	NBP-12-10	25		-75.833	166.505	552
Ophionotus	victoriae	Op818_3C_5		Ross Sea	1	FJ917337	2013	NBP-12-10	25		-75.833	166.505	552
Ophionotus	victoriae	Op818_4C_1		Ross Sea	1	FJ917337	2013	NBP-12-10	25		-75.833	166.505	552
Ophionotus	victoriae	Op818_4C_2		Ross Sea	1	FJ917337	2013	NBP-12-10	25		-75.833	166.505	552
Ophionotus	victoriae	Op818_4C_5		Ross Sea	1	FJ917337	2013	NBP-12-10	25		-75.833	166.505	552
Ophionotus	victoriae	Op826_2E		Ross Sea	1	FJ917337	2013	NBP-12-10	26		-74.708	168.408	489
Ophionotus	victoriae	Op826_3C_1		Ross Sea	1	FJ917337	2013	NBP-12-10	26		-74.708	168.408	489
Ophionotus	victoriae	Op843_2E		Ross Sea	1	FJ917337	2013	NBP-12-10	28		-74.995	165.744	1101
Ophionotus	victoriae	Op843_7C_2		Ross Sea	1	FJ917337	2013	NBP-12-10	28		-74.995	165.744	1101

Ophionotus	victoriae	Op843_7C_3		Ross Sea	1	FJ917337	2013	NBP-12-10	28		-74.995	165.744	1101
Ophionotus	victoriae	PDIVA-A	SIOBICE4766	Ross Sea	1		2010	SIO McMurdo		IVA	-77.572	163.512	
Ophionotus	victoriae	PDIVA-C	SIOBICE4766	Ross Sea	1		2010	SIO McMurdo		IVA	-77.572	163.512	
Ophionotus	victoriae	PDIVA-D	SIOBICE4766	Ross Sea	1		2010	SIO McMurdo		IVA	-77.572	163.512	
Ophionotus	victoriae	PDIVA-E	SIOBICE4766	Ross Sea	1		2010	SIO McMurdo		IVA	-77.572	163.512	
Ophionotus	victoriae	PDIVA-F	SIOBICE4766	Ross Sea	1		2010	SIO McMurdo		IVA	-77.572	163.512	
Ophionotus	victoriae	PDIVA-G	SIOBICE4766	Ross Sea	1		2010	SIO McMurdo		IVA	-77.572	163.512	
Ophionotus	victoriae	PDIVA-I	SIOBICE4766	Ross Sea	1		2010	SIO McMurdo		IVA	-77.572	163.512	
Ophionotus	victoriae	PDIVA-J	SIOBICE4766	Ross Sea	1		2010	SIO McMurdo		IVA	-77.572	163.512	
Ophionotus	victoriae	PDIVA-K	SIOBICE4766	Ross Sea	1		2010	SIO McMurdo		IVA	-77.572	163.512	
Ophionotus	victoriae	PDIVA-O	SIOBICE4766	Ross Sea	1		2010	SIO McMurdo		IVA	-77.572	163.512	
Ophionotus	victoriae	PDIVA-P	SIOBICE4766	Ross Sea	1		2010	SIO McMurdo		IVA	-77.572	163.512	
Ophionotus	victoriae	PDIVA-Q	SIOBICE4766	Ross Sea	1		2010	SIO McMurdo		IVA	-77.572	163.512	
Ophionotus	victoriae	PDIVA-R	SIOBICE4766	Ross Sea	1		2010	SIO McMurdo		IVA	-77.572	163.512	
Ophionotus	victoriae	PDIVA-S	SIOBICE4766	Ross Sea	1		2010	SIO McMurdo		IVA	-77.572	163.512	
Ophionotus	victoriae	PDIVA-T	SIOBICE4766	Ross Sea	1		2010	SIO McMurdo		IVA	-77.572	163.512	
Ophionotus	victoriae	94869B	NIWA94869	Ross Sea	24		2004	TAN0402		174	-71.494	171.604	483
Ophionotus	victoriae	A04N.01		Ross Sea	24	GU227093	2008				Cape Harlett		
Ophionotus	victoriae	N0077	NIWA85184	Ross Sea	24		2008	TAN0802		61	-75.622	169.805	521
Ophionotus	victoriae	N0110	NIWA84672	Ross Sea	24		2008	TAN0802		77	-76.833	179.950	664
Ophionotus	victoriae	N0102	NIWA84672	Ross Sea	43		2008	TAN0802		77	-76.833	179.950	664
Ophionotus	victoriae	140217A	NIWA140217	Ross Sea	49		2019	TAN1901	SRS2_7	175	-75.525	-172.992	1376
Ophionotus	victoriae	140217B	NIWA140217	Ross Sea	49		2019	TAN1901	SRS2_7	175	-75.525	-172.992	1376
Ophionotus	victoriae	N0067	NIWA85184	Ross Sea	49		2008	TAN0802		61	-75.622	169.805	521
Ophionotus	victoriae	N0070	NIWA85184	Ross Sea	49		2008	TAN0802		61	-75.622	169.805	521
Ophionotus	victoriae	N0103	NIWA84672	Ross Sea	49		2008	TAN0802		77	-76.833	179.950	664
Ophionotus	victoriae	Op803_4C_1		Ross Sea	49	KY048234	2013	NBP-12-10	23		-76.245	174.504	604
Ophionotus	victoriae	Op806_3C_2		Ross Sea	49	KY048234	2013	NBP-12-10	24		-76.904	169.965	764
Ophionotus	victoriae	PDIVA-L	SIOBICE4766	Ross Sea	50		2010	SIO McMurdo		IVA	-77.572	163.512	
Ophionotus	victoriae	36968D	NIWA36968	Ross Sea	91		2008	TAN0802		100	-76.202	176.248	447
Ophionotus	victoriae	N0071	NIWA85184	Ross Sea	91		2008	TAN0802		61	-75.622	169.805	521
Ophionotus	victoriae	N0076	NIWA85184	Ross Sea	91		2008	TAN0802		61	-75.622	169.805	521
Ophionotus	victoriae	N0109	NIWA84672	Ross Sea	91		2008	TAN0802		77	-76.833	179.950	664
Ophionotus	victoriae	Op762_3C_2		Ross Sea	91	KY048261	2013	NBP-12-10	21		-78.063	-169.991	549
Ophionotus	victoriae	Op787_6C_4		Ross Sea	91	KY048261	2013	NBP-12-10	22		-76.998	-175.093	541
Ophionotus	victoriae	Op806_3C_1		Ross Sea	91	KY048261	2013	NBP-12-10	24		-76.904	169.965	764
Ophionotus	victoriae	Op806_7C		Ross Sea	91	KY048261	2013	NBP-12-10	24		-76.904	169.965	764
Ophionotus	victoriae	Op806_8C_1		Ross Sea	91	KY048261	2013	NBP-12-10	24		-76.904	169.965	764
Ophionotus	victoriae	Op818_2E		Ross Sea	91	KY048261	2013	NBP-12-10	25		-75.833	166.505	552
Ophionotus	victoriae	Op818_3C_3		Ross Sea	91	KY048261	2013	NBP-12-10	25		-75.833	166.505	552

Ophionotus	victoriae	Op818_4C_3		Ross Sea	91	KY048261	2013	NBP-12-10	25		-75.833	166.505	552
Ophionotus	victoriae	Op818_4C_4		Ross Sea	91	KY048261	2013	NBP-12-10	25		-75.833	166.505	552
Ophionotus	victoriae	Op826_3C_2		Ross Sea	91	KY048261	2013	NBP-12-10	26		-74.708	168.408	489
Ophionotus	victoriae	Op843_3C_1		Ross Sea	91	KY048261	2013	NBP-12-10	28		-74.995	165.744	1101
Ophionotus	victoriae	Op843_7C_1		Ross Sea	91	KY048261	2013	NBP-12-10	28		-74.995	165.744	1101
Ophionotus	victoriae	Op843_7C_4		Ross Sea	91	KY048261	2013	NBP-12-10	28		-74.995	165.744	1101
Ophionotus	victoriae	N0066	NIWA85184	Ross Sea	94		2008	TAN0802		61	-75.622	169.805	521
Ophionotus	victoriae	N0074	NIWA85184	Ross Sea	95		2008	TAN0802		61	-75.622	169.805	521
Ophionotus	victoriae	94869A	NIWA94869	Ross Sea	96		2004	TAN0402		174	-71.494	171.604	483
Ophionotus	victoriae	N0104	NIWA84672	Ross Sea	102		2008	TAN0802		77	-76.833	179.950	664
Ophionotus	victoriae	PDIVA-M	SIOBICE4766	Ross Sea	109		2010	SIO McMurdo		IVA	-77.572	163.512	
Ophionotus	victoriae	PDIVA-N	SIOBICE4766	Ross Sea	110		2010	SIO McMurdo		IVA	-77.572	163.512	
Ophionotus	victoriae	93825B	NIWA93825	Ross Sea	163		2004	TAN0402		174	-71.494	171.604	483
Ophionotus	victoriae	94858A	NIWA94858	Ross Sea	164		2004	TAN0402		133	-71.645	170.219	252
Ophionotus	victoriae	94866A	NIWA94866	Ross Sea	165		2004	TAN0402		132	-71.648	170.180	172
Ophionotus	victoriae	N0111	NIWA84671	Scott Island	24		2008	TAN0802		223	-67.829	-179.587	403
Ophionotus	victoriae	N0114	NIWA84671	Scott Island	24		2008	TAN0802		223	-67.829	-179.587	403
Ophionotus	victoriae	N0115	NIWA84671	Scott Island	24		2008	TAN0802		223	-67.829	-179.587	403
Ophionotus	victoriae	N0116	NIWA84671	Scott Island	24		2008	TAN0802		223	-67.829	-179.587	403
Ophionotus	victoriae	N0119	NIWA84671	Scott Island	24		2008	TAN0802		223	-67.829	-179.587	403
Ophionotus	victoriae	N0120	NIWA84671	Scott Island	24		2008	TAN0802		223	-67.829	-179.587	403
Ophionotus	victoriae	N0121	NIWA84671	Scott Island	24		2008	TAN0802		223	-67.829	-179.587	403
Ophionotus	victoriae	N0123	NIWA84675	Scott Island	24		2008	TAN0802		247	-67.388	-179.897	144
Ophionotus	victoriae	N0124	NIWA84675	Scott Island	24		2008	TAN0802		247	-67.388	-179.897	144
Ophionotus	victoriae	N0125	NIWA84675	Scott Island	24		2008	TAN0802		247	-67.388	-179.897	144
Ophionotus	victoriae	N0126	NIWA84675	Scott Island	24		2008	TAN0802		247	-67.388	-179.897	144
Ophionotus	victoriae	N0127	NIWA84675	Scott Island	24		2008	TAN0802		247	-67.388	-179.897	144
Ophionotus	victoriae	N0128	NIWA84675	Scott Island	24		2008	TAN0802		247	-67.388	-179.897	144
Ophionotus	victoriae	N0129	NIWA84675	Scott Island	24		2008	TAN0802		247	-67.388	-179.897	144
Ophionotus	victoriae	N0133	NIWA84675	Scott Island	24		2008	TAN0802		247	-67.388	-179.897	144
Ophionotus	victoriae	N0134	NIWA84675	Scott Island	24		2008	TAN0802		247	-67.388	-179.897	144
Ophionotus	victoriae	N0113	NIWA84671	Scott Island	46		2008	TAN0802		223	-67.829	-179.587	403
Ophionotus	victoriae	N0132	NIWA84675	Scott Island	46		2008	TAN0802		247	-67.388	-179.897	144
Ophionotus	victoriae	N0136	NIWA84675	Scott Island	100		2008	TAN0802		247	-67.388	-179.897	144
Ophionotus	victoriae	N0112	NIWA84671	Scott Island	103		2008	TAN0802		223	-67.829	-179.587	403
Ophionotus	victoriae	N0118	NIWA84671	Scott Island	104		2008	TAN0802		223	-67.829	-179.587	403
Ophionotus	victoriae	N0122	NIWA84671	Scott Island	105		2008	TAN0802		223	-67.829	-179.587	403
Ophionotus	victoriae	N0130	NIWA84675	Scott Island	106		2008	TAN0802		247	-67.388	-179.897	144
Ophionotus	victoriae	N0131	NIWA84675	Scott Island	107		2008	TAN0802		247	-67.388	-179.897	144
Ophionotus	victoriae	N0138	NIWA84675	Scott Island	108		2008	TAN0802		247	-67.388	-179.897	144
Ophionotus	victoriae	DSOPH1908		Shetland Islands	1	FJ917337	2006	JR144	EI-AGT-4		-61.334	-55.195	201

Ophionotus	victoriae	DSOPH2154		Shetland Islands	1	FJ917337	2006	JR144	ST-EBS-4		-59.470	-27.276	308
Ophionotus	victoriae	DSOPH2327		Shetland Islands	1	FJ917339	2006	JR144	EI-AGT-3		-61.386	-55.193	483
Ophionotus	victoriae	DSOPH721		Shetland Islands	1	FJ917337	2006	JR144	EI-AGT-3		-61.386	-55.193	483
Ophionotus	victoriae	DSOPH722		Shetland Islands	1	FJ917337	2006	JR144	EI-AGT-3		-61.386	-55.193	483
Ophionotus	victoriae	DSOPH724		Shetland Islands	1	FJ917339	2006	JR144	EI-AGT-3		-61.386	-55.193	483
Ophionotus	victoriae	DSOPH725		Shetland Islands	1	FJ917337	2006	JR144	EI-AGT-3		-61.386	-55.193	483
Ophionotus	victoriae	DSOPH1756		Shetland Islands	3	FJ917340	2006	JR144	EI-AGT-4		-61.334	-55.195	201
Ophionotus	victoriae	DSOPH2155		Shetland Islands	3	FJ917340	2006	JR144	LI-AGT-4		-62.525	-61.827	193
Ophionotus	victoriae	SIOBICS5741E	SIOBICE7575	Shetland Islands	4		2011	Scotia 2011	SSH1	94	-62.337	-60.744	183
Ophionotus	victoriae	114.3C		Shetland Islands	5	FJ917320	2004	LMG-04-14	64		-62.934	-60.660	161
Ophionotus	victoriae	E73.2C.10		Shetland Islands	5	FJ917320	2004	LMG-04-14	44		-62.100	-58.393	276
Ophionotus	victoriae	SIOBICS5741B	SIOBICE7575	Shetland Islands	5		2011	Scotia 2011	SSH1	94	-62.337	-60.744	183
Ophionotus	victoriae	SIOBICS5741H	SIOBICE7575	Shetland Islands	5		2011	Scotia 2011	SSH1	94	-62.337	-60.744	183
Ophionotus	victoriae	AP46 (haplotype ID)		Shetland Islands	6	FJ917352		Laurence M. Gould			-62.283	-58.450	192
Ophionotus	victoriae	DSOPH2156		Shetland Islands	6	FJ917309	2006	JR144	LI-AGT-4		-62.525	-61.827	193
Ophionotus	victoriae	E73.2C.01		Shetland Islands	6	FJ917309	2004	LMG-04-14	44		-62.100	-58.393	276
Ophionotus	victoriae	E73.2C.05		Shetland Islands	6	FJ917309	2004	LMG-04-14	44		-62.100	-58.393	276
Ophionotus	victoriae	SIOBICS5741K	SIOBICE7575	Shetland Islands	6		2011	Scotia 2011	SSH1	94	-62.337	-60.744	183
Ophionotus	victoriae	SIOBICS5741O	SIOBICE7575	Shetland Islands	6		2011	Scotia 2011	SSH1	94	-62.337	-60.744	183
Ophionotus	victoriae	SIOBICS5741P	SIOBICE7575	Shetland Islands	6		2011	Scotia 2011	SSH1	94	-62.337	-60.744	183
Ophionotus	victoriae	SIOBICS5743	SIOBICE5023	Shetland Islands	6		2011	Scotia 2011	SSH1	94	-62.337	-60.744	183
Ophionotus	victoriae	114.13C		Shetland Islands	7	FJ917322	2004	LMG-04-14	64		-62.934	-60.660	161
Ophionotus	victoriae	114.6C		Shetland Islands	7	FJ917322	2004	LMG-04-14	64		-62.934	-60.660	161
Ophionotus	victoriae	DSOPH1910		Shetland Islands	7	FJ917322	2006	JR144	EI-AGT-4		-61.334	-55.195	201
Ophionotus	victoriae	E73.2C.06		Shetland Islands	7	FJ917322	2004	LMG-04-14	44		-62.100	-58.393	276
Ophionotus	victoriae	SIOBICS5741C	SIOBICE7575	Shetland Islands	7		2011	Scotia 2011	SSH1	94	-62.337	-60.744	183
Ophionotus	victoriae	SIOBICS5741I	SIOBICE7575	Shetland Islands	7		2011	Scotia 2011	SSH1	94	-62.337	-60.744	183
Ophionotus	victoriae	114.10C		Shetland Islands	8	FJ917316	2004	LMG-04-14	64		-62.934	-60.660	161
Ophionotus	victoriae	114.4C		Shetland Islands	8	FJ917316	2004	LMG-04-14	64		-62.934	-60.660	161
Ophionotus	victoriae	114.7C		Shetland Islands	8	FJ917316	2004	LMG-04-14	64		-62.934	-60.660	161
Ophionotus	victoriae	114.8C		Shetland Islands	8	FJ917316	2004	LMG-04-14	64		-62.934	-60.660	161
Ophionotus	victoriae	E73.2C.09		Shetland Islands	8	FJ917316	2004	LMG-04-14	44		-62.100	-58.393	276
Ophionotus	victoriae	SIOBICS5741N	SIOBICE7575	Shetland Islands	8		2011	Scotia 2011	SSH1	94	-62.337	-60.744	183
Ophionotus	victoriae	114.5C		Shetland Islands	10	FJ917312	2004	LMG-04-14	64		-62.934	-60.660	161
Ophionotus	victoriae	DSOPH1909		Shetland Islands	10	FJ917312	2006	JR144	EI-AGT-4		-61.334	-55.195	201
Ophionotus	victoriae	DSOPH1912		Shetland Islands	14	FJ917310	2006	JR144	EI-AGT-4		-61.334	-55.195	201
Ophionotus	victoriae	DSOPH2161		Shetland Islands	14	FJ917310	2006	JR144	LI-AGT-1		-62.276	-61.596	1511
Ophionotus	victoriae	SIOBICS5741Q	SIOBICE7575	Shetland Islands	14		2011	Scotia 2011	SSH1	94	-62.337	-60.744	183
Ophionotus	victoriae	SIOBICS5742	SIOBICE5171	Shetland Islands	14		2011	Scotia 2011	SSH1	94	-62.337	-60.744	183
Ophionotus	victoriae	AP44 (haplotype ID)		Shetland Islands	24	FJ917350	2008	JR179	BIO6-AGT-2A		-62.283	-58.450	192

Ophionotus	victoriae	E73.2C.02		Shetland Islands	24	FJ917318	2004	LMG-04-14	44		-62.100	-58.393	276
Ophionotus	victoriae	E73.2C.11		Shetland Islands	24	FJ917318	2004	LMG-04-14	44		-62.100	-58.393	276
Ophionotus	victoriae	SIOBICS5741M	SIOBICE7575	Shetland Islands	24		2011	Scotia 2011	SSH1	94	-62.337	-60.744	183
Ophionotus	victoriae	DSOPH1898		Shetland Islands	25	FJ917319	2006	JR144	EI-AGT-4		-61.334	-55.195	201
Ophionotus	victoriae	E73.2C.08		Shetland Islands	25	FJ917319	2004	LMG-04-14	44		-62.100	-58.393	276
Ophionotus	victoriae	SIOBICS5741R	SIOBICE7575	Shetland Islands	25		2011	Scotia 2011	SSH1	94	-62.337	-60.744	183
Ophionotus	victoriae	114.2C		Shetland Islands	26	FJ917321	2004	LMG-04-14	64		-62.934	-60.660	161
Ophionotus	victoriae	114.11C		Shetland Islands	27	FJ917323	2004	LMG-04-14	64		-62.934	-60.660	161
Ophionotus	victoriae	SIOBICS5741F	SIOBICE7575	Shetland Islands	32		2011	Scotia 2011	SSH1	94	-62.337	-60.744	183
Ophionotus	victoriae	SIOBICS5741A	SIOBICE7575	Shetland Islands	39		2011	Scotia 2011	SSH1	94	-62.337	-60.744	183
Ophionotus	victoriae	SIOBICS5741D	SIOBICE7575	Shetland Islands	39		2011	Scotia 2011	SSH1	94	-62.337	-60.744	183
Ophionotus	victoriae	SIOBICS5741G	SIOBICE7575	Shetland Islands	40		2011	Scotia 2011	SSH1	94	-62.337	-60.744	183
Ophionotus	victoriae	SIOBICS5741J	SIOBICE7575	Shetland Islands	40		2011	Scotia 2011	SSH1	94	-62.337	-60.744	183
Ophionotus	victoriae	E73.2C.03		Shetland Islands	45	FJ917351	2004	LMG-04-14	44		-62.100	-58.393	276
Ophionotus	victoriae	E73.2C.12		Shetland Islands	46	FJ917353	2004	LMG-04-14	44		-62.100	-58.393	276
Ophionotus	victoriae	DSOPH1899		Shetland Islands	55	KY048218	2006	JR144	EI-AGT-4		-61.334	-55.195	201
Ophionotus	victoriae	DSOPH1900		Shetland Islands	55	KY048218	2006	JR144	EI-AGT-4		-61.334	-55.195	201
Ophionotus	victoriae	DSOPH1911		Shetland Islands	56	KY048219	2006	JR144	EI-AGT-4		-61.334	-55.195	201
Ophionotus	victoriae	DSOPH2157		Shetland Islands	60	KY048223	2006	JR144	RGBT-02		-61.966	-57.244	129.76
Ophionotus	victoriae	DSOPH3528		Shetland Islands	83	KY048252	2011	Polarstern ANT-XXVII/3	PS77_222-5		-62.297	-58.678	873
Ophionotus	victoriae	SIOBICS5741L	SIOBICE7575	Shetland Islands	136		2011	Scotia 2011	SSH1	94	-62.337	-60.744	183
Ophionotus	victoriae	SIOBICS5741S	SIOBICE7575	Shetland Islands	137		2011	Scotia 2011	SSH1	94	-62.337	-60.744	183
Ophionotus	victoriae	SIOBICS20231	SIOBICE6408	South Georgia	18		2013	Scotia 2013	SG4b	9	-53.634	-37.307	167
Ophionotus	victoriae	SIOBICS20237	SIOBICE6420	South Georgia	19		2013	Scotia 2013	SG4	5	-53.715	-36.836	190
Ophionotus	victoriae	DSOPH1904		South Orkney Island	31	FJ917328	2006	JR144	PB-AGT-1B		-61.036	-46.955	1630
Ophionotus	victoriae	SIOBICS0990J	SIOBICE4784	South Sandwich Islands	10		2011	Scotia 2011	SS1	25	-57.034	-26.759	118
Ophionotus	victoriae	DSOPH2160		South Sandwich Islands	14	KY048225	2006	JR144	LI-AGT-1		-62.276	-61.596	1511
Ophionotus	victoriae	194.1E.01		South Sandwich Islands	31	FJ917328	2004	LMG-04-14	34		-58.784	-26.343	270
Ophionotus	victoriae	194.1E.06		South Sandwich Islands	31	FJ917328	2004	LMG-04-14	34		-58.784	-26.343	270
Ophionotus	victoriae	194.1E.09		South Sandwich Islands	31	FJ917335	2004	LMG-04-14	34		-58.784	-26.343	270
Ophionotus	victoriae	195.1E.03		South Sandwich Islands	31	FJ917328	2006	LMG-04-14	32		-57.089	-30.399	130
Ophionotus	victoriae	195.1E.06		South Sandwich Islands	31	FJ917328	2006	LMG-04-14	32		-57.089	-30.399	130
Ophionotus	victoriae	195.1E.08		South Sandwich Islands	31	FJ917328	2006	LMG-04-14	32		-57.089	-30.399	130
Ophionotus	victoriae	DSOPH2149		South Sandwich Islands	31	FJ917328	2006	JR144	ST-AGT-1		-59.518	-27.436	1545
Ophionotus	victoriae	SIOBICS0539A	SIOBICE4802	South Sandwich Islands	31		2011	Scotia 2011	SS2	33	-58.475	-26.205	161

Ophionotus	victoriae	SIOBICS0539C	SIOBICE4802	South Sandwich Islands	31	2011	Scotia 2011	SS2	33	-58.475	-26.205	161
Ophionotus	victoriae	SIOBICS0539E	SIOBICE4802	South Sandwich Islands	31	2011	Scotia 2011	SS2	33	-58.475	-26.205	161
Ophionotus	victoriae	SIOBICS0539F	SIOBICE4802	South Sandwich Islands	31	2011	Scotia 2011	SS2	33	-58.475	-26.205	161
Ophionotus	victoriae	SIOBICS0539L	SIOBICE4802	South Sandwich Islands	31	2011	Scotia 2011	SS2	33	-58.475	-26.205	161
Ophionotus	victoriae	SIOBICS0539M	SIOBICE4802	South Sandwich Islands	31	2011	Scotia 2011	SS2	33	-58.475	-26.205	161
Ophionotus	victoriae	SIOBICS0539Q	SIOBICE4802	South Sandwich Islands	31	2011	Scotia 2011	SS2	33	-58.475	-26.205	161
Ophionotus	victoriae	SIOBICS0539R	SIOBICE4802	South Sandwich Islands	31	2011	Scotia 2011	SS2	33	-58.475	-26.205	161
Ophionotus	victoriae	SIOBICS0539S	SIOBICE4802	South Sandwich Islands	31	2011	Scotia 2011	SS2	33	-58.475	-26.205	161
Ophionotus	victoriae	SIOBICS0539T	SIOBICE4802	South Sandwich Islands	31	2011	Scotia 2011	SS2	33	-58.475	-26.205	161
Ophionotus	victoriae	SIOBICS0554N	SIOBICE4786	South Sandwich Islands	31	2011	Scotia 2011	SS3	41	-59.394	-27.323	110
Ophionotus	victoriae	SIOBICS0554P	SIOBICE4786	South Sandwich Islands	31	2011	Scotia 2011	SS3	41	-59.394	-27.323	110
Ophionotus	victoriae	SIOBICS0554Q	SIOBICE4786	South Sandwich Islands	31	2011	Scotia 2011	SS3	41	-59.394	-27.323	110
Ophionotus	victoriae	SIOBICS0554R	SIOBICE4786	South Sandwich Islands	31	2011	Scotia 2011	SS3	41	-59.394	-27.323	110
Ophionotus	victoriae	SIOBICS0554S	SIOBICE4786	South Sandwich Islands	31	2011	Scotia 2011	SS3	41	-59.394	-27.323	110
Ophionotus	victoriae	SIOBICS0990A	SIOBICE4784	South Sandwich Islands	31	2011	Scotia 2011	SS1	25	-57.034	-26.759	118
Ophionotus	victoriae	SIOBICS0990D	SIOBICE4784	South Sandwich Islands	31	2011	Scotia 2011	SS1	25	-57.034	-26.759	118
Ophionotus	victoriae	SIOBICS0990L	SIOBICE4784	South Sandwich Islands	31	2011	Scotia 2011	SS1	25	-57.034	-26.759	118
Ophionotus	victoriae	SIOBICS0990M	SIOBICE4784	South Sandwich Islands	31	2011	Scotia 2011	SS1	25	-57.034	-26.759	118
Ophionotus	victoriae	SIOBICS0990P	SIOBICE4784	South Sandwich Islands	31	2011	Scotia 2011	SS1	25	-57.034	-26.759	118
Ophionotus	victoriae	SIOBICS0990T	SIOBICE4784	South Sandwich Islands	31	2011	Scotia 2011	SS1	25	-57.034	-26.759	118
Ophionotus	victoriae	WAMZ44932	WAMZ44932	South Sandwich Islands	31	2017	ACE 2016/17	90	2590	-59.472	-27.264	230
Ophionotus	victoriae	WAMZ44934	WAMZ44934	South Sandwich Islands	31	2017	ACE 2016/17	90	2590	-59.472	-27.264	230
Ophionotus	victoriae	WAMZ44935	WAMZ44935	South Sandwich Islands	31	2017	ACE 2016/17	90	2590	-59.472	-27.264	230
Ophionotus	victoriae	WAMZ44936	WAMZ44936	South Sandwich Islands	31	2017	ACE 2016/17	90	2590	-59.472	-27.264	230
Ophionotus	victoriae	WAMZ44938	WAMZ44938	South Sandwich Islands	31	2017	ACE 2016/17	90	2590	-59.472	-27.264	230
Ophionotus	victoriae	WAMZ44939	WAMZ44939	South Sandwich Islands	31	2017	ACE 2016/17	90	2590	-59.472	-27.264	230
Ophionotus	victoriae	WAMZ44941	WAMZ44941	South Sandwich Islands	31	2017	ACE 2016/17	90	2590	-59.472	-27.264	230
Ophionotus	victoriae	WAMZ44942	WAMZ44942	South Sandwich Islands	31	2017	ACE 2016/17	90	2590	-59.472	-27.264	230

Ophionotus	victoriae	WAMZ44944	WAMZ44944	South Sandwich Islands	31		2017	ACE 2016/17	90	2590	-59.472	-27.264	230
Ophionotus	victoriae	WAMZ44945	WAMZ44945	South Sandwich Islands	31		2017	ACE 2016/17	90	2590	-59.472	-27.264	230
Ophionotus	victoriae	WAMZ44946	WAMZ44946	South Sandwich Islands	31		2017	ACE 2016/17	90	2590	-59.472	-27.264	230
Ophionotus	victoriae	194.1E.02		South Sandwich Islands	32	FJ917329	2004	LMG-04-14	34		-58.784	-26.343	270
Ophionotus	victoriae	194.1E.05		South Sandwich Islands	32	FJ917332	2004	LMG-04-14	34		-58.784	-26.343	270
Ophionotus	victoriae	195.1E.05		South Sandwich Islands	32	FJ917329	2006	LMG-04-14	32		-57.089	-30.399	130
Ophionotus	victoriae	195.1E.07		South Sandwich Islands	32	FJ917332	2006	LMG-04-14	32		-57.089	-30.399	130
Ophionotus	victoriae	DSOPH1903		South Sandwich Islands	32	FJ917329	2006	JR144	ST-AGT-3		-59.481	-27.279	550
Ophionotus	victoriae	DSOPH2142		South Sandwich Islands	32	FJ917329	2006	JR144	ST-AGT-3		-59.481	-27.279	550
Ophionotus	victoriae	DSOPH2143		South Sandwich Islands	32	FJ917329	2006	JR144	ST-AGT-1		-59.518	-27.436	1545
Ophionotus	victoriae	DSOPH2144		South Sandwich Islands	32	FJ917329	2006	JR144	ST-AGT-1		-59.518	-27.436	1545
Ophionotus	victoriae	DSOPH2145		South Sandwich Islands	32	FJ917332	2006	JR144	ST-AGT-1		-59.518	-27.436	1545
Ophionotus	victoriae	DSOPH2148		South Sandwich Islands	32	FJ917329	2006	JR144	ST-AGT-1		-59.518	-27.436	1545
Ophionotus	victoriae	DSOPH2152		South Sandwich Islands	32	FJ917329	2006	JR144	ST-AGT-1		-59.518	-27.436	1545
Ophionotus	victoriae	SIOBICS0185	SIOBICE5232	South Sandwich Islands	32		2011	Scotia 2011	SS1A	30	-56.723	-27.036	134
Ophionotus	victoriae	SIOBICS0554T	SIOBICE4786	South Sandwich Islands	32		2011	Scotia 2011	SS3	41	-59.394	-27.323	110
Ophionotus	victoriae	SIOBICS0594A	SIOBICE4790	South Sandwich Islands	32		2011	Scotia 2011	SS3a	43	-59.383	-27.345	926
Ophionotus	victoriae	SIOBICS0594B	SIOBICE4790	South Sandwich Islands	32		2011	Scotia 2011	SS3a	43	-59.383	-27.345	926
Ophionotus	victoriae	SIOBICS0594C	SIOBICE4790	South Sandwich Islands	32		2011	Scotia 2011	SS3a	43	-59.383	-27.345	926
Ophionotus	victoriae	SIOBICS0594E	SIOBICE4790	South Sandwich Islands	32		2011	Scotia 2011	SS3a	43	-59.383	-27.345	926
Ophionotus	victoriae	SIOBICS0594G	SIOBICE4790	South Sandwich Islands	32		2011	Scotia 2011	SS3a	43	-59.383	-27.345	926
Ophionotus	victoriae	SIOBICS0594H	SIOBICE4790	South Sandwich Islands	32		2011	Scotia 2011	SS3a	43	-59.383	-27.345	926
Ophionotus	victoriae	SIOBICS0990G	SIOBICE4784	South Sandwich Islands	32		2011	Scotia 2011	SS1	25	-57.034	-26.759	118
Ophionotus	victoriae	SIOBICS0990I	SIOBICE4784	South Sandwich Islands	32		2011	Scotia 2011	SS1	25	-57.034	-26.759	118
Ophionotus	victoriae	SIOBICS0990Q	SIOBICE4784	South Sandwich Islands	32		2011	Scotia 2011	SS1	25	-57.034	-26.759	118
Ophionotus	victoriae	WAMZ44590	WAMZ44590	South Sandwich Islands	32		2017	ACE 2016/17	90	2590	-59.472	-27.264	230
Ophionotus	victoriae	WAMZ44937	WAMZ44937	South Sandwich Islands	32		2017	ACE 2016/17	90	2590	-59.472	-27.264	230
Ophionotus	victoriae	WAMZ44940	WAMZ44940	South Sandwich Islands	32		2017	ACE 2016/17	90	2590	-59.472	-27.264	230

Ophionotus	victoriae	WAMZ44943	WAMZ44943	South Sandwich Islands	32		2017	ACE 2016/17	90	2590	-59.472	-27.264	230
Ophionotus	victoriae	194.1E.03		South Sandwich Islands	33	FJ917330	2004	LMG-04-14	34		-58.784	-26.343	270
Ophionotus	victoriae	194.1E.04		South Sandwich Islands	34	FJ917331	2004	LMG-04-14	34		-58.784	-26.343	270
Ophionotus	victoriae	SIOBICS0539J	SIOBICE4802	South Sandwich Islands	34		2011	Scotia 2011	SS2	33	-58.475	-26.205	161
Ophionotus	victoriae	194.1E.07		South Sandwich Islands	35	FJ917333	2004	LMG-04-14	34		-58.784	-26.343	270
Ophionotus	victoriae	195.1E.04		South Sandwich Islands	35	FJ917333	2004	LMG-04-14	32		-57.089	-30.399	130
Ophionotus	victoriae	SIOBICS0539I	SIOBICE4802	South Sandwich Islands	35		2011	Scotia 2011	SS2	33	-58.475	-26.205	161
Ophionotus	victoriae	SIOBICS0554K	SIOBICE4786	South Sandwich Islands	35		2011	Scotia 2011	SS3	41	-59.394	-27.323	110
Ophionotus	victoriae	SIOBICS0990B	SIOBICE4784	South Sandwich Islands	35		2011	Scotia 2011	SS1	25	-57.034	-26.759	118
Ophionotus	victoriae	WAMZ44933	WAMZ44933	South Sandwich Islands	35		2017	ACE 2016/17	90	2590	-59.472	-27.264	230
Ophionotus	victoriae	194.1E.08		South Sandwich Islands	36	FJ917334	2004	LMG-04-14	34		-58.784	-26.343	270
Ophionotus	victoriae	SIOBICS0539N	SIOBICE4802	South Sandwich Islands	36		2011	Scotia 2011	SS2	33	-58.475	-26.205	161
Ophionotus	victoriae	SIOBICS0539O	SIOBICE4802	South Sandwich Islands	36		2011	Scotia 2011	SS2	33	-58.475	-26.205	161
Ophionotus	victoriae	SIOBICS0554M	SIOBICE4786	South Sandwich Islands	36		2011	Scotia 2011	SS3	41	-59.394	-27.323	110
Ophionotus	victoriae	SIOBICS0554O	SIOBICE4786	South Sandwich Islands	36		2011	Scotia 2011	SS3	41	-59.394	-27.323	110
Ophionotus	victoriae	SIOBICS0990R	SIOBICE4784	South Sandwich Islands	36		2011	Scotia 2011	SS1	25	-57.034	-26.759	118
Ophionotus	victoriae	DSOPH2146		South Sandwich Islands	57	KY048220	2006	JR144	ST-AGT-1		-59.518	-27.436	1545
Ophionotus	victoriae	DSOPH2150		South Sandwich Islands	58	KY048221	2006	JR144	ST-AGT-1		-59.518	-27.436	1545
Ophionotus	victoriae	DSOPH2151		South Sandwich Islands	59	KY048222	2006	JR144	ST-AGT-1		-59.518	-27.436	1545
Ophionotus	victoriae	DSOPH2159		South Sandwich Islands	60	KY048223	2006	JR144	LI-AGT-1		-62.276	-61.596	1511
Ophionotus	victoriae	DSOPH2158		South Sandwich Islands	61	KY048224	2006	JR144	LI-AGT-1		-62.276	-61.596	1511
Ophionotus	victoriae	SIOBICS0460	SIOBICE5187	South Sandwich Islands	113		2011	Scotia 2011	SS1A	32	-56.709	-27.049	116
Ophionotus	victoriae	SIOBICS0539B	SIOBICE4802	South Sandwich Islands	114		2011	Scotia 2011	SS2	33	-58.475	-26.205	161
Ophionotus	victoriae	SIOBICS0539D	SIOBICE4802	South Sandwich Islands	115		2011	Scotia 2011	SS2	33	-58.475	-26.205	161
Ophionotus	victoriae	SIOBICS0539G	SIOBICE4802	South Sandwich Islands	116		2011	Scotia 2011	SS2	33	-58.475	-26.205	161
Ophionotus	victoriae	SIOBICS0539H	SIOBICE4802	South Sandwich Islands	117		2011	Scotia 2011	SS2	33	-58.475	-26.205	161
Ophionotus	victoriae	SIOBICS0539K	SIOBICE4802	South Sandwich Islands	118		2011	Scotia 2011	SS2	33	-58.475	-26.205	161
Ophionotus	victoriae	SIOBICS0539P	SIOBICE4802	South Sandwich Islands	119		2011	Scotia 2011	SS2	33	-58.475	-26.205	161

Ophionotus	victoriae	SIOBICS0554L	SIOBICE4786	South Sandwich Islands	120		2011	Scotia 2011	SS3	41	-59.394	-27.323	110
Ophionotus	victoriae	SIOBICS0594D	SIOBICE4790	South Sandwich Islands	121		2011	Scotia 2011	SS3a	43	-59.383	-27.345	926
Ophionotus	victoriae	SIOBICS0594I	SIOBICE4790	South Sandwich Islands	122		2011	Scotia 2011	SS3a	43	-59.383	-27.345	926
Ophionotus	victoriae	SIOBICS0594J	SIOBICE4790	South Sandwich Islands	123		2011	Scotia 2011	SS3a	43	-59.383	-27.345	926
Ophionotus	victoriae	SIOBICS0990C	SIOBICE4784	South Sandwich Islands	124		2011	Scotia 2011	SS1	25	-57.034	-26.759	118
Ophionotus	victoriae	SIOBICS0990E	SIOBICE4784	South Sandwich Islands	125		2011	Scotia 2011	SS1	25	-57.034	-26.759	118
Ophionotus	victoriae	SIOBICS0990F	SIOBICE4784	South Sandwich Islands	126		2011	Scotia 2011	SS1	25	-57.034	-26.759	118
Ophionotus	victoriae	SIOBICS0990K	SIOBICE4784	South Sandwich Islands	127		2011	Scotia 2011	SS1	25	-57.034	-26.759	118
Ophionotus	victoriae	SIOBICS0990N	SIOBICE4784	South Sandwich Islands	128		2011	Scotia 2011	SS1	25	-57.034	-26.759	118
Ophionotus	victoriae	SIOBICS0990O	SIOBICE4784	South Sandwich Islands	129		2011	Scotia 2011	SS1	25	-57.034	-26.759	118
Ophionotus	victoriae	DSOPH2962		Weddell Sea	1	FJ917337	2011	Polarstern ANT-XXVII/3	PS77_265-2		-70.794	-10.670	634
Ophionotus	victoriae	DSOPH2963		Weddell Sea	1	FJ917337	2011	Polarstern ANT-XXVII/3	PS77_265-2		-70.794	-10.670	634
Ophionotus	victoriae	DSOPH3033		Weddell Sea	1	FJ917337	2011	Polarstern ANT-XXVII/3	PS77_260-6		-70.840	-10.597	260
Ophionotus	victoriae	DSOPH3035		Weddell Sea	1	FJ917337	2011	Polarstern ANT-XXVII/3	PS77_260-6		-70.840	-10.597	260
Ophionotus	victoriae	DSOPH3185		Weddell Sea	1	FJ917337	2011	Polarstern ANT-XXVII/3	PS77_308-1		-70.855	-10.589	224
Ophionotus	victoriae	DSOPH3216		Weddell Sea	1	FJ917337	2011	Polarstern ANT-XXVII/3	PS77_301-1		-70.851	-10.588	226
Ophionotus	victoriae	DSOPH3239		Weddell Sea	1	FJ917337	2011	Polarstern ANT-XXVII/3	PS77_284-1		-70.972	-10.504	290
Ophionotus	victoriae	308-1.7	WAMZ88554	Weddell Sea	1		2011	Polarstern ANT-XXVII/3	PS77_308-1		-70.858	-10.593	250
Ophionotus	victoriae	265-2.12	WAMZ88558	Weddell Sea	1		2011	Polarstern ANT-XXVII/3	PS77_265-2		-70.793	-10.678	615
Ophionotus	victoriae	265-2.11	WAMZ88576	Weddell Sea	1		2011	Polarstern ANT-XXVII/3	PS77_265-2		-70.793	-10.678	615
Ophionotus	victoriae	308-1.10	WAMZ88584	Weddell Sea	1		2011	Polarstern ANT-XXVII/3	PS77_308-10		-70.858	-10.593	250
Ophionotus	victoriae	1.140.3	WAMZ88587	Weddell Sea	1		2014	Polarstern ANT-XXIX/9	PS82_191-1		-74.666	-33.733	592
Ophionotus	victoriae	1.83.2	WAMZ88590	Weddell Sea	1		2014	Polarstern ANT-XXIX/9	PS82_67-1		-77.101	-36.546	1101
Ophionotus	victoriae	DSOPH3120		Weddell Sea	2	KY048248	2011	Polarstern ANT-XXVII/3	PS77_286-1		-70.844	-10.602	248
Ophionotus	victoriae	DSOPH2971		Weddell Sea	3	FJ917340	2011	Polarstern ANT-XXVII/3	PS77_265-2		-70.794	-10.670	634
Ophionotus	victoriae	DSOPH3098		Weddell Sea	3	FJ917340	2011	Polarstern ANT-XXVII/3	PS77_291-1		-70.842	-10.587	268
Ophionotus	victoriae	265-2.10	WAMZ88570	Weddell Sea	3		2011	Polarstern ANT-XXVII/3	PS77_265-2		-70.793	-10.678	615
Ophionotus	victoriae	1.140.4	WAMZ88588	Weddell Sea	14		2014	Polarstern ANT-XXIX/9	PS82_67-1		-77.101	-36.546	1101

Ophionotus	victoriae	265-2.11	WAMZ88559	Weddell Sea	24		2011	Polarstern ANT-XXVII/3	PS77_265-2	-70.793	-10.678	615
Ophionotus	victoriae	1.140.1	WAMZ88585	Weddell Sea	24		2014	Polarstern ANT-XXIX/9	PS82_191-1	-74.666	-33.733	592
Ophionotus	victoriae	1.140.2	WAMZ88586	Weddell Sea	24		2014	Polarstern ANT-XXIX/9	PS82_191-1	-74.666	-33.733	592
Ophionotus	victoriae	1.158	WAMZ88595	Weddell Sea	24		2014	Polarstern ANT-XXIX/9	PS82_126-1	-75.512	-27.487	282
Ophionotus	victoriae	1.158.1	WAMZ88596	Weddell Sea	24		2014	Polarstern ANT-XXIX/9	PS82_126-1	-75.512	-27.487	282
Ophionotus	victoriae	DSOPH2964		Weddell Sea	43	FJ917348	2011	Polarstern ANT-XXVII/3	PS77_265-2	-70.794	-10.670	634
Ophionotus	victoriae	265-2.13	WAMZ88577	Weddell Sea	43		2011	Polarstern ANT-XXVII/3	PS77_265-2	-70.793	-10.678	615
Ophionotus	victoriae	1.164.1	WAMZ88591	Weddell Sea	64		2014	Polarstern ANT-XXIX/9	PS82_151-1	-74.541	-28.531	1750
Ophionotus	victoriae	1.152.1	WAMZ88597	Weddell Sea	64		2014	Polarstern ANT-XXIX/9	PS82_115-1	-77.611	-38.939	1058
Ophionotus	victoriae	1.164.2	WAMZ88592	Weddell Sea	68		2014	Polarstern ANT-XXIX/9	PS82_151-1	-74.541	-28.531	1750
Ophionotus	victoriae	1.152.3	WAMZ88599	Weddell Sea	68		2014	Polarstern ANT-XXIX/9	PS82_115-1	-77.611	-38.939	1058
Ophionotus	victoriae	DSOPH3096		Weddell Sea	78	KY048246	2011	Polarstern ANT-XXVII/3	PS77_291-1	-70.842	-10.587	268
Ophionotus	victoriae	DSOPH3311		Weddell Sea	78	KY048246	2011	Polarstern ANT-XXVII/3	PS77_275-3	-70.934	-10.496	238
Ophionotus	victoriae	274-3.14	WAMZ88571	Weddell Sea	78		2011	Polarstern ANT-XXVII/3	PS77_274-3	-70.949	-10.574	333
Ophionotus	victoriae	308-1.8	WAMZ88583	Weddell Sea	78		2011	Polarstern ANT-XXVII/3	PS77_308-1	-70.858	-10.593	250
Ophionotus	victoriae	DSOPH3097		Weddell Sea	79	KY048247	2011	Polarstern ANT-XXVII/3	PS77_291-1	-70.842	-10.587	268
Ophionotus	victoriae	291-1.3	WAMZ88579	Weddell Sea	79		2011	Polarstern ANT-XXVII/3	PS77_291-1	-70.847	-10.590	284
Ophionotus	victoriae	1.164.3	WAMZ88593	Weddell Sea	160		2014	Polarstern ANT-XXIX/9	PS82_151-1	-74.541	-28.531	1750
Ophionotus	victoriae	1.164.4	WAMZ88594	Weddell Sea	161		2014	Polarstern ANT-XXIX/9	PS82_151-1	-74.541	-28.531	1750
Ophionotus	victoriae	1.152.2	WAMZ88598	Weddell Sea	162		2014	Polarstern ANT-XXIX/9	PS82_115-1	-77.611	-38.939	1058
Ophionotus	victoriae	312.3C.01		West Antarctic Peninsula	1	FJ917337	2006	LMG-06-05	17	-64.350	-61.760	334
Ophionotus	victoriae	312.3C.03		West Antarctic Peninsula	1	FJ917337	2006	LMG-06-05	17	-64.350	-61.760	334
Ophionotus	victoriae	312.3C.07		West Antarctic Peninsula	1	FJ917339	2006	LMG-06-05	17	-64.350	-61.760	334
Ophionotus	victoriae	312.3C.09		West Antarctic Peninsula	1	FJ917339	2006	LMG-06-05	17	-64.350	-61.760	334
Ophionotus	victoriae	312.3C.16		West Antarctic Peninsula	1	FJ917337	2006	LMG-06-05	17	-64.350	-61.760	334
Ophionotus	victoriae	398.1E.12		West Antarctic Peninsula	1	FJ917337	2006	LMG-06-05	47	-67.717	-68.243	170
Ophionotus	victoriae	398.1E.13		West Antarctic Peninsula	1	FJ917345	2006	LMG-06-05	47	-67.717	-68.243	170
Ophionotus	victoriae	422.1C.01		West Antarctic Peninsula	1	FJ917339	2006	LMG-06-05	58	-65.184	-64.243	285

Ophionotus	victoriae	422.1C.03	West Antarctic Peninsula	1	FJ917337	2006	LMG-06-05	58	-65.184	-64.243	285
Ophionotus	victoriae	422.1C.04	West Antarctic Peninsula	1	FJ917339	2006	LMG-06-05	58	-65.184	-64.243	285
Ophionotus	victoriae	422.1C.05	West Antarctic Peninsula	1	FJ917339	2006	LMG-06-05	58	-65.184	-64.243	285
Ophionotus	victoriae	422.1C.06	West Antarctic Peninsula	1	FJ917337	2006	LMG-06-05	58	-65.184	-64.243	285
Ophionotus	victoriae	422.1C.08	West Antarctic Peninsula	1	FJ917339	2006	LMG-06-05	58	-65.184	-64.243	285
Ophionotus	victoriae	422.1C.14	West Antarctic Peninsula	1	FJ917339	2006	LMG-06-05	58	-65.184	-64.243	285
Ophionotus	victoriae	DSOPH446	West Antarctic Peninsula	1	FJ917337	2009	JR230	AGT-2B	-67.983	-68.438	586
Ophionotus	victoriae	Op1042_3E_1	West Antarctic Peninsula	1	FJ917337	2013	LMG-13-12	26	-64.846	-62.959	301
Ophionotus	victoriae	Op1042_3E_2	West Antarctic Peninsula	1	FJ917339	2013	LMG-13-12	26	-64.846	-62.959	301
Ophionotus	victoriae	Op1042_3E_3	West Antarctic Peninsula	1	FJ917339	2013	LMG-13-12	26	-64.846	-62.959	301
Ophionotus	victoriae	Op1042_3E_4	West Antarctic Peninsula	1	FJ917339	2013	LMG-13-12	26	-64.846	-62.959	301
Ophionotus	victoriae	Op1042_3E_6	West Antarctic Peninsula	1	FJ917337	2013	LMG-13-12	26	-64.846	-62.959	301
Ophionotus	victoriae	Op1042_3E_9	West Antarctic Peninsula	1	FJ917339	2013	LMG-13-12	26	-64.846	-62.959	301
Ophionotus	victoriae	Op867_4E_10	West Antarctic Peninsula	1	FJ917339	2013	LMG-13-12	3	-63.806	-60.479	428
Ophionotus	victoriae	Op867_4E_2	West Antarctic Peninsula	1	FJ917339	2013	LMG-13-12	3	-63.806	-60.479	428
Ophionotus	victoriae	Op867_4E_3	West Antarctic Peninsula	1	FJ917339	2013	LMG-13-12	3	-63.806	-60.479	428
Ophionotus	victoriae	Op867_4E_5	West Antarctic Peninsula	1	FJ917337	2013	LMG-13-12	3	-63.806	-60.479	428
Ophionotus	victoriae	Op867_4E_6	West Antarctic Peninsula	1	FJ917339	2013	LMG-13-12	3	-63.806	-60.479	428
Ophionotus	victoriae	Op867_4E_7	West Antarctic Peninsula	1	FJ917337	2013	LMG-13-12	3	-63.806	-60.479	428
Ophionotus	victoriae	Op867_4E_8	West Antarctic Peninsula	1	FJ917339	2013	LMG-13-12	3	-63.806	-60.479	428
Ophionotus	victoriae	Op867_4E_9	West Antarctic Peninsula	1	FJ917339	2013	LMG-13-12	3	-63.806	-60.479	428
Ophionotus	victoriae	312.3C.05	West Antarctic Peninsula	3	FJ917338	2006	LMG-06-05	17	-64.350	-61.760	334
Ophionotus	victoriae	312.3C.15	West Antarctic Peninsula	3	FJ917340	2006	LMG-06-05	17	-64.350	-61.760	334
Ophionotus	victoriae	Op1042_3E_5	West Antarctic Peninsula	3	FJ917340	2013	LMG-13-12	26	-64.846	-62.959	301
Ophionotus	victoriae	Op867_4E_1	West Antarctic Peninsula	3	FJ917340	2013	LMG-13-12	3	-63.806	-60.479	428
Ophionotus	victoriae	362.1C.02	West Antarctic Peninsula	6	FJ917309	2006	LMG-06-05	33	-67.734	-69.293	122
Ophionotus	victoriae	362.1C.03	West Antarctic Peninsula	6	FJ917309	2006	LMG-06-05	33	-67.734	-69.293	122
Ophionotus	victoriae	362.1C.04	West Antarctic Peninsula	6	FJ917309	2006	LMG-06-05	33	-67.734	-69.293	122

Ophionotus	victoriae	362.1C.05		West Antarctic Peninsula	6	FJ917309	2006	LMG-06-05	33		-67.734	-69.293	122
Ophionotus	victoriae	362.1C.11		West Antarctic Peninsula	6	FJ917344	2006	LMG-06-05	33		-67.734	-69.293	122
Ophionotus	victoriae	DSOPH1263		West Antarctic Peninsula	6	FJ917309	2009	JR230	AGT-21A		-67.546	-70.189	508
Ophionotus	victoriae	312.3C.02		West Antarctic Peninsula	7	FJ917322	2006	LMG-06-05	17		-64.350	-61.760	334
Ophionotus	victoriae	398.1E.07		West Antarctic Peninsula	7	FJ917322	2006	LMG-06-05	47		-67.717	-68.243	170
Ophionotus	victoriae	362.1C.09		West Antarctic Peninsula	8	FJ917316	2006	LMG-06-05	33		-67.734	-69.293	122
Ophionotus	victoriae	362.1C.12		West Antarctic Peninsula	8	FJ917316	2006	LMG-06-05	33		-67.734	-69.293	122
Ophionotus	victoriae	398.1E.02		West Antarctic Peninsula	8	FJ917316	2006	LMG-06-05	47		-67.717	-68.243	170
Ophionotus	victoriae	398.1E.14		West Antarctic Peninsula	8	FJ917316	2006	LMG-06-05	47		-67.717	-68.243	170
Ophionotus	victoriae	362.1C.01		West Antarctic Peninsula	39	FJ917342	2006	LMG-06-05	33		-67.734	-69.293	122
Ophionotus	victoriae	362.1C.10		West Antarctic Peninsula	39	FJ917342	2006	LMG-06-05	33		-67.734	-69.293	122
Ophionotus	victoriae	362.1C.07		West Antarctic Peninsula	40	FJ917343	2006	LMG-06-05	33		-67.734	-69.293	122
Ophionotus	victoriae	398.1E.01		West Antarctic Peninsula	40	FJ917343	2006	LMG-06-05	47		-67.717	-68.243	170
Ophionotus	victoriae	398.1E.15		West Antarctic Peninsula	40	FJ917343	2006	LMG-06-05	47		-67.717	-68.243	170
Ophionotus	victoriae	422.1C.02		West Antarctic Peninsula	41	FJ917346	2006	LMG-06-05	58		-65.184	-64.243	285
Ophionotus	victoriae	422.1C.07		West Antarctic Peninsula	42	FJ917347	2006	LMG-06-05	58		-65.184	-64.243	285
Ophionotus	victoriae	422.1C.10		West Antarctic Peninsula	43	FJ917348	2006	LMG-06-05	58		-65.184	-64.243	285
Ophionotus	victoriae	Op1042_3E_7		West Antarctic Peninsula	83	KY048252	2013	LMG-13-12	26		-64.846	-62.959	301
Ophionotus	victoriae	Op1042_3E_10		West Antarctic Peninsula	86	KY048256	2013	LMG-13-12	26		-64.846	-62.959	301
Ophionotus	victoriae	Op1042_3E_8		West Antarctic Peninsula	87	KY048257	2013	LMG-13-12	26		-64.846	-62.959	301
Ophionotus	hexactis	SIOBICE5493A	SIOBICE5493	Bransfield Strait	11		2012	Polarstern ANT-XXVIII/4		79279	-62.278	-55.833	302
Ophionotus	hexactis	SIOBICE5493B	SIOBICE5493	Bransfield Strait	11		2012	Polarstern ANT-XXVIII/4		79279	-62.278	-55.833	302
Ophionotus	hexactis	SIOBICE5493C	SIOBICE5493	Bransfield Strait	11		2012	Polarstern ANT-XXVIII/4		79279	-62.278	-55.833	302
Ophionotus	hexactis	SIOBICE5493E	SIOBICE5493	Bransfield Strait	11		2012	Polarstern ANT-XXVIII/4		79279	-62.278	-55.833	302
Ophionotus	hexactis	SIOBICE5493G	SIOBICE5493	Bransfield Strait	11		2012	Polarstern ANT-XXVIII/4		79279	-62.278	-55.833	302
Ophionotus	hexactis	SIOBICE5493H	SIOBICE5493	Bransfield Strait	11		2012	Polarstern ANT-XXVIII/4		79279	-62.278	-55.833	302
Ophionotus	hexactis	SIOBICE5493I	SIOBICE5493	Bransfield Strait	11		2012	Polarstern ANT-XXVIII/4		79279	-62.278	-55.833	302
Ophionotus	hexactis	SIOBICE5493J	SIOBICE5493	Bransfield Strait	11		2012	Polarstern ANT-XXVIII/4		79279	-62.278	-55.833	302

Ophionotus	hexactis	SIOBICE5493K	SIOBICE5493	Bransfield Strait	11		2012	Polarstern ANT-XXVIII/4		79279	-62.278	-55.833	302
Ophionotus	hexactis	SIOBICE5493L	SIOBICE5493	Bransfield Strait	11		2012	Polarstern ANT-XXVIII/4		79279	-62.278	-55.833	302
Ophionotus	hexactis	SIOBICE5493D	SIOBICE5493	Bransfield Strait	12		2012	Polarstern ANT-XXVIII/4		79279	-62.278	-55.833	302
Ophionotus	hexactis	SIOBICE5493F	SIOBICE5493	Bransfield Strait	13		2012	Polarstern ANT-XXVIII/4		79279	-62.278	-55.833	302
Ophionotus	hexactis	WAMZ43230	WAMZ43230	Heard Island	111		2017	ACE 2016/17	18	279	-52.355	74.801	203
Ophionotus	hexactis	WAMZ43231	WAMZ43231	Heard Island	111		2017	ACE 2016/17	18	279	-52.355	74.801	203
Ophionotus	hexactis	WAMZ43232	WAMZ43232	Heard Island	111		2017	ACE 2016/17	18	279	-52.355	74.801	203
Ophionotus	hexactis	WAMZ43233	WAMZ43233	Heard Island	111		2017	ACE 2016/17	18	279	-52.355	74.801	203
Ophionotus	hexactis	WAMZ43234	WAMZ43234	Heard Island	111		2017	ACE 2016/17	18	279	-52.355	74.801	203
Ophionotus	hexactis	WAMZ43235	WAMZ43235	Heard Island	111		2017	ACE 2016/17	18	279	-52.355	74.801	203
Ophionotus	hexactis	WAMZ43236	WAMZ43236	Heard Island	111		2017	ACE 2016/17	18	279	-52.355	74.801	203
Ophionotus	hexactis	WAMZ43237	WAMZ43237	Heard Island	111		2017	ACE 2016/17	18	279	-52.355	74.801	203
Ophionotus	hexactis	WAMZ43238	WAMZ43238	Heard Island	111		2017	ACE 2016/17	18	279	-52.355	74.801	203
Ophionotus	hexactis	WAMZ43239	WAMZ43239	Heard Island	144		2017	ACE 2016/17	18	279	-52.355	74.801	203
Ophionotus	hexactis	PS133-4		Larsen Ice Shelf	48	KU895454	2007	Polarstern ANT-XIX/4	PS61_113-4		-65.329	-54.242	1113
Ophionotus	hexactis	SIOBICS3753	SIOBICE5236	Shag Rocks	144		2011	Scotia 2011	SR1	4	-53.453	-42.058	174
Ophionotus	hexactis	SIOBICS3755	SIOBICE5225	Shag Rocks	144		2011	Scotia 2011	SR1	4	-53.453	-42.058	174
Ophionotus	hexactis	SIOBICS3756	SIOBICE5180	Shag Rocks	144		2011	Scotia 2011	SR1	4	-53.453	-42.058	174
Ophionotus	hexactis	SIOBICS3757	SIOBICE5230	Shag Rocks	144		2011	Scotia 2011	SR1	4	-53.453	-42.058	174
Ophionotus	hexactis	SIOBICS3758	SIOBICE5246	Shag Rocks	144		2011	Scotia 2011	SR1	4	-53.453	-42.058	174
Ophionotus	hexactis	SIOBICS3759	SIOBICE5283	Shag Rocks	144		2011	Scotia 2011	SR1	4	-53.453	-42.058	174
Ophionotus	hexactis	SIOBICS3760	SIOBICE5227	Shag Rocks	144		2011	Scotia 2011	SR1	4	-53.453	-42.058	174
Ophionotus	hexactis	SIOBICS3761	SIOBICE5184	Shag Rocks	144		2011	Scotia 2011	SR1	4	-53.453	-42.058	174
Ophionotus	hexactis	SIOBICS3762	SIOBICE5219	Shag Rocks	144		2011	Scotia 2011	SR1	4	-53.453	-42.058	174
Ophionotus	hexactis	SIOBICS3754	SIOBICE5251	Shag Rocks	151		2011	Scotia 2011	SR1	4	-53.453	-42.058	174
Ophionotus	hexactis	SIOBICS0036A	SIOBICE4798	South Georgia	144		2011	Scotia 2011	SG3	21	-55.052	-35.396	119
Ophionotus	hexactis	SIOBICS0036C	SIOBICE4798	South Georgia	144		2011	Scotia 2011	SG3	21	-55.052	-35.396	119
Ophionotus	hexactis	SIOBICS0036D	SIOBICE4798	South Georgia	144		2011	Scotia 2011	SG3	21	-55.052	-35.396	119
Ophionotus	hexactis	SIOBICS0036E	SIOBICE4798	South Georgia	144		2011	Scotia 2011	SG3	21	-55.052	-35.396	119
Ophionotus	hexactis	SIOBICS0036F	SIOBICE4798	South Georgia	144		2011	Scotia 2011	SG3	21	-55.052	-35.396	119
Ophionotus	hexactis	SIOBICS0036H	SIOBICE4798	South Georgia	144		2011	Scotia 2011	SG3	21	-55.052	-35.396	119
Ophionotus	hexactis	SIOBICS0036I	SIOBICE4798	South Georgia	144		2011	Scotia 2011	SG3	21	-55.052	-35.396	119
Ophionotus	hexactis	SIOBICS0036J	SIOBICE4798	South Georgia	144		2011	Scotia 2011	SG3	21	-55.052	-35.396	119
Ophionotus	hexactis	SIOBICS0037A	SIOBICE4780	South Georgia	144		2011	Scotia 2011	SG3	21	-55.052	-35.396	119
Ophionotus	hexactis	SIOBICS0037B	SIOBICE4780	South Georgia	144		2011	Scotia 2011	SG3	21	-55.052	-35.396	119
Ophionotus	hexactis	SIOBICS0037D	SIOBICE4780	South Georgia	144		2011	Scotia 2011	SG3	21	-55.052	-35.396	119
Ophionotus	hexactis	SIOBICS0037H	SIOBICE4780	South Georgia	144		2011	Scotia 2011	SG3	21	-55.052	-35.396	119
Ophionotus	hexactis	SIOBICS0037I	SIOBICE4780	South Georgia	144		2011	Scotia 2011	SG3	21	-55.052	-35.396	119

Ophionotus	hexactis	SIOBICS0037J	SIOBICE4780	South Georgia	144	2011	Scotia 2011	SG3	21	-55.052	-35.396	119
Ophionotus	hexactis	SIOBICS3354B	SIOBICE4774	South Georgia	144	2011	Scotia 2011	SG2a	18	-53.801	-37.219	145
Ophionotus	hexactis	SIOBICS3354C	SIOBICE4774	South Georgia	144	2011	Scotia 2011	SG2a	18	-53.801	-37.219	145
Ophionotus	hexactis	SIOBICS3354D	SIOBICE4774	South Georgia	144	2011	Scotia 2011	SG2a	18	-53.801	-37.219	145
Ophionotus	hexactis	SIOBICS3354E	SIOBICE4774	South Georgia	144	2011	Scotia 2011	SG2a	18	-53.801	-37.219	145
Ophionotus	hexactis	SIOBICS3354I	SIOBICE4774	South Georgia	144	2011	Scotia 2011	SG2a	18	-53.801	-37.219	145
Ophionotus	hexactis	SIOBICS3355A	SIOBICE4782	South Georgia	144	2011	Scotia 2011	SG2a	18	-53.801	-37.219	145
Ophionotus	hexactis	SIOBICS3355C	SIOBICE4782	South Georgia	144	2011	Scotia 2011	SG2a	18	-53.801	-37.219	145
Ophionotus	hexactis	SIOBICS3355D	SIOBICE4782	South Georgia	144	2011	Scotia 2011	SG2a	18	-53.801	-37.219	145
Ophionotus	hexactis	SIOBICS3355E	SIOBICE4782	South Georgia	144	2011	Scotia 2011	SG2a	18	-53.801	-37.219	145
Ophionotus	hexactis	SIOBICS3355F	SIOBICE4782	South Georgia	144	2011	Scotia 2011	SG2a	18	-53.801	-37.219	145
Ophionotus	hexactis	SIOBICS3355G	SIOBICE4782	South Georgia	144	2011	Scotia 2011	SG2a	18	-53.801	-37.219	145
Ophionotus	hexactis	SIOBICS3355I	SIOBICE4782	South Georgia	144	2011	Scotia 2011	SG2a	18	-53.801	-37.219	145
Ophionotus	hexactis	SIOBICS3355J	SIOBICE4782	South Georgia	144	2011	Scotia 2011	SG2a	18	-53.801	-37.219	145
Ophionotus	hexactis	SIOBICS0036B	SIOBICE4798	South Georgia	145	2011	Scotia 2011	SG3	21	-55.052	-35.396	119
Ophionotus	hexactis	SIOBICS0036G	SIOBICE4798	South Georgia	145	2011	Scotia 2011	SG3	21	-55.052	-35.396	119
Ophionotus	hexactis	SIOBICS0037E	SIOBICE4780	South Georgia	145	2011	Scotia 2011	SG3	21	-55.052	-35.396	119
Ophionotus	hexactis	SIOBICS0037F	SIOBICE4780	South Georgia	145	2011	Scotia 2011	SG3	21	-55.052	-35.396	119
Ophionotus	hexactis	SIOBICS0037C	SIOBICE4780	South Georgia	146	2011	Scotia 2011	SG3	21	-55.052	-35.396	119
Ophionotus	hexactis	SIOBICS0037G	SIOBICE4780	South Georgia	147	2011	Scotia 2011	SG3	21	-55.052	-35.396	119
Ophionotus	hexactis	SIOBICS3354J	SIOBICE4774	South Georgia	147	2011	Scotia 2011	SG2a	18	-53.801	-37.219	145
Ophionotus	hexactis	SIOBICS3355B	SIOBICE4782	South Georgia	147	2011	Scotia 2011	SG2a	18	-53.801	-37.219	145
Ophionotus	hexactis	SIOBICS3354A	SIOBICE4774	South Georgia	148	2011	Scotia 2011	SG2a	18	-53.801	-37.219	145
Ophionotus	hexactis	SIOBICS3354F	SIOBICE4774	South Georgia	149	2011	Scotia 2011	SG2a	18	-53.801	-37.219	145
Ophionotus	hexactis	SIOBICS3354G	SIOBICE4774	South Georgia	149	2011	Scotia 2011	SG2a	18	-53.801	-37.219	145
Ophionotus	hexactis	SIOBICS3355H	SIOBICE4782	South Georgia	149	2011	Scotia 2011	SG2a	18	-53.801	-37.219	145
Ophionotus	hexactis	SIOBICS3354H	SIOBICE4774	South Georgia	150	2011	Scotia 2011	SG2a	18	-53.801	-37.219	145

Supplementary Table 2.2. Analysis of molecular variable (AMOVA) between sample localities and species in *Ophionotus victoriae* and *O. hexactis*.

Source of variation	Degrees of freedom	Sums of squares	Variance components	Percentage of variation
Among species	1	15.393	0.08441 V_a	15.86
Among locations within species	23	108.136	0.12071 V_b	22.67
Within locations	910	297.784	0.32724 V_c	61.47
Total	934	421.313	0.53235	
Fixation indices				
F_{ST}	0.26947			
F_{SC}	0.38530			
F_{CT}	0.15856			
Significant tests (1023 permutations)				
V_c and F_{ST}	p <0.0000 ± 0.0000			
V_b and F_{SC}	p <0.0000 ± 0.0000			
V_a and F_{CT}	p = 0.00293 ± 0.00164			

Supplementary Table 2.3. Pairwise F_{ST} between *Ophionotus victoriae* and *O. hexactis*. *significant value with p < 0.0001, with significant tests performed with 1,023 permutations.

	O. victoriae	*O. hexactis*
O. hexactis	0	
O. victoriae	0.20345*	0

Supplementary Table 3.1 Sample information of all Southern Ocean octopod samples (n = 440, including 22 technical replicates) sequenced with ddRAD sequencing and target capture sequencing of ddRAD loci

Genus	Species	Study ID	Field ID	Museum ID	Sample location	BOLD ID	Expedition	Station ID	Event number	Latitude	Longitude	Collection depth (m)	Collection date	Technical replicate for ddRADseq?	Ind with >80% missing data after Stacks?	ddRADseq data used for comparing with target capture data?	Samples re-sequenced with target capture sequencing?
Pareledone	turqueti	44117			Ross Sea	CANTA079-08	TAN0802			-75.63	169.85	525	01/02/2008		yes		yes
Pareledone	turqueti	44122			Ross Sea	CANTA039-08	TAN0802			-73.12	174.32	321	01/02/2008		yes		yes
Pareledone	turqueti	44130			Ross Sea	CANTA087-08	TAN0802			-76.59	176.83	369	01/02/2008		yes		yes
Pareledone	turqueti	44255			Ross Sea	CANTA105-08	TAN0802			-76.60	176.80	360	01/02/2008		yes		yes
Pareledone	turqueti	09_0713			West Antarctic Peninsula		JR230			-67.75	-70.06	586	09/12/2009		yes		yes
Pareledone	turqueti	09_0814			West Antarctic Peninsula		JR230			-67.73	-70.24	536	09/12/2009			yes	
Pareledone	aequipapillae	09_3			West Antarctic Peninsula										yes		
Adelieledone	sp	09_4			West Antarctic Peninsula										yes		
Pareledone	aequipapillae	09_6			West Antarctic Peninsula										yes		
Pareledone	aequipapillae	44059			Ross Sea	CANTA077-08	TAN0802	26		-74.58	170.25	285	01/02/2008				
Pareledone	aequipapillae	44064_1	44064.1		Ross Sea	CANTA048-08	TAN0802	61		-75.62	169.81	520	01/02/2008		yes		
Pareledone	aequipapillae	44067_2	44067.2		Ross Sea	CANTA032-08	TAN0802	94		-76.19	176.30	447	01/02/2008				
Pareledone	aequipapillae	44067_4	44067.4		Ross Sea	CANTA034-08	TAN0802	94		-76.19	176.30	447	01/02/2008		yes		
Pareledone	aequipapillae	44067_5	44067.5		Ross Sea	CANTA035-08	TAN0802	94		-76.19	176.30	447	01/02/2008				
Pareledone	aequipapillae	44067_6	44067.6		Ross Sea	CANTA036-08	TAN0802	94		-76.19	176.30	447	01/02/2008		yes		
Pareledone	aequipapillae	44071_1	44071.1		Ross Sea	CANTA098-08	TAN0802	70		-76.78	167.84	724	01/02/2008		yes		
Pareledone	cf. aequipapillae	44072_1	44072.1		Ross Sea	CANTA058-08	TAN0802	81		-76.59	176.83	369	01/02/2008		yes		
Pareledone	cf. aequipapillae	44072_2	44072.2		Ross Sea	CANTA059-08	TAN0802	81		-76.59	176.83	369	01/02/2008				
Pareledone	aequipapillae	44074_1	44074.1		Ross Sea	CANTA110-08	TAN0802	94		-76.19	176.30	447	01/02/2008		yes		
Pareledone	turqueti	44074_4	44074.4		Ross Sea	CANTA113-08	TAN0802	94		-76.19	176.30	447	01/02/2008			yes	
Pareledone	turqueti	44074_5	44074.5		Ross Sea	CANTA114-08	TAN0802	94		-76.19	176.30	447	01/02/2008		yes		yes
Pareledone	aequipapillae	44091_1	44091.1		Ross Sea	CANTA066-08	TAN0802	100		-76.20	176.25	451	01/02/2008		yes		
Pareledone	aequipapillae	44091_2	44091.2		Ross Sea	CANTA067-08	TAN0802	100		-76.20	176.25	451	01/02/2008		yes		
Pareledone	cf. aequipapillae	44091_4	44091.4		Ross Sea	CANTA069-08	TAN0802	100		-76.20	176.25	451	01/02/2008		yes		

Pareledone	cf. prydzensis	44104_2	44104.2	Ross Sea	CANTA085-08	TAN0802	161	-72.08	172.90	535	01/02/2008	yes		
Pareledone	turqueti	44112	44112	Ross Sea	CANTA011-08	TAN0802	84	-76.60	176.80	360	01/02/2008		yes	
Pareledone	turqueti	44113_1	44113.1	Ross Sea	CANTA042-08	TAN0802	94	-76.19	176.30	447	01/02/2008		yes	
Pareledone	turqueti	44113_3	44113.3	Ross Sea	CANTA044-08	TAN0802	94	-76.19	176.30	447	01/02/2008	yes		yes
Pareledone	turqueti	44113_4	44113.3	Ross Sea	CANTA045-08	TAN0802	94	-76.19	176.30	447	01/02/2008	yes		yes
Pareledone	turqueti	44118_1	44118.1	Ross Sea	CANTA090-08	TAN0802	94	-76.19	176.30	447	01/02/2008		yes	
Pareledone	turqueti	44118_2	44118.2	Ross Sea	CANTA091-08	TAN0802	94	-76.19	176.30	447	01/02/2008		yes	
Pareledone	turqueti	44118_3	44118.3	Ross Sea	CANTA092-08	TAN0802	94	-76.19	176.30	447	01/02/2008	yes		yes
Pareledone	turqueti	44121	44121	Ross Sea	CANTA095-08	TAN0802	223	-67.83	-179.59	405	01/02/2008		yes	
Pareledone	turqueti	44132	44132	Ross Sea	CANTA101-08	TAN0802	41	-74.73	167.01	916	01/02/2008		yes	
Pareledone	turqueti	44253_2	44253.2	Ross Sea	CANTA103-08	TAN0802	17	-73.12	174.32	321	01/02/2008		yes	
Pareledone	turqueti	44256_1	44256.1	Ross Sea	CANTA107-08	TAN0802	109	-72.35	175.50	850	01/02/2008	yes		yes
Pareledone	turqueti	44258_1	44258.1	Ross Sea	CANTA115-08	TAN0802	167	-71.86	174.03	1990	01/02/2008		yes	
Pareledone	turqueti	44258_4	44258.4	Ross Sea	CANTA118-08	TAN0802	167	-71.86	174.03	1990	01/02/2008		yes	
Pareledone	turqueti	AD_01_6		Casey Station		Antarctic Discovery	Longline trawl 67	-65.23	118.53	913	26/02/2016	yes		yes
Pareledone	sp	AD_01_7		Casey Station		Antarctic Discovery		-64.79	114.21	1678	15/02/2016	yes		
Megaleledone	setebos	AD01A		Casey Station		Antarctic Discovery		-64.74	132.16	1038	06/02/2016			
Pareledone	turqueti	AND138	ANTXIX-3_138	Elephant Is	CAOII043-09	ANTXIX-3		-61.07	-54.61	190			yes	
Pareledone	turqueti	AND145	ANTXIX-3_145	Elephant Is	CAOII045-09	ANTXIX-3		-61.07	-54.61	190		yes		yes
Pareledone	sp	AND226		Elephant Is				-61.16	-54.56	343				
Pareledone	turqueti	AND2414		Livingston Is				-62.39	-61.40	363			yes	
Pareledone	turqueti	AND271	ANTXIX-3_271	Elephant Is	CAOII066-09	ANTXIX-3		-61.16	-54.56	343		yes		yes
Pareledone	aequipapillae	AND432		Elephant Is				-61.20	-54.84	94				
Pareledone	subtilis	AND449		Elephant Is				-61.35	-55.23	264		yes		
Adelieledone	sp	CB10_1		Falkland Islands		Corinthian Bay		-53.02	73.45	898	19/10/2017	yes		
Megaleledone	setebos	CB10_2		Falkland Islands		Corinthian Bay		-53.02	73.45	1200	22/10/2017	yes		
Pareledone	turqueti	CT816	CEAMARC_CT816	Adélie Land	CAOII685-09	CEAMARC		-66.75	143.95	641	29/12/2007		yes	
Pareledone	turqueti	CT827	CEAMARC_CT827	Adélie Land	CAOII695-09	CEAMARC		-66.00	139.68	196	14/01/2008		yes	
Pareledone	turqueti	CT828	CEAMARC_CT828	Adélie Land	CAOII696-09	CEAMARC		-66.33	140.65	165	13/01/2008		yes	
Pareledone	turqueti	CT846	CEAMARC_CT846	Adélie Land	CAOII714-09	CEAMARC		-66.56	140.80	361	13/01/2008		yes	

Pareledone	turqueti	CT864	CEAMARC_CT864	Adélie Land	CAOII732-09	CEAMARC	-66.34	140.45	444	14/01/2008		yes		
Pareledone	turqueti	CT883	CEAMARC_CT883	Adélie Land	CAOII751-09	CEAMARC	-65.71	140.60	424	18/01/2008		yes		
Pareledone	turqueti	CT895	CEAMARC_CT895	Adélie Land	CAOII763-09	CEAMARC	-65.71	140.60	424	18/01/2008		yes		
Pareledone	turqueti	CT898	CEAMARC_CT898	Adélie Land	CAOII766-09	CEAMARC	-65.71	140.60	424	18/01/2008		yes		
Pareledone	sp	CT900	CEAMARC_CT900	Adélie Land	CAOII768-09	CEAMARC	-65.99	139.31	472	15/01/2008	yes			
Adelieledone	cf. adelieana	CT903	CEAMARC_CT903	Adélie Land	CAOII771-09	CEAMARC	-66.00	139.68	196	15/01/2008				
Pareledone	turqueti	CT905	CEAMARC_CT905	Adélie Land	CAOII773-09	CEAMARC	-66.00	139.68	196	15/01/2008	yes		yes	
Pareledone	turqueti	CT906	CEAMARC_CT906	Adélie Land	CAOII774-09	CEAMARC	-65.71	140.60	424	18/01/2008		yes		
Pareledone	aequipapillae	CT908	CEAMARC_CT908	Adélie Land	CAOII776-09	CEAMARC	-66.34	140.45	444	14/01/2008	yes			
Pareledone	turqueti	CT909	CEAMARC_CT909	Adélie Land	CAOII777-09	CEAMARC	-66.56	141.26	177	13/01/2008	yes		yes	
Pareledone	sp	CT910	CEAMARC_CT910	Adélie Land	CAOII778-09	CEAMARC	-66.34	140.45	444	14/01/2008	yes			
Adelieledone	cf. adelieana	CT914	CEAMARC_CT914	Adélie Land	CAOII782-09	CEAMARC	-65.49	139.31	411	17/01/2008	yes			
Adelieledone	polymorpha	CT915	CEAMARC_CT915	Adélie Land	GBMIN2699-12	CEAMARC	-65.51	139.36	398	17/01/2008	yes			
Pareledone	sp	CT916	CEAMARC_CT916	Adélie Land	CAOII784-09	CEAMARC	-65.51	139.36	398	17/01/2008				
Pareledone	turqueti	CT917	CEAMARC_CT917	Adélie Land	CAOII785-09	CEAMARC	-66.34	141.27	207	13/01/2008	yes		yes	
Pareledone	sp	CT918	CEAMARC_CT918	Adélie Land	CAOII786-09	CEAMARC	-66.34	140.45	444	14/01/2008				
Adelieledone	cf. adelieana	CT919	CEAMARC_CT919	Adélie Land	CAOII787-09	CEAMARC	-66.34	140.45	444	14/01/2008				
Adelieledone	cf. adelieana	CT920	CEAMARC_CT920	Adélie Land	CAOII788-09	CEAMARC	-65.48	139.26	433	16/01/2008				
Pareledone	aequipapillae	CT921	CEAMARC_CT921	Adélie Land	CAOII789-09	CEAMARC	-65.99	140.00	192	15/01/2008				
Adelieledone	polymorpha	CT922	CEAMARC_CT922	Adélie Land	GBMIN2698-12	CEAMARC	-65.49	139.31	308	17/01/2008				
Pareledone	sp	CT923	CEAMARC_CT923	Adélie Land	CAOII791-09	CEAMARC	-65.99	140.00	192	15/01/2008	yes			

Pareledone	aequipapillae	CT924	CEAMARC_CT924		Adélie Land	CAOII792-09	CEAMARC	-65.51	139.36	398	17/01/2008				
Pareledone	sp	CT925	CEAMARC_CT925		Adélie Land	CAOII793-09	CEAMARC	-65.51	139.36	398	17/01/2008	yes			
Pareledone	sp	CT926	CEAMARC_CT926		Adélie Land	CAOII794-09	CEAMARC	-65.51	139.36	398	17/01/2008				
Pareledone	sp	CT927	CEAMARC_CT927		Adélie Land	CAOII795-09	CEAMARC	-65.51	139.36	398	17/01/2008				
Pareledone	turqueti	CT928	CEAMARC_CT928		Adélie Land	CAOII796-09	CEAMARC	-66.17	139.93	150	15/01/2008		yes		
Pareledone	cornuta	CT931	CEAMARC_CT931		Adélie Land	CAOII799-09	CEAMARC	-66.40	139.79	444	14/01/2008	yes			
Adelieledone	cf. adelieana	CT932	CEAMARC_CT932		Adélie Land	CAOII800-09	CEAMARC	-65.49	139.31	408	17/01/2008				
Pareledone	turqueti	CT933	CEAMARC_CT933		Adélie Land	CAOII801-09	CEAMARC	-66.40	139.79		15/01/2008	yes			yes
Pareledone	subtilis	CT935	CEAMARC_CT935		Adélie Land	CAOII803-09	CEAMARC	-65.51	139.36	398	17/01/2008	yes			
Adelieledone	polymorpha	CT936	CEAMARC_CT936		Adélie Land	GBMIN2719-12	CEAMARC	65 28.706 S	139 15.665 E	433	16/01/2008	yes			
Pareledone	turqueti	CT937	CEAMARC_CT937		Adélie Land		CEAMARC	-66.34	141.34	230	13/01/2008		yes		
Pareledone	sp	CT938	CEAMARC_CT938		Adélie Land		CEAMARC	-65.27	-139.25	1138	16/01/2008				
Pareledone	turqueti	CT939	CEAMARC_CT939		Adélie Land	CAOII807-09	CEAMARC	-66.00	139.68	196	15/01/2008	yes			yes
Pareledone	aequipapillae	CT941	CEAMARC_CT941		Adélie Land	CAOII809-09	CEAMARC	-65.51	139.36	398	17/01/2008	yes			
Pareledone	sp	CT943	CEAMARC_CT943		Adélie Land	CAOII811-09	CEAMARC	-65.99	139.31	472	15/01/2008	yes			
Pareledone	sp	CT945	CEAMARC_CT945		Adélie Land	CAOII813-09	CEAMARC	-65.51	139.36	398	17/01/2008	yes			
Pareledone	sp	CT946	CEAMARC_CT946		Adélie Land	CAOII814-09	CEAMARC	-65.99	139.31	472	15/01/2008				
Pareledone	sp	CT947	CEAMARC_CT947		Adélie Land	CAOII815-09	CEAMARC	-65.51	139.36	398	17/01/2008				
Pareledone	sp	CT948	CEAMARC_CT948		Adélie Land		CEAMARC								
Adelieledone	sp	CT951	CEAMARC_CT951		Adélie Land		CEAMARC					yes			
Pareledone	sp	JCR1529			South Orkney Is			-60.36	-46.52	1122					
Pareledone	turqueti	JR179_141	JR179_141	NMSZ 2008090.1	Amundsen Sea	CAOII421-09	JCR 179	-71.81	-106.33	577	04/03/2008	yes			yes

Pareledone	turqueti	JR179_403	JR179_403	NMSZ2008090.3	Amundsen Sea	CAOII424-09	JCR 179	-74.41	-104.65	502	06/03/2008		yes		
Pareledone	turqueti	JR179_674	JR179_674	NMSZ2008090.8	Amundsen Sea	CAOII430-09	JCR 179	-73.98	-107.41	536	10/03/2008		yes		
Pareledone	turqueti	JR179_797	JR179_797	NMSZ2008090.11	Amundsen Sea	CAOII433-09	JCR 179	-71.35	-110.00	476	11/03/2008		yes		
Adelieledone	sp	JS_15			South Weddell Sea		RV Polarstern PS82	-77.00	-34.16		15/01/2014				
Pareledone	subtilis	JS_16			South Weddell Sea		RV Polarstern PS82	-75.20	-27.54	371	18/01/2014	yes			
Pareledone	turqueti	JS_18			South Weddell Sea		RV Polarstern PS82	-74.59	-26.89	642	03/02/2014		yes		
Pareledone	turqueti	JS_19			South Weddell Sea		RV Polarstern PS82	-74.54	-37.38	366	06/02/2014		yes		
Pareledone	aequipapillae	JS_20			South Weddell Sea		RV Polarstern PS82	-74.51	-37.47	368	08/02/2014	yes			
Adelieledone	sp	JS_22			South Weddell Sea		RV Polarstern PS82	-76.07	-30.15	442	12/02/2014				
Adelieledone	sp	JS_23			South Weddell Sea		RV Polarstern PS82	-74.67	-28.70		12/02/2014	yes			
Pareledone	aequipapillae	JS_24			South Weddell Sea		RV Polarstern PS82	-74.31	-32.83	685	04/01/2014				
Megaleledone	setebos	JS_25			South Weddell Sea		RV Polarstern PS82	-77.72	-35.98	613	17/02/2014	yes			
Pareledone	turqueti	JS_26			South Weddell Sea		RV Polarstern PS82	-77.72	-35.98	613	04/01/2014	yes			yes
Megaleledone	setebos	JS_27			South Weddell Sea		RV Polarstern PS82	-77.02	-34.44	520	11/01/2014				
Megaleledone	setebos	JS_28			South Weddell Sea		RV Polarstern PS82	-70.91	-10.74	353	01/11/2014	yes			
Pareledone	aequipapillae	JS_29			South Weddell Sea		RV Polarstern PS82	-77.61	-38.94	1026	12/01/2014				
Adelieledone	sp	JS_30			South Weddell Sea		RV Polarstern PS82	-77.00	-34.16		13/01/2014				
Pareledone	turqueti	JS_31			South Weddell Sea		RV Polarstern PS82				06/07/1905		yes		
Adelieledone	sp	JS_32			South Weddell Sea		RV Polarstern PS82				06/07/1905	yes			
Pareledone	aequipapillae	JS_35			South Weddell Sea		RV Polarstern PS82				06/07/1905				
Pareledone	sp	JS_36			South Weddell Sea		RV Polarstern PS82				06/07/1905				
Adelieledone	sp	JS_37			South Weddell Sea		RV Polarstern PS82				06/07/1905				

Adelieledone	sp	JS_38		South Weddell Sea	RV Polarstern PS82	-77.02	-33.70	403	10/02/2014					
Pareledone	turqueti	JS_39		South Weddell Sea	RV Polarstern PS82	-77.02	-33.70	403	10/02/2014		yes			
Pareledone	turqueti	JS_40		South Weddell Sea	RV Polarstern PS82				06/07/1905	yes		yes		
Pareledone	aequipapillae	JS_41		South Weddell Sea	RV Polarstern PS82				06/07/1905					
Pareledone	aequipapillae	JS_42		South Weddell Sea	RV Polarstern PS82				06/07/1905	yes				
Pareledone	aequipapillae	JS_43		South Weddell Sea	RV Polarstern PS82				06/07/1905					
Pareledone	turqueti	JS_44		South Weddell Sea	RV Polarstern PS82				08/07/1905	yes		yes		
Pareledone	turqueti	JS_46		South Weddell Sea	RV Polarstern PS82				06/07/1905		yes			
Pareledone	aequipapillae	JS_47		South Weddell Sea	RV Polarstern PS82				06/07/1905					
Pareledone	aequipapillae	JS_48		South Weddell Sea	RV Polarstern PS82				06/07/1905					
Adelieledone	sp	JS_49		South Weddell Sea	RV Polarstern PS82				06/07/1905					
Adelieledone	sp	JS_50		South Weddell Sea						yes				
Adelieledone	sp	JS_51		South Weddell Sea										
Pareledone	aequipapillae	JS_52		South Weddell Sea										
Adelieledone	sp	JS_53		South Weddell Sea										
Pareledone	turqueti	JS091	GJ_JS91	Prydz Bay	CAOII321-09	-66.93	65.92	185	26/01/2001		yes			
Pareledone	turqueti	JS096	GJ_JS96	Prydz Bay	CAOII326-09	-66.93	65.92	185	26/01/2001	yes		yes		
Pareledone	turqueti	JS097	GJ_JS97	Prydz Bay	CAOII327-09	-66.93	65.92	185	26/01/2001	yes		yes		
Pareledone	turqueti	JS099		Prydz Bay	CAOII329-09	-66.93	65.92	185	26/01/2001		yes			
Pareledone	subtilis	JS1		South Weddell Sea	RV Polarstern PS96	-70.90	-11.14	293	24/12/2015	yes				
Pareledone	turqueti	JS10		South Weddell Sea	RV Polarstern PS96	-72.31	-16.86	762	29/01/2016	yes		yes		
Pareledone	aequipapillae	JS11		South Weddell Sea	RV Polarstern PS96				Aquarium L10					
Pareledone	sp.	JS12		South Weddell Sea	RV Polarstern PS96				Aquarium L9	yes				
Pareledone	turqueti	JS13		South Weddell Sea	RV Polarstern PS96	-76.19	-30.36	420	21/01/2016		yes			

Pareledone	aequipapillae	JS14			South Weddell Sea		RV Polarstern PS82	-75.52	-28.99	442	15/01/2014				
Pareledone	aequipapillae	JS2			South Weddell Sea		RV Polarstern PS96	-70.90	-11.14	293	24/12/2015				
Pareledone	aequipapillae	JS3			South Weddell Sea		RV Polarstern PS96	-76.19	-30.06	379	21/01/2016	yes			
Adelieledone	sp	JS4			South Weddell Sea		RV Polarstern PS96	-74.95	-32.46	587	04/01/2016	yes			
Pareledone	turqueti	JS5			South Weddell Sea		RV Polarstern PS96	-72.59	-18.07	406	31/01/2016	yes			yes
Megaleledone	setebos	JS6			South Weddell Sea		RV Polarstern PS96	-72.31	-16.86	762	29/01/2016	yes			
Adelieledone	sp	JS7			South Weddell Sea		RV Polarstern PS96	-75.68	-42.47	375	17/01/2016	yes			
Pareledone	turqueti	JS8			South Weddell Sea		RV Polarstern PS96	-72.31	-16.86	762	29/01/2016		yes		
Adelieledone	sp	JS9			South Weddell Sea		RV Polarstern PS96	-74.95	-32.46	587	29/01/2016	yes			
Pareledone	sp	KL05_0779			Larsen Ice Shelves		ANT-XXII/3	-69.51	-50.40	1827	10/02/2005				
Pareledone	sp	KL05_0780			Larsen Ice Shelves		ANT-XXII/3	-63.58	-50.70	2617	14/03/2005				
Adelieledone	sp	KL05_0785			East Weddell Sea		ANT-XXII/3	-70.50	-14.53		24/02/2005				
Pareledone	sp	KL05_0787			Larsen Ice Shelves		ANT-XXII/3	-71.31	-13.97	1055	20/02/2005				
Pareledone	aequipapillae	KL05_0788			East Weddell Sea		ANT-XXII/3	-62.78	-53.07	1854	16/03/2005	yes			
Graneledone	sp.	KLO5_0783			Larsen Ice Shelves		ANT-XXII/3	-63.58	-50.70	2617	14/03/2005				
Pareledone	turqueti	LS117			South Shetland Is			-63.02	-61.15	352		yes			
Pareledone	turqueti	LS14	ANTXVII-3_14	NMSZ 20000815	East Weddell Sea	CAOII130-09	ANT-XVII/3	-71.19	-12.26	309	02/04/2000	yes			yes
Pareledone	turqueti	LS149	ANTXVII-3_149	NMSZ 20000810	Robert Is	CAOII159-09	ANT-XVII/3	-61.98	-60.31	804	02/05/2000	yes			yes
Pareledone	turqueti	LS15	ANTXVII-3_15	NMSZ 20000815	East Weddell Sea	CAOII131-09	ANT-XVII/3	-71.19	-12.26	309	02/04/2000	yes			yes
Pareledone	turqueti	LS151	ANTXVII-3_151	NMSZ 20000810	Robert Is	CAOII160-09	ANT-XVII/3	-61.98	-60.31	804	02/05/2000	yes			
Pareledone	turqueti	LS152	ANTXVII-3_152	NMSZ 20000810	Robert Is	CAOII161-09	ANT-XVII/3	-61.98	-60.31	804	02/05/2000	yes			yes
Pareledone	turqueti	LS154	ANTXVII-3_154[	NMSZ 20000810	Robert Is	CAOII163-09	ANT-XVII/3	-61.98	-60.31	804	02/05/2000	yes			yes
Pareledone	turqueti	LS155	ANTXVII-3_155	NMSZ 20000810	Robert Is	CAOII164-09	ANT-XVII/3	-61.98	-60.31	804	02/05/2000		yes		
Pareledone	turqueti	LS156	ANTXVII-3_156	NMSZ 20000810	Robert Is	CAOII165-09	ANT-XVII/3	-61.98	-60.31	804	02/05/2000	yes			

Pareledone	turqueti	LS157	ANTXVII-3_157[	NMSZ 20000081.50	Robert Is	CAOII166-09	ANT-XVII/3	-61.98	-60.31	804	02/05/2000		yes	
Pareledone	turqueti	LS158	ANTXVII-3_158	NMSZ 20000081.50	Robert Is	CAOII167-09	ANT-XVII/3	-61.98	-60.31	804	02/05/2000		yes	
Pareledone	turqueti	LS16	ANTXVII-3_16	NMSZ 20000081.15	East Weddell Sea	CAOII132-09	ANT-XVII/3	-71.19	-12.26	309	02/04/2000		yes	
Pareledone	turqueti	LS161	ANTXVII-3_161	NMSZ 20000081.50	Robert Is	CAOII169-09	ANT-XVII/3	-61.98	-60.31	804	02/05/2000	yes		yes
Pareledone	turqueti	LS162	ANTXVII-3_162	NMSZ 20000081.50	Robert Is	CAOII170-09	ANT-XVII/3	-61.98	-60.31	804	02/05/2000		yes	
Pareledone	turqueti	LS3	ANTXVII-3_3	NMSZ 20000081.2	East Weddell Sea	CAOII128-09	ANT-XVII/3	-71.29	-13.80	615	31/03/2000	yes		yes
Pareledone	turqueti	LS5	ANTXVII-3_5	NMSZ 20000081.1	East Weddell Sea	CAOII129-09	ANT-XVII/3	-71.29	-13.80	615	31/03/2000		yes	
Pareledone	turqueti	LS74	ANTXVII-3_74	NMSZ 20000081.27	Bransfield Strait	CAOII143-09	ANT-XVII/3	-63.01	-59.12	621	28/04/2000		yes	
Pareledone	turqueti	LS84	ANTXVII-3_84	NMSZ 20000081.28	Bransfield Strait	CAOII148-09	ANT-XVII/3	-63.04	-59.17	666	28/04/2000		yes	
Pareledone	turqueti	NIWA87970			Ross Sea		Kat Bolstad					yes		yes
Megaleledone	setebos	Oct03A			Prydz Bay		Aurora Australis	-66.84	-65.49	600	27/02/2015			
Megaleledone	setebos	Oct05A			Prydz Bay		Aurora Australis	-66.87	-66.70	580	28/02/2015	yes		
Adelieledone	sp	Oct06			Prydz Bay		Aurora Australis	-66.84	-65.49	600	27/02/2015	yes		
Adelieledone	sp	Oct07			Prydz Bay		Aurora Australis	-66.84	-65.49	600	27/02/2015	yes		
Pareledone	sp	Oct09			Prydz Bay		Aurora Australis	-66.87	-66.70	580	28/02/2015	yes		
Adelieledone	sp	Oct10			Prydz Bay		Aurora Australis	-66.84	-65.49	600	27/02/2015			
Pareledone	aequipapillae	Octo1			East Weddell Sea		ANTXX1/2	-70.81	-11.37	1342	10/12/2003			
Pareledone	aequipapillae	Octo10			East Weddell Sea		ANTXX1/2	-70.95	-10.53	303	10/12/2003			
Pareledone	turqueti	Octo13			East Weddell Sea		ANTXX1/2	-71.58	-13.95	844	21/12/2003	yes		yes
Pareledone	aequipapillae	Octo14			East Weddell Sea		ANTXX1/2	-71.58	-13.95	844	21/12/2003			
Pareledone	aequipapillae	Octo17			East Weddell Sea		ANTXX1/2	-71.12	-13.49	77	28/02/2003			
Adelieledone	sp	Octo18			East Weddell Sea		ANTXX1/2	-70.94	-10.53	304	10/12/2003			
Pareledone	aequipapillae	Octo19			East Weddell Sea		ANTXX1/2	-70.95	-10.53	303	10/12/2003			
Pareledone	turqueti	Octo2			East Weddell Sea		ANTXX1/2	-70.81	-11.37	1342	10/12/2003	yes		yes
Pareledone	aequipapillae	Octo20			East Weddell Sea		ANTXX1/2	-70.95	-10.53	303	10/12/2003			
Pareledone	aequipapillae	Octo21			East Weddell Sea		ANTXX1/2				aquarium			
Pareledone	sp	Octo23			East Weddell Sea		ANTXX1/2	-71.32	-13.96	848	21/12/2003	yes		
Pareledone	turqueti	Octo24			East Weddell Sea		ANTXX1/2	-70.87	-10.70	288	28/12/2003		yes	
Pareledone	turqueti	Octo3			East Weddell Sea		ANTXX1/2	-70.81	-11.37	1342	10/12/2003		yes	

Pareledone	turqueti	Octo4			East Weddell Sea		ANTXX1/2	-70.81	-11.37	1342	10/12/2003			yes		
Adelieledone	sp	Octo8			East Weddell Sea		ANTXX1/2	-70.95	-10.53	303	10/12/2003		yes			
Pareledone	aequipapillae	Octo9			East Weddell Sea		ANTXX1/2	-70.95	-10.53	303	10/12/2003					
Adelieledone	sp	P322_16			Kerguelen Is		ALC	-48.87	66.45				yes			
Pareledone	sp	P322_7			Kerguelen Is		ALC	-48.88	71.32	938						
Pareledone	sp	Pineislandbay			Amundsen Sea		BENDEX	-74.83	-102.67				yes			
Pareledone	aequipapillae	PT102			Elephant Is		JR147	-61.00	-56.00	337		yes				
Adelieledone	sp	PT103			Elephant Is			-61.00	-56.00	337		yes				
Pareledone	turqueti	PT104SG	SG05_104		South Georgia	CAOII541-09		-54.33	-39.04	226	16/01/2005			yes		
Pareledone	turqueti	PT108			Elephant Is			-61.20	-55.90	108			yes			yes
Pareledone	turqueti	PT10SG	SG05_10		South Georgia	CAOII450-09		-53.76	-39.05	238	15/01/2005			yes		
Pareledone	turqueti	PT111			Elephant Is			-61.20	-55.90	108		yes		yes		
Pareledone	turqueti	PT117AP	ANTXVII-3_117	NMSZ 2000081.36	Deception Is	CAOII153-09	ANTXVII/3	-63.02	-61.15	352	30/04/2000		yes			yes
Pareledone	turqueti	PT119AP41			Deception Is		ANTXVII/3	-63.02	-61.15	352	30/04/2000		yes			yes
Pareledone	turqueti	PT11SG	SG05_11		South Georgia	CAOII451-09		-53.76	-39.05	238	15/01/2005			yes		
Pareledone	turqueti	PT145AP	ANTXIX-3_145	NMSZ 2002037.45	Elephant Is	CAOII045-09	ANTXIX/3	-61.07	-54.61	190	30/01/2002			yes		
Pareledone	turqueti	PT149AP	ANTXVII-3_149	NMSZ 2000081.50	Robert Is	CAOII159-09	ANTXVII/3	-61.98	-60.31	804	02/05/2000			yes		
Pareledone	turqueti	PT14SG	SG05_14		South Georgia	CAOII454-09		-53.76	-39.05	238	15/01/2005			yes		
Pareledone	turqueti	PT14WS	ANTXVII-3_14		East Weddell Sea	CAOII130-09	ANTXVII/3	-71.19	-12.26	309	02/04/2000		yes			
Pareledone	turqueti	PT151AP	ANTXVII-3_151	NMSZ 2000081.50	Robert Is	CAOII160-09	ANTXVII/3	-61.98	-60.31	804	02/05/2000		yes			yes
Pareledone	turqueti	PT152AP	ANTXVII-3_152	NMSZ 2000081.50	Robert Is	CAOII161-09	ANTXVII/3	-61.98	-60.31	804	02/05/2000			yes		
Pareledone	turqueti	PT154			Elephant Is			-61.20	-55.70	103		yes	yes			yes
Pareledone	turqueti	PT154AP			Robert Is			-61.98	-60.31	804				yes		
Pareledone	turqueti	PT155			Elephant Is			-61.20	-55.70	103				yes		
Pareledone	turqueti	PT156AP			Robert Is			-61.98	-60.31	804			yes			yes
Pareledone	turqueti	PT157AP	ANTXVII-3_157	NMSZ 2000081.50	Robert Is	CAOII166-09	ANTXVII/3	-61.98	-60.31	804	02/05/2000		yes			
Pareledone	turqueti	PT15WS	ANTXVII-3_15	NMSZ 2000081.15	East Weddell Sea	CAOII131-09	ANTXVII/3	-71.19	-12.26	309	02/04/2000			yes		
Pareledone	turqueti	PT163AP			Robert Is			-61.98	-60.31	804				yes		
Pareledone	turqueti	PT165AP			Robert Is			-61.98	-60.31	804				yes		
Pareledone	turqueti	PT16WS	ANTXVII-3_16	NMSZ 2000081.15	East Weddell Sea	CAOII132-09	ANTXVII/3	-71.19	-12.26	309	02/04/2000		yes			yes

Pareledone	turqueti	PT186	JR147_186		Elephant Is	CAOII355-09		-61.20	-55.70	103	14/03/2006	yes		yes	
Pareledone	turqueti	PT18SG	SG05_18		South Georgia	CAOII458-09		-54.97	-35.32	103	24/01/2005			yes	
Pareledone	turqueti	PT191			Elephant Is			-61.20	-55.70	103		yes		yes	
Pareledone	turqueti	PT192	JR147_192		Elephant Is	CAOII358-09		-61.20	-55.70	103	14/03/2006	yes	yes		yes
Pareledone	aequipapillae	PT201			Elephant Is			-61.20	-55.70	103	14/03/2006				
Pareledone	turqueti	PT201_1	JR147_201a		Elephant Is	CAOII362-09		-61.20	-55.70	103	14/03/2006			yes	
Pareledone	aequipapillae	PT201_2	JR147_201b		Elephant Is	CAOII363-09		-61.20	-55.70	103	14/03/2006				
Pareledone	turqueti	PT209SG			South Georgia			-54.30	-37.89	149				yes	
Pareledone	turqueti	PT20SG	SG05_20		Shag Rocks	CAOII460-09		-53.81	-40.32	533	20/01/2005			yes	
Pareledone	turqueti	PT210SG	SG06_210		South Georgia	CAOII560-09		-54.30	-37.89	149	16/01/2006			yes	
Pareledone	turqueti	PT211SG	SG06_211		South Georgia	CAOII561-09		-54.30	-37.89	149	16/01/2006			yes	
Pareledone	turqueti	PT212SG	SG06_212		South Georgia	CAOII562-09		-54.30	-37.89	149	16/01/2006			yes	
Pareledone	turqueti	PT213SG	SG06_213		South Georgia	CAOII563-09		-54.30	-37.89	149	16/01/2006			yes	
Pareledone	turqueti	PT214SG	SG06_214		Shag Rocks	CAOII564-09		-53.74	-41.46	164	11/01/2006		yes		yes
Pareledone	turqueti	PT215SG	SG06_215		Shag Rocks	CAOII565-09		-53.74	-41.46	164	11/01/2006			yes	
Pareledone	turqueti	PT217SG	SG06_217		Shag Rocks	CAOII567-09		-53.79	-40.96	130	14/01/2006			yes	
Pareledone	turqueti	PT218SG	SG06_218		Shag Rocks	CAOII568-09		-53.79	-40.96	130	14/01/2006			yes	
Pareledone	turqueti	PT219SG	SG06_219		Shag Rocks	CAOII569-09		-53.79	-40.96	130	14/01/2006			yes	
Pareledone	turqueti	PT220SG	SG06_220		Shag Rocks	CAOII570-09		-53.79	-40.96	130	14/01/2006			yes	
Pareledone	turqueti	PT221SG	SG06_221		South Georgia	CAOII571-09		-54.30	-37.89	149	16/01/2006			yes	
Pareledone	turqueti	PT222SG	SG06_222		South Georgia	CAOII572-09		-54.30	-37.89	149	16/01/2006			yes	
Pareledone	turqueti	PT223SG	SG06_223		South Georgia	CAOII573-09		-54.30	-37.89	149	16/01/2006			yes	
Pareledone	turqueti	PT224SG	SG06_224		South Georgia	CAOII574-09		-54.30	-37.89	149	16/01/2006			yes	
Pareledone	turqueti	PT225SG	SG06_225		South Georgia	CAOII575-09		-54.30	-37.89	149	16/01/2006			yes	
Pareledone	turqueti	PT22SG	SG05_22		Shag Rocks	CAOII462-09		-53.81	-40.32	533	20/01/2005			yes	
Pareledone	turqueti	PT24			Robert Is			-62.00	-57.20	111			yes		yes
Pareledone	turqueti	PT2407AP			Livingston Is			-62.18	-60.80	413				yes	
Pareledone	turqueti	PT2414AP	ANTXIX-3_2414	NMSZ 2002037.6	Robert Is	CAOII087-09	ANTXIX/3	-62.39	-61.40	363	19/02/2002		yes		yes
Pareledone	turqueti	PT2429AP	ANTXIX-3_2429	NMSZ 2002037.48	Bransfield Strait	CAOII088-09	ANTXIX/3	-62.58	-55.67	158	21/02/2002			yes	
Pareledone	turqueti	PT243SG	SG06_243		South Georgia	CAOII579-09		-54.73	-35.19	294	19/01/2006			yes	
Pareledone	turqueti	PT244			South Orkney Is			-61.00	-46.80	505		yes		yes	
Pareledone	turqueti	PT244SG	SG06_244		South Georgia	CAOII580-09		-54.63	-35.58	100	19/01/2006			yes	

Pareledone	turqueti	PT245SG	SG06_245		South Georgia	CAOII581-09		-54.63	-35.58	100	19/01/2006			yes		
Pareledone	turqueti	PT246	JR147_246		South Orkney Is	CAOII381-09		-61.00	-46.80	505	18/03/2006	yes		yes		
Pareledone	turqueti	PT246SG	SG06_246		South Georgia	CAOII582-09		-54.63	-35.58	100	19/01/2006			yes		
Pareledone	turqueti	PT247SG	SG06_247		South Georgia	CAOII583-09		-54.63	-35.58	100	19/01/2006			yes		
Pareledone	turqueti	PT248	JR147_248		South Orkney Is	CAOII382-09		-60.80	-46.50	219	18/03/2006			yes		
Pareledone	turqueti	PT248SG	SG06_248		South Georgia	CAOII584-09		-53.87	-38.61	165	10/01/2006			yes		
Pareledone	turqueti	PT249SG	SG06_249		South Georgia	CAOII585-09		-53.87	-38.61	165	10/01/2006			yes		
Pareledone	turqueti	PT24SG	SG05_24		Shag Rocks	CAOII464-09		-53.92	-41.56	314	18/01/2005		yes		yes	
Pareledone	turqueti	PT25			Robert Is			-62.00	-57.20	111		yes	yes		yes	
Pareledone	turqueti	PT250			South Orkney Is			-61.00	-45.90	240			yes		yes	
Pareledone	turqueti	PT250SG	SG06_250		South Georgia	CAOII586-09		-53.87	-38.61	165	10/01/2006			yes		
Pareledone	turqueti	PT251	JR147_251		South Orkney Is	CAOII384-09		-61.00	-45.90	240	23/03/2006	yes		yes		
Pareledone	turqueti	PT251SG	SG06_251		South Georgia	CAOII587-09		-53.87	-38.61	165	10/01/2006			yes		
Pareledone	turqueti	PT252SG	SG06_252		South Georgia	CAOII588-09		-53.87	-38.61	165	10/01/2006			yes		
Pareledone	turqueti	PT255			South Orkney Is			-62.00	-57.20	111			yes		yes	
Pareledone	turqueti	PT25SG	SG05_25		Shag Rocks	CAOII465-09		-53.92	-41.56	314	18/01/2005			yes		
Pareledone	turqueti	PT26			South Orkney Is			-62.00	-57.20	111		yes		yes		
Pareledone	turqueti	PT262	JR147_262		South Orkney Is	CAOII395-09		-61.00	-45.90	240	23/03/2006	yes		yes		
Pareledone	turqueti	PT263	JR147_270		South Orkney Is	CAOII402-09		-61.00	-45.90	240	24/03/2006	yes		yes		
Pareledone	turqueti	PT263SG	SG06_263		South Georgia	CAOII594-09		-54.33	-39.03	221	15/01/2006			yes		
Pareledone	turqueti	PT264	JR147_264		South Orkney Is	CAOII396-09		-61.00	-45.90	240	23/03/2006	yes		yes		
Pareledone	turqueti	PT264SG	SG06_264		South Georgia	CAOII595-09		-54.55	-35.24	230	19/01/2006			yes		
Pareledone	turqueti	PT265SG	SG06_265		South Georgia	CAOII596-09		-54.55	-35.24	230	19/01/2006			yes		
Pareledone	turqueti	PT266SG	SG06_266		South Georgia	CAOII597-09		-54.55	-35.24	230	19/01/2006			yes		
Pareledone	turqueti	PT267AP	ANTXIX-3_267	NMSZ 2002037.46	Elephant Is	CAOII064-09	ANTXIX/3	-61.16	-54.56	343	30/01/2002		yes		yes	
Pareledone	turqueti	PT268AP			Elephant Is			-61.16	-54.56	343	30/01/2002			yes		
Pareledone	turqueti	PT26SG	SG05_26		Shag Rocks	CAOII466-09		-53.92	-41.56	314	18/01/2005			yes		
Pareledone	turqueti	PT27			King George Is			-62.00	-57.20	111		yes		yes		
Pareledone	turqueti	PT270			South Orkney Is			-60.90	-46.50	236		yes		yes		
Pareledone	turqueti	PT271AP	ANTXIX-3_271	NMSZ 2002037.46	Elephant Is	CAOII066-09	ANTXIX/3	-61.16	-54.56	343	30/01/2002			yes		
Pareledone	turqueti	PT272AP	ANTXIX-3_272	NMSZ 2002037.46	Elephant Is	CAOII067-09	ANTXIX/3	-61.16	-54.56	343	30/01/2002		yes		yes	

Pareledone	turqueti	PT27SG	SG05_27	Shag Rocks	CAOII467-09	-53.92	-41.56	314	18/01/2005			yes	
Pareledone	turqueti	PT28		King George Is		-62.00	-57.20	111		yes		yes	
Pareledone	turqueti	PT280SG		South Georgia		-54.96	-35.31	103				yes	
Pareledone	turqueti	PT281SG		South Georgia		-54.96	-35.31	103				yes	
Pareledone	turqueti	PT297_1		Shag Rocks		-53.60	-40.90	212				yes	
Pareledone	turqueti	PT299SG	SG06_299	South Georgia	CAOII606-09	-53.84	-38.35	166	09/01/2006			yes	
Pareledone	turqueti	PT301SG	SG06_301	South Georgia	CAOII607-09	-54.58	-35.44	150	19/01/2006			yes	
Pareledone	turqueti	PT302SG	SG06_301	South Georgia	CAOII608-09	-54.58	-35.44	150	19/01/2006			yes	
Pareledone	turqueti	PT303SG	SG06_303	South Georgia	CAOII609-09	-54.58	-35.44	150	19/01/2006			yes	
Pareledone	turqueti	PT304SG	SG06_304	South Georgia	CAOII610-09	-54.58	-35.44	150	19/01/2006			yes	
Pareledone	turqueti	PT305SG		South Georgia		-54.58	-35.44	150	19/01/2006		yes		yes
Pareledone	turqueti	PT306SG		South Georgia		-54.58	-35.44	150	19/01/2006			yes	
Pareledone	turqueti	PT307SG		South Georgia		-54.58	-35.44	150	19/01/2006			yes	
Pareledone	turqueti	PT30SG	SG05_30	South Georgia	CAOII470-09	-54.01	-38.53	154	15/01/2005			yes	
Pareledone	turqueti	PT310SG	SG06_310	Shag Rocks	CAOII611-09	-53.90	-41.15	265	13/01/2006			yes	
Pareledone	turqueti	PT312SG	SG06_312	South Georgia	CAOII613-09	-53.90	-38.30	109	10/01/2006			yes	
Pareledone	turqueti	PT314SG		South Georgia		-53.93	-35.79	265				yes	
Pareledone	turqueti	PT317SG		South Georgia		-54.24	-37.98	135	16/01/2006			yes	
Pareledone	turqueti	PT318SG		South Georgia		-54.24	-37.98	135	16/01/2006			yes	
Pareledone	turqueti	PT31SG	SG05_31	South Georgia	CAOII471-09	-54.01	-38.53	154	15/01/2005			yes	
Pareledone	turqueti	PT320SG	SG06_320	South Georgia	CAOII614-09	-54.24	-37.98	135	16/01/2006			yes	
Pareledone	turqueti	PT321SG	SG06_321	South Georgia	CAOII615-09	-54.24	-37.98	135	16/01/2006			yes	
Pareledone	turqueti	PT322SG	SG06_322	South Georgia	CAOII616-09	-54.24	-37.98	135	16/01/2006			yes	
Pareledone	turqueti	PT323SG	SG06_323	South Georgia	CAOII617-09	-54.24	-37.98	135	16/01/2006			yes	
Pareledone	turqueti	PT325SG	SG06_325	South Georgia	CAOII619-09	-55.06	-36.07	149	17/01/2006			yes	
Pareledone	turqueti	PT327SG	SG06_327	South Georgia	CAOII621-09	-55.06	-36.07	149	17/01/2006			yes	
Pareledone	turqueti	PT328SG	SG06_328	South Georgia	CAOII622-09	-55.06	-36.07	149	17/01/2006		yes		yes
Pareledone	turqueti	PT32SG	SG06_32	South Georgia	CAOII472-09	-54.01	-38.53	154	15/01/2005			yes	
Pareledone	turqueti	PT33		Robert Is		-62.00	-57.20	111		yes	yes		yes
Pareledone	turqueti	PT330SG		South Georgia		-55.06	-36.07	149				yes	
Pareledone	turqueti	PT331SG		South Georgia		-55.06	-36.07	149				yes	
Pareledone	turqueti	PT336SG	SG06_336	South Georgia	CAOII623-09	-54.32	-39.29	328	15/01/2006			yes	
Pareledone	turqueti	PT339SG	SG06_339	Shag Rocks	CAOII626-09	-53.80	-40.97	132	13/01/2006			yes	

Pareledone	turqueti	PT34			King George Is			-62.00	-57.20	111		yes		yes		
Pareledone	turqueti	PT341SG	SG06_341		Shag Rocks	CAOII629-09		-53.78	-41.02	129	14/01/2006			yes		
Pareledone	turqueti	PT342SG	SG06_342		Shag Rocks	CAOII630-09		-53.78	-41.02	129	14/01/2006			yes		
Pareledone	turqueti	PT343SG	SG06_343		Shag Rocks	CAOII631-09		-53.65	-40.88	220	13/01/2006			yes		
Pareledone	turqueti	PT354SG	PC_354		South Georgia	CAOII632-09		-54.07	-35.67	205	09/02/1991		yes		yes	
Pareledone	turqueti	PT355SG	PC_355		South Georgia	CAOII633-09		-54.07	-35.67	205	09/02/1991		yes		yes	
Pareledone	turqueti	PT356SG	PC_356		South Georgia	CAOII634-09		-54.07	-35.67	205	09/02/1991		yes		yes	
Pareledone	turqueti	PT357SG	PC_357		South Georgia			-54.07	-35.67	205	09/02/1991		yes		yes	
Pareledone	turqueti	PT36			Robert Is			-62.00	-57.20	111		yes	yes		yes	
Pareledone	turqueti	PT366SG	PC_366		South Georgia	CAOII638-09		-54.78	-34.92	349	01/02/1991		yes		yes	
Pareledone	turqueti	PT367SG	PC_367		South Georgia	CAOII639-09		-54.78	-34.92	349	01/02/1991		yes		yes	
Pareledone	turqueti	PT375SG			South Georgia			-53.76	-38.33	181				yes		
Pareledone	turqueti	PT376SG	SG90_376		Shag Rocks	CAOII646-09		-53.57	-41.63	120	08/01/1990		yes		yes	
Pareledone	turqueti	PT377SG	SG90_377		Shag Rocks	CAOII647-09		-53.57	-41.63	120	08/01/1990		yes		yes	
Pareledone	turqueti	PT378SG	SG90_378		Shag Rocks	CAOII648-09		-53.57	-41.63	120	08/01/1990			yes		
Pareledone	turqueti	PT378WS	ANTXIII-3_378		East Weddell Sea	CAOII021-09	ANTXIII/3	-71.53	-12.43	504			yes		yes	
Pareledone	turqueti	PT379SG	SG90_379		Shag Rocks	CAOII649-09		-53.57	-41.63	120	08/01/1990			yes		
Pareledone	turqueti	PT381SG			Shag Rocks			-53.57	-41.63	120	08/01/1990		yes		yes	
Pareledone	turqueti	PT382SG			Shag Rocks			-53.57	-41.63	120	08/01/1990		yes		yes	
Pareledone	turqueti	PT383SG			Shag Rocks			-53.57	-41.63	120	08/01/1990			yes		
Pareledone	turqueti	PT385SG			Shag Rocks			-53.57	-41.63	120	08/01/1990			yes		
Pareledone	turqueti	PT386SG			Shag Rocks			-53.57	-41.63	120	08/01/1990		yes		yes	
Pareledone	turqueti	PT3WS	ANTXVII-3_3	NMSZ 2000081.2	East Weddell Sea	CAOII128-09	ANTXVII/3	-71.29	-13.80	615				yes		
Pareledone	turqueti	PT401SG			South Georgia			-55.06	-35.38	124			yes		yes	
Pareledone	turqueti	PT402SG			South Georgia			-55.06	-35.38	124				yes		
Pareledone	turqueti	PT404SG			South Georgia			-55.06	-35.38	124				yes		
Pareledone	turqueti	PT415SG			South Georgia			-54.62	-35.53	113			yes		yes	
Pareledone	turqueti	PT420SG			South Georgia			-54.62	-35.53	113			yes		yes	
Pareledone	turqueti	PT421SG			South Georgia			-54.62	-35.53	113			yes		yes	
Pareledone	turqueti	PT42SG	SG05_42		Shag Rocks	CAOII481-09		-53.72	-41.28	130	19/01/2005		yes		yes	
Pareledone	turqueti	PT430SG			South Georgia			-53.67	-38.07	154	19/01/2005			yes		
Pareledone	turqueti	PT432SG			South Georgia			-53.67	-38.07	154			yes		yes	
Pareledone	turqueti	PT437SG			South Georgia			-53.65	-37.22	168				yes		

Pareledone	turqueti	PT43SG			Shag Rocks			-53.72	-41.28	130			yes			
Pareledone	turqueti	PT440SG			South Georgia			-53.65	-37.22	168		yes		yes		
Pareledone	turqueti	PT441SG			South Georgia			-53.65	-37.22	168			yes			
Pareledone	turqueti	PT442SG			South Georgia			-53.65	-37.22	168			yes			
Pareledone	turqueti	PT443SG			South Georgia			-53.65	-37.22	168			yes			
Pareledone	turqueti	PT444SG			South Georgia			-53.65	-37.22	168			yes			
Pareledone	turqueti	PT445SG			South Georgia			-53.65	-37.22	168		yes		yes		
Pareledone	turqueti	PT446SG			South Georgia			-53.65	-37.22	168		yes		yes		
Pareledone	turqueti	PT447SG			South Georgia			-53.65	-37.22	168			yes			
Pareledone	turqueti	PT449SG			South Georgia			-53.65	-37.22	168		yes		yes		
Pareledone	turqueti	PT452SG	SG06_452		Shag Rocks	CAOII653-09		-53.33	-43.02	378	12/01/2006		yes			
Pareledone	turqueti	PT453SG	SG06_453		Shag Rocks	CAOII654-09		-53.41	-42.45	220	12/01/2006		yes			
Pareledone	turqueti	PT454SG	SG06_454		Shag Rocks	CAOII655-09		-53.41	-42.45	220	12/01/2006		yes			
Pareledone	turqueti	PT463SG			South Georgia			-53.77	-39.03	238			yes			
Pareledone	turqueti	PT465SG			Shag Rocks			-53.73	-41.29	154			yes			
Pareledone	turqueti	PT466SG			South Georgia			-55.01	-36.39	272			yes			
Pareledone	turqueti	PT473SG			Shag Rocks			-53.84	-41.56	213			yes			
Pareledone	turqueti	PT474SG			Shag Rocks			-53.84	-41.56	213			yes			
Pareledone	turqueti	PT475SG			Shag Rocks			-53.84	-41.56	213			yes			
Pareledone	turqueti	PT484SG			South Georgia			-54.77	-35.34	240			yes			
Pareledone	turqueti	PT486SG			South Georgia			-54.77	-35.34	240			yes			
Pareledone	turqueti	PT487SG			Shag Rocks			-53.55	-41.33	171			yes			
Pareledone	turqueti	PT488SG			Shag Rocks			-53.55	-41.33	171			yes			
Pareledone	turqueti	PT489SG			Shag Rocks			-53.55	-41.33	171			yes			
Pareledone	turqueti	PT490SG			Shag Rocks			-53.55	-41.33	171			yes			
Pareledone	turqueti	PT492SG			South Georgia			-54.05	-38.61	176			yes			
Pareledone	turqueti	PT493SG			South Georgia			-54.05	-38.61	176			yes			
Pareledone	turqueti	PT495SG			South Georgia			-54.05	-38.61	176			yes			
Pareledone	turqueti	PT496SG			Shag Rocks			-53.62	-41.06	144			yes			
Pareledone	turqueti	PT497SG			Shag Rocks			-53.62	-41.06	144			yes			
Pareledone	turqueti	PT498SG			Shag Rocks			-53.62	-41.06	144			yes			
Pareledone	turqueti	PT499SG			Shag Rocks			-53.62	-41.06	144			yes			
Pareledone	turqueti	PT49WS	ANTXVII-3_49	NMSZ 20000081.20	East Weddell Sea	CAOII137-09	ANTXVII/3	-70.84	-10.59	237	07/04/2000	yes		yes		
Pareledone	turqueti	PT500SG			Shag Rocks			-53.63	-41.45	112			yes			

Pareledone	turqueti	PT501SG		Shag Rocks		-53.63	-41.45	112				yes	
Pareledone	turqueti	PT502SG		Shag Rocks		-53.63	-41.45	112				yes	
Pareledone	turqueti	PT503SG		Shag Rocks		-53.63	-41.45	112				yes	
Pareledone	turqueti	PT504SG		Shag Rocks		-53.63	-41.45	112				yes	
Pareledone	turqueti	PT505SG		Shag Rocks		-53.63	-41.45	112				yes	
Pareledone	turqueti	PT506SG	SG06_506	Shag Rocks	CAOII656-09	-53.53	-42.22	158	12/01/2006			yes	
Pareledone	turqueti	PT507SG	SG06_507	Shag Rocks	CAOII657-09	-53.53	-42.22	158	12/01/2006			yes	
Pareledone	turqueti	PT508SG	SG06_508	South Georgia	CAOII658-09	-53.53	-42.22	158	12/01/2006		yes		yes
Pareledone	turqueti	PT509SG	SG06_509	Shag Rocks	CAOII659-09	-53.53	-42.22	158	12/01/2006			yes	
Pareledone	turqueti	PT50SG		South Georgia		-54.33	-38.26	233				yes	
Pareledone	turqueti	PT510SG		Shag Rocks		-53.53	-42.22	158	12/01/2006			yes	
Pareledone	turqueti	PT511SG		Shag Rocks		-53.53	-42.22	158	12/01/2006		yes		yes
Pareledone	turqueti	PT51SG	SG05_51	Shag Rocks	CAOII490-09	-53.62	-41.11	145	19/01/2005			yes	
Pareledone	turqueti	PT52SG	SG05_52	Shag Rocks	CAOII491-09	-53.76	-40.95	133	17/01/2005			yes	
Pareledone	turqueti	PT53SG	SG05_53	Shag Rocks	CAOII492-09	-53.76	-40.95	133	17/01/2005			yes	
Pareledone	turqueti	PT54SG	SG05_54	Shag Rocks	CAOII493-09	-53.76	-40.95	133	17/01/2005			yes	
Pareledone	turqueti	PT5SG	SG05_5	South Georgia	CAOII445-09	-53.79	-38.22	178	14/01/2005			yes	
Pareledone	turqueti	PT5WS		East Weddell Sea		-71.29	-13.80	615				yes	
Pareledone	turqueti	PT60WS		East Weddell Sea		-70.84	-10.58	274			yes		yes
Pareledone	turqueti	PT61WS		East Weddell Sea		-70.84	-10.58	274			yes		yes
Pareledone	turqueti	PT62SG	SG05_62	South Georgia	CAOII501-09	-54.01	-38.53	154	15/01/2005			yes	
Pareledone	turqueti	PT6SG	SG05_6	South Georgia	CAOII446-09	53.79	38.22	178	14/01/2005			yes	
Pareledone	turqueti	PT70		Elephant Is		-61.20	-55.70	95		yes		yes	
Pareledone	turqueti	PT70SG	SG05_70	Shag Rocks	CAOII508-09	-53.73	-41.49	172	18/01/2005			yes	
Pareledone	turqueti	PT71SG	SG05_71	Shag Rocks	CAOII509-09	-53.73	-41.49	172	18/01/2005			yes	
Pareledone	turqueti	PT72SG	SG05_72	Shag Rocks	CAOII510-09	-53.73	-41.49	172	18/01/2005			yes	
Pareledone	turqueti	PT73SG	SG05_73	South Georgia	CAOII511-09	-53.79	-39.29	401	15/01/2005		yes		yes
Pareledone	turqueti	PT76	JR147_76	Elephant Is	CAOII341-09	-61.00	-55.90	154	13/03/2006			yes	
Pareledone	turqueti	PT7SG	SG05_7	South Georgia	CAOII447-09	-53.59	-37.29	258	13/01/2005			yes	
Pareledone	turqueti	PT80SG	SG05_80	Shag Rocks	CAOII518-09	-53.76	-40.95	133	17/01/2005			yes	
Pareledone	turqueti	PT81SG		Shag Rocks		-53.81	-40.91	198				yes	
Pareledone	turqueti	PT82SG		Shag Rocks		-53.81	-40.91	198				yes	
Pareledone	turqueti	PT83SG	SG05_83	Shag Rocks	CAOII521-09	-53.81	-40.72	320	17/01/2005			yes	

Pareledone	turqueti	PT84AP	ANTXVII-3_84	NMSZ 20000081.28	Bransfield Strait	CAOII148-09	ANTXVII/3	-63.04	-59.17	666	28/04/2000	yes		yes
Pareledone	turqueti	PT86SG	SG05_86		South Georgia	CAOII524-09		-53.59	-37.10	394	21/01/2005		yes	
Pareledone	turqueti	PT88SG	SG05_88		South Georgia	CAOII526-09		-53.59	-37.10	394	21/01/2005		yes	
Pareledone	turqueti	PT8SG	SG05_8		South Georgia	CAOII448-09		-53.76	-39.05	238	15/01/2005		yes	
Pareledone	turqueti	PT94SG	SG05_94		South Georgia	CAOII532-09		-53.75	-38.62	242	14/01/2005		yes	
Pareledone	turqueti	PT96SG	SG05_96		South Georgia	CAOII534-09		-53.75	-38.62	242			yes	
Adelieledone	sp	PT97			Elephant Is			-61.00	-56.00	337				
Pareledone	turqueti	WS112	ANTXIII-3_112		East Weddell Sea	CAOII010-09	ANTXIII/3	-71.67	-12.70	254	14/02/1996	yes		yes
Pareledone	turqueti	WS241	ANTXIII-3_241		East Weddell Sea	CAOII014-09	ANTXIII/3	-73.61	-22.32	620	14/02/1996		yes	
Pareledone	turqueti	WS49			East Weddell Sea			-71.05	-11.43	462			yes	
Pareledone	sp	KL05_0778										yes		
Pareledone	sp	KL05_0786										yes		
Pareledone	sp	KL05_0784										yes		
Pareledone	sp	JS_17										yes		
Pareledone	sp	P329_10										yes		
Pareledone	sp	P329_2										yes		
Pareledone	sp	P329_5										yes		
Pareledone	sp	P329_7										yes		

Supplementary Table 3.2 Sample information of Southern Ocean octopod samples (n = 285, including 17 technical replicates) sequenced with ddRAD sequencing and selected for the discovery of ddRAD loci for target capture sequencing

Study ID	Location	Species	Latitude	Longitude	Collection depth (m)
09_0814	West Antarctic Peninsula	Pareledone turqueti	-67.73	-70.24	536
44059	Ross Sea	Pareledone aequipapillae	-74.58	170.25	285
44067_2	Ross Sea	Pareledone aequipapillae	-76.19	176.30	447
44067_5	Ross Sea	Pareledone aequipapillae	-76.19	176.30	447
44072_2	Ross Sea	Pareledone cf. aequipapillae	-76.59	176.83	369
44074_4	Ross Sea	Pareledone turqueti	-76.19	176.30	447
44112	Ross Sea	Pareledone turqueti	-76.60	176.80	360
44113_1	Ross Sea	Pareledone turqueti	-76.19	176.30	447
44118_1	Ross Sea	Pareledone turqueti	-76.19	176.30	447
44118_2	Ross Sea	Pareledone turqueti	-76.19	176.30	447
44121	Ross Sea	Pareledone turqueti	-67.83	-179.59	405
44132	Ross Sea	Pareledone turqueti	-74.73	167.01	916
44253_2	Ross Sea	Pareledone turqueti	-73.12	174.32	321
44258_1	Ross Sea	Pareledone turqueti	-71.86	174.03	1990
44258_4	Ross Sea	Pareledone turqueti	-71.86	174.03	1990
AD01A	Casey Station	Megaleledone setebos	-64.74	132.16	1038
AND138	Elephant Is	Pareledone turqueti	-61.07	-54.61	190
AND226	Elephant Is	Pareledone sp	-61.16	-54.56	343
AND2414	Livingston Is	Pareledone turqueti	-62.39	-61.40	363
AND432	Elephant Is	Pareledone aequipapillae	-61.20	-54.84	94
CT816	Adélie Land	Pareledone turqueti	-66.75	143.95	641
CT827	Adélie Land	Pareledone turqueti	-66.00	139.68	196
CT828	Adélie Land	Pareledone turqueti	-66.33	140.65	165
CT846	Adélie Land	Pareledone turqueti	-66.56	140.80	361
CT864	Adélie Land	Pareledone turqueti	-66.34	140.45	444
CT883	Adélie Land	Pareledone turqueti	-65.71	140.60	424
CT895	Adélie Land	Pareledone turqueti	-65.71	140.60	424
CT898	Adélie Land	Pareledone turqueti	-65.71	140.60	424
CT903	Adélie Land	Adelieledone cf. adelieana	-66.00	139.68	196
CT906	Adélie Land	Pareledone turqueti	-65.71	140.60	424
CT916	Adélie Land	Pareledone sp	-65.51	139.36	398
CT918	Adélie Land	Pareledone sp	-66.34	140.45	444
CT919	Adélie Land	Adelieledone cf. adelieana	-66.34	140.45	444
CT920	Adélie Land	Adelieledone cf. adelieana	-65.48	139.26	433
CT921	Adélie Land	Pareledone aequipapillae	-65.99	140.00	192
CT922	Adélie Land	Adelieledone polymorpha	-65.49	139.31	408
CT924	Adélie Land	Pareledone aequipapillae	-65.51	139.36	398
CT926	Adélie Land	Pareledone sp	-65.51	139.36	398

CT927	Adélie Land	Pareledone sp	-65.51	139.36	398
CT928	Adélie Land	Pareledone turqueti	-66.17	139.93	150
CT932	Adélie Land	Adelieledone cf. adelieana	-65.49	139.31	408
CT937	Adélie Land	Pareledone turqueti	-66.34	141.34	230
CT938	Adélie Land	Pareledone sp	-65.27	139.25	1231
CT946	Adélie Land	Pareledone sp	-65.99	139.31	472
CT947	Adélie Land	Pareledone sp	-65.51	139.36	398
CT948	Adélie Land	Pareledone sp			
JCR1529	South Orkney Is	Pareledone sp	-60.36	-46.52	1122
JR179_403	Amundsen Sea	Pareledone turqueti	-74.41	-104.65	502
JR179_674	Amundsen Sea	Pareledone turqueti	-73.98	-107.41	536
JR179_797	Amundsen Sea	Pareledone turqueti	-71.35	-110.00	476
JS_15	South Weddell Sea	Adelieledone sp	-77.00	-34.16	
JS_18	South Weddell Sea	Pareledone turqueti	-74.59	-26.89	642
JS_19	South Weddell Sea	Pareledone turqueti	-74.54	-37.38	366
JS_22	South Weddell Sea	Adelieledone sp	-76.07	-30.15	442
JS_24	South Weddell Sea	Pareledone aequipapillae	-74.31	-32.83	685
JS_27	South Weddell Sea	Megaleledone setebos	-77.02	-34.44	520
JS_29	South Weddell Sea	Pareledone aequipapillae	-77.61	-38.94	1026
JS_30	South Weddell Sea	Adelieledone sp	-77.00	-34.16	
JS_31	South Weddell Sea	Pareledone turqueti			
JS_35	South Weddell Sea	Pareledone aequipapillae			
JS_36	South Weddell Sea	Pareledone sp			
JS_37	South Weddell Sea	Adelieledone sp			
JS_38	South Weddell Sea	Adelieledone sp	-77.02	-33.70	403
JS_39	South Weddell Sea	Pareledone turqueti	-77.02	-33.70	403
JS_41	South Weddell Sea	Pareledone aequipapillae			
JS_43	South Weddell Sea	Pareledone aequipapillae			
JS_46	South Weddell Sea	Pareledone turqueti			
JS_47	South Weddell Sea	Pareledone aequipapillae			
JS_48	South Weddell Sea	Pareledone aequipapillae			
JS_49	South Weddell Sea	Adelieledone sp			
JS_51	South Weddell Sea	Adelieledone sp			
JS_52	South Weddell Sea	Pareledone aequipapillae			
JS_53	South Weddell Sea	Adelieledone sp			
JS091	Prydz Bay	Pareledone turqueti	-66.93	65.92	185
JS099	Prydz Bay	Pareledone turqueti	-66.93	65.92	185
JS11	South Weddell Sea	Pareledone aequipapillae			
JS13	South Weddell Sea	Pareledone turqueti	-76.19	-30.36	420
JS14	South Weddell Sea	Pareledone aequipapillae	-75.52	-28.99	442
JS2	South Weddell Sea	Pareledone aequipapillae	-70.90	-11.14	293
JS8	South Weddell Sea	Pareledone turqueti	-72.31	-16.86	762
KL05_0779	Larsen Ice Shelves	Pareledone sp	-69.51	-50.40	1827

KL05_0780	Larsen Ice Shelves	Pareledone sp	-63.58	-50.70	2617
KL05_0785	East Weddell Sea	Adelieledone sp	-70.50	-14.53	4448
KL05_0787	Larsen Ice Shelves	Pareledone sp	-71.31	-13.97	1055
KLO5_0783	Larsen Ice Shelves	Graneledone sp.	-63.58	-50.70	2617
LS155	Robert Is	Pareledone turqueti	-61.98	-60.31	804
LS157	Robert Is	Pareledone turqueti	-61.98	-60.31	804
LS158	Robert Is	Pareledone turqueti	-61.98	-60.31	804
LS16	East Weddell Sea	Pareledone turqueti	-71.19	-12.26	309
LS162	East Weddell Sea	Pareledone turqueti	-61.98	-60.31	804
LS5	East Weddell Sea	Pareledone turqueti	-71.29	-13.80	615
LS74	Bransfield Strait	Pareledone turqueti	-63.01	-59.12	621
LS84	Bransfield Strait	Pareledone turqueti	-63.04	-59.17	666
Oct03A	Prydz Bay	Megaleledone setebos	-66.84	-65.49	600
Oct10	Prydz Bay	Adelieledone sp	-66.84	-65.49	600
Octo1	East Weddell Sea	Pareledone aequipapillae	-70.81	-11.37	1342
Octo10	East Weddell Sea	Pareledone aequipapillae	-70.95	-10.53	303
Octo14	East Weddell Sea	Pareledone aequipapillae	-71.58	-13.95	844
Octo17	East Weddell Sea	Pareledone aequipapillae	-71.12	-13.49	77
Octo18	East Weddell Sea	Adelieledone sp	-70.94	-10.53	304
Octo19	East Weddell Sea	Pareledone aequipapillae	-70.95	-10.53	303
Octo20	East Weddell Sea	Pareledone aequipapillae	-70.95	-10.53	303
Octo21	East Weddell Sea	Pareledone aequipapillae			
Octo24	East Weddell Sea	Pareledone turqueti	-70.87	-10.70	288
Octo3	East Weddell Sea	Pareledone turqueti	-70.81	-11.37	1342
Octo4	East Weddell Sea	Pareledone turqueti	-70.81	-11.37	1342
Octo9	East Weddell Sea	Pareledone aequipapillae	-70.95	-10.53	303
P322_7	Kerguelen Is	Pareledone sp	-48.88	71.32	938
PT102	Elephant Is	Pareledone aequipapillae	-61.00	-56.00	337
PT103	Elephant Is	Adelieledone sp	-61.00	-56.00	337
PT104SG	South Georgia	Pareledone turqueti	-54.33	-39.04	226
PT10SG	South Georgia	Pareledone turqueti	-53.76	-39.05	238
PT111	Elephant Is	Pareledone turqueti	-61.20	-55.90	108
PT11SG	South Georgia	Pareledone turqueti	-53.76	-39.05	238
PT145AP	Elephant Is	Pareledone turqueti	-61.07	-54.61	190
PT149AP	Robert Is	Pareledone turqueti	-61.98	-60.31	804
PT14SG	South Georgia	Pareledone turqueti	-53.76	-39.05	238
PT152AP	Robert Is	Pareledone turqueti	-61.98	-60.31	804
PT154AP	Robert Is	Pareledone turqueti	-61.98	-60.31	804
PT155	Elephant Is	Pareledone turqueti	-61.20	-55.70	103
PT15WS	East Weddell Sea	Pareledone turqueti	-71.19	-12.26	309
PT163AP	Robert Is	Pareledone turqueti	-61.98	-60.31	804
PT165AP	Robert Is	Pareledone turqueti	-61.98	-60.31	804
PT186	Elephant Is	Pareledone turqueti	-61.20	-55.70	103

PT18SG	South Georgia	Pareledone turqueti	-54.97	-35.32	103
PT191	Elephant Is	Pareledone turqueti	-61.20	-55.70	103
PT201	Elephant Is	Pareledone aequipapillae	-61.20	-55.70	103
PT201_1	Elephant Is	Pareledone turqueti	-61.20	-55.70	103
PT201_2	Elephant Is	Pareledone aequipapillae	-61.20	-55.70	103
PT209SG	South Georgia	Pareledone turqueti	-54.30	-37.89	149
PT20SG	Shag Rocks	Pareledone turqueti	-53.81	-40.32	533
PT210SG	South Georgia	Pareledone turqueti	-54.30	-37.89	149
PT211SG	South Georgia	Pareledone turqueti	-54.30	-37.89	149
PT212SG	South Georgia	Pareledone turqueti	-54.30	-37.89	149
PT213SG	South Georgia	Pareledone turqueti	-54.30	-37.89	149
PT215SG	Shag Rocks	Pareledone turqueti	-53.74	-41.46	164
PT217SG	Shag Rocks	Pareledone turqueti	-53.79	-40.96	130
PT218SG	Shag Rocks	Pareledone turqueti	-53.79	-40.96	130
PT219SG	Shag Rocks	Pareledone turqueti	-53.79	-40.96	130
PT220SG	Shag Rocks	Pareledone turqueti	-53.79	-40.96	130
PT221SG	South Georgia	Pareledone turqueti	-54.30	-37.89	149
PT222SG	South Georgia	Pareledone turqueti	-54.30	-37.89	149
PT223SG	South Georgia	Pareledone turqueti	-54.30	-37.89	149
PT224SG	South Georgia	Pareledone turqueti	-54.30	-37.89	149
PT225SG	South Georgia	Pareledone turqueti	-54.30	-37.89	149
PT22SG	Shag Rocks	Pareledone turqueti	-53.81	-40.32	533
PT2407AP	Livingston Is	Pareledone turqueti	-62.18	-60.80	413
PT2429AP	Bransfield Strait	Pareledone turqueti	-62.58	-55.67	158
PT243SG	South Georgia	Pareledone turqueti	-54.73	-35.19	294
PT244	South Orkney Is	Pareledone turqueti	-61.00	-46.80	505
PT244SG	South Georgia	Pareledone turqueti	-54.63	-35.58	100
PT245SG	South Georgia	Pareledone turqueti	-54.63	-35.58	100
PT246	South Orkney Is	Pareledone turqueti	-61.00	-46.80	505
PT246SG	South Georgia	Pareledone turqueti	-54.63	-35.58	100
PT247SG	South Georgia	Pareledone turqueti	-54.63	-35.58	100
PT248	South Orkney Is	Pareledone turqueti	-60.80	-46.50	219
PT248SG	South Georgia	Pareledone turqueti	-53.87	-38.61	165
PT249SG	South Georgia	Pareledone turqueti	-53.87	-38.61	165
PT250SG	South Georgia	Pareledone turqueti	-53.87	-38.61	165
PT251	South Orkney Is	Pareledone turqueti	-61.00	-45.90	240
PT251SG	South Georgia	Pareledone turqueti	-53.87	-38.61	165
PT252SG	South Georgia	Pareledone turqueti	-53.87	-38.61	165
PT25SG	Shag Rocks	Pareledone turqueti	-53.92	-41.56	314
PT26	South Orkney Is	Pareledone turqueti	-62.00	-57.20	111
PT262	South Orkney Is	Pareledone turqueti	-61.00	-45.90	240
PT263	South Orkney Is	Pareledone turqueti	-61.00	-45.90	240
PT263SG	South Georgia	Pareledone turqueti	-54.33	-39.03	221

PT264	South Orkney Is	Pareledone turqueti	-61.00	-45.90	240
PT264SG	South Georgia	Pareledone turqueti	-54.55	-35.24	230
PT265SG	South Georgia	Pareledone turqueti	-54.55	-35.24	230
PT266SG	South Georgia	Pareledone turqueti	-54.55	-35.24	230
PT268AP	Elephant Is	Pareledone turqueti	-61.16	-54.56	343
PT26SG	Shag Rocks	Pareledone turqueti	-53.92	-41.56	314
PT27	KingGeorgeIs	Pareledone turqueti	-62.00	-57.20	111
PT270	South Orkney Is	Pareledone turqueti	-60.90	-46.50	236
PT271AP	Elephant Is	Pareledone turqueti	-61.16	-54.56	343
PT27SG	Shag Rocks	Pareledone turqueti	-53.92	-41.56	314
PT28	KingGeorgeIs	Pareledone turqueti	-62.00	-57.20	111
PT280SG	South Georgia	Pareledone turqueti	-54.96	-35.31	103
PT281SG	South Georgia	Pareledone turqueti	-54.96	-35.31	103
PT297_1	Shag Rocks	Pareledone turqueti	-53.60	-40.90	212
PT299SG	South Georgia	Pareledone turqueti	-53.84	-38.35	166
PT301SG	South Georgia	Pareledone turqueti	-54.58	-35.44	150
PT302SG	South Georgia	Pareledone turqueti	-54.58	-35.44	150
PT303SG	South Georgia	Pareledone turqueti	-54.58	-35.44	150
PT304SG	South Georgia	Pareledone turqueti	-54.58	-35.44	150
PT306SG	South Georgia	Pareledone turqueti	-54.58	-35.44	150
PT307SG	South Georgia	Pareledone turqueti	-54.58	-35.44	150
PT30SG	South Georgia	Pareledone turqueti	-54.01	-38.53	154
PT310SG	Shag Rocks	Pareledone turqueti	-53.90	-41.15	265
PT312SG	South Georgia	Pareledone turqueti	-53.90	-38.30	109
PT314SG	South Georgia	Pareledone turqueti	-53.93	-35.79	265
PT317SG	South Georgia	Pareledone turqueti	-54.24	-37.98	135
PT318SG	South Georgia	Pareledone turqueti	-54.24	-37.98	135
PT31SG	South Georgia	Pareledone turqueti	-54.01	-38.53	154
PT320SG	South Georgia	Pareledone turqueti	-54.24	-37.98	135
PT321SG	South Georgia	Pareledone turqueti	-54.24	-37.98	135
PT322SG	South Georgia	Pareledone turqueti	-54.24	-37.98	135
PT323SG	South Georgia	Pareledone turqueti	-54.24	-37.98	135
PT325SG	South Georgia	Pareledone turqueti	-55.06	-36.07	149
PT327SG	South Georgia	Pareledone turqueti	-55.06	-36.07	149
PT32SG	South Georgia	Pareledone turqueti	-54.01	-38.53	154
PT330SG	South Georgia	Pareledone turqueti	-55.06	-36.07	149
PT331SG	South Georgia	Pareledone turqueti	-55.06	-36.07	149
PT336SG	South Georgia	Pareledone turqueti	-54.32	-39.29	328
PT339SG	Shag Rocks	Pareledone turqueti	-53.80	-40.97	132
PT34	KingGeorgeIs	Pareledone turqueti	-62.00	-57.20	111
PT341SG	Shag Rocks	Pareledone turqueti	-53.78	-41.02	129
PT342SG	Shag Rocks	Pareledone turqueti	-53.78	-41.02	129
PT343SG	Shag Rocks	Pareledone turqueti	-53.65	-40.88	220

PT375SG	South Georgia	Pareledone turqueti	-53.76	-38.33	181
PT378SG	Shag Rocks	Pareledone turqueti	-53.57	-41.63	120
PT379SG	Shag Rocks	Pareledone turqueti	-53.57	-41.63	120
PT383SG	Shag Rocks	Pareledone turqueti	-53.57	-41.63	120
PT385SG	Shag Rocks	Pareledone turqueti	-53.57	-41.63	120
PT3WS	East Weddell Sea	Pareledone turqueti	-71.29	-13.80	615
PT402SG	South Georgia	Pareledone turqueti	-55.06	-35.38	124
PT404SG	South Georgia	Pareledone turqueti	-55.06	-35.38	124
PT430SG	South Georgia	Pareledone turqueti	-53.67	-38.07	154
PT437SG	South Georgia	Pareledone turqueti	-53.65	-37.22	168
PT43SG	Shag Rocks	Pareledone turqueti	-53.72	-41.28	130
PT441SG	South Georgia	Pareledone turqueti	-53.65	-37.22	168
PT442SG	South Georgia	Pareledone turqueti	-53.65	-37.22	168
PT443SG	South Georgia	Pareledone turqueti	-53.65	-37.22	168
PT444SG	South Georgia	Pareledone turqueti	-53.65	-37.22	168
PT447SG	South Georgia	Pareledone turqueti	-53.65	-37.22	168
PT452SG	Shag Rocks	Pareledone turqueti	-53.33	-43.02	378
PT453SG	Shag Rocks	Pareledone turqueti	-53.41	-42.45	220
PT454SG	Shag Rocks	Pareledone turqueti	-53.41	-42.45	220
PT463SG	South Georgia	Pareledone turqueti	-53.77	-39.03	238
PT465SG	Shag Rocks	Pareledone turqueti	-53.73	-41.29	154
PT466SG	South Georgia	Pareledone turqueti	-55.01	-36.39	272
PT473SG	Shag Rocks	Pareledone turqueti	-53.84	-41.56	213
PT474SG	Shag Rocks	Pareledone turqueti	-53.84	-41.56	213
PT475SG	Shag Rocks	Pareledone turqueti	-53.84	-41.56	213
PT484SG	South Georgia	Pareledone turqueti	-54.77	-35.34	240
PT486SG	South Georgia	Pareledone turqueti	-54.77	-35.34	240
PT487SG	Shag Rocks	Pareledone turqueti	-53.55	-41.33	171
PT488SG	Shag Rocks	Pareledone turqueti	-53.55	-41.33	171
PT489SG	Shag Rocks	Pareledone turqueti	-53.55	-41.33	171
PT490SG	Shag Rocks	Pareledone turqueti	-53.55	-41.33	171
PT492SG	South Georgia	Pareledone turqueti	-54.05	-38.61	176
PT493SG	South Georgia	Pareledone turqueti	-54.05	-38.61	176
PT495SG	South Georgia	Pareledone turqueti	-54.05	-38.61	176
PT496SG	Shag Rocks	Pareledone turqueti	-53.62	-41.06	144
PT497SG	Shag Rocks	Pareledone turqueti	-53.62	-41.06	144
PT498SG	Shag Rocks	Pareledone turqueti	-53.62	-41.06	144
PT499SG	Shag Rocks	Pareledone turqueti	-53.62	-41.06	144
PT500SG	Shag Rocks	Pareledone turqueti	-53.63	-41.45	112
PT501SG	Shag Rocks	Pareledone turqueti	-53.63	-41.45	112
PT502SG	Shag Rocks	Pareledone turqueti	-53.63	-41.45	112
PT503SG	Shag Rocks	Pareledone turqueti	-53.63	-41.45	112
PT504SG	Shag Rocks	Pareledone turqueti	-53.63	-41.45	112

PT505SG	Shag Rocks	Pareledone turqueti	-53.63	-41.45	112
PT506SG	Shag Rocks	Pareledone turqueti	-53.53	-42.22	158
PT507SG	Shag Rocks	Pareledone turqueti	-53.53	-42.22	158
PT509SG	Shag Rocks	Pareledone turqueti	-53.53	-42.22	158
PT50SG	South Georgia	Pareledone turqueti	-54.33	-38.26	233
PT510SG	Shag Rocks	Pareledone turqueti	-53.53	-42.22	158
PT51SG	Shag Rocks	Pareledone turqueti	-53.62	-41.11	145
PT52SG	Shag Rocks	Pareledone turqueti	-53.76	-40.95	133
PT53SG	Shag Rocks	Pareledone turqueti	-53.76	-40.95	133
PT54SG	Shag Rocks	Pareledone turqueti	-53.76	-40.95	133
PT5SG	South Georgia	Pareledone turqueti	-53.79	-38.22	178
PT5WS	East Weddell Sea	Pareledone turqueti	-71.29	-13.80	615
PT62SG	South Georgia	Pareledone turqueti	-54.01	-38.53	154
PT6SG	South Georgia	Pareledone turqueti	53.79	38.22	178
PT70	Elephant Is	Pareledone turqueti	-61.20	-55.70	95
PT70SG	Shag Rocks	Pareledone turqueti	-53.73	-41.49	172
PT71SG	Shag Rocks	Pareledone turqueti	-53.73	-41.49	172
PT72SG	Shag Rocks	Pareledone turqueti	-53.73	-41.49	172
PT76	Elephant Is	Pareledone turqueti	-61.00	-55.90	154
PT7SG	South Georgia	Pareledone turqueti	-53.59	-37.29	258
PT80SG	Shag Rocks	Pareledone turqueti	-53.76	-40.95	133
PT81SG	Shag Rocks	Pareledone turqueti	-53.81	-40.91	198
PT82SG	Shag Rocks	Pareledone turqueti	-53.81	-40.91	198
PT83SG	Shag Rocks	Pareledone turqueti	-53.81	-40.72	320
PT86SG	South Georgia	Pareledone turqueti	-53.59	-37.10	394
PT88SG	South Georgia	Pareledone turqueti	-53.59	-37.10	394
PT8SG	South Georgia	Pareledone turqueti	-53.76	-39.05	238
PT94SG	South Georgia	Pareledone turqueti	-53.75	-38.62	242
PT96SG	South Georgia	Pareledone turqueti	-53.75	-38.62	242
PT97	Elephant Is	Adelieledone sp	-61.00	-56.00	337
WS241	East Weddell Sea	Pareledone turqueti	-73.61	-22.32	620
WS49	East Weddell Sea	Pareledone turqueti	-71.05	-11.43	462

Supplementary Table 3.3 Sample information of *Pareledone turqueti* (n = 87) sequenced with target capture sequencing of ddRAD loci

Species	Study ID	Sample Location	Latitude	Longitude	Collection depth (m)
Pareledone turqueti	JR179_141	Amundsen Sea	-71.81	-106.33	577
Pareledone turqueti	PT84AP	Bransfield Strait	-63.04	-59.17	666
Pareledone turqueti	PT117AP	Deception Is	-63.02	-61.15	352
Pareledone turqueti	PT119AP/41	Deception Is	-63.02	-61.15	352
Pareledone turqueti	CT905	Adélie Land	-66.00	139.68	196
Pareledone turqueti	CT909	Adélie Land	-66.56	141.26	177
Pareledone turqueti	CT917	Adélie Land	-66.34	141.27	207
Pareledone turqueti	CT933	Adélie Land	-66.40	139.79	896
Pareledone turqueti	CT939	Adélie Land	-66.00	139.68	196
Pareledone turqueti	AD_01_6	Casey Station	-65.23	118.53	913
Pareledone turqueti	JS096	Mawson Station	-66.93	65.92	185
Pareledone turqueti	JS097	Mawson Station	-66.93	65.92	185
Pareledone turqueti	LS14	East Weddell Sea	-71.19	-12.26	309
Pareledone turqueti	LS15	East Weddell Sea	-71.19	-12.26	309
Pareledone turqueti	LS3	East Weddell Sea	-71.29	-13.80	615
Pareledone turqueti	Octo13	East Weddell Sea	-71.58	-13.95	844
Pareledone turqueti	Octo2	East Weddell Sea	-70.81	-11.37	1342
Pareledone turqueti	PT16WS	East Weddell Sea	-71.19	-12.26	309
Pareledone turqueti	PT378WS	East Weddell Sea	-71.53	-12.43	504
Pareledone turqueti	PT49WS	East Weddell Sea	-70.84	-10.59	237
Pareledone turqueti	PT60WS	East Weddell Sea	-70.84	-10.58	274
Pareledone turqueti	PT61WS	East Weddell Sea	-70.84	-10.58	274
Pareledone turqueti	WS112	East Weddell Sea	-71.67	-12.70	254
Pareledone turqueti	AND145	Elephant Is	-61.07	-54.61	190
Pareledone turqueti	AND271	Elephant Is	-61.16	-54.56	343
Pareledone turqueti	PT108	Elephant Is	-61.20	-55.90	108
Pareledone turqueti	PT154	Elephant Is	-61.20	-55.70	103
Pareledone turqueti	PT192	Elephant Is	-61.20	-55.70	103
Pareledone turqueti	PT267AP	Elephant Is	-61.16	-54.56	343
Pareledone turqueti	PT272AP	Elephant Is	-61.16	-54.56	343
Pareledone turqueti	09_0713	West Antarctic Peninsula	-67.75	-70.06	586
Pareledone turqueti	LS149	Robert Is	-61.98	-60.31	804
Pareledone turqueti	LS152	Robert Is	-61.98	-60.31	804
Pareledone turqueti	LS154	Robert Is	-61.98	-60.31	804

Pareledone turqueti	LS161	Robert Is	-61.98	-60.31	804
Pareledone turqueti	PT151AP	Robert Is	-61.98	-60.31	804
Pareledone turqueti	PT156AP	Robert Is	-61.98	-60.31	804
Pareledone turqueti	PT24	KingGeorge Is	-62.00	-57.20	111
Pareledone turqueti	PT2414AP	Livingston Is	-62.39	-61.40	363
Pareledone turqueti	PT25	KingGeorge Is	-62.00	-57.20	111
Pareledone turqueti	PT33	KingGeorge Is	-62.00	-57.20	111
Pareledone turqueti	PT36	KingGeorge Is	-62.00	-57.20	111
Pareledone turqueti	44117	Ross Sea	-75.63	169.85	525
Pareledone turqueti	44122	Ross Sea	-73.12	174.32	321
Pareledone turqueti	44130	Ross Sea	-76.59	176.83	369
Pareledone turqueti	44255	Ross Sea	-76.60	176.80	360
Pareledone turqueti	44074_5	Ross Sea	-76.19	176.30	447
Pareledone turqueti	44113_3	Ross Sea	-76.19	176.30	447
Pareledone turqueti	44113_4	Ross Sea	-76.19	176.30	447
Pareledone turqueti	44118_3	Ross Sea	-76.19	176.30	447
Pareledone turqueti	44256_1	Ross Sea	-72.35	175.50	850
Pareledone turqueti	NIWA87970	Ross Sea			
Pareledone turqueti	PT214SG	Shag Rocks	-53.74	-41.46	164
Pareledone turqueti	PT24SG	Shag Rocks	-53.92	-41.56	314
Pareledone turqueti	PT376SG	Shag Rocks	-53.57	-41.63	120
Pareledone turqueti	PT377SG	Shag Rocks	-53.57	-41.63	120
Pareledone turqueti	PT381SG	Shag Rocks	-53.57	-41.63	120
Pareledone turqueti	PT382SG	Shag Rocks	-53.57	-41.63	120
Pareledone turqueti	PT386SG	Shag Rocks	-53.57	-41.63	120
Pareledone turqueti	PT42SG	Shag Rocks	-53.72	-41.28	130
Pareledone turqueti	PT511SG	Shag Rocks	-53.53	-42.22	158
Pareledone turqueti	PT305SG	South Georgia	-54.58	-35.44	150
Pareledone turqueti	PT328SG	South Georgia	-55.06	-36.07	149
Pareledone turqueti	PT354SG	South Georgia	-54.07	-35.67	205
Pareledone turqueti	PT355SG	South Georgia	-54.07	-35.67	205
Pareledone turqueti	PT356SG	South Georgia	-54.07	-35.67	205
Pareledone turqueti	PT357SG	South Georgia	-54.07	-35.67	205
Pareledone turqueti	PT366SG	South Georgia	-54.78	-34.92	349
Pareledone turqueti	PT367SG	South Georgia	-54.78	-34.92	349
Pareledone turqueti	PT401SG	South Georgia	-55.06	-35.38	124
Pareledone turqueti	PT415SG	South Georgia	-54.62	-35.53	113

Pareledone turqueti	PT420SG	South Georgia	-54.62	-35.53	113
Pareledone turqueti	PT421SG	South Georgia	-54.62	-35.53	113
Pareledone turqueti	PT432SG	South Georgia	-53.67	-38.07	154
Pareledone turqueti	PT440SG	South Georgia	-53.65	-37.22	168
Pareledone turqueti	PT445SG	South Georgia	-53.65	-37.22	168
Pareledone turqueti	PT446SG	South Georgia	-53.65	-37.22	168
Pareledone turqueti	PT449SG	South Georgia	-53.65	-37.22	168
Pareledone turqueti	PT508SG	South Georgia	-53.53	-42.22	158
Pareledone turqueti	PT73SG	South Georgia	-53.79	-39.29	401
Pareledone turqueti	PT250	South Orkney Is	-61.00	-45.90	240
Pareledone turqueti	PT255	South Orkney Is	-62.00	-57.20	111
Pareledone turqueti	JS_26	South Weddell Sea	-77.72	-35.98	613
Pareledone turqueti	JS_40	South Weddell Sea			
Pareledone turqueti	JS_44	South Weddell Sea			
Pareledone turqueti	JS10	South Weddell Sea	-72.31	-16.86	762
Pareledone turqueti	JS5	South Weddell Sea	-72.59	-18.07	406

Supplementary Table 3.4 Number of SNPs or sites retained after different variant filtering thresholds applied on ddRAD loci data of *Pareledone turqueti*. ddRAD loci data were sequenced with ddRADseq and target capture sequencing. Reads derived from ddRADseq and target capture sequencing were combined and processed in two bioinformatic pipelines. Pipelines include *bcftools mpileup* and *ANGSD*.

			mpileup	***ANGSD***
% missing data allowed (--max-missing)	Minimum % of minor allele frequency filtered (--maf)	Filter for hardy-Weinberg equilibrium departure with p < 0.05	Number of SNPs retained	number of sites retained
20 (0.8)	2 (0.02)	No	4714	243619
10 (0.9)	5 (0.05)	No	3585	100258
20 (0.8)	5 (0.05)	No	4376	168939
20 (0.8)	5 (0.05)	Yes	2293	26960
30 (0.7)	5 (0.05)	No	4617	204579
40 (0.6)	5 (0.05)	No	4711	223940
50 (0.5)	5 (0.05)	No	4807	235950
20 (0.8)	10 (0.10)	No	3895	120898

Supplementary Table 4.1 Sample information of *Ophionotus victoriae* (n = 158) and *O. hexactis* (n = 40) sequenced with target capture sequencing of ddRAD loci

Genus	Species	Field ID	Registration ID	Sample locality (defined in this study)	Collection date	Expedition	Station ID	Event number	Latitude	Longitude	Collection depth (m)
Ophionotus	victoriae	140217A	NIWA140217	Ross Sea	01/02/2019	TAN1901	SRS2_7	175	-75.525	-172.992	1376
Ophionotus	victoriae	140217B	NIWA140217	Ross Sea	01/02/2019	TAN1901	SRS2_7	175	-75.525	-172.992	1376
Ophionotus	victoriae	140217C	NIWA140217	Ross Sea	01/02/2019	TAN1901	SRS2_7	175	-75.525	-172.992	1376
Ophionotus	victoriae	36968A	NIWA36968	Ross Sea	18/02/2008	TAN0802		100	-76.202	176.248	447
Ophionotus	victoriae	36968B	NIWA36968	Ross Sea	18/02/2008	TAN0802		100	-76.202	176.248	447
Ophionotus	victoriae	36968C	NIWA36968	Ross Sea	18/02/2008	TAN0802		100	-76.202	176.248	447
Ophionotus	victoriae	36968E	NIWA36968	Ross Sea	18/02/2008	TAN0802		100	-76.202	176.248	447
Ophionotus	victoriae	36968F	NIWA36968	Ross Sea	18/02/2008	TAN0802		100	-76.202	176.248	447
Ophionotus	victoriae	37157A	NIWA37157	Ross Sea	21/02/2008	TAN0802		117	-72.590	175.342	175
Ophionotus	victoriae	93825B	NIWA93825	Ross Sea	27/02/2004	TAN0402		174	-71.494	171.604	483
Ophionotus	victoriae	93825C	NIWA93825	Ross Sea	27/02/2004	TAN0402		174	-71.494	171.604	483
Ophionotus	victoriae	93825A	NIWA93825	Ross Sea	27/02/2004	TAN0402		174	-71.494	171.604	483
Ophionotus	victoriae	94858A	NIWA94858	Ross Sea	23/02/2004	TAN0402		133	-71.645	170.219	252
Ophionotus	victoriae	94866A	NIWA94866	Ross Sea	23/02/2004	TAN0402		132	-71.648	170.180	172
Ophionotus	victoriae	94866B	NIWA94866	Ross Sea	23/02/2004	TAN0402		132	-71.648	170.180	172
Ophionotus	victoriae	94869A	NIWA94869	Ross Sea	27/02/2004	TAN0402		174	-71.494	171.604	483
Ophionotus	victoriae	94869B	NIWA94869	Ross Sea	27/02/2004	TAN0402		174	-71.494	171.604	483
Ophionotus	victoriae	N0071	NIWA85184	Ross Sea	14/02/2008	TAN0802		61	-75.622	169.805	521
Ophionotus	victoriae	N0072	NIWA85184	Ross Sea	14/02/2008	TAN0802		61	-75.622	169.805	521
Ophionotus	victoriae	N0073	NIWA85184	Ross Sea	14/02/2008	TAN0802		61	-75.622	169.805	521
Ophionotus	victoriae	N0074	NIWA85184	Ross Sea	14/02/2008	TAN0802		61	-75.622	169.805	521
Ophionotus	victoriae	N0075	NIWA85184	Ross Sea	14/02/2008	TAN0802		61	-75.622	169.805	521
Ophionotus	victoriae	PDIVA-C	SIOBICE4766	Ross Sea	11/20/2010	SIO McMurdo		IVA	-77.572	163.512	Scuba diver
Ophionotus	victoriae	PDIVA-D	SIOBICE4766	Ross Sea	11/20/2010	SIO McMurdo		IVA	-77.572	163.512	Scuba diver
Ophionotus	victoriae	PDIVA-E	SIOBICE4766	Ross Sea	11/20/2010	SIO McMurdo		IVA	-77.572	163.512	Scuba diver
Ophionotus	victoriae	PDIVA-G	SIOBICE4766	Ross Sea	11/20/2010	SIO McMurdo		IVA	-77.572	163.512	Scuba diver
Ophionotus	victoriae	PDIVA-I	SIOBICE4766	Ross Sea	11/20/2010	SIO McMurdo		IVA	-77.572	163.512	Scuba diver
Ophionotus	victoriae	250	250	Amundsen Sea	05/03/2008	JR179	BIO4-AGT-2A		-74.479	-104.237	1203.06

Ophionotus	victoriae	251	251	Amundsen Sea	05/03/2008	JR179	BIO4-AGT-2A		-74.479	-104.237	1203.06
Ophionotus	victoriae	830	830	Amundsen Sea	12/03/2008	JR179	BIO6-AGT-2A		-71.175	-109.863	1005.79
Ophionotus	victoriae	811.11	811.11	Amundsen Sea	12/03/2008	JR179	BIO6-AGT-2A		-71.175	-109.863	1005.79
Ophionotus	victoriae	881.19	881.19	Amundsen Sea	12/03/2008	JR179	BIO6-AGT-2A		-71.175	-109.863	1005.79
Ophionotus	victoriae	903	903	Amundsen Sea	12/03/2008	JR179	BIO6-AGT-2B		-71.179	-109.894	988.93
Ophionotus	victoriae	94857A	NIWA94857	Balleny Islands	04/03/2008	TAN0402		233	-67.418	163.915	227
Ophionotus	victoriae	94857B	NIWA94857	Balleny Islands	04/03/2008	TAN0402		233	-67.418	163.915	227
Ophionotus	victoriae	N0078	NIWA84670	Balleny Islands	11/03/2006	TAN0602		448	-66.557	162.570	85
Ophionotus	victoriae	N0079	NIWA84670	Balleny Islands	11/03/2006	TAN0602		448	-66.557	162.570	85
Ophionotus	victoriae	N0080	NIWA84670	Balleny Islands	11/03/2006	TAN0602		448	-66.557	162.570	85
Ophionotus	victoriae	WAMZ44965	WAMZ44965	Balleny Islands	02/03/2017	ACE 2016/17	46	1209	-66.174	162.203	350
Ophionotus	victoriae	WAMZ44962	WAMZ44962	Balleny Islands	02/03/2017	ACE 2016/17	46	1209	-66.174	162.203	350
Ophionotus	victoriae	WAMZ44963	WAMZ44963	Balleny Islands	02/03/2017	ACE 2016/17	46	1209	-66.174	162.203	350
Ophionotus	victoriae	AAD107	AAD107	Prydz Bay	28/01/2001	AAD	AL27-130	58.4.2	-66.791	62.442	213
Ophionotus	victoriae	AAD141	AAD141	Prydz Bay	27/01/2001	AAD	AL27-127	58.4.2	-66.792	62.096	270
Ophionotus	victoriae	SIOBICP00496A	SIOBICE5492	Bransfield Strait	04/02/2012	Polarstern ANT-XXVIII/4		79273	-62.367	-55.961	349
Ophionotus	victoriae	SIOBICP00496B	SIOBICE5492	Bransfield Strait	04/02/2012	Polarstern ANT-XXVIII/4		79273	-62.367	-55.961	349
Ophionotus	victoriae	SIOBICP00496C	SIOBICE5492	Bransfield Strait	04/02/2012	Polarstern ANT-XXVIII/4		79273	-62.367	-55.961	349
Ophionotus	victoriae	SIOBICP00496D	SIOBICE5492	Bransfield Strait	04/02/2012	Polarstern ANT-XXVIII/4		79273	-62.367	-55.961	349
Ophionotus	victoriae	SIOBICP00496E	SIOBICE5492	Bransfield Strait	04/02/2012	Polarstern ANT-XXVIII/4		79273	-62.367	-55.961	349
Ophionotus	victoriae	SIOBICP00524A	SIOBICE5524	Bransfield Strait	04/02/2012	Polarstern ANT-XXVIII/4		79279	-62.278	-55.833	324
Ophionotus	victoriae	SIOBICP00524B	SIOBICE5524	Bransfield Strait	04/02/2012	Polarstern ANT-XXVIII/4		79279	-62.278	-55.833	324
Ophionotus	victoriae	SIOBICP00524C	SIOBICE5524	Bransfield Strait	04/02/2012	Polarstern ANT-XXVIII/4		79279	-62.278	-55.833	324
Ophionotus	victoriae	SIOBICP00524D	SIOBICE5524	Bransfield Strait	04/02/2012	Polarstern ANT-XXVIII/4		79279	-62.278	-55.833	324
Ophionotus	victoriae	SIOBICP00524E	SIOBICE5524	Bransfield Strait	04/02/2012	Polarstern ANT-XXVIII/4		79279	-62.278	-55.833	324
Ophionotus	victoriae	SIOBICS20231	SIOBICE6408	South Georgia	17/04/2013	Scotia 2013	SG4b	9	-53.634	-37.307	167
Ophionotus	victoriae	SIOBICS20237	SIOBICE6420	South Georgia	16/04/2013	Scotia 2013	SG4	5	-53.715	-36.836	190
Ophionotus	victoriae	IE.2009.4672	IE.2009. 04672	Adelie Land	14/01/2008	CEAMARC	70EV451		-66.409	140.508	1204
Ophionotus	victoriae	IE.2009.4675	IE.2009. 06259	Adelie Land	15/01/2008	CEAMARC	22EV503		-65.991	139.307	485

Ophionotus	victoriae	IE.2009.4676	IE.2009. 04676	Adelie Land	14/01/2008	CEAMARC	70EV451		-66.409	140.508	1204
Ophionotus	victoriae	IE.2009.4679	IE.2009. 04679	Adelie Land	14/01/2008	CEAMARC	70EV451		-66.409	140.508	1204
Ophionotus	victoriae	IE.2009.4687A	IE.2009. 06154	Adelie Land	13/01/2008	CEAMARC	10EV420		-66.335	141.273	227
Ophionotus	victoriae	IE.2009.4690	IE.2009. 06478	Adelie Land	28/12/2007	CEAMARC	40EV152		-66.651	142.957	637
Ophionotus	victoriae	IE.2009.4702	IE.2009. 06736	Adelie Land	26/12/2007	CEAMARC	9EV117		-66.535	141.983	521
Ophionotus	victoriae	IE.2009.4703	IE.2009. 06468	Adelie Land	12/01/2008	CEAMARC	3EV411		-66.000	142.014	248
Ophionotus	victoriae	IE.2009.4707	IE.2009. 06232	Adelie Land	12/01/2008	CEAMARC	1EV405		-66.004	142.314	240
Ophionotus	victoriae	IE.2009.4713	IE.2009. 06736	Adelie Land	26/12/2007	CEAMARC	9EV117		-66.535	141.983	521
Ophionotus	victoriae	IE.2009.4726	IE.2009. 04726	Adelie Land	27/12/2007	CEAMARC	39EV141		-66.550	142.959	875
Ophionotus	victoriae	IE.2009.4731	IE.2009. 04731	Adelie Land	24/12/2007	CEAMARC	30EV66		-66.004	143.716	440
Ophionotus	victoriae	IE.2009.4734	IE.2009. 06386	Adelie Land	03/01/2008	CEAMARC	31EV268		-66.539	144.973	451
Ophionotus	victoriae	IE.2009.4753	IE.2009. 06662	Adelie Land	14/01/2008	CEAMARC	71EV447		-66.389	140.429	791
Ophionotus	victoriae	IE.2009.4754	IE.2009. 06381	Adelie Land	24/12/2007	CEAMARC	30EV66		-66.004	143.716	440
Ophionotus	victoriae	IE.2009.4763	IE.2009. 04763	Adelie Land	02/01/2008	CEAMARC	59EV259		-66.739	144.307	954
Ophionotus	victoriae	IE.2009.4767	IE.2009. 06523	Adelie Land	26/12/2007	CEAMARC	4EV112		-66.316	142.000	257
Ophionotus	victoriae	N0121	NIWA84671	Scott Island	04/03/2008	TAN0802		223	-67.829	-179.587	403
Ophionotus	victoriae	N0122	NIWA84671	Scott Island	04/03/2008	TAN0802		223	-67.829	-179.587	403
Ophionotus	victoriae	N0123	NIWA84675	Scott Island	07/03/2008	TAN0802		247	-67.388	-179.897	144
Ophionotus	victoriae	N0125	NIWA84675	Scott Island	07/03/2008	TAN0802		247	-67.388	-179.897	144
Ophionotus	victoriae	PNG703	PNG703	Tressler Bank	03/01/2010	AAD	Tressler2	BTC17	-64.560	95.320	758
Ophionotus	victoriae	PNG708	PNG708	Tressler Bank	03/01/2010	AAD	Tressler2	BTC15	-64.560	95.317	779
Ophionotus	victoriae	PNG710	PNG710	Tressler Bank	03/01/2010	AAD	Tressler2	BTC15	-64.560	95.317	779
Ophionotus	victoriae	SIOBICS0185	SIOBICE5232	South Sandwich Islands	03/10/2011	Scotia 2011	SS1A	30	-56.723	-27.036	134
Ophionotus	victoriae	SIOBICS0460	SIOBICE5187	South Sandwich Islands	03/10/2011	Scotia 2011	SS1A	32	-56.709	-27.049	116
Ophionotus	victoriae	SIOBICS0539B	SIOBICE4802	South Sandwich Islands	05/10/2011	Scotia 2011	SS2	33	-58.475	-26.205	161
Ophionotus	victoriae	SIOBICS0539D	SIOBICE4802	South Sandwich Islands	05/10/2011	Scotia 2011	SS2	33	-58.475	-26.205	161
Ophionotus	victoriae	SIOBICS0990A	SIOBICE4784	South Sandwich Islands	03/10/2011	Scotia 2011	SS1	25	-57.034	-26.759	118
Ophionotus	victoriae	SIOBICS0990C	SIOBICE4784	South Sandwich Islands	03/10/2011	Scotia 2011	SS1	25	-57.034	-26.759	118
Ophionotus	victoriae	WAMZ44590	WAMZ44590	South Sandwich Islands	03/08/2017	ACE 2016/17	90	2590	-59.472	-27.264	230
Ophionotus	victoriae	WAMZ44932	WAMZ44932	South Sandwich Islands	03/08/2017	ACE 2016/17	90	2590	-59.472	-27.264	230
Ophionotus	victoriae	SIOBICS1312H	SIOBICE4771	Elephant Island	22/10/2011	Scotia 2011	EI1	81	-61.218	-54.255	202
Ophionotus	victoriae	SIOBICS1312I	SIOBICE4771	Elephant Island	22/10/2011	Scotia 2011	EI1	81	-61.218	-54.255	202

Ophionotus	victoriae	SIOBICS6741	SIOBICE5209	Elephant Island	23/10/2011	Scotia 2011	EI2	83	-61.339	-55.625	143
Ophionotus	victoriae	SIOBICS6743	SIOBICE5237	Elephant Island	23/10/2011	Scotia 2011	EI2	83	-61.339	-55.625	143
Ophionotus	victoriae	SIOBICS6775A	SIOBICE4803	Elephant Island	23/10/2011	Scotia 2011	EI2	84	-61.304	-55.708	170
Ophionotus	victoriae	SIOBICS4306	SIOBICE5221	Discovery Bank	13/10/2011	Scotia 2011	DB1	58	-60.111	-34.827	439
Ophionotus	victoriae	SIOBICS4307	SIOBICE5169	Discovery Bank	13/10/2011	Scotia 2011	DB1	58	-60.111	-34.827	439
Ophionotus	victoriae	SIOBICS4308	SIOBICE5194	Discovery Bank	13/10/2011	Scotia 2011	DB1	58	-60.111	-34.827	439
Ophionotus	victoriae	SIOBICS4309	SIOBICE5168	Discovery Bank	13/10/2011	Scotia 2011	DB1	58	-60.111	-34.827	439
Ophionotus	victoriae	SIOBICS4310	SIOBICE5183	Discovery Bank	13/10/2011	Scotia 2011	DB1	58	-60.111	-34.827	439
Ophionotus	victoriae	SIOBICS4472K	SIOBICE4791	Herdman Bank	10/10/2011	Scotia 2011	HB1	50	-59.863	-32.470	600
Ophionotus	victoriae	SIOBICS4472L	SIOBICE4791	Herdman Bank	10/10/2011	Scotia 2011	HB1	50	-59.863	-32.470	600
Ophionotus	victoriae	SIOBICS4472M	SIOBICE4791	Herdman Bank	10/10/2011	Scotia 2011	HB1	50	-59.863	-32.470	600
Ophionotus	victoriae	SIOBICS4472N	SIOBICE4791	Herdman Bank	10/10/2011	Scotia 2011	HB1	50	-59.863	-32.470	600
Ophionotus	victoriae	SIOBICS4472O	SIOBICE4791	Herdman Bank	10/10/2011	Scotia 2011	HB1	50	-59.863	-32.470	600
Ophionotus	victoriae	SIOBICS5741B	SIOBICE7575	Shetland Islands	27/10/2011	Scotia 2011	SSH1	94	-62.337	-60.744	183
Ophionotus	victoriae	SIOBICS5741C	SIOBICE7575	Shetland Islands	27/10/2011	Scotia 2011	SSH1	94	-62.337	-60.744	183
Ophionotus	victoriae	SIOBICS5741F	SIOBICE7575	Shetland Islands	27/10/2011	Scotia 2011	SSH1	94	-62.337	-60.744	183
Ophionotus	victoriae	SIOBICS5742	SIOBICE5171	Shetland Islands	27/10/2011	Scotia 2011	SSH1	94	-62.337	-60.744	183
Ophionotus	victoriae	SIOBICS5743	SIOBICE5023	Shetland Islands	27/10/2011	Scotia 2011	SSH1	94	-62.337	-60.744	183
Ophionotus	victoriae	SIOBICS6316A	SIOBICE4770	Bransfield Strait	25/10/2011	Scotia 2011	BS2	89	-63.343	-59.910	213
Ophionotus	victoriae	SIOBICS6316B	SIOBICE4770	Bransfield Strait	25/10/2011	Scotia 2011	BS2	89	-63.343	-59.910	213
Ophionotus	victoriae	SIOBICS6338A	SIOBICE4781	Bransfield Strait	25/10/2011	Scotia 2011	BS2	90	-63.283	-59.903	290
Ophionotus	victoriae	SIOBICS6338B	SIOBICE4781	Bransfield Strait	25/10/2011	Scotia 2011	BS2	90	-63.283	-59.903	290
Ophionotus	victoriae	SIOBICS6760A	SIOBICE4777	Bransfield Strait	24/10/2011	Scotia 2011	BS1	87	-62.753	-57.322	292
Ophionotus	victoriae	SIOBICS6760B	SIOBICE4777	Bransfield Strait	24/10/2011	Scotia 2011	BS1	87	-62.753	-57.322	292
Ophionotus	victoriae	SIOBICS6905A	SIOBICE5162	Bransfield Strait	24/10/2011	Scotia 2011	BS1	86	-62.870	-57.217	247
Ophionotus	victoriae	SIOBICS6905B	SIOBICE5162	Bransfield Strait	24/10/2011	Scotia 2011	BS1	86	-62.870	-57.217	247
Ophionotus	victoriae	WAMZ44948	WAMZ44948	Bouvet Island	03/11/2017	ACE 2016/17	98	2765	-54.419	-3.494	300
Ophionotus	victoriae	WAMZ44949	WAMZ44949	Bouvet Island	03/11/2017	ACE 2016/17	98	2765	-54.419	-3.494	300
Ophionotus	victoriae	WAMZ44950	WAMZ44950	Bouvet Island	03/11/2017	ACE 2016/17	98	2765	-54.419	-3.494	300
Ophionotus	victoriae	WAMZ44951	WAMZ44951	Bouvet Island	03/11/2017	ACE 2016/17	98	2765	-54.419	-3.494	300
Ophionotus	victoriae	WAMZ44953	WAMZ44953	Bouvet Island	03/11/2017	ACE 2016/17	98	2765	-54.419	-3.494	300
Ophionotus	victoriae	WAMZ44954	WAMZ44954	Bouvet Island	03/11/2017	ACE 2016/17	98	2765	-54.419	-3.494	300
Ophionotus	victoriae	WAMZ44955	WAMZ44955	Bouvet Island	03/11/2017	ACE 2016/17	98	2765	-54.419	-3.494	300
Ophionotus	victoriae	WAMZ44956	WAMZ44956	Bouvet Island	03/11/2017	ACE 2016/17	98	2765	-54.419	-3.494	300
Ophionotus	victoriae	WAMZ44957	WAMZ44957	Bouvet Island	03/11/2017	ACE 2016/17	98	2765	-54.419	-3.494	300
Ophionotus	victoriae	WAMZ44958	WAMZ44958	Bouvet Island	03/11/2017	ACE 2016/17	98	2765	-54.419	-3.494	300
Ophionotus	victoriae	308-1.7	WAMZ88554	Weddell Sea	04/04/2011	Polarstern ANT-XXVII/3	PS77_30 8-1		-70.858	-10.593	250

Ophionotus	victoriae	265-2.12	WAMZ88558	Weddell Sea	22/03/2011	Polarstern ANT-XXVII/3	PS77_26 5-2	-70.793	-10.678	615
Ophionotus	victoriae	265-2.11	WAMZ88559	Weddell Sea	22/03/2011	Polarstern ANT-XXVII/3	PS77_26 5-2	-70.793	-10.678	615
Ophionotus	victoriae	265-2.10	WAMZ88570	Weddell Sea	22/03/2011	Polarstern ANT-XXVII/3	PS77_26 5-2	-70.793	-10.678	615
Ophionotus	victoriae	274-3.14	WAMZ88571	Weddell Sea	25/03/2011	Polarstern ANT-XXVII/3	PS77_27 4-3	-70.949	-10.574	333
Ophionotus	victoriae	265-2.11	WAMZ88576	Weddell Sea	22/03/2011	Polarstern ANT-XXVII/3	PS77_26 5-2	-70.793	-10.678	615
Ophionotus	victoriae	265-2.13	WAMZ88577	Weddell Sea	22/03/2011	Polarstern ANT-XXVII/3	PS77_26 5-2	-70.793	-10.678	615
Ophionotus	victoriae	291-1.3	WAMZ88579	Weddell Sea	30/03/2011	Polarstern ANT-XXVII/3	PS77_29 1-1	-70.847	-10.590	284
Ophionotus	victoriae	308-1.8	WAMZ88583	Weddell Sea	04/04/2011	Polarstern ANT-XXVII/3	PS77_30 8-1	-70.858	-10.593	250
Ophionotus	victoriae	308-1.10	WAMZ88584	Weddell Sea	04/04/2011	Polarstern ANT-XXVII/3	PS77_30 8-10	-70.858	-10.593	250
Ophionotus	victoriae	WAMZ88555	WAMZ88555	Larsen Ice Shelf	12/03/2011	Polarstern ANT-XXVII/3	PS77_25 5-3	-64.833	-60.597	682
Ophionotus	victoriae	WAMZ88556	WAMZ88556	Larsen Ice Shelf	03/03/2011	Polarstern ANT-XXVII/3	PS77_23 7-2	-66.208	-60.161	362
Ophionotus	victoriae	WAMZ88563	WAMZ88563	Larsen Ice Shelf	27/02/2011	Polarstern ANT-XXVII/3	PS77_22 8-3	-64.903	-60.490	570
Ophionotus	victoriae	WAMZ88568	WAMZ88568	Larsen Ice Shelf	10/03/2011	Polarstern ANT-XXVII/3	PS77_25 2-7	-64.704	-60.530	343
Ophionotus	victoriae	WAMZ88572	WAMZ88572	Larsen Ice Shelf	07/03/2011	Polarstern ANT-XXVII/3	PS77_24 8-3	-65.928	-60.335	433
Ophionotus	victoriae	WAMZ88573	WAMZ88573	Larsen Ice Shelf	07/03/2011	Polarstern ANT-XXVII/3	PS77_24 8-3	-65.928	-60.335	433
Ophionotus	victoriae	WAMZ88574	WAMZ88574	Larsen Ice Shelf	01/03/2011	Polarstern ANT-XXVII/3	PS77_23 3-3	-65.558	-61.623	320
Ophionotus	victoriae	WAMZ88575	WAMZ88575	Larsen Ice Shelf	01/03/2011	Polarstern ANT-XXVII/3	PS77_23 3-3	-65.558	-61.623	320
Ophionotus	victoriae	WAMZ88578	WAMZ88578	Larsen Ice Shelf	01/03/2011	Polarstern ANT-XXVII/3	PS77_25 0-6	-65.381	-61.557	581
Ophionotus	victoriae	1.140.1	WAMZ88585	Weddell Sea	26/01/2014	Polarstern ANT-XXIX/9	PS82_19 1-1	-74.666	-33.733	592
Ophionotus	victoriae	1.140.2	WAMZ88586	Weddell Sea	26/01/2014	Polarstern ANT-XXIX/9	PS82_19 1-1	-74.666	-33.733	592
Ophionotus	victoriae	1.140.3	WAMZ88587	Weddell Sea	26/01/2014	Polarstern ANT-XXIX/9	PS82_19 1-1	-74.666	-33.733	592
Ophionotus	victoriae	1.140.4	WAMZ88588	Weddell Sea	26/01/2014	Polarstern ANT-XXIX/9	PS82_67 -1	-77.101	-36.546	1101
Ophionotus	victoriae	1.83.2	WAMZ88590	Weddell Sea	26/01/2014	Polarstern ANT-XXIX/9	PS82_67 -1	-77.101	-36.546	1101
Ophionotus	victoriae	1.164.1	WAMZ88591	Weddell Sea	22/01/2014	Polarstern ANT-XXIX/9	PS82_15 1-1	-74.541	-28.531	1750

Ophionotus	victoriae	1.164.2	WAMZ88592	Weddell Sea	22/01/2014	Polarstern ANT-XXIX/9	PS82_15 1-1		-74.541	-28.531	1750
Ophionotus	victoriae	1.164.3	WAMZ88593	Weddell Sea	22/01/2014	Polarstern ANT-XXIX/9	PS82_15 1-1		-74.541	-28.531	1750
Ophionotus	victoriae	1.164.4	WAMZ88594	Weddell Sea	22/01/2014	Polarstern ANT-XXIX/9	PS82_15 1-1		-74.541	-28.531	1750
Ophionotus	victoriae	1.158	WAMZ88595	Weddell Sea	19/01/2014	Polarstern ANT-XXIX/9	PS82_12 6-1		-75.512	-27.487	282
Ophionotus	victoriae	1.158.1	WAMZ88596	Weddell Sea	19/01/2014	Polarstern ANT-XXIX/9	PS82_12 6-1		-75.512	-27.487	282
Ophionotus	victoriae	1.152.1	WAMZ88597	Weddell Sea	17/01/2014	Polarstern ANT-XXIX/9	PS82_11 5-1		-77.611	-38.939	1058
Ophionotus	victoriae	1.152.2	WAMZ88598	Weddell Sea	17/01/2014	Polarstern ANT-XXIX/9	PS82_11 5-1		-77.611	-38.939	1058
Ophionotus	victoriae	1.152.3	WAMZ88599	Weddell Sea	17/01/2014	Polarstern ANT-XXIX/9	PS82_11 5-1		-77.611	-38.939	1058
Ophionotus	hexactis	SIOBICE5493A	SIOBICE5493	Bransfield Strait	04/04/2012	Polarstern ANT-XXVIII/4		79279	-62.278	-55.833	302
Ophionotus	hexactis	SIOBICE5493B	SIOBICE5493	Bransfield Strait	04/04/2012	Polarstern ANT-XXVIII/4		79279	-62.278	-55.833	302
Ophionotus	hexactis	SIOBICE5493C	SIOBICE5493	Bransfield Strait	04/04/2012	Polarstern ANT-XXVIII/4		79279	-62.278	-55.833	302
Ophionotus	hexactis	SIOBICE5493D	SIOBICE5493	Bransfield Strait	04/04/2012	Polarstern ANT-XXVIII/4		79279	-62.278	-55.833	302
Ophionotus	hexactis	SIOBICE5493E	SIOBICE5493	Bransfield Strait	04/04/2012	Polarstern ANT-XXVIII/4		79279	-62.278	-55.833	302
Ophionotus	hexactis	SIOBICE5493F	SIOBICE5493	Bransfield Strait	04/04/2012	Polarstern ANT-XXVIII/4		79279	-62.278	-55.833	302
Ophionotus	hexactis	SIOBICE5493G	SIOBICE5493	Bransfield Strait	04/04/2012	Polarstern ANT-XXVIII/4		79279	-62.278	-55.833	302
Ophionotus	hexactis	SIOBICE5493H	SIOBICE5493	Bransfield Strait	04/04/2012	Polarstern ANT-XXVIII/4		79279	-62.278	-55.833	302
Ophionotus	hexactis	SIOBICE5493I	SIOBICE5493	Bransfield Strait	04/04/2012	Polarstern ANT-XXVIII/4		79279	-62.278	-55.833	302
Ophionotus	hexactis	SIOBICE5493J	SIOBICE5493	Bransfield Strait	04/04/2012	Polarstern ANT-XXVIII/4		79279	-62.278	-55.833	302
Ophionotus	hexactis	SIOBICS0036A	SIOBICE4798	South Georgia	29/09/2011	Scotia 2011	SG3	21	-55.052	-35.396	119
Ophionotus	hexactis	SIOBICS0036B	SIOBICE4798	South Georgia	29/09/2011	Scotia 2011	SG3	21	-55.052	-35.396	119
Ophionotus	hexactis	SIOBICS0036C	SIOBICE4798	South Georgia	29/09/2011	Scotia 2011	SG3	21	-55.052	-35.396	119
Ophionotus	hexactis	SIOBICS0036D	SIOBICE4798	South Georgia	29/09/2011	Scotia 2011	SG3	21	-55.052	-35.396	119
Ophionotus	hexactis	SIOBICS0036E	SIOBICE4798	South Georgia	29/09/2011	Scotia 2011	SG3	21	-55.052	-35.396	119
Ophionotus	hexactis	SIOBICS0036F	SIOBICE4798	South Georgia	29/09/2011	Scotia 2011	SG3	21	-55.052	-35.396	119
Ophionotus	hexactis	SIOBICS0036G	SIOBICE4798	South Georgia	29/09/2011	Scotia 2011	SG3	21	-55.052	-35.396	119
Ophionotus	hexactis	SIOBICS0036H	SIOBICE4798	South Georgia	29/09/2011	Scotia 2011	SG3	21	-55.052	-35.396	119
Ophionotus	hexactis	SIOBICS0036I	SIOBICE4798	South Georgia	29/09/2011	Scotia 2011	SG3	21	-55.052	-35.396	119
Ophionotus	hexactis	SIOBICS0036J	SIOBICE4798	South Georgia	29/09/2011	Scotia 2011	SG3	21	-55.052	-35.396	119

Ophionotus	hexactis	SIOBICS3070	SIOBICE5201	Shag Rocks	23/09/2011	Scotia 2011	SR2-5		-53.532	-41.628	131
Ophionotus	hexactis	SIOBICS3533O	SIOBICE4775	Shag Rocks	23/09/2011	Scotia 2011	SR3-9		-53.722	-41.466	180
Ophionotus	hexactis	SIOBICS3753	SIOBICE5236	Shag Rocks	23/09/2011	Scotia 2011	SR1	4	-53.453	-42.058	174
Ophionotus	hexactis	SIOBICS3754	SIOBICE5251	Shag Rocks	23/09/2011	Scotia 2011	SR1	4	-53.453	-42.058	174
Ophionotus	hexactis	SIOBICS3755	SIOBICE5225	Shag Rocks	23/09/2011	Scotia 2011	SR1	4	-53.453	-42.058	174
Ophionotus	hexactis	SIOBICS3756	SIOBICE5180	Shag Rocks	23/09/2011	Scotia 2011	SR1	4	-53.453	-42.058	174
Ophionotus	hexactis	SIOBICS3757	SIOBICE5230	Shag Rocks	23/09/2011	Scotia 2011	SR1	4	-53.453	-42.058	174
Ophionotus	hexactis	SIOBICS3758	SIOBICE5246	Shag Rocks	23/09/2011	Scotia 2011	SR1	4	-53.453	-42.058	174
Ophionotus	hexactis	SIOBICS3759	SIOBICE5283	Shag Rocks	23/09/2011	Scotia 2011	SR1	4	-53.453	-42.058	174
Ophionotus	hexactis	SIOBICS3760	SIOBICE5227	Shag Rocks	23/09/2011	Scotia 2011	SR1	4	-53.453	-42.058	174
Ophionotus	hexactis	WAMZ43230	WAMZ43230	Heard Island	01/08/2017	ACE 2016/17	18	279	-52.355	74.801	203
Ophionotus	hexactis	WAMZ43231	WAMZ43231	Heard Island	01/08/2017	ACE 2016/17	18	279	-52.355	74.801	203
Ophionotus	hexactis	WAMZ43232	WAMZ43232	Heard Island	01/08/2017	ACE 2016/17	18	279	-52.355	74.801	203
Ophionotus	hexactis	WAMZ43233	WAMZ43233	Heard Island	01/08/2017	ACE 2016/17	18	279	-52.355	74.801	203
Ophionotus	hexactis	WAMZ43234	WAMZ43234	Heard Island	01/08/2017	ACE 2016/17	18	279	-52.355	74.801	203
Ophionotus	hexactis	WAMZ43235	WAMZ43235	Heard Island	01/08/2017	ACE 2016/17	18	279	-52.355	74.801	203
Ophionotus	hexactis	WAMZ43236	WAMZ43236	Heard Island	01/08/2017	ACE 2016/17	18	279	-52.355	74.801	203
Ophionotus	hexactis	WAMZ43237	WAMZ43237	Heard Island	01/08/2017	ACE 2016/17	18	279	-52.355	74.801	203
Ophionotus	hexactis	WAMZ43238	WAMZ43238	Heard Island	01/08/2017	ACE 2016/17	18	279	-52.355	74.801	203
Ophionotus	hexactis	WAMZ43239	WAMZ43239	Heard Island	01/08/2017	ACE 2016/17	18	279	-52.355	74.801	203

Supplementary Table 4.2 Results of the three-population test (*f*3-statistic) from *TreeMix* analysis of *Ophionotus victoriae* with *O. hexactis* as outgroup. Significant negative Z-score (< -3) indicates population A is admixed between two source populations of B and C. Abbreviations represent different geographical locations; BM = Bransfield Mouth, SG = South Georgia, DB = Discovery Bank, HB = Herdman Bank, SSI = South Sandwich Is., BOU = Bouvet Is., SHE = South Shetland Is., EI = Elephant Is., BS = Bransfield Strait, LAR = Larsen Ice Shelves, EWS = East Weddell Sea, SWS = South Weddell Sea, PB = Prydz Bay, TB = Tressler Bank, SCO = Scott Is, BAL = Balleny Is., AL = Adélie Land, RS = Ross Sea, AS = Amundsen Sea.

Population A	Population B	Population C	*f*3-statistic	Standard Error	Z-score
LAR	EI+SHE+BS	EWS	-0.0011399	0.00024258	-4.69914
AL+RS	O. hexactis	EWS	-0.0007226	0.00015512	-4.65848
LAR	O. hexactis	EWS	-0.0011020	0.00024523	-4.49369
LAR	SG+DB+HB+SSI	EWS	-0.0011905	0.00027813	-4.28037
LAR	AL+RS	EI+SHE+BS	-0.0008236	0.00019273	-4.27359
LAR	AL+RS	SCO+BAL	-0.0009675	0.00022691	-4.26395
AL+RS	EI+SHE+BS	EWS	-0.0006043	0.00014719	-4.10554
LAR	AL+RS	SG+DB+HB+SSI	-0.0008261	0.00021313	-3.87619
AL+RS	SG+DB+HB+SSI	EWS	-0.0006524	0.00017243	-3.78337
LAR	PB_DS	EI+SHE+BS	-0.0011025	0.00032713	-3.37006
LAR	AL+RS	O. hexactis	-0.0006674	0.00019936	-3.34778
LAR	SCO+BAL	EWS	-0.0010127	0.00030321	-3.33985
SWS	AS	EI+SHE+BS	-0.0010075	0.00030539	-3.29916
LAR	SCO+BAL	PB_DS	-0.0012411	0.00040333	-3.07713
LAR	PB_DS	BM	-0.0012112	0.00041622	-2.91011
SWS	AS	BM	-0.0011135	0.00038284	-2.90857
LAR	PB_DS	SG+DB+HB+SSI	-0.0011323	0.00039309	-2.88058
AL+RS	BOU	EWS	-0.0006042	0.00021576	-2.80012
SWS	AS	SCO+BAL	-0.0009686	0.00035847	-2.70199
LAR	BOU	EWS	-0.0009002	0.00033509	-2.68637
LAR	BM	EWS	-0.0008074	0.00030124	-2.68035
SWS	AS	O. hexactis	-0.0008189	0.00030742	-2.66392
AL+RS	PB_DS	BM	-0.0008647	0.00032761	-2.63945
SWS	AS	LAR	-0.0008063	0.00030814	-2.61662
LAR	AL+RS	SWS	-0.0005517	0.00021084	-2.61653
SWS	AS	SG+DB+HB+SSI	-0.0008792	0.00033911	-2.59279
SWS	SG+DB+HB+SSI	EWS	-0.0006577	0.00025534	-2.57574
LAR	PB_DS	O. hexactis	-0.0008432	0.00033419	-2.52300
EI+SHE+BS	BM	O. hexactis	-0.0004874	0.00019731	-2.47026
LAR	AL+RS	BM	-0.0005903	0.00023897	-2.47004
SWS	O. hexactis	EWS	-0.0005317	0.00021763	-2.44315
AL+RS	BM	EWS	-0.0005052	0.00021218	-2.38084
SWS	PB_DS	BM	-0.0008398	0.00035958	-2.33538
AL+RS	PB_DS	EI+SHE+BS	-0.0005226	0.00022681	-2.30393
LAR	EWS	SWS	-0.0005812	0.00025346	-2.29312
LAR	AL+RS	BOU	-0.0005840	0.00026247	-2.22517
SWS	BM	EWS	-0.0005524	0.00025649	-2.15381
AL+RS	EWS	SWS	-0.0003176	0.00014762	-2.15138
SWS	AL+RS	AS	-0.0005433	0.00026133	-2.07888
AL+RS	EWS	LAR	-0.0002880	0.00014019	-2.05446
SWS	EI+SHE+BS	EWS	-0.0004550	0.00022320	-2.03846
LAR	PB_DS	SWS	-0.0006977	0.00034600	-2.01657
EI+SHE+BS	SCO+BAL	O. hexactis	-0.0003796	0.00018852	-2.01389
EI+SHE+BS	SCO+BAL	BOU	-0.0005078	0.00026288	-1.93188
EWS	PB_DS	BM	-0.0008373	0.00045536	-1.83880
SWS	AL+RS	BM	-0.0003649	0.00019935	-1.83022
AL+RS	PB_DS	SG+DB+HB+SSI	-0.0005499	0.00030523	-1.80165
AL+RS	SCO+BAL	EWS	-0.0003332	0.00018571	-1.79401
SWS	AL+RS	SCO+BAL	-0.0003363	0.00018752	-1.79332
PB_DS	O. hexactis	EWS	-0.0013228	0.00074135	-1.78430
EI+SHE+BS	BOU	LAR	-0.0004211	0.00023783	-1.77057
AL+RS	SCO+BAL	PB_DS	-0.0005173	0.00031181	-1.65909
AL+RS	PB_DS	O. hexactis	-0.0004195	0.00025284	-1.65909
PB_DS	BOU	EWS	-0.0013242	0.00080191	-1.65126
LAR	AS	EI+SHE+BS	-0.0005728	0.00035104	-1.63162
AL+RS	PB_DS	SWS	-0.0003898	0.00024001	-1.62407
SWS	AL+RS	SG+DB+HB+SSI	-0.0003229	0.00019952	-1.61843
SWS	AS	BOU	-0.0007185	0.00045192	-1.58988
SWS	AS	PB_DS	-0.0008268	0.00052329	-1.57995
LAR	EI+SHE+BS	SWS	-0.0003715	0.00023589	-1.57502
EWS	SCO+BAL	PB_DS	-0.0006620	0.00042754	-1.54829

EWS	AL+RS	PB_DS	-0.0004778	0.00031337	-1.52472
SWS	AS	EWS	-0.0005538	0.00036399	-1.52154
EI+SHE+BS	BOU	SWS	-0.0003495	0.00023321	-1.49847
PB_DS	EI+SHE+BS	EWS	-0.0011014	0.00073741	-1.49363
PB_DS	SG+DB+HB+SSI	EWS	-0.0011221	0.00075520	-1.48586
EWS	PB_DS	SWS	-0.0005500	0.00037604	-1.46265
PB_DS	EWS	LAR	-0.0010640	0.00073990	-1.43800
SWS	PB_DS	SG+DB+HB+SSI	-0.0004830	0.00033796	-1.42926
AL+RS	AS	PB_DS	-0.0006733	0.00047363	-1.42156
PB_DS	AL+RS	EWS	-0.0010197	0.00072395	-1.40850
SWS	SCO+BAL	EWS	-0.0003519	0.00025324	-1.38947
EWS	AS	PB_DS	-0.0008230	0.00059701	-1.37845
LAR	PB_DS	BOU	-0.0006400	0.00046591	-1.37360
SWS	BM	LAR	-0.0003262	0.00024068	-1.35547
SWS	SCO+BAL	PB_DS	-0.0004638	0.00035607	-1.30259
LAR	SCO+BAL	SWS	-0.0003474	0.00027222	-1.27615
PB_DS	EWS	SWS	-0.0009475	0.00074249	-1.27607
LAR	AS	SCO+BAL	-0.0005097	0.00040276	-1.26551
LAR	AS	PB_DS	-0.0007182	0.00056900	-1.26224
EWS	PB_DS	LAR	-0.0004335	0.00037079	-1.16913
LAR	SCO+BAL	O. hexactis	-0.0003099	0.00026658	-1.16261
AL+RS	AS	EWS	-0.0003281	0.00029675	-1.10579
PB_DS	SCO+BAL	EWS	-0.0008355	0.00076218	-1.09623
SWS	BM	O. hexactis	-0.0002605	0.00023977	-1.08642
LAR	O. hexactis	SWS	-0.0002569	0.00023959	-1.07219
AL+RS	PB_DS	LAR	-0.0002437	0.00022970	-1.06109
EWS	PB_DS	EI+SHE+BS	-0.0003961	0.00038559	-1.02714
EI+SHE+BS	O. hexactis	LAR	-0.0001692	0.00017014	-0.99451
SWS	PB_DS	EI+SHE+BS	-0.0003010	0.00030383	-0.99077
LAR	BOU	SWS	-0.0002999	0.00030725	-0.97605
EI+SHE+BS	BM	LAR	-0.0002187	0.00022522	-0.97084
LAR	AL+RS	AS	-0.0002887	0.00029966	-0.96326
SWS	AL+RS	EI+SHE+BS	-0.0001683	0.00017911	-0.93947
EI+SHE+BS	PB_DS	BM	-0.0003274	0.00035249	-0.92892
PB_DS	AL+RS	LAR	-0.0006541	0.00072497	-0.90224
SWS	BOU	EWS	-0.0002869	0.00032183	-0.89142
LAR	AS	EWS	-0.0003288	0.00038135	-0.86213
EWS	PB_DS	SG+DB+HB+SSI	-0.0003753	0.00044915	-0.83569
LAR	SG+DB+HB+SSI	SWS	-0.0002194	0.00026475	-0.82866
PB_DS	BM	EWS	-0.0006602	0.00080187	-0.82327
AL+RS	PB_DS	BOU	-0.0002997	0.00037572	-0.79759
EI+SHE+BS	BM	SG+DB+HB+SSI	-0.0001950	0.00024560	-0.79409
PB_DS	AS	EWS	-0.0006745	0.00086457	-0.78019
EI+SHE+BS	AL+RS	BOU	-0.0001815	0.00023473	-0.77324
LAR	AS	SG+DB+HB+SSI	-0.0002923	0.00038241	-0.76447
PB_DS	AL+RS	BOU	-0.0005982	0.00078972	-0.75742
LAR	AS	O. hexactis	-0.0002695	0.00036982	-0.72885
SWS	AL+RS	O. hexactis	-0.0001267	0.00017655	-0.71759
EI+SHE+BS	BM	BOU	-0.0002116	0.00029509	-0.71719
PB_DS	AL+RS	SWS	-0.0005080	0.00073075	-0.69521
PB_DS	AL+RS	O. hexactis	-0.0004783	0.00073946	-0.64687
LAR	BM	O. hexactis	-0.0001911	0.00029677	-0.64407
EI+SHE+BS	AL+RS	SCO+BAL	-0.0001360	0.00021973	-0.61894
EI+SHE+BS	O. hexactis	EWS	-0.0001313	0.00022103	-0.59395
EI+SHE+BS	BOU	EWS	-0.0001814	0.00030841	-0.58804
LAR	AL+RS	PB_DS	-0.0001781	0.00030791	-0.57837
LAR	AL+RS	EWS	-0.0001338	0.00023708	-0.56435
EI+SHE+BS	SG+DB+HB+SSI	EWS	-0.0001455	0.00026972	-0.53935
LAR	AS	BM	-0.0002488	0.00047277	-0.52634
LAR	SCO+BAL	BOU	-0.0001862	0.00035854	-0.51942
PB_DS	AL+RS	EI+SHE+BS	-0.0003753	0.00073425	-0.51108
SWS	PB_DS	O. hexactis	-0.0001564	0.00030847	-0.50697
PB_DS	AL+RS	SCO+BAL	-0.0003805	0.00075435	-0.50441
AL+RS	AS	LAR	-0.0001332	0.00026454	-0.50338
EI+SHE+BS	SG+DB+HB+SSI	LAR	-0.0000949	0.00019334	-0.49085
PB_DS	AL+RS	SG+DB+HB+SSI	-0.0003479	0.00075937	-0.45816
EI+SHE+BS	AL+RS	SG+DB+HB+SSI	-0.0000974	0.00021348	-0.45631
LAR	AS	BOU	-0.0002121	0.00047040	-0.45093
EWS	PB_DS	O. hexactis	-0.0001747	0.00041806	-0.41786
EI+SHE+BS	PB_DS	SG+DB+HB+SSI	-0.0001248	0.00032645	-0.38219
EI+SHE+BS	SCO+BAL	PB_DS	-0.0001308	0.00035046	-0.37310
LAR	SCO+BAL	EI+SHE+BS	-0.0000995	0.00027365	-0.36354
EWS	PB_DS	BOU	-0.0001733	0.00050068	-0.34615
EI+SHE+BS	O. hexactis	SWS	-0.0000546	0.00017612	-0.30977
SWS	BM	SG+DB+HB+SSI	-0.0000799	0.00026680	-0.29952

PB_DS	AL+RS	AS	-0.0002245	0.00084712	-0.26505
EWS	AL+RS	LAR	-0.0000679	0.00027979	-0.24274
SWS	SG+DB+HB+SSI	LAR	-0.0000484	0.00021217	-0.22829
PB_DS	BOU	LAR	-0.0001922	0.00088102	-0.21816
EI+SHE+BS	SCO+BAL	SG+DB+HB+SSI	-0.0000438	0.00024064	-0.18217
PB_DS	LAR	SWS	-0.0001345	0.00079333	-0.16948
LAR	SCO+BAL	SG+DB+HB+SSI	-0.0000484	0.00029529	-0.16397
EI+SHE+BS	AS	BOU	-0.0000604	0.00042465	-0.14232
EWS	AL+RS	SWS	-0.0000384	0.00029278	-0.13100
PB_DS	AS	LAR	-0.0001140	0.00090804	-0.12551
SCO+BAL	BM	LAR	-0.0000354	0.00036847	-0.09613
EI+SHE+BS	AL+RS	O. hexactis	-0.0000130	0.00017333	-0.07492
EWS	AL+RS	AS	-0.0000278	0.00041056	-0.06771
EWS	AL+RS	SCO+BAL	-0.0000228	0.00033666	-0.06767
SWS	O. hexactis	LAR	-0.0000109	0.00021269	-0.05145
PB_DS	AL+RS	BM	-0.0000331	0.00077897	-0.04252
SCO+BAL	PB_DS	BM	-0.0000056	0.00050106	-0.01109
SWS	AL+RS	BOU	-0.0000003	0.00024983	-0.00124
LAR	SG+DB+HB+SSI	EI+SHE+BS	0.0000033	0.00026673	0.01242
PB_DS	O. hexactis	LAR	0.0000110	0.00081308	0.01352
EI+SHE+BS	SCO+BAL	LAR	0.0000079	0.00020503	0.03851
EI+SHE+BS	AL+RS	BM	0.0000147	0.00021938	0.06701
LAR	BM	SG+DB+HB+SSI	0.0000269	0.00031804	0.08469
EI+SHE+BS	PB_DS	BOU	0.0000414	0.00041750	0.09914
SCO+BAL	BM	SG+DB+HB+SSI	0.0000399	0.00038240	0.10443
SWS	BOU	LAR	0.0000321	0.00027334	0.11730
SWS	SCO+BAL	O. hexactis	0.0000265	0.00022504	0.11787
SCO+BAL	SG+DB+HB+SSI	EWS	0.0000551	0.00037532	0.14681
EI+SHE+BS	SCO+BAL	SWS	0.0000320	0.00021789	0.14699
BM	SCO+BAL	BOU	0.0000793	0.00052912	0.14980
EI+SHE+BS	AS	SCO+BAL	0.0000710	0.00038643	0.18365
LAR	BM	SWS	0.0000584	0.00029307	0.19931
SWS	PB_DS	BOU	0.0000898	0.00044994	0.19962
SCO+BAL	BM	O. hexactis	0.0000834	0.00039914	0.20888
PB_DS	BOU	SWS	0.0002056	0.00092695	0.22184
EI+SHE+BS	AS	BM	0.0001053	0.00043729	0.24076
BM	BOU	SWS	0.0001271	0.00052714	0.24114
EWS	AS	LAR	0.0001271	0.00049953	0.25436
EI+SHE+BS	SG+DB+HB+SSI	SWS	0.0000572	0.00020672	0.27689
PB_DS	AS	BOU	0.0003139	0.00107935	0.29082
LAR	O. hexactis	EI+SHE+BS	0.0000776	0.00024383	0.31831
EI+SHE+BS	PB_DS	O. hexactis	0.0000901	0.00027579	0.32665
PB_DS	EI+SHE+BS	LAR	0.0002703	0.00079522	0.33988
SWS	SCO+BAL	LAR	0.0000796	0.00022775	0.34937
PB_DS	SG+DB+HB+SSI	LAR	0.0003001	0.00085025	0.35301
EI+SHE+BS	SCO+BAL	BM	0.0001008	0.00026717	0.37711
EI+SHE+BS	BM	EWS	0.0001138	0.00029367	0.38763
AL+RS	AS	EI+SHE+BS	0.0001177	0.00029505	0.39890
SCO+BAL	BM	EWS	0.0001698	0.00042547	0.39912
SCO+BAL	AS	BM	0.0002254	0.00054487	0.41375
SCO+BAL	EI+SHE+BS	EWS	0.0001567	0.00036508	0.42931
BM	SCO+BAL	SWS	0.0001962	0.00045661	0.42971
EWS	AL+RS	BM	0.0001492	0.00034070	0.43801
PB_DS	AS	EI+SHE+BS	0.0004157	0.00094785	0.43859
LAR	BM	EI+SHE+BS	0.0001271	0.00028825	0.44081
PB_DS	BM	LAR	0.0003791	0.00084098	0.45074
EI+SHE+BS	AS	O. hexactis	0.0001340	0.00029457	0.45498
PB_DS	AS	O. hexactis	0.0004597	0.00098094	0.46860
EI+SHE+BS	SCO+BAL	EWS	0.0001351	0.00028712	0.47069
PB_DS	SCO+BAL	LAR	0.0004089	0.00085180	0.48007
BM	AL+RS	SCO+BAL	0.0002248	0.00046601	0.48233
AL+RS	PB_DS	EWS	0.0001219	0.00024602	0.49532
SCO+BAL	BM	EI+SHE+BS	0.0001911	0.00037967	0.50340
SCO+BAL	AS	EI+SHE+BS	0.0002209	0.00043512	0.50770
SWS	EI+SHE+BS	LAR	0.0001037	0.00020060	0.51696
AL+RS	AS	BM	0.0002083	0.00039819	0.52305
PB_DS	O. hexactis	SWS	0.0004518	0.00085191	0.53038
AL+RS	AS	BOU	0.0002388	0.00043723	0.54607
EI+SHE+BS	AS	SG+DB+HB+SSI	0.0001855	0.00033751	0.54970
LAR	PB_DS	EWS	0.0002318	0.00041668	0.55628
BM	AS	SCO+BAL	0.0003412	0.00061085	0.55850
BM	EI+SHE+BS	SWS	0.0002649	0.00045639	0.58050
PB_DS	AS	SCO+BAL	0.0006175	0.00103036	0.59925
SWS	SCO+BAL	BOU	0.0001932	0.00030481	0.63392
LAR	SCO+BAL	BM	0.0002199	0.00033786	0.65092

BM	AS	EI+SHE+BS	0.0003709	0.00056319	0.65864
EWS	AL+RS	BOU	0.0002482	0.00036429	0.68137
SCO+BAL	SG+DB+HB+SSI	LAR	0.0002329	0.00034055	0.68394
BM	BOU	EWS	0.0003927	0.00056964	0.68933
SWS	BM	EI+SHE+BS	0.0001724	0.00024494	0.70367
PB_DS	AS	SG+DB+HB+SSI	0.0007260	0.00103167	0.70373
PB_DS	EI+SHE+BS	SWS	0.0005965	0.00083476	0.71455
AL+RS	BOU	LAR	0.0001622	0.00022348	0.72586
BM	AS	BOU	0.0005221	0.00069335	0.75307
BM	EI+SHE+BS	EWS	0.0003624	0.00047891	0.75670
SCO+BAL	EI+SHE+BS	SWS	0.0002599	0.00033976	0.76481
BM	SCO+BAL	EWS	0.0003968	0.00051856	0.76516
SCO+BAL	PB_DS	SG+DB+HB+SSI	0.0003417	0.00044613	0.76593
EWS	AL+RS	EI+SHE+BS	0.0002484	0.00031898	0.77861
BM	SG+DB+HB+SSI	EWS	0.0004120	0.00051941	0.79311
AL+RS	AS	SCO+BAL	0.0003247	0.00039808	0.81556
SWS	SCO+BAL	BM	0.0002411	0.00029550	0.81584
BM	SCO+BAL	EI+SHE+BS	0.0003755	0.00045729	0.82108
EI+SHE+BS	BM	SWS	0.0002113	0.00025703	0.82204
PB_DS	AS	BM	0.0008484	0.00102910	0.82445
PB_DS	SCO+BAL	BOU	0.0008627	0.00103873	0.83051
PB_DS	SCO+BAL	SWS	0.0007593	0.00090420	0.83970
LAR	BM	BOU	0.0003365	0.00040049	0.84027
PB_DS	SG+DB+HB+SSI	SWS	0.0007785	0.00091185	0.85374
SWS	BM	BOU	0.0003102	0.00036009	0.86138
AL+RS	AS	O. hexactis	0.0002647	0.00030402	0.87069
AL+RS	BM	LAR	0.0001685	0.00019288	0.87339
SCO+BAL	EI+SHE+BS	LAR	0.0002840	0.00032446	0.87524
EWS	AL+RS	SG+DB+HB+SSI	0.0002964	0.00033636	0.88127
AL+RS	LAR	SWS	0.0001299	0.00014665	0.88541
BM	BOU	LAR	0.0004854	0.00053906	0.90048
SCO+BAL	AL+RS	BM	0.0003418	0.00037683	0.90711
BM	AL+RS	BOU	0.0004917	0.00053993	0.91060
SCO+BAL	AS	SG+DB+HB+SSI	0.0004503	0.00047956	0.93894
SCO+BAL	PB_DS	EI+SHE+BS	0.0004226	0.00044744	0.94456
SCO+BAL	BM	SWS	0.0003704	0.00039169	0.94560
EWS	AS	SCO+BAL	0.0006300	0.00065961	0.95514
BM	SCO+BAL	PB_DS	0.0005722	0.00059821	0.95644
SCO+BAL	BOU	LAR	0.0003707	0.00038606	0.96030
SCO+BAL	SG+DB+HB+SSI	SWS	0.0003609	0.00036115	0.99937
BM	AL+RS	EI+SHE+BS	0.0004615	0.00046114	1.00082
SCO+BAL	SG+DB+HB+SSI	EI+SHE+BS	0.0003357	0.00033487	1.00252
PB_DS	SCO+BAL	O. hexactis	0.0009422	0.00093926	1.00310
BM	SCO+BAL	O. hexactis	0.0004832	0.00048153	1.00351
EWS	LAR	SWS	0.0003795	0.00037161	1.02128
SCO+BAL	BOU	SWS	0.0004182	0.00040935	1.02172
SWS	SCO+BAL	SG+DB+HB+SSI	0.0002505	0.00024513	1.02206
LAR	EI+SHE+BS	BOU	0.0003295	0.00032043	1.02833
SCO+BAL	BM	BOU	0.0004873	0.00046741	1.04264
SCO+BAL	O. hexactis	EWS	0.0004051	0.00038729	1.04599
EWS	AS	BM	0.0006857	0.00065006	1.05475
BM	SG+DB+HB+SSI	SWS	0.0005172	0.00048305	1.07070
BM	SCO+BAL	SG+DB+HB+SSI	0.0005267	0.00048115	1.09459
SCO+BAL	BOU	EWS	0.0004832	0.00043797	1.10333
SCO+BAL	AL+RS	SG+DB+HB+SSI	0.0003743	0.00033696	1.11081
EWS	AL+RS	O. hexactis	0.0003667	0.00032724	1.12048
AL+RS	AS	SG+DB+HB+SSI	0.0004006	0.00035714	1.12178
BM	AL+RS	SG+DB+HB+SSI	0.0005591	0.00049104	1.13867
PB_DS	BM	O. hexactis	0.0010311	0.00090547	1.13874
PB_DS	AS	SWS	0.0011222	0.00096767	1.15971
SCO+BAL	AS	BOU	0.0006683	0.00057376	1.16480
EWS	AS	BOU	0.0008151	0.00069567	1.17169
EWS	AS	EI+SHE+BS	0.0006942	0.00058152	1.19376
BM	AS	SG+DB+HB+SSI	0.0007515	0.00061675	1.21849
BM	SCO+BAL	LAR	0.0006020	0.00047919	1.25631
PB_DS	BM	SWS	0.0011352	0.00089354	1.27045
SCO+BAL	AL+RS	EI+SHE+BS	0.0004279	0.00033377	1.28194
BM	EI+SHE+BS	BOU	0.0006879	0.00052598	1.30776
PB_DS	EI+SHE+BS	BOU	0.0012398	0.00093964	1.31940
SWS	EWS	LAR	0.0003134	0.00023675	1.32374
SWS	PB_DS	LAR	0.0004299	0.00032435	1.32545
PB_DS	BM	BOU	0.0013556	0.00099742	1.35907
PB_DS	O. hexactis	EI+SHE+BS	0.0011911	0.00086929	1.37016
BM	SG+DB+HB+SSI	EI+SHE+BS	0.0006713	0.00047337	1.41803
EWS	BM	LAR	0.0006057	0.00042663	1.41977

BM	O. hexactis	SWS	0.0006978	0.00048907	1.42676
BM	O. hexactis	EWS	0.0007185	0.00050300	1.42845
SCO+BAL	O. hexactis	LAR	0.0004944	0.00034572	1.43014
EI+SHE+BS	LAR	SWS	0.0002799	0.00019485	1.43667
EI+SHE+BS	AS	LAR	0.0004812	0.00033480	1.43723
BM	EI+SHE+BS	LAR	0.0006949	0.00048068	1.44562
BM	PB_DS	SG+DB+HB+SSI	0.0008739	0.00059432	1.47047
PB_DS	SCO+BAL	SG+DB+HB+SSI	0.0014928	0.00101415	1.47200
LAR	AS	SWS	0.0005385	0.00036379	1.48010
BM	PB_DS	EI+SHE+BS	0.0008037	0.00054278	1.48065
SWS	SG+DB+HB+SSI	EI+SHE+BS	0.0003264	0.00021985	1.48471
EWS	BOU	LAR	0.0006985	0.00046534	1.50096
SCO+BAL	AS	LAR	0.0006942	0.00046203	1.50249
EI+SHE+BS	AS	PB_DS	0.0008654	0.00056964	1.51926
AL+RS	O. hexactis	LAR	0.0002456	0.00016097	1.52572
PB_DS	SG+DB+HB+SSI	EI+SHE+BS	0.0014059	0.00091777	1.53188
SWS	SCO+BAL	EI+SHE+BS	0.0003516	0.00022876	1.53704
SWS	AL+RS	LAR	0.0002838	0.00018349	1.54684
PB_DS	SCO+BAL	EI+SHE+BS	0.0014119	0.00091245	1.54737
SCO+BAL	LAR	SWS	0.0005319	0.00034214	1.55460
SCO+BAL	O. hexactis	SWS	0.0005849	0.00037584	1.55637
EWS	AS	SG+DB+HB+SSI	0.0010252	0.00065492	1.56537
BM	PB_DS	BOU	0.0010567	0.00067449	1.56665
BM	LAR	SWS	0.0007635	0.00048524	1.57351
EWS	AS	O. hexactis	0.0009595	0.00060784	1.57854
SCO+BAL	AS	O. hexactis	0.0007346	0.00046001	1.59689
AL+RS	BOU	SWS	0.0004140	0.00025882	1.59953
PB_DS	BM	SG+DB+HB+SSI	0.0015383	0.00095868	1.60462
BM	SG+DB+HB+SSI	LAR	0.0007950	0.00049058	1.62053
BM	AS	O. hexactis	0.0009924	0.00059618	1.66454
SG+DB+HB+SSI	SCO+BAL	BOU	0.0005346	0.00032044	1.66817
BM	AL+RS	SWS	0.0008021	0.00048032	1.67002
SG+DB+HB+SSI	AS	BOU	0.0007526	0.00044090	1.70697
SCO+BAL	PB_DS	BOU	0.0009719	0.00054968	1.76807
PB_DS	BM	EI+SHE+BS	0.0016086	0.00090449	1.77844
BM	AS	LAR	0.0010708	0.00059888	1.78795
PB_DS	O. hexactis	BOU	0.0017892	0.00098888	1.80930
SCO+BAL	AS	PB_DS	0.0012171	0.00066671	1.82552
EWS	BOU	SWS	0.0009798	0.00052477	1.86708
SCO+BAL	PB_DS	O. hexactis	0.0008924	0.00047082	1.89535
BM	AL+RS	O. hexactis	0.0009359	0.00049288	1.89893
SCO+BAL	O. hexactis	EI+SHE+BS	0.0006715	0.00035355	1.89938
EWS	SCO+BAL	LAR	0.0008110	0.00042605	1.90342
PB_DS	SCO+BAL	BM	0.0018401	0.00096581	1.90522
BM	O. hexactis	EI+SHE+BS	0.0009636	0.00050383	1.91259
SCO+BAL	AL+RS	BOU	0.0007542	0.00038826	1.94255
BM	EWS	SWS	0.0009897	0.00050895	1.94466
SG+DB+HB+SSI	BOU	SWS	0.0005919	0.00029913	1.97863
SWS	O. hexactis	EI+SHE+BS	0.0004382	0.00022049	1.98737
AS	EWS	SWS	0.0020008	0.00100343	1.99392
SCO+BAL	EI+SHE+BS	BOU	0.0007997	0.00040001	1.99924
BM	O. hexactis	LAR	0.0010131	0.00050536	2.00466
AS	AL+RS	SWS	0.0019902	0.00099250	2.00526
BM	AS	PB_DS	0.0015638	0.00076867	2.03442
AS	BOU	SWS	0.0021655	0.00105350	2.05547
EWS	SCO+BAL	SWS	0.0010448	0.00050059	2.08708
AS	PB_DS	SWS	0.0022737	0.00108529	2.09502
AL+RS	SG+DB+HB+SSI	LAR	0.0004043	0.00019027	2.12497
AS	SG+DB+HB+SSI	EWS	0.0022223	0.00104355	2.12956
SG+DB+HB+SSI	BOU	LAR	0.0006724	0.00030635	2.19479
AS	PB_DS	BM	0.0025475	0.00115904	2.19792
SCO+BAL	AL+RS	O. hexactis	0.0007945	0.00036138	2.19862
EWS	O. hexactis	LAR	0.0009003	0.00040909	2.20068
EWS	AS	SWS	0.0012467	0.00056615	2.20211
AS	O. hexactis	SWS	0.0022659	0.00102814	2.20386
AS	LAR	SWS	0.0022532	0.00101635	2.21697
AS	O. hexactis	EWS	0.0022880	0.00102962	2.22217
SCO+BAL	PB_DS	SWS	0.0010753	0.00047953	2.24237
AS	BOU	EWS	0.0024324	0.00107993	2.25236
AS	SG+DB+HB+SSI	SWS	0.0023262	0.00103243	2.25311
BM	PB_DS	SWS	0.0012770	0.00056394	2.26449
PB_DS	O. hexactis	SG+DB+HB+SSI	0.0021743	0.00095725	2.27136
EWS	SG+DB+HB+SSI	LAR	0.0009888	0.00043344	2.28122
PB_DS	SG+DB+HB+SSI	BOU	0.0024475	0.00105875	2.31163
EI+SHE+BS	PB_DS	SWS	0.0006847	0.00029597	2.31329

AS	PB_DS	SG+DB+HB+SSI	0.0026699	0.00115230	2.31703
BM	PB_DS	O. hexactis	0.0013812	0.00059586	2.31792
SWS	AL+RS	PB_DS	0.0008035	0.00034579	2.32358
AS	SCO+BAL	SWS	0.0024155	0.00102070	2.36654
BM	AL+RS	AS	0.0013724	0.00057450	2.38885
EWS	SCO+BAL	BOU	0.0015249	0.00063530	2.40027
BM	AS	EWS	0.0015494	0.00064497	2.40232
EWS	EI+SHE+BS	LAR	0.0009382	0.00038993	2.40608
AS	SCO+BAL	PB_DS	0.0027785	0.00115321	2.40935
AS	BM	EWS	0.0025619	0.00105618	2.42559
SCO+BAL	EWS	SWS	0.0009633	0.00039668	2.42848
AS	BM	SWS	0.0025605	0.00104878	2.44139
AS	EI+SHE+BS	SWS	0.0024545	0.00100358	2.44572
AS	AL+RS	SG+DB+HB+SSI	0.0025465	0.00103724	2.45510
BOU	PB_DS	SG+DB+HB+SSI	0.0014741	0.00059082	2.49505
AS	SCO+BAL	EWS	0.0026175	0.00103752	2.52282
AS	EI+SHE+BS	EWS	0.0025533	0.00101174	2.52367
AS	AL+RS	BOU	0.0027084	0.00106538	2.54219
AS	PB_DS	BOU	0.0030820	0.00121061	2.54584
AS	AL+RS	SCO+BAL	0.0026225	0.00102349	2.56231
AL+RS	SCO+BAL	BOU	0.0009435	0.00036821	2.56239
SCO+BAL	AS	EWS	0.0013781	0.00053483	2.57667
AS	PB_DS	O. hexactis	0.0029363	0.00113854	2.57898
BM	AS	SWS	0.0015508	0.00059829	2.59208
AS	AL+RS	O. hexactis	0.0026825	0.00103364	2.59517
SWS	PB_DS	EWS	0.0012429	0.00047597	2.61135
AL+RS	EI+SHE+BS	LAR	0.0004018	0.00015387	2.61143
SCO+BAL	AL+RS	SWS	0.0009478	0.00036290	2.61160
SG+DB+HB+SSI	PB_DS	BOU	0.0011647	0.00044550	2.61440
AS	AL+RS	BM	0.0027389	0.00104520	2.62046
EWS	EI+SHE+BS	SWS	0.0011479	0.00043741	2.62429
EWS	BM	SWS	0.0012454	0.00047284	2.63374
SWS	EI+SHE+BS	BOU	0.0007331	0.00027790	2.63798
EWS	SG+DB+HB+SSI	SWS	0.0013506	0.00050806	2.65833
SG+DB+HB+SSI	BM	BOU	0.0009820	0.00036933	2.65871
AL+RS	BM	O. hexactis	0.0006447	0.00024111	2.67404
AS	PB_DS	EI+SHE+BS	0.0029802	0.00111054	2.68356
EWS	O. hexactis	SWS	0.0012246	0.00045500	2.69149
EI+SHE+BS	O. hexactis	BOU	0.0006395	0.00023607	2.70895
SWS	AL+RS	EWS	0.0007313	0.00026938	2.71461
AL+RS	SCO+BAL	LAR	0.0005457	0.00020057	2.72084
AS	BOU	LAR	0.0030038	0.00109378	2.74624
AS	AL+RS	EI+SHE+BS	0.0028295	0.00100939	2.80314
SG+DB+HB+SSI	BOU	EWS	0.0009627	0.00034107	2.82248
SCO+BAL	PB_DS	LAR	0.0014256	0.00050440	2.82635
SCO+BAL	EWS	LAR	0.0011972	0.00042152	2.84013
SG+DB+HB+SSI	O. hexactis	BOU	0.0007796	0.00027449	2.84028
BM	AL+RS	LAR	0.0014122	0.00049526	2.85144
AL+RS	O. hexactis	SWS	0.0005404	0.00018901	2.85901
AS	BM	LAR	0.0030405	0.00106303	2.86023
EI+SHE+BS	AL+RS	SWS	0.0005519	0.00019247	2.86757
AS	BM	O. hexactis	0.0031189	0.00108019	2.88738
EWS	BM	O. hexactis	0.0015166	0.00052247	2.90268
AS	SG+DB+HB+SSI	LAR	0.0030840	0.00105895	2.91233
AS	O. hexactis	LAR	0.0030612	0.00105047	2.91415
EWS	SCO+BAL	O. hexactis	0.0016030	0.00054895	2.92013
BOU	BM	SG+DB+HB+SSI	0.0016569	0.00055946	2.96158
AS	EWS	LAR	0.0031204	0.00105245	2.96493
AS	SCO+BAL	BOU	0.0033273	0.00110937	2.99921
EI+SHE+BS	AS	EWS	0.0012923	0.00043026	3.00359
SCO+BAL	AL+RS	AS	0.0013731	0.00045706	3.00414
EWS	BM	BOU	0.0018424	0.00061235	3.00874
AS	AL+RS	LAR	0.0030803	0.00102368	3.00908
AS	SCO+BAL	O. hexactis	0.0032610	0.00107301	3.03910
AL+RS	SCO+BAL	SWS	0.0007500	0.00024569	3.05255
BOU	AS	SG+DB+HB+SSI	0.0018862	0.00061590	3.06257
EI+SHE+BS	PB_DS	LAR	0.0010109	0.00032893	3.07320
AL+RS	SG+DB+HB+SSI	SWS	0.0007366	0.00023957	3.07471
BM	EWS	LAR	0.0016294	0.00052853	3.08281
AS	BM	SG+DB+HB+SSI	0.0033598	0.00108285	3.10274
AS	PB_DS	LAR	0.0035099	0.00113115	3.10295
BM	O. hexactis	BOU	0.0018148	0.00058442	3.10525
AL+RS	AS	SWS	0.0009570	0.00030782	3.10885
BOU	SG+DB+HB+SSI	EWS	0.0016762	0.00053888	3.11047
AS	SCO+BAL	LAR	0.0033014	0.00105634	3.12530

SCO+BAL	AL+RS	LAR	0.0011520	0.00036781	3.13209
AS	AL+RS	EWS	0.0032753	0.00104530	3.13336
BOU	SG+DB+HB+SSI	EI+SHE+BS	0.0016403	0.00052223	3.14089
AS	BM	BOU	0.0035891	0.00113332	3.16694
AL+RS	BM	BOU	0.0010890	0.00034321	3.17304
SCO+BAL	AS	SWS	0.0015800	0.00049729	3.17734
EWS	SCO+BAL	SG+DB+HB+SSI	0.0019530	0.00061034	3.19987
EI+SHE+BS	AL+RS	AS	0.0010162	0.00031650	3.21059
SG+DB+HB+SSI	AL+RS	BOU	0.0009145	0.00028421	3.21761
AS	AL+RS	PB_DS	0.0036205	0.00112467	3.21914
BOU	BM	O. hexactis	0.0018079	0.00055954	3.23111
AS	EI+SHE+BS	LAR	0.0033644	0.00103296	3.25708
AS	SCO+BAL	SG+DB+HB+SSI	0.0035453	0.00108162	3.27778
AL+RS	EI+SHE+BS	SWS	0.0005820	0.00017673	3.29291
SG+DB+HB+SSI	BM	O. hexactis	0.0009307	0.00028260	3.29333
BOU	AL+RS	SG+DB+HB+SSI	0.0017244	0.00052078	3.31115
SG+DB+HB+SSI	SCO+BAL	O. hexactis	0.0008873	0.00026705	3.32240
BM	SG+DB+HB+SSI	BOU	0.0019658	0.00059125	3.32487
EWS	BM	SG+DB+HB+SSI	0.0018231	0.00054702	3.33284
SG+DB+HB+SSI	EI+SHE+BS	BOU	0.0009986	0.00029880	3.34186
EWS	SCO+BAL	BM	0.0018383	0.00054637	3.36456
BM	PB_DS	LAR	0.0020332	0.00060194	3.37774
AS	PB_DS	EWS	0.0040705	0.00119986	3.39243
AL+RS	SCO+BAL	O. hexactis	0.0009032	0.00026601	3.39529
AS	SG+DB+HB+SSI	EI+SHE+BS	0.0036601	0.00106102	3.44960
SG+DB+HB+SSI	AS	O. hexactis	0.0011716	0.00033767	3.46954
LAR	O. hexactis	BOU	0.0011382	0.00032737	3.47687
AS	SCO+BAL	BM	0.0037701	0.00108238	3.48320
AS	O. hexactis	EI+SHE+BS	0.0037116	0.00106114	3.49775
AS	BM	EI+SHE+BS	0.0037404	0.00106732	3.50441
EI+SHE+BS	EWS	SWS	0.0008386	0.00023851	3.51614
BOU	PB_DS	BM	0.0025660	0.00072380	3.54522
AS	EI+SHE+BS	BOU	0.0039061	0.00109902	3.55413
EWS	SCO+BAL	EI+SHE+BS	0.0018514	0.00051817	3.57294
AS	SCO+BAL	EI+SHE+BS	0.0037747	0.00105333	3.58355
EI+SHE+BS	AL+RS	LAR	0.0007320	0.00020405	3.58752
AL+RS	BM	SWS	0.0007785	0.00021625	3.60018
LAR	O. hexactis	SG+DB+HB+SSI	0.0010309	0.00028510	3.61604
BOU	PB_DS	O. hexactis	0.0021324	0.00058945	3.61760
SCO+BAL	PB_DS	EWS	0.0026701	0.00073798	3.61805
BOU	AS	O. hexactis	0.0022782	0.00062514	3.64425
SCO+BAL	AL+RS	PB_DS	0.0022150	0.00060618	3.65407
BOU	SG+DB+HB+SSI	LAR	0.0019665	0.00053346	3.68626
AL+RS	BM	SG+DB+HB+SSI	0.0010215	0.00027642	3.69566
EWS	BM	EI+SHE+BS	0.0018727	0.00050343	3.71983
BOU	SG+DB+HB+SSI	SWS	0.0020470	0.00054451	3.75926
BOU	O. hexactis	SG+DB+HB+SSI	0.0018592	0.00049351	3.76731
EI+SHE+BS	SG+DB+HB+SSI	BOU	0.0010829	0.00028674	3.77666
BOU	SCO+BAL	SG+DB+HB+SSI	0.0021043	0.00055715	3.77687
BM	O. hexactis	SG+DB+HB+SSI	0.0020171	0.00053003	3.80560
BOU	O. hexactis	EWS	0.0021338	0.00055610	3.83703
BM	AL+RS	EWS	0.0020858	0.00054205	3.84803
EI+SHE+BS	AS	SWS	0.0013912	0.00036027	3.86141
O. hexactis	AS	BOU	0.0017863	0.00046171	3.86890
AL+RS	SCO+BAL	SG+DB+HB+SSI	0.0013234	0.00034146	3.87585
LAR	SG+DB+HB+SSI	BOU	0.0015073	0.00038664	3.89858
AS	O. hexactis	BOU	0.0044115	0.00113131	3.89951
EWS	EI+SHE+BS	BOU	0.0021679	0.00055378	3.91471
BOU	O. hexactis	EI+SHE+BS	0.0020837	0.00052365	3.97921
AS	O. hexactis	SG+DB+HB+SSI	0.0043845	0.00110046	3.98423
BOU	SCO+BAL	O. hexactis	0.0022119	0.00055417	3.99138
EI+SHE+BS	EWS	LAR	0.0010483	0.00026193	4.00225
SCO+BAL	AL+RS	EWS	0.0020309	0.00050503	4.02130
BM	AL+RS	PB_DS	0.0024454	0.00060537	4.03946
SCO+BAL	O. hexactis	SG+DB+HB+SSI	0.0015738	0.00038943	4.04131
EWS	SG+DB+HB+SSI	EI+SHE+BS	0.0021320	0.00052321	4.07481
SG+DB+HB+SSI	O. hexactis	EWS	0.0012373	0.00030183	4.09914
O. hexactis	PB_DS	SG+DB+HB+SSI	0.0015470	0.00037635	4.11054
BOU	AS	BM	0.0031006	0.00075405	4.11188
BOU	PB_DS	EI+SHE+BS	0.0026818	0.00064945	4.12934
SCO+BAL	O. hexactis	BOU	0.0018189	0.00044037	4.13034
SG+DB+HB+SSI	PB_DS	O. hexactis	0.0014379	0.00034558	4.16089
AS	SG+DB+HB+SSI	BOU	0.0048035	0.00115305	4.16587
EI+SHE+BS	O. hexactis	SG+DB+HB+SSI	0.0008584	0.00020604	4.16641
O. hexactis	PB_DS	BOU	0.0019321	0.00046281	4.17465

SCO+BAL	SG+DB+HB+SSI	BOU	0.0019265	0.00046038	4.18456
BOU	AS	EI+SHE+BS	0.0027836	0.00066479	4.18723
SG+DB+HB+SSI	O. hexactis	SWS	0.0011113	0.00026403	4.20885
SG+DB+HB+SSI	O. hexactis	LAR	0.0011488	0.00027269	4.21270
BOU	AL+RS	O. hexactis	0.0022522	0.00053149	4.23755
SG+DB+HB+SSI	PB_DS	BM	0.0020738	0.00048798	4.24987
BOU	O. hexactis	LAR	0.0023356	0.00054807	4.26145
EWS	O. hexactis	EI+SHE+BS	0.0021178	0.00048958	4.32576
SG+DB+HB+SSI	AS	BM	0.0021963	0.00050764	4.32644
BM	PB_DS	EWS	0.0030724	0.00070288	4.37115
BOU	AS	PB_DS	0.0036077	0.00082229	4.38734
BOU	O. hexactis	SWS	0.0023786	0.00053903	4.41271
BOU	SCO+BAL	PB_DS	0.0030589	0.00068875	4.44121
AL+RS	SCO+BAL	BM	0.0013559	0.00030452	4.45265
SG+DB+HB+SSI	AS	SCO+BAL	0.0020108	0.00044431	4.52554
BOU	AS	SCO+BAL	0.0033625	0.00073535	4.57262
EI+SHE+BS	AL+RS	PB_DS	0.0016564	0.00036098	4.58863
AL+RS	BM	EI+SHE+BS	0.0011192	0.00024016	4.65999
SG+DB+HB+SSI	O. hexactis	EI+SHE+BS	0.0012231	0.00026211	4.66629
EI+SHE+BS	PB_DS	EWS	0.0023826	0.00050994	4.67224
SG+DB+HB+SSI	AS	PB_DS	0.0028862	0.00061743	4.67444
BOU	BM	EI+SHE+BS	0.0029348	0.00062762	4.67612
SG+DB+HB+SSI	AS	EI+SHE+BS	0.0018960	0.00040010	4.73876
SWS	O. hexactis	BOU	0.0014272	0.00030081	4.74441
O. hexactis	BOU	SWS	0.0016859	0.00035512	4.74734
AL+RS	EI+SHE+BS	BOU	0.0013154	0.00027272	4.82308
O. hexactis	SCO+BAL	BOU	0.0018526	0.00038294	4.83779
SG+DB+HB+SSI	AL+RS	O. hexactis	0.0013075	0.00027022	4.83862
BOU	EI+SHE+BS	EWS	0.0029046	0.00060000	4.84091
SG+DB+HB+SSI	SCO+BAL	PB_DS	0.0021193	0.00043239	4.90146
BOU	BM	EWS	0.0032300	0.00065803	4.90864
O. hexactis	AS	SG+DB+HB+SSI	0.0018134	0.00036879	4.91707
BOU	BM	LAR	0.0031373	0.00063792	4.91802
O. hexactis	BOU	LAR	0.0017289	0.00034926	4.95020
EWS	O. hexactis	BOU	0.0029387	0.00059128	4.97004
O. hexactis	BOU	EWS	0.0019307	0.00038648	4.99563
EWS	SG+DB+HB+SSI	BOU	0.0033963	0.00067751	5.01287
AL+RS	SG+DB+HB+SSI	EI+SHE+BS	0.0012313	0.00024379	5.05050
BOU	AL+RS	BM	0.0031310	0.00061685	5.07588
BOU	AL+RS	EI+SHE+BS	0.0029047	0.00057129	5.08442
AL+RS	SCO+BAL	EI+SHE+BS	0.0012699	0.00024868	5.10639
SWS	SG+DB+HB+SSI	BOU	0.0017588	0.00033944	5.18148
BOU	AS	LAR	0.0036859	0.00070976	5.19315
BOU	EI+SHE+BS	SWS	0.0030727	0.00058758	5.22931
SWS	O. hexactis	SG+DB+HB+SSI	0.0012394	0.00023438	5.28798
BOU	SCO+BAL	BM	0.0035434	0.00066757	5.30798
O. hexactis	BM	BOU	0.0022566	0.00042140	5.35487
BOU	SCO+BAL	EI+SHE+BS	0.0032311	0.00060324	5.35614
O. hexactis	AL+RS	BOU	0.0018123	0.00033691	5.37906
BOU	AL+RS	SCO+BAL	0.0032766	0.00060615	5.40551
BOU	PB_DS	SWS	0.0037159	0.00068608	5.41618
O. hexactis	SG+DB+HB+SSI	EWS	0.0017477	0.00032119	5.44129
BOU	EI+SHE+BS	LAR	0.0031443	0.00057753	5.44436
AL+RS	O. hexactis	EI+SHE+BS	0.0011468	0.00021021	5.45579
BOU	BM	SWS	0.0034956	0.00063913	5.46929
EWS	O. hexactis	SG+DB+HB+SSI	0.0031217	0.00057005	5.47615
BOU	SCO+BAL	EWS	0.0035476	0.00064284	5.51860
SG+DB+HB+SSI	PB_DS	EI+SHE+BS	0.0022063	0.00039909	5.52822
O. hexactis	AS	PB_DS	0.0032616	0.00058609	5.56504
BOU	AS	EWS	0.0042573	0.00076066	5.59685
O. hexactis	PB_DS	BM	0.0026902	0.00047677	5.64251
O. hexactis	AS	BM	0.0030790	0.00053768	5.72631
BOU	PB_DS	LAR	0.0041138	0.00071803	5.72926
BOU	SCO+BAL	SWS	0.0036125	0.00063054	5.72928
SG+DB+HB+SSI	AS	LAR	0.0024720	0.00043064	5.74042
EI+SHE+BS	AL+RS	EWS	0.0017382	0.00030157	5.76373
O. hexactis	AL+RS	SG+DB+HB+SSI	0.0016774	0.00029036	5.77705
BOU	AL+RS	AS	0.0039813	0.00068698	5.79532
O. hexactis	EI+SHE+BS	BOU	0.0019808	0.00034138	5.80228
BOU	SCO+BAL	LAR	0.0036600	0.00062885	5.82025
O. hexactis	BM	SG+DB+HB+SSI	0.0020542	0.00035199	5.83605
BOU	AL+RS	PB_DS	0.0045197	0.00076891	5.87810
BOU	PB_DS	EWS	0.0052457	0.00088303	5.94061
SG+DB+HB+SSI	BM	EWS	0.0025358	0.00041695	6.08187
O. hexactis	SG+DB+HB+SSI	EI+SHE+BS	0.0017619	0.00028889	6.09867

SG+DB+HB+SSI	BM	LAR	0.0021528	0.00035256	6.10617
O. hexactis	SG+DB+HB+SSI	SWS	0.0018737	0.00030486	6.14606
BOU	LAR	SWS	0.0037737	0.00061364	6.14968
O. hexactis	AS	SCO+BAL	0.0029369	0.00047539	6.17790
O. hexactis	SG+DB+HB+SSI	LAR	0.0018362	0.00029439	6.23713
BOU	AS	SWS	0.0045243	0.00072048	6.27949
AL+RS	SG+DB+HB+SSI	BOU	0.0024957	0.00039573	6.30662
O. hexactis	SCO+BAL	PB_DS	0.0027791	0.00044045	6.30973
O. hexactis	AS	EI+SHE+BS	0.0024863	0.00039393	6.31143
BOU	AL+RS	SWS	0.0038061	0.00060140	6.32873
SG+DB+HB+SSI	SCO+BAL	BM	0.0024211	0.00038249	6.32980
O. hexactis	SG+DB+HB+SSI	BOU	0.0022053	0.00034331	6.42358
O. hexactis	SCO+BAL	SG+DB+HB+SSI	0.0020977	0.00032623	6.43003
BOU	EWS	SWS	0.0040926	0.00063330	6.46242
AL+RS	O. hexactis	BOU	0.0019678	0.00030370	6.47958
SG+DB+HB+SSI	EI+SHE+BS	EWS	0.0022270	0.00034175	6.51627
SG+DB+HB+SSI	SCO+BAL	SWS	0.0021001	0.00032017	6.55944
BOU	AL+RS	LAR	0.0040578	0.00061655	6.58148
BOU	EWS	LAR	0.0043740	0.00066225	6.60468
SG+DB+HB+SSI	BM	EI+SHE+BS	0.0022765	0.00034419	6.61413
SG+DB+HB+SSI	SCO+BAL	EWS	0.0024059	0.00036340	6.62066
SG+DB+HB+SSI	PB_DS	EWS	0.0047343	0.00071310	6.63907
SG+DB+HB+SSI	AS	EWS	0.0033338	0.00050082	6.65658
SG+DB+HB+SSI	PB_DS	SWS	0.0028337	0.00042072	6.73536
SG+DB+HB+SSI	AL+RS	SCO+BAL	0.0020867	0.00030974	6.73696
O. hexactis	PB_DS	EI+SHE+BS	0.0025302	0.00037311	6.78138
SG+DB+HB+SSI	SCO+BAL	LAR	0.0022281	0.00032834	6.78596
SG+DB+HB+SSI	SCO+BAL	EI+SHE+BS	0.0021253	0.00031106	6.83259
BOU	AL+RS	EWS	0.0048242	0.00070588	6.83432
SG+DB+HB+SSI	EI+SHE+BS	SWS	0.0020243	0.00029271	6.91547
SG+DB+HB+SSI	PB_DS	LAR	0.0033120	0.00047751	6.93601
SG+DB+HB+SSI	AL+RS	PB_DS	0.0039601	0.00056806	6.97123
SG+DB+HB+SSI	AL+RS	BM	0.0023886	0.00034167	6.99097
SG+DB+HB+SSI	BM	SWS	0.0024306	0.00034440	7.05742
SG+DB+HB+SSI	AL+RS	AS	0.0030095	0.00041024	7.33603
SG+DB+HB+SSI	EI+SHE+BS	LAR	0.0021764	0.00029544	7.36649
O. hexactis	AS	LAR	0.0031367	0.00042524	7.37617
SG+DB+HB+SSI	AL+RS	EI+SHE+BS	0.0021789	0.00029526	7.37965
AL+RS	O. hexactis	SG+DB+HB+SSI	0.0021027	0.00028034	7.50045
SG+DB+HB+SSI	AS	SWS	0.0032299	0.00043020	7.50788
SG+DB+HB+SSI	LAR	SWS	0.0023991	0.00031180	7.69430
O. hexactis	BM	EWS	0.0033528	0.00042640	7.86309
O. hexactis	AS	EWS	0.0039099	0.00049593	7.88385
O. hexactis	PB_DS	SWS	0.0032694	0.00041093	7.95621
O. hexactis	BM	LAR	0.0030582	0.00038361	7.97218
SG+DB+HB+SSI	EWS	LAR	0.0033702	0.00041763	8.06974
SG+DB+HB+SSI	AL+RS	EWS	0.0040625	0.00049518	8.20415
O. hexactis	EI+SHE+BS	EWS	0.0027516	0.00033474	8.22008
O. hexactis	AL+RS	SCO+BAL	0.0028769	0.00034359	8.37316
O. hexactis	PB_DS	LAR	0.0037103	0.00044142	8.40536
O. hexactis	PB_DS	EWS	0.0050441	0.00059792	8.43601
O. hexactis	BM	EI+SHE+BS	0.0031077	0.00036820	8.44016
O. hexactis	SCO+BAL	EWS	0.0032664	0.00038667	8.44737
O. hexactis	AL+RS	BM	0.0031354	0.00036899	8.49716
O. hexactis	SCO+BAL	BM	0.0035881	0.00042181	8.50636
O. hexactis	EI+SHE+BS	SWS	0.0026748	0.00031443	8.50689
O. hexactis	AL+RS	EI+SHE+BS	0.0026333	0.00030884	8.52632
SG+DB+HB+SSI	AL+RS	LAR	0.0030058	0.00035252	8.52680
SG+DB+HB+SSI	EWS	SWS	0.0030083	0.00035241	8.53641
O. hexactis	BM	SWS	0.0033735	0.00039427	8.55652
O. hexactis	SCO+BAL	EI+SHE+BS	0.0029999	0.00034922	8.59029
SG+DB+HB+SSI	AL+RS	SWS	0.0026736	0.00031095	8.59810
O. hexactis	EI+SHE+BS	LAR	0.0027895	0.00032365	8.61889
O. hexactis	SCO+BAL	LAR	0.0031770	0.00036744	8.64634
O. hexactis	AL+RS	PB_DS	0.0041996	0.00047209	8.89576
O. hexactis	AL+RS	AS	0.0035154	0.00039499	8.89996
O. hexactis	SCO+BAL	SWS	0.0030865	0.00034650	8.90781
O. hexactis	AS	SWS	0.0039320	0.00043345	9.07128
O. hexactis	LAR	SWS	0.0031240	0.00033141	9.42649
O. hexactis	AL+RS	SWS	0.0032397	0.00032707	9.90549
O. hexactis	EWS	SWS	0.0036448	0.00036577	9.96462
O. hexactis	EWS	LAR	0.0039691	0.00038509	10.30680
O. hexactis	AL+RS	LAR	0.0035345	0.00034039	10.38380
O. hexactis	AL+RS	EWS	0.0045027	0.00041593	10.82560

Supplementary Table 4.3 Results of the four-population test (*f*4-statistic) from TreeMix analysis of *Ophionotus victoriae* with *O. hexactis* as outgroup. Significant negative Z-score (< -3) indicates gene flow between either population A and D, or population B and C. Abbreviations represent different geographical locations; BM = Bransfield Mouth, SG = South Georgia, DB = Discovery Bank, HB = Herdman Bank, SSI = South Sandwich Is., BOU = Bouvet Is., SHE = South Shetland Is., EI = Elephant Is., BS = Bransfield Strait, LAR = Larsen Ice Shelves, EWS = East Weddell Sea, SWS = South Weddell Sea, PB = Prydz Bay, TB = Tressler Bank, SCO = Scott Is, BAL = Balleny Is., AL = Adélie Land, RS = Ross Sea, AS = Amundsen Sea.

Population A	Population B	Population C	Population D	*f*4-statistic	Standard Error	Z-score
AL+RS	O. hexactis	SG+DB+HB+SSI	SWS	-0.0015623	0.0001909	-8.18379
AL+RS	O. hexactis	SG+DB+HB+SSI	EWS	-0.0028253	0.0003510	-8.04823
AL+RS	O. hexactis	SG+DB+HB+SSI	LAR	-0.0018571	0.0002360	-7.86871
AL+RS	SG+DB+HB+SSI	O. hexactis	LAR	-0.0016984	0.0002272	-7.47379
AL+RS	SG+DB+HB+SSI	O. hexactis	EWS	-0.0027550	0.0003704	-7.43745
AL+RS	O. hexactis	BOU	EWS	-0.0026904	0.0003632	-7.40822
AL+RS	SG+DB+HB+SSI	O. hexactis	SWS	-0.0013661	0.0001935	-7.06111
AL+RS	BOU	SG+DB+HB+SSI	SWS	-0.0020817	0.0002976	-6.99433
AL+RS	BOU	SG+DB+HB+SSI	LAR	-0.0023335	0.0003431	-6.80063
AL+RS	BOU	O. hexactis	LAR	-0.0018056	0.0002673	-6.75519
AL+RS	SG+DB+HB+SSI	BOU	EWS	-0.0031481	0.0004720	-6.66955
AL+RS	O. hexactis	EI+SHE+BS	EWS	-0.0018694	0.0002850	-6.55882
AL+RS	BOU	O. hexactis	SWS	-0.0015539	0.0002398	-6.47874
AL+RS	O. hexactis	BOU	LAR	-0.0017223	0.0002677	-6.43321
AL+RS	BOU	O. hexactis	EWS	-0.0025720	0.0003999	-6.43170
AL+RS	EI+SHE+BS	O. hexactis	EWS	-0.0017511	0.0002762	-6.34024
AL+RS	BOU	SG+DB+HB+SSI	EWS	-0.0030999	0.0004893	-6.33544
AL+RS	SG+DB+HB+SSI	BOU	LAR	-0.0020914	0.0003331	-6.27953
AL+RS	EI+SHE+BS	SCO+BAL	EWS	-0.0018742	0.0002997	-6.25355
AS	SG+DB+HB+SSI	O. hexactis	SWS	-0.0020583	0.0003294	-6.24940
AL+RS	O. hexactis	BOU	SWS	-0.0014275	0.0002286	-6.24532
AS	BOU	SG+DB+HB+SSI	SWS	-0.0026380	0.0004346	-6.06966
SCO+BAL	SG+DB+HB+SSI	O. hexactis	EI+SHE+BS	-0.0012381	0.0002040	-6.06796
AS	O. hexactis	SG+DB+HB+SSI	SWS	-0.0021186	0.0003495	-6.06263
AL+RS	EI+SHE+BS	SG+DB+HB+SSI	EWS	-0.0018356	0.0003060	-5.99960
AL+RS	SG+DB+HB+SSI	BOU	SWS	-0.0017591	0.0002964	-5.93468
AL+RS	EI+SHE+BS	BM	EWS	-0.0017235	0.0002917	-5.90849
PB_DS	BOU	SG+DB+HB+SSI	LAR	-0.0026397	0.0004478	-5.89465
BM	BOU	O. hexactis	SWS	-0.0016877	0.0002881	-5.85887
AS	BOU	O. hexactis	SWS	-0.0022461	0.0003841	-5.84724
AL+RS	EI+SHE+BS	BOU	EWS	-0.0019197	0.0003298	-5.82011
PB_DS	O. hexactis	SG+DB+HB+SSI	EWS	-0.0034970	0.0006110	-5.72322
BM	SG+DB+HB+SSI	O. hexactis	SWS	-0.0014999	0.0002639	-5.68444
AL+RS	SG+DB+HB+SSI	EI+SHE+BS	EWS	-0.0018836	0.0003327	-5.66226
SCO+BAL	SG+DB+HB+SSI	O. hexactis	LAR	-0.0013409	0.0002387	-5.61821
PB_DS	SG+DB+HB+SSI	O. hexactis	EWS	-0.0032964	0.0005868	-5.61757
BM	SG+DB+HB+SSI	O. hexactis	EI+SHE+BS	-0.0013458	0.0002420	-5.56070
BM	BOU	SG+DB+HB+SSI	SWS	-0.0018387	0.0003322	-5.53581
PB_DS	BOU	SG+DB+HB+SSI	SWS	-0.0022418	0.0004060	-5.52240
PB_DS	BOU	SG+DB+HB+SSI	EWS	-0.0037716	0.0006962	-5.41737
SCO+BAL	SG+DB+HB+SSI	O. hexactis	EWS	-0.0015187	0.0002822	-5.38097
SCO+BAL	SG+DB+HB+SSI	O. hexactis	SWS	-0.0012129	0.0002278	-5.32355
SG+DB+HB+SSI	LAR	EI+SHE+BS	BOU	-0.0015040	0.0002870	-5.24101
PB_DS	O. hexactis	SG+DB+HB+SSI	LAR	-0.0021633	0.0004165	-5.19454
PB_DS	BOU	O. hexactis	LAR	-0.0019814	0.0003816	-5.19226
SCO+BAL	BOU	O. hexactis	SWS	-0.0014006	0.0002704	-5.17903
PB_DS	BOU	O. hexactis	EWS	-0.0031134	0.0006042	-5.15331
AL+RS	BOU	EI+SHE+BS	EWS	-0.0019195	0.0003739	-5.13382
PB_DS	SG+DB+HB+SSI	O. hexactis	LAR	-0.0018741	0.0003652	-5.13241
AS	SG+DB+HB+SSI	O. hexactis	EWS	-0.0021622	0.0004215	-5.12939
SCO+BAL	BOU	O. hexactis	LAR	-0.0014481	0.0002850	-5.08189
SG+DB+HB+SSI	SWS	EI+SHE+BS	BOU	-0.0014324	0.0002824	-5.07290
SCO+BAL	SG+DB+HB+SSI	BOU	LAR	-0.0016936	0.0003344	-5.06397
SCO+BAL	SG+DB+HB+SSI	BOU	EWS	-0.0018714	0.0003696	-5.06373
PB_DS	O. hexactis	EI+SHE+BS	EWS	-0.0025139	0.0004966	-5.06172
AL+RS	BM	SCO+BAL	EWS	-0.0018611	0.0003683	-5.05309

PB_DS	EI+SHE+BS	BM	EWS	-0.0027100	0.0005371	-5.04522
PB_DS	SG+DB+HB+SSI	BOU	EWS	-0.0035696	0.0007143	-4.99765
SCO+BAL	BOU	SG+DB+HB+SSI	SWS	-0.0015082	0.0003025	-4.98557
SCO+BAL	SG+DB+HB+SSI	BOU	SWS	-0.0015656	0.0003144	-4.97983
AL+RS	BM	EI+SHE+BS	EWS	-0.0016243	0.0003281	-4.95077
AS	O. hexactis	SG+DB+HB+SSI	EWS	-0.0020965	0.0004258	-4.92392
AS	SG+DB+HB+SSI	BOU	SWS	-0.0024773	0.0005078	-4.87838
PB_DS	O. hexactis	SG+DB+HB+SSI	SWS	-0.0017224	0.0003540	-4.86532
AL+RS	O. hexactis	SG+DB+HB+SSI	EI+SHE+BS	-0.0009558	0.0001970	-4.85164
AL+RS	O. hexactis	EI+SHE+BS	LAR	-0.0009012	0.0001862	-4.84018
PB_DS	O. hexactis	BOU	EWS	-0.0031120	0.0006455	-4.82087
AL+RS	O. hexactis	SCO+BAL	EWS	-0.0016258	0.0003379	-4.81136
AL+RS	SG+DB+HB+SSI	O. hexactis	EI+SHE+BS	-0.0008714	0.0001813	-4.80776
AS	BOU	EI+SHE+BS	SWS	-0.0017406	0.0003624	-4.80363
AL+RS	BM	SCO+BAL	PB_DS	-0.0022206	0.0004626	-4.80059
AL+RS	SCO+BAL	EI+SHE+BS	EWS	-0.0016030	0.0003341	-4.79822
BM	O. hexactis	SG+DB+HB+SSI	SWS	-0.0013193	0.0002752	-4.79364
SCO+BAL	BOU	SG+DB+HB+SSI	LAR	-0.0015558	0.0003249	-4.78825
AL+RS	EI+SHE+BS	SCO+BAL	PB_DS	-0.0017924	0.0003745	-4.78684
AL+RS	SG+DB+HB+SSI	BM	EWS	-0.0016739	0.0003524	-4.74993
AL+RS	BOU	EI+SHE+BS	LAR	-0.0011531	0.0002436	-4.73367
AL+RS	SG+DB+HB+SSI	SCO+BAL	EWS	-0.0019758	0.0004209	-4.69455
BM	SG+DB+HB+SSI	O. hexactis	EWS	-0.0016051	0.0003421	-4.69235
AS	SG+DB+HB+SSI	BOU	EWS	-0.0025812	0.0005540	-4.65927
PB_DS	SG+DB+HB+SSI	EI+SHE+BS	EWS	-0.0025280	0.0005450	-4.63847
PB_DS	BOU	O. hexactis	SWS	-0.0015836	0.0003431	-4.61544
O. hexactis	LAR	EI+SHE+BS	BOU	-0.0010606	0.0002304	-4.60369
PB_DS	SG+DB+HB+SSI	BM	EWS	-0.0026605	0.0005793	-4.59239
AS	O. hexactis	BOU	SWS	-0.0021457	0.0004676	-4.58856
PB_DS	BOU	EI+SHE+BS	EWS	-0.0025639	0.0005607	-4.57291
BM	SG+DB+HB+SSI	O. hexactis	LAR	-0.0012221	0.0002706	-4.51628
AS	BOU	SG+DB+HB+SSI	EWS	-0.0023711	0.0005251	-4.51562
BM	BOU	O. hexactis	LAR	-0.0013294	0.0002952	-4.50352
AL+RS	O. hexactis	BM	EWS	-0.0013673	0.0003045	-4.49123
PB_DS	EI+SHE+BS	O. hexactis	EWS	-0.0022925	0.0005123	-4.47496
AL+RS	SCO+BAL	BM	EWS	-0.0016891	0.0003776	-4.47310
SCO+BAL	EWS	PB_DS	EI+SHE+BS	-0.0025133	0.0005706	-4.40470
AS	O. hexactis	EI+SHE+BS	SWS	-0.0014457	0.0003311	-4.36583
PB_DS	O. hexactis	BM	EWS	-0.0023539	0.0005425	-4.33889
PB_DS	BM	EI+SHE+BS	EWS	-0.0022687	0.0005234	-4.33469
PB_DS	SG+DB+HB+SSI	BOU	LAR	-0.0021473	0.0004956	-4.33303
PB_DS	EI+SHE+BS	SG+DB+HB+SSI	EWS	-0.0025073	0.0005795	-4.32673
SCO+BAL	O. hexactis	BOU	EWS	-0.0014138	0.0003284	-4.30500
BM	BOU	O. hexactis	EI+SHE+BS	-0.0011269	0.0002623	-4.29597
AL+RS	SG+DB+HB+SSI	EI+SHE+BS	LAR	-0.0008269	0.0001932	-4.27985
AL+RS	BOU	SG+DB+HB+SSI	EI+SHE+BS	-0.0011803	0.0002790	-4.23002
SCO+BAL	O. hexactis	BOU	SWS	-0.0012339	0.0002924	-4.22038
AL+RS	BM	SG+DB+HB+SSI	EWS	-0.0015267	0.0003625	-4.21192
AL+RS	BM	EI+SHE+BS	LAR	-0.0009507	0.0002260	-4.20594
PB_DS	SG+DB+HB+SSI	O. hexactis	SWS	-0.0013958	0.0003319	-4.20543
BM	BOU	SG+DB+HB+SSI	LAR	-0.0014804	0.0003523	-4.20222
SCO+BAL	O. hexactis	SG+DB+HB+SSI	LAR	-0.0010794	0.0002571	-4.19756
PB_DS	BOU	EI+SHE+BS	LAR	-0.0014320	0.0003416	-4.19226
PB_DS	BOU	BM	EWS	-0.0026797	0.0006426	-4.17014
SCO+BAL	O. hexactis	BOU	LAR	-0.0013245	0.0003183	-4.16156
AS	O. hexactis	BOU	EWS	-0.0021235	0.0005137	-4.13418
SCO+BAL	BOU	O. hexactis	EWS	-0.0013357	0.0003236	-4.12735
BM	BOU	O. hexactis	EWS	-0.0014221	0.0003466	-4.10362
AS	BOU	SG+DB+HB+SSI	LAR	-0.0017997	0.0004399	-4.09113
SCO+BAL	BOU	O. hexactis	EI+SHE+BS	-0.0010192	0.0002492	-4.08968
AS	BOU	O. hexactis	EWS	-0.0019792	0.0004842	-4.08745
AL+RS	BOU	EI+SHE+BS	SWS	-0.0009014	0.0002210	-4.07793
SCO+BAL	O. hexactis	SG+DB+HB+SSI	SWS	-0.0009888	0.0002425	-4.07736
AL+RS	BM	SCO+BAL	LAR	-0.0011874	0.0002925	-4.05926
BM	O. hexactis	SG+DB+HB+SSI	EWS	-0.0012986	0.0003212	-4.04238
O. hexactis	SWS	EI+SHE+BS	BOU	-0.0009890	0.0002448	-4.03983
AS	SG+DB+HB+SSI	EI+SHE+BS	SWS	-0.0013339	0.0003303	-4.03858
SCO+BAL	EWS	PB_DS	BM	-0.0025002	0.0006244	-4.00408
PB_DS	SWS	BM	EWS	-0.0020827	0.0005244	-3.97156
AL+RS	SWS	BM	EWS	-0.0010961	0.0002761	-3.96944
AL+RS	EI+SHE+BS	SG+DB+HB+SSI	LAR	-0.0008295	0.0002093	-3.96404
AL+RS	BOU	BM	EWS	-0.0016932	0.0004338	-3.90316

AL+RS	SCO+BAL	SG+DB+HB+SSI	EWS	-0.0016566	0.0004245	-3.90275
AL+RS	EI+SHE+BS	SCO+BAL	LAR	-0.0008680	0.0002225	-3.90133
SCO+BAL	EWS	PB_DS	SG+DB+HB+SSI	-0.0026150	0.0006706	-3.89973
SCO+BAL	O. hexactis	SG+DB+HB+SSI	EWS	-0.0011687	0.0002999	-3.89699
AS	SCO+BAL	EI+SHE+BS	SWS	-0.0013591	0.0003493	-3.89093
AL+RS	EI+SHE+BS	O. hexactis	LAR	-0.0007450	0.0001930	-3.85981
AS	EI+SHE+BS	O. hexactis	SWS	-0.0012571	0.0003268	-3.84713
BM	BOU	SG+DB+HB+SSI	EI+SHE+BS	-0.0012780	0.0003325	-3.84305
SCO+BAL	O. hexactis	SG+DB+HB+SSI	EI+SHE+BS	-0.0009023	0.0002366	-3.81378
AS	SG+DB+HB+SSI	O. hexactis	LAR	-0.0013005	0.0003415	-3.80848
BM	BOU	SG+DB+HB+SSI	EWS	-0.0015731	0.0004133	-3.80607
AL+RS	EI+SHE+BS	BOU	LAR	-0.0009135	0.0002402	-3.80305
PB_DS	EI+SHE+BS	BOU	EWS	-0.0023412	0.0006158	-3.80176
BM	SG+DB+HB+SSI	BOU	SWS	-0.0014486	0.0003824	-3.78834
SCO+BAL	EWS	PB_DS	O. hexactis	-0.0022650	0.0005990	-3.78158
BM	O. hexactis	SG+DB+HB+SSI	EI+SHE+BS	-0.0010535	0.0002789	-3.77672
SCO+BAL	BOU	SG+DB+HB+SSI	EWS	-0.0014433	0.0003845	-3.75318
AL+RS	BM	BOU	EWS	-0.0015942	0.0004260	-3.74197
AS	O. hexactis	SG+DB+HB+SSI	LAR	-0.0013233	0.0003551	-3.72614
PB_DS	O. hexactis	BOU	LAR	-0.0017782	0.0004779	-3.72084
SCO+BAL	BOU	SG+DB+HB+SSI	EI+SHE+BS	-0.0011268	0.0003066	-3.67514
AL+RS	SWS	EI+SHE+BS	EWS	-0.0008995	0.0002452	-3.66920
PB_DS	BM	SG+DB+HB+SSI	EWS	-0.0021985	0.0006003	-3.66219
O. hexactis	LAR	EWS	SWS	-0.0008451	0.0002324	-3.63672
PB_DS	O. hexactis	EI+SHE+BS	LAR	-0.0011801	0.0003247	-3.63495
SG+DB+HB+SSI	EWS	EI+SHE+BS	BOU	-0.0012643	0.0003484	-3.62936
AL+RS	SG+DB+HB+SSI	SCO+BAL	PB_DS	-0.0018733	0.0005207	-3.59774
AL+RS	SWS	AS	EWS	-0.0012745	0.0003549	-3.59081
AS	BOU	O. hexactis	LAR	-0.0014078	0.0003936	-3.57635
AL+RS	O. hexactis	EI+SHE+BS	SWS	-0.0006065	0.0001702	-3.56337
AL+RS	LAR	SCO+BAL	EWS	-0.0008337	0.0002348	-3.55138
PB_DS	BM	EI+SHE+BS	LAR	-0.0012295	0.0003473	-3.53978
AL+RS	SWS	SCO+BAL	EWS	-0.0010676	0.0003039	-3.51340
EI+SHE+BS	LAR	EWS	SWS	-0.0007684	0.0002189	-3.51108
BM	SG+DB+HB+SSI	BOU	EWS	-0.0015539	0.0004427	-3.50999
AS	SG+DB+HB+SSI	BOU	LAR	-0.0017194	0.0004917	-3.49716
AS	EI+SHE+BS	SG+DB+HB+SSI	SWS	-0.0012056	0.0003456	-3.48835
AL+RS	EI+SHE+BS	SCO+BAL	SWS	-0.0006879	0.0001973	-3.48704
AL+RS	SG+DB+HB+SSI	SCO+BAL	LAR	-0.0009191	0.0002645	-3.47439
AL+RS	SWS	SG+DB+HB+SSI	EWS	-0.0010542	0.0003036	-3.47182
SG+DB+HB+SSI	LAR	EWS	SWS	-0.0009711	0.0002803	-3.46486
PB_DS	SG+DB+HB+SSI	BOU	SWS	-0.0016690	0.0004819	-3.46352
AS	O. hexactis	EI+SHE+BS	EWS	-0.0014236	0.0004112	-3.46249
BM	O. hexactis	SG+DB+HB+SSI	LAR	-0.0010040	0.0002908	-3.45313
AS	SG+DB+HB+SSI	EI+SHE+BS	EWS	-0.0014378	0.0004165	-3.45187
PB_DS	SG+DB+HB+SSI	EI+SHE+BS	LAR	-0.0011058	0.0003211	-3.44340
AL+RS	SCO+BAL	EI+SHE+BS	LAR	-0.0007241	0.0002111	-3.43070
AL+RS	EI+SHE+BS	SG+DB+HB+SSI	SWS	-0.0006493	0.0001904	-3.41049
AL+RS	SCO+BAL	O. hexactis	EWS	-0.0012364	0.0003632	-3.40411
AL+RS	BM	O. hexactis	EWS	-0.0011499	0.0003406	-3.37652
AL+RS	LAR	EI+SHE+BS	EWS	-0.0006898	0.0002051	-3.36294
AL+RS	BOU	SCO+BAL	EWS	-0.0015477	0.0004626	-3.34548
AL+RS	EI+SHE+BS	O. hexactis	SWS	-0.0005649	0.0001692	-3.33820
AS	LAR	EI+SHE+BS	SWS	-0.0011112	0.0003342	-3.32511
PB_DS	SWS	EI+SHE+BS	EWS	-0.0015440	0.0004645	-3.32401
PB_DS	BOU	SG+DB+HB+SSI	EI+SHE+BS	-0.0012077	0.0003636	-3.32132
AS	EI+SHE+BS	SCO+BAL	SWS	-0.0013202	0.0003980	-3.31675
PB_DS	EI+SHE+BS	BM	LAR	-0.0013383	0.0004057	-3.29846
AL+RS	SWS	O. hexactis	EWS	-0.0008580	0.0002604	-3.29429
PB_DS	BOU	EI+SHE+BS	SWS	-0.0010341	0.0003143	-3.29036
AL+RS	SWS	AS	PB_DS	-0.0013468	0.0004096	-3.28794
AL+RS	SWS	BM	LAR	-0.0006487	0.0001978	-3.28033
BM	LAR	EWS	SWS	-0.0008658	0.0002650	-3.26747
AL+RS	EI+SHE+BS	BOU	SWS	-0.0007334	0.0002246	-3.26552
PB_DS	BOU	BM	LAR	-0.0015478	0.0004746	-3.26098
BM	O. hexactis	BOU	SWS	-0.0011170	0.0003433	-3.25339
AS	BM	EI+SHE+BS	SWS	-0.0011799	0.0003629	-3.25107
PB_DS	SWS	BM	LAR	-0.0012697	0.0003946	-3.21727
AL+RS	EI+SHE+BS	BM	LAR	-0.0007173	0.0002238	-3.20479
AS	EWS	LAR	SWS	-0.0011197	0.0003495	-3.20398
PB_DS	LAR	EI+SHE+BS	EWS	-0.0013343	0.0004167	-3.20170
SCO+BAL	LAR	PB_DS	BM	-0.0014610	0.0004585	-3.18636

SCO+BAL	EWS	PB_DS	BOU	-0.0021868	0.0006915	-3.16261
AL+RS	O. hexactis	SCO+BAL	PB_DS	-0.0013227	0.0004184	-3.16168
AL+RS	BM	SG+DB+HB+SSI	LAR	-0.0008531	0.0002703	-3.15654
AS	EI+SHE+BS	BOU	SWS	-0.0014516	0.0004628	-3.13629
AS	SCO+BAL	BM	SWS	-0.0013546	0.0004372	-3.09809
AS	EWS	PB_DS	SWS	-0.0020697	0.0006697	-3.09055
AS	EI+SHE+BS	BM	SWS	-0.0012859	0.0004195	-3.06543
AS	PB_DS	EWS	SWS	-0.0017967	0.0005865	-3.06374
PB_DS	BM	O. hexactis	EWS	-0.0016913	0.0005531	-3.05803
PB_DS	O. hexactis	BOU	SWS	-0.0013373	0.0004375	-3.05716
AS	BOU	EI+SHE+BS	EWS	-0.0014737	0.0004830	-3.05142
AL+RS	BOU	O. hexactis	EI+SHE+BS	-0.0006525	0.0002143	-3.04550
BM	O. hexactis	BOU	EWS	-0.0010963	0.0003609	-3.03731
PB_DS	O. hexactis	SG+DB+HB+SSI	EI+SHE+BS	-0.0009832	0.0003237	-3.03718
AS	SG+DB+HB+SSI	SCO+BAL	SWS	-0.0012191	0.0004020	-3.03279
PB_DS	SWS	SG+DB+HB+SSI	EWS	-0.0017260	0.0005702	-3.02673
PB_DS	LAR	BM	EWS	-0.0014430	0.0004824	-2.99145
BM	SG+DB+HB+SSI	BOU	LAR	-0.0011708	0.0003915	-2.99074
PB_DS	EI+SHE+BS	SG+DB+HB+SSI	LAR	-0.0011356	0.0003802	-2.98722
AL+RS	SWS	SG+DB+HB+SSI	LAR	-0.0006068	0.0002032	-2.98564
SCO+BAL	EWS	PB_DS	SWS	-0.0017067	0.0005721	-2.98319
AL+RS	SWS	SCO+BAL	PB_DS	-0.0011398	0.0003847	-2.96311
AS	O. hexactis	BOU	LAR	-0.0013503	0.0004558	-2.96271
PB_DS	BM	BOU	EWS	-0.0020157	0.0006805	-2.96202
AS	BOU	BM	SWS	-0.0014237	0.0004832	-2.94642
SCO+BAL	PB_DS	EWS	SWS	-0.0015948	0.0005420	-2.94237
AS	SCO+BAL	SG+DB+HB+SSI	SWS	-0.0011298	0.0003842	-2.94085
AS	PB_DS	LAR	SWS	-0.0012362	0.0004204	-2.94067
PB_DS	SG+DB+HB+SSI	BM	LAR	-0.0012382	0.0004214	-2.93824
AL+RS	SWS	EI+SHE+BS	LAR	-0.0004521	0.0001539	-2.93749
SCO+BAL	EWS	PB_DS	LAR	-0.0014729	0.0005017	-2.93603
AL+RS	SWS	SCO+BAL	LAR	-0.0006201	0.0002113	-2.93532
AL+RS	LAR	SG+DB+HB+SSI	EWS	-0.0006923	0.0002364	-2.92915
AL+RS	SWS	AS	LAR	-0.0008271	0.0002826	-2.92722
SG+DB+HB+SSI	SWS	EWS	LAR	-0.0006093	0.0002099	-2.90233
EI+SHE+BS	SWS	EWS	LAR	-0.0005587	0.0001925	-2.90208
AL+RS	SCO+BAL	SG+DB+HB+SSI	LAR	-0.0007777	0.0002683	-2.89828
AL+RS	O. hexactis	SCO+BAL	LAR	-0.0006576	0.0002269	-2.89772
SCO+BAL	LAR	PB_DS	EI+SHE+BS	-0.0011416	0.0003941	-2.89667
AS	SG+DB+HB+SSI	SCO+BAL	EWS	-0.0013230	0.0004605	-2.87299
BM	EI+SHE+BS	O. hexactis	SWS	-0.0006987	0.0002438	-2.86644
AL+RS	EWS	PB_DS	O. hexactis	-0.0008445	0.0002965	-2.84786
AL+RS	SCO+BAL	BM	LAR	-0.0008102	0.0002850	-2.84236
PB_DS	EI+SHE+BS	BM	SWS	-0.0010121	0.0003566	-2.83825
AL+RS	EI+SHE+BS	BM	SWS	-0.0005372	0.0001901	-2.82592
AL+RS	SCO+BAL	BOU	EWS	-0.0012767	0.0004529	-2.81892
PB_DS	SWS	O. hexactis	EWS	-0.0013993	0.0004965	-2.81841
AL+RS	BOU	BM	LAR	-0.0009268	0.0003290	-2.81663
O. hexactis	EWS	EI+SHE+BS	BOU	-0.0008209	0.0002929	-2.80287
AS	BM	SCO+BAL	SWS	-0.0012097	0.0004321	-2.79955
PB_DS	SG+DB+HB+SSI	O. hexactis	EI+SHE+BS	-0.0007683	0.0002762	-2.78234
SCO+BAL	LAR	PB_DS	SG+DB+HB+SSI	-0.0011927	0.0004289	-2.78106
AS	EI+SHE+BS	O. hexactis	EWS	-0.0011583	0.0004171	-2.77720
PB_DS	BM	SG+DB+HB+SSI	LAR	-0.0011593	0.0004229	-2.74118
AS	EI+SHE+BS	LAR	SWS	-0.0009100	0.0003320	-2.74087
PB_DS	EI+SHE+BS	O. hexactis	LAR	-0.0009208	0.0003389	-2.71733
SCO+BAL	PB_DS	EWS	LAR	-0.0012445	0.0004618	-2.69465
AL+RS	SG+DB+HB+SSI	EI+SHE+BS	SWS	-0.0004947	0.0001838	-2.69100
AS	BM	EI+SHE+BS	EWS	-0.0011785	0.0004380	-2.69047
AL+RS	O. hexactis	AS	EWS	-0.0009873	0.0003678	-2.68421
AL+RS	SG+DB+HB+SSI	SCO+BAL	SWS	-0.0005868	0.0002189	-2.68148
PB_DS	LAR	SG+DB+HB+SSI	EWS	-0.0013641	0.0005105	-2.67198
AL+RS	BM	BOU	LAR	-0.0009206	0.0003463	-2.65796
AS	SCO+BAL	EI+SHE+BS	EWS	-0.0011572	0.0004366	-2.65044
AS	EI+SHE+BS	SCO+BAL	EWS	-0.0012214	0.0004617	-2.64543
AS	LAR	SCO+BAL	SWS	-0.0010482	0.0003963	-2.64496
AS	BOU	SCO+BAL	SWS	-0.0011618	0.0004407	-2.63645
AS	EWS	PB_DS	O. hexactis	-0.0017825	0.0006794	-2.62345
AS	EI+SHE+BS	SG+DB+HB+SSI	EWS	-0.0011068	0.0004239	-2.61084
AL+RS	BM	SCO+BAL	O. hexactis	-0.0007112	0.0002741	-2.59500
PB_DS	BOU	BM	SWS	-0.0011499	0.0004459	-2.57887
AS	EI+SHE+BS	BOU	EWS	-0.0013528	0.0005263	-2.57046
AL+RS	SCO+BAL	EI+SHE+BS	SWS	-0.0005199	0.0002024	-2.56921
AL+RS	SCO+BAL	SG+DB+HB+SSI	SWS	-0.0005735	0.0002237	-2.56376

AL+RS	SWS	O. hexactis	LAR	-0.0004105	0.0001604	-2.56018
PB_DS	O. hexactis	EI+SHE+BS	SWS	-0.0007392	0.0002891	-2.55708
AL+RS	EWS	PB_DS	SG+DB+HB+SSI	-0.0007742	0.0003041	-2.54586
AS	BM	SCO+BAL	EWS	-0.0012083	0.0004770	-2.53322
AS	O. hexactis	SCO+BAL	SWS	-0.0009951	0.0003934	-2.52925
AS	EWS	PB_DS	SG+DB+HB+SSI	-0.0018481	0.0007326	-2.52271
AL+RS	LAR	SCO+BAL	PB_DS	-0.0007894	0.0003130	-2.52187
AS	SCO+BAL	O. hexactis	SWS	-0.0008455	0.0003366	-2.51158
AL+RS	SG+DB+HB+SSI	BM	LAR	-0.0006172	0.0002462	-2.50707
AS	O. hexactis	LAR	SWS	-0.0007953	0.0003217	-2.47246
AS	BOU	EI+SHE+BS	LAR	-0.0009023	0.0003653	-2.47002
AS	LAR	O. hexactis	SWS	-0.0008080	0.0003273	-2.46836
O. hexactis	SWS	EWS	LAR	-0.0005208	0.0002113	-2.46510
AS	SCO+BAL	LAR	SWS	-0.0008858	0.0003596	-2.46364
PB_DS	O. hexactis	BM	LAR	-0.0010201	0.0004156	-2.45442
AS	SG+DB+HB+SSI	BM	SWS	-0.0010336	0.0004217	-2.45109
AL+RS	SG+DB+HB+SSI	AS	EWS	-0.0010530	0.0004297	-2.45057
PB_DS	SWS	EI+SHE+BS	LAR	-0.0007309	0.0002983	-2.45027
PB_DS	EI+SHE+BS	SG+DB+HB+SSI	SWS	-0.0008094	0.0003305	-2.44936
AL+RS	BOU	SCO+BAL	LAR	-0.0007813	0.0003192	-2.44802
AS	EI+SHE+BS	BM	EWS	-0.0011870	0.0004878	-2.43372
BM	EWS	LAR	SWS	-0.0006396	0.0002636	-2.42681
AL+RS	LAR	O. hexactis	EWS	-0.0005336	0.0002201	-2.42416
AS	LAR	SG+DB+HB+SSI	SWS	-0.0008308	0.0003431	-2.42135
PB_DS	LAR	O. hexactis	EWS	-0.0010750	0.0004448	-2.41677
AL+RS	EWS	PB_DS	EI+SHE+BS	-0.0007262	0.0003009	-2.41351
PB_DS	SWS	SG+DB+HB+SSI	LAR	-0.0009129	0.0003911	-2.33429
AS	SG+DB+HB+SSI	LAR	SWS	-0.0007578	0.0003268	-2.31920
AS	SG+DB+HB+SSI	O. hexactis	EI+SHE+BS	-0.0007244	0.0003136	-2.30969
AS	SG+DB+HB+SSI	BM	EWS	-0.0011375	0.0004926	-2.30901
SCO+BAL	LAR	PB_DS	BOU	-0.0010549	0.0004579	-2.30390
AS	BOU	SG+DB+HB+SSI	EI+SHE+BS	-0.0008974	0.0003913	-2.29353
AS	SCO+BAL	BM	EWS	-0.0011527	0.0005029	-2.29209
AS	BOU	LAR	SWS	-0.0008383	0.0003662	-2.28914
SCO+BAL	LAR	PB_DS	O. hexactis	-0.0009312	0.0004071	-2.28713
AL+RS	SCO+BAL	BM	SWS	-0.0006059	0.0002651	-2.28580
AL+RS	SWS	BOU	EWS	-0.0007316	0.0003201	-2.28565
SCO+BAL	LAR	EWS	SWS	-0.0006653	0.0002912	-2.28447
SCO+BAL	LAR	PB_DS	SWS	-0.0008937	0.0003928	-2.27520
SCO+BAL	SWS	PB_DS	EI+SHE+BS	-0.0008154	0.0003585	-2.27464
AL+RS	LAR	SCO+BAL	SWS	-0.0004159	0.0001839	-2.26194
BM	O. hexactis	BOU	LAR	-0.0008017	0.0003564	-2.24974
AS	EWS	PB_DS	EI+SHE+BS	-0.0015172	0.0006751	-2.24738
AS	LAR	PB_DS	SWS	-0.0012567	0.0005696	-2.20613
AS	LAR	EWS	SWS	-0.0008672	0.0003968	-2.18580
AL+RS	EWS	PB_DS	BOU	-0.0007260	0.0003334	-2.17780
PB_DS	EI+SHE+BS	BOU	LAR	-0.0009695	0.0004470	-2.16869
AL+RS	BOU	BM	SWS	-0.0006750	0.0003116	-2.16662
BM	SWS	O. hexactis	EI+SHE+BS	-0.0004328	0.0002005	-2.15875
AS	EWS	PB_DS	BOU	-0.0016381	0.0007601	-2.15497
AS	O. hexactis	SCO+BAL	EWS	-0.0009730	0.0004527	-2.14944
AL+RS	BOU	SCO+BAL	PB_DS	-0.0012432	0.0005838	-2.12947
SCO+BAL	EI+SHE+BS	O. hexactis	SWS	-0.0004117	0.0001945	-2.11717
AL+RS	EWS	SCO+BAL	O. hexactis	-0.0003894	0.0001848	-2.10761
BM	BOU	EI+SHE+BS	SWS	-0.0005607	0.0002676	-2.09573
PB_DS	SG+DB+HB+SSI	EI+SHE+BS	SWS	-0.0006274	0.0003018	-2.07884
AS	O. hexactis	BM	SWS	-0.0008530	0.0004113	-2.07382
AL+RS	BM	SCO+BAL	SWS	-0.0005774	0.0002797	-2.06423
BM	SWS	O. hexactis	BOU	-0.0005707	0.0002768	-2.06151
AS	O. hexactis	EI+SHE+BS	LAR	-0.0006504	0.0003157	-2.06003
AL+RS	EI+SHE+BS	AS	EWS	-0.0007220	0.0003510	-2.05693
AS	BM	EI+SHE+BS	LAR	-0.0006998	0.0003407	-2.05434
AS	BOU	BM	EWS	-0.0011568	0.0005631	-2.05432
AS	BM	SG+DB+HB+SSI	SWS	-0.0007993	0.0003916	-2.04113
BM	EI+SHE+BS	O. hexactis	EWS	-0.0006012	0.0002955	-2.03471
AS	SCO+BAL	SG+DB+HB+SSI	EWS	-0.0009278	0.0004565	-2.03260
AS	EWS	PB_DS	BM	-0.0015086	0.0007495	-2.01277
SCO+BAL	O. hexactis	PB_DS	BM	-0.0008090	0.0004032	-2.00664
SCO+BAL	EI+SHE+BS	BOU	SWS	-0.0005399	0.0002722	-1.98377
PB_DS	EI+SHE+BS	O. hexactis	SWS	-0.0005946	0.0003011	-1.97443
SCO+BAL	EI+SHE+BS	O. hexactis	EWS	-0.0005148	0.0002609	-1.97310
AL+RS	BM	AS	PB_DS	-0.0010730	0.0005443	-1.97122
PB_DS	SG+DB+HB+SSI	BM	SWS	-0.0007598	0.0003866	-1.96523
BM	EI+SHE+BS	LAR	SWS	-0.0004299	0.0002191	-1.96210
SCO+BAL	EI+SHE+BS	BOU	EWS	-0.0006430	0.0003296	-1.95073
AL+RS	BOU	SCO+BAL	SWS	-0.0005295	0.0002729	-1.94053

AS	O. hexactis	SG+DB+HB+SSI	EI+SHE+BS	-0.0006729	0.0003471	-1.93887
AS	BM	BOU	SWS	-0.0010287	0.0005319	-1.93414
AL+RS	LAR	EI+SHE+BS	SWS	-0.0002720	0.0001408	-1.93143
SCO+BAL	EI+SHE+BS	O. hexactis	LAR	-0.0003875	0.0002019	-1.91947
AL+RS	BM	O. hexactis	LAR	-0.0004763	0.0002486	-1.91615
AS	LAR	BM	SWS	-0.0007873	0.0004113	-1.91401
O. hexactis	BOU	SG+DB+HB+SSI	SWS	-0.0005194	0.0002726	-1.90506
PB_DS	SWS	BOU	EWS	-0.0011531	0.0006055	-1.90452
AL+RS	LAR	BM	EWS	-0.0004565	0.0002404	-1.89853
PB_DS	SWS	BM	BOU	-0.0009296	0.0004911	-1.89267
AS	BM	SCO+BAL	PB_DS	-0.0012227	0.0006466	-1.89076
SCO+BAL	EI+SHE+BS	BOU	LAR	-0.0005157	0.0002745	-1.87914
AL+RS	EWS	PB_DS	BM	-0.0006270	0.0003339	-1.87820
PB_DS	BOU	O. hexactis	EI+SHE+BS	-0.0005494	0.0002937	-1.87083
SCO+BAL	SWS	PB_DS	SG+DB+HB+SSI	-0.0007144	0.0003837	-1.86177
PB_DS	BM	BOU	LAR	-0.0009765	0.0005245	-1.86175
SCO+BAL	PB_DS	O. hexactis	SG+DB+HB+SSI	-0.0005507	0.0002962	-1.85912
SCO+BAL	EI+SHE+BS	O. hexactis	SG+DB+HB+SSI	-0.0003358	0.0001808	-1.85736
BOU	LAR	EWS	SWS	-0.0006003	0.0003254	-1.84480
AL+RS	O. hexactis	SCO+BAL	SWS	-0.0003628	0.0001969	-1.84243
AS	SCO+BAL	BOU	SWS	-0.0009117	0.0004966	-1.83603
AS	PB_DS	EI+SHE+BS	SWS	-0.0007065	0.0003853	-1.83358
AS	SG+DB+HB+SSI	EI+SHE+BS	LAR	-0.0005761	0.0003156	-1.82542
PB_DS	SWS	O. hexactis	LAR	-0.0005863	0.0003230	-1.81489
SG+DB+HB+SSI	BOU	EI+SHE+BS	SWS	-0.0004067	0.0002241	-1.81448
AL+RS	SG+DB+HB+SSI	AS	PB_DS	-0.0009505	0.0005254	-1.80917
AS	BM	BOU	EWS	-0.0010273	0.0005714	-1.79781
PB_DS	SWS	BM	O. hexactis	-0.0006834	0.0003809	-1.79416
SCO+BAL	SWS	EWS	LAR	-0.0004314	0.0002408	-1.79191
BM	EI+SHE+BS	SG+DB+HB+SSI	SWS	-0.0004063	0.0002298	-1.76796
AL+RS	LAR	SCO+BAL	BM	-0.0003772	0.0002151	-1.75364
AS	BM	SCO+BAL	LAR	-0.0007296	0.0004163	-1.75269
PB_DS	EWS	BM	O. hexactis	-0.0006626	0.0003787	-1.74962
AL+RS	SWS	SG+DB+HB+SSI	BOU	-0.0003226	0.0001853	-1.74124
AL+RS	LAR	SG+DB+HB+SSI	SWS	-0.0002745	0.0001581	-1.73666
BM	LAR	O. hexactis	BOU	-0.0005277	0.0003052	-1.72884
AL+RS	SWS	AS	BOU	-0.0005430	0.0003147	-1.72523
AS	BOU	SCO+BAL	EWS	-0.0008949	0.0005196	-1.72219
AL+RS	SCO+BAL	BM	O. hexactis	-0.0004527	0.0002629	-1.72200
AS	O. hexactis	BM	EWS	-0.0008309	0.0004842	-1.71613
PB_DS	BM	O. hexactis	LAR	-0.0006520	0.0003800	-1.71583
AL+RS	LAR	SCO+BAL	BOU	-0.0003835	0.0002247	-1.70671
AS	BM	SG+DB+HB+SSI	EWS	-0.0007979	0.0004678	-1.70580
AL+RS	LAR	BOU	EWS	-0.0004502	0.0002666	-1.68879
AL+RS	EWS	SCO+BAL	SG+DB+HB+SSI	-0.0003192	0.0001893	-1.68668
SCO+BAL	PB_DS	O. hexactis	EI+SHE+BS	-0.0004697	0.0002788	-1.68464
AL+RS	O. hexactis	BM	LAR	-0.0003991	0.0002381	-1.67618
AS	EWS	EI+SHE+BS	SWS	-0.0005525	0.0003329	-1.65978
SCO+BAL	SWS	O. hexactis	EI+SHE+BS	-0.0003251	0.0001963	-1.65639
SCO+BAL	SWS	PB_DS	BM	-0.0007049	0.0004268	-1.65170
AL+RS	BOU	AS	EWS	-0.0008429	0.0005111	-1.64927
AL+RS	SCO+BAL	SG+DB+HB+SSI	BOU	-0.0003799	0.0002312	-1.64328
SCO+BAL	BOU	EI+SHE+BS	LAR	-0.0004290	0.0002620	-1.63747
AS	LAR	BOU	SWS	-0.0007506	0.0004586	-1.63673
O. hexactis	BOU	SG+DB+HB+SSI	LAR	-0.0004764	0.0002918	-1.63287
AL+RS	EWS	SCO+BAL	EI+SHE+BS	-0.0002711	0.0001665	-1.62847
PB_DS	LAR	BOU	EWS	-0.0008718	0.0005368	-1.62404
AS	PB_DS	O. hexactis	SWS	-0.0006626	0.0004084	-1.62244
PB_DS	O. hexactis	BM	SWS	-0.0005793	0.0003599	-1.60944
AL+RS	AS	SCO+BAL	PB_DS	-0.0009980	0.0006210	-1.60709
AL+RS	EI+SHE+BS	AS	PB_DS	-0.0006403	0.0004001	-1.60014
AS	BM	O. hexactis	SWS	-0.0005584	0.0003496	-1.59742
O. hexactis	SG+DB+HB+SSI	BOU	EWS	-0.0004576	0.0002876	-1.59141
SCO+BAL	SWS	PB_DS	BOU	-0.0006570	0.0004136	-1.58862
AL+RS	LAR	SCO+BAL	O. hexactis	-0.0003001	0.0001890	-1.58812
PB_DS	SWS	BM	EI+SHE+BS	-0.0005387	0.0003409	-1.58018
AL+RS	BM	AS	EWS	-0.0007134	0.0004598	-1.55150
AL+RS	PB_DS	EWS	SWS	-0.0005117	0.0003306	-1.54791
AL+RS	EWS	PB_DS	SWS	-0.0004394	0.0002841	-1.54677
SCO+BAL	SWS	PB_DS	LAR	-0.0005434	0.0003514	-1.54629
AL+RS	O. hexactis	AS	PB_DS	-0.0006842	0.0004426	-1.54597
AL+RS	SWS	SCO+BAL	BOU	-0.0003360	0.0002173	-1.54589
AL+RS	BM	EI+SHE+BS	SWS	-0.0003406	0.0002203	-1.54587
AL+RS	AS	SG+DB+HB+SSI	LAR	-0.0005338	0.0003473	-1.53723

AL+RS	SWS	AS	O. hexactis	-0.0004166	0.0002726	-1.52802
AS	BM	SCO+BAL	O. hexactis	-0.0006512	0.0004264	-1.52742
AL+RS	SCO+BAL	O. hexactis	LAR	-0.0003575	0.0002351	-1.52058
AS	EWS	PB_DS	LAR	-0.0009500	0.0006251	-1.51983
AS	BOU	PB_DS	SWS	-0.0009166	0.0006043	-1.51683
AS	BOU	O. hexactis	EI+SHE+BS	-0.0005055	0.0003337	-1.51499
AL+RS	AS	SG+DB+HB+SSI	EWS	-0.0007288	0.0004812	-1.51463
AS	EWS	SCO+BAL	SWS	-0.0006167	0.0004074	-1.51368
AL+RS	SCO+BAL	AS	PB_DS	-0.0008420	0.0005565	-1.51298
PB_DS	LAR	EI+SHE+BS	SWS	-0.0004047	0.0002684	-1.50781
PB_DS	EI+SHE+BS	BOU	SWS	-0.0006433	0.0004268	-1.50715
AL+RS	EWS	PB_DS	LAR	-0.0004099	0.0002729	-1.50182
SG+DB+HB+SSI	BOU	EWS	SWS	-0.0003708	0.0002472	-1.50006
PB_DS	SWS	SG+DB+HB+SSI	BOU	-0.0005728	0.0003835	-1.49366
SCO+BAL	O. hexactis	PB_DS	EWS	-0.0004873	0.0003264	-1.49308
AS	SCO+BAL	O. hexactis	EWS	-0.0006435	0.0004335	-1.48434
BM	LAR	O. hexactis	EI+SHE+BS	-0.0003182	0.0002154	-1.47717
AL+RS	SWS	BM	BOU	-0.0003645	0.0002470	-1.47597
PB_DS	LAR	BM	SWS	-0.0005135	0.0003483	-1.47423
SCO+BAL	BOU	EI+SHE+BS	SWS	-0.0003815	0.0002601	-1.46662
SG+DB+HB+SSI	EWS	LAR	SWS	-0.0003618	0.0002468	-1.46608
AS	SG+DB+HB+SSI	SCO+BAL	PB_DS	-0.0008754	0.0005972	-1.46590
SCO+BAL	EWS	O. hexactis	SG+DB+HB+SSI	-0.0003500	0.0002395	-1.46142
SG+DB+HB+SSI	BOU	EI+SHE+BS	LAR	-0.0003262	0.0002237	-1.45825
BM	EWS	O. hexactis	EI+SHE+BS	-0.0003561	0.0002443	-1.45773
PB_DS	LAR	SG+DB+HB+SSI	BOU	-0.0004923	0.0003422	-1.43878
AL+RS	SCO+BAL	AS	EWS	-0.0006578	0.0004593	-1.43214
PB_DS	BM	EI+SHE+BS	SWS	-0.0004734	0.0003326	-1.42318
SCO+BAL	BM	BOU	LAR	-0.0005228	0.0003678	-1.42126
SCO+BAL	BOU	PB_DS	LAR	-0.0006011	0.0004262	-1.41034
AS	PB_DS	BOU	SWS	-0.0008083	0.0005749	-1.40607
PB_DS	EWS	BM	BOU	-0.0006640	0.0004736	-1.40214
AS	SCO+BAL	EI+SHE+BS	LAR	-0.0004733	0.0003395	-1.39401
BM	EI+SHE+BS	BOU	SWS	-0.0004229	0.0003040	-1.39127
AS	BM	LAR	SWS	-0.0004800	0.0003497	-1.37274
O. hexactis	SG+DB+HB+SSI	BOU	LAR	-0.0003691	0.0002698	-1.36827
O. hexactis	BOU	EI+SHE+BS	SWS	-0.0002949	0.0002166	-1.36170
AL+RS	LAR	SG+DB+HB+SSI	BOU	-0.0002421	0.0001781	-1.35976
AS	EI+SHE+BS	SCO+BAL	PB_DS	-0.0007945	0.0005865	-1.35466
SCO+BAL	LAR	O. hexactis	SG+DB+HB+SSI	-0.0002615	0.0001932	-1.35355
SCO+BAL	SWS	PB_DS	O. hexactis	-0.0004903	0.0003626	-1.35227
BM	EI+SHE+BS	O. hexactis	SG+DB+HB+SSI	-0.0002924	0.0002168	-1.34891
AL+RS	SWS	AS	EI+SHE+BS	-0.0003750	0.0002803	-1.33795
O. hexactis	EWS	LAR	SWS	-0.0003243	0.0002445	-1.32648
AS	EWS	BM	SWS	-0.0005611	0.0004236	-1.32450
AL+RS	LAR	EI+SHE+BS	BOU	-0.0002396	0.0001820	-1.31646
PB_DS	LAR	SG+DB+HB+SSI	SWS	-0.0004346	0.0003318	-1.30988
AL+RS	AS	SCO+BAL	EWS	-0.0006528	0.0004993	-1.30755
AL+RS	AS	O. hexactis	EWS	-0.0005928	0.0004536	-1.30706
AS	SCO+BAL	BOU	EWS	-0.0007098	0.0005452	-1.30180
PB_DS	EWS	BM	EI+SHE+BS	-0.0004413	0.0003393	-1.30041
BM	SWS	SG+DB+HB+SSI	BOU	-0.0003901	0.0003006	-1.29783
AL+RS	SCO+BAL	BM	BOU	-0.0004124	0.0003180	-1.29696
AL+RS	EWS	AS	O. hexactis	-0.0003945	0.0003052	-1.29266
BM	EWS	O. hexactis	SG+DB+HB+SSI	-0.0003066	0.0002414	-1.27008
AL+RS	BM	SCO+BAL	SG+DB+HB+SSI	-0.0003344	0.0002637	-1.26809
AL+RS	SG+DB+HB+SSI	BM	SWS	-0.0002849	0.0002251	-1.26604
BM	O. hexactis	LAR	SWS	-0.0003153	0.0002505	-1.25867
AL+RS	SWS	BM	O. hexactis	-0.0002382	0.0001898	-1.25504
SCO+BAL	BOU	PB_DS	SWS	-0.0005536	0.0004415	-1.25409
AL+RS	SCO+BAL	EI+SHE+BS	BOU	-0.0003263	0.0002605	-1.25285
AS	BM	O. hexactis	EWS	-0.0005571	0.0004468	-1.24688
PB_DS	LAR	EI+SHE+BS	BOU	-0.0004625	0.0003710	-1.24671
O. hexactis	SG+DB+HB+SSI	BOU	SWS	-0.0003316	0.0002663	-1.24515
AS	O. hexactis	PB_DS	SWS	-0.0006704	0.0005386	-1.24462
AL+RS	AS	O. hexactis	LAR	-0.0003979	0.0003218	-1.23647
BM	BOU	LAR	SWS	-0.0003583	0.0002900	-1.23533
AL+RS	SCO+BAL	BOU	LAR	-0.0003978	0.0003224	-1.23380
PB_DS	LAR	BM	BOU	-0.0005713	0.0004637	-1.23206
AS	SG+DB+HB+SSI	SCO+BAL	LAR	-0.0004613	0.0003745	-1.23158
AS	SWS	BM	EWS	-0.0005597	0.0004578	-1.22249
AS	EI+SHE+BS	BOU	LAR	-0.0005416	0.0004435	-1.22117
AL+RS	SWS	BOU	LAR	-0.0002841	0.0002340	-1.21437
AL+RS	AS	SCO+BAL	LAR	-0.0004578	0.0003815	-1.19993
AS	O. hexactis	PB_DS	EWS	-0.0006483	0.0005405	-1.19928

AL+RS	SG+DB+HB+SSI	SCO+BAL	BM	-0.0003019	0.0002520	-1.19823
PB_DS	EWS	BM	SG+DB+HB+SSI	-0.0004620	0.0003859	-1.19726
AS	SWS	EI+SHE+BS	EWS	-0.0004537	0.0003791	-1.19681
SG+DB+HB+SSI	BOU	EWS	LAR	-0.0002903	0.0002456	-1.18201
AS	BOU	BM	LAR	-0.0005854	0.0004972	-1.17738
AL+RS	SWS	SCO+BAL	O. hexactis	-0.0002096	0.0001790	-1.17093
SCO+BAL	O. hexactis	PB_DS	LAR	-0.0003979	0.0003408	-1.16781
BM	EI+SHE+BS	O. hexactis	LAR	-0.0002688	0.0002312	-1.16231
AL+RS	PB_DS	EWS	LAR	-0.0003656	0.0003179	-1.14994
BM	SG+DB+HB+SSI	LAR	SWS	-0.0002778	0.0002420	-1.14775
AL+RS	O. hexactis	PB_DS	EWS	-0.0003031	0.0002657	-1.14102
O. hexactis	BOU	EI+SHE+BS	LAR	-0.0002519	0.0002209	-1.14032
SCO+BAL	EWS	O. hexactis	EI+SHE+BS	-0.0002484	0.0002198	-1.12999
SCO+BAL	BOU	PB_DS	EWS	-0.0004886	0.0004330	-1.12863
BOU	SWS	EWS	LAR	-0.0003189	0.0002830	-1.12695
AL+RS	SWS	BM	EI+SHE+BS	-0.0001966	0.0001756	-1.11951
BM	SWS	SG+DB+HB+SSI	EI+SHE+BS	-0.0002523	0.0002276	-1.10829
AL+RS	O. hexactis	SCO+BAL	BM	-0.0002585	0.0002332	-1.10817
SCO+BAL	LAR	O. hexactis	EI+SHE+BS	-0.0002104	0.0001910	-1.10170
AS	SCO+BAL	BM	O. hexactis	-0.0005091	0.0004639	-1.09747
AL+RS	EWS	SCO+BAL	BOU	-0.0002710	0.0002472	-1.09637
AS	BM	BOU	LAR	-0.0005486	0.0005033	-1.09016
AL+RS	EWS	AS	SG+DB+HB+SSI	-0.0003242	0.0002981	-1.08766
SCO+BAL	SWS	O. hexactis	SG+DB+HB+SSI	-0.0002240	0.0002061	-1.08704
BM	EI+SHE+BS	SG+DB+HB+SSI	EWS	-0.0003089	0.0002848	-1.08452
AS	PB_DS	EWS	LAR	-0.0005606	0.0005206	-1.07675
AS	PB_DS	SCO+BAL	SWS	-0.0005048	0.0004688	-1.07666
AS	BOU	PB_DS	EWS	-0.0006496	0.0006070	-1.07017
AS	EI+SHE+BS	SCO+BAL	LAR	-0.0004102	0.0003840	-1.06827
PB_DS	EI+SHE+BS	BM	O. hexactis	-0.0004175	0.0003914	-1.06677
AS	EI+SHE+BS	O. hexactis	LAR	-0.0003472	0.0003273	-1.06067
PB_DS	BM	SG+DB+HB+SSI	SWS	-0.0004031	0.0003809	-1.05838
AL+RS	AS	BM	EWS	-0.0005364	0.0005080	-1.05592
O. hexactis	BOU	EWS	SWS	-0.0002448	0.0002326	-1.05264
AL+RS	EWS	BM	O. hexactis	-0.0002174	0.0002082	-1.04416
BM	EWS	O. hexactis	BOU	-0.0003258	0.0003123	-1.04345
SCO+BAL	SG+DB+HB+SSI	EI+SHE+BS	EWS	-0.0002806	0.0002704	-1.03786
AL+RS	AS	BOU	EWS	-0.0005669	0.0005471	-1.03617
BM	EI+SHE+BS	O. hexactis	BOU	-0.0002758	0.0002671	-1.03257
BM	O. hexactis	EI+SHE+BS	SWS	-0.0002658	0.0002581	-1.02991
PB_DS	EWS	BM	LAR	-0.0004038	0.0003922	-1.02961
AL+RS	AS	EI+SHE+BS	EWS	-0.0004458	0.0004371	-1.02004
AS	SCO+BAL	BM	LAR	-0.0004688	0.0004652	-1.00775
SCO+BAL	O. hexactis	EI+SHE+BS	EWS	-0.0002664	0.0002646	-1.00711
PB_DS	O. hexactis	SG+DB+HB+SSI	BOU	-0.0003851	0.0003828	-1.00588
SCO+BAL	PB_DS	LAR	SWS	-0.0003503	0.0003500	-1.00104
AS	SCO+BAL	EI+SHE+BS	BOU	-0.0004474	0.0004493	-0.99587
BM	LAR	SG+DB+HB+SSI	BOU	-0.0003096	0.0003111	-0.99513
AL+RS	BM	SG+DB+HB+SSI	SWS	-0.0002430	0.0002464	-0.98628
BOU	EWS	LAR	SWS	-0.0002813	0.0002857	-0.98461
AS	EWS	SCO+BAL	SG+DB+HB+SSI	-0.0003952	0.0004023	-0.98227
AS	SWS	SCO+BAL	EWS	-0.0004148	0.0004238	-0.97874
PB_DS	SWS	EI+SHE+BS	BOU	-0.0003908	0.0003994	-0.97854
PB_DS	LAR	BM	O. hexactis	-0.0003681	0.0003765	-0.97760
BM	EI+SHE+BS	BOU	EWS	-0.0003255	0.0003344	-0.97317
AL+RS	PB_DS	SCO+BAL	BM	-0.0003474	0.0003576	-0.97151
BM	LAR	O. hexactis	SWS	-0.0002495	0.0002575	-0.96903
AS	EI+SHE+BS	PB_DS	SWS	-0.0005257	0.0005497	-0.95635
SCO+BAL	BOU	EI+SHE+BS	EWS	-0.0003165	0.0003315	-0.95466
AS	BM	SCO+BAL	SG+DB+HB+SSI	-0.0004103	0.0004311	-0.95180
BM	SWS	EWS	LAR	-0.0002262	0.0002381	-0.95004
SCO+BAL	BOU	PB_DS	BM	-0.0004845	0.0005107	-0.94875
EI+SHE+BS	EWS	LAR	SWS	-0.0002097	0.0002212	-0.94818
BM	LAR	O. hexactis	SG+DB+HB+SSI	-0.0002181	0.0002317	-0.94107
EI+SHE+BS	BOU	EWS	LAR	-0.0002397	0.0002576	-0.93078
SCO+BAL	BM	EI+SHE+BS	LAR	-0.0002265	0.0002440	-0.92859
AL+RS	BM	BOU	SWS	-0.0003105	0.0003344	-0.92844
AS	EWS	BOU	SWS	-0.0004316	0.0004743	-0.91012
AL+RS	BM	SCO+BAL	EI+SHE+BS	-0.0002368	0.0002605	-0.90895
AL+RS	SWS	SCO+BAL	EI+SHE+BS	-0.0001680	0.0001851	-0.90758
AL+RS	AS	SG+DB+HB+SSI	EI+SHE+BS	-0.0002829	0.0003118	-0.90746
O. hexactis	BOU	SG+DB+HB+SSI	EI+SHE+BS	-0.0002245	0.0002478	-0.90601
SCO+BAL	O. hexactis	PB_DS	SWS	-0.0003074	0.0003394	-0.90570

AS	PB_DS	SG+DB+HB+SSI	SWS	-0.0003962	0.0004395	-0.90157
SCO+BAL	EI+SHE+BS	PB_DS	EWS	-0.0002659	0.0002957	-0.89931
AL+RS	EWS	AS	EI+SHE+BS	-0.0002762	0.0003078	-0.89735
SCO+BAL	EWS	LAR	SWS	-0.0002338	0.0002621	-0.89201
AS	LAR	EI+SHE+BS	BOU	-0.0003607	0.0004059	-0.88844
AS	EI+SHE+BS	SG+DB+HB+SSI	LAR	-0.0002957	0.0003349	-0.88274
AL+RS	BOU	AS	PB_DS	-0.0005384	0.0006183	-0.87086
AS	EWS	O. hexactis	SWS	-0.0002872	0.0003308	-0.86837
PB_DS	SWS	BM	SG+DB+HB+SSI	-0.0003567	0.0004113	-0.86736
BM	BOU	EI+SHE+BS	EWS	-0.0002952	0.0003451	-0.85549
AL+RS	AS	BOU	LAR	-0.0003719	0.0004355	-0.85399
AL+RS	LAR	SCO+BAL	EI+SHE+BS	-0.0001439	0.0001693	-0.85003
AS	EI+SHE+BS	BM	LAR	-0.0003759	0.0004422	-0.85000
AL+RS	SWS	SG+DB+HB+SSI	EI+SHE+BS	-0.0001547	0.0001830	-0.84507
AS	BM	SG+DB+HB+SSI	LAR	-0.0003193	0.0003780	-0.84459
BM	SWS	O. hexactis	SG+DB+HB+SSI	-0.0001806	0.0002144	-0.84210
O. hexactis	BOU	SG+DB+HB+SSI	EWS	-0.0002746	0.0003262	-0.84164
AS	EWS	SCO+BAL	O. hexactis	-0.0003295	0.0003918	-0.84090
SCO+BAL	SG+DB+HB+SSI	PB_DS	EWS	-0.0002866	0.0003426	-0.83647
SCO+BAL	O. hexactis	EI+SHE+BS	LAR	-0.0001771	0.0002125	-0.83329
SG+DB+HB+SSI	EI+SHE+BS	LAR	SWS	-0.0001521	0.0001830	-0.83130
AL+RS	AS	EI+SHE+BS	LAR	-0.0002509	0.0003018	-0.83129
SG+DB+HB+SSI	EI+SHE+BS	EWS	SWS	-0.0002027	0.0002445	-0.82913
AL+RS	LAR	SCO+BAL	SG+DB+HB+SSI	-0.0001414	0.0001713	-0.82519
AL+RS	SWS	EI+SHE+BS	BOU	-0.0001680	0.0002044	-0.82152
AL+RS	AS	BM	LAR	-0.0003414	0.0004174	-0.81809
AS	SWS	SG+DB+HB+SSI	EWS	-0.0003254	0.0004003	-0.81282
AS	LAR	PB_DS	BOU	-0.0005061	0.0006246	-0.81025
AS	LAR	PB_DS	O. hexactis	-0.0004487	0.0005560	-0.80699
BM	O. hexactis	EI+SHE+BS	EWS	-0.0002451	0.0003045	-0.80506
PB_DS	EWS	BM	SWS	-0.0002873	0.0003575	-0.80375
BM	SG+DB+HB+SSI	EI+SHE+BS	EWS	-0.0002593	0.0003239	-0.80059
BM	BOU	EWS	SWS	-0.0002656	0.0003325	-0.79860
AS	SG+DB+HB+SSI	PB_DS	EWS	-0.0004476	0.0005627	-0.79547
AL+RS	EWS	AS	BOU	-0.0002760	0.0003471	-0.79532
O. hexactis	BOU	EWS	LAR	-0.0002018	0.0002539	-0.79501
AS	SWS	BM	BOU	-0.0003950	0.0005038	-0.78403
AS	SCO+BAL	BM	BOU	-0.0004429	0.0005658	-0.78271
AL+RS	SCO+BAL	O. hexactis	SWS	-0.0001532	0.0001962	-0.78106
AL+RS	BOU	PB_DS	EWS	-0.0003045	0.0003900	-0.78076
AL+RS	SWS	AS	SG+DB+HB+SSI	-0.0002204	0.0002827	-0.77939
AS	EI+SHE+BS	PB_DS	EWS	-0.0004269	0.0005478	-0.77934
AL+RS	BM	SCO+BAL	BOU	-0.0002669	0.0003440	-0.77574
AL+RS	LAR	O. hexactis	SWS	-0.0001158	0.0001495	-0.77410
PB_DS	EI+SHE+BS	BM	BOU	-0.0003688	0.0004828	-0.76393
O. hexactis	SWS	SG+DB+HB+SSI	BOU	-0.0001878	0.0002466	-0.76157
SCO+BAL	BM	BOU	EWS	-0.0003175	0.0004188	-0.75820
PB_DS	SWS	BOU	LAR	-0.0003401	0.0004525	-0.75165
BM	BOU	EI+SHE+BS	LAR	-0.0002024	0.0002703	-0.74892
SCO+BAL	SG+DB+HB+SSI	PB_DS	BM	-0.0003018	0.0004031	-0.74861
AS	BOU	SCO+BAL	LAR	-0.0003235	0.0004323	-0.74828
AS	SWS	BM	LAR	-0.0003072	0.0004111	-0.74744
AL+RS	EWS	SCO+BAL	BM	-0.0001720	0.0002330	-0.73835
AS	LAR	PB_DS	SG+DB+HB+SSI	-0.0004259	0.0005783	-0.73647
AS	SWS	EI+SHE+BS	BOU	-0.0002890	0.0003936	-0.73426
AS	SWS	BM	O. hexactis	-0.0002946	0.0004022	-0.73238
AS	LAR	PB_DS	BM	-0.0004694	0.0006576	-0.71375
AL+RS	SWS	AS	SCO+BAL	-0.0002070	0.0002903	-0.71298
AL+RS	SWS	O. hexactis	BOU	-0.0001264	0.0001777	-0.71129
AS	PB_DS	O. hexactis	SG+DB+HB+SSI	-0.0002664	0.0003768	-0.70691
AS	LAR	PB_DS	EWS	-0.0003894	0.0005515	-0.70610
AS	EWS	BM	SG+DB+HB+SSI	-0.0003396	0.0004827	-0.70343
AL+RS	SCO+BAL	BOU	SWS	-0.0001935	0.0002797	-0.69198
SCO+BAL	BM	EWS	LAR	-0.0002052	0.0002966	-0.69186
AS	SWS	O. hexactis	EWS	-0.0002651	0.0003849	-0.68876
PB_DS	SWS	O. hexactis	BOU	-0.0002462	0.0003586	-0.68658
SCO+BAL	LAR	PB_DS	EWS	-0.0002284	0.0003357	-0.68059
BM	LAR	EI+SHE+BS	BOU	-0.0002095	0.0003091	-0.67755
SCO+BAL	SWS	O. hexactis	BOU	-0.0001667	0.0002479	-0.67254
O. hexactis	EI+SHE+BS	LAR	SWS	-0.0001146	0.0001723	-0.66541
AL+RS	EWS	BM	SG+DB+HB+SSI	-0.0001472	0.0002219	-0.66328
AS	SCO+BAL	SG+DB+HB+SSI	LAR	-0.0002439	0.0003682	-0.66246

AL+RS	O. hexactis	SG+DB+HB+SSI	BOU	-0.0001348	0.0002057	-0.65539
BM	O. hexactis	SG+DB+HB+SSI	BOU	-0.0002023	0.0003103	-0.65199
AL+RS	EI+SHE+BS	SCO+BAL	BM	-0.0001507	0.0002316	-0.65078
BM	SG+DB+HB+SSI	EI+SHE+BS	SWS	-0.0001541	0.0002377	-0.64807
AS	SWS	EI+SHE+BS	LAR	-0.0002012	0.0003106	-0.64799
SCO+BAL	O. hexactis	PB_DS	EI+SHE+BS	-0.0002208	0.0003410	-0.64770
AS	LAR	SCO+BAL	O. hexactis	-0.0002402	0.0003764	-0.63797
AS	SCO+BAL	PB_DS	SWS	-0.0003630	0.0005700	-0.63678
AS	SG+DB+HB+SSI	BM	LAR	-0.0002758	0.0004365	-0.63186
AS	BOU	EWS	SWS	-0.0002669	0.0004291	-0.62206
SCO+BAL	EI+SHE+BS	SG+DB+HB+SSI	EWS	-0.0001790	0.0002879	-0.62178
AS	EWS	BM	O. hexactis	-0.0002739	0.0004419	-0.61976
AL+RS	EI+SHE+BS	SCO+BAL	O. hexactis	-0.0001230	0.0001999	-0.61554
AS	SG+DB+HB+SSI	PB_DS	SWS	-0.0003437	0.0005601	-0.61373
AS	LAR	SCO+BAL	BOU	-0.0002976	0.0004857	-0.61264
AL+RS	SWS	AS	BM	-0.0001784	0.0002919	-0.61115
AS	EWS	SG+DB+HB+SSI	SWS	-0.0002215	0.0003671	-0.60342
SCO+BAL	EI+SHE+BS	PB_DS	BM	-0.0002315	0.0003845	-0.60215
PB_DS	EWS	EI+SHE+BS	BOU	-0.0002227	0.0003770	-0.59089
EI+SHE+BS	BOU	EWS	SWS	-0.0001681	0.0002854	-0.58900
AS	LAR	EI+SHE+BS	EWS	-0.0002440	0.0004151	-0.58785
AS	LAR	SCO+BAL	SG+DB+HB+SSI	-0.0002174	0.0003719	-0.58442
PB_DS	SWS	SG+DB+HB+SSI	EI+SHE+BS	-0.0001820	0.0003150	-0.57786
AS	O. hexactis	SCO+BAL	PB_DS	-0.0003247	0.0005645	-0.57525
PB_DS	LAR	O. hexactis	BOU	-0.0002032	0.0003545	-0.57314
PB_DS	EWS	SG+DB+HB+SSI	BOU	-0.0002020	0.0003535	-0.57157
AL+RS	AS	SCO+BAL	EI+SHE+BS	-0.0002070	0.0003644	-0.56800
AS	PB_DS	BM	SWS	-0.0002738	0.0004924	-0.55600
AS	LAR	SCO+BAL	BM	-0.0002609	0.0004694	-0.55569
AL+RS	AS	O. hexactis	EI+SHE+BS	-0.0001470	0.0002682	-0.54816
AS	SWS	BM	SG+DB+HB+SSI	-0.0002343	0.0004294	-0.54565
AL+RS	PB_DS	O. hexactis	SG+DB+HB+SSI	-0.0001304	0.0002393	-0.54503
PB_DS	BM	EI+SHE+BS	BOU	-0.0002530	0.0004663	-0.54263
AL+RS	PB_DS	LAR	SWS	-0.0001461	0.0002700	-0.54100
AL+RS	O. hexactis	BM	SWS	-0.0001044	0.0001942	-0.53734
AS	SWS	SCO+BAL	BOU	-0.0002501	0.0004742	-0.52743
AS	O. hexactis	SCO+BAL	LAR	-0.0001998	0.0003788	-0.52736
AL+RS	EWS	AS	BM	-0.0001770	0.0003361	-0.52666
AS	SWS	PB_DS	EWS	-0.0002729	0.0005200	-0.52493
AS	SCO+BAL	SG+DB+HB+SSI	BOU	-0.0002180	0.0004277	-0.50987
AL+RS	LAR	AS	EWS	-0.0001549	0.0003079	-0.50296
AS	SCO+BAL	EWS	SWS	-0.0002020	0.0004031	-0.50106
AL+RS	EWS	BM	EI+SHE+BS	-0.0000991	0.0002002	-0.49530
PB_DS	LAR	O. hexactis	SWS	-0.0001454	0.0002959	-0.49150
SCO+BAL	SG+DB+HB+SSI	EI+SHE+BS	LAR	-0.0001028	0.0002103	-0.48888
SCO+BAL	EI+SHE+BS	PB_DS	SWS	-0.0001628	0.0003383	-0.48120
PB_DS	EI+SHE+BS	BM	SG+DB+HB+SSI	-0.0002027	0.0004240	-0.47805
AL+RS	PB_DS	O. hexactis	EI+SHE+BS	-0.0001031	0.0002168	-0.47549
SCO+BAL	LAR	O. hexactis	BOU	-0.0001237	0.0002632	-0.46989
AS	SCO+BAL	BM	SG+DB+HB+SSI	-0.0002248	0.0004805	-0.46791
BM	SWS	EI+SHE+BS	BOU	-0.0001378	0.0002969	-0.46417
SCO+BAL	SWS	SG+DB+HB+SSI	EI+SHE+BS	-0.0001011	0.0002200	-0.45947
O. hexactis	LAR	SG+DB+HB+SSI	BOU	-0.0001073	0.0002366	-0.45335
PB_DS	EI+SHE+BS	SG+DB+HB+SSI	BOU	-0.0001662	0.0003676	-0.45195
SCO+BAL	BM	O. hexactis	LAR	-0.0001188	0.0002646	-0.44900
AS	SWS	SCO+BAL	LAR	-0.0001623	0.0003657	-0.44384
AL+RS	LAR	O. hexactis	BOU	-0.0000834	0.0001886	-0.44204
SCO+BAL	EI+SHE+BS	PB_DS	LAR	-0.0001387	0.0003190	-0.43468
AS	SWS	SCO+BAL	O. hexactis	-0.0001496	0.0003463	-0.43211
PB_DS	BM	BOU	SWS	-0.0002204	0.0005144	-0.42836
AL+RS	AS	SG+DB+HB+SSI	BOU	-0.0001619	0.0003797	-0.42629
PB_DS	BM	SG+DB+HB+SSI	BOU	-0.0001828	0.0004335	-0.42157
SCO+BAL	SWS	BM	EI+SHE+BS	-0.0001105	0.0002655	-0.41630
AL+RS	SG+DB+HB+SSI	SCO+BAL	EI+SHE+BS	-0.0000922	0.0002222	-0.41477
AS	SWS	SG+DB+HB+SSI	BOU	-0.0001607	0.0003921	-0.40991
BM	LAR	SG+DB+HB+SSI	EI+SHE+BS	-0.0001001	0.0002448	-0.40901
BM	EI+SHE+BS	EWS	SWS	-0.0000975	0.0002388	-0.40807
SCO+BAL	O. hexactis	EI+SHE+BS	SWS	-0.0000866	0.0002154	-0.40200
AS	SG+DB+HB+SSI	SCO+BAL	BM	-0.0001855	0.0004722	-0.39283
O. hexactis	EI+SHE+BS	EWS	SWS	-0.0000767	0.0001955	-0.39255

SCO+BAL	BOU	PB_DS	EI+SHE+BS	-0.0001721	0.0004421	-0.38938
AS	PB_DS	SCO+BAL	BM	-0.0002310	0.0005944	-0.38861
AL+RS	EWS	BM	BOU	-0.0000990	0.0002564	-0.38610
AS	LAR	SCO+BAL	EWS	-0.0001809	0.0004728	-0.38269
SCO+BAL	BOU	EWS	LAR	-0.0001125	0.0003032	-0.37097
AS	BOU	SCO+BAL	PB_DS	-0.0002452	0.0006663	-0.36805
AS	EWS	SCO+BAL	BOU	-0.0001851	0.0005108	-0.36239
AL+RS	SCO+BAL	BM	EI+SHE+BS	-0.0000861	0.0002392	-0.35972
PB_DS	SG+DB+HB+SSI	BM	EI+SHE+BS	-0.0001324	0.0003717	-0.35619
SG+DB+HB+SSI	BOU	LAR	SWS	-0.0000805	0.0002269	-0.35482
SCO+BAL	EI+SHE+BS	SG+DB+HB+SSI	SWS	-0.0000759	0.0002143	-0.35397
AL+RS	PB_DS	AS	BM	-0.0001914	0.0005516	-0.34701
AS	SWS	BOU	EWS	-0.0001647	0.0004762	-0.34585
AL+RS	EI+SHE+BS	PB_DS	EWS	-0.0000817	0.0002382	-0.34316
SCO+BAL	SWS	PB_DS	EWS	-0.0001119	0.0003338	-0.33536
AL+RS	SG+DB+HB+SSI	PB_DS	EWS	-0.0001024	0.0003061	-0.33466
SCO+BAL	EWS	BM	SG+DB+HB+SSI	-0.0001147	0.0003445	-0.33300
PB_DS	LAR	BM	EI+SHE+BS	-0.0001088	0.0003300	-0.32969
SCO+BAL	BM	BOU	SWS	-0.0001169	0.0003605	-0.32440
SCO+BAL	SG+DB+HB+SSI	PB_DS	LAR	-0.0001088	0.0003379	-0.32194
AS	BM	SCO+BAL	BOU	-0.0001810	0.0005706	-0.31721
AL+RS	LAR	AS	PB_DS	-0.0001106	0.0003515	-0.31460
AS	BM	EI+SHE+BS	BOU	-0.0001512	0.0004847	-0.31196
SCO+BAL	BOU	BM	LAR	-0.0001166	0.0003745	-0.31137
PB_DS	BOU	BM	EI+SHE+BS	-0.0001158	0.0003983	-0.29071
AS	EI+SHE+BS	SCO+BAL	SG+DB+HB+SSI	-0.0001146	0.0003945	-0.29038
AS	O. hexactis	SCO+BAL	BM	-0.0001421	0.0004894	-0.29028
AS	SCO+BAL	PB_DS	EWS	-0.0001610	0.0005763	-0.27939
SCO+BAL	BM	SG+DB+HB+SSI	LAR	-0.0000754	0.0002716	-0.27744
AS	SWS	BM	EI+SHE+BS	-0.0001060	0.0003892	-0.27237
AS	SWS	O. hexactis	BOU	-0.0001004	0.0003743	-0.26834
AS	EWS	EI+SHE+BS	BOU	-0.0001209	0.0004566	-0.26485
AS	SWS	SCO+BAL	PB_DS	-0.0001418	0.0005356	-0.26479
AS	LAR	PB_DS	EI+SHE+BS	-0.0001454	0.0005619	-0.25883
AS	EI+SHE+BS	EWS	SWS	-0.0000988	0.0003825	-0.25844
AL+RS	AS	SCO+BAL	BM	-0.0001164	0.0004540	-0.25633
SG+DB+HB+SSI	EI+SHE+BS	EWS	LAR	-0.0000506	0.0002072	-0.24408
SCO+BAL	EI+SHE+BS	PB_DS	SG+DB+HB+SSI	-0.0000869	0.0003607	-0.24095
AS	SWS	SCO+BAL	SG+DB+HB+SSI	-0.0000894	0.0003720	-0.24022
AL+RS	PB_DS	BOU	SWS	-0.0000901	0.0003777	-0.23860
AS	EWS	BM	BOU	-0.0001295	0.0005436	-0.23819
AL+RS	SCO+BAL	SG+DB+HB+SSI	EI+SHE+BS	-0.0000536	0.0002271	-0.23595
SCO+BAL	EI+SHE+BS	SG+DB+HB+SSI	LAR	-0.0000517	0.0002198	-0.23540
AS	EWS	O. hexactis	SG+DB+HB+SSI	-0.0000657	0.0002791	-0.23536
AL+RS	AS	BM	EI+SHE+BS	-0.0000906	0.0003863	-0.23449
AS	PB_DS	SCO+BAL	SG+DB+HB+SSI	-0.0001086	0.0004762	-0.22800
SCO+BAL	SWS	O. hexactis	LAR	-0.0000530	0.0002331	-0.22754
AS	SWS	SG+DB+HB+SSI	LAR	-0.0000730	0.0003323	-0.21955
AS	BM	O. hexactis	LAR	-0.0000784	0.0003610	-0.21718
SCO+BAL	BOU	EWS	SWS	-0.0000650	0.0003013	-0.21567
AL+RS	LAR	BM	SWS	-0.0000386	0.0001814	-0.21288
AL+RS	EI+SHE+BS	SCO+BAL	SG+DB+HB+SSI	-0.0000386	0.0001903	-0.20281
AS	LAR	SG+DB+HB+SSI	BOU	-0.0000802	0.0003957	-0.20277
PB_DS	LAR	BM	SG+DB+HB+SSI	-0.0000789	0.0003936	-0.20051
AL+RS	SWS	BM	SG+DB+HB+SSI	-0.0000419	0.0002158	-0.19434
AS	SWS	PB_DS	BOU	-0.0001083	0.0005676	-0.19075
SCO+BAL	BM	O. hexactis	SG+DB+HB+SSI	-0.0000434	0.0002282	-0.19032
O. hexactis	BOU	LAR	SWS	-0.0000430	0.0002265	-0.18985
O. hexactis	BOU	EI+SHE+BS	EWS	-0.0000501	0.0002656	-0.18855
SCO+BAL	BOU	BM	SWS	-0.0000691	0.0003682	-0.18765
AL+RS	EWS	LAR	SWS	-0.0000296	0.0001602	-0.18450
AL+RS	LAR	PB_DS	EWS	-0.0000443	0.0002414	-0.18350
AL+RS	AS	SCO+BAL	BOU	-0.0000859	0.0004731	-0.18158
AL+RS	BOU	AS	LAR	-0.0000765	0.0004264	-0.17951
AS	EI+SHE+BS	O. hexactis	SG+DB+HB+SSI	-0.0000515	0.0002872	-0.17931
AS	EI+SHE+BS	BM	SG+DB+HB+SSI	-0.0000802	0.0004530	-0.17714
BM	EWS	SG+DB+HB+SSI	EI+SHE+BS	-0.0000496	0.0002883	-0.17188
AL+RS	AS	SCO+BAL	O. hexactis	-0.0000600	0.0003584	-0.16728
AS	EWS	SCO+BAL	EI+SHE+BS	-0.0000642	0.0003976	-0.16142
AS	EI+SHE+BS	SCO+BAL	O. hexactis	-0.0000631	0.0003913	-0.16114

BM	SG+DB+HB+SSI	O. hexactis	BOU	-0.0000513	0.0003274	-0.15660
AL+RS	LAR	BOU	SWS	-0.0000324	0.0002085	-0.15527
AS	LAR	O. hexactis	BOU	-0.0000574	0.0003970	-0.14467
SG+DB+HB+SSI	BOU	EI+SHE+BS	EWS	-0.0000359	0.0002673	-0.13424
AS	BOU	PB_DS	LAR	-0.0000782	0.0006011	-0.13015
AS	O. hexactis	BM	LAR	-0.0000577	0.0004475	-0.12894
BM	LAR	SG+DB+HB+SSI	SWS	-0.0000315	0.0002545	-0.12367
SCO+BAL	EI+SHE+BS	LAR	SWS	-0.0000241	0.0001979	-0.12192
AS	EWS	SCO+BAL	BM	-0.0000556	0.0004885	-0.11387
AL+RS	SCO+BAL	BM	SG+DB+HB+SSI	-0.0000325	0.0002856	-0.11372
SCO+BAL	EI+SHE+BS	BM	EWS	-0.0000344	0.0003038	-0.11319
AL+RS	PB_DS	SCO+BAL	SG+DB+HB+SSI	-0.0000326	0.0003095	-0.10530
PB_DS	LAR	SG+DB+HB+SSI	EI+SHE+BS	-0.0000299	0.0002895	-0.10317
AL+RS	BM	EI+SHE+BS	BOU	-0.0000301	0.0003018	-0.09986
AL+RS	BM	AS	LAR	-0.0000398	0.0004023	-0.09896
BM	O. hexactis	EWS	SWS	-0.0000207	0.0002466	-0.08405
AL+RS	SWS	SCO+BAL	SG+DB+HB+SSI	-0.0000134	0.0001703	-0.07852
AS	BM	SCO+BAL	EI+SHE+BS	-0.0000298	0.0004050	-0.07354
SCO+BAL	BM	PB_DS	LAR	-0.0000299	0.0004123	-0.07244
AS	LAR	BM	BOU	-0.0000367	0.0005149	-0.07133
AS	EI+SHE+BS	SCO+BAL	BM	-0.0000343	0.0004828	-0.07107
AL+RS	AS	O. hexactis	BOU	-0.0000259	0.0003701	-0.07010
O. hexactis	SG+DB+HB+SSI	EI+SHE+BS	EWS	-0.0000142	0.0002122	-0.06688
SCO+BAL	BM	EI+SHE+BS	EWS	-0.0000213	0.0003218	-0.06623
AL+RS	O. hexactis	AS	LAR	-0.0000191	0.0002932	-0.06518
AS	EI+SHE+BS	BM	O. hexactis	-0.0000287	0.0004528	-0.06348
AS	O. hexactis	EWS	SWS	-0.0000221	0.0003703	-0.05973
BM	EWS	SG+DB+HB+SSI	BOU	-0.0000193	0.0003405	-0.05660
AS	SCO+BAL	BOU	LAR	-0.0000259	0.0004821	-0.05368
SCO+BAL	EWS	BM	EI+SHE+BS	-0.0000131	0.0002783	-0.04700
AS	SWS	O. hexactis	LAR	-0.0000127	0.0003119	-0.04059
AS	SWS	PB_DS	LAR	-0.0000205	0.0005189	-0.03948
SCO+BAL	SWS	BM	SG+DB+HB+SSI	-0.0000095	0.0002951	-0.03207
AL+RS	LAR	BM	BOU	-0.0000062	0.0002352	-0.02654
AS	EWS	BM	EI+SHE+BS	-0.0000086	0.0004206	-0.02033
AL+RS	PB_DS	SCO+BAL	EI+SHE+BS	-0.0000052	0.0002725	-0.01925
AL+RS	LAR	SG+DB+HB+SSI	EI+SHE+BS	-0.0000025	0.0001422	-0.01768
SCO+BAL	SG+DB+HB+SSI	PB_DS	EI+SHE+BS	-0.0000060	0.0003412	-0.01756
AL+RS	EWS	AS	SCO+BAL	-0.0000050	0.0003085	-0.01627
AS	SWS	PB_DS	O. hexactis	-0.0000078	0.0005125	-0.01527
SCO+BAL	BOU	BM	EWS	-0.0000041	0.0004163	-0.00987
PB_DS	EWS	O. hexactis	BOU	-0.0000014	0.0003549	-0.00388
AS	BM	EWS	SWS	-0.0000014	0.0004113	-0.00337
AL+RS	EWS	EI+SHE+BS	BOU	0.0000001	0.0002036	0.00071
AS	SCO+BAL	BM	EI+SHE+BS	0.0000045	0.0004351	0.01041
AL+RS	SG+DB+HB+SSI	AS	LAR	0.0000037	0.0003248	0.01135
AS	BM	PB_DS	SWS	0.0000130	0.0005920	0.02194
BM	EI+SHE+BS	BOU	LAR	0.0000070	0.0003050	0.02300
AS	BM	PB_DS	EWS	0.0000144	0.0006081	0.02364
AL+RS	EWS	AS	SWS	0.0000106	0.0002914	0.03622
AS	LAR	BM	O. hexactis	0.0000207	0.0004398	0.04708
SCO+BAL	SG+DB+HB+SSI	BM	EWS	0.0000152	0.0003126	0.04851
SCO+BAL	SG+DB+HB+SSI	PB_DS	SWS	0.0000192	0.0003417	0.05625
BM	EI+SHE+BS	SG+DB+HB+SSI	BOU	0.0000166	0.0002862	0.05803
AL+RS	AS	BM	BOU	0.0000305	0.0004915	0.06202
AS	O. hexactis	SG+DB+HB+SSI	BOU	0.0000270	0.0003948	0.06850
PB_DS	EWS	SG+DB+HB+SSI	EI+SHE+BS	0.0000207	0.0002958	0.07000
AS	LAR	SG+DB+HB+SSI	EWS	0.0000364	0.0004381	0.08316
BM	EWS	EI+SHE+BS	BOU	0.0000303	0.0003576	0.08469
AS	LAR	O. hexactis	SG+DB+HB+SSI	0.0000228	0.0002669	0.08542
AL+RS	EWS	SCO+BAL	SWS	0.0000156	0.0001792	0.08693
BM	EI+SHE+BS	SG+DB+HB+SSI	LAR	0.0000236	0.0002451	0.09638
AS	LAR	BM	SG+DB+HB+SSI	0.0000435	0.0004428	0.09825
AS	SWS	PB_DS	SG+DB+HB+SSI	0.0000525	0.0005300	0.09900
SCO+BAL	BM	PB_DS	SG+DB+HB+SSI	0.0000455	0.0004360	0.10434
AL+RS	PB_DS	SG+DB+HB+SSI	EI+SHE+BS	0.0000274	0.0002501	0.10934
AL+RS	PB_DS	O. hexactis	SWS	0.0000297	0.0002628	0.11301
AS	SWS	SCO+BAL	EI+SHE+BS	0.0000389	0.0003413	0.11411
AS	SCO+BAL	O. hexactis	LAR	0.0000404	0.0003531	0.11437
AL+RS	EI+SHE+BS	BM	O. hexactis	0.0000277	0.0002336	0.11855

SCO+BAL	SG+DB+HB+SSI	EI+SHE+BS	SWS	0.0000252	0.0002103	0.11986
AS	PB_DS	O. hexactis	EI+SHE+BS	0.0000439	0.0003626	0.12119
AL+RS	EWS	AS	LAR	0.0000401	0.0003084	0.13008
AL+RS	SWS	SCO+BAL	BM	0.0000286	0.0002173	0.13142
PB_DS	EI+SHE+BS	O. hexactis	BOU	0.0000487	0.0003629	0.13421
PB_DS	EWS	EI+SHE+BS	LAR	0.0000374	0.0002766	0.13538
AS	LAR	O. hexactis	EWS	0.0000592	0.0004335	0.13663
PB_DS	LAR	BOU	SWS	0.0000578	0.0004160	0.13884
AL+RS	AS	BM	O. hexactis	0.0000564	0.0004032	0.13997
SCO+BAL	SWS	BM	BOU	0.0000479	0.0003369	0.14206
AL+RS	PB_DS	BOU	LAR	0.0000559	0.0003792	0.14753
AS	SCO+BAL	O. hexactis	BOU	0.0000663	0.0004294	0.15432
AS	LAR	BM	EWS	0.0000799	0.0004948	0.16156
PB_DS	EWS	SG+DB+HB+SSI	LAR	0.0000582	0.0003411	0.17052
SCO+BAL	LAR	O. hexactis	SWS	0.0000375	0.0002183	0.17161
AL+RS	SCO+BAL	O. hexactis	BOU	0.0000403	0.0002343	0.17206
AS	LAR	SCO+BAL	EI+SHE+BS	0.0000631	0.0003599	0.17524
SCO+BAL	BOU	LAR	SWS	0.0000475	0.0002686	0.17685
PB_DS	BM	SG+DB+HB+SSI	EI+SHE+BS	0.0000703	0.0003712	0.18931
AS	PB_DS	EI+SHE+BS	BOU	0.0001018	0.0005376	0.18939
O. hexactis	EI+SHE+BS	EWS	LAR	0.0000379	0.0001995	0.19012
AL+RS	EI+SHE+BS	SCO+BAL	BOU	0.0000455	0.0002326	0.19565
AS	SWS	BOU	LAR	0.0000878	0.0004288	0.20471
AL+RS	AS	SCO+BAL	SG+DB+HB+SSI	0.0000760	0.0003652	0.20805
SCO+BAL	PB_DS	O. hexactis	BOU	0.0000795	0.0003821	0.20806
BM	O. hexactis	EI+SHE+BS	LAR	0.0000494	0.0002342	0.21117
O. hexactis	SG+DB+HB+SSI	LAR	SWS	0.0000375	0.0001773	0.21143
AS	PB_DS	BM	SG+DB+HB+SSI	0.0001224	0.0005789	0.21149
SCO+BAL	PB_DS	BOU	SWS	0.0001034	0.0004761	0.21718
SCO+BAL	BM	PB_DS	O. hexactis	0.0000889	0.0004071	0.21843
AS	LAR	BOU	EWS	0.0001167	0.0005131	0.22735
SCO+BAL	LAR	SG+DB+HB+SSI	EI+SHE+BS	0.0000511	0.0002183	0.23394
AL+RS	EWS	SCO+BAL	LAR	0.0000451	0.0001927	0.23423
SCO+BAL	PB_DS	SG+DB+HB+SSI	EI+SHE+BS	0.0000809	0.0003402	0.23787
AS	O. hexactis	PB_DS	LAR	0.0001250	0.0005182	0.24115
AL+RS	PB_DS	AS	SG+DB+HB+SSI	0.0001234	0.0005111	0.24142
AL+RS	BM	SG+DB+HB+SSI	BOU	0.0000675	0.0002763	0.24425
AS	SWS	O. hexactis	SG+DB+HB+SSI	0.0000603	0.0002448	0.24625
SCO+BAL	SWS	SG+DB+HB+SSI	BOU	0.0000573	0.0002324	0.24668
AL+RS	EWS	SG+DB+HB+SSI	BOU	0.0000482	0.0001923	0.25065
SCO+BAL	BM	O. hexactis	EWS	0.0000864	0.0003334	0.25925
AS	EI+SHE+BS	SCO+BAL	BOU	0.0001314	0.0005038	0.26081
SCO+BAL	EWS	O. hexactis	BOU	0.0000781	0.0002934	0.26631
AS	SG+DB+HB+SSI	EWS	SWS	0.0001039	0.0003879	0.26777
SCO+BAL	EI+SHE+BS	BM	SWS	0.0000687	0.0002545	0.27007
BM	SWS	O. hexactis	LAR	0.0000657	0.0002390	0.27506
BM	BOU	EWS	LAR	0.0000927	0.0003285	0.28237
AS	O. hexactis	PB_DS	BM	0.0001827	0.0006450	0.28321
BM	LAR	EI+SHE+BS	SWS	0.0000687	0.0002370	0.28969
AS	PB_DS	O. hexactis	BOU	0.0001458	0.0005016	0.29060
AL+RS	SWS	PB_DS	EWS	0.0000722	0.0002467	0.29276
PB_DS	BM	O. hexactis	SWS	0.0001041	0.0003526	0.29529
AL+RS	SWS	O. hexactis	EI+SHE+BS	0.0000416	0.0001401	0.29665
AL+RS	AS	EI+SHE+BS	BOU	0.0001211	0.0004058	0.29832
AL+RS	PB_DS	AS	SCO+BAL	0.0001560	0.0005225	0.29850
AL+RS	EWS	SG+DB+HB+SSI	EI+SHE+BS	0.0000481	0.0001591	0.30214
AS	SG+DB+HB+SSI	SCO+BAL	EI+SHE+BS	0.0001148	0.0003781	0.30364
AL+RS	PB_DS	AS	EI+SHE+BS	0.0001507	0.0004958	0.30403
AS	EI+SHE+BS	BM	BOU	0.0001657	0.0005399	0.30695
EI+SHE+BS	BOU	LAR	SWS	0.0000716	0.0002174	0.32947
SCO+BAL	LAR	EI+SHE+BS	BOU	0.0000868	0.0002623	0.33069
AS	SWS	SCO+BAL	BM	0.0001450	0.0004369	0.33174
AL+RS	PB_DS	SCO+BAL	O. hexactis	0.0000978	0.0002919	0.33513
SCO+BAL	EI+SHE+BS	BM	LAR	0.0000929	0.0002715	0.34200
AS	PB_DS	SCO+BAL	O. hexactis	0.0001578	0.0004549	0.34683
AS	LAR	SCO+BAL	PB_DS	0.0002085	0.0006006	0.34719
AS	SWS	PB_DS	EI+SHE+BS	0.0001808	0.0005181	0.34891
AS	EWS	O. hexactis	BOU	0.0001444	0.0004109	0.35138
SCO+BAL	O. hexactis	EWS	LAR	0.0000893	0.0002518	0.35471
BM	SG+DB+HB+SSI	EWS	SWS	0.0001053	0.0002967	0.35472
SCO+BAL	EWS	SG+DB+HB+SSI	EI+SHE+BS	0.0001016	0.0002810	0.36172
AL+RS	PB_DS	O. hexactis	BOU	0.0001198	0.0003203	0.37415
AL+RS	LAR	BM	O. hexactis	0.0000771	0.0002027	0.38049

SCO+BAL	BM	SG+DB+HB+SSI	EWS	0.0001299	0.0003397	0.38239
SCO+BAL	SWS	BOU	LAR	0.0001137	0.0002943	0.38617
SCO+BAL	O. hexactis	LAR	SWS	0.0000905	0.0002337	0.38729
AL+RS	BM	SG+DB+HB+SSI	EI+SHE+BS	0.0000976	0.0002504	0.38982
PB_DS	EWS	LAR	SWS	0.0001165	0.0002944	0.39570
SCO+BAL	BOU	O. hexactis	SG+DB+HB+SSI	0.0001076	0.0002673	0.40259
SCO+BAL	EI+SHE+BS	EWS	SWS	0.0001031	0.0002480	0.41574
AL+RS	PB_DS	SCO+BAL	SWS	0.0001275	0.0003054	0.41761
SCO+BAL	BM	PB_DS	EWS	0.0001754	0.0004110	0.42670
AS	SWS	SG+DB+HB+SSI	EI+SHE+BS	0.0001283	0.0003001	0.42749
AL+RS	BOU	SCO+BAL	BM	0.0001455	0.0003359	0.43320
AL+RS	BOU	AS	SWS	0.0001752	0.0003978	0.44054
AL+RS	EI+SHE+BS	SG+DB+HB+SSI	BOU	0.0000841	0.0001900	0.44266
AL+RS	AS	BM	SG+DB+HB+SSI	0.0001924	0.0004336	0.44363
AS	PB_DS	SCO+BAL	EI+SHE+BS	0.0002017	0.0004539	0.44444
O. hexactis	SG+DB+HB+SSI	EI+SHE+BS	LAR	0.0000743	0.0001622	0.45820
PB_DS	O. hexactis	BM	EI+SHE+BS	0.0001600	0.0003459	0.46250
O. hexactis	SG+DB+HB+SSI	EWS	LAR	0.0000885	0.0001913	0.46256
AL+RS	EI+SHE+BS	BM	SG+DB+HB+SSI	0.0001121	0.0002413	0.46467
SCO+BAL	BM	O. hexactis	EI+SHE+BS	0.0001078	0.0002296	0.46928
AS	BOU	SCO+BAL	BM	0.0002619	0.0005457	0.47993
SCO+BAL	BM	PB_DS	EI+SHE+BS	0.0001967	0.0004068	0.48343
AS	SWS	PB_DS	BM	0.0002868	0.0005877	0.48795
AS	BM	SG+DB+HB+SSI	BOU	0.0002294	0.0004694	0.48864
AS	PB_DS	SCO+BAL	BOU	0.0003036	0.0006149	0.49367
AS	EI+SHE+BS	O. hexactis	BOU	0.0001945	0.0003890	0.49992
SCO+BAL	EI+SHE+BS	BM	SG+DB+HB+SSI	0.0001446	0.0002884	0.50135
AL+RS	EI+SHE+BS	O. hexactis	SG+DB+HB+SSI	0.0000844	0.0001679	0.50281
AL+RS	EWS	O. hexactis	SG+DB+HB+SSI	0.0000702	0.0001389	0.50555
AS	EWS	SG+DB+HB+SSI	BOU	0.0002101	0.0004115	0.51049
AL+RS	PB_DS	AS	O. hexactis	0.0002538	0.0004895	0.51847
BM	SG+DB+HB+SSI	EI+SHE+BS	LAR	0.0001238	0.0002382	0.51944
AL+RS	AS	EWS	LAR	0.0001950	0.0003717	0.52450
AL+RS	AS	O. hexactis	SG+DB+HB+SSI	0.0001359	0.0002512	0.54105
SCO+BAL	EI+SHE+BS	O. hexactis	BOU	0.0001282	0.0002354	0.54456
SCO+BAL	EI+SHE+BS	EWS	LAR	0.0001273	0.0002333	0.54539
BM	BOU	O. hexactis	SG+DB+HB+SSI	0.0001511	0.0002735	0.55223
SCO+BAL	LAR	BOU	SWS	0.0001612	0.0002914	0.55305
AL+RS	PB_DS	SCO+BAL	BOU	0.0002177	0.0003929	0.55397
SCO+BAL	LAR	SG+DB+HB+SSI	BOU	0.0001378	0.0002480	0.55582
AL+RS	PB_DS	EI+SHE+BS	SWS	0.0001328	0.0002379	0.55815
PB_DS	EWS	SG+DB+HB+SSI	SWS	0.0001747	0.0003125	0.55886
PB_DS	SWS	O. hexactis	EI+SHE+BS	0.0001446	0.0002576	0.56156
SCO+BAL	PB_DS	O. hexactis	SWS	0.0001829	0.0003257	0.56167
SCO+BAL	BM	SG+DB+HB+SSI	EI+SHE+BS	0.0001512	0.0002688	0.56248
AL+RS	PB_DS	SG+DB+HB+SSI	SWS	0.0001601	0.0002843	0.56318
SCO+BAL	SWS	BM	LAR	0.0001615	0.0002849	0.56700
SCO+BAL	SG+DB+HB+SSI	LAR	SWS	0.0001280	0.0002212	0.57874
PB_DS	EWS	EI+SHE+BS	SWS	0.0001540	0.0002636	0.58407
AL+RS	SCO+BAL	AS	LAR	0.0002211	0.0003770	0.58630
AL+RS	SCO+BAL	PB_DS	EWS	0.0001842	0.0003129	0.58861
O. hexactis	SG+DB+HB+SSI	EI+SHE+BS	SWS	0.0001118	0.0001872	0.59709
AL+RS	BM	O. hexactis	SWS	0.0001338	0.0002222	0.60228
AL+RS	PB_DS	AS	SWS	0.0002835	0.0004704	0.60266
SCO+BAL	SWS	EI+SHE+BS	BOU	0.0001584	0.0002619	0.60474
AS	EI+SHE+BS	SG+DB+HB+SSI	BOU	0.0002460	0.0003948	0.62302
AL+RS	EWS	O. hexactis	BOU	0.0001184	0.0001857	0.63797
AS	SCO+BAL	SG+DB+HB+SSI	EI+SHE+BS	0.0002294	0.0003564	0.64353
PB_DS	EWS	BOU	LAR	0.0002602	0.0003972	0.65503
AL+RS	PB_DS	EI+SHE+BS	BOU	0.0002229	0.0003402	0.65518
AL+RS	PB_DS	O. hexactis	LAR	0.0001758	0.0002679	0.65617
O. hexactis	SG+DB+HB+SSI	EWS	SWS	0.0001260	0.0001909	0.65988
AS	BOU	BM	EI+SHE+BS	0.0003169	0.0004760	0.66580
SCO+BAL	SG+DB+HB+SSI	BM	LAR	0.0001930	0.0002896	0.66630
O. hexactis	EWS	SG+DB+HB+SSI	BOU	0.0001830	0.0002699	0.67810
AL+RS	AS	PB_DS	EWS	0.0003452	0.0005082	0.67916
AL+RS	PB_DS	AS	BOU	0.0003736	0.0005478	0.68206
PB_DS	SG+DB+HB+SSI	O. hexactis	BOU	0.0002732	0.0003985	0.68556
AS	PB_DS	BM	O. hexactis	0.0003888	0.0005586	0.69598

AS	BOU	PB_DS	BM	0.0005071	0.0007184	0.70590
SCO+BAL	BM	EWS	SWS	0.0002006	0.0002816	0.71236
SCO+BAL	SWS	BM	O. hexactis	0.0002146	0.0002991	0.71730
AS	PB_DS	BOU	LAR	0.0004279	0.0005943	0.71993
AS	EI+SHE+BS	PB_DS	LAR	0.0003842	0.0005326	0.72139
SCO+BAL	BM	EI+SHE+BS	SWS	0.0001793	0.0002482	0.72239
AS	SWS	O. hexactis	EI+SHE+BS	0.0001886	0.0002604	0.72425
AS	SG+DB+HB+SSI	BM	EI+SHE+BS	0.0003003	0.0004144	0.72466
SCO+BAL	SWS	SG+DB+HB+SSI	LAR	0.0001710	0.0002342	0.73007
SCO+BAL	SG+DB+HB+SSI	EWS	LAR	0.0001778	0.0002422	0.73414
PB_DS	EWS	O. hexactis	SG+DB+HB+SSI	0.0002007	0.0002717	0.73865
AS	PB_DS	SG+DB+HB+SSI	EI+SHE+BS	0.0003103	0.0004195	0.73964
AS	SWS	EWS	LAR	0.0002525	0.0003385	0.74589
AS	SG+DB+HB+SSI	PB_DS	LAR	0.0004141	0.0005517	0.75061
SCO+BAL	EI+SHE+BS	PB_DS	O. hexactis	0.0002489	0.0003299	0.75435
SCO+BAL	O. hexactis	EWS	SWS	0.0001798	0.0002368	0.75950
AL+RS	PB_DS	SG+DB+HB+SSI	BOU	0.0002502	0.0003280	0.76290
SCO+BAL	EWS	BM	O. hexactis	0.0002353	0.0003055	0.77025
PB_DS	BM	O. hexactis	BOU	0.0003245	0.0004211	0.77043
AS	BM	O. hexactis	SG+DB+HB+SSI	0.0002409	0.0003124	0.77093
PB_DS	EI+SHE+BS	O. hexactis	SG+DB+HB+SSI	0.0002149	0.0002774	0.77455
AL+RS	EI+SHE+BS	BM	BOU	0.0001962	0.0002533	0.77460
BM	LAR	BOU	SWS	0.0002781	0.0003561	0.78103
AS	LAR	BM	EI+SHE+BS	0.0003239	0.0004126	0.78505
AS	PB_DS	SG+DB+HB+SSI	BOU	0.0004121	0.0005192	0.79370
SCO+BAL	PB_DS	BM	SG+DB+HB+SSI	0.0003473	0.0004372	0.79423
AS	PB_DS	BM	BOU	0.0005345	0.0006694	0.79857
SCO+BAL	EWS	BM	BOU	0.0003134	0.0003895	0.80468
AL+RS	EWS	O. hexactis	EI+SHE+BS	0.0001183	0.0001448	0.81687
AS	BM	PB_DS	LAR	0.0004930	0.0006009	0.82046
AL+RS	BOU	BM	EI+SHE+BS	0.0002263	0.0002738	0.82654
AS	SCO+BAL	PB_DS	BOU	0.0005488	0.0006605	0.83089
AS	PB_DS	BM	EI+SHE+BS	0.0004327	0.0005042	0.85820
AL+RS	PB_DS	AS	LAR	0.0004296	0.0005005	0.85836
AS	SCO+BAL	PB_DS	O. hexactis	0.0004825	0.0005620	0.85856
AL+RS	EI+SHE+BS	O. hexactis	BOU	0.0001685	0.0001954	0.86243
AL+RS	PB_DS	SCO+BAL	LAR	0.0002736	0.0003146	0.86965
PB_DS	EWS	O. hexactis	LAR	0.0002588	0.0002973	0.87068
PB_DS	EWS	O. hexactis	EI+SHE+BS	0.0002214	0.0002506	0.88340
AS	EWS	O. hexactis	EI+SHE+BS	0.0002653	0.0003002	0.88377
SCO+BAL	PB_DS	BOU	LAR	0.0004537	0.0005081	0.89294
AL+RS	PB_DS	BM	SG+DB+HB+SSI	0.0003148	0.0003489	0.90236
SCO+BAL	BM	PB_DS	SWS	0.0003759	0.0004155	0.90477
AS	SCO+BAL	PB_DS	LAR	0.0005229	0.0005748	0.90968
AL+RS	SCO+BAL	LAR	SWS	0.0002043	0.0002237	0.91305
SCO+BAL	BM	EI+SHE+BS	BOU	0.0002962	0.0003244	0.91318
AS	SCO+BAL	O. hexactis	SG+DB+HB+SSI	0.0002843	0.0003105	0.91561
SCO+BAL	O. hexactis	SG+DB+HB+SSI	BOU	0.0002451	0.0002674	0.91665
PB_DS	EWS	BOU	SWS	0.0003767	0.0004092	0.92066
AS	LAR	SG+DB+HB+SSI	EI+SHE+BS	0.0002804	0.0003027	0.92642
SCO+BAL	LAR	BM	SG+DB+HB+SSI	0.0002683	0.0002892	0.92774
AL+RS	EWS	BM	SWS	0.0001876	0.0002016	0.93032
AS	BM	PB_DS	O. hexactis	0.0005714	0.0006087	0.93880
AL+RS	PB_DS	BOU	EWS	0.0004215	0.0004482	0.94054
SCO+BAL	BOU	BM	EI+SHE+BS	0.0003124	0.0003303	0.94572
AS	EWS	SG+DB+HB+SSI	EI+SHE+BS	0.0003310	0.0003500	0.94574
BM	SWS	SG+DB+HB+SSI	LAR	0.0002463	0.0002573	0.95753
AL+RS	LAR	AS	BOU	0.0002954	0.0003076	0.96026
AL+RS	SG+DB+HB+SSI	BM	EI+SHE+BS	0.0002097	0.0002183	0.96067
PB_DS	BOU	BM	O. hexactis	0.0004336	0.0004490	0.96572
SCO+BAL	EI+SHE+BS	PB_DS	BOU	0.0003771	0.0003901	0.96679
AL+RS	PB_DS	SG+DB+HB+SSI	LAR	0.0003062	0.0003106	0.98584
SCO+BAL	EWS	EI+SHE+BS	BOU	0.0003265	0.0003301	0.98912
AL+RS	EWS	BM	LAR	0.0002172	0.0002188	0.99226
AL+RS	EI+SHE+BS	AS	LAR	0.0002841	0.0002860	0.99332
AS	SG+DB+HB+SSI	O. hexactis	BOU	0.0004190	0.0004195	0.99883
PB_DS	LAR	O. hexactis	EI+SHE+BS	0.0002593	0.0002582	1.00429
AL+RS	BM	PB_DS	EWS	0.0003595	0.0003574	1.00583
AL+RS	AS	PB_DS	LAR	0.0005401	0.0005304	1.01838
SCO+BAL	O. hexactis	BM	EWS	0.0003217	0.0003138	1.02512
AL+RS	BOU	PB_DS	LAR	0.0004619	0.0004485	1.02995
AS	BM	O. hexactis	BOU	0.0004702	0.0004553	1.03288

SCO+BAL	BM	PB_DS	BOU	0.0004929	0.0004768	1.03383
PB_DS	LAR	O. hexactis	SG+DB+HB+SSI	0.0002892	0.0002794	1.03496
AL+RS	BOU	LAR	SWS	0.0002518	0.0002404	1.04747
BM	EWS	O. hexactis	SWS	0.0002712	0.0002570	1.05553
AS	SG+DB+HB+SSI	PB_DS	BM	0.0006899	0.0006521	1.05799
O. hexactis	EI+SHE+BS	SG+DB+HB+SSI	BOU	0.0002189	0.0002058	1.06389
PB_DS	EI+SHE+BS	LAR	SWS	0.0003262	0.0003058	1.06660
AL+RS	LAR	AS	BM	0.0003016	0.0002827	1.06694
AL+RS	LAR	AS	SWS	0.0002630	0.0002464	1.06750
BM	SWS	O. hexactis	EWS	0.0002920	0.0002733	1.06829
AS	BM	SG+DB+HB+SSI	EI+SHE+BS	0.0003806	0.0003561	1.06855
AS	LAR	O. hexactis	EI+SHE+BS	0.0003032	0.0002832	1.07057
AL+RS	LAR	O. hexactis	EI+SHE+BS	0.0001562	0.0001456	1.07309
AL+RS	O. hexactis	AS	SWS	0.0002757	0.0002533	1.08826
SCO+BAL	SG+DB+HB+SSI	BM	EI+SHE+BS	0.0002958	0.0002706	1.09313
AL+RS	PB_DS	EI+SHE+BS	LAR	0.0002788	0.0002550	1.09359
AL+RS	BM	AS	O. hexactis	0.0004365	0.0003965	1.10078
BM	O. hexactis	EWS	LAR	0.0002946	0.0002672	1.10226
SCO+BAL	BM	O. hexactis	SWS	0.0002870	0.0002600	1.10390
SG+DB+HB+SSI	LAR	EI+SHE+BS	SWS	0.0002227	0.0002002	1.11254
AL+RS	PB_DS	BM	EI+SHE+BS	0.0003421	0.0003062	1.11736
PB_DS	BOU	LAR	SWS	0.0003978	0.0003560	1.11752
AL+RS	EI+SHE+BS	LAR	SWS	0.0001801	0.0001601	1.12483
PB_DS	SWS	O. hexactis	SG+DB+HB+SSI	0.0003266	0.0002886	1.13167
SCO+BAL	SG+DB+HB+SSI	BM	SWS	0.0003210	0.0002821	1.13807
AS	EWS	SCO+BAL	LAR	0.0005030	0.0004413	1.13984
AS	BOU	O. hexactis	SG+DB+HB+SSI	0.0003919	0.0003413	1.14817
AL+RS	EWS	AS	PB_DS	0.0004500	0.0003918	1.14863
AL+RS	SG+DB+HB+SSI	AS	SWS	0.0003360	0.0002902	1.15765
AL+RS	LAR	O. hexactis	SG+DB+HB+SSI	0.0001587	0.0001366	1.16184
AL+RS	LAR	BM	SG+DB+HB+SSI	0.0002359	0.0002003	1.17788
AS	EI+SHE+BS	PB_DS	BM	0.0007601	0.0006446	1.17923
AS	O. hexactis	SCO+BAL	EI+SHE+BS	0.0004506	0.0003804	1.18451
SCO+BAL	LAR	EI+SHE+BS	SWS	0.0002479	0.0002085	1.18930
AS	EI+SHE+BS	PB_DS	SG+DB+HB+SSI	0.0006799	0.0005670	1.19907
SCO+BAL	LAR	BM	EI+SHE+BS	0.0003194	0.0002634	1.21284
SCO+BAL	LAR	BM	BOU	0.0004062	0.0003348	1.21327
SCO+BAL	PB_DS	BM	EI+SHE+BS	0.0004282	0.0003523	1.21558
AS	EWS	BM	LAR	0.0005586	0.0004593	1.21631
SCO+BAL	SG+DB+HB+SSI	O. hexactis	BOU	0.0003527	0.0002892	1.21962
SCO+BAL	PB_DS	EI+SHE+BS	BOU	0.0005492	0.0004418	1.24333
AS	BM	EWS	LAR	0.0004787	0.0003804	1.25827
AL+RS	LAR	PB_DS	BOU	0.0004060	0.0003220	1.26076
SCO+BAL	BM	SG+DB+HB+SSI	SWS	0.0003305	0.0002613	1.26488
AS	SCO+BAL	PB_DS	SG+DB+HB+SSI	0.0007668	0.0006048	1.26782
AL+RS	SCO+BAL	AS	SWS	0.0004253	0.0003336	1.27495
PB_DS	EWS	O. hexactis	SWS	0.0003753	0.0002926	1.28266
AS	PB_DS	BOU	EWS	0.0009884	0.0007690	1.28533
AL+RS	O. hexactis	SCO+BAL	EI+SHE+BS	0.0002437	0.0001892	1.28777
AL+RS	O. hexactis	AS	BM	0.0003800	0.0002945	1.29060
SCO+BAL	SG+DB+HB+SSI	EWS	SWS	0.0003058	0.0002365	1.29296
AS	BM	PB_DS	SG+DB+HB+SSI	0.0008123	0.0006277	1.29404
SCO+BAL	BM	O. hexactis	BOU	0.0004040	0.0003119	1.29515
AL+RS	EWS	BOU	SWS	0.0002866	0.0002199	1.30311
AL+RS	PB_DS	BM	O. hexactis	0.0004452	0.0003410	1.30563
AL+RS	PB_DS	BM	BOU	0.0005650	0.0004308	1.31151
AL+RS	LAR	BM	EI+SHE+BS	0.0002334	0.0001778	1.31264
AL+RS	SWS	O. hexactis	SG+DB+HB+SSI	0.0001962	0.0001485	1.32114
SCO+BAL	SWS	EI+SHE+BS	LAR	0.0002720	0.0002052	1.32606
AS	BOU	PB_DS	EI+SHE+BS	0.0008240	0.0006212	1.32653
SCO+BAL	LAR	SG+DB+HB+SSI	SWS	0.0002990	0.0002253	1.32680
AL+RS	LAR	PB_DS	BM	0.0004122	0.0003099	1.33019
AS	EI+SHE+BS	PB_DS	O. hexactis	0.0007314	0.0005488	1.33270
BM	EI+SHE+BS	EWS	LAR	0.0003325	0.0002485	1.33809
AS	PB_DS	EI+SHE+BS	LAR	0.0005297	0.0003950	1.34083
PB_DS	O. hexactis	LAR	SWS	0.0004409	0.0003283	1.34266
AS	PB_DS	O. hexactis	LAR	0.0005736	0.0004259	1.34684
AS	O. hexactis	BM	EI+SHE+BS	0.0005927	0.0004348	1.36306
AL+RS	LAR	PB_DS	SWS	0.0003736	0.0002735	1.36601
SCO+BAL	O. hexactis	BM	LAR	0.0004111	0.0002993	1.37353
BM	SG+DB+HB+SSI	EWS	LAR	0.0003831	0.0002784	1.37597
AS	BOU	SCO+BAL	EI+SHE+BS	0.0005788	0.0004203	1.37725
AL+RS	AS	PB_DS	BM	0.0008816	0.0006397	1.37800
PB_DS	SG+DB+HB+SSI	LAR	SWS	0.0004783	0.0003462	1.38168

AL+RS	BOU	SCO+BAL	EI+SHE+BS	0.0003719	0.0002691	1.38170
AL+RS	AS	PB_DS	EI+SHE+BS	0.0007910	0.0005642	1.40188
AL+RS	EWS	BOU	LAR	0.0003161	0.0002254	1.40281
SCO+BAL	EWS	BOU	SWS	0.0004801	0.0003418	1.40482
AS	O. hexactis	PB_DS	EI+SHE+BS	0.0007753	0.0005509	1.40742
SCO+BAL	SWS	O. hexactis	EWS	0.0003784	0.0002682	1.41083
AS	BOU	EWS	LAR	0.0005714	0.0004047	1.41195
AS	EWS	BOU	LAR	0.0006881	0.0004841	1.42124
SCO+BAL	BM	SG+DB+HB+SSI	BOU	0.0004474	0.0003148	1.42127
AL+RS	EWS	SCO+BAL	PB_DS	0.0004550	0.0003193	1.42489
AS	PB_DS	SCO+BAL	LAR	0.0007314	0.0005096	1.43531
AL+RS	AS	PB_DS	BOU	0.0009121	0.0006349	1.43651
AL+RS	BOU	PB_DS	SWS	0.0007137	0.0004939	1.44495
AL+RS	LAR	AS	O. hexactis	0.0003788	0.0002620	1.44581
SCO+BAL	EWS	SG+DB+HB+SSI	BOU	0.0004281	0.0002957	1.44779
SCO+BAL	PB_DS	O. hexactis	LAR	0.0005332	0.0003679	1.44928
AL+RS	SCO+BAL	AS	BOU	0.0006188	0.0004255	1.45458
AS	SCO+BAL	PB_DS	BM	0.0009917	0.0006816	1.45479
PB_DS	O. hexactis	EI+SHE+BS	BOU	0.0005981	0.0004071	1.46918
AL+RS	SG+DB+HB+SSI	O. hexactis	BOU	0.0003930	0.0002674	1.46985
AL+RS	PB_DS	AS	EWS	0.0007952	0.0005369	1.48112
AL+RS	PB_DS	BM	SWS	0.0004749	0.0003178	1.49455
AL+RS	PB_DS	O. hexactis	EWS	0.0005414	0.0003610	1.49952
BM	EWS	BOU	SWS	0.0005971	0.0003978	1.50102
AS	BM	PB_DS	BOU	0.0010417	0.0006916	1.50626
AS	EI+SHE+BS	PB_DS	BOU	0.0009259	0.0006127	1.51117
PB_DS	SG+DB+HB+SSI	BM	O. hexactis	0.0006359	0.0004188	1.51832
AL+RS	BOU	AS	SCO+BAL	0.0007048	0.0004619	1.52582
PB_DS	BM	O. hexactis	SG+DB+HB+SSI	0.0005072	0.0003298	1.53800
SCO+BAL	PB_DS	SG+DB+HB+SSI	BOU	0.0006302	0.0004019	1.56813
AL+RS	SCO+BAL	AS	O. hexactis	0.0005785	0.0003689	1.56827
PB_DS	O. hexactis	BM	BOU	0.0007581	0.0004829	1.56986
AL+RS	BM	AS	SWS	0.0005703	0.0003607	1.58118
AS	BOU	BM	O. hexactis	0.0008224	0.0005181	1.58738
BM	SWS	SG+DB+HB+SSI	EWS	0.0004725	0.0002911	1.62345
AL+RS	PB_DS	SCO+BAL	EWS	0.0006392	0.0003933	1.62538
AL+RS	AS	BOU	SWS	0.0007182	0.0004400	1.63242
AS	SCO+BAL	O. hexactis	EI+SHE+BS	0.0005137	0.0003123	1.64457
AS	EWS	EI+SHE+BS	LAR	0.0005671	0.0003437	1.64990
AL+RS	AS	PB_DS	O. hexactis	0.0009380	0.0005672	1.65378
SCO+BAL	BM	LAR	SWS	0.0004058	0.0002443	1.66142
AL+RS	BM	O. hexactis	BOU	0.0004443	0.0002671	1.66324
AS	O. hexactis	EI+SHE+BS	BOU	0.0006999	0.0004168	1.67940
AL+RS	PB_DS	SG+DB+HB+SSI	EWS	0.0006718	0.0003998	1.68015
AL+RS	SG+DB+HB+SSI	LAR	SWS	0.0003323	0.0001974	1.68358
AL+RS	AS	SG+DB+HB+SSI	SWS	0.0005563	0.0003298	1.68675
SCO+BAL	SWS	BOU	EWS	0.0005451	0.0003211	1.69736
AS	PB_DS	BM	LAR	0.0009624	0.0005665	1.69894
AL+RS	O. hexactis	LAR	SWS	0.0002948	0.0001734	1.69983
AS	SCO+BAL	PB_DS	EI+SHE+BS	0.0009962	0.0005859	1.70040
AL+RS	AS	SCO+BAL	SWS	0.0006323	0.0003689	1.71402
AL+RS	LAR	PB_DS	O. hexactis	0.0004893	0.0002837	1.72462
AS	SG+DB+HB+SSI	PB_DS	EI+SHE+BS	0.0009902	0.0005735	1.72649
AL+RS	BM	O. hexactis	SG+DB+HB+SSI	0.0003768	0.0002180	1.72824
AS	PB_DS	SG+DB+HB+SSI	LAR	0.0008400	0.0004852	1.73129
AL+RS	PB_DS	BM	LAR	0.0006210	0.0003572	1.73868
PB_DS	SG+DB+HB+SSI	BM	BOU	0.0009091	0.0005207	1.74583
SCO+BAL	O. hexactis	BM	SWS	0.0005016	0.0002865	1.75074
SCO+BAL	EI+SHE+BS	BM	O. hexactis	0.0004804	0.0002740	1.75319
AS	SCO+BAL	EWS	LAR	0.0006839	0.0003893	1.75653
O. hexactis	LAR	EI+SHE+BS	SWS	0.0003345	0.0001893	1.76678
AS	PB_DS	O. hexactis	EWS	0.0011342	0.0006403	1.77133
AL+RS	SWS	PB_DS	LAR	0.0005196	0.0002928	1.77469
AL+RS	AS	PB_DS	SG+DB+HB+SSI	0.0010739	0.0006042	1.77751
AL+RS	SG+DB+HB+SSI	AS	BM	0.0006209	0.0003471	1.78890
AL+RS	EI+SHE+BS	AS	SWS	0.0004643	0.0002577	1.80139
AS	PB_DS	SCO+BAL	EWS	0.0012920	0.0007164	1.80353
AS	PB_DS	EI+SHE+BS	EWS	0.0010903	0.0006034	1.80699
SCO+BAL	EWS	BOU	LAR	0.0007139	0.0003948	1.80840
AL+RS	BOU	AS	BM	0.0008503	0.0004679	1.81720
BM	SWS	BOU	LAR	0.0006364	0.0003490	1.82372
SCO+BAL	O. hexactis	PB_DS	SG+DB+HB+SSI	0.0006814	0.0003701	1.84130
AL+RS	PB_DS	EI+SHE+BS	EWS	0.0006444	0.0003431	1.87830
SCO+BAL	LAR	BM	O. hexactis	0.0005299	0.0002808	1.88700

SCO+BAL	EI+SHE+BS	SG+DB+HB+SSI	BOU	0.0004640	0.0002459	1.88707
BM	LAR	O. hexactis	EWS	0.0006163	0.0003262	1.88935
PB_DS	BM	O. hexactis	EI+SHE+BS	0.0005775	0.0003054	1.89107
AL+RS	EWS	EI+SHE+BS	SWS	0.0002867	0.0001509	1.90036
O. hexactis	SG+DB+HB+SSI	EI+SHE+BS	BOU	0.0004434	0.0002316	1.91442
SCO+BAL	SWS	BM	EWS	0.0005929	0.0003092	1.91796
SCO+BAL	PB_DS	BM	BOU	0.0009774	0.0005080	1.92396
SG+DB+HB+SSI	SWS	EI+SHE+BS	LAR	0.0003748	0.0001936	1.93599
AS	EWS	SCO+BAL	PB_DS	0.0014530	0.0007480	1.94255
AL+RS	BM	AS	BOU	0.0008807	0.0004532	1.94344
AS	BM	PB_DS	EI+SHE+BS	0.0011929	0.0006134	1.94468
AS	BM	O. hexactis	EI+SHE+BS	0.0006214	0.0003185	1.95130
SCO+BAL	EI+SHE+BS	BM	BOU	0.0006086	0.0003116	1.95337
AL+RS	EWS	EI+SHE+BS	LAR	0.0003163	0.0001615	1.95802
AL+RS	AS	BM	SWS	0.0007487	0.0003817	1.96122
AS	PB_DS	SG+DB+HB+SSI	EWS	0.0014005	0.0007070	1.98088
SCO+BAL	BOU	PB_DS	O. hexactis	0.0008470	0.0004271	1.98326
SCO+BAL	BOU	PB_DS	SG+DB+HB+SSI	0.0009546	0.0004797	1.99001
AL+RS	LAR	AS	SG+DB+HB+SSI	0.0005375	0.0002690	1.99836
BM	EWS	SG+DB+HB+SSI	SWS	0.0005778	0.0002891	1.99849
PB_DS	SWS	EWS	LAR	0.0008130	0.0004057	2.00379
AL+RS	BM	AS	SG+DB+HB+SSI	0.0008133	0.0004056	2.00499
AL+RS	SCO+BAL	O. hexactis	EI+SHE+BS	0.0003667	0.0001824	2.00988
PB_DS	BOU	O. hexactis	SG+DB+HB+SSI	0.0006583	0.0003244	2.02896
AL+RS	BOU	O. hexactis	SG+DB+HB+SSI	0.0005279	0.0002598	2.03214
AL+RS	EWS	SG+DB+HB+SSI	LAR	0.0003643	0.0001791	2.03458
SCO+BAL	PB_DS	SG+DB+HB+SSI	SWS	0.0007336	0.0003604	2.03573
AL+RS	LAR	AS	EI+SHE+BS	0.0005350	0.0002604	2.05423
AL+RS	EWS	SG+DB+HB+SSI	SWS	0.0003348	0.0001625	2.05969
AL+RS	SWS	PB_DS	BOU	0.0008038	0.0003869	2.07733
SCO+BAL	PB_DS	EI+SHE+BS	SWS	0.0006526	0.0003135	2.08160
AL+RS	LAR	EWS	SWS	0.0004179	0.0002006	2.08312
AS	SG+DB+HB+SSI	SCO+BAL	O. hexactis	0.0008392	0.0004020	2.08770
SCO+BAL	LAR	BM	SWS	0.0005673	0.0002690	2.10907
AL+RS	SWS	EWS	LAR	0.0004474	0.0002115	2.11572
SCO+BAL	O. hexactis	BM	EI+SHE+BS	0.0005882	0.0002759	2.13194
AL+RS	LAR	PB_DS	SG+DB+HB+SSI	0.0006481	0.0003034	2.13611
PB_DS	BM	LAR	SWS	0.0007561	0.0003538	2.13725
SCO+BAL	LAR	BOU	EWS	0.0008264	0.0003864	2.13867
AL+RS	SCO+BAL	O. hexactis	SG+DB+HB+SSI	0.0004202	0.0001965	2.13869
AL+RS	O. hexactis	PB_DS	LAR	0.0006651	0.0003109	2.13927
AS	BOU	PB_DS	O. hexactis	0.0013295	0.0006196	2.14591
AL+RS	O. hexactis	AS	SCO+BAL	0.0006385	0.0002963	2.15518
SCO+BAL	LAR	O. hexactis	EWS	0.0007027	0.0003226	2.17867
AS	O. hexactis	EWS	LAR	0.0007732	0.0003543	2.18269
AS	PB_DS	BM	EWS	0.0015230	0.0006974	2.18373
PB_DS	BOU	BM	SG+DB+HB+SSI	0.0010919	0.0004975	2.19483
AS	BOU	BM	SG+DB+HB+SSI	0.0012143	0.0005513	2.20259
SCO+BAL	SWS	SG+DB+HB+SSI	EWS	0.0006024	0.0002718	2.21654
AL+RS	BM	O. hexactis	EI+SHE+BS	0.0004744	0.0002126	2.23204
SCO+BAL	PB_DS	BM	O. hexactis	0.0008979	0.0004017	2.23554
AS	EWS	SG+DB+HB+SSI	LAR	0.0008981	0.0004015	2.23682
AS	SG+DB+HB+SSI	BM	O. hexactis	0.0010247	0.0004565	2.24451
PB_DS	LAR	EWS	SWS	0.0009295	0.0004128	2.25160
AS	O. hexactis	SCO+BAL	BOU	0.0011506	0.0005103	2.25455
AS	EWS	O. hexactis	LAR	0.0008325	0.0003686	2.25872
AL+RS	BM	AS	EI+SHE+BS	0.0009109	0.0004021	2.26533
AL+RS	AS	O. hexactis	SWS	0.0006923	0.0003034	2.28155
PB_DS	BM	EWS	LAR	0.0010392	0.0004548	2.28513
AS	EI+SHE+BS	EWS	LAR	0.0008111	0.0003527	2.29968
AL+RS	O. hexactis	BM	EI+SHE+BS	0.0005021	0.0002174	2.31007
SCO+BAL	EWS	O. hexactis	SWS	0.0005582	0.0002402	2.32366
AL+RS	LAR	AS	SCO+BAL	0.0006789	0.0002916	2.32838
BM	SWS	BOU	EWS	0.0008626	0.0003695	2.33430
BM	SWS	EI+SHE+BS	LAR	0.0004986	0.0002125	2.34691
AL+RS	LAR	PB_DS	EI+SHE+BS	0.0006455	0.0002746	2.35126
SCO+BAL	PB_DS	BOU	EWS	0.0016982	0.0007185	2.36348
O. hexactis	SWS	EI+SHE+BS	LAR	0.0004491	0.0001895	2.37038
AS	O. hexactis	BM	BOU	0.0012926	0.0005440	2.37605
AS	SG+DB+HB+SSI	SCO+BAL	BOU	0.0012582	0.0005269	2.38794
PB_DS	SG+DB+HB+SSI	EI+SHE+BS	BOU	0.0010415	0.0004346	2.39634

AS	BOU	SCO+BAL	O. hexactis	0.0010843	0.0004512	2.40315
AL+RS	BM	EWS	LAR	0.0006736	0.0002793	2.41190
SCO+BAL	O. hexactis	PB_DS	BOU	0.0009265	0.0003826	2.42189
PB_DS	BOU	EWS	LAR	0.0011320	0.0004668	2.42505
AL+RS	BOU	EWS	LAR	0.0007664	0.0003157	2.42744
AS	SG+DB+HB+SSI	EWS	LAR	0.0008617	0.0003529	2.44202
AL+RS	PB_DS	BM	EWS	0.0009866	0.0004039	2.44255
AS	O. hexactis	PB_DS	BOU	0.0014753	0.0006030	2.44654
AL+RS	SG+DB+HB+SSI	PB_DS	LAR	0.0009542	0.0003877	2.46142
BM	EWS	EI+SHE+BS	SWS	0.0006273	0.0002544	2.46580
AL+RS	SCO+BAL	AS	EI+SHE+BS	0.0009452	0.0003810	2.48054
AL+RS	BOU	AS	EI+SHE+BS	0.0010766	0.0004316	2.49433
AL+RS	BOU	PB_DS	BM	0.0013887	0.0005506	2.52212
AS	SG+DB+HB+SSI	EI+SHE+BS	BOU	0.0011434	0.0004492	2.54536
AS	SG+DB+HB+SSI	BM	BOU	0.0014437	0.0005661	2.55007
AL+RS	EWS	O. hexactis	LAR	0.0004346	0.0001701	2.55446
AL+RS	SCO+BAL	AS	BM	0.0010312	0.0004030	2.55897
AL+RS	EWS	O. hexactis	SWS	0.0004050	0.0001581	2.56202
AS	O. hexactis	PB_DS	SG+DB+HB+SSI	0.0014482	0.0005637	2.56933
SCO+BAL	PB_DS	SG+DB+HB+SSI	LAR	0.0010839	0.0004211	2.57411
BM	O. hexactis	EI+SHE+BS	BOU	0.0008511	0.0003292	2.58577
BM	LAR	SG+DB+HB+SSI	EWS	0.0008344	0.0003204	2.60405
AS	BOU	PB_DS	SG+DB+HB+SSI	0.0017214	0.0006606	2.60598
AL+RS	SG+DB+HB+SSI	AS	EI+SHE+BS	0.0008306	0.0003157	2.63113
AL+RS	SCO+BAL	AS	SG+DB+HB+SSI	0.0009988	0.0003782	2.64081
AL+RS	SG+DB+HB+SSI	AS	SCO+BAL	0.0009228	0.0003494	2.64107
AL+RS	SCO+BAL	PB_DS	LAR	0.0010630	0.0004023	2.64209
PB_DS	O. hexactis	BM	SG+DB+HB+SSI	0.0011432	0.0004300	2.65876
AL+RS	SCO+BAL	PB_DS	BOU	0.0014608	0.0005465	2.67298
SCO+BAL	SWS	EI+SHE+BS	EWS	0.0007035	0.0002630	2.67442
AS	O. hexactis	BM	SG+DB+HB+SSI	0.0012656	0.0004730	2.67556
EI+SHE+BS	SWS	BOU	LAR	0.0006294	0.0002335	2.69601
AL+RS	BM	PB_DS	LAR	0.0010332	0.0003820	2.70490
AL+RS	BM	AS	SCO+BAL	0.0011476	0.0004238	2.70828
SCO+BAL	EWS	O. hexactis	LAR	0.0007921	0.0002918	2.71471
SCO+BAL	PB_DS	BM	SWS	0.0010808	0.0003964	2.72692
AS	O. hexactis	SCO+BAL	SG+DB+HB+SSI	0.0011235	0.0004119	2.72752
AL+RS	BM	LAR	SWS	0.0006101	0.0002236	2.72851
AL+RS	O. hexactis	PB_DS	SWS	0.0009599	0.0003518	2.72867
AL+RS	O. hexactis	PB_DS	BM	0.0010642	0.0003897	2.73084
AL+RS	AS	EI+SHE+BS	SWS	0.0008393	0.0003072	2.73160
AL+RS	SWS	PB_DS	O. hexactis	0.0009302	0.0003379	2.75298
BM	SWS	EI+SHE+BS	EWS	0.0007248	0.0002621	2.76536
SCO+BAL	EWS	BM	SWS	0.0007935	0.0002856	2.77890
SCO+BAL	LAR	SG+DB+HB+SSI	EWS	0.0009642	0.0003448	2.79634
PB_DS	BOU	EWS	SWS	0.0015298	0.0005469	2.79699
AL+RS	BOU	EWS	SWS	0.0010182	0.0003625	2.80907
AL+RS	SCO+BAL	PB_DS	SWS	0.0012673	0.0004503	2.81417
BM	LAR	BOU	EWS	0.0011439	0.0004038	2.83288
AL+RS	BOU	BM	O. hexactis	0.0008788	0.0003100	2.83465
EI+SHE+BS	LAR	BOU	SWS	0.0007010	0.0002449	2.86307
AL+RS	AS	PB_DS	SWS	0.0016302	0.0005658	2.88150
BM	EWS	BOU	LAR	0.0012367	0.0004271	2.89578
AL+RS	SG+DB+HB+SSI	PB_DS	SWS	0.0012865	0.0004348	2.95913
AL+RS	SWS	PB_DS	SG+DB+HB+SSI	0.0011264	0.0003796	2.96735
SCO+BAL	LAR	EI+SHE+BS	EWS	0.0009132	0.0003075	2.96957
AS	SG+DB+HB+SSI	PB_DS	O. hexactis	0.0017146	0.0005716	2.99986
O. hexactis	EI+SHE+BS	BOU	SWS	0.0006941	0.0002310	3.00431
SCO+BAL	PB_DS	O. hexactis	EWS	0.0017777	0.0005880	3.02337
SCO+BAL	PB_DS	EI+SHE+BS	LAR	0.0010030	0.0003312	3.02805
AL+RS	AS	EWS	SWS	0.0012851	0.0004239	3.03158
AL+RS	SCO+BAL	PB_DS	O. hexactis	0.0014205	0.0004670	3.04172
BM	LAR	EI+SHE+BS	EWS	0.0009345	0.0003071	3.04295
AL+RS	SWS	PB_DS	EI+SHE+BS	0.0009717	0.0003188	3.04822
BM	EWS	O. hexactis	LAR	0.0009109	0.0002976	3.06035
SCO+BAL	EWS	BM	LAR	0.0010273	0.0003323	3.09138
AL+RS	O. hexactis	AS	EI+SHE+BS	0.0008821	0.0002844	3.10207
PB_DS	SG+DB+HB+SSI	EWS	LAR	0.0014223	0.0004573	3.11032
O. hexactis	EI+SHE+BS	BOU	EWS	0.0007708	0.0002468	3.12305
AS	BOU	SCO+BAL	SG+DB+HB+SSI	0.0014762	0.0004683	3.15263
PB_DS	O. hexactis	EWS	LAR	0.0013338	0.0004225	3.15673
AL+RS	SCO+BAL	EWS	LAR	0.0008789	0.0002779	3.16233
AL+RS	SG+DB+HB+SSI	SCO+BAL	O. hexactis	0.0007793	0.0002417	3.22471
SCO+BAL	PB_DS	BM	LAR	0.0014312	0.0004432	3.22897
AL+RS	SCO+BAL	EWS	SWS	0.0010831	0.0003330	3.25254

AS	SG+DB+HB+SSI	PB_DS	BOU	0.0021336	0.0006540	3.26247
AL+RS	EI+SHE+BS	PB_DS	LAR	0.0009244	0.0002831	3.26492
AL+RS	EI+SHE+BS	AS	BM	0.0010015	0.0003062	3.27017
EI+SHE+BS	EWS	BOU	SWS	0.0010200	0.0003119	3.27028
AL+RS	BOU	PB_DS	EI+SHE+BS	0.0016150	0.0004925	3.27927
PB_DS	EI+SHE+BS	EWS	LAR	0.0013717	0.0004109	3.33865
AL+RS	SWS	PB_DS	BM	0.0011683	0.0003499	3.33903
SG+DB+HB+SSI	EWS	EI+SHE+BS	SWS	0.0007814	0.0002303	3.39248
SCO+BAL	EWS	SG+DB+HB+SSI	LAR	0.0011421	0.0003365	3.39358
SCO+BAL	EWS	EI+SHE+BS	SWS	0.0008066	0.0002375	3.39561
SCO+BAL	EWS	SG+DB+HB+SSI	SWS	0.0009082	0.0002642	3.43717
SCO+BAL	PB_DS	SG+DB+HB+SSI	EWS	0.0023284	0.0006741	3.45387
SCO+BAL	LAR	BM	EWS	0.0012326	0.0003566	3.45644
AL+RS	SCO+BAL	PB_DS	SG+DB+HB+SSI	0.0018407	0.0005322	3.45875
SCO+BAL	BOU	BM	SG+DB+HB+SSI	0.0014392	0.0004139	3.47668
AL+RS	SG+DB+HB+SSI	PB_DS	BM	0.0015715	0.0004511	3.48338
O. hexactis	EI+SHE+BS	BOU	LAR	0.0008087	0.0002320	3.48585
SCO+BAL	SG+DB+HB+SSI	PB_DS	O. hexactis	0.0012321	0.0003511	3.50885
SCO+BAL	BOU	BM	O. hexactis	0.0013315	0.0003792	3.51172
AL+RS	EI+SHE+BS	PB_DS	SWS	0.0011045	0.0003144	3.51315
BM	SG+DB+HB+SSI	EI+SHE+BS	BOU	0.0012946	0.0003675	3.52294
AL+RS	AS	LAR	SWS	0.0010901	0.0003085	3.53384
AL+RS	EI+SHE+BS	AS	BOU	0.0011977	0.0003389	3.53402
AL+RS	EI+SHE+BS	AS	O. hexactis	0.0010291	0.0002900	3.54860
PB_DS	SG+DB+HB+SSI	EWS	SWS	0.0019006	0.0005351	3.55223
SG+DB+HB+SSI	EI+SHE+BS	BOU	SWS	0.0010257	0.0002876	3.56624
PB_DS	BM	EWS	SWS	0.0017954	0.0005009	3.58397
AL+RS	BM	PB_DS	O. hexactis	0.0015094	0.0004202	3.59264
AL+RS	EI+SHE+BS	AS	SCO+BAL	0.0011522	0.0003167	3.63861
AL+RS	BOU	SCO+BAL	O. hexactis	0.0010243	0.0002810	3.64554
EI+SHE+BS	EWS	BOU	LAR	0.0012297	0.0003359	3.66057
PB_DS	EI+SHE+BS	EWS	SWS	0.0016979	0.0004620	3.67506
BM	EWS	SG+DB+HB+SSI	LAR	0.0012174	0.0003296	3.69396
SG+DB+HB+SSI	EI+SHE+BS	BOU	EWS	0.0012284	0.0003315	3.70561
AL+RS	EI+SHE+BS	AS	SG+DB+HB+SSI	0.0011136	0.0003002	3.70954
PB_DS	O. hexactis	EWS	SWS	0.0017746	0.0004777	3.71536
AL+RS	O. hexactis	EI+SHE+BS	BOU	0.0008210	0.0002175	3.77525
SCO+BAL	SG+DB+HB+SSI	PB_DS	BOU	0.0015848	0.0004165	3.80483
AL+RS	SCO+BAL	PB_DS	BM	0.0018732	0.0004912	3.81340
O. hexactis	SWS	SG+DB+HB+SSI	EI+SHE+BS	0.0008012	0.0002099	3.81625
O. hexactis	EWS	EI+SHE+BS	SWS	0.0008932	0.0002311	3.86579
AL+RS	BOU	BM	SG+DB+HB+SSI	0.0014067	0.0003631	3.87464
AL+RS	BM	PB_DS	BOU	0.0019537	0.0005018	3.89383
AL+RS	SG+DB+HB+SSI	EWS	LAR	0.0010567	0.0002702	3.91128
O. hexactis	EWS	SG+DB+HB+SSI	EI+SHE+BS	0.0010039	0.0002565	3.91333
AL+RS	SG+DB+HB+SSI	SCO+BAL	BOU	0.0011723	0.0002982	3.93102
SG+DB+HB+SSI	SWS	EI+SHE+BS	EWS	0.0009841	0.0002497	3.94051
AL+RS	SCO+BAL	PB_DS	EI+SHE+BS	0.0017872	0.0004458	4.00936
SCO+BAL	EWS	EI+SHE+BS	LAR	0.0010404	0.0002578	4.03606
AL+RS	BOU	AS	O. hexactis	0.0017291	0.0004261	4.05808
AL+RS	BM	PB_DS	SWS	0.0016432	0.0004048	4.05939
SG+DB+HB+SSI	LAR	EI+SHE+BS	EWS	0.0011938	0.0002912	4.09957
SCO+BAL	PB_DS	EI+SHE+BS	EWS	0.0022474	0.0005443	4.12916
O. hexactis	SWS	EI+SHE+BS	EWS	0.0009699	0.0002341	4.14312
SCO+BAL	O. hexactis	EI+SHE+BS	BOU	0.0011474	0.0002767	4.14732
AL+RS	SG+DB+HB+SSI	PB_DS	EI+SHE+BS	0.0017812	0.0004290	4.15232
AL+RS	O. hexactis	EWS	LAR	0.0009682	0.0002327	4.16167
AL+RS	SG+DB+HB+SSI	BM	O. hexactis	0.0010811	0.0002597	4.16325
SG+DB+HB+SSI	EI+SHE+BS	BOU	LAR	0.0011778	0.0002806	4.19710
AL+RS	SG+DB+HB+SSI	EWS	SWS	0.0013890	0.0003307	4.20046
AL+RS	BM	PB_DS	SG+DB+HB+SSI	0.0018862	0.0004476	4.21424
AL+RS	BM	EWS	SWS	0.0012837	0.0003009	4.26693
AL+RS	BOU	PB_DS	O. hexactis	0.0022675	0.0005249	4.32025
AL+RS	O. hexactis	PB_DS	EI+SHE+BS	0.0015663	0.0003599	4.35264
SCO+BAL	PB_DS	BM	EWS	0.0026756	0.0006076	4.40386
O. hexactis	EI+SHE+BS	SG+DB+HB+SSI	EWS	0.0009897	0.0002223	4.45155
O. hexactis	LAR	EI+SHE+BS	EWS	0.0011796	0.0002641	4.46686
EI+SHE+BS	SWS	BOU	EWS	0.0011881	0.0002658	4.47052
SG+DB+HB+SSI	EWS	EI+SHE+BS	LAR	0.0011432	0.0002541	4.49927
AL+RS	EI+SHE+BS	PB_DS	BM	0.0016417	0.0003634	4.51742
BM	EWS	EI+SHE+BS	LAR	0.0012670	0.0002770	4.57332
AL+RS	SG+DB+HB+SSI	EI+SHE+BS	BOU	0.0012644	0.0002715	4.65783
AL+RS	O. hexactis	SCO+BAL	BOU	0.0010647	0.0002280	4.67000
AL+RS	SG+DB+HB+SSI	BM	BOU	0.0014742	0.0003150	4.68053

AL+RS	EI+SHE+BS	EWS	LAR	0.0010061	0.0002142	4.69751
O. hexactis	EI+SHE+BS	SG+DB+HB+SSI	SWS	0.0009130	0.0001940	4.70557
AL+RS	BM	PB_DS	EI+SHE+BS	0.0019839	0.0004208	4.71465
SCO+BAL	O. hexactis	BM	SG+DB+HB+SSI	0.0014904	0.0003150	4.73198
AL+RS	BOU	AS	SG+DB+HB+SSI	0.0022569	0.0004755	4.74642
O. hexactis	EWS	EI+SHE+BS	LAR	0.0012175	0.0002564	4.74805
AL+RS	EI+SHE+BS	PB_DS	SG+DB+HB+SSI	0.0017538	0.0003670	4.77865
AL+RS	BOU	PB_DS	SG+DB+HB+SSI	0.0027954	0.0005840	4.78687
AL+RS	O. hexactis	EWS	SWS	0.0012630	0.0002620	4.82144
AL+RS	EI+SHE+BS	PB_DS	BOU	0.0018379	0.0003799	4.83837
AL+RS	EI+SHE+BS	EWS	SWS	0.0011863	0.0002442	4.85879
SCO+BAL	O. hexactis	BM	BOU	0.0017355	0.0003509	4.94633
AL+RS	EI+SHE+BS	PB_DS	O. hexactis	0.0016694	0.0003373	4.94906
O. hexactis	LAR	SG+DB+HB+SSI	EI+SHE+BS	0.0009533	0.0001914	4.97987
EI+SHE+BS	LAR	BOU	EWS	0.0014694	0.0002941	4.99630
AL+RS	BOU	SCO+BAL	SG+DB+HB+SSI	0.0015522	0.0003107	4.99660
SCO+BAL	SG+DB+HB+SSI	BM	O. hexactis	0.0015339	0.0003068	4.99911
SCO+BAL	SG+DB+HB+SSI	BM	BOU	0.0018866	0.0003748	5.03301
AL+RS	O. hexactis	AS	BOU	0.0017031	0.0003381	5.03689
AL+RS	SG+DB+HB+SSI	AS	BOU	0.0020951	0.0004097	5.11345
SCO+BAL	SG+DB+HB+SSI	EI+SHE+BS	BOU	0.0015908	0.0003049	5.21764
AL+RS	O. hexactis	BM	BOU	0.0013231	0.0002530	5.22946
AL+RS	SG+DB+HB+SSI	AS	O. hexactis	0.0017020	0.0003227	5.27403
O. hexactis	EI+SHE+BS	SG+DB+HB+SSI	LAR	0.0010276	0.0001939	5.30125
O. hexactis	SWS	BOU	LAR	0.0014381	0.0002698	5.32994
O. hexactis	LAR	BOU	SWS	0.0013951	0.0002580	5.40720
SG+DB+HB+SSI	LAR	BOU	SWS	0.0017267	0.0003193	5.40723
AL+RS	O. hexactis	PB_DS	BOU	0.0023873	0.0004340	5.50060
SG+DB+HB+SSI	EWS	BOU	SWS	0.0020457	0.0003649	5.60566
O. hexactis	EWS	BOU	LAR	0.0020384	0.0003628	5.61916
AL+RS	SG+DB+HB+SSI	PB_DS	BOU	0.0030456	0.0005386	5.65500
O. hexactis	SWS	SG+DB+HB+SSI	LAR	0.0012503	0.0002210	5.65865
O. hexactis	EWS	BOU	SWS	0.0017140	0.0003027	5.66170
AL+RS	SG+DB+HB+SSI	PB_DS	O. hexactis	0.0026526	0.0004674	5.67501
SG+DB+HB+SSI	EWS	BOU	LAR	0.0024075	0.0004208	5.72070
AL+RS	O. hexactis	BM	SG+DB+HB+SSI	0.0014579	0.0002534	5.75270
SG+DB+HB+SSI	SWS	BOU	LAR	0.0018072	0.0003083	5.86269
AL+RS	O. hexactis	SCO+BAL	SG+DB+HB+SSI	0.0011995	0.0002015	5.95240
AL+RS	O. hexactis	PB_DS	SG+DB+HB+SSI	0.0025222	0.0004207	5.99572
AL+RS	O. hexactis	AS	SG+DB+HB+SSI	0.0018380	0.0002953	6.22339
O. hexactis	LAR	SG+DB+HB+SSI	SWS	0.0012878	0.0002054	6.27027
SG+DB+HB+SSI	LAR	BOU	EWS	0.0026978	0.0004087	6.60093
O. hexactis	EWS	SG+DB+HB+SSI	LAR	0.0022214	0.0003240	6.85610
O. hexactis	LAR	BOU	EWS	0.0022402	0.0003206	6.98801
SG+DB+HB+SSI	SWS	BOU	EWS	0.0024165	0.0003362	7.18805
O. hexactis	LAR	SG+DB+HB+SSI	EWS	0.0021329	0.0002944	7.24553
O. hexactis	SWS	BOU	EWS	0.0019589	0.0002676	7.31937
O. hexactis	SWS	SG+DB+HB+SSI	EWS	0.0017711	0.0002415	7.33397
O. hexactis	EWS	SG+DB+HB+SSI	SWS	0.0018971	0.0002536	7.48131

Supplementary Table 4.4 Results of the three-population test (*f*3-statistic) from *TreeMix* analysis of *Ophionotus hexactis* with *O. victoriae* used as outgroup. Significant negative Z-score (< -3) indicates population A is admixed between two source populations of B and C. Abbreviations represent different geographical locations; BM = Bransfield Mouth, SG = South Georgia, SR = Shag Rocks, HI = Heard Island.

Population A	Population B	Population C	*f*3-statistic	Standard Error	Z-score
SG	O. victoriae	SR	-0.0004022	0.00021401	-1.87949
SG	BM	SR	-0.0004466	0.00024175	-1.84731
SR	SG	HI	-0.0003674	0.00024448	-1.50274
SG	O. victoriae	HI	-0.0003492	0.00024241	-1.44072
SR	O. victoriae	HI	-0.0003144	0.00024576	-1.27932
SG	BM	HI	-0.0002609	0.00027289	-0.95606
SG	SR	HI	-0.0002078	0.00024954	-0.83271
SR	O. victoriae	SG	-0.0001730	0.00024763	-0.69844
SR	BM	HI	-0.0001817	0.00028160	-0.64520
SR	BM	SG	-0.0001286	0.00026835	-0.47918
HI	BM	SR	0.0000321	0.00028294	0.11356
HI	O. victoriae	SR	0.0001649	0.00027939	0.59005
HI	SG	SR	0.0002178	0.00027240	0.79967
HI	BM	SG	0.0002709	0.00028477	0.95140
HI	O. victoriae	SG	0.0003593	0.00026990	1.33116
BM	O. victoriae	HI	0.0005262	0.00029230	1.80038
BM	O. victoriae	SG	0.0006146	0.00028891	2.12733
BM	O. victoriae	SR	0.0006590	0.00028717	2.29465
SG	O. victoriae	BM	0.0008658	0.00029434	2.94158
SR	O. victoriae	BM	0.0011395	0.00031462	3.62173
HI	O. victoriae	BM	0.0014860	0.00033271	4.46640
BM	SG	HI	0.0017413	0.00035495	4.90576
BM	SG	SR	0.0019270	0.00035963	5.35832
BM	SR	HI	0.0019801	0.00036078	5.48841
O. victoriae	BM	SR	0.0020028	0.00029785	6.72417
O. victoriae	BM	SG	0.0020472	0.00029044	7.04846
O. victoriae	BM	HI	0.0021355	0.00030214	7.06804
O. victoriae	SR	HI	0.0034567	0.00035273	9.79967
O. victoriae	SG	HI	0.0032622	0.00032554	10.02080
O. victoriae	SG	SR	0.0033152	0.00032762	10.11910

Supplementary Table 4.5 Results of the four-population test (*f*4-statistic) from *TreeMix* analysis of *Ophionotus hexactis* with *O. victoriae* used as outgroup. Significant negative Z-score (< -3) indicates gene flow between either population A and D, or population B and C. Significant positive Z-score (> 3) indicates gene flow between either population A and C, or population B and D. Abbreviations represent different geographical locations; BM = Bransfield Mouth, SG = South Georgia, SR = Shag Rocks, HI = Heard Island.

Population A	Population B	Population C	Population D	*f*4-statistic	Standard Error	Z-score
BM	SG	SR	HI	-0.0001857	0.00023218	-0.799814
O. victoriae	SG	SR	HI	-0.0000530	0.00019942	-0.265644
O. victoriae	BM	SG	SR	-0.0000444	0.00018001	-0.246481
BM	SR	SG	HI	0.0000531	0.00025514	0.208130
O. victoriae	BM	SG	HI	0.0000884	0.00020098	0.439611
O. victoriae	SR	SG	HI	0.0001415	0.00021983	0.643485
O. victoriae	BM	SR	HI	0.0001327	0.00018860	0.703704
O. victoriae	HI	SG	SR	0.0001944	0.00021393	0.908830
BM	HI	SG	SR	0.0002388	0.00023486	1.016760
O. victoriae	HI	BM	SG	0.0011267	0.00025794	4.368140
O. victoriae	SG	BM	HI	0.0012151	0.00026104	4.654640
O. victoriae	HI	BM	SR	0.0013211	0.00027520	4.800680
O. victoriae	SG	BM	SR	0.0012680	0.00025793	4.916140
O. victoriae	SR	BM	SG	0.0013124	0.00025129	5.222610
O. victoriae	SR	BM	HI	0.0014539	0.00026482	5.489910

Supplementary Table 4.6 List of loci under selection identified by two or more outlier loci detection methods (PCAdapt, OutFLANK, BayeScan, RDA). Abbreviations: surface water salinity (sal_surface), bottom water salinity (sal_bottom), surface water temperature (temp_surface), bottom water temperature (temp_bottom), water depth (depth).

Locus ID	Dataset	Methods	Relevant environmental predictor identified by RDA (if applicable)
CLocus-1425		PCAdapt; RDA	temp_bottom
CLocus-14020		PCAdapt; OutFLANK; RDA	sal_bottom
CLocus-18227		PCAdapt; OutFLANK; RDA; BayeScan	sal_bottom
CLocus-52370		PCAdapt; OutFLANK; RDA	sal_bottom
CLocus-59826		PCAdapt; OutFLANK; RDA	sal_surface
CLocus-65173		PCAdapt; OutFLANK; RDA	sal_bottom
CLocus-72907		PCAdapt; OutFLANK; RDA	sal_bottom
CLocus-72989		PCAdapt; RDA	sal_surface
CLocus-73391		PCAdapt; OutFLANK; RDA; BayeScan	sal_bottom
CLocus-80182		PCAdapt; OutFLANK; RDA	sal_bottom
CLocus-88903		PCAdapt; OutFLANK; RDA	sal_bottom
CLocus-91063		PCAdapt; OutFLANK; RDA	sal_bottom
CLocus-103005		PCAdapt; OutFLANK; RDA; BayeScan	sal_bottom
CLocus-103979	*O. victoriae* VS *O. hexactis*	PCAdapt; RDA	sal_bottom
CLocus-107002		PCAdapt; OutFLANK	
CLocus-116178		PCAdapt; OutFLANK	
CLocus-122893		PCAdapt; OutFLANK; RDA	sal_bottom
CLocus-129923		PCAdapt; OutFLANK; RDA	temp_bottom
CLocus-137010		PCAdapt; OutFLANK; RDA; BayeScan	sal_bottom
CLocus-137845		PCAdapt; RDA	sal_surface
CLocus-142100		PCAdapt; RDA	temp_bottom
CLocus-145027		PCAdapt; OutFLANK; RDA	temp_bottom
CLocus-145213		PCAdapt; RDA	
CLocus-154402		PCAdapt; OutFLANK	
CLocus-156412		PCAdapt; OutFLANK	
CLocus-161631		PCAdapt; RDA	sal_surface
CLocus-186281		PCAdapt; OutFLANK	
CLocus-69131		OutFLANK; RDA	sal_surface
CLocus-72338		OutFLANK; RDA	sal_bottom
CLocus-25405	>1000 m VS <1000 m VS islands within *O. victoriae*	PCAdapt; BayeScan	
CLocus-94437		PCAdapt; BayeScan	
CLocus-123481		PCAdapt; BayeScan	
CLocus-137845		PCAdapt; RDA; BayeScan	sal_surface
CLocus-140312		PCAdapt; RDA	
CLocus-161631		PCAdapt; RDA	sal_surface
CLocus-14020		OutFLANK; RDA	sal_bottom
CLocus-18227		OutFLANK; RDA	sal_bottom
CLocus-52370		OutFLANK; RDA	sal_bottom
CLocus-59826		OutFLANK; RDA	sal_surface
CLocus-65173		OutFLANK; RDA	sal_bottom
CLocus-69131		OutFLANK; RDA	sal_surface
CLocus-72338		OutFLANK; RDA	sal_bottom
CLocus-72907		OutFLANK; RDA	sal_bottom
CLocus-73391		OutFLANK; RDA	sal_bottom
CLocus-80182		OutFLANK; RDA	sal_bottom
CLocus-88903		OutFLANK; RDA	sal_bottom
CLocus-91063		OutFLANK; RDA	sal_bottom
CLocus-103005		OutFLANK; RDA	sal_bottom
CLocus-122893		OutFLANK; RDA	sal_bottom
CLocus-129923		OutFLANK; RDA	temp_bottom
CLocus-137010		OutFLANK; RDA	sal_bottom
CLocus-145027		OutFLANK; RDA	temp_bottom
CLocus-67226		RDA; BayeScan	depth
CLocus-62747	Sample locations within *O. hexactis*	PCAdapt; RDA	temp_bottom
CLocus-72913		PCAdapt; RDA	depth
CLocus-90839		PCAdapt; RDA	temp_bottom
CLocus-98641		PCAdapt; RDA	temp_bottom
CLocus-110092		PCAdapt; RDA	temp_bottom
CLocus-129767		PCAdapt; RDA	temp_bottom
CLocus-140351		PCAdapt; RDA	sal_bottom
CLocus-141960		PCAdapt; RDA	temp_bottom
CLocus-163908		PCAdapt; RDA	temp_bottom

CLocus-184749	PCAdapt; RDA	temp_bottom

Supplementary Table 4.7 Gene ontology (GO) annotation results for outlier locus (between *Ophionotus victoriae* and *O. hexactis*) matched against InterPro protein database.

Locus ID	Dataset	Sequence Description	GO ID	GO term	GO category
Clocus-186281	*O. victoriae* VS *O. hexactis*	Ionotropic glutamate receptor (IPR001320)	GO:0015276	Ligand-gated ion channel activity	Molecular function
			GO:0016020	Membrane	Cellular component

Supplementary Table 4.8 Relative migration estimated by *divMigrate* using Nm between locations sampled within *Ophionotus victoriae*. East Antarctica include samples from Prydz Bay and Tressler Bank. Sample sizes were balanced between locations after random sub-sampling to n = 5. No significant asymmetric migration was detected (10,000 bootstrap iterations).

		Source population															
	Location	East Antarctica	Adélie Land	Ross Sea	Balleny Is.	Amundsen Sea	South Shetland Is.	Bransfield Strait	Bransfield Mouth	Elephant Is.	Discovery Bank	Herdman Bank	South Sandwich Is.	Bouvet Is.	Larsen Ice Shelf	East Weddell Sea	South Weddell Sea
Receiving population	East Antarctica	NA	0.468688419	0.489394190	0.401590300	0.306285860	0.383803520	0.417681930	0.345219190	0.399992470	0.371043990	0.334955540	0.373499460	0.299106780	0.474903870	0.596431680	0.451195520
	Adélie Land	0.557384420	NA	0.922685350	0.706961290	0.499765460	0.706180130	0.721183700	0.558210090	0.733674690	0.585688830	0.534957190	0.653878580	0.458340790	0.828427450	0.897260860	0.677398590
	Ross Sea	0.539498390	0.778132080	NA	0.562905000	0.438177960	0.559114510	0.657427880	0.487088740	0.681317390	0.519208410	0.534505530	0.561178410	0.401688000	0.774684840	0.937469460	0.638157450
	Balleny Is.	0.426527410	0.658490950	0.546656000	NA	0.398509880	0.667447540	0.656398720	0.553389370	0.768390080	0.621026790	0.598079480	0.616955090	0.449219320	0.682561160	0.719963070	0.611571220
	Amundsen Sea	0.233488940	0.289899810	0.288547710	0.266015740	NA	0.250226460	0.255060490	0.218844380	0.281996040	0.290966480	0.261739770	0.293551790	0.206512720	0.296093660	0.337008020	0.267870320
	South Shetland Is.	0.434033630	0.678737210	0.607027660	0.680685720	0.417972540	NA	0.653875780	0.493082730	0.740536690	0.584720310	0.577959490	0.623766210	0.440985410	0.698853660	0.668314410	0.593277470
	Bransfield Strait	0.470724850	0.739024320	0.595827450	0.718591340	0.425215740	0.709362350	NA	0.590157770	0.838168510	0.617087560	0.598146110	0.678474510	0.478910530	0.778059110	0.730583650	0.700064740
	Bransfield Mouth	0.306961940	0.383713260	0.398620510	0.459735480	0.299198650	0.388345190	0.457048010	NA	0.457421070	0.367436920	0.323673360	0.399178900	0.296545400	0.419023310	0.469489820	0.381911870
	Elephant Is.	0.483581520	0.808452000	0.721707490	0.835690860	0.465866760	0.773835220	0.859195010	0.584998460	NA	0.732109090	0.692361040	0.755521970	0.491228060	0.867298340	0.865920470	0.726066730
	Discovery Bank	0.426510510	0.599118910	0.555507540	0.608805560	0.422634290	0.594621300	0.573640460	0.455806360	0.651455430	NA	0.739695020	0.769787030	0.432847640	0.616059130	0.624216930	0.521169830
	Herdman Bank	0.380385360	0.541440700	0.547212890	0.605762380	0.403173910	0.532716620	0.565926770	0.425164310	0.630186580	0.800217080	NA	0.862593720	0.393758140	0.531515820	0.594895850	0.471089140
	South Sandwich Is.	0.441733710	0.606214040	0.629194030	0.646679750	0.449513410	0.609929590	0.649550220	0.482130922	0.725644470	0.887514670	0.885334420	NA	0.451744370	0.633196390	0.630414840	0.577493610
	Bouvet Is.	0.292563990	0.414514380	0.349345180	0.401605190	0.279303380	0.428178400	0.426253960	0.361689500	0.453931600	0.452711760	0.368419820	0.401052130	NA	0.356790820	0.425062960	0.366658730
	Larsen Ice Shelf	0.564684000	0.832520280	0.828705100	0.771642620	0.458403850	0.724895730	0.773475650	0.568626970	0.778867100	0.650930760	0.663741870	0.704885280	0.476679850	NA	0.999999990	0.771363050
	East Weddell Sea	0.580124960	0.835487560	0.791154540	0.604392410	0.435620190	0.569018730	0.582546080	0.492027630	0.661007260	0.535635280	0.500030850	0.578475560	0.403533000	0.782685000	NA	0.720459480
	South Weddell Sea	0.468531310	0.698219090	0.672553060	0.657564060	0.449899770	0.593092860	0.672201420	0.499747060	0.724296790	0.589569770	0.572872150	0.625251430	0.424220630	0.763385760	0.800120411	NA

Supplementary Table 4.9 Pairwise F_{ST} between locations within *Ophionotus victoriae*. East Antarctica include samples from Prydz Bay and Tressler Bank. Bold values indicate significant differentiation after Bonferroni Correction (adjusted p value = 0.00037).

	Ross Sea	Amundsen Sea	Balleny Is.	East Antarctica	Bransfield Mouth	Adélie Land	Scott Is.	South Sandwich Is.	Elephant Is.	Discovery Bank	Herdman Bank	South Shetland Is.
Amundsen Sea	**0.027**											
Balleny Is.	**0.014**	0.037										
East Antarctica	0	0.04	0.023									
Bransfield Mouth	0.008	0.032	0.005	0.012								
Adélie Land	0.001	**0.029**	**0.015**	-0.001	**0.011**							
Scott Is.	**0.06**	0.038	0.03	0.025	0.028	**0.05**						
South Sandwich Is.	**0.026**	0.045	**0.022**	0.035	**0.02**	**0.029**	0.048					
Elephant Is.	0.008	0.034	0	0.026	0.004	0.01	0.054	0.016				
Discovery Bank	**0.029**	0.048	0.022	0.037	0.024	**0.033**	0.039	0.01	0.021			
Herdman Bank	**0.032**	0.047	0.024	0.043	0.028	**0.039**	0.032	0	0.026	0.012		
South Shetland Is.	0.011	0.031	0.003	0.018	0.006	**0.012**	0.051	**0.023**	0	0.029	0.03	
Bransfield Strait	**0.015**	0.039	0.01	0.022	0.004	**0.015**	0.054	**0.022**	-0.001	0.026	0.033	0.006
Bouvet Is.	**0.027**	**0.048**	**0.025**	0.026	**0.021**	**0.026**	0.053	**0.03**	0.015	**0.023**	**0.034**	**0.02**
East Weddell Sea	0.002	**0.027**	**0.018**	-0.006	0.012	0.002	0.049	**0.037**	0.016	**0.034**	**0.043**	0.016
Larsen Ice Shelf	0.001	0.017	0.006	0.002	0.002	-0.001	0.051	**0.02**	0.003	0.022	0.026	0.008
South Weddell Sea	**0.007**	**0.024**	0.01	0.015	0.007	**0.008**	**0.05**	**0.023**	0.008	**0.028**	**0.03**	0.009

Supplementary Table 4.10 Relative migration estimated by *divMigrate* using Nm between locations sampled within *Ophionotus hexactis*. Sample sizes were balanced between locations (n = 40). No significant asymmetric migration was detected (10,000 bootstrap iterations).

	Location	**Source population**			
		Bransfield Mouth	South Georgia	Shag Rocks	Heard Is.
Receiving population	Bransfield Mouth	NA	0.63399425	0.60798016	0.54097814
	South Georgia	0.60845657	NA	1	0.9125133
	Shag Rocks	0.58269985	0.95405389	NA	0.92949542
	Heard Is.	0.59988276	0.87498068	0.85653545	NA

Supplementary Table 4.11 Pairwise F_{ST} between locations within *Ophionotus hexactis*. Bold values indicate significant differentiation after Bonferroni Correction (adjusted p value = 0.0083).

	Bransfield Mouth	South Georgia	Shag Rocks
South Georgia	**0.028**		
Shag Rocks	**0.031**	**0.005**	
Heard Island	**0.035**	**0.010**	**0.010**

Supplementary Table 4.12 Parameter values (unscaled) and model fitting of all demographic models (n = 9) used to explore the divergence and connectivity between *Ophionotus victoriae* and *O. hexactis*. Analysed dataset excluded *O. victoriae* samples from South Georgia and *O. hexactis* samples from Bransfield Mouth with strong intraspecific admixture.

Model	K	LogL	AIC	ΔAICi	Score	WAIC	theta	nu1	nu2	nu1a	nu2a	nu1b	nu2b	T	T1	T2	m12	m21	m12a	m21a	m12b	m21b
IM	5	-2797.17	5604.34	0.00	1.00	1.00	181.81	29.7679	2.3432					13.0969			0.0158	5.0511				
IM_size_asym	10	-2805.90	5631.80	27.46	1.00	0.00	371.82			0.2348	0.6507	14.2061	0.9450		0.5144	6.7415			0.3750	0.1323	0.1487	11.8250
AM	6	-3189.74	6391.48	787.14	0.98	0.00	290.33	14.3052	4.4512						8.6884	0.0517	1.6318	3.2437				
IM_size	8	-3338.14	6692.28	1087.94	0.98	0.00	853.54			0.2004	1.1655	4.8526	1.4982		2.2186	2.824	2.9414	4.9388				
SC_size	8	-3888.88	7793.76	2189.42	0.96	0.00	1578.78			25.0555	21.9847	1.4461	0.7971		0.4116	0.0891	20.9957	1.8527				
SC	6	-3996.66	8005.32	2400.98	0.95	0.00	371.26	8.0878	11.4360						0.1785	6.0360	3.1210	0.0227				
SI	3	-5280.44	10566.88	4962.54	0.90	0.00	3308.13	2.1603	0.3631					0.0144								
AM_size	8	-5490.26	10996.52	5392.18	0.89	0.00	2900.07			7.0957	1.3252	0.3929	2.7320		0.0324	0.0030	0.2745	0.2326				
SI_size	6	-27254.18	54520.36	48916.02	0.00	0.00	205.60			24.395	1.9589	28.5829	0.1695		0.2355	2.8446						

Abbreviations are as follows:
K: Number of free parameters used in the model
LogL: The best maximum log liklihood estimates in the final fourth round of *dadi_pipeline*
AIC: Akaike Information Criterion
ΔAICi: Difference in AIC between model (i) and the best model
Model score: (Δmax-ΔAICi)/Δmax, where Δmax = difference in AIC between the models with lowest and highest AIC values
WAIC: Akaike weight evaluating the probability of model I relative to the best model
Theta: 4*Nref*mu*L, the effective mutation rate of the ancestral population before split (Nref)
nu1, nu2: effective population size under constant population size model in units of 2Nref generations
nu1a, nu2a: effective population size before instantaneous size change in units of 2Nref generations
nu1a, nu2a: effective population size after instantaneous size change in units of 2Nref generations
T: unscaled time between O. victoriae and O. hexactis split and the present in units of 2Nref generations
T1: unscaled time between O. victoriae and O. hexactis split and strict isolation (SC) / ancient migration (AM)/ or before instantaneous size change (SI_size, IM_size, IM_size_asym, SC_size, AM_size) in units of 2Nref generations
T2: unscaled time between after the instantaneous size change of *O. victoriae* and *O. hexactis* and the present time in units of 2Nref generations
m12: migration rate from *O. hexactis* to *O. victoriae* in units of 2Nref generations
m21: migration rate from *O. victoriae* to *O. hexactis* in units of 2Nref generations
m12a: migration rate from *O. hexactis* to *O. victoriae* before instantaneous size change in units of 2Nref generations
m21a: migration rate from *O. victoriae* to *O. hexactis* before instantaneous size change in units of 2Nref generations
m12b: migration rate from *O. hexactis* to *O. victoriae* after instantaneous size change in units of 2Nref generations
m21b: migration rate from *O. victoriae* to *O. hexactis* after instantaneous size change in units of 2Nref generations

Supplementary Table 5.1 Sample information of all *Pareledone turqueti* (n = 87) and two outgroup samples sequenced with target capture sequencing of ddRAD loci and analysed in this study.

Genus	species	Study ID	Field ID	Museum ID	Sample location	BOLD ID from previous studies	Expedition	Station ID	Event number	Latitude	Longitude	Collection depth (m)	Collection date
Pareledone	turqueti	JR179_141	JR179_141	NMSZ 2008090.1	Amundsen Sea	CAOII421-09	JR179	38		-71.81	-106.33	577	04/03/2008
Pareledone	turqueti	PT84AP	ANTXVII-3_84	NMSZ 2000081.28	Bransfield Strait	CAOII148-09	ANT-XVII/3	56/166-1		-63.04	-59.17	666	28/04/2000
Pareledone	turqueti	PT117AP	ANTXVII-3_117	NMSZ 2000081.36	Deception Is	CAOII153-09	ANT-XVII/3	56/173-1		-63.02	-61.15	352	28/04/2000
Pareledone	turqueti	PT119AP/41			Deception Is		ANT-XVII/3	56/173-1		-63.02	-61.15	352	28/04/2000
Pareledone	turqueti	CT905	V3_3238	CT905	Adélie Land	CAOII773-09	CEAMARC		Event 496; Trawl 79	-66.00	139.68	196	15/01/2008
Pareledone	turqueti	CT909	V3_2493	CT909	Adélie Land	CAOII777-09	CEAMARC		Event 424; Trawl 62	-66.56	141.26	177	13/01/2008
Pareledone	turqueti	CT917	V3_2458	CT917	Adélie Land	CAOII785-09	CEAMARC		Event 420; Trawl 61	-66.34	141.27	207	15/01/2008
Pareledone	turqueti	CT933	V3_3076	CT933	Adélie Land	CAOII801-09	CEAMARC			-66.40	139.79	896	15/01/2008
Pareledone	turqueti	CT939	V3_3237	CT939	Adélie Land	CAOII807-09	CEAMARC		Event 496; Trawl 79	-66.00	139.68	196	15/01/2008
Pareledone	turqueti	AD_01_6	AD-01		Casey Station		Antarctic Discovery Voyage No. 1		Longline trawl 67	-65.23	118.53	913	26/02/2016
Pareledone	turqueti	JS096	GJ_JS96	Z17090-F173485	Prydz Bay	CAOII326-09	AL27		Haul 123	-66.93	65.92	185	26/01/2001
Pareledone	turqueti	JS097	GJ_JS97	Z17096-F173491	Prydz Bay	CAOII327-09	AL27		Haul 123	-66.93	65.92	185	26/01/2001
Pareledone	turqueti	LS14	ANTXVII-3_14	NMSZ 2000081.15	East Weddell Sea	CAOII130-09	ANT-XVII/3			-71.19	-12.26	309	02/04/2000
Pareledone	turqueti	LS15	ANTXVII-3_15	NMSZ 2000081.15	East Weddell Sea	CAOII131-09	ANT-XVII/3			-71.19	-12.26	309	02/04/2000
Pareledone	turqueti	LS3	ANTXVII-3_3	NMSZ 2000081.2	East Weddell Sea	CAOII128-09	ANT-XVII/3			-71.29	-13.80	615	31/03/2000
Pareledone	turqueti	Octo13	ANTXXI-2_13	ANTXXI-2_13	East Weddell Sea	CAOII178-09	ANT-XXI/2			-71.58	-13.95	844	21/12/2003
Pareledone	turqueti	Octo2	ANTXXI-2_2	ANTXXI-2_2	East Weddell Sea	CAOII172-09	ANT-XXI/2			-70.81	-11.37	1342	10/12/2003
Pareledone	turqueti	PT16WS	ANTXVII-3_16	NMSZ 2000081.15	East Weddell Sea	CAOII132-09	ANT-XVII/3			-71.19	-12.26	309	02/04/2000
Pareledone	turqueti	PT378WS	ANTXIII-3_378	ANTXIII-3_378	East Weddell Sea	CAOII021-09	ANT-XIII/3			-71.53	-12.43	504	28/02/1996
Pareledone	turqueti	PT49WS	ANTXVII-3_49	NMSZ 2000081.20	East Weddell Sea	CAOII137-09	ANT-XVII/3			-70.84	-10.59	237	07/04/2000
Pareledone	turqueti	PT60WS	ANTXVII-3_60	NMSZ 2000081.16	East Weddell Sea	CAOII139-09	ANT-XVII/3			-70.84	-10.58	274	10/04/2000

Pareledone	turqueti	PT61WS	ANTXVII-3_61	NMSZ 2000081.16	East Weddell Sea	CAOII140-09	ANT-XVII/3		-70.84	-10.58	274	10/04/2000
Pareledone	turqueti	WS112	ANTXIII-3_112	ANTXIII-3_112	East Weddell Sea	CAOII010-09	ANT-XVII/3		-71.67	-12.70	254	06/02/1996
Pareledone	turqueti	AND145	ANTXIX-3_145	NMSZ 2002037.45	Elephant Is	CAOII045-09	ANT-XIX/3		-61.07	-54.61	190	30/01/2002
Pareledone	turqueti	AND271	ANTXIX-3_271	NMSZ 2002037.46	Elephant Is	CAOII066-09	ANT-XIX/3		-61.16	-54.56	343	30/01/2002
Pareledone	turqueti	PT108	JR147_108		Elephant Is	CAOII345-09	JR147	EI-RGBT-07	-61.20	-55.90	108	14/03/2006
Pareledone	turqueti	PT154			Elephant Is		JR147	EI-RGBT-09	-61.20	-55.70	103	14/03/2006
Pareledone	turqueti	PT192	JR147_192		Elephant Is	CAOII358-09	JR147	EI-RGBT-10	-61.20	-55.70	103	14/03/2006
Pareledone	turqueti	PT267AP	ANTXIX-3_267	NMSZ 2002037.46	Elephant Is	CAOII064-09	ANT-XIX/3		-61.16	-54.56	343	30/01/2002
Pareledone	turqueti	PT272AP	ANTXIX-3_272	NMSZ 2002037.46	Elephant Is	CAOII067-09	ANT-XIX/3		-61.16	-54.56	343	30/01/2002
Pareledone	turqueti	09_0713			West Antarctic Peninsula		JR230		-67.75	-70.06	586	09/12/2009
Pareledone	turqueti	LS149	ANTXVII-3_149	NMSZ 2000081.50	Robert Is	CAOII159-09	ANT-XVII/3		-61.98	-60.31	804	02/05/2000
Pareledone	turqueti	LS152	ANTXVII-3_152	NMSZ 2000081.50	Robert Is	CAOII161-09	ANT-XVII/3		-61.98	-60.31	804	02/05/2000
Pareledone	turqueti	LS154	ANTXVII-3_154	NMSZ 2000081.50	Robert Is	CAOII163-09	ANT-XVII/3		-61.98	-60.31	804	02/05/2000
Pareledone	turqueti	LS161	ANTXVII-3_161	NMSZ 2000081.50	Robert Is	CAOII169-09	ANT-XVII/3		-61.98	-60.31	804	02/05/2000
Pareledone	turqueti	PT151AP	ANTXVII-3_151	NMSZ 2000081.50	Robert Is	CAOII160-09	ANT-XVII/3		-61.98	-60.31	804	02/05/2000
Pareledone	turqueti	PT156AP	ANTXVII-3_156	NMSZ 2000081.50	Robert Is	CAOII165-09	ANT-XVII/3		-61.98	-60.31	804	02/05/2000
Pareledone	turqueti	PT24			KingGeorge Is		JR147	EI-RGBT-02	-62.00	-57.20	111	11/03/2006
Pareledone	turqueti	PT2414AP	ANTXIX-3_2414	NMSZ 2002037.6	Livingston Is	CAOII087-09	ANT-XIX/3		-62.39	-61.40	363	19/02/2002
Pareledone	turqueti	PT25			KingGeorge Is		JR147	EI-RGBT-02	-62.00	-57.20	111	11/03/2006
Pareledone	turqueti	PT33			KingGeorge Is		JR147	EI-RGBT-02	-62.00	-57.20	111	11/03/2006
Pareledone	turqueti	PT36			KingGeorge Is		JR147	EI-RGBT-02	-62.00	-57.20	111	11/03/2006
Pareledone	turqueti	44117			Ross Sea	CANTA079-08	TAN0802		-75.63	169.85	525	01/02/2008

Pareledone	turqueti	44122		Ross Sea	CANTA039-08	TAN0802	-73.12	174.32	321	01/02/2008
Pareledone	turqueti	44130		Ross Sea	CANTA087-08	TAN0802	-76.59	176.83	369	01/02/2008
Pareledone	turqueti	44255		Ross Sea	CANTA105-08	TAN0802	-76.60	176.80	360	01/02/2008
Pareledone	turqueti	44074_5	44074.5	Ross Sea	CANTA114-08	TAN0802	-76.19	176.30	447	01/02/2008
Pareledone	turqueti	44113_3	44113.3	Ross Sea	CANTA044-08	TAN0802	-76.19	176.30	447	01/02/2008
Pareledone	turqueti	44113_4	44113.4	Ross Sea	CANTA045-08	TAN0802	-76.19	176.30	447	01/02/2008
Pareledone	turqueti	44118_3	44118.3	Ross Sea	CANTA092-08	TAN0802	-76.19	176.30	447	01/02/2008
Pareledone	turqueti	44256_1	44256.1	Ross Sea	CANTA107-08	TAN0802	-72.35	175.50	850	01/02/2008
Pareledone	turqueti	NIWA87970		Ross Sea		Kat Bolstad				
Pareledone	turqueti	PT214SG	SG06_214	Shag Rocks	CAOII564-09		-53.74	-41.46	164	11/01/2006
Pareledone	turqueti	PT24SG	SG05_24	Shag Rocks	CAOII464-09		-53.92	-41.56	314	18/01/2005
Pareledone	turqueti	PT376SG	SG90_376	Shag Rocks	CAOII646-09		-53.57	-41.63	120	08/01/1990
Pareledone	turqueti	PT377SG	SG90_377	Shag Rocks	CAOII647-09		-53.57	-41.63	120	08/01/1990
Pareledone	turqueti	PT381SG		Shag Rocks			-53.57	-41.63	120	08/01/1990
Pareledone	turqueti	PT382SG		Shag Rocks			-53.57	-41.63	120	08/01/1990
Pareledone	turqueti	PT386SG		Shag Rocks			-53.57	-41.63	120	08/01/1990
Pareledone	turqueti	PT42SG	SG05_42	Shag Rocks	CAOII481-09		-53.72	-41.28	130	19/01/2005
Pareledone	turqueti	PT511SG		Shag Rocks			-53.53	-42.22	158	
Pareledone	turqueti	PT305SG		South Georgia			-54.58	-35.44	150	
Pareledone	turqueti	PT328SG	SG06_328	South Georgia	CAOII622-09		-55.06	-36.07	149	17/01/2006
Pareledone	turqueti	PT354SG	PC_354	South Georgia	CAOII632-09		-54.07	-35.67	205	09/02/1991
Pareledone	turqueti	PT355SG	PC_355	South Georgia	CAOII633-09		-54.07	-35.67	205	09/02/1991
Pareledone	turqueti	PT356SG	PC_356	South Georgia	CAOII634-09		-54.07	-35.67	205	09/02/1991
Pareledone	turqueti	PT357SG		South Georgia			-54.07	-35.67	205	09/02/1991
Pareledone	turqueti	PT366SG	PC_366	South Georgia	CAOII638-09		-54.78	-34.92	349	01/02/1991
Pareledone	turqueti	PT367SG	PC_367	South Georgia	CAOII639-09		-54.78	-34.92	349	01/02/1991

Pareledone	turqueti	PT401SG		South Georgia				-55.06	-35.38	124		
Pareledone	turqueti	PT415SG		South Georgia				-54.62	-35.53	113		
Pareledone	turqueti	PT420SG		South Georgia				-54.62	-35.53	113		
Pareledone	turqueti	PT421SG		South Georgia				-54.62	-35.53	113		
Pareledone	turqueti	PT432SG		South Georgia				-53.67	-38.07	154		
Pareledone	turqueti	PT440SG		South Georgia				-53.65	-37.22	168		
Pareledone	turqueti	PT445SG		South Georgia				-53.65	-37.22	168		
Pareledone	turqueti	PT446SG		South Georgia				-53.65	-37.22	168		
Pareledone	turqueti	PT449SG		South Georgia				-53.65	-37.22	168		
Pareledone	turqueti	PT508SG	SG06_508	South Georgia	CAOII658-09			-53.53	-42.22	158	12/01/2006	
Pareledone	turqueti	PT73SG	SG05_73	South Georgia	CAOII511-09			-53.79	-39.29	401	15/01/2005	
Pareledone	turqueti	PT250		South Orkney Is				-61.00	-45.90	240		
Pareledone	turqueti	PT255		South Orkney Is				-62.00	-57.20	111		
Pareledone	turqueti	JS_26		South Weddell Sea		RV Polarstern PS82		-77.72	-35.98	613	04/01/2014	
Pareledone	turqueti	JS_40		South Weddell Sea		RV Polarstern PS82					2014	
Pareledone	turqueti	JS_44		South Weddell Sea		RV Polarstern PS82					2016	
Pareledone	turqueti	JS10		South Weddell Sea		RV Polarstern PS96		-72.31	-16.86	762	29/01/2016	
Pareledone	turqueti	JS5		South Weddell Sea		RV Polarstern PS96		-72.59	-18.07	406	31/01/2016	
Pareledone	turqueti	PT186	JR147_186	Elephant Is	CAOII355-09	JR147		-61.20	-55.70	103	14/03/2006	
Pareledone	turqueti	PT244	JR147_244	South Orkney Is	CAOII380-09	JR147		-61.00	-46.80	505	18/03/2006	
Pareledone	cornuta	CT931		Adélie Land	CAOII799-09	CEAMARC		-66.34	140.45	444	14/01/2008	
Pareledone	aequipapillae	44064_1	44064.1	Ross Sea	CANTA048-08	TAN0802	61	-75.62	169.81	520	01/02/2008	

Supplementary Table 5.2 Pairwise F_{ST} between locations of *Pareledone turqueti* based on ddRAD loci data. Bold values indicate significant differentiation after Bonferroni Correction (adjusted p value = 0.0013).

	Shag Rocks	South Georgia	Elephant Is.	King George Is.	Robert Is.	South Weddell Sea	East Weddell Sea	Ross Sea	Adélie Land
Shag Rocks	-	**0.036**	**0.075**	0.077	**0.124**	0.105	**0.127**	**0.139**	**0.152**
South Georgia	**0.036**	-	**0.073**	**0.074**	**0.116**	**0.097**	**0.118**	**0.127**	**0.139**
Elephant Is.	**0.075**	**0.073**	-	0.006	0.061	0.035	**0.067**	**0.068**	0.074
King George Is.	0.077	**0.074**	0.006	-	0.092	0.072	**0.091**	**0.115**	0.136
Robert Is.	**0.124**	**0.116**	0.061	0.092	-	0.021	**0.064**	**0.058**	0.078
South Weddell Sea	**0.105**	**0.097**	0.035	0.072	0.021	-	0.011	0.039	0.042
East Weddell Sea	**0.127**	**0.118**	**0.067**	**0.091**	**0.064**	0.011	-	**0.086**	**0.095**
Ross Sea	**0.139**	**0.127**	**0.068**	**0.115**	**0.058**	0.039	**0.086**	-	0.018
Adélie Land	**0.152**	**0.139**	0.074	0.136	0.078	0.042	**0.095**	0.018	-

Supplementary Table 5.3 Summary of outlier contigs detected within *Pareledone turqueti* with their associated functional annotations based on positive matches with the BLASTx databse (< E value of 1 x 10^{-5}). Outlier contigs contains outlier SNPs detected by at least two methods including FastPCA, outFLANK, pcadapt, RDA, Bayescan. Dataset ("Shelf vs Scotia") contains all *P. turqueti* samples collected around the Southern Ocean (n = 87), with samples divided between the Antarctic continental shelf and Scotia Arc. Dataset ("Location within Scotia Arc") contains only *P. turqueti* samples from the Scotia Arc (n = 52), with samples divided between sample locations.

Dataset	Contig ID	E-value	Uniport ID	% identity	Sequence length	Sequence description	Relevant environmental predictor identified by RDA (if applicable)	TE classification: Class	TE classification: Order	References of TE functions (if details are not available on the QuickGO database)
Shelf vs Scotia	ctg233	1.70E-19	P14381	33.1	287	Transposon TX1 uncharacterized 149 kDa protein	Longitude	Class I (retrotransposon)	LINE	Furano et al. (2004)
	ctg5271	3.01E-10	Q96K76	57.8	45	Ubiquitin carboxyl-terminal hydrolase 47	Salinity			
	ctg9111	3.60E-14	P03934	31.9	204	Transposable element Tc1 transposase		Class II (DNA transposons)	TIR	
	ctg695	3.43E-14	Q86UP8	34.2	155	General transcription factor II-I repeat domain-containing protein 2A		Domesticated TE	Class II	Tipney et al. (2004)
	ctg767	0.00E+00	O61363	66.9	809	Hemocyanin G-type, units Oda to Odg	Temperature, Longitude			
	ctg893	1.79E-15	P14381	39	82	Transposon TX1 uncharacterized 149 kDa protein	Longitude	Class I (retrotransposon)	LINE	Furano et al. (2004)
	ctg1213	1.86E-08	Q8TCP9	43.4	76	Protein FAM200A	Longitude	Domesticated TE		
	ctg2007	1.15E-08	Q7JQ07	32.3	96	Mariner Mos1 transposase		Class I (retrotransposon)	TIR	
	ctg4289	4.70E-45	Q9HCL0	33	437	Protocadherin-18	Longitude			
	ctg4331	1.56E-19	Q9Z2G6	68.1	69	Protein sel-1 homolog 1	Water depth			
	ctg4415	3.09E-09	A6QPH9	38.4	86	Zinc finger MYM-type protein 5	Longitude	Domesticated TE	Class II	Kojima & Jurka (2011)
	ctg2014	1.06E-07	O60825	45.9	74	6-phosphofructo-2-kinase/fructose-2,6-bisphosphatase 2				
	ctg12635	3.69E-92	Q7KRW1	47.9	334	Protein TRC8 homolog	Temperature			
	ctg15574	1.30E-19	Q14974	72.3	65	Importin subunit beta-1	Longitude			
	ctg34031	5.51E-06	Q6P1D7	40.2	82	Structure-specific endonuclease subunit SLX4	Temperature	TE repressor	SLX4	Brégnard et al. (2016)
	ctg5046	6.36E-21	P20825	35	214	Retrovirus-related Pol polyprotein from transposon 297	Longitude	Class I (retrotransposon)	LTR	Todorovska (2007)
	ctg5551	7.75E-20	Q8NFW1	33.3	192	Collagen alpha-1(XXII) chain	Longitude			
	ctg6681	4.11E-88	A6NNF4	49.4	172	Zinc finger protein 726	Longitude	TE repressor	KRAB-ZFP	

	ctg5271	3.01E-10	Q96K76	57.8	45	Ubiquitin carboxyl-terminal hydrolase 47				
	ctg9782	9.71E-07	Q6R2W3	45.1	82	SCAN domain-containing protein 3	Longitude	Domesticated TE	Class II	
	ctg9963	5.17E-87	O12944	67.8	211	DNA repair and recombination protein RAD54-like	Longitude	TE interactor		Romeijn et al. (2004)
	ctg10210	1.97E-11	P04323	41.2	114	Retrovirus-related Pol polyprotein from transposon 17.6		Class I (retrotransposon)	LTR	
	ctg10565	6.14E-22	Q9VL00	73.4	64	Ubiquitin thioesterase otubain-like	Temperature			
	ctg3397	2.72E-11	F1QCN0	58.1	62	Glutamine amidotransferase-like class 1 domain-containing protein 3A, mitochondrial				
	ctg3720	2.36E-18	Q7LHG5	33.3	87	Transposon Ty3-I Gag-Pol polyprotein	Longitude	Class I (retrotransposon)	LTR	
	ctg6923	4.84E-06	Q9NBX4	36	100	Probable RNA-directed DNA polymerase from transposon X-element	Salinity	Class I (retrotransposon)	LINE	Tudor et al. (2001)
	ctg18035	1.28E-22	Q9Y3P9	66.7	78	Rab GTPase-activating protein 1				
	ctg18731	2.26E-46	Q2S1V4	35.6	264	Tryptophanase	Longitude			
	ctg29082	3.89E-09	Q7ZXZ0	60	60	Zygotic DNA replication licensing factor mcm3				
	ctg1099	6.75E-09	Q5U560	39.8	93	THAP domain-containing protein 1 A	Longitude	Class II (DNA transposons)	TIR	Majumda & Rio (2015)
	ctg1182	9.48E-36	Q05D44	69.1	94	Eukaryotic translation initiation factor 5B	Longitude			
Location within Scotia Arc	ctg121	2.97E-20	P14381	31.9	235	Transposon TX1 uncharacterized 149 kDa	Water depth	Class I (retrotransposon)	LINE	Furano et al. (2004)
	ctg767	0.00E+00	O61363	66.9	809	Hemocyanin G-type, units Oda to Odg	Longitude			
	ctg1881	1.10E-22	P14381	28.7	307	Transposon TX1 uncharacterized 149 kDa protein	Temperature	Class I (retrotransposon)	LINE	Furano et al. (2004)
	ctg10565	6.14E-22	Q9VL00	73.4	64	Ubiquitin thioesterase otubain-like	Longitude			
	ctg9176	3.32E-18	Q6EKJ0	41.3	92	General transcription factor II-I repeat domain-containing protein 2B	Temperature	Domesticated TE		Tipney et al. (2004)
	ctg10287	4.54E-10	O88501	38.5	53	Calpain-6				
	ctg34031	5.51E-06	Q6P1D7	40.2	82	Structure-specific endonuclease subunit SLX4		TE repressor	SLX4	Brégnard et al. (2016)
	ctg3292	4.13E-13	O70244	41.6	101	Cubilin	Longitude			
	ctg3397	2.72E-11	F1QCN0	58.1	62	Glutamine amidotransferase-like class 1 domain-containing protein 3A, mitochondrial				
	ctg4458	9.09E-12	P14381	28.5	305	Transposon TX1 uncharacterized 149 kDa protein		Class I (retrotransposon)	LINE	Furano et al. (2004)
	ctg5271	3.01E-10	Q96K76	57.8	45	Ubiquitin carboxyl-terminal hydrolase 47				
	ctg12635	3.69E-92	Q7KRW1	47.9	334	Protein TRC8 homolog				
	ctg15490	7.24E-07	Q9D024	60	40	PAT complex subunit CCDC47				
	ctg27838	8.07E-13	Q03274	44.3	61	Retrovirus-related Pol polyprotein from type-1 retrotransposable element R2		Class I (retrotransposon)	LTR	

ctg22306	1.74E-15	Q9FMP4	87.2	39	Splicing factor 3B subunit 6-like protein	Temperature			
ctg23199	4.96E-06	O43663	40.8	76	Protein regulator of cytokinesis 1				
ctg23251	1.90E-23	Q62210	28.9	256	Baculoviral IAP repeat-containing protein 2	Salinity			
ctg1486	5.93E-12	Q9NBX4	34.7	95	Probable RNA-directed DNA polymerase from transposon X-element	Temperature	Class I (retrotransposon)	LINE	Tudor et al. (2001)

References:

Furano, A. V., Duvernell, D. D., & Boissinot, S. (2004) L1 (LINE-1) retrotransposon diversity differs dramatically between mammals and fish. *Trends in Genetics*, **20**(1), 9-14.

Tipney H. J., Hinsley, T. A., Brass, A., Metcalfe, K., Donnai, D., & Tassabeji. (2004) Isolation and characterisation of GTF2IRD2, a novel fusion gene and member of the TFII-I family of transcription factors, deleted in Williams–Beuren syndrome. *European Journal of Human Genetics*, **12**, 551-560.

Kojima, K. K., & Jurka, J. (2011) *Crypton* transposons: identification of new diverse families and ancient domestication events. Mobile DNA, **2**, 12.

Brégnard, C., Guerra, J., Déjardin, S., Passalacqua, F., Benkirane, M., & Laguette, N. (2016) Upregulated LINE-1 Activity in the Fanconi Anemia Cancer Susceptibility Syndrome Leads to Spontaneous Pro-inflammatory Cytokine Production. *EBioMedicine, **8**, 184-194*.

Todorovska, E. (2014) Retrotransposons and their Role in Plant—Genome Evolution. Biotechnology & Biotechnological Equipment. *Biotechnology & Biotechnological Equipment*, **21**(3), 294-305.

Romeijn, R., Gorski, M. M., van Schie, M. A., Noordermeer, J. N., Mullenders, L. H., Ferro, W., & Pastink A. (2004) Lig4 and rad54 are required for repair of DNA double-strand breaks induced by P-element excision in Drosophila. *Comparative Study*, **169**(2), 795-806.

Tudor, M., Davis, A. J., Feldman, M., Grammatikaki, M., & O'Hare, K. (2001) The X element, a novel LINE transposable element from *Drosophila melanogaster*. *Molecular Genetics and Genomics*, **265**(3), 489-496.

Majumdar, S., & Rio, D. C. (2015) P Transposable Elements in Drosophila and other Eukaryotic Organisms. *Microbiology Spectrum*, **3**(2), MDNA3-0004-2014.

Supplementary Table 6.1 Demographic parameters inferred in the best model (cc_full_col2) in *Pareledone turqueti*. Maximum-likelihood (ML) parameter estimates were extracted form the best run with the highest composite likelihood among 100 replicates. Migration rates are scaled as 2Nm (population effective sizes) looking forward in time. Effective population sizes are given in the number of haploids. Estimations of timing of events are given in the number of generations (gen) and years. The 95% confidence intervals (CI) were generated from 53 block-bootstrapped datasets. Abbreviations: Weddell Sea (WS), Amundsen Sea (AS), Ross Sea (RS), East Antarctica (EA).

			95% CI	
Parameter	**Parameter description**	**ML estimate**	**Lower bound**	**Upper bound**
T1 (gen)	Time of AS divergence from the ancestral population of WS, RS and EA (in generations)	28765	12192	82402
T3 (gen)	Time of contemporary gene flow between WS-EA-RS-AS driven by circumpolar current (in generations)	0	0	0
T2 (gen)	Time of trans-west Antarctic seaway connetivitiy between WS-AS-RS (in generations)	8249	4450	12504
T0 (gen)	Time of demographic change in the ancestral population of AS, WS, RS and EA (in generations)	212148	112701	434389
T1 (year)	Time of AS divergence from the ancestral population of WS, RS and EA (in years)	373945	158500	1071226
T3 (year)	Time of contemporary gene flow between WS-EA-RS-AS driven by circumpolar current (in years)	0	0	0
T2 (year)	Time of trans-west Antarctic seaway connectivity between WS-AS-RS (in years)	107237	57855	162553
T0 (year)	Time of demographic change in the ancestral population of AS, WS, RS and EA (in years)	2757924	1465110	5647057
NWS$	Effective population size of WS after T3	125876	133182	786884
NAS$	Effective population size of AS after T3	772896	194520	921623
NRS$	Effective population size of RS after T3	363888	98723	889109
NEA$	Effective population size of EA after T3	616843	143293	929707
NASC$	Effective population size of AS after T2	80997	24504	131860
NWSC$	Effective population size of WS after T2	298059	158262	885406
NEAC$	Effective population size of EA after T2	1776436	1057288	2487127
NRSC$	Effective population size of RS after T2	580855	140308	672322
NASA$	Effective population size of AS after T1	501680	184405	992946
NANC3$	Effective population size of the ancestral population of WS, RS and EA after T1	84068	44493	929580
NANC2$	Effective population size of the ancestral population of AS, WS, RS and EA after T0	1990827	1225870	3630281
NANC1$	Effective population size of the ancestral population of AS, WS, RS and EA before T0	79582	43182	153515
MIG10$	Migration rates from AS to RS after T3	1.76E-06	1.31E-10	4.12E-06

MIG30$	Migration rates from AS to WS after T3	1.30E-10	1.48E-10	9.96E-06
MIG01$	Migration rates from RS to AS after T3	1.96E-09	2.29E-10	7.63E-06
MIG21$	Migration rates from RS to EA after T3	2.14E-09	2.82E-10	1.38E-05
MIG12$	Migration rates from EA to RS after T3	5.73E-07	1.87E-10	1.16E-05
MIG32$	Migration rates from EA to WS after T3	7.67E-10	1.18E-10	1.41E-05
MIG03$	Migration rates from WS to AS after T3	4.03E-10	4.12E-10	1.01E-05
MIG23$	Migration rates from WS to EA after T3	9.75E-11	1.22E-10	8.44E-06
MIG10C$	Migration rates from AS to RS after T2	5.54E-08	5.23E-09	6.27E-05
MIG30C$	Migration rates from AS to WS after T2	2.84E-05	3.28E-10	6.77E-05
MIG01C$	Migration rates from RS to AS after T2	2.19E-04	1.27E-04	6.78E-04
MIG31C$	Migration rates from RS to WS after T2	1.14E-07	2.39E-10	3.21E-06
MIG03C$	Migration rates from WS to AS after T2	1.62E-04	3.72E-05	4.14E-04
MIG13C$	Migration rates from WS to RS after T2	3.72E-07	2.65E-10	2.62E-06

Supplementary Table 6.2 Demographic parameters inferred in the best model (full_col2) in *Pareledone turqueti*. Maximum-likelihood (ML) parameter estimates were extracted form the best run with the highest composite likelihood among 100 replicates. Migration rates are scaled as 2Nm (population effective sizes) looking forward in time. Effective population sizes are given in the number of haploids. Estimations of timing of events are given in the number of generations (gen) and years. The 95% confidence intervals (CI) were generated from 16 block-bootstrapped datasets. Abbreviations: Weddell Sea (WS), Amundsen Sea (AS), Ross Sea (RS), East Antarctica (EA).

Parameter	Parameter description	ML estimate	95% CI	
			Lower bound	Upper bound
T1 (gen)	Time of AS divergence from the ancestral population of WS, RS and EA (in generations)	377	274102	728068.5
T3 (gen)	Time of contemporary gene flow between WS-EA-RS-AS driven by circumpolar current (in generations)	0	0	0
T2 (gen)	Time of trans-west Antarctic seaway connectivity between WS-AS-RS (in generations)	125	29	1394
T0 (gen)	Time of demographic change in the ancestral population of AS, WS, RS and EA (in generations)	381593	314199	904736
T1 (year)	Time of AS divergence from the ancestral population of WS, RS and EA (in years)	3770	2741020	7280685
T3 (year)	Time of contemporary gene flow between WS-EA-RS-AS driven by circumpolar current (in years)	0	0	0
T2 (year)	Time of trans-west Antarctic seaway connectivity between WS-AS-RS (in years)	1250	286	13943
T0 (year)	Time of demographic change in the ancestral population of AS, WS, RS and EA (in years)	3815930	3141989	9047358
NWS$	Effective population size of WS after T3	500586	168547	957183
NAS$	Effective population size of AS after T3	368231	233240	727959
NRS$	Effective population size of RS after T3	412809	280474	938485
NEA$	Effective population size of EA after T3	693874	69835	769759
NASC$	Effective population size of AS after T2	19005	276	14823
NWSC$	Effective population size of WS after T2	643549	337271	967673
NEAC$	Effective population size of EA after T2	586448	311003	1063390
NRSC$	Effective population size of RS after T2	70774	647156	1142379
NASA$	Effective population size of AS after T1	471328	136927	906636
NANC3$	Effective population size of the ancestral population of WS, RS and EA after T1	566088	410614	915200
NANC2$	Effective population size of the ancestral population of AS, WS, RS and EA after T0	1005962	13063	106733
NANC1$	Effective population size of the ancestral population of AS, WS, RS and EA before T0	127229	328140	1076848
MIG30$	Migration rates from AS to WS after T3	1.32E-10	2.53E-10	2.55E-06

MIG01$	Migration rates from RS to AS after T3	9.07E-07	9.30E-10	3.45E-06
MIG12$	Migration rates from EA to RS after T3	1.35E-10	9.98E-11	2.08E-06
MIG23$	Migration rates from WS to EA after T3	1.61E-08	8.07E-10	6.50E-06
MIG10C$	Migration rates from AS to RS after T2	4.34E-08	2.03E-10	2.69E-06
MIG30C$	Migration rates from AS to WS after T2	3.48E-07	2.00E-09	1.48E-05
MIG01C$	Migration rates from RS to AS after T2	1.15E-07	1.25E-03	2.51E-01
MIG31C$	Migration rates from RS to WS after T2	9.97E-07	1.77E-10	3.34E-06
MIG03C$	Migration rates from WS to AS after T2	1.11E-06	1.27E-03	2.09E-01
MIG13C$	Migration rates from WS to RS after T2	5.64E-10	8.16E-10	3.60E-06

Supplementary Table 6.3 Sample information of *Pareledone turqueti* (n = 87) and outgroup (n = 2) sequenced with target capture sequencing of ddRAD loci. All samples were used for inference of population structure, demographic modelling and admixture-based statistics.

Genus	species	Sample ID	Field ID	Museum ID	Sample location	BOLD ID from previous studies	Expedition	Station ID	Event number	Latitude	Longitude	Collection depth (m)	Collection date
Pareledone	turqueti	JR179_141	JR179_141	NMSZ 2008090.1	Amundsen Sea	CAOII421-09	JR179	38		-71.81	-106.33	577	04/03/2008
Pareledone	turqueti	PT84AP	ANTXVII-3_84	NMSZ 2000081.28	Bransfield Strait	CAOII148-09	ANT-XVII/3	56/166-1		-63.04	-59.17	666	28/04/2000
Pareledone	turqueti	PT117AP	ANTXVII-3_117	NMSZ 2000081.36	Deception Is	CAOII153-09	ANT-XVII/3	56/173-1		-63.02	-61.15	352	28/04/2000
Pareledone	turqueti	PT119AP/41			Deception Is		ANT-XVII/3	56/173-1		-63.02	-61.15	352	28/04/2000
Pareledone	turqueti	CT905	V3_3238	CT905	Adélie Land	CAOII773-09	CEAMARC		Event 496; Trawl 79	-66.00	139.68	196	15/01/2008
Pareledone	turqueti	CT909	V3_2493	CT909	Adélie Land	CAOII777-09	CEAMARC		Event 424; Trawl 62	-66.56	141.26	177	13/01/2008
Pareledone	turqueti	CT917	V3_2458	CT917	Adélie Land	CAOII785-09	CEAMARC		Event 420; Trawl 61	-66.34	141.27	207	13/01/2008
Pareledone	turqueti	CT933	V3_3076	CT933	Adélie Land	CAOII801-09	CEAMARC			-66.40	139.79	896	15/01/2008
Pareledone	turqueti	CT939	V3_3237	CT939	Adélie Land	CAOII807-09	CEAMARC		Event 496; Trawl 79	-66.00	139.68	196	15/01/2008
Pareledone	turqueti	AD_01_6	AD-01		Casey Station		Antarctic Discovery Voyage No. 1		Longline trawl 67	-65.23	118.53	913	26/02/2016
Pareledone	turqueti	JS096	GJ_JS96	Z17090-F173485	Mawson Station	CAOII326-09	AL27		Haul 123	-66.93	65.92	185	26/01/2001
Pareledone	turqueti	JS097	GJ_JS97	Z17096-F173491	Mawson Station	CAOII327-09	AL27		Haul 123	-66.93	65.92	185	26/01/2001
Pareledone	turqueti	LS14	ANTXVII-3_14	NMSZ 2000081.15	East Weddell Sea	CAOII130-09	ANT-XVII/3			-71.19	-12.26	309	02/04/2000
Pareledone	turqueti	LS15	ANTXVII-3_15	NMSZ 2000081.15	East Weddell Sea	CAOII131-09	ANT-XVII/3			-71.19	-12.26	309	02/04/2000
Pareledone	turqueti	LS3	ANTXVII-3_3	NMSZ 2000081.2	East Weddell Sea	CAOII128-09	ANT-XVII/3			-71.29	-13.80	615	31/03/2000
Pareledone	turqueti	Octo13	ANTXXI-2_13	ANTXXI-2_13	East Weddell Sea	CAOII178-09	ANT-XXI/2			-71.58	-13.95	844	21/12/2003
Pareledone	turqueti	Octo2	ANTXXI-2_2	ANTXXI-2_2	East Weddell Sea	CAOII172-09	ANT-XXI/2			-70.81	-11.37	1342	10/12/2003
Pareledone	turqueti	PT16WS	ANTXVII-3_16	NMSZ 2000081.15	East Weddell Sea	CAOII132-09	ANT-XVII/3			-71.19	-12.26	309	02/04/2000
Pareledone	turqueti	PT378WS	ANTXIII-3_378	ANTXIII-3_378	East Weddell Sea	CAOII021-09	ANT-XIII/3			-71.53	-12.43	504	28/02/1996
Pareledone	turqueti	PT49WS	ANTXVII-3_49	NMSZ 2000081.20	East Weddell Sea	CAOII137-09	ANT-XVII/3			-70.84	-10.59	237	07/04/2000

Pareledone	turqueti	PT60WS	ANTXVII-3_60	NMSZ 2000081.16	East Weddell Sea	CAOII139-09	ANT-XVII/3		-70.84	-10.58	274	10/04/2000
Pareledone	turqueti	PT61WS	ANTXVII-3_61	NMSZ 2000081.16	East Weddell Sea	CAOII140-09	ANT-XVII/3		-70.84	-10.58	274	10/04/2000
Pareledone	turqueti	WS112	ANTXIII-3_112	ANTXIII-3_112	East Weddell Sea	CAOII010-09	ANT-XVII/3		-71.67	-12.70	254	06/02/1996
Pareledone	turqueti	AND145	ANTXIX-3_145	NMSZ 2002037.45	Elephant Is	CAOII045-09	ANT-XIX/3		-61.07	-54.61	190	30/01/2002
Pareledone	turqueti	AND271	ANTXIX-3_271	NMSZ 2002037.46	Elephant Is	CAOII066-09	ANT-XIX/3		-61.16	-54.56	343	30/01/2002
Pareledone	turqueti	PT108	JR147_108		Elephant Is	CAOII345-09	JR147	EI-RGBT-07	-61.20	-55.90	108	14/03/2006
Pareledone	turqueti	PT154			Elephant Is		JR147	EI-RGBT-09	-61.20	-55.70	103	14/03/2006
Pareledone	turqueti	PT192	JR147_192		Elephant Is	CAOII358-09	JR147	EI-RGBT-10	-61.20	-55.70	103	14/03/2006
Pareledone	turqueti	PT267AP	ANTXIX-3_267	NMSZ 2002037.46	Elephant Is	CAOII064-09	ANT-XIX/3		-61.16	-54.56	343	30/01/2002
Pareledone	turqueti	PT272AP	ANTXIX-3_272	NMSZ 2002037.46	Elephant Is	CAOII067-09	ANT-XIX/3		-61.16	-54.56	343	30/01/2002
Pareledone	turqueti	09_0713			West Antarctic Peninsula		JR230		-67.75	-70.06	586	09/12/2009
Pareledone	turqueti	LS149	ANTXVII-3_149	NMSZ 2000081.50	Robert Is	CAOII159-09	ANT-XVII/3		-61.98	-60.31	804	02/05/2000
Pareledone	turqueti	LS152	ANTXVII-3_152	NMSZ 2000081.50	Robert Is	CAOII161-09	ANT-XVII/3		-61.98	-60.31	804	02/05/2000
Pareledone	turqueti	LS154	ANTXVII-3_154	NMSZ 2000081.50	Robert Is	CAOII163-09	ANT-XVII/3		-61.98	-60.31	804	02/05/2000
Pareledone	turqueti	LS161	ANTXVII-3_161	NMSZ 2000081.50	Robert Is	CAOII169-09	ANT-XVII/3		-61.98	-60.31	804	02/05/2000
Pareledone	turqueti	PT151AP	ANTXVII-3_151	NMSZ 2000081.50	Robert Is	CAOII160-09	ANT-XVII/3		-61.98	-60.31	804	02/05/2000
Pareledone	turqueti	PT156AP	ANTXVII-3_156	NMSZ 2000081.50	Robert Is	CAOII165-09	ANT-XVII/3		-61.98	-60.31	804	02/05/2000
Pareledone	turqueti	PT24			KingGeorge Is		JR147	EI-RGBT-02	-62.00	-57.20	111	11/03/2006
Pareledone	turqueti	PT2414AP	ANTXIX-3_2414	NMSZ 2002037.6	Livingston Is	CAOII087-09	ANT-XIX/3		-62.39	-61.40	363	19/02/2002
Pareledone	turqueti	PT25			KingGeorge Is		JR147	EI-RGBT-02	-62.00	-57.20	111	11/03/2006
Pareledone	turqueti	PT33			KingGeorge Is		JR147	EI-RGBT-02	-62.00	-57.20	111	11/03/2006

Pareledone	turqueti	PT36		KingGeorge Is		JR147	EI-RGBT-02	-62.00	-57.20	111	11/03/2006
Pareledone	turqueti	44117		Ross Sea	CANTA079-08	TAN0802		-75.63	169.85	525	01/02/2008
Pareledone	turqueti	44122		Ross Sea	CANTA039-08	TAN0802		-73.12	174.32	321	01/02/2008
Pareledone	turqueti	44130		Ross Sea	CANTA087-08	TAN0802		-76.59	176.83	369	01/02/2008
Pareledone	turqueti	44255		Ross Sea	CANTA105-08	TAN0802		-76.60	176.80	360	01/02/2008
Pareledone	turqueti	44074_5	44074.5	Ross Sea	CANTA114-08	TAN0802		-76.19	176.30	447	01/02/2008
Pareledone	turqueti	44113_3	44113.3	Ross Sea	CANTA044-08	TAN0802		-76.19	176.30	447	01/02/2008
Pareledone	turqueti	44113_4	44113.4	Ross Sea	CANTA045-08	TAN0802		-76.19	176.30	447	01/02/2008
Pareledone	turqueti	44118_3	44118.3	Ross Sea	CANTA092-08	TAN0802		-76.19	176.30	447	01/02/2008
Pareledone	turqueti	44256_1	44256.1	Ross Sea	CANTA107-08	TAN0802		-72.35	175.50	850	01/02/2008
Pareledone	turqueti	NIWA87970		Ross Sea		Kat Bolstad					
Pareledone	turqueti	PT214SG	SG06_214	Shag Rocks	CAOII564-09			-53.74	-41.46	164	11/01/2006
Pareledone	turqueti	PT24SG	SG05_24	Shag Rocks	CAOII464-09			-53.92	-41.56	314	18/01/2005
Pareledone	turqueti	PT376SG	SG90_376	Shag Rocks	CAOII646-09			-53.57	-41.63	120	08/01/1990
Pareledone	turqueti	PT377SG	SG90_377	Shag Rocks	CAOII647-09			-53.57	-41.63	120	08/01/1990
Pareledone	turqueti	PT381SG		Shag Rocks				-53.57	-41.63	120	08/01/1990
Pareledone	turqueti	PT382SG		Shag Rocks				-53.57	-41.63	120	08/01/1990
Pareledone	turqueti	PT386SG		Shag Rocks				-53.57	-41.63	120	08/01/1990
Pareledone	turqueti	PT42SG	SG05_42	Shag Rocks	CAOII481-09			-53.72	-41.28	130	19/01/2005
Pareledone	turqueti	PT511SG		Shag Rocks				-53.53	-42.22	158	
Pareledone	turqueti	PT305SG		South Georgia				-54.58	-35.44	150	
Pareledone	turqueti	PT328SG	SG06_328	South Georgia	CAOII622-09			-55.06	-36.07	149	17/01/2006
Pareledone	turqueti	PT354SG	PC_354	South Georgia	CAOII632-09			-54.07	-35.67	205	09/02/1991
Pareledone	turqueti	PT355SG	PC_355	South Georgia	CAOII633-09			-54.07	-35.67	205	09/02/1991
Pareledone	turqueti	PT356SG	PC_356	South Georgia	CAOII634-09			-54.07	-35.67	205	09/02/1991

Pareledone	turqueti	PT357SG		South Georgia			-54.07	-35.67	205	09/02/1991
Pareledone	turqueti	PT366SG	PC_366	South Georgia	CAOII638-09		-54.78	-34.92	349	01/02/1991
Pareledone	turqueti	PT367SG	PC_367	South Georgia	CAOII639-09		-54.78	-34.92	349	01/02/1991
Pareledone	turqueti	PT401SG		South Georgia			-55.06	-35.38	124	
Pareledone	turqueti	PT415SG		South Georgia			-54.62	-35.53	113	
Pareledone	turqueti	PT420SG		South Georgia			-54.62	-35.53	113	
Pareledone	turqueti	PT421SG		South Georgia			-54.62	-35.53	113	
Pareledone	turqueti	PT432SG		South Georgia			-53.67	-38.07	154	
Pareledone	turqueti	PT440SG		South Georgia			-53.65	-37.22	168	
Pareledone	turqueti	PT445SG		South Georgia			-53.65	-37.22	168	
Pareledone	turqueti	PT446SG		South Georgia			-53.65	-37.22	168	
Pareledone	turqueti	PT449SG		South Georgia			-53.65	-37.22	168	
Pareledone	turqueti	PT508SG	SG06_508	South Georgia	CAOII658-09		-53.53	-42.22	158	12/01/2006
Pareledone	turqueti	PT73SG	SG05_73	South Georgia	CAOII511-09		-53.79	-39.29	401	15/01/2005
Pareledone	turqueti	PT250		South Orkney Is			-61.00	-45.90	240	
Pareledone	turqueti	PT255		South Orkney Is			-62.00	-57.20	111	
Pareledone	turqueti	JS_26		South Weddell Sea		RV Polarstern PS82	-77.72	-35.98	613	04/01/2014
Pareledone	turqueti	JS_40		South Weddell Sea		RV Polarstern PS82				2014
Pareledone	turqueti	JS_44		South Weddell Sea		RV Polarstern PS82				2016
Pareledone	turqueti	JS10		South Weddell Sea		RV Polarstern PS96	-72.31	-16.86	762	29/01/2016
Pareledone	turqueti	JS5		South Weddell Sea		RV Polarstern PS96	-72.59	-18.07	406	31/01/2016
Pareledone	aequipapillae	44064_1		Ross Sea		TAN0802	-74.58	170.25	285	01/02/2008
Pareledone	cornuta	CT931		Adélie Land		CEAMARC	-66.40	139.79	444	14/01/2008

Supplementary Table 6.4 Sample information of *Ophionotus victoriae* (n = 169) and outgroup (n = 1) sequenced with target capture sequencing of ddRAD loci.

Genus	Species	Field ID	Registration ID	Sample location	Collection date	Expedition	Station ID	Event number	Latitude	Longitude	Collection depth (m)	Sample used for population structure inference?	Sample used for demographic modelling and admixture-based statistics?
Ophionotus	victoriae	140217A	NIWA140217	Ross Sea	01/02/2019	TAN1901	SRS2_7	175	-75.525	-172.992	1376	Yes	Yes
Ophionotus	victoriae	140217B	NIWA140217	Ross Sea	01/02/2019	TAN1901	SRS2_7	175	-75.525	-172.992	1376	Yes	Yes
Ophionotus	victoriae	140217C	NIWA140217	Ross Sea	01/02/2019	TAN1901	SRS2_7	175	-75.525	-172.992	1376	Yes	Yes
Ophionotus	victoriae	36968A	NIWA36968	Ross Sea	18/02/2008	TAN0802		100	-76.202	176.248	447	Yes	Yes
Ophionotus	victoriae	36968B	NIWA36968	Ross Sea	18/02/2008	TAN0802		100	-76.202	176.248	447	Yes	Yes
Ophionotus	victoriae	36968C	NIWA36968	Ross Sea	18/02/2008	TAN0802		100	-76.202	176.248	447	Yes	Yes
Ophionotus	victoriae	36968E	NIWA36968	Ross Sea	18/02/2008	TAN0802		100	-76.202	176.248	447	Yes	Yes
Ophionotus	victoriae	36968F	NIWA36968	Ross Sea	18/02/2008	TAN0802		100	-76.202	176.248	447	Yes	Yes
Ophionotus	victoriae	37157A	NIWA37157	Ross Sea	21/02/2008	TAN0802		117	-72.590	175.342	175	Yes	Yes
Ophionotus	victoriae	37157B	NIWA37157	Ross Sea	21/02/2008	TAN0802		117	-72.590	175.342	175		Yes
Ophionotus	victoriae	93825B	NIWA93825	Ross Sea	27/02/2004	TAN0402		174	-71.494	171.604	483	Yes	Yes
Ophionotus	victoriae	93825C	NIWA93825	Ross Sea	27/02/2004	TAN0402		174	-71.494	171.604	483	Yes	Yes
Ophionotus	victoriae	93825A	NIWA93825	Ross Sea	27/02/2004	TAN0402		174	-71.494	171.604	483	Yes	Yes
Ophionotus	victoriae	94858A	NIWA94858	Ross Sea	23/02/2004	TAN0402		133	-71.645	170.219	252	Yes	Yes
Ophionotus	victoriae	94858B	NIWA94858	Ross Sea	23/02/2004	TAN0402		133	-71.645	170.219	252	Yes	Yes
Ophionotus	victoriae	94866A	NIWA94866	Ross Sea	23/02/2004	TAN0402		132	-71.648	170.180	172	Yes	Yes
Ophionotus	victoriae	94866B	NIWA94866	Ross Sea	23/02/2004	TAN0402		132	-71.648	170.180	172	Yes	Yes
Ophionotus	victoriae	94869A	NIWA94869	Ross Sea	27/02/2004	TAN0402		174	-71.494	171.604	483	Yes	Yes
Ophionotus	victoriae	94869B	NIWA94869	Ross Sea	27/02/2004	TAN0402		174	-71.494	171.604	483	Yes	Yes
Ophionotus	victoriae	N0071	NIWA85184	Ross Sea	14/02/2008	TAN0802		61	-75.622	169.805	521	Yes	Yes
Ophionotus	victoriae	N0072	NIWA85184	Ross Sea	14/02/2008	TAN0802		61	-75.622	169.805	521	Yes	Yes
Ophionotus	victoriae	N0073	NIWA85184	Ross Sea	14/02/2008	TAN0802		61	-75.622	169.805	521	Yes	Yes
Ophionotus	victoriae	N0074	NIWA85184	Ross Sea	14/02/2008	TAN0802		61	-75.622	169.805	521	Yes	Yes
Ophionotus	victoriae	N0075	NIWA85184	Ross Sea	14/02/2008	TAN0802		61	-75.622	169.805	521	Yes	Yes
Ophionotus	victoriae	N0103		Ross Sea	16/02/2008	TAN0802		77	-76.833	179.950	663.5		Yes
Ophionotus	victoriae	PDIVA-C	SIOBICE4766	Ross Sea	11/20/2010	SIO McMurdo		IVA	-77.572	163.512	Scuba diver	Yes	Yes
Ophionotus	victoriae	PDIVA-D	SIOBICE4766	Ross Sea	11/20/2010	SIO McMurdo		IVA	-77.572	163.512	Scuba diver	Yes	Yes

Ophionotus	victoriae	PDIVA-E	SIOBICE4766	Ross Sea	11/20/2010	SIO McMurdo		IVA	-77.572	163.512	Scuba diver	Yes	Yes
Ophionotus	victoriae	PDIVA-G	SIOBICE4766	Ross Sea	11/20/2010	SIO McMurdo		IVA	-77.572	163.512	Scuba diver	Yes	Yes
Ophionotus	victoriae	PDIVA-I	SIOBICE4766	Ross Sea	11/20/2010	SIO McMurdo		IVA	-77.572	163.512	Scuba diver	Yes	Yes
Ophionotus	victoriae	250	250	Amundsen Sea	05/03/2008	JR179	BIO4-AGT-2A		-74.479	-104.237	1203.06	Yes	Yes
Ophionotus	victoriae	251	251	Amundsen Sea	05/03/2008	JR179	BIO4-AGT-2A		-74.479	-104.237	1203.06	Yes	Yes
Ophionotus	victoriae	830	830	Amundsen Sea	12/03/2008	JR179	BIO6-AGT-2A		-71.175	-109.863	1005.79	Yes	Yes
Ophionotus	victoriae	811.11	811.11	Amundsen Sea	12/03/2008	JR179	BIO6-AGT-2A		-71.175	-109.863	1005.79	Yes	Yes
Ophionotus	victoriae	811.14	811.14	Amundsen Sea	12/03/2008	JR179	BIO6-AGT-2A		-71.175	-109.863	1005.79		Yes
Ophionotus	victoriae	811.17	811.17	Amundsen Sea	12/03/2008	JR179	BIO6-AGT-2A		-71.175	-109.863	1005.79		Yes
Ophionotus	victoriae	881.19	881.19	Amundsen Sea	12/03/2008	JR179	BIO6-AGT-2A		-71.175	-109.863	1005.79	Yes	Yes
Ophionotus	victoriae	881.2	881.2	Amundsen Sea	12/03/2008	JR179	BIO6-AGT-2A		-71.175	-109.863	1005.79		Yes
Ophionotus	victoriae	903	903	Amundsen Sea	12/03/2008	JR179	BIO6-AGT-2B		-71.179	-109.894	988.93	Yes	Yes
Ophionotus	victoriae	904	904	Amundsen Sea	12/03/2008	JR179	BIO6-AGT-2B		-71.179	-109.894	988.93		Yes
Ophionotus	victoriae	980.4	980.4	Amundsen Sea	13/03/2008	JR179	BIO6-AGT-1B		-71.152	-110.013	1491.25		Yes
Ophionotus	victoriae	94857A	NIWA94857	Balleny Islands	04/03/2008	TAN0402		233	-67.418	163.915	227	Yes	
Ophionotus	victoriae	94857B	NIWA94857	Balleny Islands	04/03/2008	TAN0402		233	-67.418	163.915	227	Yes	
Ophionotus	victoriae	N0078	NIWA84670	Balleny Islands	11/03/2006	TAN0602		448	-66.557	162.570	85	Yes	
Ophionotus	victoriae	N0079	NIWA84670	Balleny Islands	11/03/2006	TAN0602		448	-66.557	162.570	85	Yes	
Ophionotus	victoriae	N0080	NIWA84670	Balleny Islands	11/03/2006	TAN0602		448	-66.557	162.570	85	Yes	
Ophionotus	victoriae	WAMZ44965	WAMZ44965	Balleny Islands	02/03/2017	ACE 2016/17	46	1209	-66.174	162.203	350	Yes	
Ophionotus	victoriae	WAMZ44962	WAMZ44962	Balleny Islands	02/03/2017	ACE 2016/17	46	1209	-66.174	162.203	350	Yes	
Ophionotus	victoriae	WAMZ44963	WAMZ44963	Balleny Islands	02/03/2017	ACE 2016/17	46	1209	-66.174	162.203	350	Yes	
Ophionotus	victoriae	AAD107	AAD107	Prydz Bay	28/01/2001	AAD	AL27-130	58.4.2	-66.791	62.442	213	Yes	Yes
Ophionotus	victoriae	AAD139	AAD139	Prydz Bay	27/01/2001	AAD	AL27-127	58.4.2	-66.792	62.096	270		Yes
Ophionotus	victoriae	AAD141	AAD141	Prydz Bay	27/01/2001	AAD	AL27-127	58.4.2	-66.792	62.096	270	Yes	Yes
Ophionotus	victoriae	AAD143	AAD143	Prydz Bay	27/01/2001	AAD	AL27-127	58.4.2	-66.792	62.096	270		Yes
Ophionotus	victoriae	AAD144	AAD144	Prydz Bay	27/01/2001	AAD	AL27-127	58.4.2	-66.792	62.096	270		Yes
Ophionotus	victoriae	SIOBICP00496A	SIOBICE5492	Bransfield Strait	04/02/2012	Polarstern ANT-XXVIII/4		79273	-62.367	-55.961	349	Yes	
Ophionotus	victoriae	SIOBICP00496B	SIOBICE5492	Bransfield Strait	04/02/2012	Polarstern ANT-XXVIII/4		79273	-62.367	-55.961	349	Yes	
Ophionotus	victoriae	SIOBICP00496C	SIOBICE5492	Bransfield Strait	04/02/2012	Polarstern ANT-XXVIII/4		79273	-62.367	-55.961	349	Yes	
Ophionotus	victoriae	SIOBICP00496D	SIOBICE5492	Bransfield Strait	04/02/2012	Polarstern ANT-XXVIII/4		79273	-62.367	-55.961	349	Yes	
Ophionotus	victoriae	SIOBICP00496E	SIOBICE5492	Bransfield Strait	04/02/2012	Polarstern ANT-XXVIII/4		79273	-62.367	-55.961	349	Yes	
Ophionotus	victoriae	SIOBICP00524A	SIOBICE5524	Bransfield Strait	04/02/2012	Polarstern ANT-XXVIII/4		79279	-62.278	-55.833	324	Yes	

Ophionotus	victoriae	SIOBICP 00524B	SIOBICE5524	Bransfield Strait	04/02/2012	Polarstern ANT-XXVIII/4		79279	-62.278	-55.833	324	Yes		
Ophionotus	victoriae	SIOBICP 00524C	SIOBICE5524	Bransfield Strait	04/02/2012	Polarstern ANT-XXVIII/4		79279	-62.278	-55.833	324	Yes		
Ophionotus	victoriae	SIOBICP 00524D	SIOBICE5524	Bransfield Strait	04/02/2012	Polarstern ANT-XXVIII/4		79279	-62.278	-55.833	324	Yes		
Ophionotus	victoriae	SIOBICP 00524E	SIOBICE5524	Bransfield Strait	04/02/2012	Polarstern ANT-XXVIII/4		79279	-62.278	-55.833	324	Yes		
Ophionotus	victoriae	SIOBICS 20231	SIOBICE6408	South Georgia	17/04/2013	Scotia 2013	SG4b	9	-53.634	-37.307	167	Yes		
Ophionotus	victoriae	SIOBICS 20237	SIOBICE6420	South Georgia	16/04/2013	Scotia 2013	SG4	5	-53.715	-36.836	190	Yes		
Ophionotus	victoriae	IE.2009.4 672	IE.2009. 04672	Adelie Land	14/01/2008	CEAMARC	70EV451		-66.409	140.508	1204	Yes		
Ophionotus	victoriae	IE.2009.4 675	IE.2009. 06259	Adelie Land	15/01/2008	CEAMARC	22EV503		-65.991	139.307	485	Yes		
Ophionotus	victoriae	IE.2009.4 676	IE.2009. 04676	Adelie Land	14/01/2008	CEAMARC	70EV451		-66.409	140.508	1204	Yes		
Ophionotus	victoriae	IE.2009.4 679	IE.2009. 04679	Adelie Land	14/01/2008	CEAMARC	70EV451		-66.409	140.508	1204	Yes		
Ophionotus	victoriae	IE.2009.4 687A	IE.2009. 06154	Adelie Land	13/01/2008	CEAMARC	10EV420		-66.335	141.273	227	Yes		
Ophionotus	victoriae	IE.2009.4 690	IE.2009. 06478	Adelie Land	28/12/2007	CEAMARC	40EV152		-66.651	142.957	637	Yes		
Ophionotus	victoriae	IE.2009.4 702	IE.2009. 06736	Adelie Land	26/12/2007	CEAMARC	9EV117		-66.535	141.983	521	Yes		
Ophionotus	victoriae	IE.2009.4 703	IE.2009. 06468	Adelie Land	12/01/2008	CEAMARC	3EV411		-66.000	142.014	248	Yes		
Ophionotus	victoriae	IE.2009.4 707	IE.2009. 06232	Adelie Land	12/01/2008	CEAMARC	1EV405		-66.004	142.314	240	Yes		
Ophionotus	victoriae	IE.2009.4 713	IE.2009. 06736	Adelie Land	26/12/2007	CEAMARC	9EV117		-66.535	141.983	521	Yes		
Ophionotus	victoriae	IE.2009.4 726	IE.2009. 04726	Adelie Land	27/12/2007	CEAMARC	39EV141		-66.550	142.959	875	Yes		
Ophionotus	victoriae	IE.2009.4 731	IE.2009. 04731	Adelie Land	24/12/2007	CEAMARC	30EV66		-66.004	143.716	440	Yes		
Ophionotus	victoriae	IE.2009.4 734	IE.2009. 06386	Adelie Land	03/01/2008	CEAMARC	31EV268		-66.539	144.973	451	Yes		
Ophionotus	victoriae	IE.2009.4 753	IE.2009. 06662	Adelie Land	14/01/2008	CEAMARC	71EV447		-66.389	140.429	791	Yes		
Ophionotus	victoriae	IE.2009.4 754	IE.2009. 06381	Adelie Land	24/12/2007	CEAMARC	30EV66		-66.004	143.716	440	Yes		
Ophionotus	victoriae	IE.2009.4 763	IE.2009. 04763	Adelie Land	02/01/2008	CEAMARC	59EV259		-66.739	144.307	954	Yes		
Ophionotus	victoriae	IE.2009.4 767	IE.2009. 06523	Adelie Land	26/12/2007	CEAMARC	4EV112		-66.316	142.000	257	Yes		
Ophionotus	victoriae	N0121	NIWA84671	Scott Island	04/03/2008	TAN0802		223	-67.829	-179.587	403	Yes		
Ophionotus	victoriae	N0122	NIWA84671	Scott Island	04/03/2008	TAN0802		223	-67.829	-179.587	403	Yes		
Ophionotus	victoriae	N0123	NIWA84675	Scott Island	07/03/2008	TAN0802		247	-67.388	-179.897	144	Yes		
Ophionotus	victoriae	N0125	NIWA84675	Scott Island	07/03/2008	TAN0802		247	-67.388	-179.897	144	Yes		
Ophionotus	victoriae	PNG703	PNG703	Tressler Bank	03/01/2010	AAD	Tressler2	BTC17	-64.560	95.320	758	Yes	Yes	
Ophionotus	victoriae	PNG708	PNG708	Tressler Bank	03/01/2010	AAD	Tressler2	BTC15	-64.560	95.317	779	Yes	Yes	

Ophionotus	victoriae	PNG710	PNG710	Tressler Bank	03/01/2010	AAD	Tressler2	BTC15	-64.560	95.317	779	Yes	Yes
Ophionotus	victoriae	SIOBICS 0185	SIOBICE5232	South Sandwich Islands	03/10/2011	Scotia 2011	SS1A	30	-56.723	-27.036	134	Yes	
Ophionotus	victoriae	SIOBICS 0460	SIOBICE5187	South Sandwich Islands	03/10/2011	Scotia 2011	SS1A	32	-56.709	-27.049	116	Yes	
Ophionotus	victoriae	SIOBICS 0539B	SIOBICE4802	South Sandwich Islands	05/10/2011	Scotia 2011	SS2	33	-58.475	-26.205	161	Yes	
Ophionotus	victoriae	SIOBICS 0539D	SIOBICE4802	South Sandwich Islands	05/10/2011	Scotia 2011	SS2	33	-58.475	-26.205	161	Yes	
Ophionotus	victoriae	SIOBICS 0990A	SIOBICE4784	South Sandwich Islands	03/10/2011	Scotia 2011	SS1	25	-57.034	-26.759	118	Yes	
Ophionotus	victoriae	SIOBICS 0990C	SIOBICE4784	South Sandwich Islands	03/10/2011	Scotia 2011	SS1	25	-57.034	-26.759	118	Yes	
Ophionotus	victoriae	WAMZ44 590	WAMZ44590	South Sandwich Islands	03/08/2017	ACE 2016/17	90	2590	-59.472	-27.264	230	Yes	
Ophionotus	victoriae	WAMZ44 932	WAMZ44932	South Sandwich Islands	03/08/2017	ACE 2016/17	90	2590	-59.472	-27.264	230	Yes	
Ophionotus	victoriae	SIOBICS 1312H	SIOBICE4771	Elephant Island	22/10/2011	Scotia 2011	EI1	81	-61.218	-54.255	202	Yes	
Ophionotus	victoriae	SIOBICS 1312I	SIOBICE4771	Elephant Island	22/10/2011	Scotia 2011	EI1	81	-61.218	-54.255	202	Yes	
Ophionotus	victoriae	SIOBICS 6741	SIOBICE5209	Elephant Island	23/10/2011	Scotia 2011	EI2	83	-61.339	-55.625	143	Yes	
Ophionotus	victoriae	SIOBICS 6743	SIOBICE5237	Elephant Island	23/10/2011	Scotia 2011	EI2	83	-61.339	-55.625	143	Yes	
Ophionotus	victoriae	SIOBICS 6775A	SIOBICE4803	Elephant Island	23/10/2011	Scotia 2011	EI2	84	-61.304	-55.708	170	Yes	
Ophionotus	victoriae	SIOBICS 4306	SIOBICE5221	Discovery Bank	13/10/2011	Scotia 2011	DB1	58	-60.111	-34.827	439	Yes	
Ophionotus	victoriae	SIOBICS 4307	SIOBICE5169	Discovery Bank	13/10/2011	Scotia 2011	DB1	58	-60.111	-34.827	439	Yes	
Ophionotus	victoriae	SIOBICS 4308	SIOBICE5194	Discovery Bank	13/10/2011	Scotia 2011	DB1	58	-60.111	-34.827	439	Yes	
Ophionotus	victoriae	SIOBICS 4309	SIOBICE5168	Discovery Bank	13/10/2011	Scotia 2011	DB1	58	-60.111	-34.827	439	Yes	
Ophionotus	victoriae	SIOBICS 4310	SIOBICE5183	Discovery Bank	13/10/2011	Scotia 2011	DB1	58	-60.111	-34.827	439	Yes	
Ophionotus	victoriae	SIOBICS 4472K	SIOBICE4791	Herdman Bank	10/10/2011	Scotia 2011	HB1	50	-59.863	-32.470	600	Yes	
Ophionotus	victoriae	SIOBICS 4472L	SIOBICE4791	Herdman Bank	10/10/2011	Scotia 2011	HB1	50	-59.863	-32.470	600	Yes	
Ophionotus	victoriae	SIOBICS 4472M	SIOBICE4791	Herdman Bank	10/10/2011	Scotia 2011	HB1	50	-59.863	-32.470	600	Yes	
Ophionotus	victoriae	SIOBICS 4472N	SIOBICE4791	Herdman Bank	10/10/2011	Scotia 2011	HB1	50	-59.863	-32.470	600	Yes	
Ophionotus	victoriae	SIOBICS 4472O	SIOBICE4791	Herdman Bank	10/10/2011	Scotia 2011	HB1	50	-59.863	-32.470	600	Yes	
Ophionotus	victoriae	SIOBICS 5741B	SIOBICE7575	Shetland Islands	27/10/2011	Scotia 2011	SSH1	94	-62.337	-60.744	183	Yes	Yes
Ophionotus	victoriae	SIOBICS 5741C	SIOBICE7575	Shetland Islands	27/10/2011	Scotia 2011	SSH1	94	-62.337	-60.744	183	Yes	Yes
Ophionotus	victoriae	SIOBICS 5741F	SIOBICE7575	Shetland Islands	27/10/2011	Scotia 2011	SSH1	94	-62.337	-60.744	183	Yes	Yes
Ophionotus	victoriae	SIOBICS 5742	SIOBICE5171	Shetland Islands	27/10/2011	Scotia 2011	SSH1	94	-62.337	-60.744	183	Yes	Yes

Ophionotus	victoriae	SIOBICS 5743	SIOBICE5023	Shetland Islands	27/10/2011	Scotia 2011	SSH1	94	-62.337	-60.744	183	Yes	Yes
Ophionotus	victoriae	SIOBICS 6316A	SIOBICE4770	Bransfield Strait	25/10/2011	Scotia 2011	BS2	89	-63.343	-59.910	213	Yes	
Ophionotus	victoriae	SIOBICS 6316B	SIOBICE4770	Bransfield Strait	25/10/2011	Scotia 2011	BS2	89	-63.343	-59.910	213	Yes	
Ophionotus	victoriae	SIOBICS 6338A	SIOBICE4781	Bransfield Strait	25/10/2011	Scotia 2011	BS2	90	-63.283	-59.903	290	Yes	
Ophionotus	victoriae	SIOBICS 6338B	SIOBICE4781	Bransfield Strait	25/10/2011	Scotia 2011	BS2	90	-63.283	-59.903	290	Yes	
Ophionotus	victoriae	SIOBICS 6760A	SIOBICE4777	Bransfield Strait	24/10/2011	Scotia 2011	BS1	87	-62.753	-57.322	292	Yes	
Ophionotus	victoriae	SIOBICS 6760B	SIOBICE4777	Bransfield Strait	24/10/2011	Scotia 2011	BS1	87	-62.753	-57.322	292	Yes	
Ophionotus	victoriae	SIOBICS 6905A	SIOBICE5162	Bransfield Strait	24/10/2011	Scotia 2011	BS1	86	-62.870	-57.217	247	Yes	
Ophionotus	victoriae	SIOBICS 6905B	SIOBICE5162	Bransfield Strait	24/10/2011	Scotia 2011	BS1	86	-62.870	-57.217	247	Yes	
Ophionotus	victoriae	WAMZ44 948	WAMZ44948	Bouvet Island	03/11/2017	ACE 2016/17	98	2765	-54.419	-3.494	300	Yes	
Ophionotus	victoriae	WAMZ44 949	WAMZ44949	Bouvet Island	03/11/2017	ACE 2016/17	98	2765	-54.419	-3.494	300	Yes	
Ophionotus	victoriae	WAMZ44 950	WAMZ44950	Bouvet Island	03/11/2017	ACE 2016/17	98	2765	-54.419	-3.494	300	Yes	
Ophionotus	victoriae	WAMZ44 951	WAMZ44951	Bouvet Island	03/11/2017	ACE 2016/17	98	2765	-54.419	-3.494	300	Yes	
Ophionotus	victoriae	WAMZ44 953	WAMZ44953	Bouvet Island	03/11/2017	ACE 2016/17	98	2765	-54.419	-3.494	300	Yes	
Ophionotus	victoriae	WAMZ44 954	WAMZ44954	Bouvet Island	03/11/2017	ACE 2016/17	98	2765	-54.419	-3.494	300	Yes	
Ophionotus	victoriae	WAMZ44 955	WAMZ44955	Bouvet Island	03/11/2017	ACE 2016/17	98	2765	-54.419	-3.494	300	Yes	
Ophionotus	victoriae	WAMZ44 956	WAMZ44956	Bouvet Island	03/11/2017	ACE 2016/17	98	2765	-54.419	-3.494	300	Yes	
Ophionotus	victoriae	WAMZ44 957	WAMZ44957	Bouvet Island	03/11/2017	ACE 2016/17	98	2765	-54.419	-3.494	300	Yes	
Ophionotus	victoriae	WAMZ44 958	WAMZ44958	Bouvet Island	03/11/2017	ACE 2016/17	98	2765	-54.419	-3.494	300	Yes	
Ophionotus	victoriae	308-1.7	WAMZ88554	Weddell Sea	04/04/2011	Polarstern ANT-XXVII/3	PS77_308-1		-70.858	-10.593	250	Yes	Yes
Ophionotus	victoriae	265-2.12	WAMZ88558	Weddell Sea	22/03/2011	Polarstern ANT-XXVII/3	PS77_265-2		-70.793	-10.678	615	Yes	Yes
Ophionotus	victoriae	265-2.11	WAMZ88559	Weddell Sea	22/03/2011	Polarstern ANT-XXVII/3	PS77_265-2		-70.793	-10.678	615	Yes	Yes
Ophionotus	victoriae	265-2.10	WAMZ88570	Weddell Sea	22/03/2011	Polarstern ANT-XXVII/3	PS77_265-2		-70.793	-10.678	615	Yes	Yes
Ophionotus	victoriae	274-3.14	WAMZ88571	Weddell Sea	25/03/2011	Polarstern ANT-XXVII/3	PS77_274-3		-70.949	-10.574	333	Yes	Yes
Ophionotus	victoriae	265-2.11	WAMZ88576	Weddell Sea	22/03/2011	Polarstern ANT-XXVII/3	PS77_265-2		-70.793	-10.678	615	Yes	Yes
Ophionotus	victoriae	265-2.13	WAMZ88577	Weddell Sea	22/03/2011	Polarstern ANT-XXVII/3	PS77_265-2		-70.793	-10.678	615	Yes	Yes
Ophionotus	victoriae	291-1.3	WAMZ88579	Weddell Sea	30/03/2011	Polarstern ANT-XXVII/3	PS77_291-1		-70.847	-10.590	284	Yes	Yes
Ophionotus	victoriae	308-1.8	WAMZ88583	Weddell Sea	04/04/2011	Polarstern ANT-XXVII/3	PS77_308-1		-70.858	-10.593	250	Yes	Yes

Ophionotus	victoriae	308-1.10	WAMZ88584	Weddell Sea	04/04/2011	Polarstern ANT-XXVII/3	PS77_308-10		-70.858	-10.593	250	Yes	Yes
Ophionotus	victoriae	WAMZ88555	WAMZ88555	Larsen Ice Shelf	12/03/2011	Polarstern ANT-XXVII/3	PS77_255-3		-64.833	-60.597	682	Yes	
Ophionotus	victoriae	WAMZ88556	WAMZ88556	Larsen Ice Shelf	03/03/2011	Polarstern ANT-XXVII/3	PS77_237-2		-66.208	-60.161	362	Yes	
Ophionotus	victoriae	WAMZ88563	WAMZ88563	Larsen Ice Shelf	27/02/2011	Polarstern ANT-XXVII/3	PS77_228-3		-64.903	-60.490	570	Yes	
Ophionotus	victoriae	WAMZ88568	WAMZ88568	Larsen Ice Shelf	10/03/2011	Polarstern ANT-XXVII/3	PS77_252-7		-64.704	-60.530	343	Yes	
Ophionotus	victoriae	WAMZ88572	WAMZ88572	Larsen Ice Shelf	07/03/2011	Polarstern ANT-XXVII/3	PS77_248-3		-65.928	-60.335	433	Yes	
Ophionotus	victoriae	WAMZ88573	WAMZ88573	Larsen Ice Shelf	07/03/2011	Polarstern ANT-XXVII/3	PS77_248-3		-65.928	-60.335	433	Yes	
Ophionotus	victoriae	WAMZ88574	WAMZ88574	Larsen Ice Shelf	01/03/2011	Polarstern ANT-XXVII/3	PS77_233-3		-65.558	-61.623	320	Yes	
Ophionotus	victoriae	WAMZ88575	WAMZ88575	Larsen Ice Shelf	01/03/2011	Polarstern ANT-XXVII/3	PS77_233-3		-65.558	-61.623	320	Yes	
Ophionotus	victoriae	WAMZ88578	WAMZ88578	Larsen Ice Shelf	01/03/2011	Polarstern ANT-XXVII/3	PS77_250-6		-65.381	-61.557	581	Yes	
Ophionotus	victoriae	1.140.1	WAMZ88585	Weddell Sea	26/01/2014	Polarstern ANT-XXIX/9	PS82_191-1		-74.666	-33.733	592	Yes	Yes
Ophionotus	victoriae	1.140.2	WAMZ88586	Weddell Sea	26/01/2014	Polarstern ANT-XXIX/9	PS82_191-1		-74.666	-33.733	592	Yes	Yes
Ophionotus	victoriae	1.140.3	WAMZ88587	Weddell Sea	26/01/2014	Polarstern ANT-XXIX/9	PS82_191-1		-74.666	-33.733	592	Yes	Yes
Ophionotus	victoriae	1.140.4	WAMZ88588	Weddell Sea	26/01/2014	Polarstern ANT-XXIX/9	PS82_67-1		-77.101	-36.546	1101	Yes	Yes
Ophionotus	victoriae	1.83.2	WAMZ88590	Weddell Sea	26/01/2014	Polarstern ANT-XXIX/9	PS82_67-1		-77.101	-36.546	1101	Yes	Yes
Ophionotus	victoriae	1.164.1	WAMZ88591	Weddell Sea	22/01/2014	Polarstern ANT-XXIX/9	PS82_151-1		-74.541	-28.531	1750	Yes	Yes
Ophionotus	victoriae	1.164.2	WAMZ88592	Weddell Sea	22/01/2014	Polarstern ANT-XXIX/9	PS82_151-1		-74.541	-28.531	1750	Yes	Yes
Ophionotus	victoriae	1.164.3	WAMZ88593	Weddell Sea	22/01/2014	Polarstern ANT-XXIX/9	PS82_151-1		-74.541	-28.531	1750	Yes	Yes
Ophionotus	victoriae	1.164.4	WAMZ88594	Weddell Sea	22/01/2014	Polarstern ANT-XXIX/9	PS82_151-1		-74.541	-28.531	1750	Yes	Yes
Ophionotus	victoriae	1.158	WAMZ88595	Weddell Sea	19/01/2014	Polarstern ANT-XXIX/9	PS82_126-1		-75.512	-27.487	282	Yes	Yes
Ophionotus	victoriae	1.158.1	WAMZ88596	Weddell Sea	19/01/2014	Polarstern ANT-XXIX/9	PS82_126-1		-75.512	-27.487	282	Yes	Yes
Ophionotus	victoriae	1.152.1	WAMZ88597	Weddell Sea	17/01/2014	Polarstern ANT-XXIX/9	PS82_115-1		-77.611	-38.939	1058	Yes	Yes
Ophionotus	victoriae	1.152.2	WAMZ88598	Weddell Sea	17/01/2014	Polarstern ANT-XXIX/9	PS82_115-1		-77.611	-38.939	1058	Yes	Yes
Ophionotus	victoriae	1.152.3	WAMZ88599	Weddell Sea	17/01/2014	Polarstern ANT-XXIX/9	PS82_115-1		-77.611	-38.939	1058	Yes	Yes
Ophionotus	hexactis	SIOBICS 3758	SIOBICE5246	Shag Rocks	23/09/2011	Scotia 2011	SR1	4	-53.453	-42.058	174	Outgroup	Outgroup

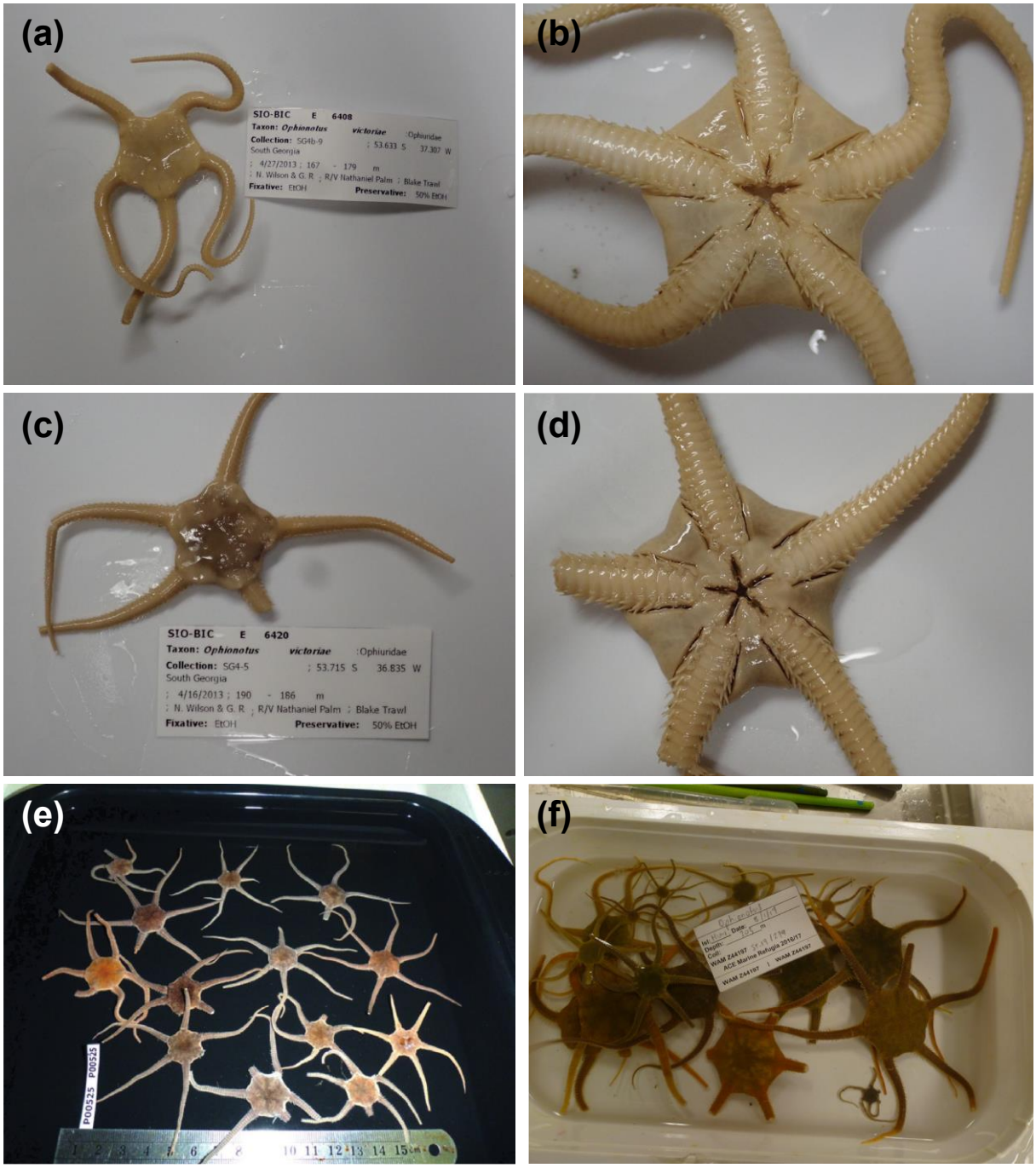

Supplementary Fig 2.1. (a, b) *Ophionotus victoriae* from South Georgia, SIO-BIC E6408 (field number S20231) and (c, d) *O. victoriae* from South Georgia, SIO-BIC 6420 (field number S20237). (e) *O. hexactis* from Bransfield Strait (SIO-BIC E5493A-E5493L). Note specimen from the top right corner of this photo was not sequenced in *Chapter 2*. (f) *O. hexactis* from Heard Island, Kerguelen Plateau (WAMZ43230-WAM43239). Note 10 out of 17 specimens were sequenced from this lot (lot number WAMZ44197) in *Chapter 2*.

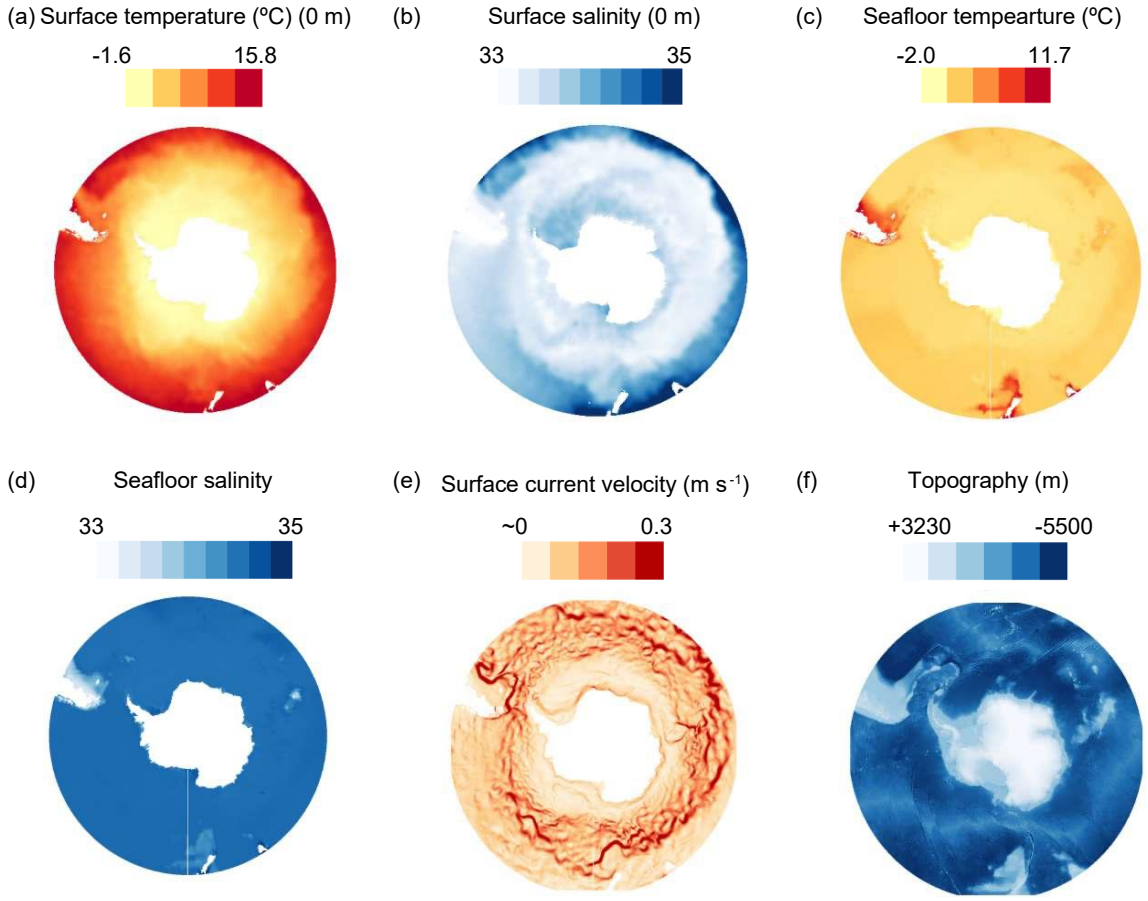

Supplementary Fig 2.2. Raster surfaces of six environmental parameters used as the input spatial predictors of spatial genetic patterns of *Ophionotus victoriae* and *O. hexactis*. The raster surfaces representing each environmental parameter were either interpolated (a-d) or resampled (f) to achieve a cell resolution of 16 km that was pre-defined in (e).

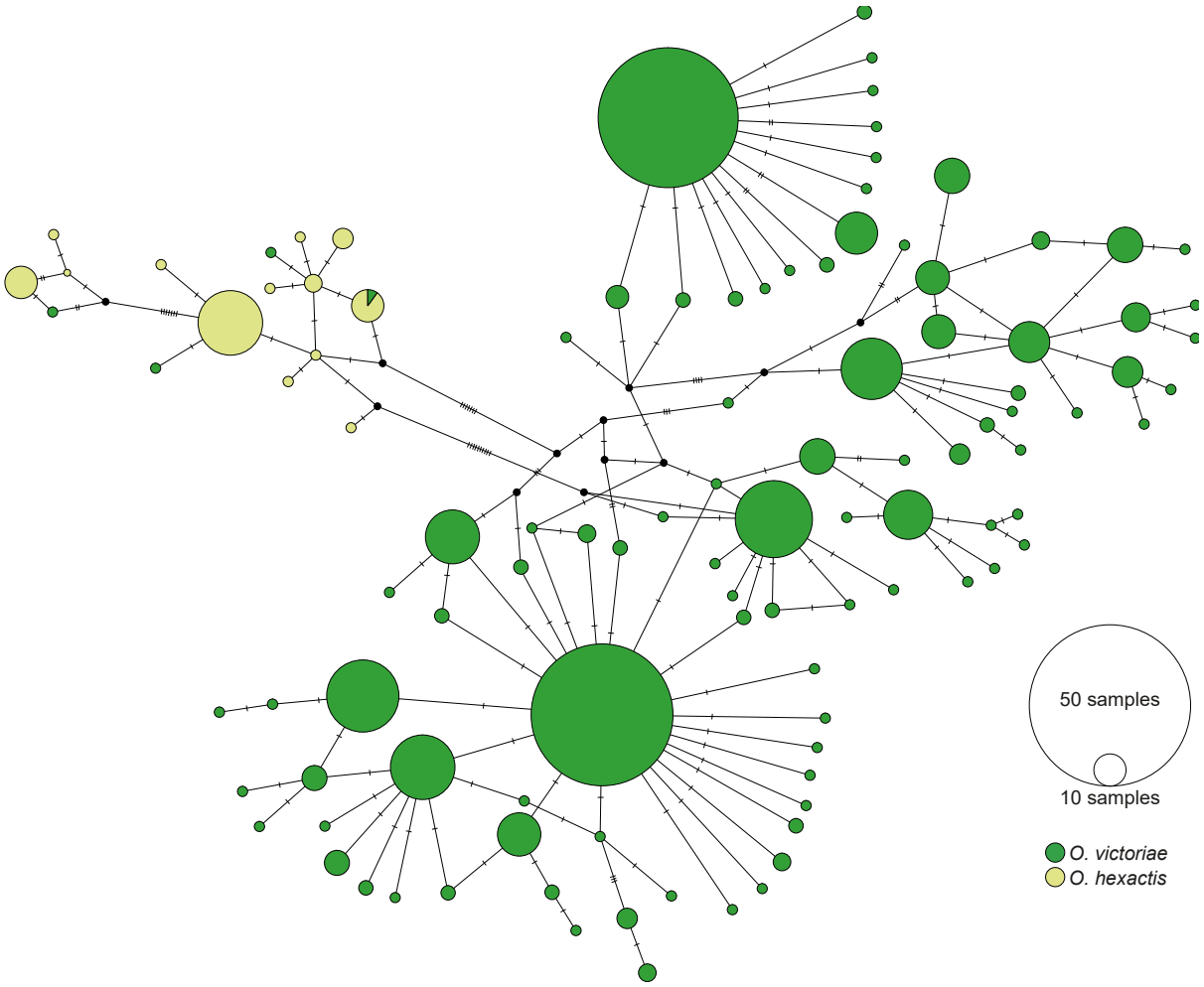

Supplementary Fig 2.3. TCS haplotype network of *Ophionotus victoriae* and *O. hexactis* COI sequences (434 bp, n = 935), separated by species. Size and colours of circle represent the number of samples and sample locations associated with each haplotype. Black circle = inferred haplotype missing in the dataset. Hatch lines = inferred mutation steps between haplotypes.

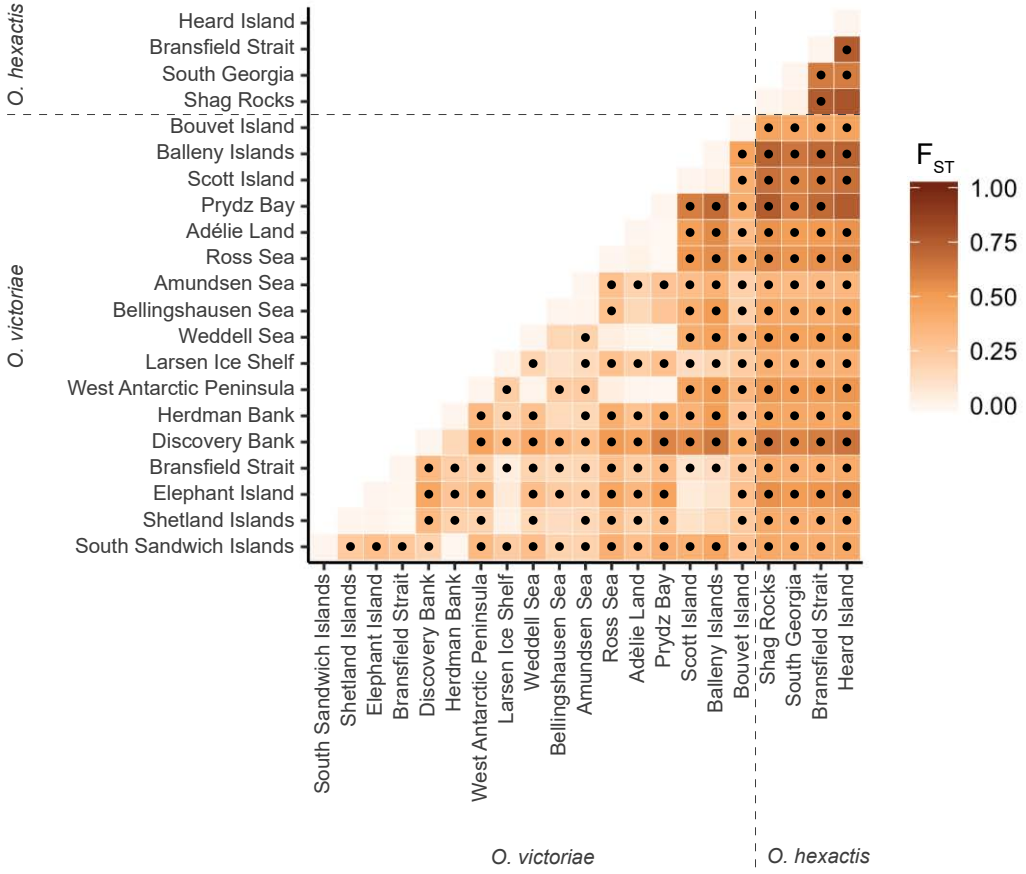

Supplementary Fig 2.4. Heatmap showing pairwise F_{ST} values estimated from COI data of *Ophionotus victoriae* and *O. hexactis*, between sample localities with sample size (n) $\geq$ 5. Dots indicate significant difference after Bonferroni corrections ($p < 0.00014$).

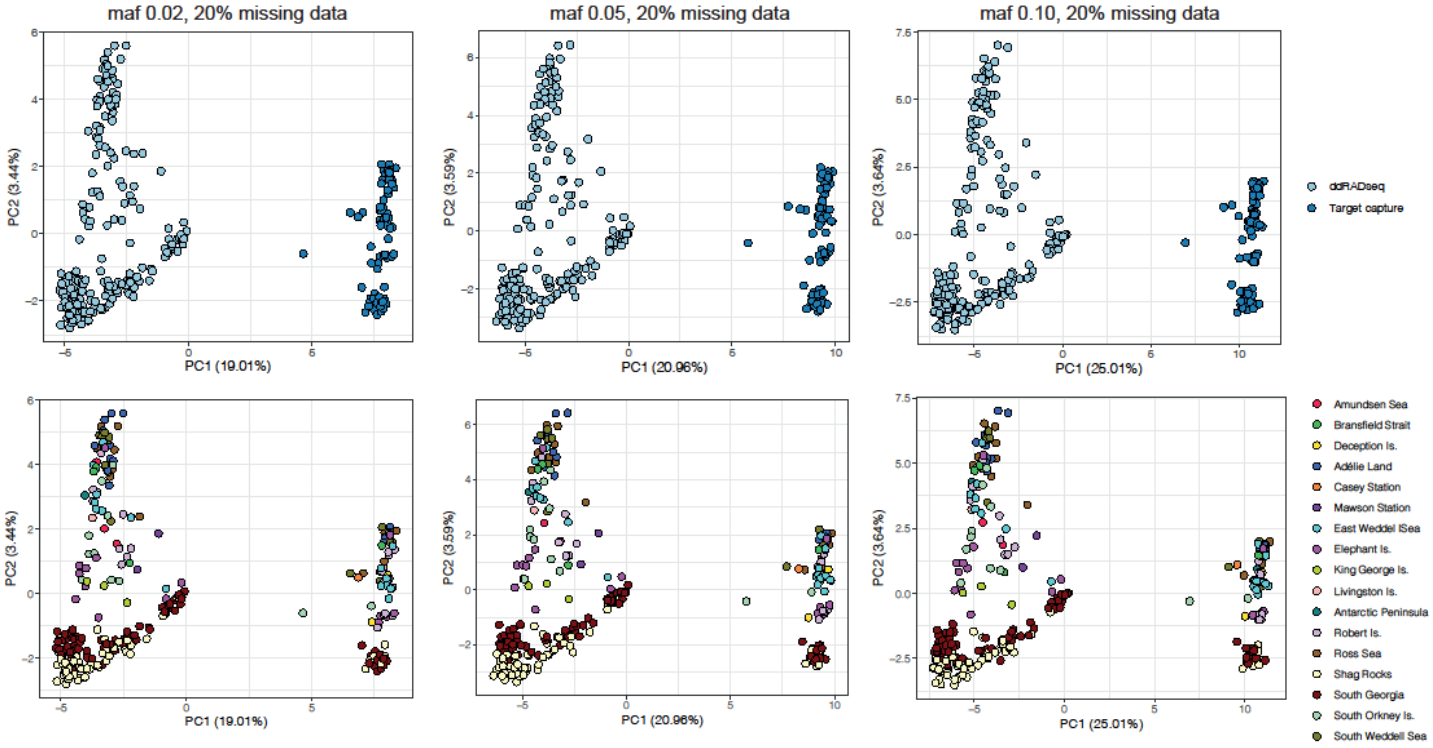

Supplementary Fig 3.1 Principal Component Analysis of ddRADseq and target capture sequencing of RAD loci in *Pareldone turqueti*. Samples are grouped by sequencing method (top panel) and location (bottom panel). Reads derived from both methods were processed together in a single bioinformatic pipeline via reference calling with *bcftools mpileup*. Data were filtered with different minor allele frequency threshold with 20% missing data allowed. No filtering for Hardy-Weinberg departure was applied.

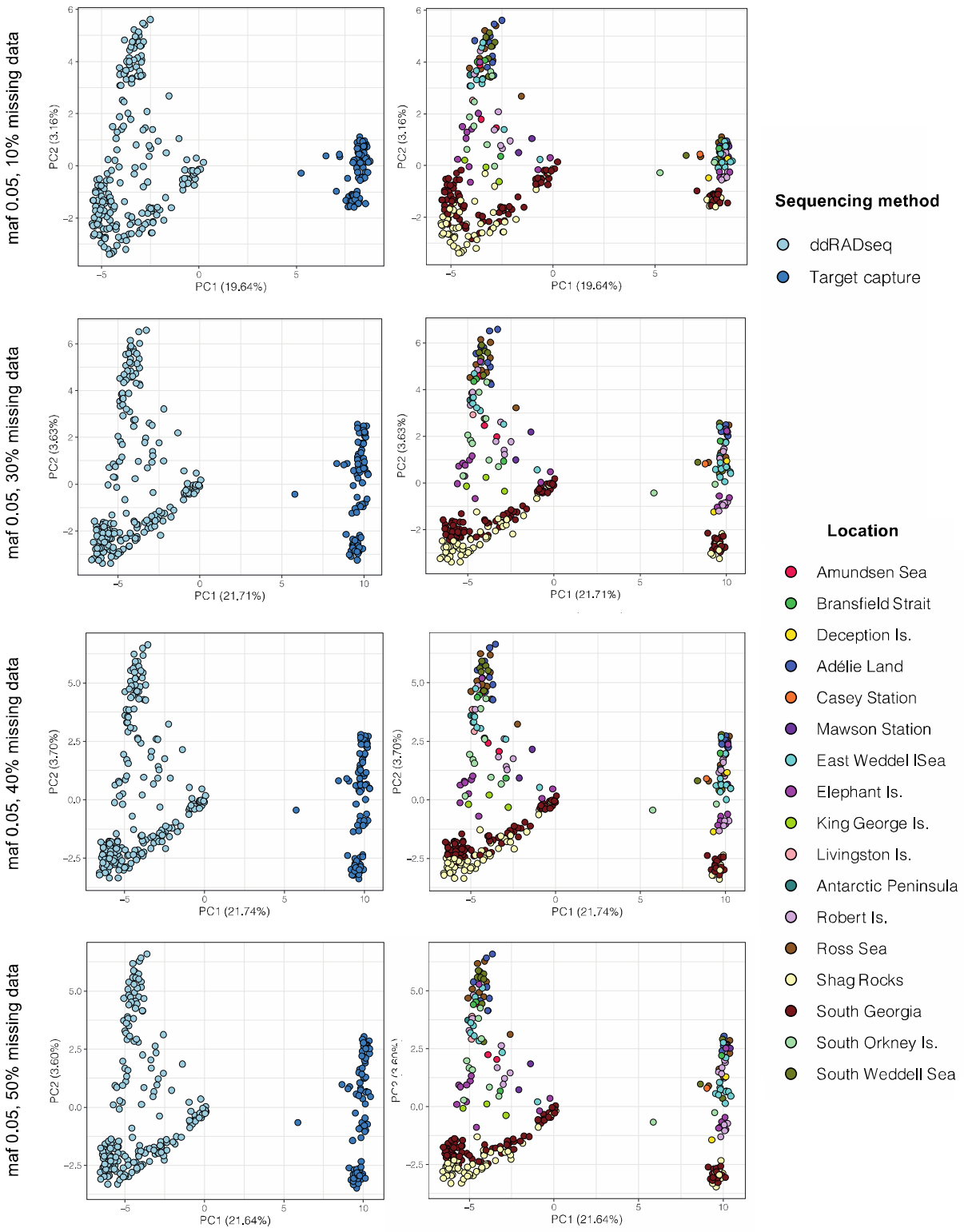

Supplementary Fig 3.2 Principal Component Analysis of ddRADseq and target capture sequencing of RAD loci in *Pareldone turqueti*. Samples are grouped by sequencing method (left panel) and location (right panel). Reads derived from both methods were processed together in a single bioinformatic pipeline via reference calling with *bcftools mpileup*. Data were filtered with different missing data threshold with at least a minor allele frequency of 0.05. No filtering for Hardy-Weinberg departure was applied, with and without filter applied for Hardy-Weinberg equilibrium (HWE) departure at $p \leq 0.05$

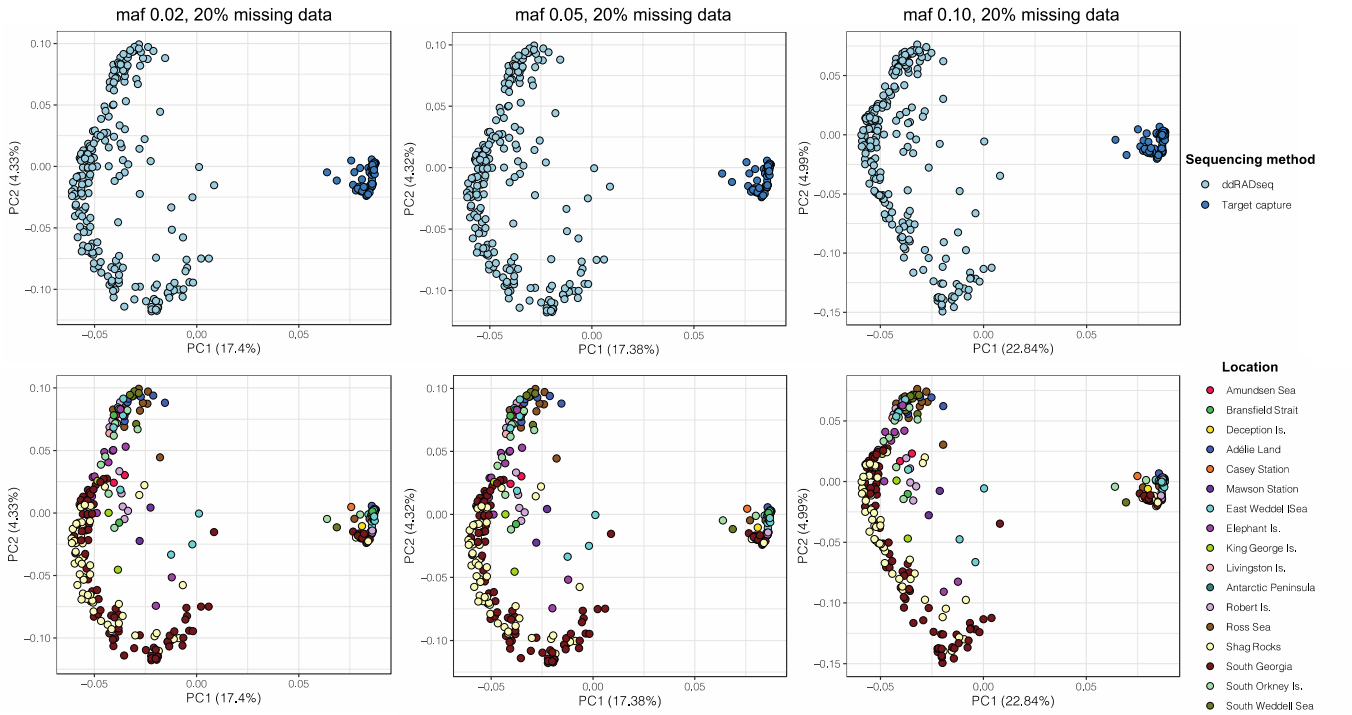

Supplementary Fig 3.3 Principal Component Analysis of ddRADseq and target capture sequencing of RAD loci in *Pareldone turqueti*. Samples are grouped by sequencing method (top panel) and location (bottom panel). Reads derived from both methods were processed together in a single bioinformatic pipeline via genotype likelihood estimation with *PCAngsd*. Data were filtered with different minor allele frequency threshold with 20% missing data allowed. No filtering for Hardy-Weinberg departure was applied.

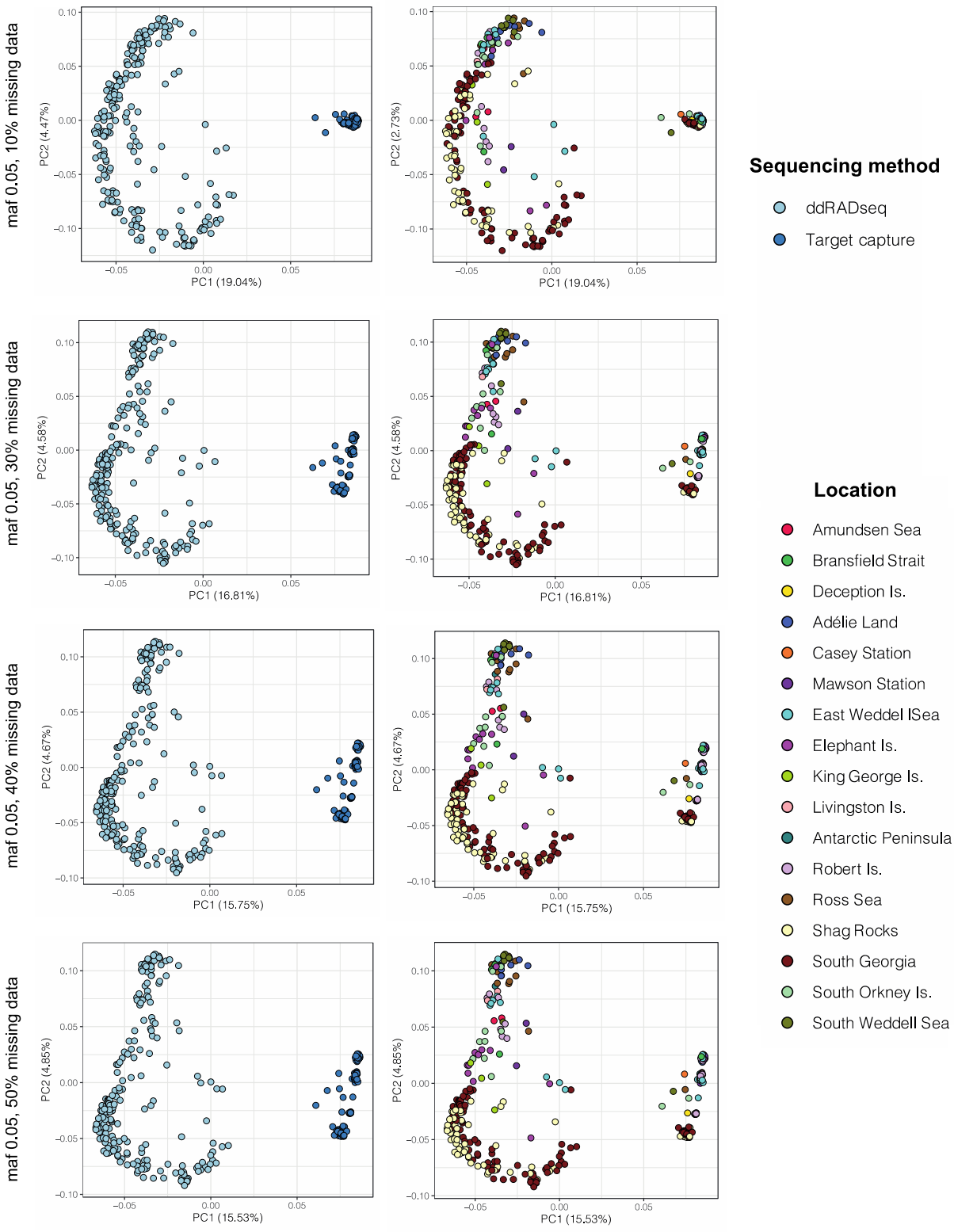

Supplementary Fig 3.4 Principal Component Analysis of ddRADseq and target capture sequencing of RAD loci in *Pareldone turqueti*. Samples are grouped by sequencing method (left panel) and location (right panel). Reads derived from both methods were processed together in a single bioinformatic pipeline via genotype likelihood estimation with *PCAngsd*. Data were filtered with different missing data threshold with a minor allele frequency of at least 0.05. No filtering for Hardy-Weinberg departure was applied.

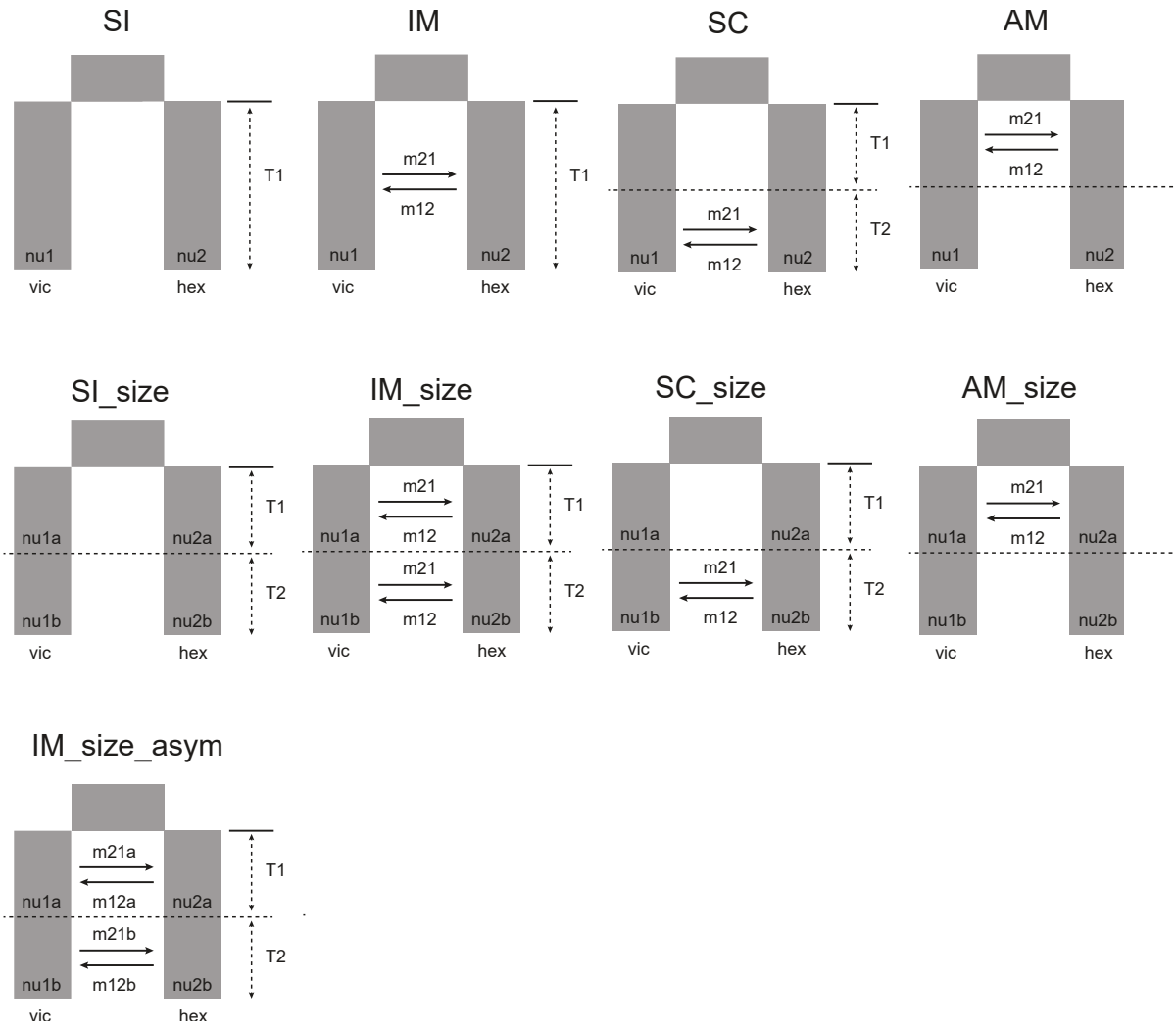

Supplementary Fig 4.1 Schematic representation of all models tested in *dadi* analyses between *Ophionotus victoriae* and *O. hexactis*. SI: strict isolation since species divergence, IM: isolation with continuous migration, SC: strict isolation followed by secondary contact, AM: ancient migration followed by strict isolation, SI_size: strict isolation with instantaneous size changes, IM_size: isolation with continuous migration and instantaneous size changes, SC_size: strict isolation followed by secondary contact and instantaneous size changes, AM_size: ancient migration followed by strict isolation and instantaneous size changes, IM_size_asym: isolation with continuous migration, followed by instantaneous size changes and another period of continuous migration.

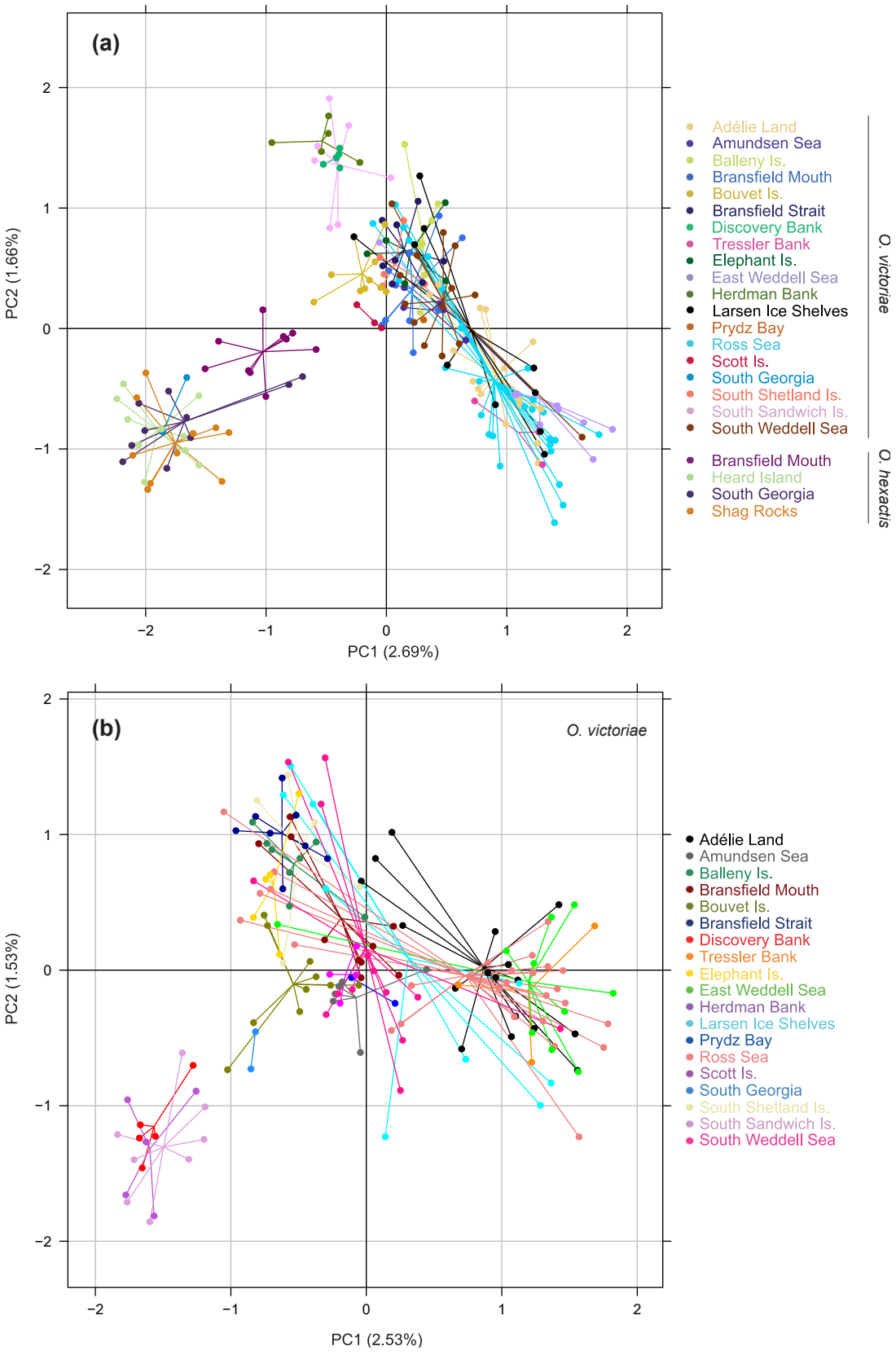

Supplementary Fig 4.2 Principal component analysis (PCA) results on the first two axes including (a) samples between *Ophionotus victoriae* and *O. hexactis* (n = 195, 1781 SNPs) grouped by geographical locations; (b) within *O. victoriae* with samples grouped by geographical locations (n = 158, 1949 SNPs).

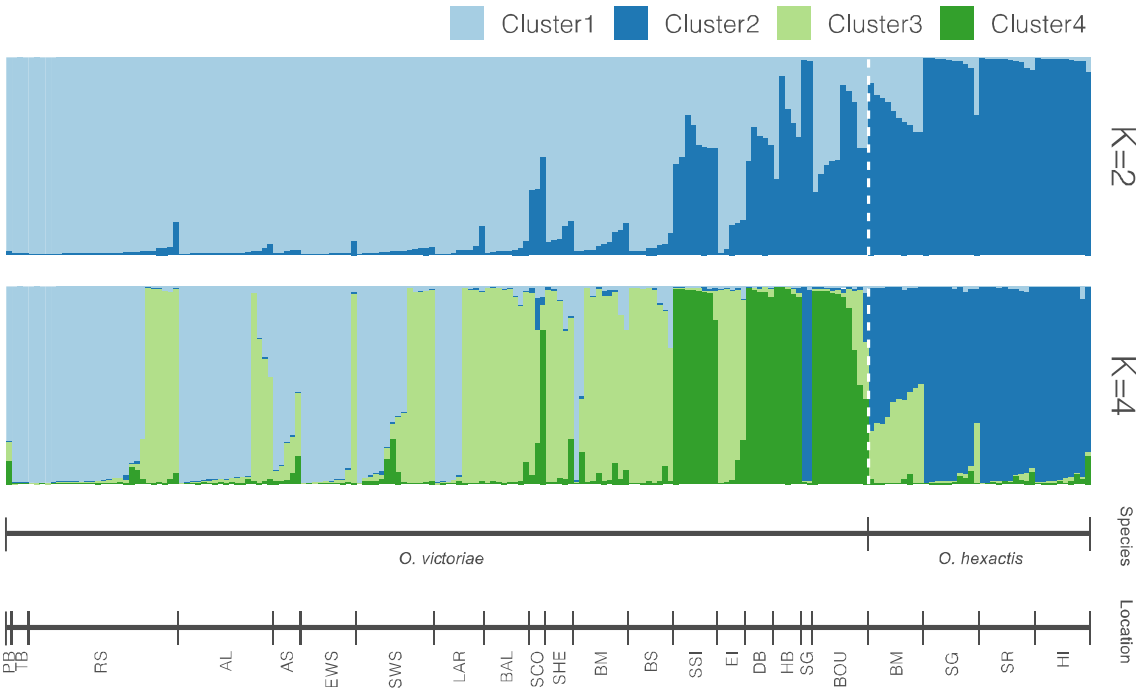

Supplementary Fig 4.3 Admixture proportions between *Ophionotus victoriae* and *O. hexactis* (n = 195) grouped by species and geographical locations. Each vertical bar represents one individual sample, colours correspond to admixture proportion estimations derived from *Structure* analyses. *K* = 2 and 4 are presented as they were highly supported by the Evanno method and highest mean log likelihood, respectively. Abbreviations represent different geographical locations; BM = Bransfield Mouth, SG = South Georgia, SR = Shag Rocks, HI = Heard Island, DB = Discovery Bank, HB = Herdman Bank, SSI = South Sandwich Is., BOU = Bouvet Is., SHE = South Shetland Is., EI = Elephant Is., BS = Bransfield Strait, LAR = Larsen Ice Shelves, EWS = East Weddell Sea, SWS = South Weddell Sea, PB = Prydz Bay, TB = Tressler Bank, SCO = Scott Is, BAL = Balleny Is., AL = Adélie Land, RS = Ross Sea, AS = Amundsen Sea.

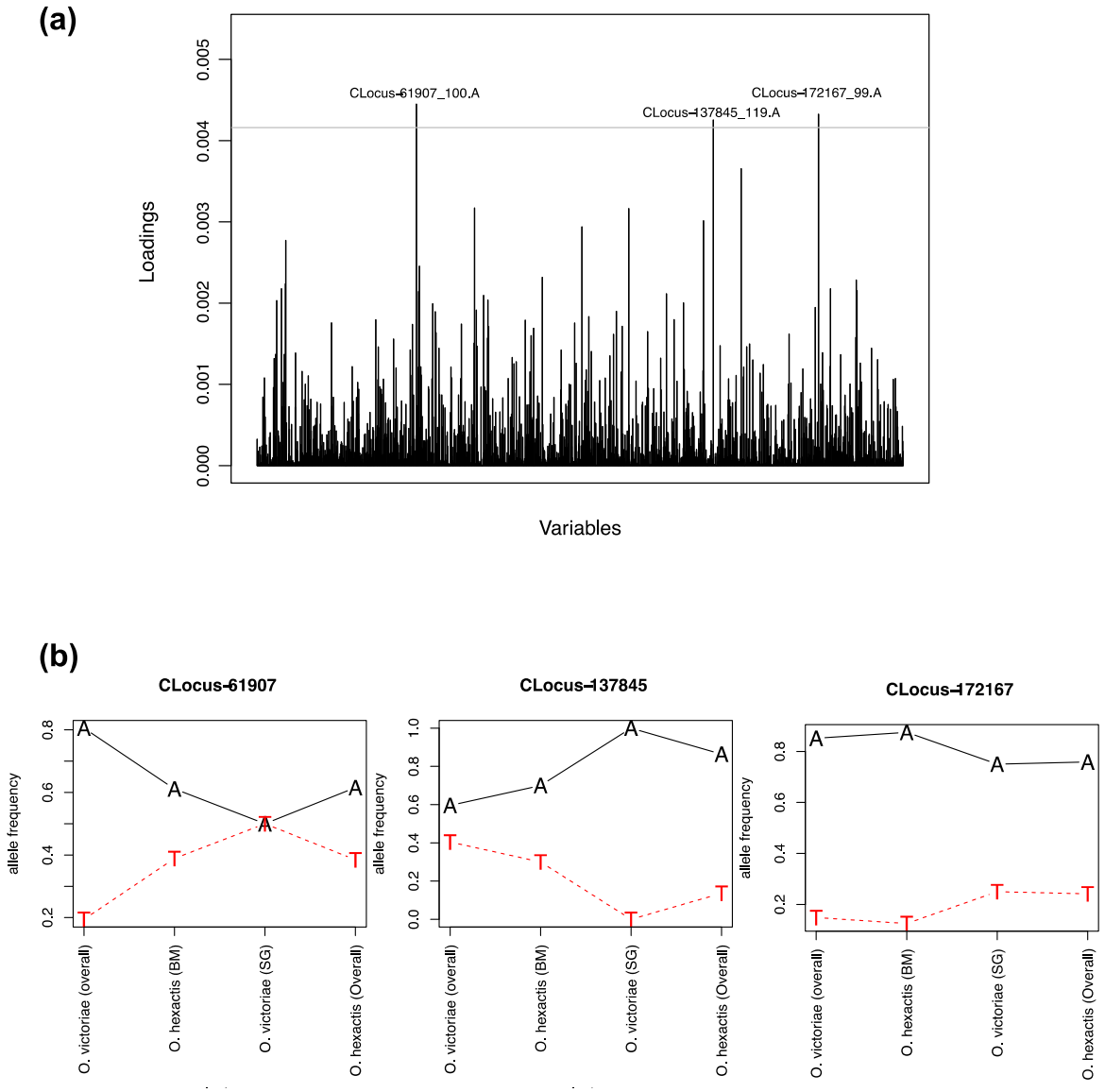

Supplementary Fig 4.4 (a) Loading plot calculated by Discriminant Analysis of Principal Components (DAPC) analysis showing the most contributing variables to the discriminant functions at 0.999 quantile among the ddRAD loci data of *Ophionotus victoriae* and *O. hexactis*. (b) The major and minor allele frequency at the three loci that contribute the most to the discriminant functions at 0.999 quantile and examined between *O. victoriae* and *O. hexactis*, with *O. victoriae* from South Georgia (SG) and *O. hexactis* from Bransfield Mouth (BM) visualised as separate clusters.

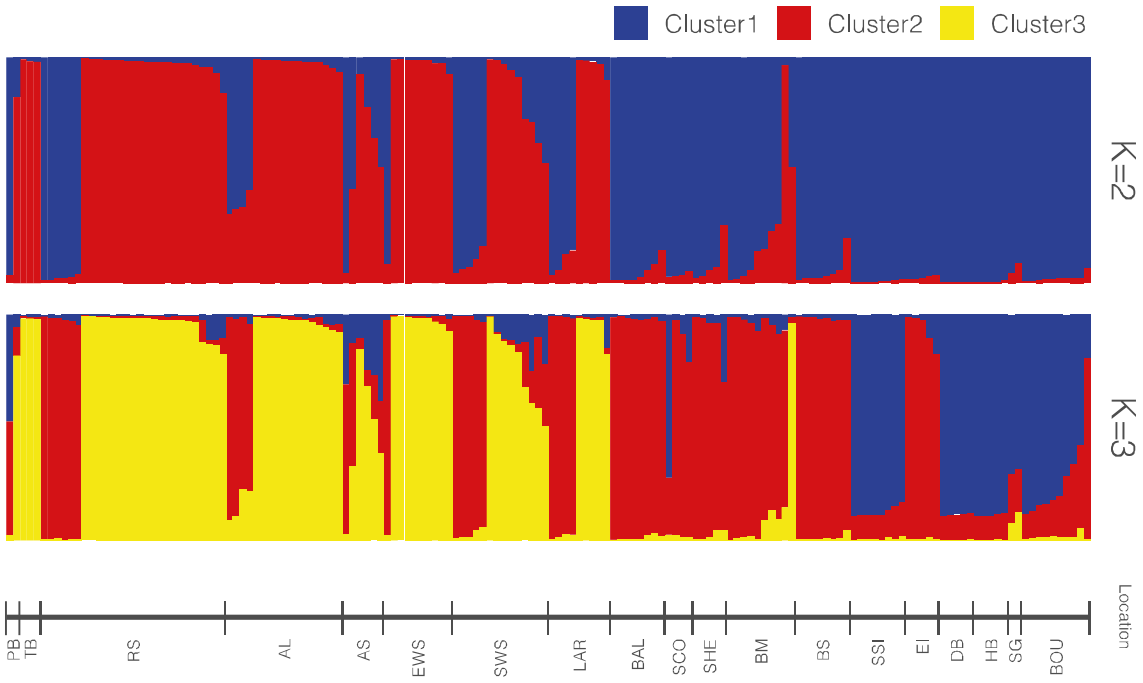

Supplementary Fig 4.5 Admixture proportions within *Ophionotus victoriae* (n = 158) grouped by locations. Each vertical bar represents one individual sample, colours correspond to admixture proportion estimations derived from *Structure* analyses. *K* = 2 and 3 are presented as they were highly supported by the Evanno method and highest mean log likelihood, respectively. Abbreviations represent different geographical locations; BM = Bransfield Mouth, SG = South Georgia, SR = Shag Rocks, HI = Heard Island, DB = Discovery Bank, HB = Herdman Bank, SSI = South Sandwich Is., BOU = Bouvet Is., SHE = South Shetland Is., EI = Elephant Is., BS = Bransfield Strait, LAR = Larsen Ice Shelves, EWS = East Weddell Sea, SWS = South Weddell Sea, PB = Prydz Bay, TB = Tressler Bank, SCO = Scott Is, BAL = Balleny Is., AL = Adélie Land, RS = Ross Sea, AS = Amundsen Sea.

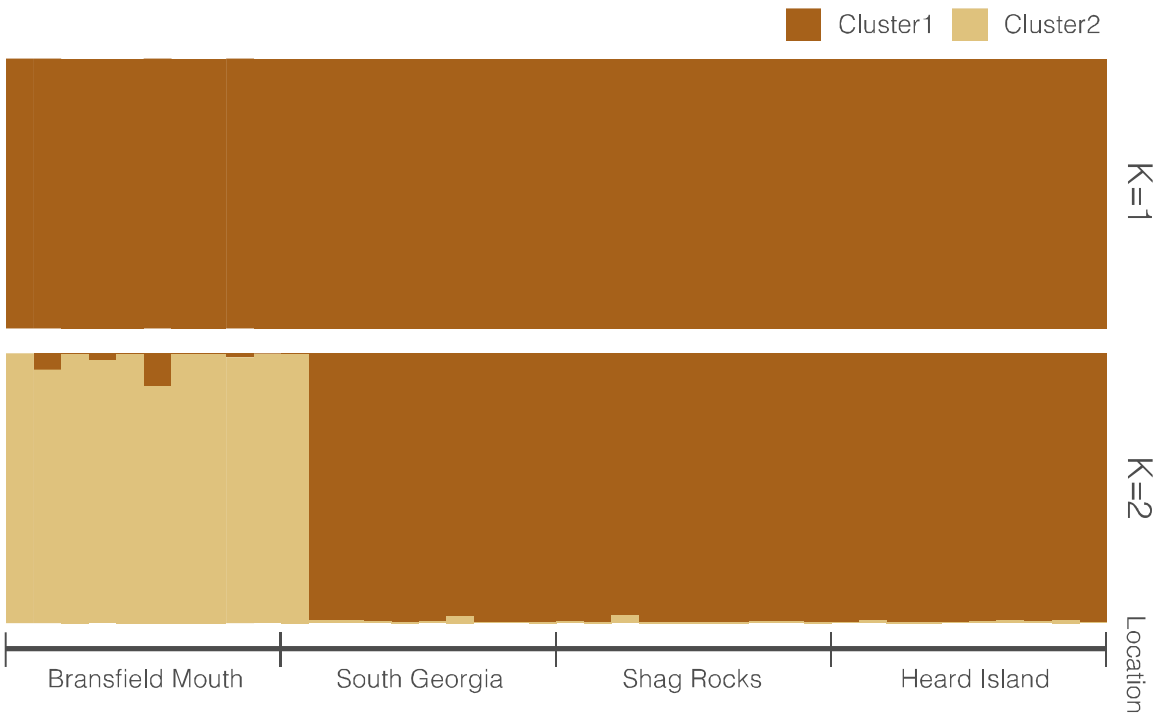

Supplementary Fig 4.6 Admixture proportions within *Ophionotus hexactis* (n = 40) grouped by locations. Each vertical bar represents one individual sample, colours correspond to admixture proportion estimations derived from *Structure* analyses. Different *K* values are presented as they were highly supported by the highest mean log likelihood (*K* = 1) and Evanno method (*K* = 2).

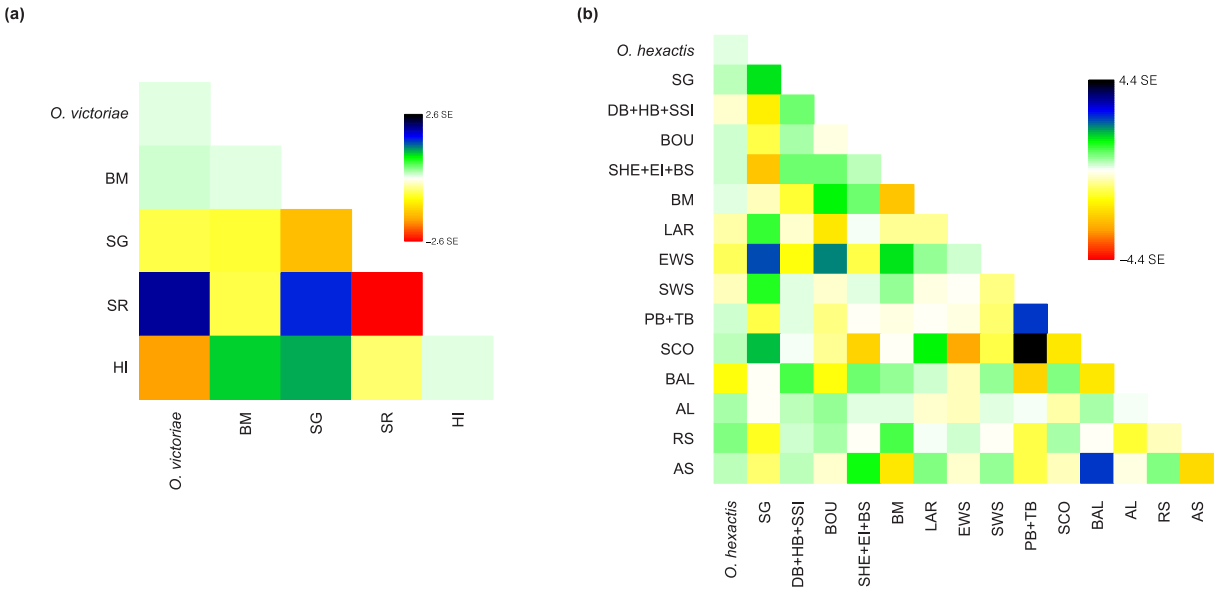

Supplementary Fig 4.7 Residual matrix visualising the fit of the *TreeMix* modelled allele frequencies (a) (maximum likelihood tree with 0 migrate edge (m)) to the observed allele frequencies in *Ophionotus hexactis*, with *O. victoriae* assigned as outgroup, and (b) (maximum likelihood tree with 1 migrate edge (m)) to the observed allele frequencies in *O. victoriae*, with *O. hexactis* assigned as outgroup. Residuals are shown as the standard error (SE) of the covariance deviation. Positive residuals (> 0) represent *TreeMix* model underestimated the observed covariance, and that the paired populations are more closely related than modelled. Negative residuals (< 0) represent *TreeMix* model overestimated the observed covariance, and that the paired populations are more distant than modelled. However, negative residuals are also products of positive residuals being present in the matrix. Here the range of the residuals are small (up to ± 4.4 SE) and most are close to zero between paired localities, suggesting the concluded *TreeMix* models were overall good fit to the observed data. Abbreviations represent different geographical locations; BM = Bransfield Mouth, SG = South Georgia, SR = Shag Rocks, HI = Heard Island, DB = Discovery Bank, HB = Herdman Bank, SSI = South Sandwich Is., BOU = Bouvet Is., SHE = South Shetland Is., EI = Elephant Is., BS = Bransfield Strait, LAR = Larsen Ice Shelves, EWS = East Weddell Sea, SWS = South Weddell Sea, PB = Prydz Bay, TB = Tressler Bank, SCO = Scott Is, BAL = Balleny Is., AL = Adélie Land, RS = Ross Sea, AS = Amundsen Sea.

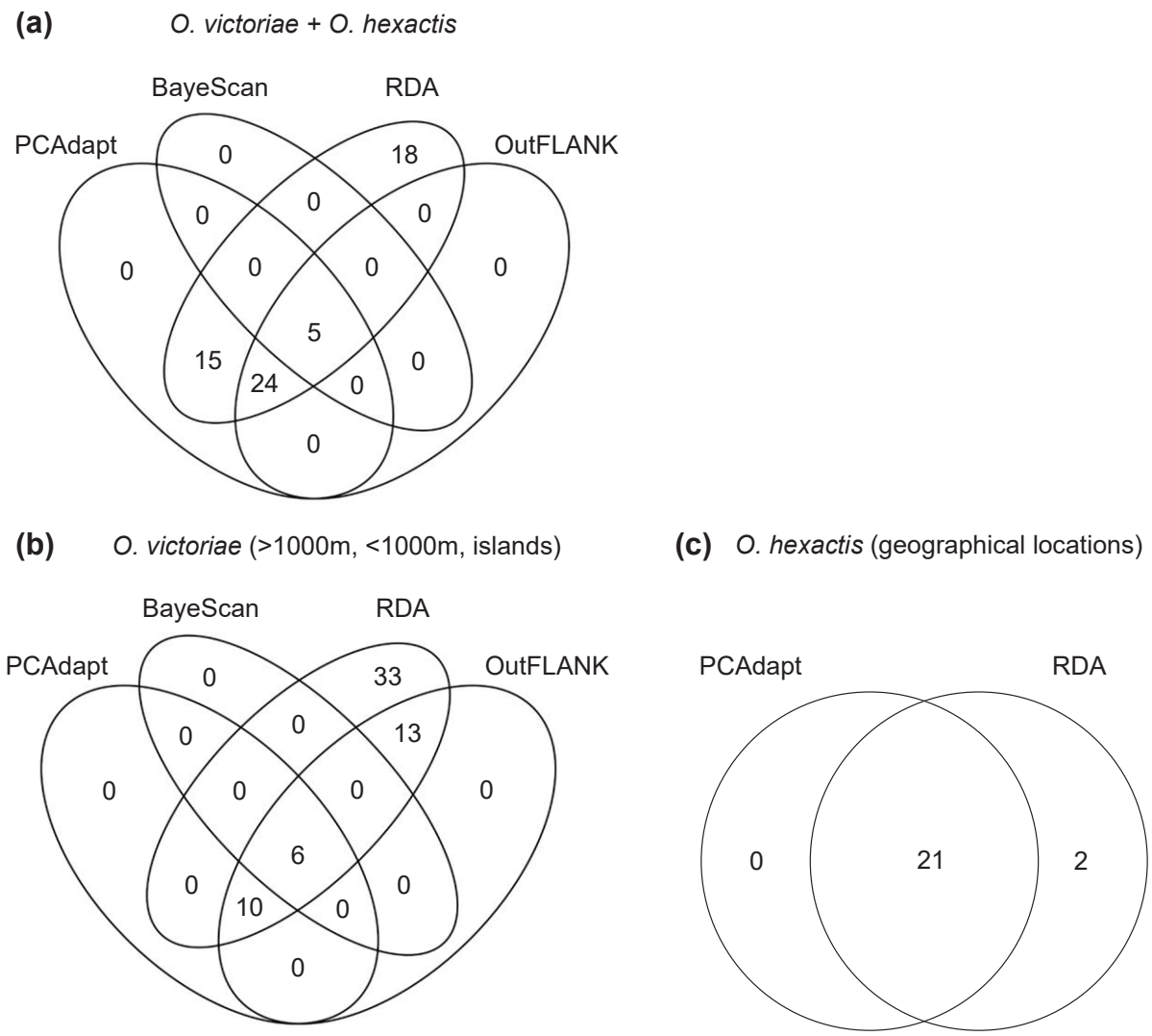

Supplementary Fig 4.8 Venn diagrams of the number of shared outlier loci identified by *PCAdapt*, *BayeScan*, Redundancy Analysis (*RDA*) and *OutFLANK*. (a) Between *Ophionotus victoriae* and *O. hexactis* (n = 195, 1,781 SNPs). (b) Within *O. victoriae* with samples defined by deep continental shelf (> 1000 m), shallow continental shelf (< 1000 m) and Antarctic islands (n = 158, 1,653 SNPs). (c) Within *O. hexactis* with samples defined by geographical locations (n = 40, 2,209 SNPs). No outlier loci were detected by *BayeScan* and *outFLANK* within *O. hexactis*.

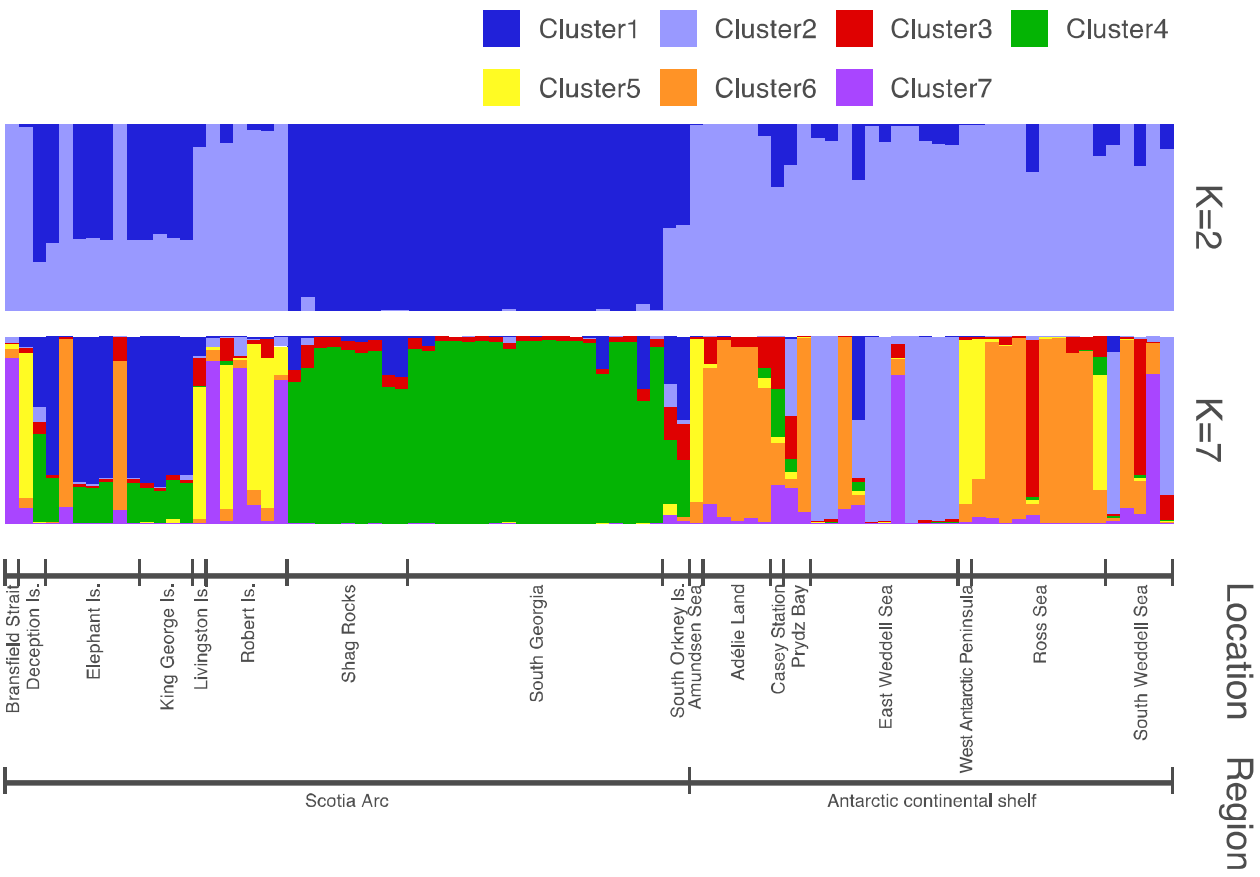

Supplementary Fig 5.1 Admixture proportions within *Pareledone turqueti* (n = 87) based on ddRAD loci data (5,437 unlinked SNPs) with samples sorted by geographical region (Scotia Arc and Antarctic Continental Shelf). Each vertical bar represents one individual sample, colours correspond to admixture proportion estimations derived from *Structure* analyses. The recommended values of *K* = 2 (by delta*K* statistics) and = 7 (by highest mean log likelihood) are presented.

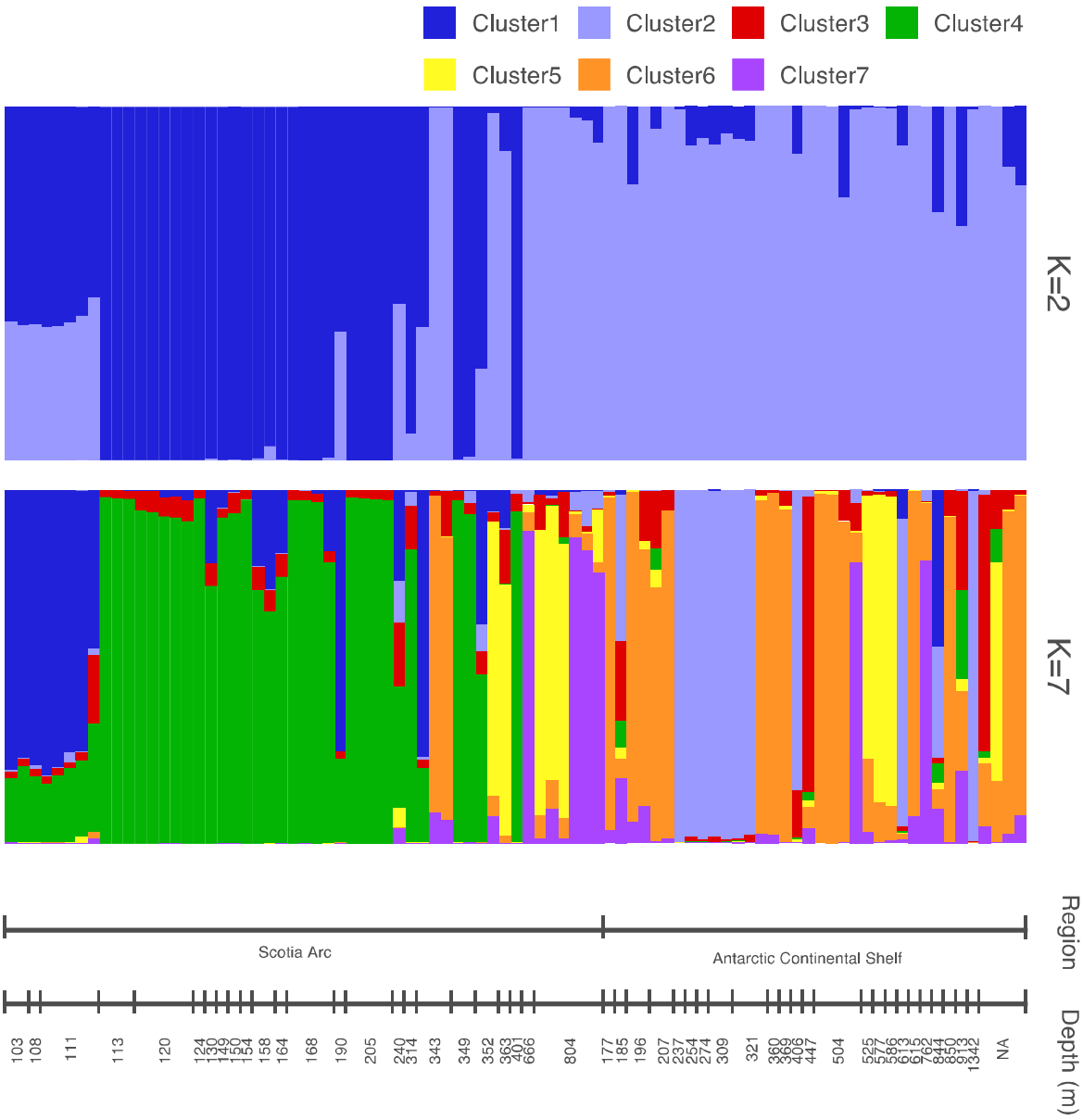

Supplementary Fig 5.2 Admixture proportions within *Pareledone turqueti* (n = 87) based on ddRAD loci data (5,437 unlinked SNPs), with samples sorted by water depth and geographical region (Scotia Arc and Antarctic Continental Shelf). Each vertical bar represents one individual sample, colours correspond to admixture proportion estimations derived from *Structure* analyses. The recommended values of *K* = 2 (by deltaK statistics) and = 7 (by highest mean log likelihood) are presented.

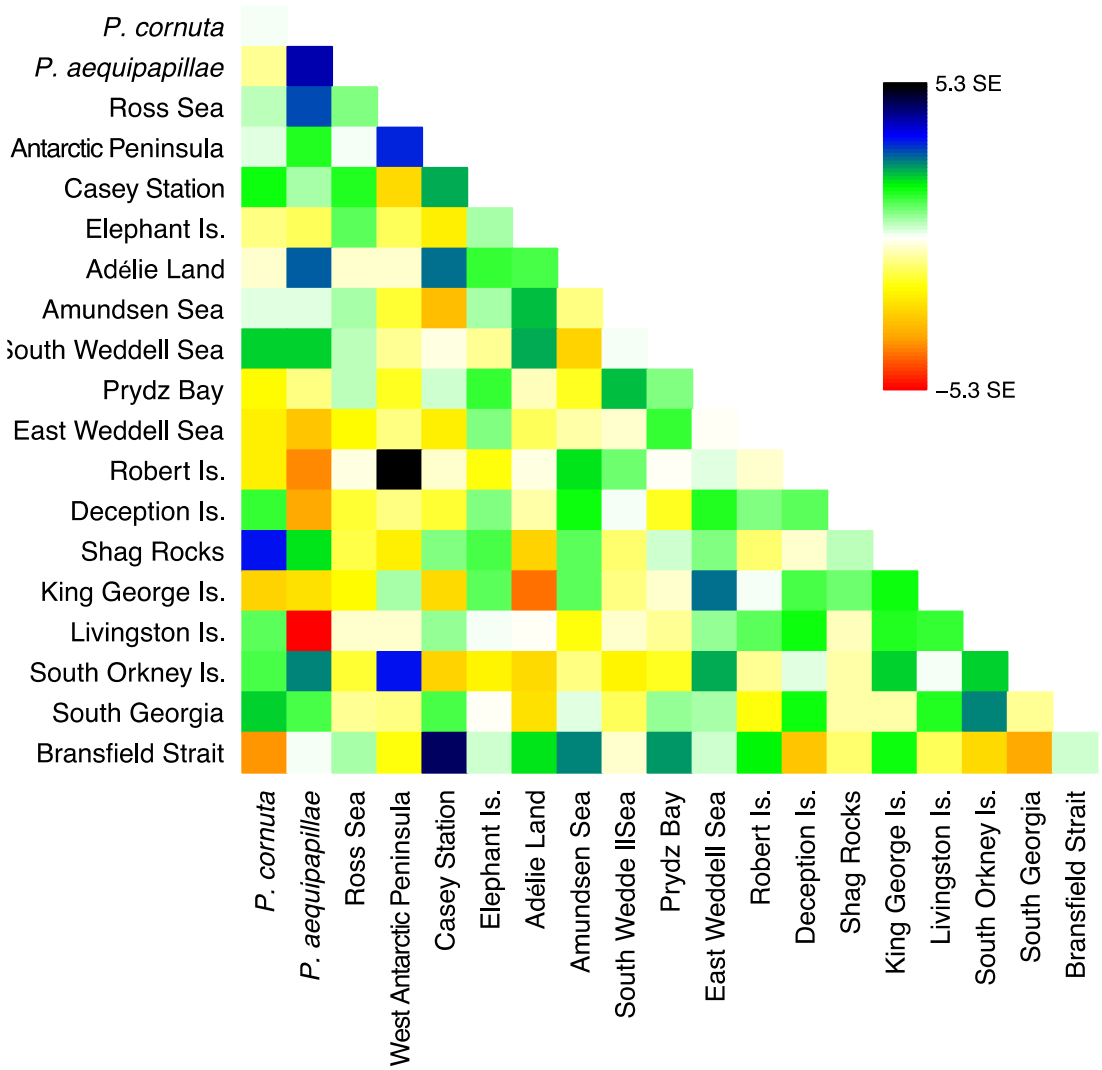

Supplementary Fig 5.3 Residual matrix visualising the fit of the *TreeMix* modelled allele frequencies (maximum likelihood tree with 6 migrate edge (m)) to the observed allele frequencies between sampled locations in *Pareledone turqueti*, with *P. cornuta* and *P. aequipapillae* assigned as outgroup, based on ddRAD loci data (5,437 SNPs). Residuals are shown as the standard error (SE) of the covariance deviation. Positive residuals (> 0) represent *TreeMix* model underestimated the observed covariance, and that the paired populations are more closely related than modelled. Negative residuals (< 0) represent *TreeMix* model overestimated the observed covariance, and that the paired populations are more distant than modelled. However, negative residuals are also products of positive residuals being present in the matrix. Here the range of the residuals are small (up to ± 5.3 SE) and most are close to zero between paired localities, suggesting the concluded *TreeMix* models were overall good fit to the observed data.

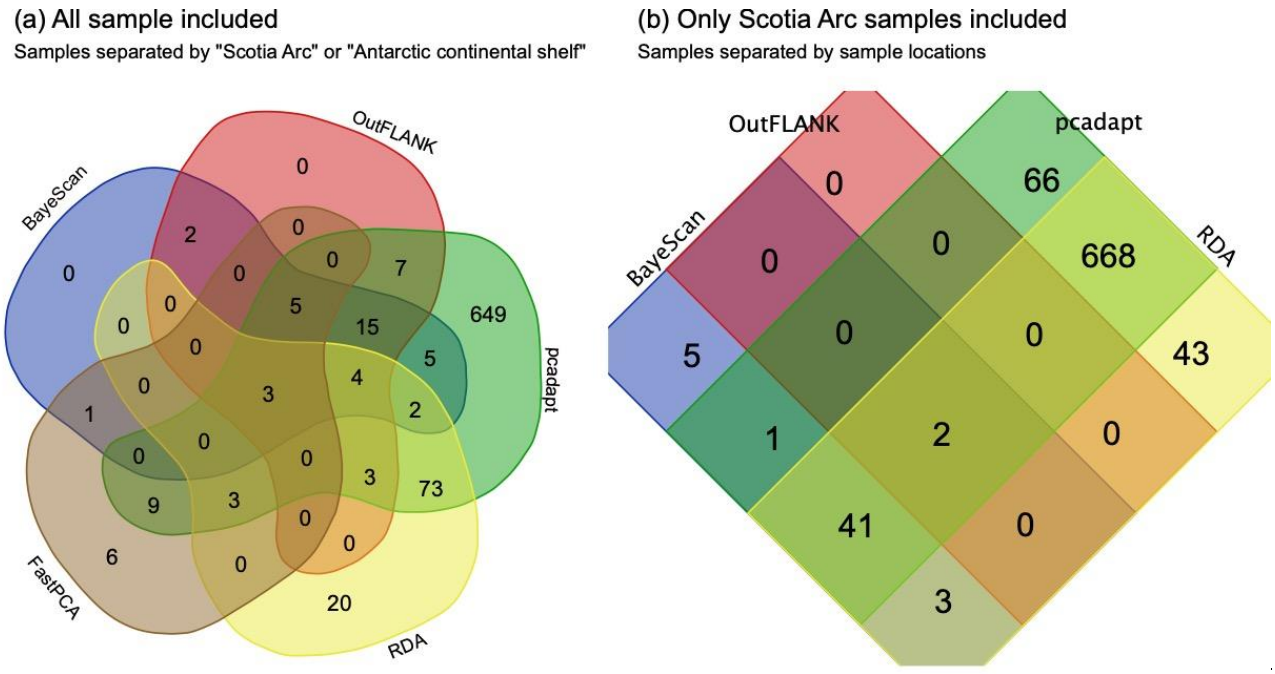

Supplementary Fig 5.4 Venn diagrams of the number of shared outlier loci identified by *PCAdapt*, *BayeScan*, Redundancy Analysis (*RDA*), *OutFLANK* and FastPCA based on ddRAD loci data. (a) Across all *Pareledone turqueti* samples collected throughout the Southern Ocean, with samples defined by the Antarctic Continental Shelf and Scotia Arc (n = 87, 5,437 SNPs). (b) Only *P. turqueti* samples collected from the Scotia Arc are included, with samples defined by sample locations (n = 52, 5,437 SNPs). No outlier loci were detected by *FactPCA*.

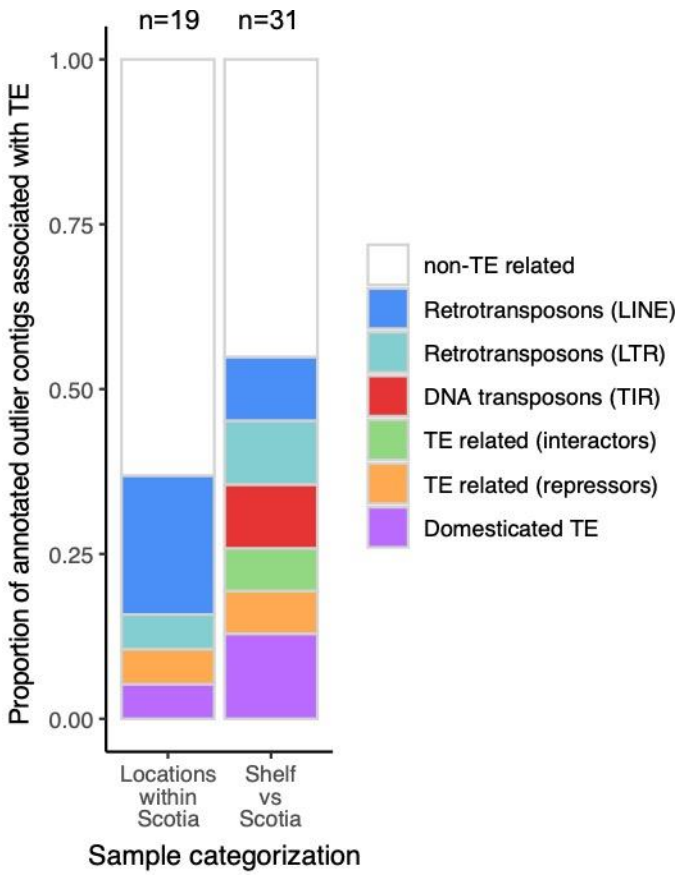

Supplementary Fig 5.5 Bar plot showing the number of outlier contigs, detected within *Pareledone turqueti*, returned with positive matches with the BLASTx database (< E value of 1 x 10^{-5}), and the proportion of annotated contigs linked to Transposable elements (TE). Sample categorization represent the datasets used in outlier loci analyses, including all *P. turqueti* samples collected across the Southern Ocean with samples divided between the Antarctic Continental Shelf and Scotia Arc ('Shelf vs Scotia'), and only *P. turqueti* samples collected from the Scotia Arc with samples divided based on sample locations ('Location within Scotia').

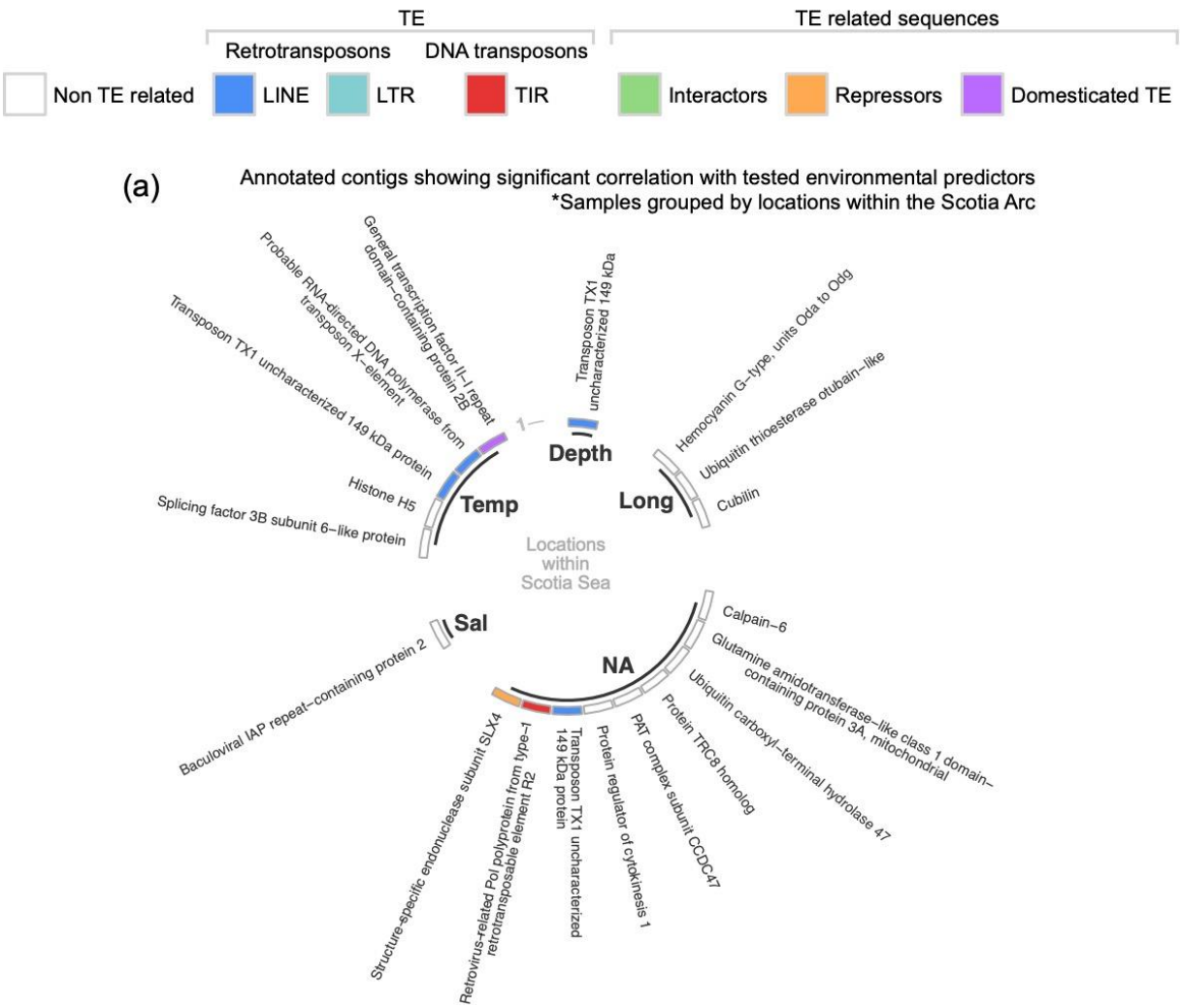
TE
Retrotransposons
DNA transposons
TE related sequences
Non TE related
LINE
LTR
TIR
Interactors
Repressors
Domesticated TE
(a)
Annotated contigs showing significant correlation with tested environmental predictors
*Samples grouped by locations within the Scotia Arc
Depth
Temp
Long
Sal
NA
Locations within Scotia Sea
Transposon TX1 uncharacterized 149 kDa
Hemocyanin G-type, units Oda to Odg
Ubiquitin thioesterase otubain-like
Cubilin
General transcription factor II-I repeat domain-containing protein 2B
Probable RNA-directed DNA polymerase from transposon X-element
Transposon TX1 uncharacterized 149 kDa protein
Histone H5
Splicing factor 3B subunit 6-like protein
Baculoviral IAP repeat-containing protein 2
Calpain-6
Glutamine amidotransferase-like class 1 domain-containing protein 3A, mitochondrial
Ubiquitin carboxyl-terminal hydrolase 47
Protein TRC8 homolog
PAT complex subunit CCDC47
Protein regulator of cytokinesis 1
Transposon TX1 uncharacterized 149 kDa protein
Retrovirus-related Pol polyprotein from type-1 retrotransposable element R2
Structure-specific endonuclease subunit SLX4
(b)
Annotated contigs showing significant correlation with tested environmental predictors
*Samples grouped by Antarctic shelf and the Scotia Arc
Depth
Temp
Sal
NA
Long
Shelf vs Scotia
Protein sel-1 homolog 1
Ubiquitin thioesterase otubain-like
Protein TRC8 homolog
Hemocyanin G-type, units Oda to Odg
Structure-specific endonuclease subunit SLX4
Ubiquitin carboxyl-terminal hydrolase 47
Probable RNA-directed DNA polymerase from transposon X-element
Hemocyanin G-type, units Oda to Odg
Protocadherin-18
Importin subunit beta-1
Collagen alpha-1(XXII) chain
Tryptophanase
Eukaryotic translation initiation factor 5B
Transposon TX1 uncharacterized 149 kDa protein
Retrovirus-related Pol polyprotein from transposon 297
Transposon Ty3-I Gag-Pol polyprotein
THAP domain-containing protein 1 A
Protein FAM200A
Zinc finger MYM-type protein 5
SCAN domain-containing protein 3
DNA repair and recombination protein RAD54-like
Zinc finger protein 726
General transcription factor II-I repeat domain-containing protein 2A
Mariner Mos1 transposase
Transposable element Tc1 transposase
Retrovirus-related Pol polyprotein from transposon 17.6
Zygotic DNA replication licensing factor mcm3
Rab GTPase-activating protein 1
Glutamine amidotransferase-like class 1 domain-containing protein 3A, mitochondrial
Ubiquitin carboxyl-terminal hydrolase 47
6-phosphofructo-2-kinase/fructose-2,6-bisphosphatase 2

Supplementary Fig 5.6 Bar plots showing the outlier contigs identified via Redundancy Analysis (RDA), as well as their association with environmental variables, detected within *Pareledone turqueti*. Only outlier contigs returned with positive matches with the BLASTx database (< E value of 1 x 10^{-5}) are shown. (a) RDA with the dataset including only *Pareledone turqueti* samples from the Scotia Arc (n = 52), with samples divided between sample locations ("Location within Scotia Arc); (b) RDA with the dataset including all *P. turqueti* samples collected around the Southern Ocean (n = 87), with samples divided between the Antarctic continental shelf and Scotia Arc ("Shelf vs Scotia"). Bar plot also represent the proportion of annotated contigs linked to Transposable elements (TE). The analysed environmental variables included water depth (Depth), bottom water temperature (Temp), bottom water salinity (Sal), longitude (Long), and not associated with any environmental variable (NA).

Supplementary Fig 5.7 A network visualising the Gene Ontology (GO) of biological processes in the annotated outlier contigs significantly matched with the BLASTx database, constructed using REVIGO with medium (0.7) semantic similarity of medium and a semantic similarity measure of SimRel under the whole UniProt database. Highly similar GO terms are linked by edges, with line width indicating the level of similarity. Outlier contigs were identified in the dataset included all *Pareledone turqueti* samples collected across the Southern Ocean (n = 87), with samples divided between the Antarctic Continental shelf and Scotia Arc.

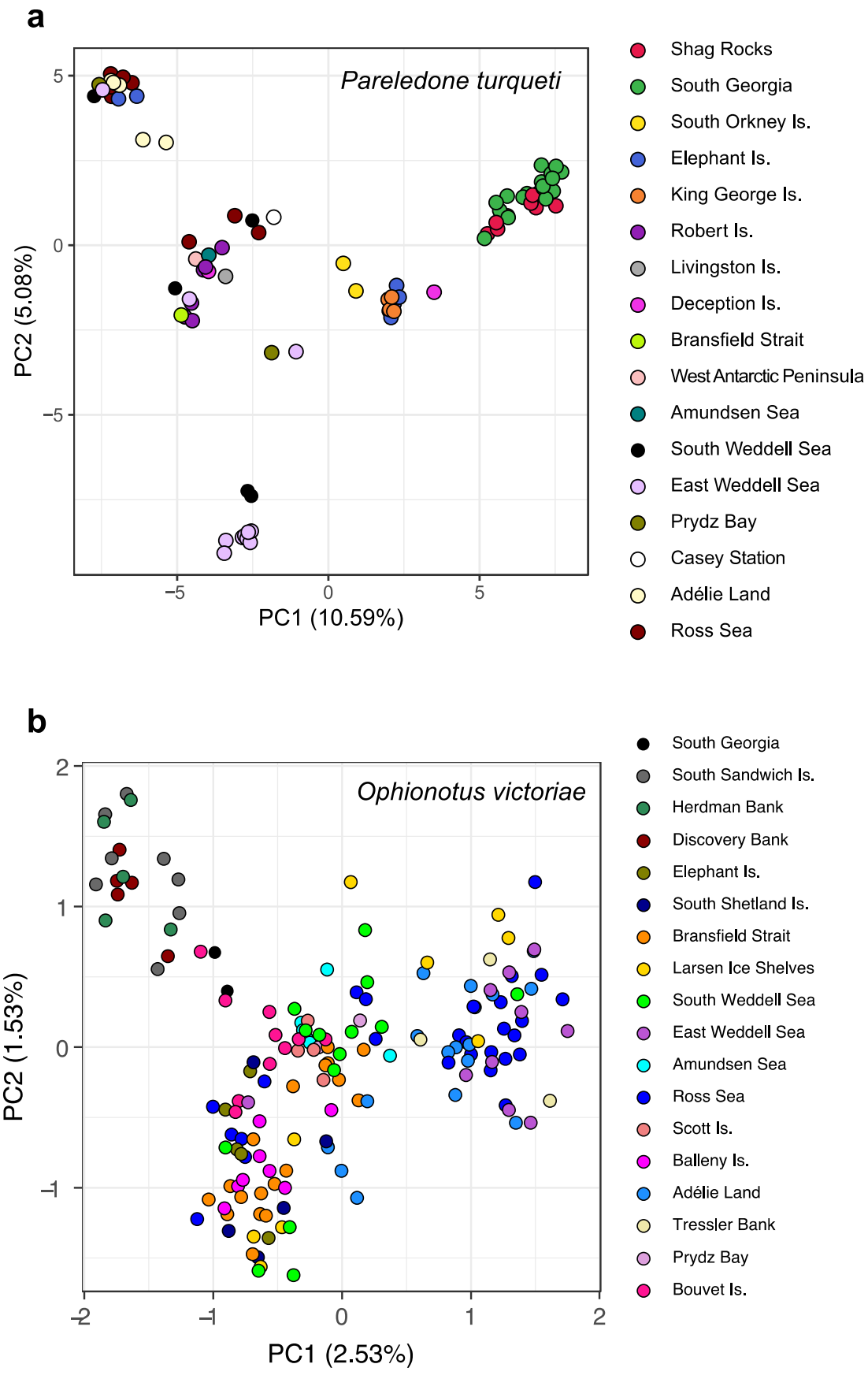

Supplementary Fig 6.1 Principal component (PC) analysis of *Pareledone turqueti* (a) and *Ophionotus victoriae* (b) showing the genetic variation on the first two PC axes.

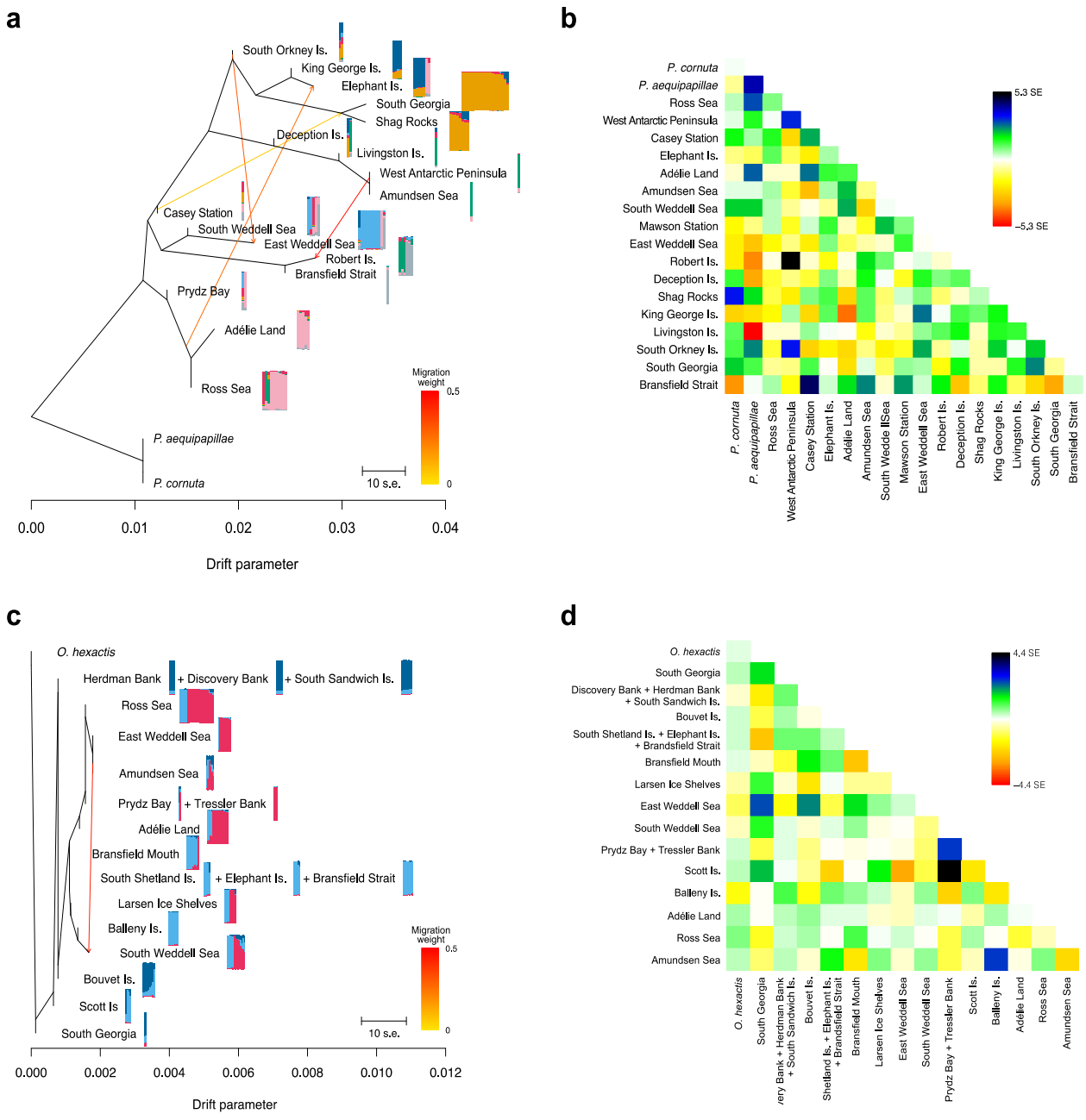

Supplementary Fig 6.2 *TreeMix* maximum likelihood (ML) tree of *Ophionotus victoriae* and *Pareledone turqueti* rooted with outgroups. Horizontal branch lengths are proportional to the amount of genetic drift that has occurred on each branch. *Structure* output is superimposed on the ML tree indicating how "populations" are defined in either species. In the bar plots, each vertical bar represents one individual sample from the corresponding geographic location(s), with colours corresponding to admixture proportion estimations. Migration edge is coloured based on migration weight, which corresponds to the % ancestry in the sink population originated from the source population. Only the edges found to be significant by jackknife significance tests were presented. (a) ML tree of *O. victoriae*. Terminal nodes are subdivided based on neighbouring geographical locations with similar admixture proportions estimated by *Structure* (preferred $K = 4$). (b) ML tree of *P. turqueti*. Terminal nodes are subdivided based on distinct geographical locations. (c, d) Residual matrix visualising the fit of the *TreeMix* modelled allele frequencies to the observed allele frequencies in *O. victoriae* (c) and *P. turqueti* (d). Residuals are shown as the standard error (SE) of the covariance deviation. Positive residuals (> 0) represent that the *TreeMix* model underestimated the observed covariance, and that the paired

populations are more closely related than modelled. Negative residuals (< 0) represent that the *TreeMix* model overestimated the observed covariance, and that the paired populations are more distant than modelled. However, negative residuals are also products of positive residuals being present in the matrix. Here the range of the residuals are small (up to ± 5.3 SE) and most are close to zero between paired localities, suggesting that the concluded *TreeMix* models were overall a good fit to the observed data.

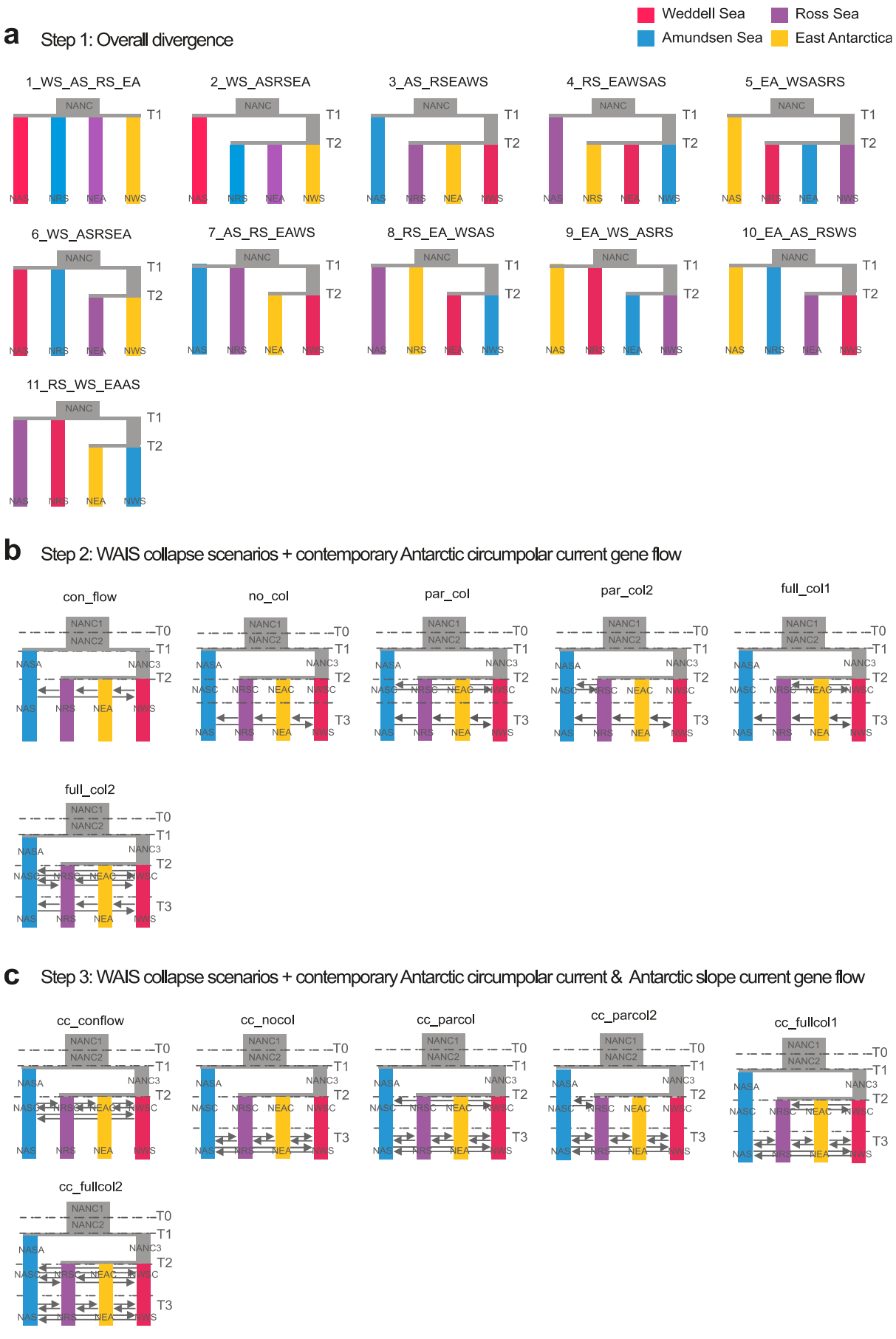

Supplementary Fig 6.3 Hierarchical demographic modelling approach to deduce signatures of historical trans-West Antarctic seaways connectivity in *Pareledone turqueti* and *Ophionotus victoriae*,

following Marques et al. (2019). (a) The phylogenetic relationship between Weddell Sea (WS), Amundsen Sea (AS), Ross Sea (RS) and East Antarctica (EA) were first determined. (b) Based on the best topology (lowest Akaike Information Criterion value) at step 1, contrasting scenarios of past WAIS configurations were compared. For the models at step 2, it was hypothesised that since population divergence, WS, AS, RS may have experienced any, partial, or complete connectivity, followed by modern circumpolar gene flow linking WS, AS, RS and EA. The possibilities of population sizes change over each time interval were also considered. For circumpolar gene flow, simpler models which only consisted of the directionality of the Antarctic circumpolar current (clockwise) were performed. (c) When necessary, step 3 models were performed, which considered more complex models that included both directionalities of the Antarctic Circumpolar Current and Antarctic Slope Current (clockwise and counter-clockwise, respectively). Each model is labelled by the text above it. Text within each model denotes the parameter labels associated with the population size change at a particular interval (Nxxx), as well as the timing of modelled events (Tx). Dashed lines represent a distinct time interval. Arrows represent migration between populations.

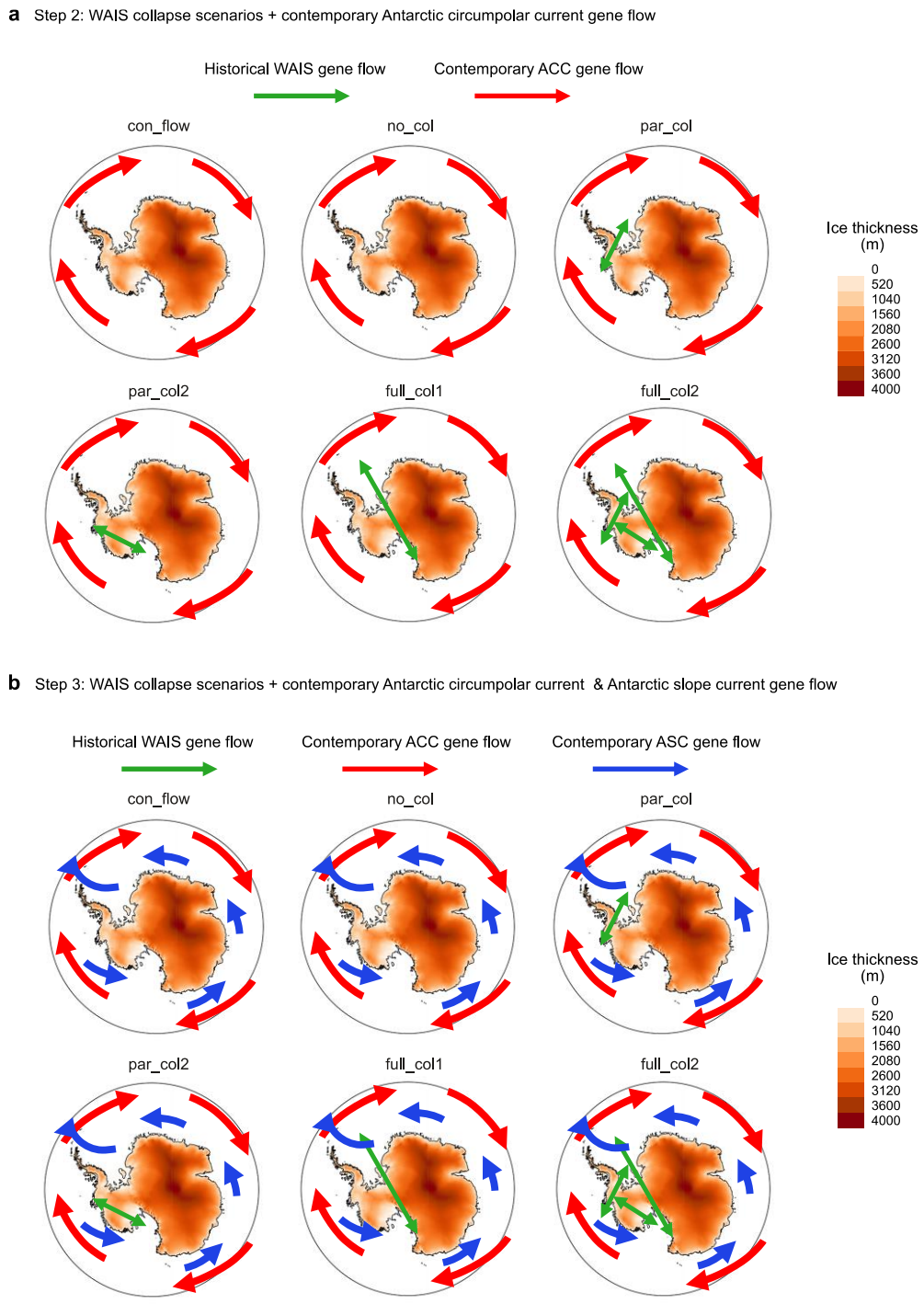

Supplementary Fig 6.4 Illustrations of the contrasting demographic models to deduce signatures of historical trans-West Antarctic seaways connectivity in *Pareledone turqueti* and *Ophionotus victoriae*. (a) At step 2 of the hierarchical demographic modelling approach, contrasting scenarios of past WAIS configurations were compared. It was hypothesised that since population divergence, the WS, AS and RS may have experienced any, partial, or complete connectivity (green arrows), followed by contemporary circumpolar gene flow driven by the Antarctic circumpolar current (ACC; red arrows) linking between the WS, AS, RS and EA. (b) At step 3, more complex models were further considered; they included both directionalities of the circumpolar gene flow, driven by the ACC (red arrows) and Antarctic slope current (ASC; blue arrows). Distinct texts are placed on top of each model as model labels. Maps illustrate ice thickness of the modern Antarctic Ice sheet and were generated using ETOPO1 Elevation model dataset from *Quantartica* (Matsuoka et al., 2021).

Supplementary Note 2.1

Additional methods for *Chapter 2* - Phylogenetic analyses and molecular species delimitation

A maximum likelihood (ML) estimate and a Bayesian inference (BI) of phylogeny were reconstructed to determine relationships between *O. victoriae* and *O. hexactis*, as well as input for tree-based species delineation analyses. For ML tree-based species delimitation analyses, sequences were first collapsed into unique haplotypes for easier presentation using *FaBox* v1.5 (Villesen 2007) (see Supplementary Table 2.1 for haplotype information). No sequences were collapsed into unique haplotypes for BI tree-based species delimitation analyses. Sequences were not collapsed into unique haplotypes for BI tree is due to the fact that, in genealogy-based approach such as *BEAST*, identical sequences are treated as different alleles coalescing back to the most common recent ancestor (Talavera et al., 2013). During this process, non-zero branch lengths will be inserted between identical sequences, which would have an effect on the overall branch length for each group (Talavera et al., 2013). Whether the sequences are collapsed or not, however, does not seem have an effect on the BI-tree based species delimitation analysis used in this study (Talavera et al., 2013). The COI sequences of *Ophiura aequalis*, *O. micracantha*, *Ophiocten ludwigi* and *Ophiocrossota multispina* were included as outgroups in order to root the tree (Hugall et al., 2016) (GenBank accession numbers: KU894989, KU894990, KU895450 and KU895449, respectively). The ML tree was generated using the *IQ-TREE* web server v1.6.11 (Trifinopoulos et al., 2016) using ultrafast bootstrap support of 1,000 iterations for node support. A substitution model of the *Ophionotus* spp. sequences (TN+F+I+G4) was determined based on Bayesian Information Criterion (BIC) using *ModelFinder* on the *IQ-TREE* web server (Kalyaanamoorthy et al., 2017). The Bayesian inference (BI) phylogenetic tree was generated using all COI sequences in BEAST under the substitution model of TN+F+I+G4, uncorrelated lognormal relaxed clock and using a constant coalescent constant population tree prior (Michonneau 2016). A Markov Chain Monte Carlo (MCMC) analysis was run for 200 million generations sampled at every 5,000 generations. Tracer used to inspect convergence values based on based on trace plots and ESS > 200. The final 20,000 trees were kept using *TreeAnnotator* v1.8.4 (from the *BEAST* pacakge). The final ML and BI consensus tree were visualised in *FigTree* v1.4.3 (Rambaut 2016).

To assess species limits within *O. victoriae*, as well as between *O. victoriae* and *O. hexactis*, four single-locus species delineation methods were used: *ABGD* algorithm (Automated Barcode Gap Discovery) (Puillandre et al., 2012), *mPTP* (multi-rate Poisson Tree Processes) (Kapli et al., 2017), *bPTP* (Bayesian implementation of PTP mode) (Zhang et al., 2013) and *sGMYC* (single-threshold General Mixed Yule Coalescent) (Fujisawa and Barraclough 2013). *ABGD* was performed using the online web server (https://bioinfo.mnhn.fr/abi/public/abgd/abgdweb.html) based on genetic p-

distance between haplotypes with a priori thresholds (P) set between 0.001 and 0.1. Both *mPTP* and *bPTP* were performed using online web servers (https://mptp.h-its.org and https://species.h-its.org/). For both *PTP* analyses, a rooted ML tree was used as input, with outgroup taxa excluded prior to species delimitation. During the search in *bPTP*, 500,000 MCMC generations were used, with a thinning parameter of 100 and the first 10% discarded as burn-in. For *sGMYC*, an unrooted BI tree with outgroup taxa excluded was used as input and *sGMYC* was performed using the R packages *SPLITS* (Ezard et al., 2009), *APE* (Paradis et al., 2004), *PARAN* (Dinno 2012) and *RNCL* (Michonneau et al., 2016).

Additional results for *Chapter 2*

Phylogenetic trees and species delimitation

The topology of ML and BI trees revealed that both *O. victoriae* and *O. hexactis* are paraphyletic species, with both trees showing *O. victoriae* plus *O. hexactis* sequences comprising a single lineage together (Fig N2.1 and Fig N2.2). The ML tree showed short internal branches for the clade containing *O. victoriae* haplotypes, with *O. hexactis* haplotypes nested within *O. victoriae* haplotypes (SH-aLRT support = 98.7%, Ultrafast BS = 99%) (Fig N2.1). In the ML tree, *O. victoriae* COI sequences were also nested within clades of *O. hexactis*. The BI tree, also with short internal branches, suggested *O. victoriae* forms two separate clades (posterior probability = 100%) (Fig N2.2). On the BI tree, *O. hexactis* is nested within one of *O. victoriae*'s clades alongside *O. victoriae* sequences (Fig N2.2).

Species delimitation analyses by genetic distance (*ABGD*) suggests *O. victoriae* and *O. hexactis* are a single species with no barcoding gap between sampled haplotypes (Fig N2.1). Tree-based species delineation analyses (*mPTP*, *bPTP* and *sGMYC*) indicate 1, 128 and 301 putative species, respectively, among *O. victoriae* and *O. hexactis*. However, no tree-based analyses distinguished *O. hexactis* and *O. victoriae* as monophyletic species; each delimitation analysis has defined at least one putative species comprised of haplotypes/or sequences from both species.

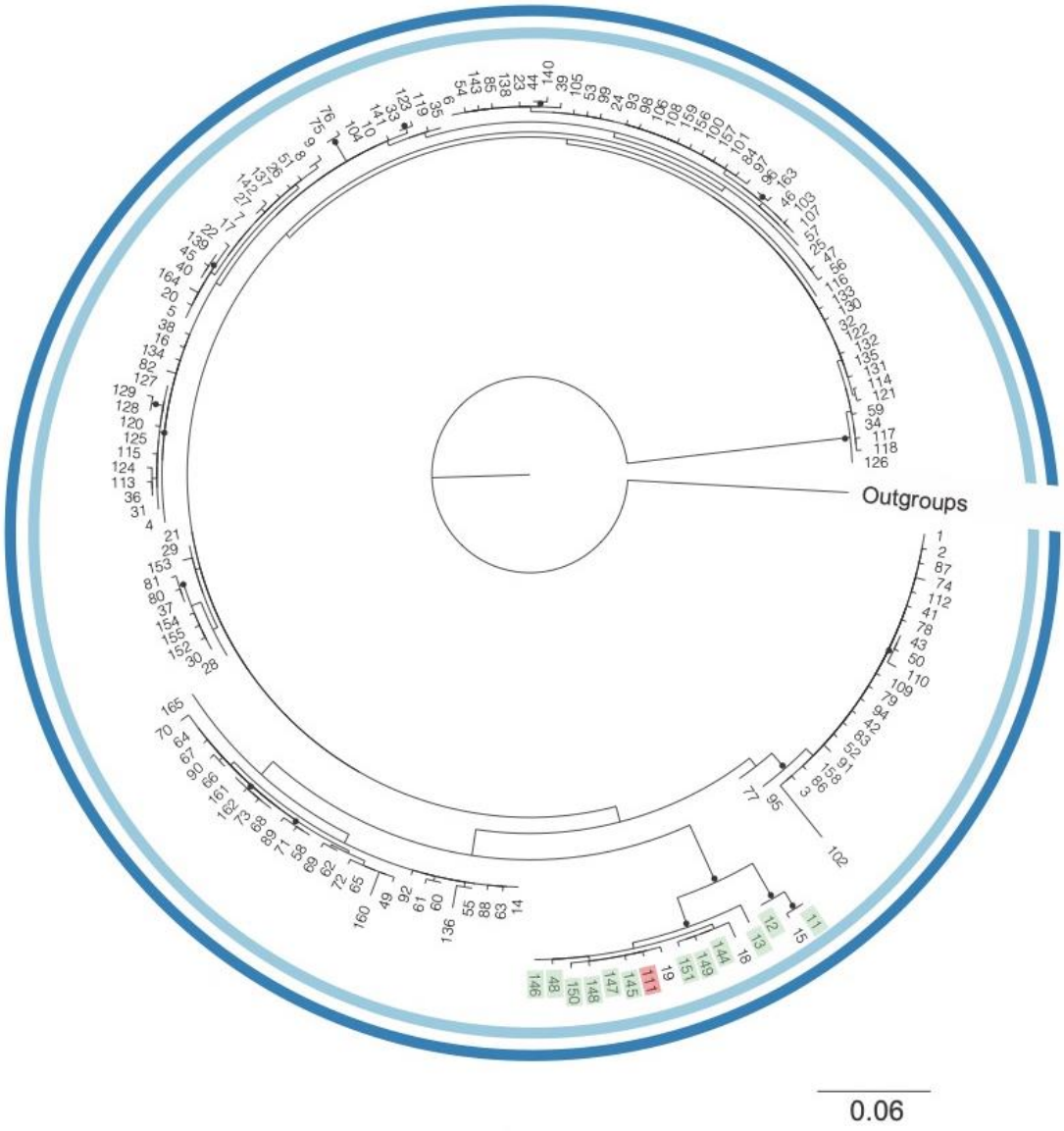

Supplementary Fig N2.1. Maximum likelihood tree of *Ophionotus victoriae* COI haplotypes (non-shaded) and *O. hexactis* (shaded in green). Haplotype ID shaded in red = shared haplotype between *O. victoriae* and *O. hexactis*. A solid circle at the node represents Shimodaira–Hasegawa approximate likelihood ratio test (SH-aLRT) >= 80% and ultrafast bootstrap (UFBoot) >= 95%. Bars indicate results proposed by species delimitation analyses: ABGD (light blue) and *mPTP* (dark blue). Results of *bPTP* and *sGMYC* not shown.

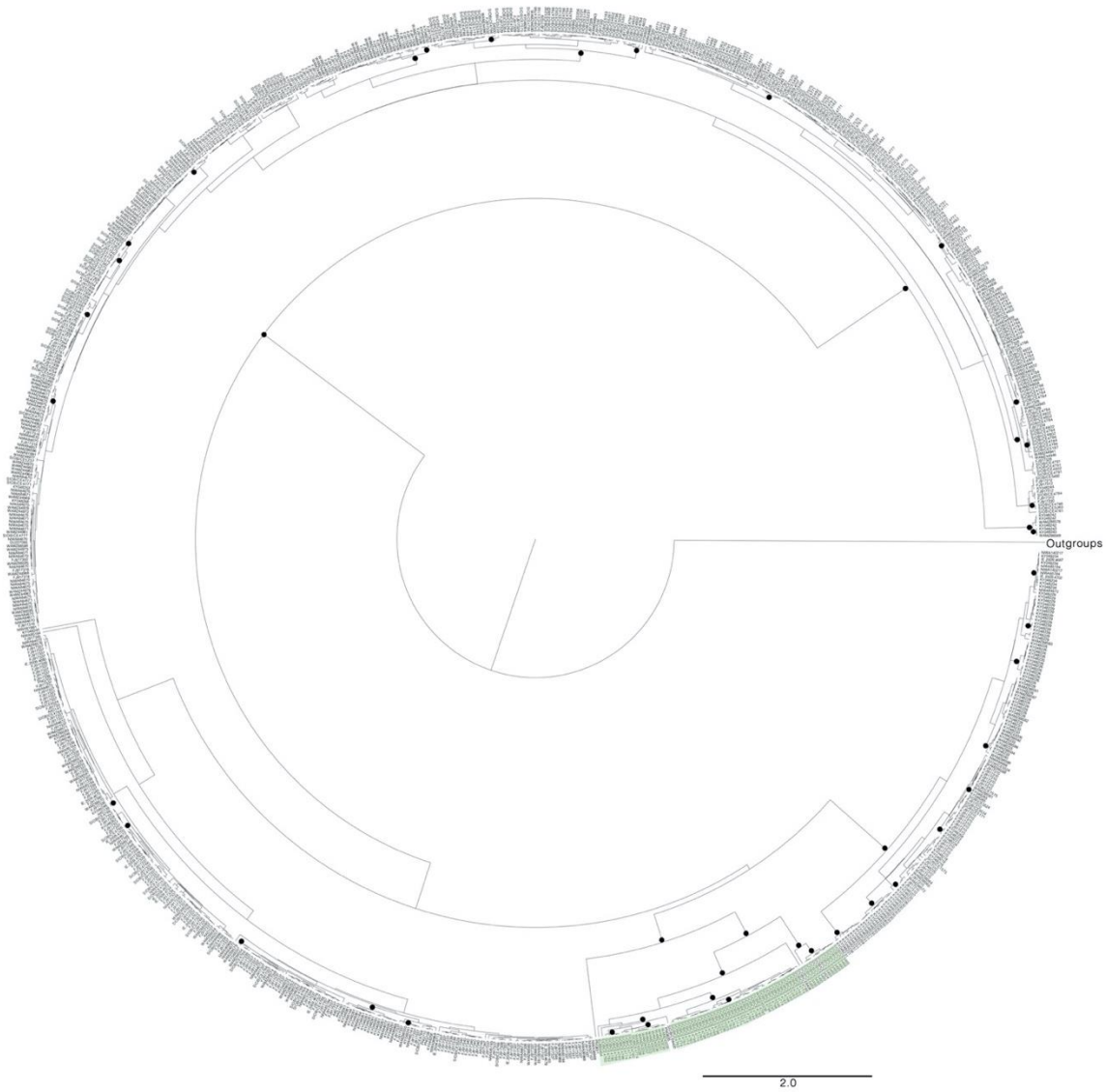

Supplementary Fig N2.2. Bayesian inference ultrametric tree of *Ophionotus victoriae* (non-shaded) and *O. hexactis* (shaded in green) COI sequences. A solid circle at the node represents posterior probability >= 90%.

Additional references

Dinno, A. (2012). paran: Horn's test of principal components/factors. [tool source] Retrieved from https://cran.r-project.org/web/packages/paran/index.html

Ezard, T., Fujisawa, T., & Barraclough, T. G. (2009). Splits: SPecies' LImits by threshold statistics. https://rdrr.io/rforge/splits/.

Fujisawa, T., & Barraclough, T. G. (2013). Delimiting species using single-locus data and the generalized mixed yule coalescent approach: A revised method and evaluation on simulated data sets. *Systematic Biology*, **62**, 707–724.

Hugall, A. F., O'Hara, T. D., Hunjan, S., Nilsen, R., & Moussalli, A. (2016). An exon-capture system for the entire class Ophiuroidea. *Molecular Biology and Evolution*, **33**, 281–294.

Kalyaanamoorthy, S., Minh, B. Q., Wong, T. K. F., Von Haeseler, A., & Jermiin, L. S. (2017). ModelFinder: Fast model selection for accurate phylogenetic estimates. *Nature Methods*, **14**, 587–589.

Kapli, P., Lutteropp, S., Zhang, J., Kobert, K., Pavlidis, P., Stamatakis, A., & Flouri, T. Multi-rate Poisson tree processes for single-locus species delimitation under maximum likelihood and Markov chain Monte Carlo. *Bioinformatics*, **33**, 1630–1638.

Michonneau, F. (2016). Using GMYC for species delineation. Zenodo.

Michonneau, F., Bolker, B., Holder, M., Lewis, P., & O'Meara, B. (2016). rncl: An interface to the Nexus Class Library. [tool source] Retrieved from https://cran.r-project.org/package=rncl

Paradis, E., Claude, J., & Strimmer, K. (2004). APE: Analyses of phylogenetics and evolution in R language. *Bioinformatics*, **20**, 289–290.

Pullandre, N., Lambert, A., Brouillet, S., & Achaz G. ABGD, Automatic Barcode Gap Discovery for primary species delimitation. *Molecular Ecology*, ***21***, 1864–1877.

Rambaut, A. (2016). FigTree v.1.4.3. [tool source] Retrieved from http://tree.bio.ed.ac.uk/software/figtree/

Zhang, J., Kapli, P., Pavlidis, P., & Stamatakis, A. (2013). A general species delimitation method with applications to phylogenetic placements. *Bioinformatics*, **29,** 2869–2876.

Talavera, G., Dincă, V., & Fila, R. (2013). Factors affecting species delimitations with the GMYC model: Insights from a butterfly survey. *Methods in Ecology and Evolution*, **4**, 1101–1110.

Trifinopoulos, J., Nguyen, L. T., von Haeseler, A., & Minh, B. Q. (2016). W-IQ-TREE: A fast online phylogenetic tool for maximum likelihood analysis. *Nucleic Acids Research*, **44**, W232–W235.

Villesen, P. (2007). FaBox: An online toolbox for FASTA sequences. *Molecular Ecology Resources*, **7**, 965–968.

Supplementary Note 4.1

Additional methods for *Chapter 4* - Population tree with admixture

TreeMix is a complementary method to *Structure*; although *Structure* can cluster individuals into populations, *TreeMix* models how the populations may have arisen and outlines the historical relationship between populations (Pickrell & Pritchard 2012). For *TreeMix* analysis within *O. victoriae*, all individuals *of O. hexactis* were assigned as outgroups for tree rooting. Populations within *O. victoriae* were classified by clustering individuals from neighbouring sample locations with similar admixture proportions based on the *Structure* analysis (optimal *K* = 4 in dataset 1). This approach was also utilised in other studies where populations are not clearly defined by discrete geographical locations (e.g. Thom et al. 2020). For *TreeMix* analysis within *O. hexactis*, all individuals *of O. victoriae* were assigned as outgroups for tree rooting. Populations within *O. hexactis* were classified by sample sites, as the genetic structure of *O. hexactis* can be defined by geographical locations (based on *Structure* analysis of dataset 1).

For each species, the input for *Treemix* was generated using the R package *dartR* v1.1.11 (Gruber and Georges 2018). Migration edges (m) were modelled between 0 and 10 in *O. victoriae*, and between 0 and 5 in *O. hexactis*. Ten replicates per each migrant edge were generated using the bootstrap option with a block size of 1 (as the input file contained a single SNP per locus, which assumes loci are unlinked). Each migration edge was weighted based on the ancestry fraction in the sink population originated from each source population (subjected to underestimation under scenarios with high level of admixture) (Pickrell & Pritchard 2012). For the analysis within *O. victoriae*, sample size correction was disabled as some user-defined populations had uneven and limited sample sizes.

Residuals of the covariance matrix were examined to determine whether modelled populations and migrations fit a strict ML tree model. The optimal number of migration edges was evaluated using the simple exponential and non-linear least square model (threshold = 0.05) using the R package *OptM* v0.1.3 (Fitak 2019). Confidence of migration events was also evaluated using jackknife p values, f_3 and f_4 statistics implemented within *TreeMix*. For f_3 statistic, a significantly negative value (Z score < -3) would indicate population A is an admixture of population B and C. For f_4 statistic, a significantly negative value (Z score < -3) would indicate gene flow between population A and D, or between population B and C; a significantly positive value (Z score > 3) would indicate gene flow between population A and C, or between B or D. Both f_3 and f_4 statistics were performed for all possible combinations of populations within each species.

Rationale for population groupings in *Treemix*

TreeMix requires samples within a dataset to be pre-defined into separate populations by the users. *TreeMix* assumes the input populations overall exhibit tree-like structure, and subsequently model migration events between populations to improve to overall data fit to the tree model. In the input dataset, if the number of admixed populations is high relative to the number of non-admixed populations, the tree-ness assumption of *TreeMix* is violated (treemix paper). This violation in *TreeMix*'s assumption is reflected in the *O. victoriae* dataset when populations within *O. victoriae* were user-defined by separate geographical locations. Even though migration edges (between m = 1 - 10) were added in an attempt to relax the assumption of tree-ness, the % variance did not improve by increasing m (Supplementary Fig N4.1A), suggesting genetic variation by locations do not exhibit a tree-like structure and many locations are likely admixed. Admixture between locations is further supported by *PCA* and *Structure* outputs, which indicated various levels of connectivity across locations within *O. victoriae*, and multiple sample locations can be clustered together based on similarity in admixture proportions.

To account for the high level of genetic connectivity across locations in *O. victoriae*, we undertook an iterative approach to cluster locations with similar genetic variation together as a single population in the input dataset. This approach 1) would reduce the number of admixed populations relative to the number of non-admixed populations, 2) enable the SNP data to be a better fit to *TreeMix*'s tree-ness assumption, and 3) minimise the potential errors in over-merging locations with different past demographic histories.

We began with clustering locations with the highest similarity in admixture proportions and stopped when the % variance of the data explained by the *TreeMix* model could be improved with increasing migration edges added. This is an indication that *TreeMix*'s assumptions were likely not violated (i.e. input populations overall exhibit tree-like structure, the number of admixed populations is lower to the number of non-admixed populations, and the model can be improved with increasing migration edges added). We also cross validated the data fit to the final *TreeMix* model with a residual matrix, jackknife p values, f_3 and f_4 statistics in order to ensure the *TreeMix* results could be corroborated by other statistics.

Based on PCA and *Structure* results (K = 4; Fig 4.1 - 4.2), we first clustered Herdman Bank, Discovery Bank and South Sandwich Islands as a single population. As the % variance explained did not noticeably improve with increasing m (Supplementary Fig N4.1b), we then clustered Elephant Island, South Shetland Islands and Bransfield Strait as a single population. While the overall % variance explained were improved, the % variance explained did not consistently improve as the m sequentially increased (Supplementary Fig N4.1c). Finally, we also clustered

Prydz Bay and Tressler Bank as a single population, which the % variance explained consistently improved and/or stabilised as m was sequentially increased (Supplementary Fig N4.1D), suggesting *TreeMix* was likely running as per the model's assumptions.

Additional references

Fitak, R. R. (2019). OptM: Estimating the Optimal Number of Migration Edges from 'Treemix.' [tool source]. Retrieved from https://cran.r-project.org/web/packages/OptM/

Gruber, B, and Georges, A. (2018). DartR: Importing and Analysing SNP and Silicodart Data Generated by Genome-Wide Restriction Fragment Analysis. [tool source]. Retrieved from https://cran.r-project.org/package=dartR

Pickrell, J. K., & Pritchard, J. K. (2012). Inference of Population Splits and Mixtures from Genome-Wide Allele Frequency Data. *PLoS Genetics*, **8**(11), e1002967.

Thom, G., Xue, A. T., Sawakuchi, A. O., Ribas, CC C., Hickerson, M. J., Aleixo, A., & Miyaki, C. (2020). Quaternary Climate Changes as Speciation Drivers in the Amazon Floodplains. *Science Advances*, **6**(11), eaax4718.

(a)

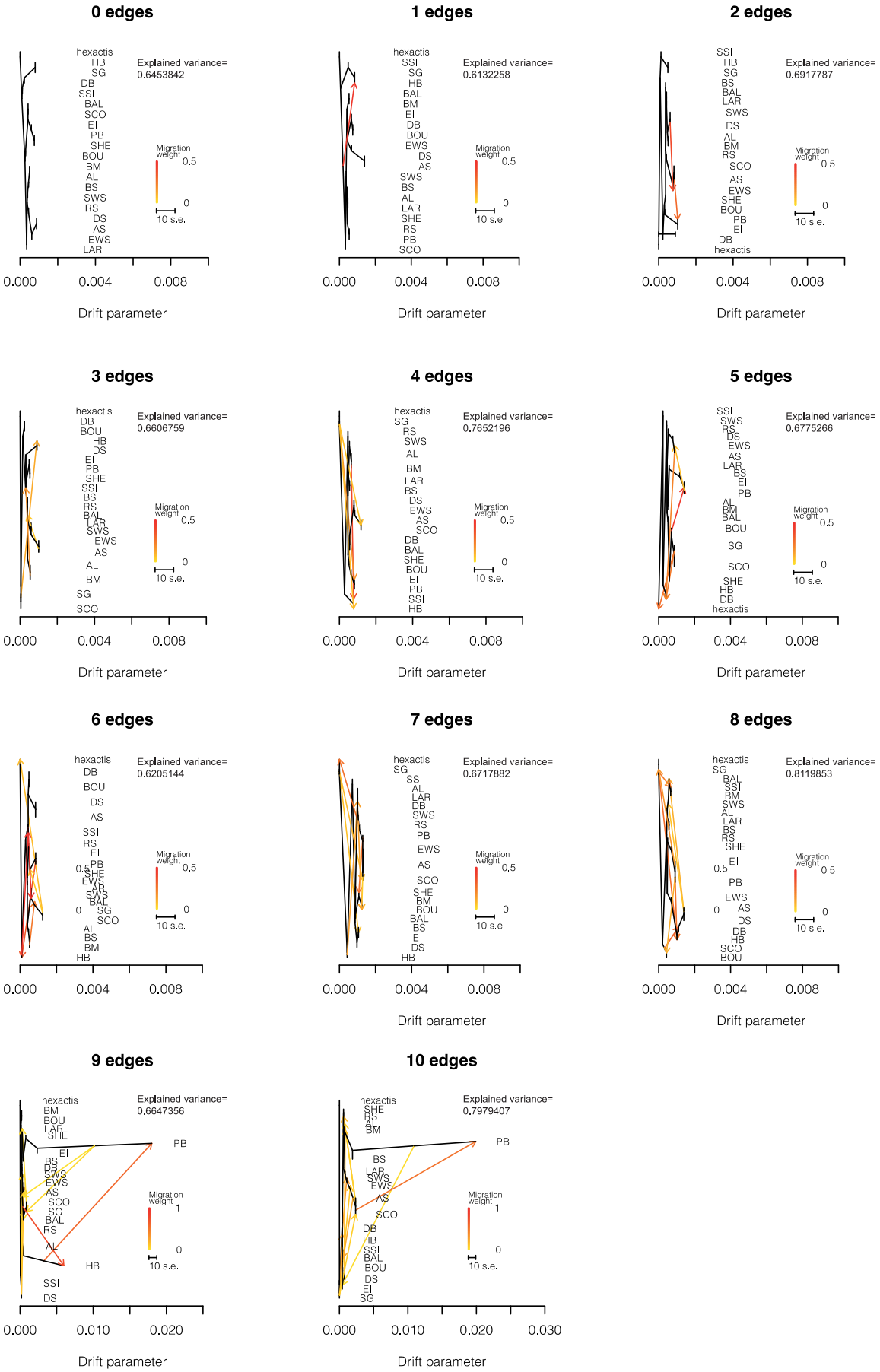
0 edges
Explained variance= 0.6453842
1 edges
Explained variance= 0.6132258
2 edges
Explained variance= 0.6917787
3 edges
Explained variance= 0.6606759
4 edges
Explained variance= 0.7652196
5 edges
Explained variance= 0.6775266
6 edges
Explained variance= 0.6205144
7 edges
Explained variance= 0.6717882
8 edges
Explained variance= 0.8119853
9 edges
Explained variance= 0.6647356
10 edges
Explained variance= 0.7979407
Migration weight
10 s.e.
Drift parameter

(b)

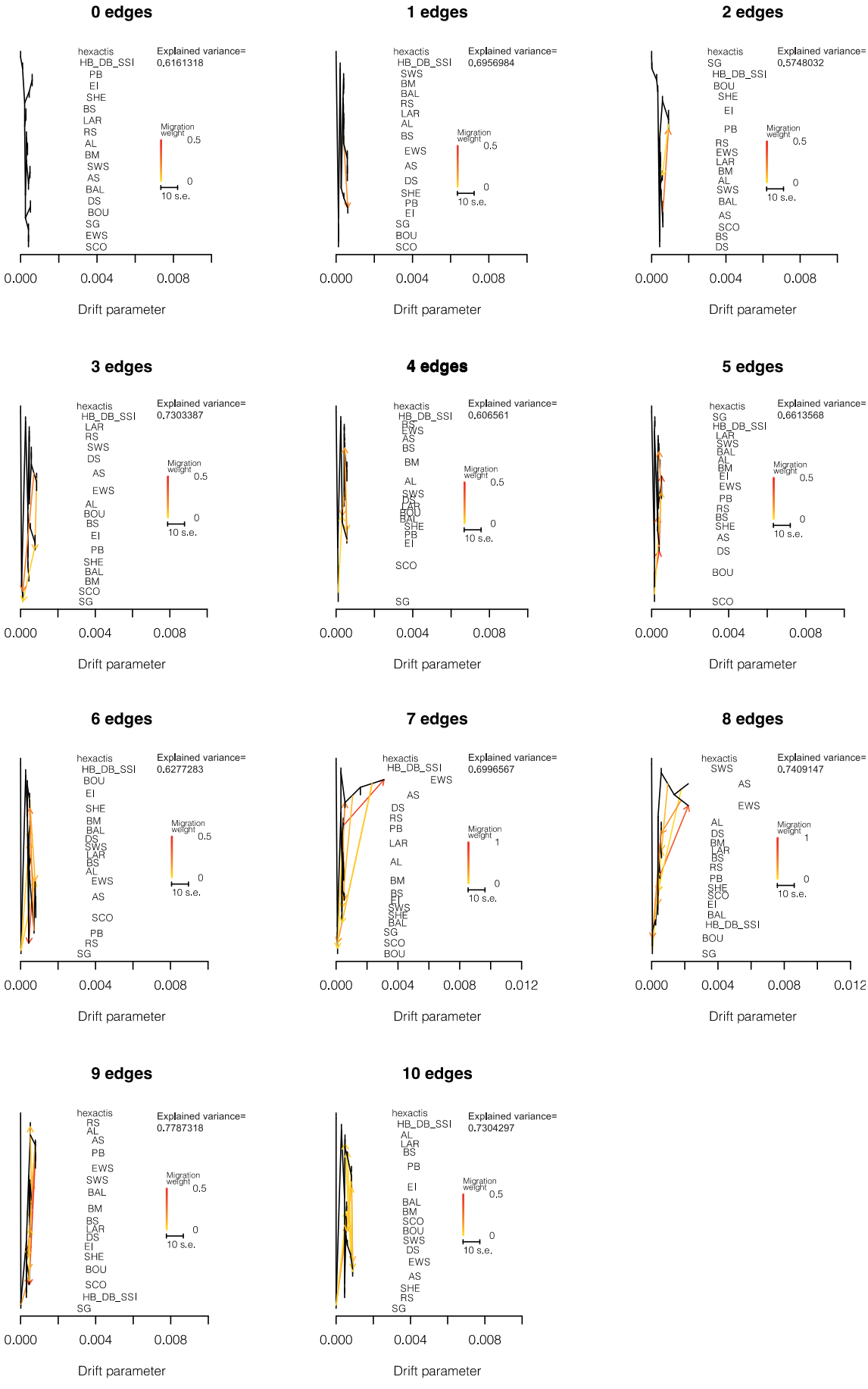
0 edges
hexactis
HB_DB_SSI
PB
EI
SHE
BS
LAR
RS
AL
BM
SWS
AS
BAL
DS
BOU
SG
EWS
SCO
Explained variance=
0.6161318
Migration weight
0.5
0
10 s.e.
0.000
0.004
0.008
Drift parameter
1 edges
hexactis
HB_DB_SSI
SWS
BM
BAL
RS
LAR
AL
BS
EWS
AS
DS
SHE
PB
EI
SG
BOU
SCO
Explained variance=
0.6956984
Migration weight
0.5
0
10 s.e.
0.000
0.004
0.008
Drift parameter
2 edges
hexactis
SG
HB_DB_SSI
BOU
SHE
EI
PB
RS
EWS
LAR
BM
AL
SWS
BAL
AS
SCO
BS
DS
Explained variance=
0.5748032
Migration weight
0.5
0
10 s.e.
0.000
0.004
0.008
Drift parameter
3 edges
hexactis
HB_DB_SSI
LAR
RS
SWS
DS
AS
EWS
AL
BOU
BS
EI
PB
SHE
BAL
BM
SCO
SG
Explained variance=
0.7303387
Migration weight
0.5
0
10 s.e.
0.000
0.004
0.008
Drift parameter
4 edges
hexactis
HB_DB_SSI
EWS
AS
BS
BM
AL
SWS
DS
LAR
BOU
BAL
SHE
PB
EI
SCO
SG
Explained variance=
0.606561
Migration weight
0.5
0
10 s.e.
0.000
0.004
0.008
Drift parameter
5 edges
hexactis
SG
HB_DB_SSI
LAR
SWS
BAL
AL
BM
EI
EWS
PB
RS
BS
SHE
AS
DS
BOU
SCO
Explained variance=
0.6613568
Migration weight
0.5
0
10 s.e.
0.000
0.004
0.008
Drift parameter
6 edges
hexactis
HB_DB_SSI
BOU
EI
SHE
BM
BAL
DS
SWS
LAR
BS
AL
EWS
AS
SCO
PB
RS
SG
Explained variance=
0.6277283
Migration weight
0.5
0
10 s.e.
0.000
0.004
0.008
Drift parameter
7 edges
hexactis
HB_DB_SSI
EWS
AS
DS
RS
PB
LAR
AL
BM
BS
EI
SWS
SHE
BAL
SG
SCO
BOU
Explained variance=
0.6996567
Migration weight
1
0
10 s.e.
0.000
0.004
0.008
0.012
Drift parameter
8 edges
hexactis
SWS
AS
EWS
AL
DS
BM
LAR
BS
RS
PB
SHE
SCO
EI
BAL
HB_DB_SSI
BOU
SG
Explained variance=
0.7409147
Migration weight
1
0
10 s.e.
0.000
0.004
0.008
0.012
Drift parameter
9 edges
hexactis
RS
AL
AS
PB
EWS
SWS
BAL
BM
BS
LAR
DS
EI
SHE
BOU
SCO
HB_DB_SSI
SG
Explained variance=
0.7787318
Migration weight
0.5
0
10 s.e.
0.000
0.004
0.008
Drift parameter
10 edges
hexactis
HB_DB_SSI
AL
LAR
BS
PB
EI
BAL
BM
SCO
BOU
SWS
DS
EWS
AS
SHE
RS
SG
Explained variance=
0.7304297
Migration weight
0.5
0
10 s.e.
0.000
0.004
0.008
Drift parameter

(c)

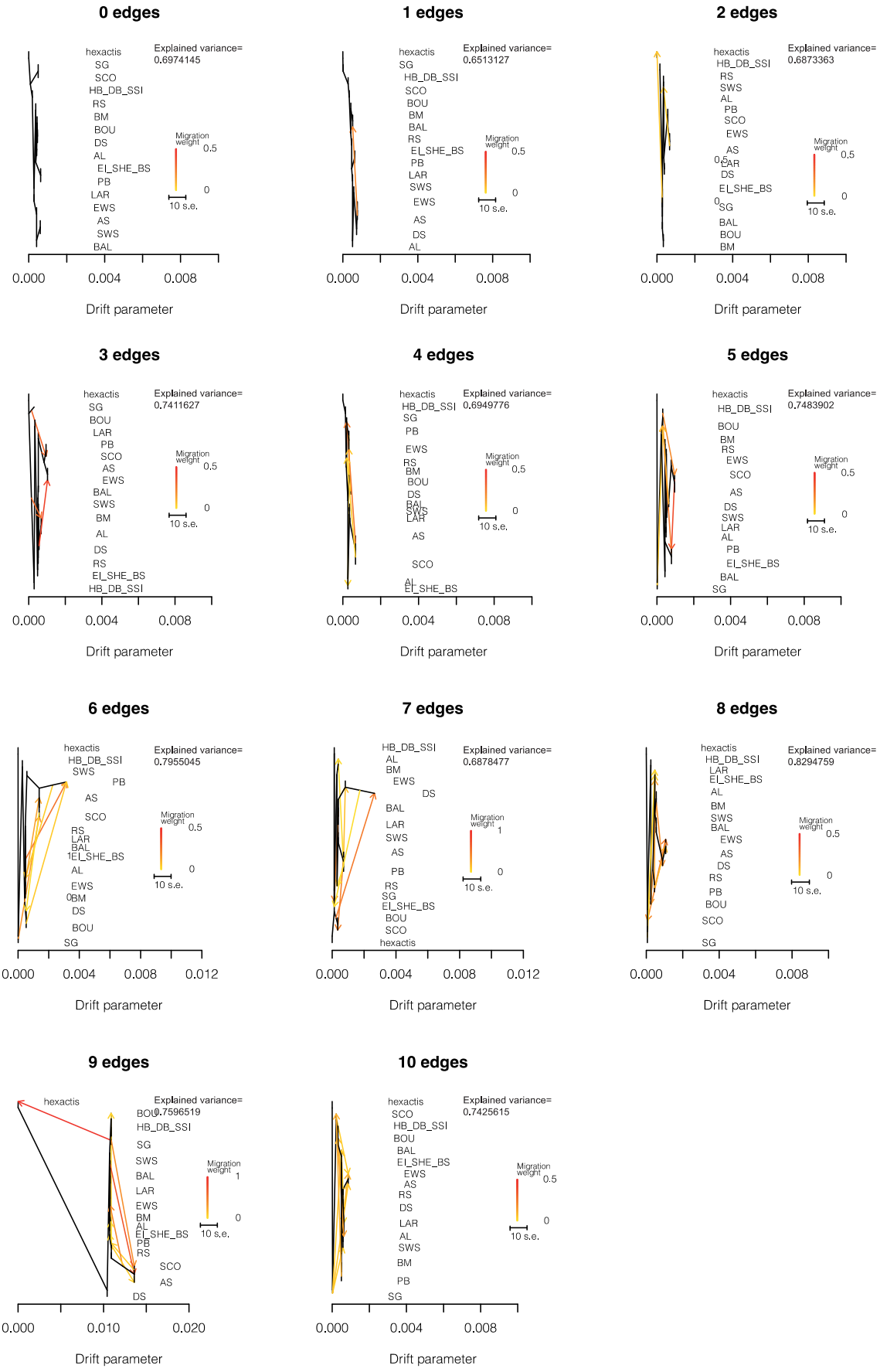
0 edges
hexactis
Explained variance=
0.6974145
SG
SCO
HB_DB_SSI
RS
BM
BOU
DS
AL
EI_SHE_BS
PB
LAR
EWS
AS
SWS
BAL
Migration weight
0.5
0
10 s.e.
0.000
0.004
0.008
Drift parameter
1 edges
hexactis
Explained variance=
0.6513127
SG
HB_DB_SSI
SCO
BOU
BM
BAL
RS
EI_SHE_BS
PB
LAR
SWS
EWS
AS
DS
AL
Migration weight
0.5
0
10 s.e.
0.000
0.004
0.008
Drift parameter
2 edges
hexactis
Explained variance=
0.6873363
HB_DB_SSI
RS
SWS
AL
PB
SCO
EWS
AS
LAR
DS
EI_SHE_BS
SG
BAL
BOU
BM
Migration weight
0.5
0
10 s.e.
0.000
0.004
0.008
Drift parameter
3 edges
hexactis
Explained variance=
0.7411627
SG
BOU
LAR
PB
SCO
AS
EWS
BAL
SWS
BM
AL
DS
RS
EI_SHE_BS
HB_DB_SSI
Migration weight
0.5
0
10 s.e.
0.000
0.004
0.008
Drift parameter
4 edges
hexactis
Explained variance=
0.6949776
HB_DB_SSI
SG
PB
EWS
RS
BM
BOU
DS
BAL
SWS
LAR
AS
SCO
AL
EI_SHE_BS
Migration weight
0.5
0
10 s.e.
0.000
0.004
0.008
Drift parameter
5 edges
hexactis
Explained variance=
0.7483902
HB_DB_SSI
BOU
BM
RS
EWS
SCO
AS
DS
SWS
LAR
AL
PB
EI_SHE_BS
BAL
SG
Migration weight
0.5
0
10 s.e.
0.000
0.004
0.008
Drift parameter
6 edges
hexactis
Explained variance=
0.7955045
HB_DB_SSI
SWS
PB
AS
SCO
RS
LAR
BAL
EI_SHE_BS
AL
EWS
BM
DS
BOU
SG
Migration weight
0.5
0
10 s.e.
0.000
0.004
0.008
0.012
Drift parameter
7 edges
HB_DB_SSI
Explained variance=
0.6878477
AL
BM
EWS
DS
BAL
LAR
SWS
AS
PB
RS
SG
EI_SHE_BS
BOU
SCO
hexactis
Migration weight
1
0
10 s.e.
0.000
0.004
0.008
0.012
Drift parameter
8 edges
hexactis
Explained variance=
0.8294759
HB_DB_SSI
LAR
EI_SHE_BS
AL
BM
SWS
BAL
EWS
AS
DS
RS
PB
BOU
SCO
SG
Migration weight
0.5
0
10 s.e.
0.000
0.004
0.008
Drift parameter
9 edges
hexactis
Explained variance=
0.7596519
BOU
HB_DB_SSI
SG
SWS
BAL
LAR
EWS
BM
AL
EI_SHE_BS
PB
RS
SCO
AS
DS
Migration weight
1
0
10 s.e.
0.000
0.010
0.020
Drift parameter
10 edges
hexactis
Explained variance=
0.7425615
SCO
HB_DB_SSI
BOU
BAL
EI_SHE_BS
EWS
AS
RS
DS
LAR
AL
SWS
BM
PB
SG
Migration weight
0.5
0
10 s.e.
0.000
0.004
0.008
Drift parameter

(d)

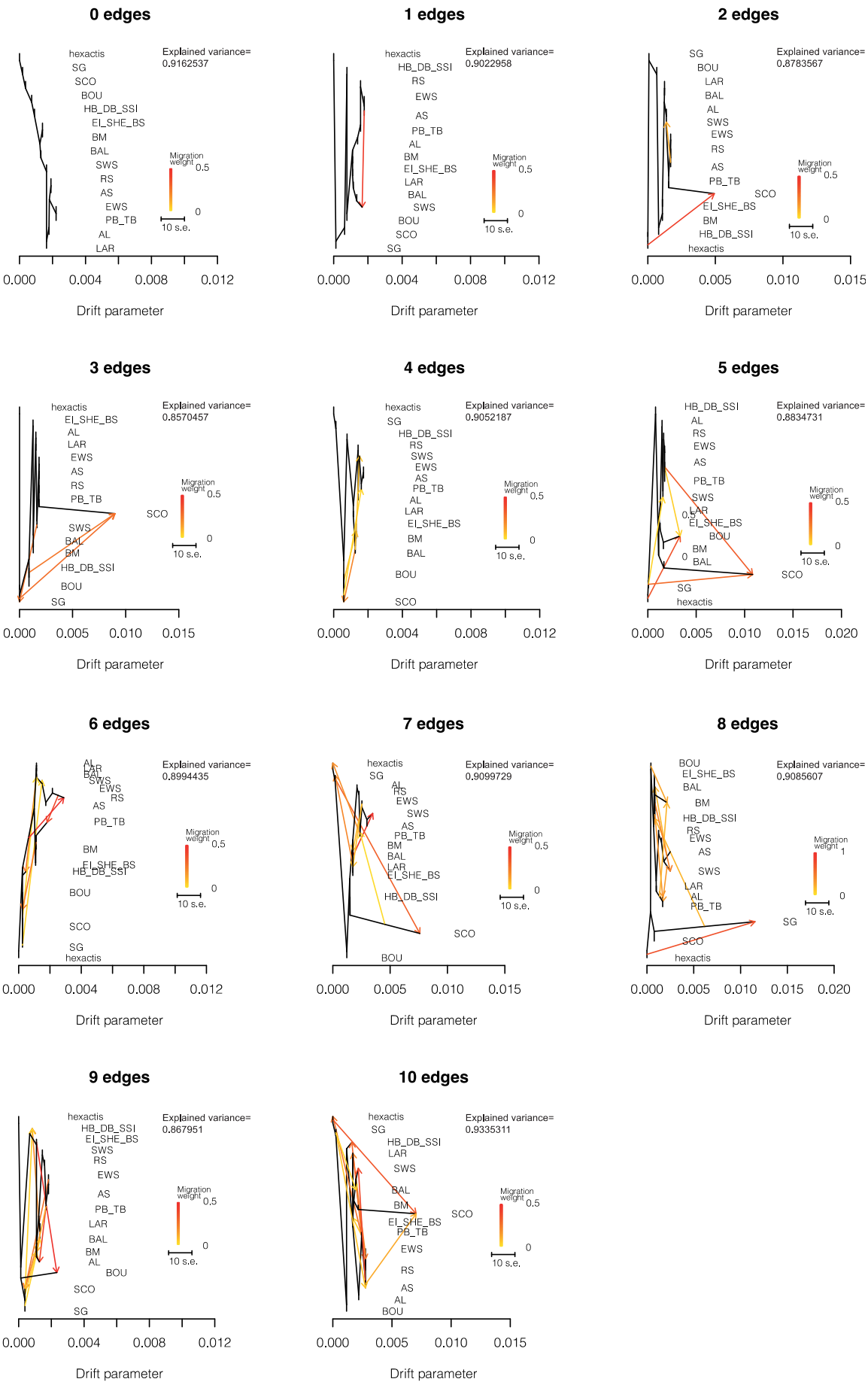
0 edges
Explained variance= 0.9162537
hexactis SG SCO BOU HB_DB_SSI EI_SHE_BS BM BAL SWS RS AS EWS PB_TB AL LAR
Migration weight 0.5 0 10 s.e.
0.000 0.004 0.008 0.012
Drift parameter
1 edges
Explained variance= 0.9022958
hexactis HB_DB_SSI RS EWS AS PB_TB AL BM EI_SHE_BS LAR BAL SWS BOU SCO SG
Migration weight 0.5 0 10 s.e.
0.000 0.004 0.008 0.012
Drift parameter
2 edges
Explained variance= 0.8783567
SG BOU LAR BAL AL SWS EWS RS AS PB_TB SCO EI_SHE_BS BM HB_DB_SSI hexactis
Migration weight 0.5 0 10 s.e.
0.000 0.005 0.010 0.015
Drift parameter
3 edges
Explained variance= 0.8570457
hexactis EI_SHE_BS AL LAR EWS AS RS PB_TB SCO SWS BAL BM HB_DB_SSI BOU SG
Migration weight 0.5 0 10 s.e.
0.000 0.005 0.010 0.015
Drift parameter
4 edges
Explained variance= 0.9052187
hexactis SG HB_DB_SSI RS SWS EWS AS PB_TB AL LAR EI_SHE_BS BM BAL BOU SCO
Migration weight 0.5 0 10 s.e.
0.000 0.004 0.008 0.012
Drift parameter
5 edges
Explained variance= 0.8834731
HB_DB_SSI AL RS EWS AS PB_TB SWS LAR EI_SHE_BS BOU BM BAL SCO SG hexactis
Migration weight 0.5 0 10 s.e.
0.000 0.005 0.010 0.015 0.020
Drift parameter
6 edges
Explained variance= 0.8994435
AL LAR BAL SWS EWS RS AS PB_TB BM EI_SHE_BS HB_DB_SSI BOU SCO SG hexactis
Migration weight 0.5 0 10 s.e.
0.000 0.004 0.008 0.012
Drift parameter
7 edges
Explained variance= 0.9099729
hexactis SG AL RS EWS SWS AS PB_TB BM BAL LAR EI_SHE_BS HB_DB_SSI SCO BOU
Migration weight 0.5 0 10 s.e.
0.000 0.005 0.010 0.015
Drift parameter
8 edges
Explained variance= 0.9085607
BOU EI_SHE_BS BAL BM HB_DB_SSI RS EWS AS SWS LAR AL PB_TB SG SCO hexactis
Migration weight 1 0 10 s.e.
0.000 0.005 0.010 0.015 0.020
Drift parameter
9 edges
Explained variance= 0.867951
hexactis HB_DB_SSI EI_SHE_BS SWS RS EWS AS PB_TB LAR BAL BM AL BOU SCO SG
Migration weight 0.5 0 10 s.e.
0.000 0.004 0.008 0.012
Drift parameter
10 edges
Explained variance= 0.9335311
hexactis SG HB_DB_SSI LAR SWS BAL BM EI_SHE_BS PB_TB SCO EWS RS AS AL BOU
Migration weight 0.5 0 10 s.e.
0.000 0.005 0.010 0.015
Drift parameter

Supplementary Fig N4.1 *TreeMix* maximum likelihood (ML) trees with migration edges (between m = 0 - 10) of *O. victoriae* (n = 165) rooted with *O. hexactis* (n = 40) (total n = 195, 1,781 loci). Terminal nodes were defined by (a) separate geographical locations; (b) Herdman Bank, Discovery Bank and South Sandwich Islands as a single population; (c) Herdman Bank, Discovery Bank and South Sandwich Islands as a single population, and Elephant Island, South Shetland Islands and Bransfield Strait as a single population; (d) Herdman Bank, Discovery Bank and South Sandwich Islands as a single population, and Elephant Island, South Shetland Islands and Bransfield Strait as a single population, and Prydz Bay and Tressler Bank as a single population.

Supplementary Note 4.2

Additional methods for *Chapter 4 - dadi* inference between *O. victoriae* and *O. hexactis*

The divergence and connectivity between *O. victoriae* and *O. hexactis* were investigated via the diffusion approximation framework within *dadi*. A total of nine demographic models were fitted against the folded 2-dimensional joint site frequency spectrum (2d-jSFS) between *O. victoriae* and *O. hexactis*. The examined demographic models ranged from simple (three parameters) to complex (ten parameters) biologically relevant scenarios, including divergence followed by strict isolation, continuous migration, ancient migration, secondary contact and past population size changes (Supplementary Fig 4.1). We explored the relationship between *O. victoriae* and *O. hexactis* using all samples of dataset 1 but excluded samples with signals of strong interspecific admixture, i.e. *O. victoriae* from South Georgia (n = 2) and *O. hexactis* from Bransfield Mouth (n = 10), thus the total number of samples = 183.

For *dadi* input, folded 2d-jSFS was generated using easySFS.py (https://github.com/isaacovercast/easySFS#easysfs). In the dataset with non-admixed samples (n = 183), SFS was down projected to 144 haploid samples (*O. victoriae*) and 32 haploid samples (*O. hexactis*).

Each *dadi* model was run with four consecutive rounds of optimisation using the *dadi_pipeline* v3.1.6 (Portik et al., 2017). Each round was run with a designated number of replicates, and the best scoring replicate (based on log-likelihood) was then used as starting values for the next round of perturbed parameters. *dadi_pipeline* was performed with replicates of 10, 20, 30, 40, iterations of 3, 5, 10, 15 and fold in parameter generation of 3, 2, 2, 1. Each parameter set was optimised using the default Nelder-Mead method. For each model, replicates in the final fourth round were compared using Akaike information criterion (AIC) and log-likelihood to assess overall convergence. Parameters of the best fit models were converted into biologically meaningful units.

dadi model evaluations

As our dataset contains linked sites, evaluations based on AIC could be associated with bias towards more complex models. However, studies that utilised linked SNPs in *dadi* have typically ranked models based on AIC methods as the first step in identifying the best fitted model (e.g. Benham & Cheviron 2019; Walsh et al., 2019). Since not all the models analysed in this study are directly nested within each other, we could not perform likelihood ratio test with a Godambe information matrix (GIM) based adjustment to account for linkage (Coffman et al. 2016), which would score the best fit model between every two models. Instead, the replicate with the highest log-likelihood of each model were compared among models based on AIC, model score, Akaike

weights (W_{AIC}), and residuals relative to the observed data, following Rougeux et al. (2017) and Silva et al. (2021).

For *dadi* model evaluations, the replicate with the highest log-likelihood of each model were compared among models based on AIC, model score, Akaike weights (W_{AIC}), and residuals relative to the observed data, following Rougeux et al. (2017) and Silva et al. (2021). Model score penalises models with more parameters, which compares models with increasing complexity and addresses overparameterisation issues (Silva et al., 2021). For each tested model (i), Score was estimated as follows:

$$model\ score = \frac{(\Delta_{max} - \Delta AIC_i)}{\Delta_{max}}$$

Where Δ_{max} = difference in AIC between the models with lowest and highest AIC values, and ΔAIC_i = AIC_i – AIC_{min}. Thus, the best and worst model would yield a model score of 1 and 0, respectively.

Akaike weights (W_{AIC}) was calculated to evaluate the relative probability of different models as follows:

$$W_{AIC} = \frac{e^{\frac{-(\Delta AIC_i)}{2}}}{\sum_{i=1}^{R} e^{\frac{-(\Delta AIC_i)}{2}}}$$

where R = 9 (total number of models tested).

To evaluate parameter uncertainties, we generated 100 replicate spectra with nonparametric bootstrapping using *dadi-cli* (https://github.com/xin-huang/dadi-CLI). We performed uncertainty analysis with GIM for each top ranking model (Coffman et al. 2016), and calculated 95% confidence intervals (CI) for each parameter estimate using the point estimate of $\pm$ 1.96 SD. Finally, parameters were also converted into biologically meaningful units following Rougeux et al. (2017) and Silva et al. (2021). Ancestral effective population size (N_{ref}) before species divergence was calculated as follows:

$$N_{ref} = \frac{\theta}{4L\mu}$$

Where θ = optimal multiplicative scaling factor scaled between model and data, μ = mutation rate (1.43×10^{-8} per site per generation), and L = effective length of the genome explored which was calculated as follows:

$$L = \frac{zy140}{x}$$

Where z = number of SNPS retained for *dadi* analysis (24,649), y = number of RAD tags (of 140 bp) retained after genotyping calling (*Stacks*/*genotypes*; 170,953), and x = number of SNPs that were originally detected from y RAD tags (307,738). Notes that while z represents the number of SNPs retained for *dadi* analyses from target capture sequencing of *O. victoriae* and *O. hexactis*, x and y represent the number of RAD loci and SNPs detected from the initial loci discovery of eight mitochondrially divergent *Ophiontous* individuals via genotyping-by-sequencing.

Additional references

Benham, P. M., & Cheviron, Z. A. (2019) Divergent Mitochondrial Lineages Arose within a Large, Panmictic Population of the Savannah Sparrow (*Passerculus Sandwichensis*). *Molecular Ecology*, **28**(7), 1765–1783.

Coffman, A. J., Hsieh, P. H., Gravel, S., & Gutenkunst, R. N. (2016) Computationally Efficient Composite Likelihood Statistics for Demographic Inference. *Molecular Biology and Evolution*, **33(**2), 591–593.

Portik, D. M., Leaché, A. D., Rivera, D., Barej, M. F., Burger, M., Hirschfeld, M., Rödel, M. O., Blackburn, D. C., & Fujita, M. K. (2017) Evaluating Mechanisms of Diversification in a Guineo-Congolian Tropical Forest Frog Using Demographic Model Selection. *Molecular Ecology*, **26**(19), 5245–5263.

Rougeux, C., Bernatchez, L., & Gagnaire, P. A. (2017) Modeling the Multiple Facets of Speciation-with-Gene-Flow toward Inferring the Divergence History of Lake Whitefish Species Pairs (*Coregonus Clupeaformis*). *Genome Biology and Evolution*, **9**(8), 2057–2074.

Silva, C. N. S., Murphy, N. P., Bell, J. J., Green, B. S., Duhamel, G., Cockcroft, A. C., Hernández, C. E., & Strugnell, J. M. (2021) Global Drivers of Recent Diversification in a Marine Species Complex. *Molecular Ecology*, **30**(5), 1223–1236.

Walsh, J., Benham, P. M., Deane-Coe, P. E., Arcese, P., Butcher, B. G., Chan, Y. L., Cheviron, Z. A., Elphick, C. S., Kovach, A. I., Olsen, B. J., Shriver, W. G., Winder, V. L. & Lovette, I. J. (2019) Genomics of Rapid Ecological Divergence and Parallel Adaptation in Four Tidal Marsh Sparrows. *Evolution Letters*, **3**(4), 324–338.

Supplementary Notes 6.1

Extended results of demographic modelling

Demographic modelling of *P. turqueti*

We used a hierarchical approach to build a demographic model of WS, AS, RS and EA populations in *P. turqueti*. We started from simple models (Step 1) and gradually increased model complexity (Step 2 and Step 3) (Supplementary Fig 6.3-6.4). The first level included estimation of the population divergence topology that acted as the baseline for Step 2 models. At Step 1, the best model was '3_AS_RSEAWS' where AS was divergent from RS, EA and WS populations (Supplementary Table N6.1). At Step 2, a limitation differentiation between AIC values (median between -153097.72 and -152294.76) was observed across competing scenarios (Supplementary Table N6.2, Supplementary Fig N6.1-N6.2). Therefore, we further evaluated Step 3 models to increase complexity and to model more ecologically realistic scenarios. After incorporating competing scenarios of historical WAIS configurations and contemporary gene flow driven by the ACC and ASC, the "cc_full_col2" model was identified as the best model (Supplementary Table N6.3, Supplementary Fig N6.3-N6.4). Under the most likely model of "cc_full_col2", The ancestral population of *P. turqueti*'s seaway and EA populations experienced a population expansion at 2.76 (95% confidence interval (CI) between 1.47 and 5.65) million years ago, corresponding to the previous estimated timing of the species' continental shelf clade emergence based on mitochondrial data (Strugnell et al. 2012). Then, the AS population was estimated to have diverged from the ancestral population of WS, RS and EA at 373,945 (95% CI between 158,500 and 1,071,226) years ago, and direct gene flow between WS-AS, AS-RS and WS-RS was detected at 107,237 (95% CI between 57,855 and 162,553) years ago. Finally, contemporary gene flow following the directionality of the ACC and ASP began in modern times (0 (95% CI between 0 and 0) years ago).

Overall, we obtained a very good fit of the expected and the observed SFS for *P. turqueti* (Supplementary Fig N6.5-N6.6). Among the entries of the joint SFS (Supplementary Fig N6.7), there is a good fit of the expected SFS for the entries with more SNPs, with the fit of the expected SFS gradually gets poorer for entries with fewer SNPs. The poorest fits of the expected SFS were observed for the entries with a high number of derived alleles in some populations (Supplementary Fig N6.7). This is expected as the modelled demographical scenarios aim to test for simple contrasting hypothesised scenarios of whether there was no, partial or complete historical WAIS collapse, as well as accounting the partners of circumpolar gene flow, across four populations (WS, AS, RS and EA). We did not model for specific population history in order to avoid over-parametrise the models in a limited dataset (i.e. RAD loci). The unmodelled high number of derived

alleles in some populations likely represent unmodelled population-level changes throughout the Quaternary glacial-interglacial cycles.

Supplementary Table N6.1 Summary of likelihoods for the model tested at Step 1 in *Pareledone turqueti*. Model label corresponds to model label in Supplementary Fig 6.3. Delta AIC and relative likelihoods were calculated following Excoffier et al. (2013). Abbreviations: Lhood = log likelihoods, AIC = Akaike Information Criterion.

Model label	log10(Lhood)	Number of parameters	AIC	Delta AIC	Relative likelihood (Akaike's weight of evidence)
3_AS_RSEAWS	-156826.6852	7	722357.712	0	1.00
2_WS_ASRSEA	-157122.1933	7	723718.822	1361.11031	0.00
4_RS_EAWSAS	-157138.3451	7	723793.218	1435.50550	0.00
9_EA_WS_ASRS	-157152.8118	7	723859.851	1502.13912	0.00
6_WS_AS_RSEA	-157202.5906	7	724089.132	1731.42027	0.00
8_RS_EA_WSAS	-157212.2655	7	724133.695	1775.98286	0.00
7_AS_RS_EAWS	-157262.5244	7	724365.187	2007.47536	0.00
1_WS_AS_RS_EA	-157264.2168	6	724370.983	2013.27055	0.00
11_RS_WS_EAAS	-157267.2098	7	724386.768	2029.05631	0.00
10_EA_AS_RSWS	-157278.2386	7	724437.567	2079.85496	0.00
5_EA_WSASRS	-157291.1285	7	724496.938	2139.22584	0.00

Supplementary Table N6.2 Summary of likelihoods for the model tested at Step 2 in *Pareledone turqueti*. Model label corresponds to model label in Supplementary Fig 6.3. Delta AIC and relative likelihoods were calculated following Excoffier et al. (2013). Abbreviations: Lhood = log likelihoods, AIC = Akaike Information Criterion.

Model label	log10(Lhood)	Number of parameters	AIC	Delta AIC	Relative likelihood (Akaike's weight of evidence)
par_col2	-152294.7570	22	701513.6507	0	1.00
par_col	-152298.8235	22	701532.3810	18.7302990	0.00
no_col	-152312.4281	20	701591.0438	77.3930866	0.00
full_col1	-152313.9543	22	701602.0735	88.4227638	0.00
full_col2	-152325.2559	26	701662.1287	148.4779334	0.00
con_flow	-153097.7213	15	705198.1043	3684.453566	0.00

Supplementary Table N6.3 Summary of likelihoods for the model tested at Step 3 in *Pareledone turqueti*. Model label corresponds to model label in Supplementary Fig 6.3. Delta AIC and relative likelihoods were calculated following Excoffier et al. (2013). Abbreviations: Lhood = log likelihoods, AIC = Akaike Information Criterion.

Model label	log10(Lhood)	Number of parameters	AIC	Delta AIC	Relative likelihood (Akaike's weight of evidence)
cc_full_col2	-152212.468	30	701150.6276	0	1.00
cc_full_col1	-152232.9408	26	701236.9253	86.2977168	0.00
cc_no_col	-152262.0371	24	701366.9429	216.3152746	0.00
cc_pa_rcol	-152262.0371	26	701370.9429	220.3152746	0.00
cc_par_col2	-152270.6446	26	701410.5890	259.9614196	0.00
cc_con_flow	-152979.9878	19	704663.8238	3513.196199	0.00

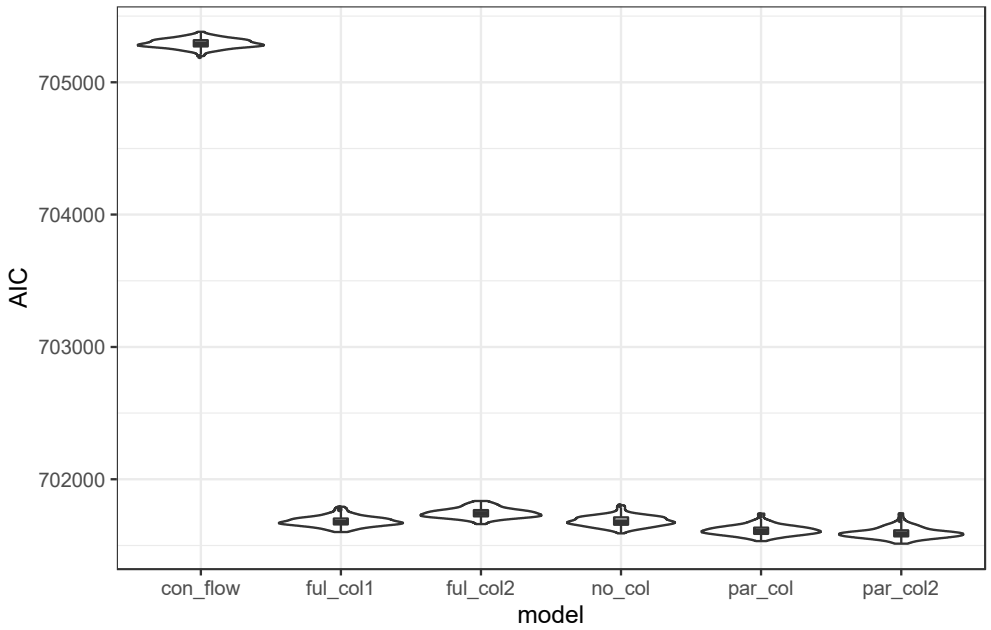

Supplementary Fig N6.1 Comparisons of demographic models at Step 2 in *Pareledone turqueti* (see Extended Data Fig 6.3 for visualisations of the models). The distributions of AIC from 100 independent expected SFS (violin plot), with each approximated using 200,000 coalescent simulations under the parameters that maximised the likelihood for each model. Each box represents the interquartile range (25th and 75th percentile), each line represents the median, each dot represents outlier values > 1.5x and < 3x the interquartile range.

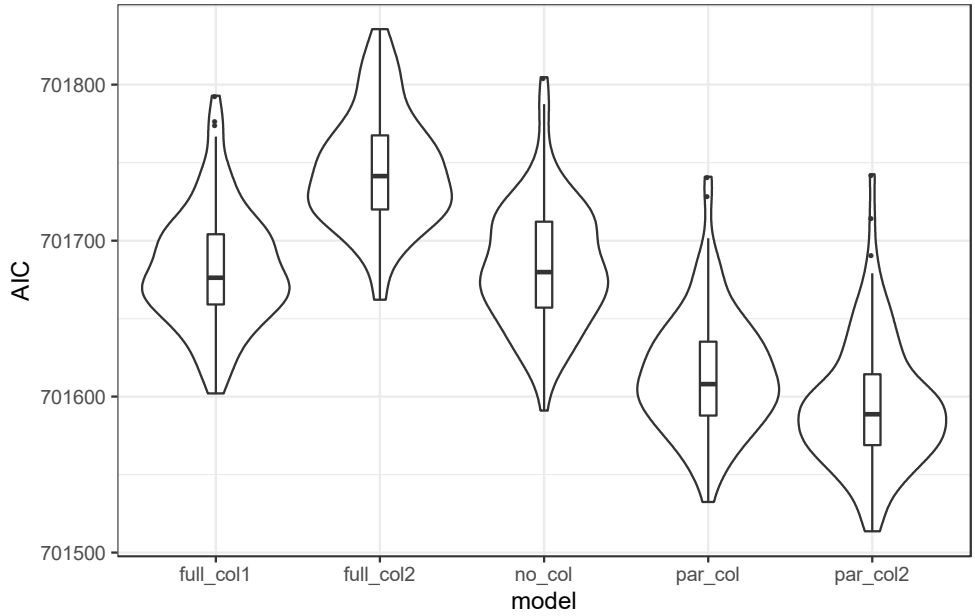

Supplementary Fig N6.2 Comparisons of demographic models at Step 2 (excluding 'conflow') in *Pareledone turqueti* (see Extended Data Fig 6.3 for visualisations of the models). The distributions of AIC from 100 independent expected SFS (violin plot), with each approximated using 200,000 coalescent simulations under the parameters that maximised the likelihood for each model. Each box represents the interquartile range (25th and 75th percentile), each line represents the median, each dot represents outlier values > 1.5x and < 3x the interquartile range.

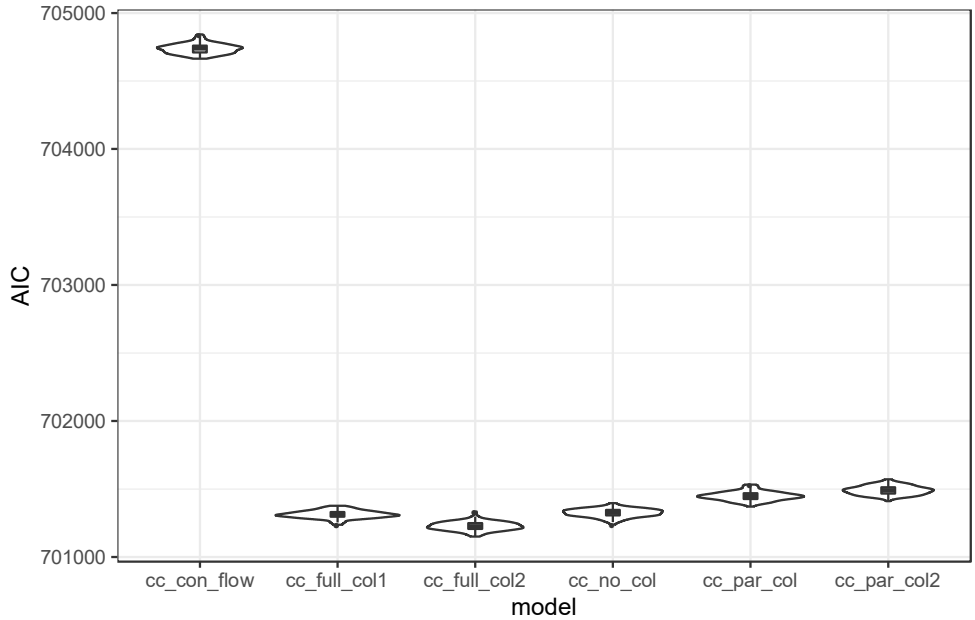

Supplementary Fig N6.3 Comparisons of demographic models at Step 3 in *Pareledone turqueti* (see Extended Data Fig 6.3 for visualisations of the models). The distributions of AIC from 100 independent expected SFS (violin plot), with each approximated using 200,000 coalescent simulations under the parameters that maximised the likelihood for each model. Each box represents the interquartile range (25th and 75th percentile), each line represents the median, each dot represents outlier values > 1.5x and < 3x the interquartile range.

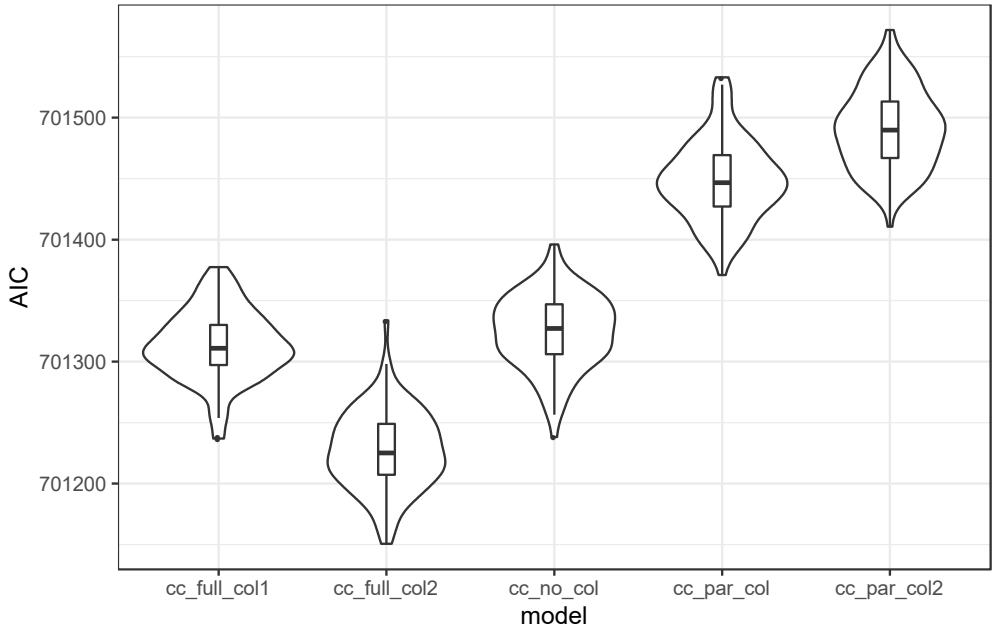

Supplementary Fig N6.4 Comparisons of demographic models at Step 3 (excluding 'cc_con_flow') in *Pareledone turqueti* (see Extended Data Fig 6.3 for visualisations of the models). The distributions of AIC from 100 independent expected SFS (violin plot), with each approximated using 200,000 coalescent simulations under the parameters that maximised the likelihood for each model. Each box represents the interquartile range (25th and 75th percentile), each line represents the median, each dot represents outlier values > 1.5x and < 3x the interquartile range.

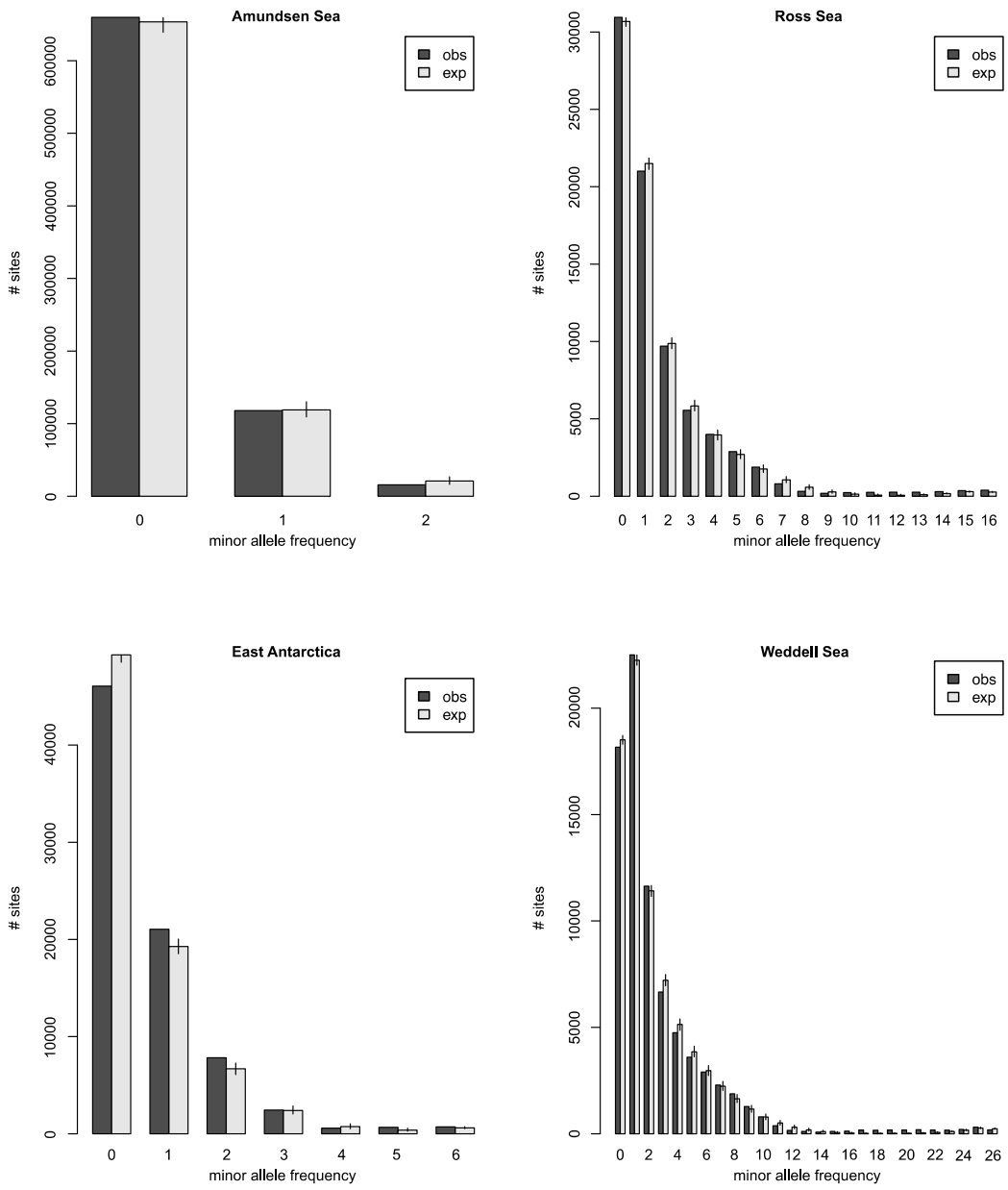

Supplementary Fig N6.5 Fit of the expected and observed one-dimensional (1d)-SFS under the best model evaluated ('cc_ful_col2') for *Pareledone turqueti*. Marginal 1d-SFS of the observed data (black bars) is compared to the averaged expected SFS (light grey bars) obtained from 100 SFS approximated with 200,000 coalescent simulations. Error bars = range of the values obtained across 100 simulated expected SFS under the parameters that maximised the likelihoods.

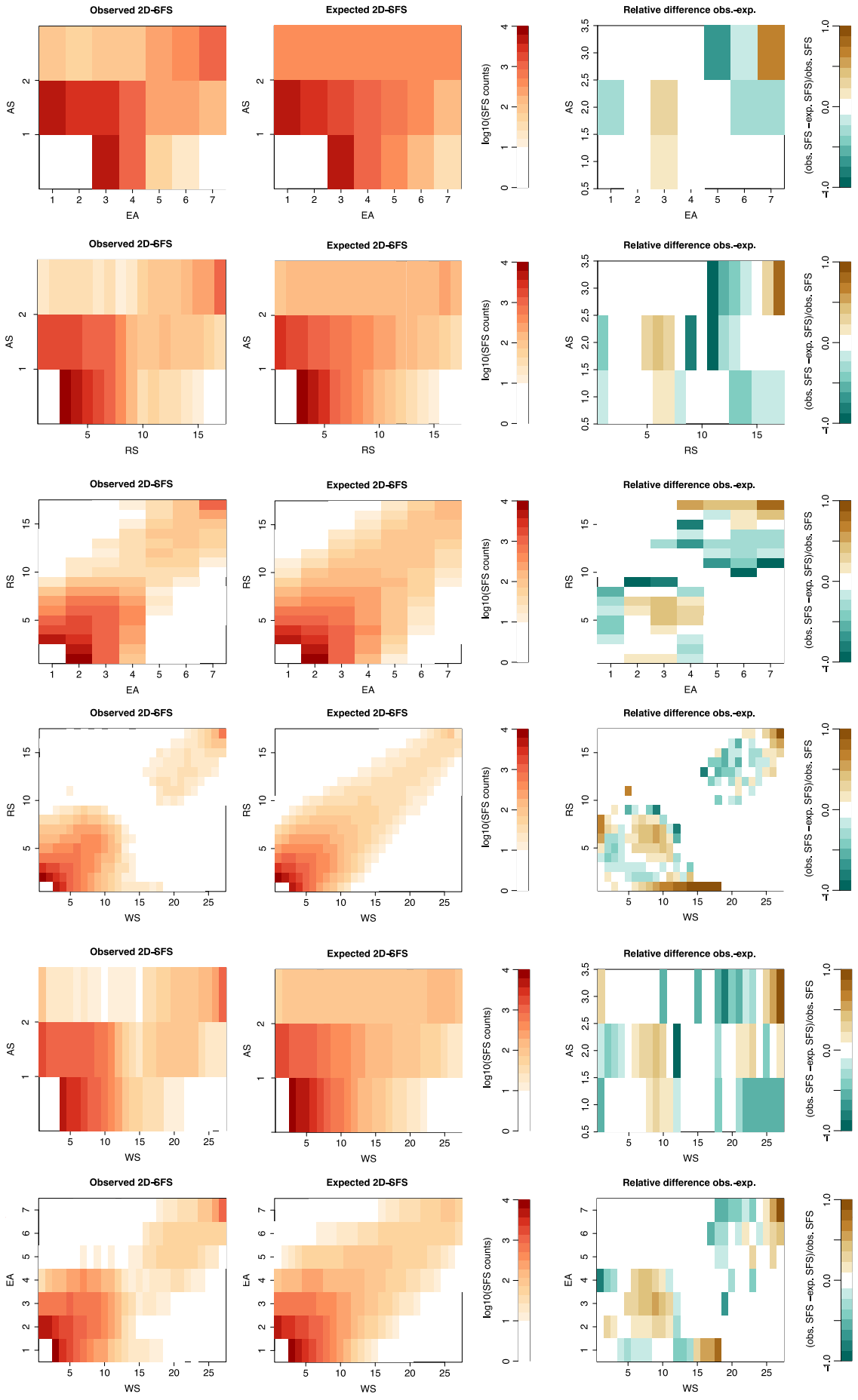
Observed 2D-SFS
Expected 2D-SFS
Relative difference obs.-exp.
log10(SFS counts)
(obs. SFS −exp. SFS)/obs. SFS
AS
EA
RS
WS

Supplementary Fig N6.6 Fit of the observed (obs) and averaged expected (exp) pairwise two-dimensional (2d)-SFS in $\log_{10}$ scale under the best model evaluated ('cc_ful_col2') for *Pareledone turqueti*. Left panel showing observed 2d-SFS, and middle panel showing expected 2d-SFS, between every two populations. Numbers in x and y axis represent SFS entries (i.e. sample size in diploids). Right panel showing the relative differences between observed and expected SFS in natural scale. Only entries with more than 10 SNPs are shown. Averaged expected SFS was obtained from 100 SFS approximated with 200,000 coalescent simulations under the parameters that maximised the likelihoods. Abbreviations: Amundsen Sea (AS), Ross Sea (RS), East Antarctica (EA) and Weddell Sea (WS).

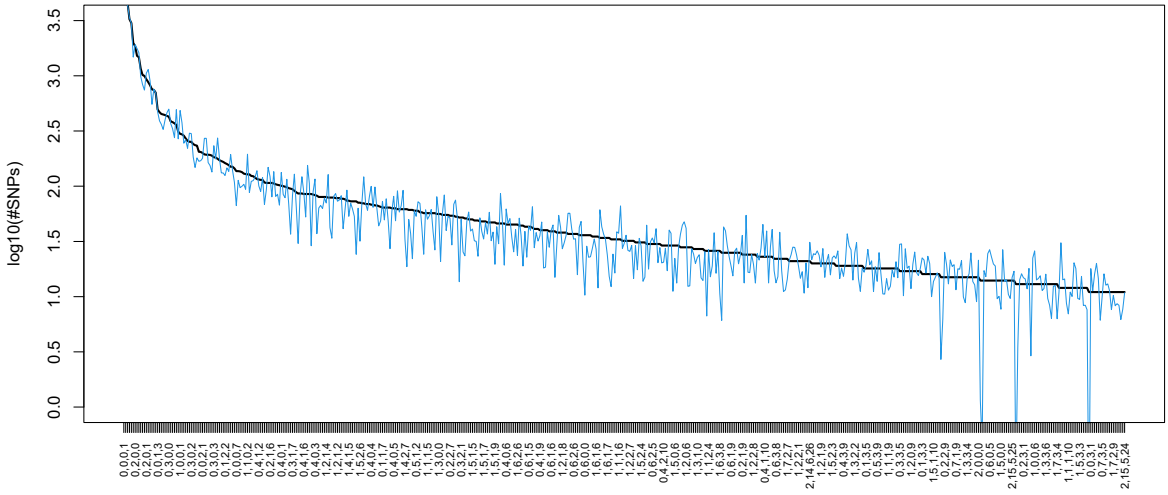

Supplementary Fig N6.7 Fit of the expected to observed four-dimensional (4d)-SFS under the best model evaluated ('cc_ful_col2') for *Pareledone turqueti*. Only entries with more than 10 SNPs are shown. Entries in the x-axis are indicated by column in the format of (AS, RS, EA, WS), and numbers within each entry correspond to the count of the derived allele in Amundsen Sea (AS), Ross Sea (RS), East Antarctica (EA) and Weddell Sea (WS). Solid black line represents observed SFS, blue line represents averaged expected SFS. Averaged expected SFS was obtained from 100 SFS approximated with 200,000 coalescent simulations under the parameters that maximised the likelihoods.

Demographic modelling of *O. victoriae*

We used a hierarchical approach to build a demographic model of WS, AS, RS and EA populations in *O. victoriae*. We started from simple models (Step 1) and gradually increased model complexity (Step 2) (Supplementary Fig 6.3-6.4). The first level included estimation of the population divergence topology that acted as the baseline for Step 2 models. At Step 1, the best model was '3_AS_RSEAWS' where AS was divergent form RS, EA and WS populations (Supplementary Table N6.4). At Step 2, after incorporating competing scenarios of historical WAIS configurations and contemporary gene flow driven by the ACC, the "full_col2" model was identified as the best model (Supplementary Table N6.5, Supplementary Fig N6.8). We did not pursue evaluating more complex models at Step 3 as models at Step 2 already addressed our hypothesis, and that we recognised the limited number of SNPs in *O. victoriae* might not offer enough information to differentiate Step 3 models. Under the most likely model of "full_col2", the ancestral population of *O. victoriae* experienced a population expansion at 3.81 (95% CI between 3.14 and 9.05) million years ago. Then, the AS population was estimated to have diverged from the ancestral population of WS, RS and EA at 3,770 years ago (95% CI between 2.74 and 7.28 million years ago). Direct gene flow between WS-AS, AS-RS and WS-RS was dated back to 1,250 (95% CI between 286 and 13,943) years ago. Finally, contemporary gene flow following the directionality of the ACC began in modern times (0 (95% CI between 0 and 0) years ago).

Interestingly, the parameter estimations of the time of divergence and the following events were very recent (< 4,000 years ago), indicating the overall very short tree length of *O. victoriae*. Nonetheless, we obtained a very good fit of expected and observed SFS (Supplementary Fig N6.9-6.10). It is known that *O. victoriae* likely diverged at ~430,000 years ago encompassing multiple interglacial cycles until now (*Chapter 4*), and following ecological and geological opportunity that would most likely enable gene flow linking to a full WAIS collapse scenario would be during the LIG.

Further investigation of population size changes using *StairwayPlot* revealed WS and RS experienced dramatic population bottleneck during the LGM, whereas AS and EA experienced population expansion followed by steady population size since the LIG (Fig 6.4). The contrasting patterns in population size changes between WS & RS and AS & EA likely revealed the different survival strategies of *O. victoriae* throughout the Pleistocene. Populations of WS and RS likely persisted on the shelf within *in situ* refugia over extreme glacial periods, resulting in population bottlenecks during the LGM. During LIG, large area of newly ice-free habitats would be available for *O. victoriae* to expand in population size. During the subsequent last glacial maximum, the AIS expanded across the Antarctic continental shelf, the shelf habitats would be reduced to small, isolated pockets of ice-free refugia. Those persisted on the shelf would experience extreme

bottleneck events, as observed in the WS and RS populations of *O. victoriae*. A previous review has also revealed the shelf habitats of WS and RS served as hotspots of *in situ* refugia for different Southern Ocean benthic taxa during the LGM (Lau et al. 2020). However, *O. victoriae* is also known to persist in deep-sea refugia, where the recent population expansion observed in AS and EA populations of *O. victoriae* likely support such scenario (Lau et al. 2021). Overall, the current evidence suggests contrasting refugial choice in different populations of *O. victoriae*, which would be associated with different rates of coalescence that bias the estimation of tree length. The shallow tree length was likely caused by the signatures of recent severe bottlenecks WS and RS. A severe recent bottleneck can be associated with many coalescence events at this single recent time point, leading to a reduction in the overall tree length (Excoffier et al. 2013; Terhorst and Song 2015), thus confounding the parameter scaling of time, population size and migration rates (Excoffier et al. 2013). Nonetheless, variation in tree length does not preclude the conclusion of genealogy (i.e. model choice) (Excoffier et al. 2013; Gattepaille et al., 2013).

Overall, we obtained a good fit of expected and observed SFS for *O. victoriae*, particularly for AS and EA populations (Supplementary Fig N6.9-6.10). For RS and WS populations, there are some unmodeled signatures of population size change, evident by the deviation between expected and observed SFS at intermediate and low frequency SNPs. This deviation was likely caused by unmodelled bottleneck (see Schraiber and Akey (2015) for a review on how bottleneck can influence the shape of an SFS). Signatures of bottleneck in RS and WS was also detected by *StairwayPlot*. However, *fastsimcoal* was unable to detect signatures of bottleneck in RS and WS, likely due to the simplistic model framework tested in this study. Among the entries of the joint SFS (Supplementary Fig N6.11), there is a very good fit of the expected SFS for the entries with more SNPs, with the fit of the expected SFS gradually gets poorer for entries with less SNPs. Similar to the case of *P. turqueti*, the poorest fits of the expected SFS were observed for the entries with high number of derived alleles in some populations (Supplementary Fig N6.11). This is expected as the modelled demographical scenarios aim to test for simple contrasting hypothesised scenarios of whether there was no, partial or complete historical WAIS collapse, as well as accounting the partners of circumpolar gene flow, across four populations (WS, AS, RS and EA). We did not model for specific population history in order to avoid over-parametrise the models in a limited dataset (i.e. RAD loci). The unmodelled high number of derived alleles in some populations likely represent unmodelled demography in the linked to unique population-level changes throughout the Quaternary glacial-interglacial cycles.

Supplementary Table N6.4 Summary of likelihoods for the model tested at Step 1 in *Ophionotus victoriae*. Model label correspond to model label in Supplementary Fig 6.3. Delta AIC and relative likelihoods were calculated following Excoffier et al. (2013). Abbreviations: Lhood = log likelihoods, AIC = Akaike Information Criterion.

Model label	log10(Lhood)	Number of parameters	AIC	Delta AIC	Relative likelihood (Akaike's weight of evidence)
3_AS_RSEAWS	-38899.39227	7	179184.601	0	1.00
5_EA_WSASRS	-38903.76809	7	179204.756	20.15502692	0.00
10_EA_AS_RSWS	-38905.74580	7	179213.865	29.26435918	0.00
2_WS_ASRSEA	-38914.76379	7	179255.402	70.80122112	0.00
11_RS_WS_EAAS	-38915.12245	7	179257.054	72.45320908	0.00
7_AS_RS_EAWS	-38916.28520	7	179262.410	77.80883558	0.00
8_RS_EA_WSAS	-38916.32230	7	179262.581	77.97971818	0.00
1_WS_AS_RS_EA	-38917.71713	6	179267.005	82.40430516	0.00
6_WS_AS_RSEA	-38917.60894	7	179268.507	83.90598202	0.00
9_EA_WS_ASRS	-38917.73057	7	179269.067	84.46620980	0.00
4_RS_EAWSAS	-38918.20016	7	179271.230	86.62914134	0.00

Supplementary Table N6.5 Summary of likelihoods for the model tested at Step 2 in *Ophionotus victoriae*. Model label correspond to model label in Supplementary Fig 6.3. Delta AIC and relative likelihoods were calculated following Excoffier et al. (2013). Abbreviations: Lhood = log likelihoods, AIC = Akaike Information Criterion.

Model label	log10(Lhood)	Number of parameters	AIC	Delta AIC	Relative likelihood (Akaike's weight of evidence)
full_col2	-36446.27016	26	167923.5204	0	1.00
par_col2	-36484.64353	22	168092.2681	168.7477320	0.00
full_col1	-36486.32053	22	168099.9924	176.4720042	0.00
no_col	-36490.59859	20	168115.6971	192.1767486	0.00
par_col	-36495.06466	22	168140.2678	216.7474670	0.00
con_flow	-36501.07430	15	168153.9482	230.4278688	0.00

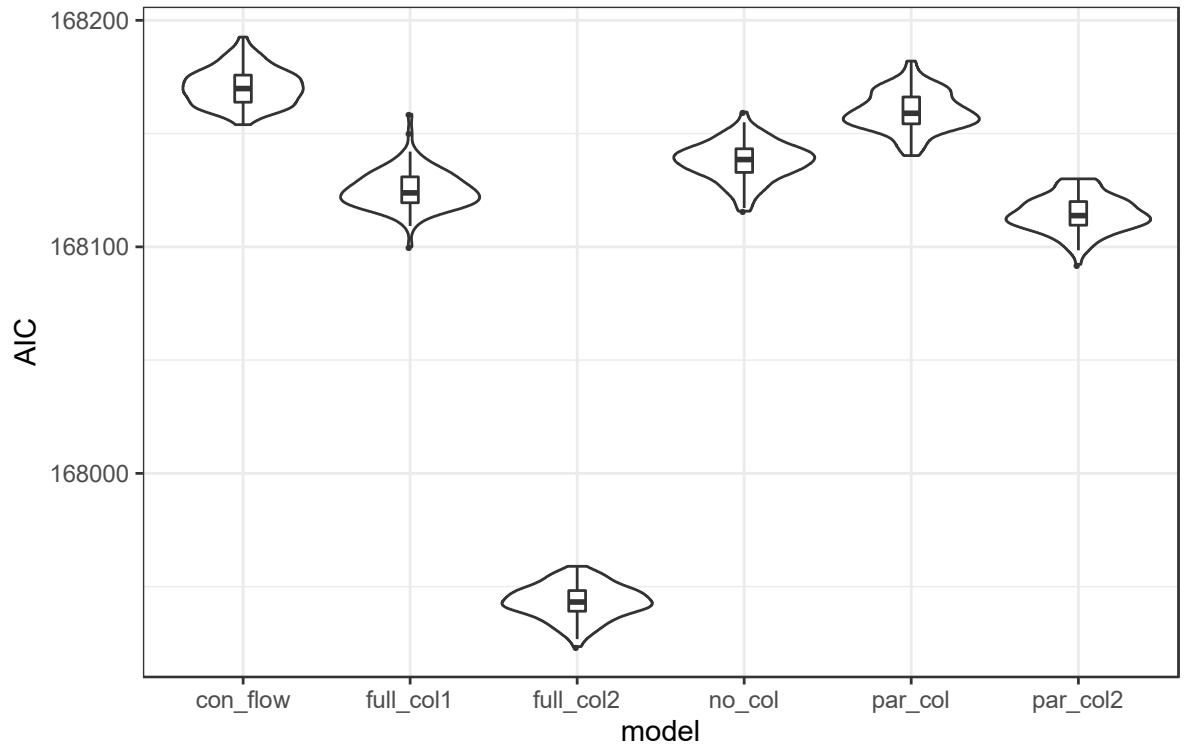

Supplementary Fig N6.8 Comparisons of demographic models at Step 2 in *Ophionotus victoriae* (see Supplementary Fig 6.3 for visualisations of the models). The distributions of AIC from 100 independent expected SFS (violin plot), with each approximated using 200,000 coalescent simulations under the parameters that maximised the likelihood for each model. Each box represents the interquartile range (25^{th} and 75^{th} percentile), each line represents the median, each dot represents outlier values > 1.5x and < 3x the interquartile range.

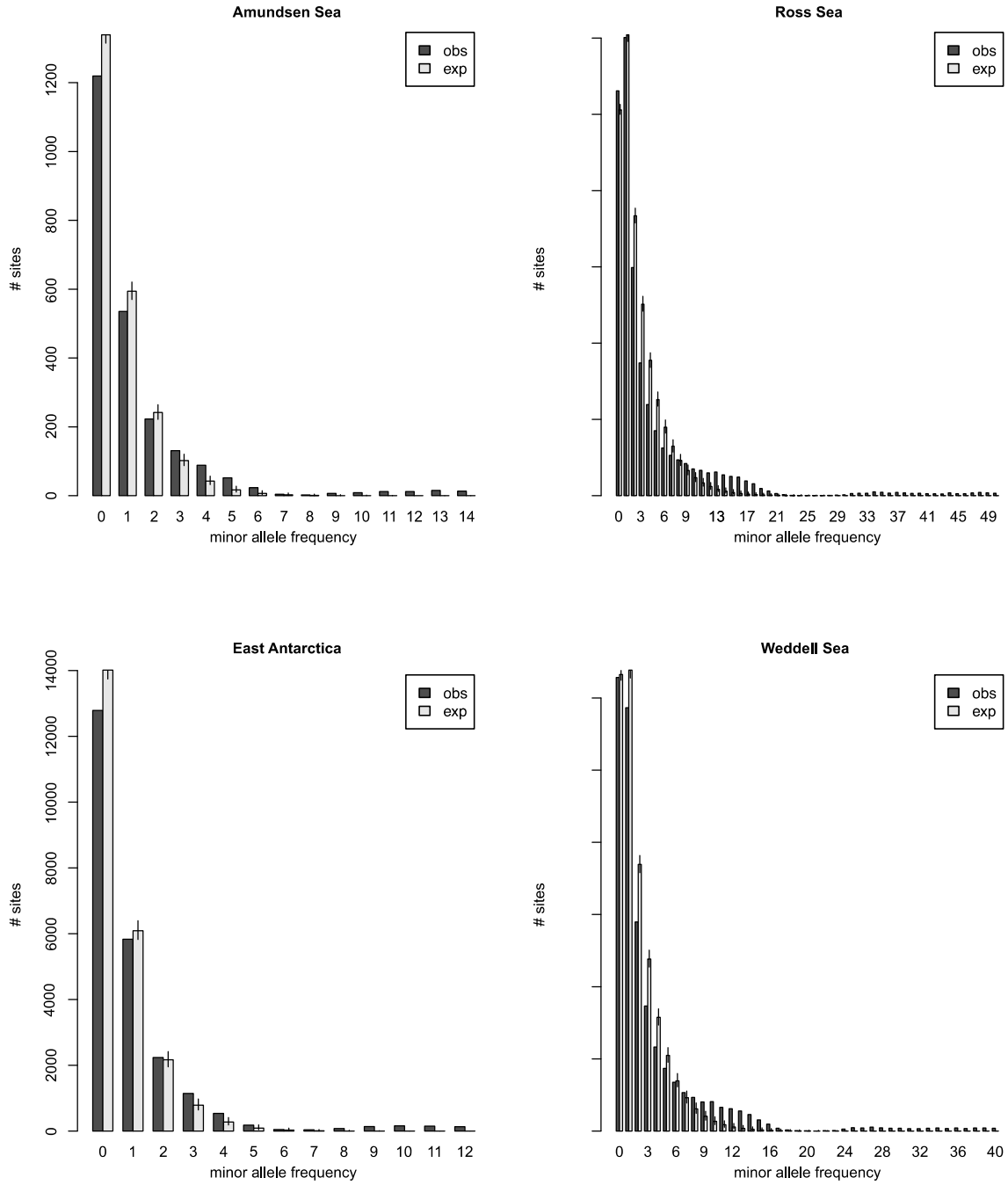

Supplementary Fig N6.9 Fit of the expected and observed one-dimensional (1d)-SFS under the best model evaluated ('ful_col2') for *Ophionotus victoriae*. Marginal 1d-SFS of the observed data (black bars) is compared to the averaged expected SFS (light grey bars) obtained from 100 SFS approximated with 200,000 coalescent simulations. Error bars = range of the values obtained across 100 simulated expected SFS under the parameters that maximised the likelihoods.

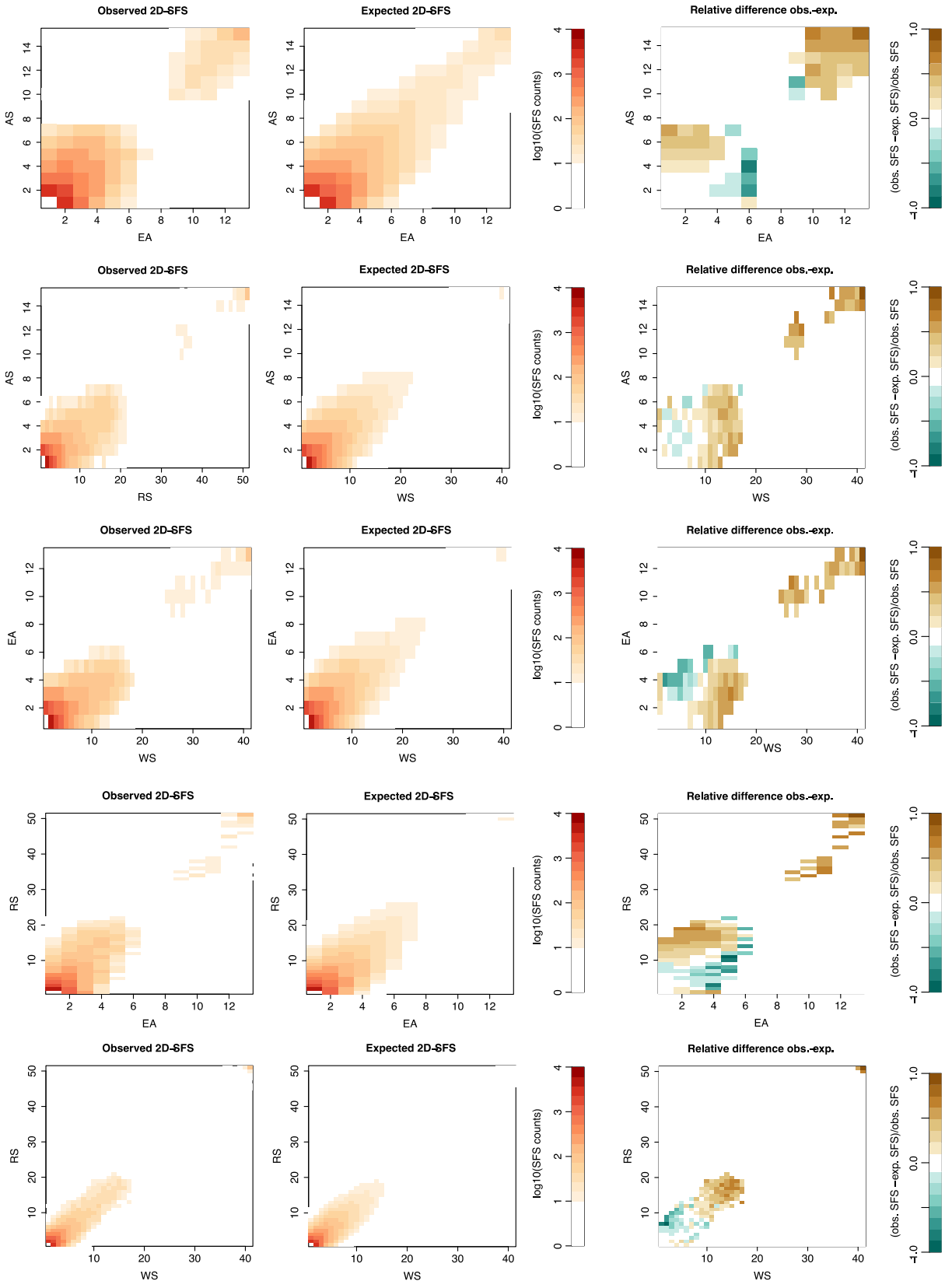

Supplementary Fig N6.10 Fit of the observed (obs) and averaged expected (exp) pairwise two-dimensional (2d)-SFS in $\log_{10}$ scale under the best model evaluated ('ful_col2') for *Ophionotus victoriae*. Left panel showing observed 2D-SFS, and middle panel showing expected 2D-SFS, between every two populations. Numbers in x and y axis represent SFS entries (i.e. sample size in diploids). Right panel showing the relative differences between observed and expected SFS in natural scale.

Only entries with more than 10 SNPs are shown. Averaged expected SFS was obtained from 100 SFS approximated with 200,000 coalescent simulations under the parameters that maximised the likelihoods. Abbreviations: Amundsen Sea (AS), Ross Sea (RS), East Antarctica (EA) and Weddell Sea (WS).

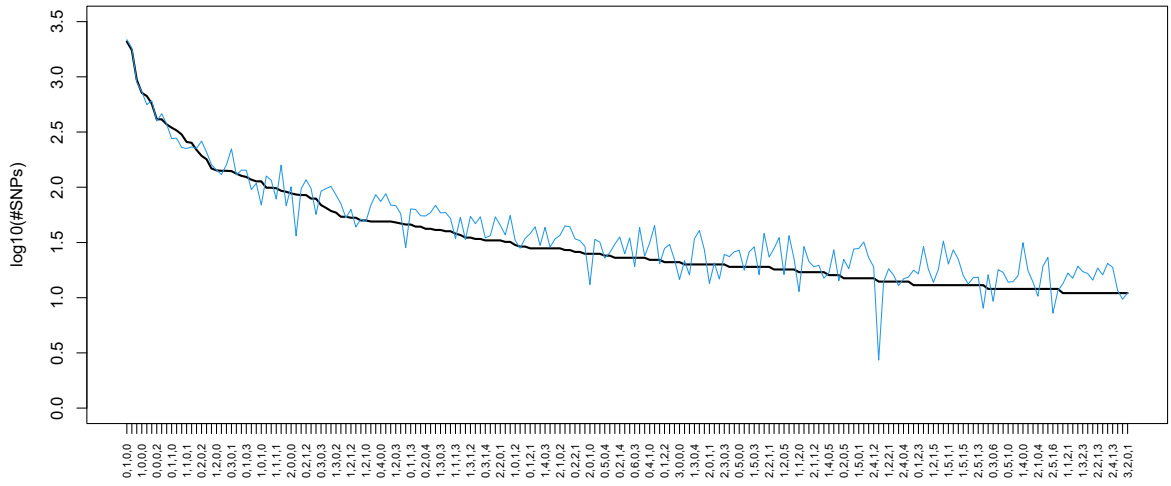

Supplementary Fig N6.11 Fit of the expected to observed four-dimensional (4d)-SFS under the best model evaluated ('ful_col2') for *Ophionotus victoriae*. Only entries with more than 10 SNPs are shown. Entries in the x-axis are indicated by column in the format of (AS, RS, EA, WS), and numbers within each entire correspond to the count of the derived allele in Amundsen Sea (AS), Ross Sea (RS), East Antarctica (EA) and Weddell Sea (WS). Solid black line represents observed SFS, blue line represents averaged expected SFS. Averaged expected SFS was obtained from 100 SFS approximated with 200,000 coalescent simulations under the parameters that maximised the likelihoods.

Additional references

Excoffier, L., Dupanloup, I., Huerta-Sánchez, E., Sousa, V. C., & Foll, M. (2013). Robust Demographic Inference from Genomic and SNP Data. *PLoS Genetics*, **9**(10), e1003905.

Gattepaille, L. M., Jakobsson, M., & Blum, M. G. B. (2013). Inferring population size changes with sequence and SNP data: Lessons from human bottlenecks. *Heredity*, **110**, 409–419.

Lau, S. C. Y., Strugnell, J. M., Sands, C. J., Silva, C. N. S., & Wilson, N. G. (2021). Evolutionary innovations in Antarctic brittle stars linked to glacial refugia. *Ecology and Evolution*, **11**(23), 17428–17446.

Lau, S. C. Y., Wilson, N. G., Silva, C. N. S., & Strugnell, J. M. (2020). Detecting glacial refugia in the Southern Ocean. *Ecography*, **43**(11), 1639–1656.

Terhorst, J., & Song, Y. S. (2015). Fundamental limits on the accuracy of demographic inference based on the sample frequency spectrum. *Proceedings of the National Academy of Sciences of the United States of America*, **112**(25), 7677–7682.